Alterations of Blood-Brain Barrier Functions and Gene Expression during *Toxoplasma gondii* Infection

By

Mohammad Syamsul Reza Harun (BSc, MSc)

Thesis submitted to the University of Nottingham

for the degree of Doctor of Philosophy

March 2019

Abstract

The apicomplexan protozoan parasite *Toxoplasma gondii* is the causative agent of toxoplasmosis, a major zoonotic infection that can infect roughly one-third of the world's human population. *T. gondii* is remarkable in its ability to rapidly disseminate *via* the bloodstream or within immune cells to immune-privileged sites distant from the site of initial infection. It can cross the blood-brain, blood-retinal and blood-placental barriers. A better understanding of the mechanisms underpinning the parasite's interaction with these barriers is crucial for the development of therapeutic interventions. Initial work in this thesis characterises the interaction of *T. gondii* with human brain microvascular endothelial cells (hBMECs) evaluated using Alamar blue viability assay, FITC-dextran flux-based permeability assay, transendothelial electrical resistance (TEER) measurements for tight junction integrity evaluation, viability, early/late apoptosis and cell cycle analyses using NC-3000™ image-based flow cytometry and tight junction genes (Occludin, PRKCA and ZO-1) and inflammatory genes (IL-6, P-GP and TNF-alpha) genes expression using RT-PCR. These experiments were performed at 3, 6, 24, 48 and 72 hours post infection (h.p.i) to represent early (3 and 6 h.p.i), middle (24 h.p.i) and late (48 and 72 h.p.i) stages of infection at blood brain barrier (BBB). During the early and middle stages of infection, *T. gondii* maintained host cells' viability, suppressed cell apoptosis by halting cells at the G0/G1 stage, induced up-regulation of IL-6 gene, reduced the permeability of infected cells compared to non-infected cells. Late stage of infection was marked by significant reduction of the cell integrity and vitality, and by significant increase of fragmented DNA.

Initial data lead to the hypothesis that analysis of the transcriptomic changes in hBMECs in response to *T. gondii* infection would reveal some facets of the molecular mechanisms underlying signalling mechanisms that mediate the parasite-hBMECs interaction. To test this hypothesis, global transcriptome (i.e. gene expression) of both host hBMECs and the parasite during infection were examined in a time course study. Total RNA samples from *T. gondii* RH-infected hBMECs were obtained at 6, 24 and 48 h.p.i where messenger RNA (mRNA) and small RNA were sequenced using Illumina™ next-generation sequencing. MRNA and small RNA sequencing reads were mapped to the annotated human and *T. gondii* reference genomes before conducting differential expression analysis on control (uninfected) versus infected cell reads. Genes expressed with false discovery rate (FDR) < 0.01 and > 1 $\log_2$ fold change were identified. Differently expressed genes were then validated with microarray and quantitative real-time PCR (RT-PCR). This study confirmed previous findings that *T. gondii* infection halts cell cycle progression and modulates the expression of cancer-like genes in infected cells. Integrated mRNA/miRNA expression profiling and pathway analysis showed multiple signalling pathways including, ATF4 activation, TP53 regulation, selenoamino acid metabolism and selenocysteine synthesis as key pathways regulated during *T. gondii* infection. Small RNA study identified increased expression of miR-7, miR-19, miR-20 families and expression of the miR-17-92 family that possibly determine the fate of host cells in *T. gondii* infection. Also, *T. gondii*'s ribosomal proteins L36 and S12 were identified as key players in its pathogenesis and have good potential as vaccine candidates.

Because Wnt signalling pathway was one of the most affected pathways, its role of Wnt pathway in *T. gondii* infection was further investigated by examining the anti-parasitic effects of Monensin, an inhibitor of the host cell WNT signalling pathway, on *T. gondii* tachyzoites and the proliferation of

hBMECs and microglial cells. Monensin showed significant anti-*T. gondii* activity against the tachyzoite grown in cerebral endothelial cell and microglial cell cultures. However, inhibition of *T. gondii* infection in hBMECs was not directly achieved through blocking WNT signalling. Interestingly, monensin had more lethal effect against the parasite compared to its mild and reversible toxic effect on host cells at 0.1 μM concentration. Data from this study encourage further exploration of monovalent ionophores for repurposing as novel anti-toxoplasmosis leads.

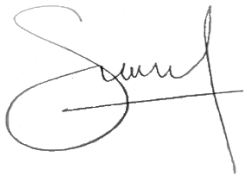
Using cell culture techniques, transwell system and two quorum sensing (QS) molecules produced by *Pseudomonas aeruginosa* (3-Oxo and PQS), a leading agent of nosocomial infection, the effect of exposure to these QS molecules on the ability of the parasite to cross the BBB endothelial cells was evaluated. The effects of 3-Oxo and PQS at a low and high concentration with and without *T. gondii* infection on hBMECs were also characterised. Both 3-Oxo and PQS increased hBMEC monolayer permeability and integrity through *PRKCA* gene up-regulation, slowly induced cell apoptosis and halted cell proliferation at the G0/G1 stage. Overall, these results did not support the hypothesis that QS molecules from *P. aeruginosa* facilitate *T. gondii* crossing of BBB into the brain.

Taken together, this thesis has presented new findings on *T. gondii* interaction with a 2D BBB model represented by hBMEC culture in a Transwell system, identified new genes and miRNAs altered by infection, and showed the potential of monensin as treatment for *T. gondii* infection. These findings should facilitate further analysis of host-pathogen interactions in toxoplasmosis in preclinical animal models.

.

Declaration

I declare that the work in this dissertation was carried out in accordance with the regulations of the University of Nottingham. The work is original and has not been submitted for any other degree at the University of Nottingham or elsewhere.



_____

Name: Mohammad Syamsul Reza Harun

Student ID: 4223081

Date: 16 March 2019

Conferences and Presentations

Oral Presentation

Sutton Bonington Campus Postgraduate Wide Symposium

16 & 17 May 2017, Sutton Bonington Campus

Early Careers Researcher Presentation Day

Tuesday 6th Dec 2016, B02/B02 Gateway Building, Sutton Bonington Campus, University of Nottingham.

Early Careers Researcher Presentation Day

Friday 3rd July 2015, A29 School of Veterinary Medicine and Science, Sutton Bonington Campus, University of Nottingham.

Poster Presentation

Early Career UK and Ireland Blood-Brain Barrier Symposium 2015

Friday 27th November 2015, Highfield Campus, University of Southampton.

Course/Conference attended

EMBL Course: Whole Transcriptome Data Analysis

4 - 7 Oct 2016, EMBL Heidelberg, Germany

Early Career UK and Ireland Blood-Brain Barrier Symposium 2015

Friday 27th November 2015

Highfield Campus, University of Southampton

Acknowledgements

All praise to Allah, for his blessings by surrounding me with wonderful people. I would like to express my deepest gratitude to my main supervisor Associate Professor Hany M. Elsheikha for his scientific supervision and academic support. I am immeasurably grateful for his unlimited support and continuous guidance, which helped me tremendously in all aspects of research and completion of this thesis.

Also, I would like to thank my co-supervisor Dr Gareth Cave for his support and suggestions in this research. I would like to acknowledge the support of the technicians at the School of Veterinary Medicine and Science, notably Mrs Catherine Williams, Mrs Belinda Wang and Mr Scott Hulme for their help and support. Not to forget Dr Robin Flynn who provided useful comments on my research progress in my first year review and the Anton Enright research group at EBI, Hinxton for helping me with sequencing and microarray data analysis.

I am also very grateful to the school administrative staff and postgraduate communities within the school for their help, interactions, support and advice. Their support has made my experience during my PhD an invaluable experience.

I gratefully acknowledge the financial support from the Malaysia Ministry of Higher Education and Advanced Medical and Dental Institute, Universiti Sains Malaysia.

Finally, I would like to say a huge thank you to my parents, my in-laws, my siblings, my wife, and my two beautiful daughters for their patience, prayers and support throughout my study.

Table of Contents

Chapter 1 General Introduction 1

1.1 The Organism 1

1.2 Biology and Life Cycle Forms 2

1.3 Routes of Infection 3

1.4 Genetic structure of *T. gondii* 4

1.5 Impact of Toxoplasmosis on Animals 6

1.6 Clinical Significance of Toxoplasmosis in Human 7

1.7 Disease forms of Toxoplasmosis 7

1.7.1 Congenital Toxoplasmosis 8

1.7.2 Ocular Toxoplasmosis 9

1.7.3 Cerebral Toxoplasmosis 9

1.7.4 Pulmonary Toxoplasmosis 11

1.8 Diagnosis of Toxoplasmosis 11

1.9 Treatment of Toxoplasmosis 13

1.9.1 Monensin 14

1.10 Breaching the Biological Barriers 15

1.10.1 Bronchial Epithelial Barrier (BEB) 15

1.10.2 Blood Brain Barrier (BBB) 15

1.10.3 Blood-Retinal Barrier (BRB) 16

1.11 Tight Junction 17

1.11.1 Claudin and Occludin 19

1.11.2 Junctional Adhesion Molecules (JAMs) 20

1.11.3 Zona Occludens (ZO) 20

1.12 Mechanisms of Penetration of BBB by Microbes 21

1.13 Molecular Pathogenesis and Host-Parasite Interaction 24

1.13.1 Metabolism 24

1.13.2 Apoptosis 25

1.13.3 Immunity 26

1.14 Transcriptomics in *T. gondii*-host Interaction Research 29
1.15 The Role of miRNA in *T. gondii* Infection 30
1.16 *Toxoplasma gondii* and *Pseudomonas aeruginosa* Quorum Sensing Molecules 31
1.17 Thesis: Hypothesis and Aims 32

Chapter 2 The Response of Human Brain Microvascular Endothelial Cells (hBMECs) to *Toxoplasma gondii* Infection 34
2.1 Abstract 34
2.2 Introduction 34
2.3 Materials and Methods 36
2.3.1 Growth Media Formulation 36
2.3.2 Maintenance of Cell Culture 37
2.3.3 Cell Counting 38
2.3.4 Counting the Tachyzoites 39
2.3.5 Cell Seeding Optimisation 39
2.3.6 Cell Insert Count 40
2.3.7 Cell Viability Assays 40
2.3.8 *T. gondii* Infection Titration 41
2.3.9 Measurement of Cellular Thiols 41
2.3.10 Mitochondrial Potential Assay 42
2.3.11 DNA Fragmentation Assay 44
2.3.12 Two-Step Cell Cycle Analysis 44
2.3.13 EVOM Voltohmmeter Calibration 45
2.3.14 Measurement of TEER 46
2.3.15 HBMECs Monolayer Permeability 48
2.3.16 Extracting total RNA using Qiagen RNeasy Kit 48
2.3.17 Total RNA Quality Analysis 49
2.3.18 Converting RNA to cDNA 49

2.3.19 Real time PCR using Roche Lightcycler 480 II and SYBR Green Mastermix.....51
2.3.20 Primers.....52
2.3.21 Statistical analysis.....54
2.4 Results.....54
2.4.1 Optimisation of Cell Seeding and Multiplicity of Infection.....54
2.4.2 The Effect of Long-term Culture on Membrane Integrity.....56
2.4.3 *Toxoplasma gondii* Titration.....57
2.4.4 Characteristics of *T. gondii* Infection of hBMECs.....61
2.4.5 Tight Junction and Inflammatory Genes Expression following *T. gondii* Infection.....75
2.5 Discussion.....79
2.5.1 Optimisation Experiments.....79
2.5.2 Parasite Effects on Host Cell Viability and Vitality.....81
2.5.3 Effects on Host Cell Apoptosis.....81
2.5.4 Effects on Host Cell Cycle.....83
2.5.5 Effects on Host Cell Junction and Inflammatory Gene Expression.....83
2.5.6 Conclusion.....86

Chapter 3 Integrated Genome-wide mRNA and miRNA Expression Profiling of *Toxoplasma gondii*-Infected HBME Cells.....87
3.1 Abstract.....87
3.2 Introduction.....88
3.3 Materials and Methods.....90
3.3.1 Cell Growth and Maintenance.....90
3.3.2 Extracting total RNA and miRNA using Qiagen RNeasy Kit.....90
3.3.3 RNA Quality Analysis: Illumina® Agilent® 2100 Bioanalyzer.....91
3.3.4 Messenger RNA: Library Preparation and Sequencing.....93
3.3.5 Messenger RNA: Sequence Data and Differential Expression Analysis.....94

3.3.6 Microarray Experiment and Data Analysis 96
3.3.7 Gene Ontology (GO) with Protein Analysis Through Evolutionary Relationships Classification System (PANTHER) Analysis 97
3.3.8 Reactome Pathway Analysis 99
3.3.9 ToxoDB.org Gene Analysis 100
3.3.10 Small RNA: Library Preparation and Sequencing 100
3.3.11 Small RNA: Sequence Data Analysis 101
3.3.12 Diana Tools – mirPath v.3 103
3.3.13 Converting RNA to cDNA 104
3.3.14 Real-time PCR using Roche LightCycler® 480 II and SYBR Green Mastermix 106
3.3.15 Primers 107
3.3.16 Statistical Analysis 109
3.4 Results 109
3.4.1 Transcriptomes Based on mRNA Sequencing: Mapped to Human Reference Genome 109
3.4.2 Transcriptomes Based on mRNA Sequencing: Mapped to *T. gondii* Reference Genome 145
3.4.3 Transcriptomes Based on miRNA: Mapped to Human Reference Genome 154
3.4.4 Transcriptomes Based on miRNA: Mapped to *T. gondii* Reference Genome 163
3.4.5 Transcriptomes Based on Microarray Data 168
3.4.6 Validation of genes using RT-PCR 194
3.5 Discussion 198
3.5.1 Host Gene Expression Profile in *T. gondii* Infection 198
3.5.2 Expression Profile of *T. gondii* Genes During Infection 207
3.5.3 Host Small RNA Expression Profile in *T. gondii* Infection 210
3.5.4 *T. gondii* Small RNA Expression Profile During Infection 214
3.5.5 Sequencing Data Validation with qPCR 216
3.5.6 Conclusion 217

Chapter 4 Chapter 4 Cytotoxic and Anti-*Toxoplasma gondii* Activities of Monensin (a WNT Signalling Inhibitor) 218
4.1 Abstract 218
4.2 Introduction 219
4.3 Materials and Methods 221
4.3.1 Chemicals 221
4.3.2 Cell Lines 221
4.3.3 Parasite Strain and Culture Conditions 222
4.3.4 Efficacy of Monensin on the In vitro Growth of *T. gondii* 223
4.3.5 Parasite Count 223
4.3.6 Colorimetric SRB Assay 224
4.3.7 Effects of Monensin on Host Cell Viability 225
4.3.8 Monensin Cytoxicity using Nucleic Acid Double Staining 225
4.3.9 Mitochondrial Potential, DNA Fragmentation, Cell Cycle Analyses 226
4.3.10 Effect of Monensin on BBB Integrity 226
4.3.11 Microarray Data Analysis 227
4.3.12 Gene Ontology (GO) with Protein Analysis Through Evolutionary Relationships Classification System (PANTHER) Analysis 229
4.3.13 Reactome Pathway Analysis 229
4.3.14 Statistical Analysis 230
4.4 Results 230
4.4.1 Cytotoxicity of Monensin 230
4.4.2 The Antiparasitic Effect of Monensin 233
4.4.3 Effects on Mitochondrial Potential, DNA Fragmentation and Cell Cycle Assays 236
4.4.4 Assessment of hBMEC Monolayer Integrity 242
4.4.5 Microarray Quality Control and Normalisation 244
4.4.6 Venn Diagrams 249
4.4.7 Patterns of Altered Gene Expression: Control vs Monensin_only 249

4.4.8 Patterns of Altered Genes Expression: Control vs TG_only 256
4.4.9 Patterns of Altered Genes Expression: Control vs TG_Monensin.....262
4.4.10 Gene Ontology (GO) and Pathway Analysis 269
4.5 Discussion 290
4.5.1 Conclusion.....295

Chapter 5 Assessment of Quorum Sensing Molecules Roles in *Toxoplasma gondii* Infection 297
5.1 Abstract 297
5.2 Introduction.....298
5.3 Material and Methods.....301
5.3.1 Preparation of 3-Oxo and PQS Solutions.....301
5.3.2 HBMEC Monolayer Permeability Assessment by FITC-Dextran Flux Assay.....301
5.3.3 HBMEC Monolayer Integrity Assessment by TEER Measurement.....302
5.3.4 Cell Viability Assay by Alamar Blue 302
5.3.5 The Effect of 3-Oxo and PQS on hBMEC Cells Mitochondrial Potential, DNA Fragmentation and Cell Cycle. 302
5.3.6 Tight Junction Genes Expression Study 303
5.3.7 Effect of Quorum Sensing Molecules on *T. gondii* Infection.....303
5.3.8 Statistical analysis 304
5.4 Results.....304
5.4.1 Cytotoxic Effects of PQS and 3-Oxo 304
5.4.2 Monolayer Permeability Assay 306
5.4.3 Membrane Integrity Assay 307
5.4.4 Mitochondrial Potential Assay 308
5.4.5 DNA Fragmentation 309
5.4.6 Cell Cycle Assay 309
5.4.7 Tight Junction Genes Expression 310

5.4.8 The Effect of Quorum Sensing Molecules on *T. gondii* Infection on hBMECs 314

5.5 Discussion 319

5.5.1 Effects of QS Molecules on hBMEC viability and Cell Cycle 319

5.5.2 Effects of QS Molecules on hBMEC Permeability and Integrity 321

5.5.3 Conclusion 324

Chapter 6 General Discussion 325

6.1 Introduction 325

6.2 Phenotypic and Functional Changes in hBMECs following *T. gondii* Infection 329

6.3 Effects on Host Cell Junction and Inflammatory Gene Expression 331

6.4 HBMECs Immune Response to *T. gondii* Infection 334

6.5 Key Pathways in *T. gondii* Invasion of hBMECs 335

6.6 Potential Use of Monensin as Anti-*T. gondii* Treatment at BBB 337

6.7 Quorum Sensing Molecules Reduce hBMECs Permeability Possibly by Inducing PRKCA Expression 341

6.8 Quorum Sensing Molecules Induce Apoptosis and Halt Cell Cycle Stage Progression in hBMECs 344

6.9 Limitations of Study 346

6.10 Future Work and Conclusion 347

Chapter 7 Appendices 350

Chapter 8 References 402

List of Figures

Figure 1-1 Electron micrographic representation of a tachyzoite (left) and a bradyzoite (right) of *T. gondii*. 2

Figure 1-2 Life cycle of *Toxoplasma gondii*. 3

Figure 1-3 Components of TJ and adherens junction.....18

Figure 1-4 Breaching blood-brain barrier.....22

Figure 1-5 Innate and adaptive immunity interplay in intracellular *Toxoplasma gondii* infection.....28

Figure 2-1 TEER value of hBMEC monolayer resistance in Ωcm^2 unit measured over 168 hours (7 days). 55

Figure 2-2 TEER value of hBMECs membrane resistance in Ωcm unit measured over 216 hours (*i.e*. nine days).....57

Figure 2-3 Temporal changes in hBMEC's viability. 58

Figure 2-4 The effect of a multiplicity of infection on hBMEC monolayer integrity.....59

Figure 2-5 The effect of a multiplicity of infection on hBMECs monolayer permeability.....60

Figure 2-6 The number of *T. gondii* tachyzoites that passed through hBMECs monolayer in the Transwell system. 61

Figure 2-7 The effect of *T. gondii* infection on hBMECs monolayer permeability.....62

Figure 2-8 The effect of *T. gondii* infection on hBMECs' monolayer integrity.....63

Figure 2-9 A: Scatter plots of uninfected hBMECs vitality (left) and infected hBMECs vitality (right) from 3 to 72 hours. B: Bar chart showing hBMECs vitality cells population following *T. gondii* infection. h.p.i. 65

Figure 2-10 A: Scatter plots of uninfected hBMECs' mitochondrial potential (left) and infected hBMECs' mitochondrial potential (right), from 3 to 72 hours. B: Bar chart showing the mitochondrial potential state of hBMECs following *T. gondii* infection. 68

Figure 2-11 A: Histograms of uninfected hBMECs with fragmented DNA (left) and infected hBMECs with fragmented DNA (right), from 3 to 72 hours. B: Bar chart showing hBMECs with fragmented DNA following *T. gondii* infection……71

Figure 2-12 A: Histograms of uninfected hBMECs' cell cycle stage population (left) and infected hBMECs' cell cycle stage population (right) from 3 to 72 hours. B: Bar chart showing cell cycle stage population of hBMECs following *T. gondii* infection. 74

Figure 2-13 Normalised fold change of Occludin, PRKCA, ZO-1, IL-6, P-GP and TNF-alpha genes at 3, 6, 24, 48 and 72 h.p.i……78

Figure 3-1 An electropherogram showing a successful sample total RNA run peaks complete with ladder electropherogram. 92

Figure 3-2 Pre and post-normalised counts of mRNA sequencing data after alignment to the human reference genome. 111

Figure 3-3 Correlation heatmap of all mRNA transcriptome expression profiles after mapping to the human reference genome.. 113

Figure 3-4 Principal component analysis (PCA) plot showing all samples transcriptome dataset variation. 114

Figure 3-5 Volcano plots of DEGs (control *vs* infected) at 6, 24 and 48 h.p.i. ……116

Figure 3-6 Venn diagram of DEGs at 6, 24 and 48 h.p.i from mRNA sequencing…... 117

Figure 3-7 PANTHER GO-Slim molecular function ontology hits for significantly DEGs at 6 h.p.i... 122

Figure 3-8 PANTHER GO-Slim biological processes ontology hits for significantly DEGs at 6 h.p.i. 123

Figure 3-9 PANTHER GO-Slim cellular components ontology hits for significantly DEGs at 6 h.p.i.. 125

Figure 3-10 PANTHER GO-Slim molecular function ontology hits for significantly DEGs at 24 h.p.i.....128

Figure 3-11 PANTHER GO-Slim biological processes ontology hits for significantly DEGs at 24 h.p.i.....129

Figure 3-12 PANTHER GO-Slim cellular components ontology hits for significantly DEGs at 24 h.p.i.....130

Figure 3-13 PANTHER GO-Slim molecular function ontology hits for significantly DEGs at 48 h.p.i.....135

Figure 3-14 PANTHER GO-Slim biological processes ontology hits for significantly DEGs at 48 h.p.i.....136

Figure 3-15 PANTHER GO-Slim cellular components ontology hits for significantly DEGs at 48 h.p.i.....137

Figure 3-16 Pre and post-normalised counts of mRNA sequencing data after alignment to *T. gondii* ME49 reference genome.. 146

Figure 3-17 Correlation heatmap of all mRNA transcriptome expression profiles after mapping to *T. gondii* reference genome. 147

Figure 3-18 Principal component analysis (PCA) plot is showing all samples transcriptome dataset variation. 148

Figure 3-19 Venn diagram of DEGs at 6, 24 and 48 hours from transcriptome reads mapped to *T. gondii* genome.. 149

Figure 3-20 Venn diagram comparing up-regulated miRNAs (panel A) and precursors (panel B) at 6 and 48 h.p.i.. 158

Figure 3-21 Venn diagram comparing down-regulated miRNAs (panel A) and precursors (panel B) at 6 and 48 h.p.i. 159

Figure 3-22 Venn Diagram of DEGs at 6, 24 and 48 h.p.i based on mapping to *T. gondii* reference genome. 167

Figure 3-23 Box plots of expressed genes of all samples pre and post-normalisation of microarray samples. 169

Figure 3-24 Correlation heatmap of all microarray sequencing samples.....170

Figure 3-25 Volcano plot of DEGs (control *vs* infected) at 6, 24, and 48 h.p.i.....172

Figure 3-26 Venn diagram of DEGs at 6, 24, and 48 hours from a microarray experiment.....173

Figure 3-27 PANTHER GO-Slim molecular function ontology hits for significantly DEGs at 6 h.p.i.. 177

Figure 3-28 PANTHER GO-Slim biological process ontology hits for significantly DEGs at 6 h.p.i. 179

Figure 3-29 PANTHER GO-Slim cellular component ontology hits for significantly DEGs at 6 h.p.i.. 180

Figure 3-30 PANTHER GO-Slim molecular function ontology hits for significantly DEGs at 24 h.p.i.....183

Figure 3-31 PANTHER GO-Slim biological process ontology hits for significantly DEGs at 24 h.p.i.....184

Figure 3-32 PANTHER GO-Slim cellular component ontology hits for significantly DEGs at 24 h.p.i.....185

Figure 3-33 PANTHER GO-Slim molecular function ontology hits for significantly DEGs at 48 h.p.i.....189

Figure 3-34 PANTHER GO-Slim biological process ontology hits for significantly DEGs at 48 h.p.i.....191

Figure 3-35 PANTHER GO-Slim cellular component ontology hits for significantly DEGs at 48 h.p.i.....192

Figure 3-36 Normalised FC of CXCR4, IFI6, HSP90AAP, NR4A2, TXNIP, ZNF451, and ZNF467 genes at 6, 24 and 48 h.p.i at MOI of 5 by SYBR green RT-qPCR.....196

Figure 4-1 *Toxoplasma gondii* tachyzoite growth inhibition in microglial and hBMEC cultures is dependent on monensin concentration.. 234

Figure 4-2 Microglial and hBMEC cultures showed different sensitivity to monensin concentration.....235

Figure 4-3 Cytotoxic effect of monensin on hBMECs and microglial cells…231

Figure 4-4 The effects of 24 hours treatment with 0.01 µM and 0.1 µM monensin on hBMEC's viability.. 233

Figure 4-5 The effects of 24 hours treatment with 0.1 µM monensin on hBMEC's mitochondrial potential. 238

Figure 4-6 The effects of 24 hours treatment with 0.1 µM monensin on hBMECs DNA fragmentation. 240

Figure 4-7 The effects of 24 hours treatment with 0.1 µM monensin on hBMECs G0/G1, S and G2/M cell cycle stages.....242

Figure 4-8 The effect of 0.1 μM monensin treatment on transendothelial electrical resistance (TEER) of the hBMECs monolayer.. 243

Figure 4-9 Box plots of pre (top) and post-normalisation (bottom) for all samples…….....245

Figure 4-10 Correlation heatmap for all 12 microarray transcriptome expression profiles.. 247

Figure 4-11 Principal component analysis (PCA) plot is showing all samples transcriptome dataset variation.. 248

Figure 4-12 Venn diagram comparing expression profiles of Control *vs* TG_only, Control *vs* Monensin_only and Control *vs* TG_Monensin.....249

Figure 4-13 Volcano plot showing the expression profile of hBMECs after treatment with 0.1 μM monensin (Monensin_only).. 251

Figure 4-14 Correlation heatmap of the top 30 most significant DEGs following 24 hours treatment with 0.1 μM monensin.. 252

Figure 4-15 Volcano plot showing the expression profile of hBMEC after being infected with *T. gondii* for 24 hours (TG_only).. 256

Figure 4-16 Correlation heatmap of the top 30 most significant DEGs from 24 hours of *T. gondii* infection (TG_only).. 257

Figure 4-17 Volcano plot showing the expression profile of hBMECs infected with *T. gondii* then treated with 0.1 μM monensin (TG_Monensin).....262

Figure 4-18 Correlation heatmap of the top 30 most significant DEGs from hBMECs infected with *T. gondii* then treated with 0.1 μM monensin (TG_Monensin).....263

Figure 4-19 PANTHER GO-Slim biological process ontology hits for significantly DEGs due to treatment with 0.1 μM monensin for 24 hours (Monensin_only).....271

Figure 4-20 PANTHER GO-Slim molecular function ontology hits for significantly DEGs due to treatment with 0.1 μM monensin for 24 hours (Monensin_only).....272

Figure 4-21 PANTHER GO-Slim cellular component ontology hits for significantly DEGs due to treatment with 0.1 μM monensin for 24 hours (Monensin_only).....272

Figure 4-22 PANTHER GO-Slim biological process ontology hits for significantly DEGs due to *T. gondii* infection (TG_only)…….277

Figure 4-23 PANTHER GO-Slim molecular function ontology hits for significantly DEGs due to *T. gondii* infection (TG_only)……278

Figure 4-24 PANTHER GO-Slim cellular component ontology hits for significantly DEGs due to *T. gondii* infection (TG_only)……278

Figure 4-25 PANTHER GO-Slim biological process ontology hits for significantly DEGs due to *T. gondii* infection and treatment with monensin (TG_Monensin)……284

Figure 4-26 PANTHER GO-Slim molecular function ontology hits for significantly DEGs due to *T. gondii* infection and treatment with monensin (TG_Monensin)..... 285

Figure 4-27 PANTHER GO-Slim cellular component ontology hits for significantly DEGs due to *T. gondii* infection and treatment with monensin (TG_Monensin)..... 285

Figure 5-1 The effect of 3-Oxo and PQS treatment on hBMECs cell viability assessed using Alamar blue assay..... 305

Figure 5-2 The effect of quorum sensing molecules on hBMEC monolayer permeability..... 306

Figure 5-3 The effect of quorum sensing molecules on hBMEC monolayer integrity……307

Figure 5-4 The effect of 3-Oxo and PQS at 10 μM and 100 μM on hBMECs mitochondrial potential..... 308

Figure 5-5 DNA fragmentation in hBMECs following treatment with quorum sensing molecules..... 309

Figure 5-6 Cell cycle assay following treatment with quorum sensing molecules on hBMECs..... 310

Figure 5-7 The effect of 10 and 100 μM 3-Oxo on TJ genes expression in hBMECs……312

Figure 5-8 The effect of 10 and 100 μM PQS on TJ genes expression in hBMECs……313

Figure 5-9 The effect of treatment with quorum sensing molecules and *T. gondii* infection on hBMEC monolayer permeability..... 314

Figure 5-10 The effect of quorum sensing treatment on hBMECs monolayer and *T. gondii* infection on hBMEC monolayer integrity.. 315

Figure 5-11 The combined effect of 3-Oxo at 10 and 100 μM concentration and *T. gondii* infection on TJ genes expression in hBMECs. 316

Figure 5-12 The combined effect of PQS and *T. gondii* infection on TJ genes expression in hBMECs. 318

List of Tables

Table 1-1 List of genomes of 11 strains of *T. gondii* readily available on ToxoDB website. 5

Table 1-2 Interaction of pathogens and host ligands used in binding, penetration and invasion of the BBB. 23

Table 1-3 List of transcriptome studies performed on different human cells and different strains of *T. gondii*. 29

Table 2-1 List of primers with their description, GenBank accession number, forward and reverse sequences, and their ID number from sourced databases.....53

Table 2-2 Counted hBMECs in Millicell Inserts (24 well 0.33 cm surface area) after 120 hours at 10^4 cells seeding.....56

Table 2-3 Calculation of primer pairs' efficiency using the Pfaffl method (Pfaffl 2001).....75

Table 2-4 Descriptive statistics of 2 housekeeping genes (3-72 hours) 76

Table 3-1 List of genes analysed by qPCR and their respective primer pair sequences.....108

Table 3-2 List of top 30 significantly down-regulated genes at 6 h.p.i. ...119

Table 3-3 List of top 30 significantly up-regulated genes at 6 h.p.i. 120

Table 3-4 List of top 30 up-regulated genes at 24 h.p.i. 126

Table 3-5 List of all seven down-regulated genes at 24 h.p.i. 127

Table 3-6 List of top 30 down-regulated genes at 48 h.p.i. 132

Table 3-7 List of top 30 up-regulated genes at 48 h.p.i. 133

Table 3-8 List of the 14 DEGs shared between all time points. 139

Table 3-9 List of top 30 pathways affected by DEGs at 6 h.p.i (Entities FDR < 0.01) sorted with the most significant pathway at the top. 141

Table 3-10 List of all eight pathways affected by DEGs at 24 h.p.i (Entities FDR < 0.01) sorted with the most significant pathway at the top. 142

Table 3-11 List of top 30 pathways affected by DEGs at 48 h.p.i (Entities FDR < 0.01) sorted with the most significant pathway at the top. 144

Table 3-12 List of all five pathways affected by fourteen DEGs at all time points (Minimum three entities/pathway, entities FDR < 0.01) sorted with the most significant pathway at the top. 145

Table 3-13 List of 30 highly expressed *T. gondii* genes with ≥ 2000 baseMean counts, $\log_2$ FC ≥ 5 and *P*-value < 0.01 at 6, 24 and 48 h.p.i. ...151

Table 3-14 Gene ontology for all 94 miRNA up-regulated at 6, 24 and 48 h.p.i.....152

Table 3-15 List of pathways associated with 94 up-regulated *T. gondii* genes (*P*-value < 0.05).....153

Table 3-16 The percentage of sequenced reads mapped to the human genome.....154

Table 3-17 The percentage of sequenced reads mapped to the miRBase database.....154

Table 3-18 List of all 31 up-regulated miRNAs at 6 hours sorted with the most significant on top.....155

Table 3-19 List of all five down-regulated miRNAs at 6 hours sorted with the lowest $\log_2$ FC on top.....156

Table 3-20 List of top 30 out of 531 up-regulated miRNAs at 48 hours.157

Table 3-21 List of all 15 down-regulated miRNAs at 48 hours. 157

Table 3-22 List of all 24 up-regulated plus three down-regulated miRNAs shared between 6 and 48 h.p.i. 158

Table 3-23 Consensus pathways from priori – genes intersection and posteriori – pathway/categories union methods associated with up-regulated miRNAs at 6 h.p.i.....160

Table 3-24 Consensus pathway from priori – genes intersection and posteriori – pathway/categories union methods associated with up-regulated miRNAs at 48 h.p.i. 162

Table 3-25 The percentage of sequenced reads mapped to the *T. gondii* genome.....163

Table 3-26 Gene Ontology of 138 genes at 24 h.p.i. 165

Table 3-27 Gene ontology of 164 genes at 48 h.p.i 166

Table 3-28 List of the top 30 down-regulated genes at 6 h.p.i. 175

Table 3-29 List of the top 30 up-regulated genes at 6 h.p.i. 176

Table 3-30 List of all 24 down-regulated genes at 24 h.p.i. 181

Table 3-31 List of all 21 up-regulated genes at 24 hours.. 182

Table 3-32 List of the top 30 down-regulated genes at 48 h.p.i. 186

Table 3-33 List of the top 30 up-regulated genes at 48 h.p.i. 187

Table 3-34 List of the pathways affected by DEGs at 6 and 24 h.p.i (Entities FDR < 0.01) sorted with the most significant pathway at the top. 194

Table 3-35 Calculation of primer pairs efficiency using the Pfaffl method (Pfaffl, 2001) 194

Table 3-36 Validation of RNA-seq and microarray data by RT-PCR. 197

Table 4-1 List of the top 30 significant DEGs induced by 24 hours treatment with 0.1 μM monensin (Monensin_only) with the most highly significant at the top.....253

Table 4-2 List of top 30 up-regulated genes sorted with the highest log_2 FC at the top.....254

Table 4-3 List of top 30 down-regulated genes sorted with the lowest log_2 FC at the top.....255

Table 4-4 List of top 30 most significant DEGs from 24 hours of *T. gondii* infection (TG_only) with the most highly significant at the top. 259

Table 4-5 List of top 30 up-regulated genes following 24 hours *T. gondii* infection sorted with the highest log_2 FC values at the top. 260

Table 4-6 List of top 30 down-regulated genes following 24 hours *T. gondii* infection sorted with the lowest log_2 FC value at the top. 261

Table 4-7 List of the top 30 most significant DEGs in hBMECs infected with *T. gondii* and treated with 0.1 μM monensin (TG_Monensin) with the most highly significant at the top. 265

Table 4-8 List of top 30 up-regulated genes from 24 hours treatment with 0.1 uM monensin and *T. gondii* infection sorted with the highest log_2 FC values at the top.....267

Table 4-9 List of top 30 down-regulated genes from 24 hours treatment with 0.1 uM monensin and *T. gondii* infection sorted with the lowest log_2 FC values at the top.....268

Table 4-10 List of all 23 Reactome pathways affected by 24 hours treatment with 0.1 μM monensin (Monensin_only) with FDR < 0.05 sorted with the lowest FDR values at the top.....275

Table 4-11 List of WNT signalling related pathways with the matched genes, average log_2 FC and FDR values. 276

Table 4-12 List of all four Reactome pathways affected by 24 hours infection with *T. gondii* (TG_only) with FDR < 0.05 sorted with the lowest FDR values at the top.....280

Table 4-13 List of WNT signalling related pathways with the matched genes, average log_2 FC and FDR values. 281

Table 4-14 List of all 25 significantly enriched biological processes from 101 annotated up-regulated genes sorted with the most significant at the top.....283

Table 4-15 List of top 30 out of 55 Reactome pathways affected by 24 hours *T. gondii* infection and treatment with 0.1 μM monensin (TG_Monensin) sorted with the lowest FRD values at the top.....288

Table 4-16 List of WNT signalling related pathways with the matched genes, average log_2 FC and FDR values affected by 198 DEGs. 289

List of Abbreviations

3-Oxo	N-(3-oxododecanoyl)-L-homoserine lactone
°C	degrees Celsius
ANOVA	one-way analysis of variance
APC	antigen presenting cell
ATP	adenosine triphosphate
AUC	area under the curve
BBB	blood brain barrier
bp	base pair
BRB	blood retinal barrier
DC	dendritic cells
DEG	differentially expressed genes
DMEM	Dulbecco's modified eagle medium
DNA	deoxyribose nucleic acid
EDTA	ethylene-diamine-tetra-acetic acid
FBS	foetal bovine serum
FC	fold change
FDR	false discovery rate
FI	fluorescent intensities
g	acceleration due to gravity
hBMECs	human brain microvascular endothelial cells
HFF	human foreskin fibroblast
h.p.i	hours post infection
JAMs	junction adhesion molecules
IFN-γ	interferon-gamma
IL	interleukin
log_2 FC	log_2 fold change
MC	monocyte
mg	milligrams
miRNA	microRNA
mL	millilitres
mm	millimetres
mM	millimolar
MOI	multiplicity of infection
MP	macrophage
mRNA	messenger RNA

NF-κB	nuclear factor-kappa-beta
NGS	next-generation sequencing
NK	natural killer
NO	nitrus oxide
nt	nucleotide
PCR	polymerase chain reaction
PQS	2-Heptyl-3-hydroxy-4(1H)-quinolone
qRT-PCR	real-time quantitative reverse transcriptase polymerase chain reaction
QS	quorum sensing
RIN	RNA integrity number
RNA	ribonucleic acid
ROS	reactive oxygen species
rRNA	ribosomal RNA
RT	real-time
RT	room temperature
SD	standard deviation
SEM	standard error of mean
SNP	single nucleotide polymorphism
TEER	trans-endothelial electrical resistance
TH1	type 1 T helper
TJ	tight junction
TLR	toll-like receptors
TNF-α	tumour necrosis factor alpha
tRNA	transfer RNA
UTR	untranslated region
µL	microliter
µm	micrometre
ZO	zona occluden

Chapter 1 General Introduction

1.1 The Organism

The obligate apicomplexan intracellular protozoan parasite *Toxoplasma gondii* (*T. gondii*) is the causative agent of a disease known as toxoplasmosis (**Figure** 1-1). This disease ranks among the most common infectious diseases in the world, infecting almost all warm-blooded mammals and birds (Pulzova, Bhide and Andrej 2009). It has been estimated that 30–50% of the human population is infected with this parasite (Pulzova, Bhide and Andrej 2009)(Pulzova, Bhide and Andrej, 2009). Humans or animals become infected congenitally from an infected mother to the foetus, by ingestion of the parasite tissue cysts from undercooked or uncooked meat or by drinking water contaminated with oocysts shed in feline faeces (Elsheikha, 2008). The clinical spectrum of the disease varies, depending on the host genetic background and genotype of the infecting strain, from asymptomatic infection in immune-competent people to severe illness in pregnant women and immunocompromised individuals (Yarovinsky, 2014).

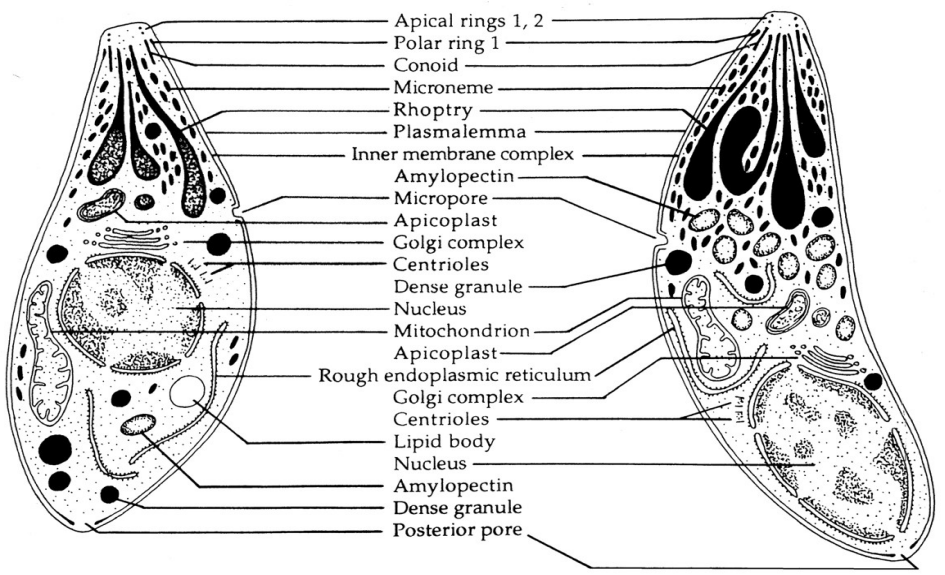


Figure 1-1 Electron micrographic representation of a tachyzoite (left) and a bradyzoite (right) of *T. gondii*. Three obvious differences between the two stages are bradyzoites have a looped rhoptry, their nucleus is located posteriorly and contain more amylopectin bodies. Image credit: Dubey, Lindsay, & Speer, (1998).

1.2 Biology and Life Cycle Forms

This parasite has a complex, indirect, life cycle that alternates between definitive hosts which are members of the family Felidae (**Figure** 1-1), the only animals capable of forming and shedding oocysts in their faeces and transmitting the parasite to intermediate hosts which are all non-felid, vertebrate animals. The other two life cycle forms of *T. gondii* are tachyzoite and bradyzoites (**Figure** 1-2). Tachyzoites, the rapidly replicating form, cause an acute infection that rapidly spreads throughout the body. In response to immune pressure, tachyzoites differentiate to slow-growing bradyzoites within tissues forming tissue cysts, which mark a long-term chronic stage of infection.

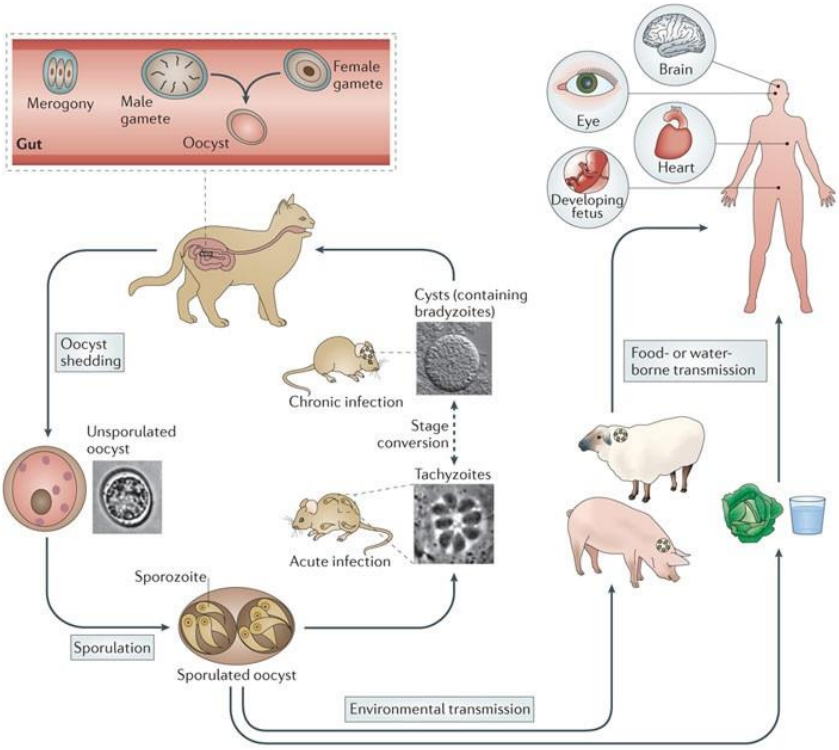


Figure 1-2 Life cycle of *Toxoplasma gondii*. Cats are the definitive host of *T. gondii* where sexual replication takes place. In the cat gut cells, tachyzoites differentiate into merozoites which then replicate to produce male and female *T. gondii* gametes. Gametes then are fused forming diploid un-sporulated oocysts that are shed in cat faeces and undergo meiosis in the environment to yield eight haploid progeny sporozoites. In the intermediate hosts which are human, mouse and farm animals, asexual replication occurs. Image credit: Hunter & Sibley, (2012)

1.3 Routes of Infection

Ingestion of tissue cysts can lead to infection. In cats, the parasite undergoes the sexual phase of the life cycle with un-sporulated oocyst as the end product being passed through with faeces. Un-sporulated oocysts are resistant to stresses in the environment for long periods of time and will undergo sporulation forming infectious sporulated oocysts ready for infection of intermediate hosts *via* contaminating the food or the water. Among intermediate hosts for *T. gondii* are farm animals and humans. Humans commonly become infected by ingesting undercooked meat containing tissue

cysts or by drinking water contaminated with sporulated oocysts (Hunter and Sibley, 2012). Most human infections are mild but in immunocompromised people and developing foetus toxoplasmosis can cause serious damage to the brain and other organs.

1.4 Genetic structure of *T. gondii*

Genetically, *T. gondii* is highly variable with three major genetic types I, II and III, together with many additional recombinant and atypical strains. Genotype I of *T. gondii* is most virulent for mice, causing far-reaching parasite dissemination and sudden death. One example of genotype I, the RH strain originally isolated by Sabin (Sabin and Warren, 1942), is extremely pathogenic to mice, LD_{100} by intraperitoneal infection is below ten tachyzoites (Ruskin and Remington, 1968). In contrast, genotype II causes non-fatal infection with less tachyzoite spreading (Dardé, 2004). However, strain-specific virulence varied between mice and rats (Dubey *et al.*, 2012). As such, it is safe to assume that there are some differences in *T. gondii* strain virulence between mice and humans. *T. gondii* type II strains are present in some European countries and the United States and cause congenital toxoplasmosis with lethal consequences, severe neuro-ocular infection, chorioretinitis, and/or latent toxoplasmosis (Flegr, Klapilova and Kankova, 2014). Type I *T. gondii* strains have higher proliferation rates than type II strains, and this has been attributed to upregulation of genes related to pyrimidine biosynthesis, TCA cycle and pentose phosphate shunt that are responsible for higher ATP production relative to type II strains (Song *et al.*, 2014).

The genomes of about 18 strains of *T. gondii* have been published and deposited at NCBI and can be assessed from the ToxoDB (www.toxodb.org; Gajria *et al.*, 2007). Recently published genomes ranging from 2013 to 2016

are listed in **Table** 1-1. Among these, *T. gondii* ME49 is considered the reference genome because this strain has been studied extensively using genomics, proteomics and CHIP-seq sequencing. Completely sequenced *T. gondii* genomes are around 65 mega base pairs (Mbp) in size consisting of around 10,000 genes.

Table 1-1 List of genomes of 11 strains of *T. gondii* readily available on ToxoDB website.

Parasite strain (Strain Type)	NCBI taxon ID	Genome version	Genome size (Mbp)	Total gene count
Toxoplasma gondii ARI	1074872	2016	64.69	10148
Toxoplasma gondii COUG	1074873	2013	63.7	-
Toxoplasma gondii FOU	943167	2014	64.53	10297
Toxoplasma gondii GT1	507601	2013	63.95	8637
Toxoplasma gondii MAS	943118	2014	63.32	10176
Toxoplasma gondii ME49	508771	2015	65.67	8920
Toxoplasma gondii p89	943119	2014	64.16	9874
Toxoplasma gondii RH	383379	2006	69.35	7860
Toxoplasma gondii TgCatPRC2	1130821	2016	64.19	10300
Toxoplasma gondii VAND	933077	2014	64.27	9426
Toxoplasma gondii VEG	432359	2013	64.52	8563

Note: Greyed row denotes the reference genome.

T. gondii GT1 is the type I reference strain while *T. gondii* ME49 is the type II reference strain (Pomares *et al.*, 2018). *T. gondii* VEG strain is a type III strain (Pomares *et al.*, 2018). TgCatPRC2 (cat) were atypical strain isolated from cat in China (Wang *et al.*, 2013). The exotic strain COUG is efficiently transmitted by the oral route while another two exotic strains MAS and FOU, are defective in oral transmission (Fux *et al.*, 2007). P89 were also an atypical strain with low mortality rate on mice (Jensen *et al.*, 2015) while another

atypical strain VAND, is highly virulent in mice (Behnke *et al.*, 2015). Generally, atypical strains isolated from an infected human have more gene counts compared to established typical strain of I, II and III (**Table** 1-1). These extra genes expression may contribute the parasite virulency. For example, *T. gondii* ROP5 and ROP18 allelles were found in several virulent atypical strains from South America (Behnke *et al.*, 2015; Jensen *et al.*, 2015). These two proteins block IFN-γ expression in murine hosts (Behnke *et al.*, 2015; Jensen *et al.*, 2015).

1.5 Impact of Toxoplasmosis on Animals

Toxoplasma gondii is the second leading cause of abortion, after Campylobacter species, causing significant economic loss to the UK sheep industry (Agency *et al.*, 2012). The loss of over 0.5 million lambs each year due to toxoplasmosis was estimated to cost the UK sheep industry £12-24 million (Agency *et al.*, 2012). Toxoplasmosis was responsible for 204 (23%) of 904 ovine abortions in England and Wales in 2009 (Agency *et al.*, 2012). Veterinary Investigation Diagnosis and Analysis (VIDA) data for incidents of ovine abortion in Great Britain from 2011 to 2015 reported confirmed Toxoplasmosis responsible for 23.7% of ovine abortion ('Focus on ovine abortions', 2017).

Toxoplasma gondii infection has also been reported in marine mammal species, indicating that the organism has entered the marine environment, but with unknown consequences as yet (Dubey *et al.*, 2003). For example, 34.1% of common dolphins in British waters, *Delphinus delphis*, were found infected with *T. gondii* (Forman *et al.*, 2009). Toxoplasmosis also impacts the meat industries where PCR studies on 67 UK cured meat products revealed an overall prevalence of 38%, including 25% of beef samples, 33% of pork samples and 67% of lamb samples (Warnekulasuriya, Johnson and Holliman, 1998). Though

this study did not determine cyst viability, viable parasites were found in one sample. Meanwhile, in the USA, *T. gondii* is responsible for approximately 24% of deaths attributed to foodborne pathogens (Belluco *et al.*, 2016).

1.6 Clinical Significance of Toxoplasmosis in Human

Toxoplasmosis has been reported in nearly all countries, and seropositivity rates vary from < 10% to > 90% (Pappas, Roussos and Falagas, 2009). Whilst this disease severity is low, and the infection is also self-limiting, in key vulnerable groups such as the immunosuppressed, immunodeficient, and during pregnancy (*i.e.* congenital infection), the severe or life-threatening disease can occur. In the USA, toxoplasmosis is the second leading cause of death from foodborne diseases (Belluco *et al.*, 2016). In European countries, the prevalence ranges between 10% and 60%, and in some regions is as high as 90% (Flegr, Klapilova and Kankova, 2014). In the United Kingdom, toxoplasmosis incidence is 2.6 times higher in children than in adults (Welton and Ades, 2005). The *Toxoplasma* Reference Unit of England and Wales reported 310 cases of human toxoplasmosis in 2013 and 351 in 2014 (Halsby *et al.*, 2014). There is limited UK data on toxoplasmosis in AIDS patients and cases in organ graft recipients. However, toxoplasma encephalitis is estimated to occur in 7% of AIDS patients (Agency *et al.*, 2012).

1.7 Disease forms of Toxoplasmosis

Typically, in the intermediate host, tachyzoites that can infect all nucleated cells enter the cells before replicating inside a parasitophorous vacuole. Once matured they egress, killing the cell while disseminating to

neighbouring cells. In the immunocompetent host with a strong inflammatory response pressure, tachyzoites to turn into bradyzoites, a slowly replicating form of the parasite. Bradyzoites stay inside cysts that are commonly found in skeletal muscle tissue and the brain tissue for the host lifetime. An important aspect of *T. gondii* infections is the capability of the parasite to cross restrictive biological barriers such as blood intestinal barrier, blood-brain barrier, blood-retina barrier and blood-placental barrier. This allows the parasite to gain access to immuno privileged organs and tissues. Active parasite motility and tightly regulated interactions between cell receptors and parasite proteins contribute to their success. In addition, the parasite can also regulate and control infected leukocytes like macrophages (Da Gama *et al.*, 2004), monocytes (Courret *et al.*, 2006) and dendritic cells (Lambert *et al.*, 2006) by using them as "Trojan horses" to evade the immune system and to reach to immune privileged sites. ADAM10 and MMP-9, secreted metalloprotease that is central in the migratory molecular complex, and were observed to be essential in increased migration of infected human macrophages (Niehus *et al.*, 2014).

1.7.1 *Congenital Toxoplasmosis*

Infected pregnant women can transmit the parasite to their unborn foetus causing congenital toxoplasmosis (Elsheikha, 2008). Transmission rate from infected pregnant women to their babies is 28.1% (Pappas, Roussos and Falagas, 2009). The global estimated incidence of congenital toxoplasmosis is 190,100 annual cases while the incidence rate is about 1.5 cases of congenital toxoplasmosis per 1,000 live births (Pappas, Roussos and Falagas, 2009). The highest seroprevalence, more than 90%, was found in some parts of European and South American countries while the lowest, ~1%, was found in some countries in the Far East (Flegr, Klapilova and Kankova, 2014). Meanwhile, in

the last national survey in the UK performed between 2002 and 2004, 22 cases of congenital toxoplasmosis were found resulting in a mean incidence of 11 cases annually (Gilbert and Dezateux, 2006).

1.7.2 *Ocular Toxoplasmosis*

Ocular toxoplasmosis or also known as 'toxoplasmic retinochoroiditis' is a common inflammatory eye disease caused by *T. gondii*. Ocular toxoplasmosis has an incidence rate of 0.4 per 100,000 of patients born in Britain (Halsby *et al.*, 2014). Approximately 1.25 million U.S. residents suffer from ocular toxoplasmosis, and in certain parts of the world, this eye disease is believed to affect over 15% of the population (Holland, 2003). Statistically, 2% of individuals with toxoplasmosis were diagnosed with ocular toxoplasmosis in the USA, (Furtado *et al.*, 2013) while in the UK, the incidence was reported to be at 0.8/100,000 people per year (Halsby *et al.*, 2014). Ocular toxoplasmosis is more common in Latin America where it had 17.7% prevalence in Brazil and was responsible for 40% of uveitis in Colombia (Furtado *et al.*, 2013). The parasite usually infects retina' cells, but in severe cases will also infect choroid and glial cells (Holland, 2003). Complications from this disease range from blurred vision and unusual floaters to glaucoma and loss of vision due to scarring if the disease is untreated (Furtado *et al.*, 2013).

1.7.3 *Cerebral Toxoplasmosis*

Infection with the protozoan parasite *T. gondii* can result in an invasion of the brain and the formation of tissue cysts that persist throughout the life of the host without causing symptoms (Montoya and Liesenfeld, 2004). However, in immunocompromised patients, reactivation of latent infection may result in the release of rapidly multiplying tachyzoites from tissue cysts and lethal

encephalitis, if left untreated (Dellacasa-Lindberg, Hitziger and Barragan, 2007). Reactivated toxoplasmosis is among the most frequent CNS manifestations in seropositive AIDS and transplant patients (Montoya and Liesenfeld, 2004; Dellacasa-Lindberg, Hitziger and Barragan, 2007). Cerebral toxoplasmosis is a potentially life-threatening disease characterised by the infiltration of *T. gondii* parasites to the brain parenchyma and the persistence of parasites in cysts (Feustel, Meissner and Liesenfeld, 2012). In healthy individuals, infection severity ranges from mild to asymptomatic while in immunocompromised individuals, rapidly proliferating tachyzoites can cause lethal encephalitis if left untreated.

The latest studies have suggested that *T. gondii* cross BBB by a 'Trojan horse' pathway (Lachenmaier *et al.*, 2011), *via* a paracellular pathway by targeting tight junction (TJ) proteins (Elsheikha and Khan, 2010) and/or by a transcellular pathway (Däubener *et al.*, 2001). Lachenmaier *et al.*, (2011) study of transcriptional regulation in rat brain endothelial cells after the infection showed an increased expression of E- and P-selectins, ICAM-1 and enhanced adhesion molecule expression. The same study also found that CD11b+ monocytes/dendritic cells induced up-regulation of ICAM-1 and VCAM-1 and a stronger IL-6 and MCP-1 secretion, promoting infected inflammatory cell migration. It is unclear how this parasite can reach the brain from the onset of infection. The capability of *T. gondii* to spread out seems to differ between strains. Type I strains have high migratory capability while type II strains have been shown to markedly induce infected dendritic cells migratory capability (Lambert *et al.*, 2006, 2009).

1.7.4 *Pulmonary Toxoplasmosis*

Another rare form of toxoplasmosis is pulmonary toxoplasmosis (also known as toxoplasmosis pneumonia), which is an inflammation of the lungs caused by *T. gondii* infection. Polymerase chain reaction-based assay in bronchoalveolar lavage fluid has been reported in HIV positive patients. Common symptoms of this disease are lymphadenopathy and fever. Pulmonary toxoplasmosis is responsible for 4% of pulmonary complication in HIV patients (Gingo *et al.*, 2010; Chiang *et al.*, 2011).

1.8 Diagnosis of Toxoplasmosis

Current laboratory methods for confirmation of *T. gondii* infection include (a) direct detection of the parasites in tissues or body fluids using histology staining and/or PCR (b) isolation of *T. gondii* in mice or tissue culture and (c) serological methods (Montoya and Liesenfeld, 2004). Histology staining and isolation methods are time-consuming, and some specimens like cerebrospinal fluid are risky and difficult to obtain. As such, common diagnosis of toxoplasmosis is made by serology through detection of specific anti-*Toxoplasma* immunoglobulin in the form of IgM and IgG. Following *T. gondii* infection, IgM antibodies are produced by the host as the first defensive mechanism. IgM will last about two weeks before it falls, to below detectable levels after a couple of months. Following that, IgG will be produced by the host for long-term protection. A person who has been infected with *T. gondii* will usually have a detectable level of IgG for the rest of their life. The limitation of antibody testing is that in an immunocompromised individual strong antibody response to *T. gondii* may not occur, or if it is produced the level maybe low and this leads to the wrong conclusion, as a chronic infection is interpreted as weak infection due to low antibody titre. In addition, antibody testing can

produce a false positive result. Hence, a definitive diagnosis can only be made by direct detection, typically by PCR technique. The quantitative real-time PCR method is very sensitive, in parasite detection as low as 0.5 toxo/mL of blood with 529bp target primers were more sensitive, compared to using B1 gene as a target (Edvinsson *et al.*, 2006; Veronesi *et al.*, 2017).

Ocular toxoplasmosis is commonly diagnosed by the serological test of ocular fluids, and clinical finding by ophthalmologic examination followed by *Toxoplasma*-specific antibodies by ELISA technique and confirmation is made by detection of *T. gondii* DNA in aqueous and/or vitreous humor (Holland, 2003; Montoya and Liesenfeld, 2004).

Diagnosis of congenital toxoplasmosis is depended on the period of pregnancy. At the gestation stage, ultrasonography and parasite detection by PCR of amniotic fluid is the most common method (Gilbert and Dezateux, 2006; Elsheikha, 2008). At the post-natal period, the best diagnosis method is the serological detection of *Toxoplasma* IgM, IgA and IgG for 12 months while a less common method is parasite detection by PCR from peripheral blood or urine samples (Gilbert and Dezateux, 2006; Elsheikha, 2008).

Meanwhile, diagnosis of cerebral toxoplasmosis can be done by detection of mass lesions in the brain by radiographic imaging, such as computerised tomography (CT) or magnetic resonance imaging (MRI) and/or detection of *T. gondii* in cerebrospinal fluid (CSF) by PCR (Mesquita *et al.*, 2010). Finally, common diagnosis of pulmonary toxoplasmosis is made by detection of the parasite in bronchoalveolar lavage fluid using PCR techniques (Petersen *et al.*, 2006).

1.9 Treatment of Toxoplasmosis

A healthy or immunocompetent person generally recovers from toxoplasmosis without treatment. While there is no 100% effective treatment for toxoplasmosis, some medicines have been prescribed for treatment, such as spiramycin, azithromycin, pyrimethamine-sulfadiazine combo, trimethoprim-sulfamethoxazole combo and pyrimethamine-clindamycin combo (Wei *et al.*, 2015). Traditional Chinese medicine is formulated primarily from *Astragalus membranaceus*, *Scutellaria baicalensis*, *Artemisia annua*, *Ginkgo biloba* herbs (Wei *et al.*, 2015). Susceptible individuals such as pregnant women, new-borns, infants, HIV patients and individuals undergoing immunosuppression treatment can be treated with several drugs in combination, e.g. pyrimethamine and sulfadiazine and folinic acid for 4-6 weeks (Kongsaengdao *et al.*, 2008; Wei *et al.*, 2015). Even after drug treatment, it is unlikely that total parasite eradication can be achieved because *T. gondii* can form bradyzoite and tissue cysts in immunoprevileged sites, such as the brain where a biological barrier prevents many drugs from diffusing freely.

A systemic review conducted by Wei *et al.*, (2015) on toxoplasma encephalitis treatment, the pyrimethamine-clindamycin combo was found to be the most effective followed by trimethoprim-sulfamethoxazole combo then pyrimethamine-sulfadiazine combo with cure rates of 64.7%, 59.9% and 49.8% respectively, albeit with no statistically significant difference found between the different treatment protocols. However, the best choice of treatment is pyrimethamine-sulfadiazine combo because treatment with the other two combos have more recurrence rate and side effects on patients (Kongsaengdao *et al.*, 2008).

1.9.1 *Monensin*

Ionophores are a class of antiparasitic agents widely used in veterinary medicine (Lavine and Arrizabalaga, 2011, 2012). Among them is monensin, a broad-spectrum anti-parasite that is widely used to treat animals infected with *Plasmodium* sp, *Toxoplasma* sp, and *Eimeria*. Monensin was discovered and isolated by Lilly Research Laboratories, and the Department of Biochemistry of Indiana University School of Medicine (Chapman, Jeffers and Williams, 2010). Lavine & Arrizabalaga, (2011, 2012) reported monensin mode of action where it causes the arrest of *T. gondii* in the late phase of the cell cycle. Monensin's effect on *T. gondii* morphology can be seen after 6 hours exposure. After 24 hours of exposure, the sickle-like parasite shape can be no longer be seen. However, about 31% of *T. gondii* manage to survive exposure to monensin suggesting that the monensin effect is reversible and dependent on the length of exposure (Lavine and Arrizabalaga, 2012). Prolonged cell cycle arrest from monensin exposure resulted in parasite cell death by autophagy (Lavine and Arrizabalaga, 2012). The specific signalling mechanism for autophagy induction by monensin is unclear. It was suggested that resistance has been slow to develop against monensin compared with earlier synthetic drugs (Chapman, Jeffers and Williams, 2010).

Another effect of monensin is disruption of the *T. gondii* mitochondrial membrane potential (Charvat and Arrizabalaga, 2016). Mitochondrial membrane potential is an intact electrochemical gradient across the inner mitochondrial membrane that is constantly maintained for oxidative phosphorylation and ATP generation (Kroemer, Galluzzi and Brenner, 2007). Disruption of mitochondrial membrane potential is an early process of cell death (Kroemer, Galluzzi and Brenner, 2007). Thus, there are two ways where monensin can cause cell death, either by autophagy or apoptosis.

1.10 Breaching the Biological Barriers

1.10.1 *Bronchial Epithelial Barrier (BEB)*

Toxoplasma gondii infection of the lung is rare in immunocompetent persons, but several cases have been reported when the route of infection is by ingestion (Petersen *et al.*, 2006; Gingo *et al.*, 2010). Typically for any lung infection, the site of infection is at the bronchoalveolar area. Here, there is a bronchial epithelial barrier is formed by polarised tight epithelial cell layer that serves as a selective, protective barrier between the air and the lung. The best model for this barrier is the Calu-3 cell line, which is an immortalised cell line that can be easily maintained in culture and has been shown to demonstrate many characteristics of functional bronchial epithelium *in vivo* (Grainger *et al.*, 2006). The cell line also forms tight polarised monolayers with tight junctions, high TEER values and displays, microvilli, as well as expressing the lung surfactant-specific protein, TJ protein' occludin and adherens junction protein' E-cadherin (Kreft *et al.*, 2015). TEER of the Calu-3 reached maximal TEER values > 500 ohm/cm^2 in one week after reaching confluence (Kreft *et al.*, 2015).

1.10.2 *Blood Brain Barrier (BBB)*

The BBB is a unique barrier that separates the brain from the intravascular compartment (Deli, 2007). Generally, the functions of BBB include regulating ion composition for synaptic signalling, keeping the central and peripheral neurotransmitters pools separate, preventing damaging macromolecules like pro-thrombin and plasminogen from entering the brain, shielding the brain from neurotoxins circulating in the blood and transporting nutrients into the brain (Deli, 2007). The base of BBB is the TJs of brain

microvascular endothelial cells. The microvessels are surrounded by pericytes and the end-feet of astrocytes. The unique characteristics of brain microvascular endothelial cells are they have a high electrical resistance between cells which are around 1000+ ohm/cm^2 (200-500 ohm/cm2 in other human cells), a low number of pinocytotic vesicles, slow rate of fluid-phase endocytosis and high densities of mitochondria (Deli, 2007). The BBB is tightly regulated by pericytes, astrocytes and neurons through cell to cell interactions (Luissint *et al.*, 2012). Both astrocytes and pericytes have been documented to regulate BBB formation and integrity (Abbott, Rönnbäck and Hansson, 2006; Cabezas *et al.*, 2014). Specifically, astrocytes release soluble factors that are important in maintaining the phenotype of brain endothelial cells while pericytes release growth factors and morphogens which are signalling molecules that governs the pattern of tissue development (Abbott, Rönnbäck and Hansson, 2006; Cabezas *et al.*, 2014). The impacts of these characteristics are that BBB is selective against certain molecules like lipid, glucose and amino acids, in addition to shielding the brain from blood components homeostasis and dangerous components in the blood. That, however, can change if there are infections to the central nervous system or circulatory system. Inflammation induces brain micro-endothelial cells to express cell adhesion molecules such as ICAM-1, VCAM-1 and selectins (Vries *et al.*, 1997; Deli, 2007). The molecules allow leukocyte to penetrate the barrier for immune action.

1.10.3 *Blood-Retinal Barrier (BRB)*

The BRB is a similar type of barrier to BBB, but it exists at the posterior part of the eye. The BRB is made up of retinal capillary endothelial cells (inner BRB) and retinal pigment epithelial cells (RPE, outer BRB). Just like in the BBB, retinal capillary endothelial cells are surrounded by pericyte and glial cell foot

processes. At both layers, tight-junctions between retinal endothelial and epithelial cells prevent large molecules from the choriocapillaris going into the retina. The main function of outer BRB is to control the exchange of nutrients with the choroidal vessels, which in turn maintain the specialised environment of the neural retina. Both the vascular endothelium and pigment epithelium possess a well-developed junctional complex that includes both adherens and TJs conferring a high degree of control of solute and fluid permeability (Runkle and Antonetti, 2011).

1.11 Tight Junction

The tight junction is one of the intercellular junctions located between the apical and basolateral membranes of the cell formed as a congregation of transmembrane proteins consisting of occludin, claudins and junctional adhesion molecules (JAM) together with cytoplasmic proteins, which are zonula occludens (ZO-1), ZO-2, ZO-3 and cingulin (Matter and Balda, 2003). The tight junction is closely associated with the adherens junction, as important intercellular junctions as shown in **Figure** 1-3. The functions of TJs are to regulate the passage of molecules (ions, water, macromolecules), pathogens and cells through the cells and to maintain cell shape and structure (Wolburg and Lippoldt, 2002; Luissint *et al.*, 2012). Tight junctions between endothelial cells of brain capillaries are the most important structural elements of the BBB. Brain endothelial TJs are composed of transmembrane proteins which include occludin, claudins and JAMs plus cytoplasmic scaffolding proteins, such as ZO proteins, actin cytoskeleton and associated proteins, such as protein kinases small GTPases and G-proteins (Luissint *et al.*, 2012). HBMECs were shown to express TJs and cell adhesion proteins, which are claudin-1 (Fletcher *et al.*, 2012), ICAM-1, VCAM-1, claudin-3 (Buttmann *et al.*, 2007; Eigenmann *et al.*,

2016), ZO-1, occludin (Buttmann *et al.*, 2007; Fletcher *et al.*, 2012), and ß-catenin (Gallego-Delgado *et al.*, 2016). Also, adherens junction proteins' VE-cadherin and were also expressed by hBMECs together with claudin-5 but at a lower level than VE-cadherin and ZO-1 (Eigenmann *et al.*, 2013, 2016).

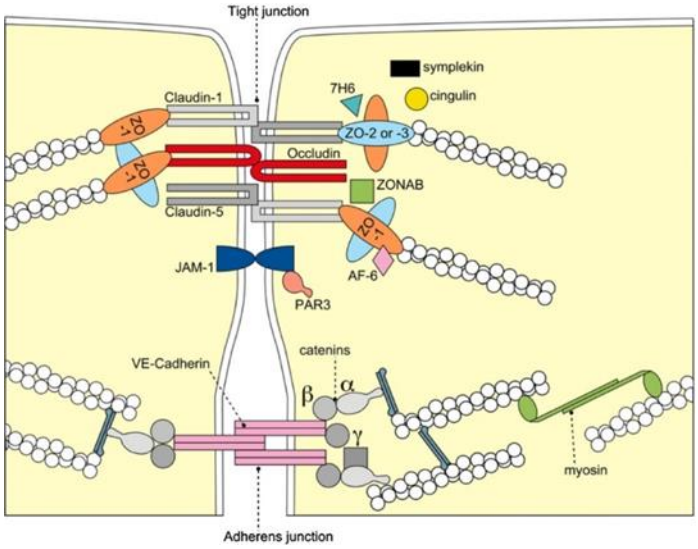


Figure 1-3 Components of a TJ and an adherens junction. Three transmembrane proteins of a TJ claudin-1, occludin and claudin-5 from neighbouring cells bind to each at paracellular space forming a seal. ZO protein family bound to one of these can shuttle into cells' nuclei to promote cellular differentiation and/or proliferation. Cingulin is responsible for actomyosin activation in the cellular process while symplekin and 7H6 functions are not clear. In endothelial cells, these two junctions interact with each other while in other cell types they do not. For example, according to Taddei *et al.*, (2008). VE-cadherin can stimulate claudin-5 expression only in endothelial cells. Figure credit: Förster, (2008)

Transepithelial/transendothelial electrical resistance (TEER) is the measurement of electrical resistance across a cellular monolayer that is employed as a very sensitive and reliable method to indicate the integrity of the TJs and permeability of the monolayer (Srinivasan *et al.*, 2015). It reflects the ionic conductance of the paracellular pathway in the epithelial monolayer. The TEER value for hBMECs after 2.5 days is at 30 Ωcm^2 with cells already expressing ZO-1, VE-cadherin, and actin and low expression of claudin-5 (Eigenmann *et al*., 2013; 2016). The same study also found that contact co-

culture models with HBPCT (human pericyte cell line) cells, have maximal TEER values that are lower than those for hBMECs mono-cultures on day 12. They concluded that among four human endothelial cell lines tested, hBMECs proved to be the best cell line for a human *in vitro* BBB model, regarding barrier tightness and paracellular permeability in a 24-well mono-culture system.

1.11.1 *Claudin and Occludin*

Claudin and occludin are considered the mainstay of the TJ and together with several cytosolic proteins such as ZO-1, ZO-2 and cingulin they contribute to the electrical resistance across the BBB (Razakandrainibe *et al.*, 2013). Claudins constitute a family of 24 proteins 20-27 kDa in size with four transmembrane domains in TJs in different cell types (Furuse *et al.*, 1998; Gunzel and Yu, 2013). Substantial data identified the key contribution of claudin-3 and claudin-5 to TJ formation and integrity of the BBB (Luissint *et al.*, 2012). Claudin-5 and G-proteins 2 interact with each other in controlling TJ integrity (Luissint *et al.*, 2012). Claudin-1, -2, -3, -5, -11, and -12 are found in brain endothelial cells, but only claudin- 5 is expressed in the endothelial cells in almost all segments of the brain (Ueno, 2007).

Occludin was the first TJ specific protein identified in epithelial cells that is important for barrier function (Luissint *et al.*, 2012). Occludin degradation induced by viruses like HIV-1 or bacteria (i.e. *Neisseria meningitides*) was shown to increase the permeability of primary and immortalised hBMECs (Schubert-Unkmeir *et al.*, 2007). Occludin has a molecular weight of 60-65 kDa and consists of four transmembrane domains, two extracellular domains, three cytoplasmic domains and has a unique feature where it binds to F-actin (Kniesel and Wolburg, 2000; Ueno, 2007). Occludin deficient mice produce histological abnormalities for example calcification in the brain and thinning of the compact

bone suggesting that the functions of occludin are more complex than just a building block in the TJ (Kniesel and Wolburg, 2000; Ueno, 2007).

1.11.2 *Junctional Adhesion Molecules (JAMs)*

JAMs are involved in assisting the TJ components' assembly and in the establishment of cell shape and structure (Ueno, 2007; Razakandrainibe *et al.*, 2013). JAMs contribute to permeability control as well as monocyte extravasation (Kniesel and Wolburg, 2000; Ueno, 2007). JAMs belong to the immunoglobulin superfamily, and have a molecular weight at about 40 kDa (W. Jia *et al.*, 2013). JAM can be categorised into JAM-A, JAM-B, JAM-C and JAM-D but only JAM-B, and -C are found in endothelial cells (W. Jia *et al.*, 2013). Both JAM-A and JAM-C maintain the stability of a TJ, and JAM-B maintains the stability of a TJ by interacting with JAM-C (Ueno, 2007; W. Jia *et al.*, 2013).

1.11.3 *Zona Occludens (ZO)*

ZO-1 is a 220 kDa phosphoprotein that binds to actin cytoskeleton and transmembrane proteins acting as a bridge for a TJ stability and permeability (Greene and Campbell, 2016). Dissociation of ZO-1 from the junctional complex often leads to increased permeability of BBB (Ueno, 2007; Greene and Campbell, 2016). ZO proteins play a role in connecting transmembrane proteins to skeleton proteins and interact directly with most of the transmembrane proteins like occludin, claudins and JAM while at the same time are involved in signal transduction and transcriptional modulation (W. Jia *et al.*, 2013; Greene and Campbell, 2016). CCR2 can bind to MCP-1 receptor resulting in redistribution of ZO-1, ZO-2, occludin and claudin-5 leading to an increase of endothelial permeability (Gunzel and Yu, 2013; Greene and Campbell, 2016). Besides being connected to the transmembrane proteins, ZO-1 is thought to

help recruit other cytosolic components to the TJ, including the actin cytoskeleton (Kniesel and Wolburg, 2000; Luissint *et al.*, 2012). Among additional TJs-associated proteins, G-proteins were first described to contribute to the TJ formation and maintenance in epithelial and brain endothelial cells, together with ZO-1 (Luissint *et al.*, 2012; Greene and Campbell, 2016).

1.12 Mechanisms of Penetration of BBB by Microbes

Various mechanisms exist *via* which pathogens can cross the BBB (**Figure** 1-4). The TJ can be disrupted by oxidative stress, pathogens and proinflammatory cytokines (Matter and Balda, 2003; Steed, Balda and Matter, 2010). The opening of TJs, increased pinocytotic activity and/or formation of transendothelial channels can increase BBB permeability (Kniesel and Wolburg, 2000; Greene and Campbell, 2016). Transcellular invasion of BBB has been demonstrated for bacteria *Escherichia coli* (Kim, 2002, 2012), *Listeria monocytogenes* (Greiffenberg *et al.*, 2000), *Streptococcus pneumoniae* (Iovino *et al.*, 2013), for fungal pathogens such as *Candida albicans* (Jong *et al.*, 2001) and *Cryptococcus neoformans* (Tseng *et al.*, 2015) and for viruses including HIV virus (Chiang *et al.*, 2011; Atluri *et al.*, 2015) and West Nile virus (Winkelmann, Luo and Wang, 2016).

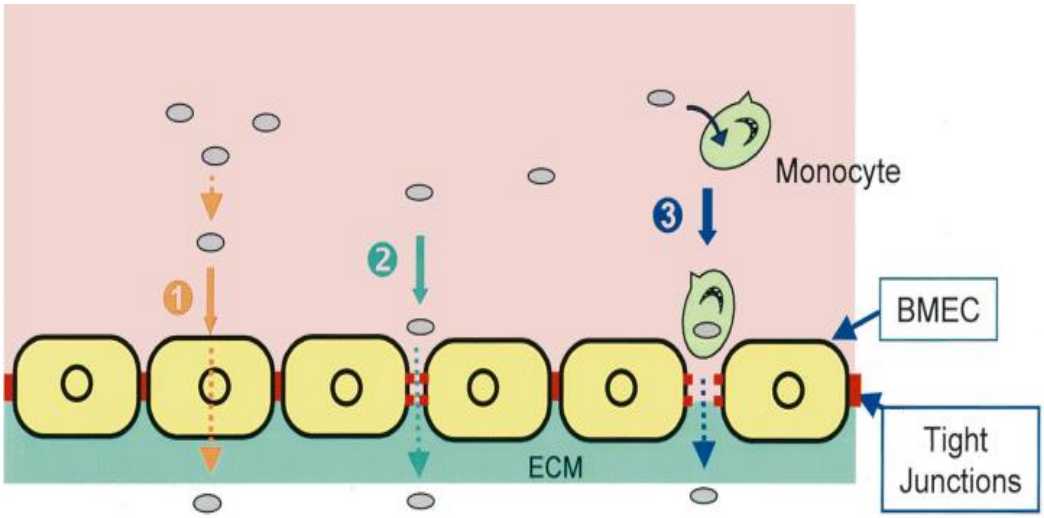


Figure 1-4 Breaching the blood-brain barrier. There are three pathways for pathogens to pass through BBB which are; 1-transcellular pathway, 2-paracellular pathway following disruption of the TJ of the BBB and 3- being transported within circulating phagocytic cells such as monocytes also known as Trojan horse mechanism. The Trojan horse mechanism also requires disruption of TJ proteins. Image credit: Huang & Jong, (2001)

There are several published reviews on the microbial invasion of the BBB and the key virulence factors together with cellular mechanisms of microbial proteins contributing to invasion of the BBB *in vitro* and *in vivo* (Huang and Jong, 2001; Pulzova, Bhide and Andrej, 2009). Crossing mechanisms of the neuro-invasive pathogens are described below and the ligand-receptor interactions are summarised in **Table** 1-2.

Table 1-2 Interaction of pathogens and host ligands used in binding, penetration and invasion of the BBB.

Pathogen	Mechanism	Ligand (pathogen)	Ligand (host)
E. coli	Transcellular	CNF1 (cytotoxic necrotising factor 1)	37 LRP (laminin receptor precursor) 67 LRP CD48 Gp96 45-kDa protein
S. pneumoniae	Transcellular	Phosphorylcholine	Platelet-activating factor receptor
L. monocytogenes	Transcellular Trojan horse mechanism	Internalin B	gC1q-R (receptor for the globular head of the complement component C1q) Met receptor tyrosine kinase gp96 (glycoprotein 96) ND
Neisseria meningitides	Transcellular	Opc (outer membrane protein) Pili (Pil A and Pil B) LOS (lipooligosaccharide)	Fibronectin (anchoring to the integrin-α5β1 receptor) CD46
Treponema pallidum	Paracellular	ND	ND
Haemophilus influenzae type B	ND	phosphorylcholine	PAF receptor
Mycobacterium tuberculosis	Transcellular Trojan horse mechanism	Upregulation of genes Rv0980c, Rv0987c, Rv0989c, Rv1801	ND
Candida albicans	Transcellular	Enolase	Plasmin(ogen)
Cryptococcus neoformans	Transcellular	Hyaluronic acid Phospholipase B Urease Isc1	CD44
West Nile virus	Transcellular	ND	ND
Trypanosoma spp.	Paracellular	ND	ND
Plasmodium falciparum	ND	Pf-IRBCs or PfEMP1	Thrombospondin, CD36, ICAM1 (intercellular adhesion molecule), PECAM, VCAM1, ELAM, chondroitin sulfate A
Acanthomoeba	Paracellular	Mannose-binding protein	ND
Toxoplasma gondii	ND	SAG1	ND
HIV	Trojan horse mechanism Transcellular	Tat protein	CD4 and CCR5

Note: Table modified from Pulzova et al., (2009). ND – No data

Usage of transgenic parasites to infect transgenic mice plus intravital imaging have highlighted a new mechanism for parasite entry into the brain where replication in and lysis of endothelial cells precedes invasion of the central nervous system (Konradt *et al.*, 2016). Tachyzoites can be found in the blood of acute and chronically infected humans and mice in free form, but predominantly in infected monocytes (Harker, Ueno and Lodoen, 2015). This suggests that *T. gondii* disseminate throughout the host via various strategies to maximise their survival. In chronically infected mice, parasite infection is localised around the microvasculature of frontal and parietal lobes, suggesting that the infection occurs *via* the bloodstream and across the BBB (Dellacasa-Lindberg, Hitziger and Barragan, 2007).

1.13 Molecular Pathogenesis and Host-Parasite Interaction

1.13.1 *Metabolism*

Like other parasite infections, *T. gondii* infection induces a metabolic alteration in infected cells that lead to an increase in both glycolysis and mitochondrial respiration (Tymoshenko *et al.*, 2015). A genomic scale metabolic model of *T. gondii* infection within the human host cell, ToxoNet1, was developed by Tymoshenko *et al*., (2015) that predicts a set of 53 enzyme-coding genes and 76 reactions to be essential for parasite replication. A validation experiment from the prediction confirms that cytosolic acetyl-CoA biosynthesis, ATP-citrate lyase and acetyl-CoA synthase enzymes are indispensable for the parasite growth. Acetyl-CoA is an important molecule in many biochemical processes such as fatty acid synthesis, fatty acid chain elongation and acetylation of proteins. The set of *T. gondii* proteins that are responsible for acetyl-CoA biosynthesis are designated TGME49_266640,

TGME49_223840, TGME49_219230 and TGME49_301120 in the parasite genome (Tymoshenko *et al.*, 2015). Another set of enzymes essential for *T. gondii* survival are TGME49_318580 and TGME49_285980 genes that encode glucose-1-phosphate production in the cytosol which is an indispensable precursor for starch and nucleotide-sugar metabolism. In addition to fatty acid biosynthesis, *T. gondii* can also salvage fatty acids for the host cells (Ramakrishnan *et al.*, 2012). In this process, exogenous fatty acids are incorporated into complex lipids or degraded all the way to acetyl-CoA *via* mitochondrial β-oxidation which then are used for new fatty acid biosynthesis (Coppens, Asai and Tomavo, 2013).

It has been established by various studies that *T. gondii* has both *de novo* and salvage pyrimidine nucleotide biosynthetic pathways for DNA/RNA biosynthesis (Kim and Weiss, 2004; Coppens, Asai and Tomavo, 2013). The *de novo* pyrimidine biosynthetic pathway is more important than the salvage pathway and is essential for *T. gondii* growth and virulence (Coppens, Asai and Tomavo, 2013).

1.13.2 *Apoptosis*

Toxoplasma gondii has been shown to interfere with apoptosis induction in human cells ensuring their survival even in the presence of apoptosis stimuli like actinomycin D and TNF-alpha. Goebel, Gross, & Lüder, (2001) observed in infected human-derived HL-60 and U937 cells treated with actinomycin D or TNF-alpha in combination with cycloheximide that *T. gondii* downregulate host cell apoptosis by inhibition of cytochrome c release and subsequent caspase activation as well as downregulation of poly(ADP-ribose) polymerase protein levels. Meanwhile, Keller *et al*., (2006) found that *T. gondii* directly inhibits cytochrome c-mediated activation of the caspase cascade while Carmen, Hardi,

and Sinai, (2006) found that the parasite alters the balance between pro- and anti-apoptotic Bcl-2 proteins in their favour. *T. gondii* can also interfere with the death receptor where it has been shown that it can significantly reduce Fas/CD95-triggered apoptosis by impairing activation of the initiator caspase 8 (Sinai *et al*., 2004).

Toxoplasma gondii infected cells mimics apoptotic cells by exposing phosphatidylserine, inducing secretion of TGF-β1 by infected activated macrophages, which leads to the degradation of inducible nitric oxide synthase and inhibition of nitric oxide production, and consequently parasite persistence in macrophages (dos Santos *et al.*, 2011). Phosphatidylserine exposure by *T. gondii* is essential for the escape mechanism for a successful infection (Kim and Weiss, 2004; Coppens, Asai and Tomavo, 2013). Therefore, interfering with the phosphatidylserine biosynthetic pathways would hypothetically reduce the parasite burden in their hosts. There are no published data so far on whether *T. gondii* also inhibits apoptosis in hBMECs.

1.13.3 *Immunity*

Following challenge with *T. gondii*, monocytes, neutrophils and dendritic cells (DCs) are recruited to the site of infection (Dupont, Christian and Hunter, 2012). One of the most critical functions of the innate immune response to *T. gondii* is the ability to sense the pathogen and produce the cytokine IL-12, which stimulates natural killer (NK) cells and T cells to produce the cytokine IFN-γ (Yarovinsky, 2014). IFN-γ is the major mediator of resistance to *T. gondii* and promotes multiple intracellular mechanisms to kill the parasite and inhibit its replication. This Th1 immune response, defined by the production of IL-12 and IFN-γ, is characteristic of infection with many intracellular pathogens including *T. gondii* (Dupont, Christian and Hunter, 2012; Yarovinsky, 2014).

The adapter molecule MyD88, which is required for downstream signalling from most Toll-like receptors is essential for the detection of the *T. gondii* antigen. Among the cells responsible for the production of IL-12 *in vivo* are neutrophils, inflammatory monocytes, macrophages and DCs (Dupont, Christian and Hunter, 2012; Yarovinsky, 2014). CD4+ T cells are critical for regulating functions involved in mediating resistance during toxoplasmosis. At early stages of infection, they contribute to optimal B and CD8+ T cell responses and the ability of these cells to control chronic infection by cytokine production and expression of CD40L (Coombes and Hunter, 2015).

IFN-γ mediates protective effects by initiating tryptophan degradation through upregulation of indolamine 2,3-dioxygenase-1 and -2 genes (Yarovinsky, 2014; Coombes and Hunter, 2015). Tryptophan is essential for *T. gondii* growth in a variety of infected cell types. Another key cytokine, TNF-α, is produced by several cell populations in response to *T. gondii* or *T. gondii* antigens. This includes neutrophils, DCs, macrophages, microglial, and T cells (Yarovinsky, 2014; Coombes and Hunter, 2015). TNF-α together with IFN-γ promote anti-parasitic mechanisms in macrophages, as well as non-hematopoietic cells, through the production of nitric oxide (Yarovinsky, 2014; Coombes and Hunter, 2015).

The balance of the immune response in *T. gondii* infection is juggled by IL-10 that is produced by several cell types, including macrophages, NK cells, T cells and B cells. IL-10 can inhibit the activation of accessory cells, inhibit adaptive immune responses and limiting inflammation (Coombes and Hunter, 2015). *T. gondii* has also been shown to interfere with STAT1 signalling, resulting in blockage of interferon regulatory factor 1 (Irf1), p65 GBPs, inducible nitric oxide synthase (iNOS/Nos2), indoleamine 2,3-dioxygenase 1 and MHC increasing their survivability (Zimmermann *et al.*, 2006; Brasil *et al.*, 2017).

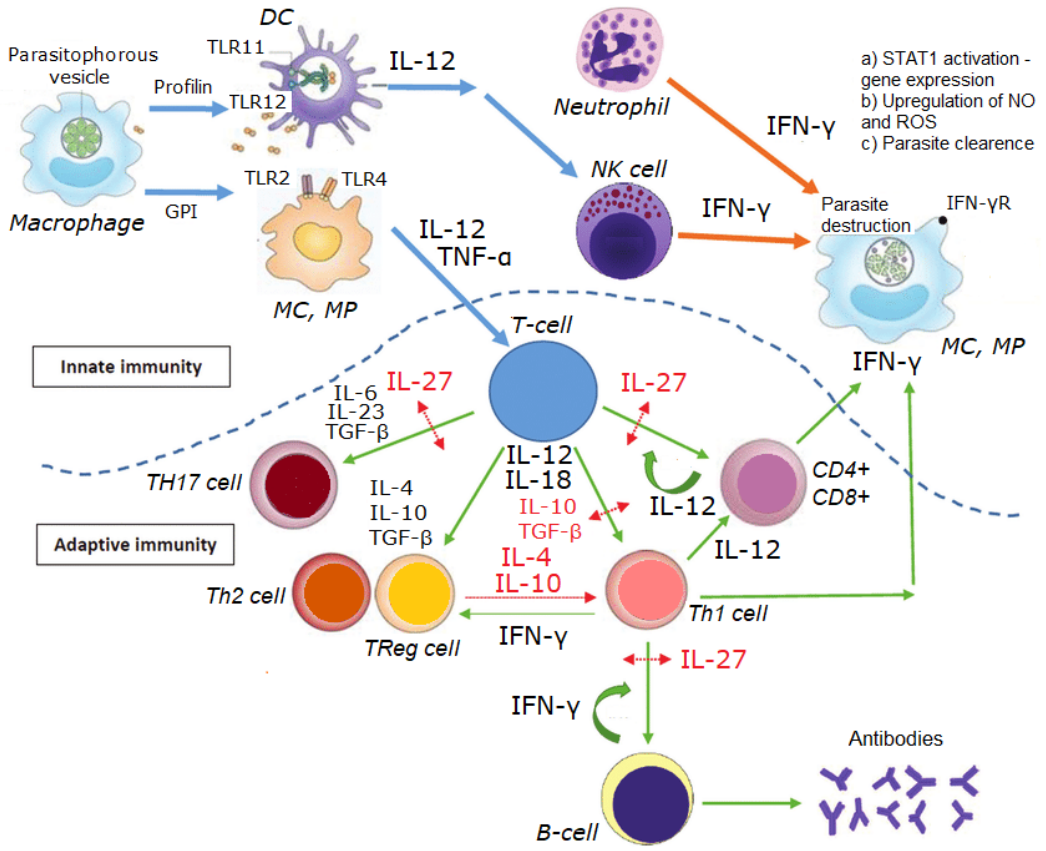


Figure 1-5 Innate and adaptive immunity interplay in intracellular *Toxoplasma gondii* infection. Dendritic cells (DC), monocytes (MC), and macrophages (MP) are the first cells to respond to *T. gondii* infection. *T. gondii* profilin interacts with Toll-like receptor (TLR) 11 and TLR12 on dendritic cells while *T. gondii* GPI protein interacts with TLR2 and TLR4 on MC/MP. Interation leads to IL-12 production by DC and MC/MP. In addition, macrophages also induce TNF-α. The innate immune response results in the production of IFN-γ from natural NK cells. These inflammatory mediators then direct the developing adaptive immune system, resulting in the differentiation of T-cells into T helper cells (Th), T regulatory (TReg) and/or CD4+/CD8+. Adaptive immune response is regulated by Th2 and TReg cells primarily through IL-4 and IL-10 production. IL-10 and IL-27 are key to modulating these pathways and prevent the overproduction of Th1-type cytokines. IFN-γ production is the key mediator during the innate and adaptive responses for activating cells to control parasite infection. IFN-γ induces signal transducer and activator of transcription 1 (STAT1, a nuclear transcription factor) for genes expression leading to production of NO and reactive oxygen species (ROS) for parasite destruction or limiting parasite replication intracellularly. (Image credit:Molan *et al.*, 2017)

1.14 Transcriptomics in *T. gondii*-host Interaction Research

The transcriptomes of three different strains of *T. gondii* representing three common genotypes RH (type I), PLK (type II) and CTG (type III) tachyzoite and bradyzoite stages have also been sequenced (Croken *et al.*, 2014). Among significant findings are that in steady state, extracellularly, all strains differ greatly in gene expression, despite limited genetic differences. Also, for *T. gondii* RH, a high level of AP2IX-9, a transcription regulator, is essential to the parasite's ability to withstand stress and its inability to differentiate to bradyzoite stage (Croken *et al.*, 2014).

Transcriptome sequencing studies from *T. gondii* infected human cells have also been conducted and are listed in **Table** 1-3. The list suggested the lack of large-scale gene expression investigation on human brain cells. Therefore, it is an area that has been explored in this thesis.

Table 1-3 List of transcriptome studies performed on different human cells and different strains of *T. gondii*.

Type	Strain	Cell Type	Transcriptome	Reference
I	RH, GT1	Human foreskin fibroblast	RNA seq - mRNA	Yang *et al*., (2013)
I	RH	Human foreskin fibroblast	RNA seq - mRNA	Radke *et al*., (2005)
I	RH	Monocytes & macrophage	Microarray - mRNA	Chaussabel *et al*., (2003)
II	Prugniaud (Pru)	Human foreskin fibroblast	RNA seq - mRNA	Skariah & Mordue, (2012)
II	Prugniaud (Pru)	Human foreskin fibroblast	Microarray – miRNA and mRNA	Pope & Lässer, (2013)
II	PDS	Human foreskin fibroblast	Microarray - mRNA	Blader, Manger, & Boothroyd, (2001)
II	Prugniaud (Pru)	Human foreskin fibroblast	Microarray - mRNA	Fouts & Boothroyd, (2007)

1.15 The Role of miRNA in *T. gondii* Infection

Micro RNA (miRNA) or also known as small non-coding RNA (ncRNA) are non-coding RNAs that modulate gene expression regulation by inhibition, activation, modification or decay of messenger RNA (Aalto and Pasquinelli, 2012). miRNA of *T. gondii* infection have been sequenced from infected primary human foreskin fibroblasts (Zeiner *et al.*, 2010), human macrophage (Cai *et al.*, 2014) and human neuro-like cells (Xiao *et al.*, 2014). A study on *T. gondii* infected human neuron-like cells, showed that miRNA-132 that controls the dopamine level in the brain was upregulated to the level similar to those seen in schizophrenia patients (Xiao *et al.*, 2014). Meanwhile, a study on human macrophages revealed a selection of miRNAs that were regulated by STAT3 and are involved in the anti-apoptosis response to *T. gondii* infection (Cai *et al.*, 2013). A study on human fibroblasts discovered that *T. gondii* specifically modulates miR-17~92 and miR-106b~25 expression, which is central to mammalian cell regulation and has been associated with several hyperproliferative diseases (Zeiner *et al.*, 2010) It was predicted that *T. gondii* RH contains 117,315 small RNAs while *T. gondii* ME49 contains 67,623 small RNAs (J. Wang *et al.*, 2012). Among small RNAs of *T. gondii* ME49, 336 of them are miRNAs while for *T. gondii* RH, 201 of them are miRNAs (J. Wang *et al.*, 2012). Unfortunately, there is no specific database cataloguing *T. gondii* miRNA that can be used to BLAST all mapped reads even at ToxoDB.org. In addition, the latest analysis using the *T. gondii* genome only managed to confirm a limited selection of three types of noncoding RNA, namely 181 copies of tRNA, 18 copies of rRNA and four copies of miRNA (Lau *et al.*, 2016).

1.16 *Toxoplasma gondii* and *Pseudomonas aeruginosa* Quorum Sensing Molecules

The *Pseudomonas aeruginosa* (*P. aeruginosa*) quorum-sensing signalling molecule *N*-(3-oxododecanoyl)-L-homoserine lactone (3-Oxo) is bacterial virulence factor that can induce proinflammatory cytokine production in different cell types in addition to suppressing the function of key immune responses responsible for bacterial clearance (Mayer *et al.*, 2011). It is also capable of inducing apoptosis in certain cell types, such as mammary epithelial cells and Caco-2 cell (Li *et al.*, 2004; Taguchi *et al.*, 2014). Additionally, 3-Oxo disrupts epithelial barrier integrity in Caco-2 cells by the degradation of TJs (Vikström, Tafazoli and Magnusson, 2006). So far, there is no report on whether this molecule affects BBB membrane integrity.

The 2-Heptyl-3-hydroxy-4(1H)-quinolone (PQS) is another quorum sensing molecule produced by *P. aeruginosa* (Pesci *et al.*, 1999). Both 3-Oxo and PQS suppress T-cell proliferation, but only 3-Oxo was able to suppress human peripheral blood mononuclear cell proliferation (hPBMC) and IL-2 release (Hooi *et al.*, 2004). It is still not known whether PQS can affect hBMEC viability and/or BBB integrity. Thus, if 3-Oxo and PQS can open up TJs in the BBB, there is a potential for them to carry drugs intended for the brain, easing their entry. Both *T. gondii* and *P. aeruginosa* can cross BBB to cause encephalitis (Pulzova *et al.,* 2009) suggesting that they have similar tissue tropism. However, there had been no previous studies that specifically, and directly, assessed the impact of co- or pre-infection with *P. aeruginosa* on *T. gondii* infection at the BBB interface. Co-infection of *T. gondii* and *P. aeruginosa* while uncommon, have been reported in at least two cases in French Guiana (Carme *et al.*, 2002; Demar *et al.*, 2012) and Peru (Nunura *et al.*, 2010).

1.17 Thesis: Hypothesis and Aims

Despite the significant strides that have been achieved over the last few decades in toxoplasmosis research, much remains to be investigated especially in the area of host-parasite interaction and the molecular mechanisms that underpin the pathophysiology of disease caused by *T. gondii* infection at the blood-brain barrier interface. Additionally, despite the availability of many anti-*T. gondii* drugs, current chemotherapeutic interventions do not provide a full cure, and some can generate side-effects. A better knowledge of the host-pathogen interaction is needed to understand the molecular mechanisms that underpin the pathogenesis of toxoplasmosis.

Therefore, this thesis tested the hypothesis that *T. gondii* infection with human brain microvascular endothelial cells (hBMECs) cells induces molecular alterations in gene expression that can be used as biomarkers or biosignatures specific to infection. In this work, an integrated approach was adopted, encompassing transcriptomics and multiple cell-based assays, to identify biosignatures of *T. gondii* infection of hBMECs. Specific aims of the study included:

(i) studying the alterations in the BBB barrier function in response to infection;
(ii) profiling the transcriptomic changes that occur in hBMECs subsequent to infection;
(iii) identifying the differentially expressed miRNAs that are altered by *T. gondii* infection;
(iv) investigating the antiparasitic effect of monensin on *T. gondii* infecting hBMECs;
(v) investigating the effect of quorum sensing (QS) molecules known to modulate BBB permeability on the ability of *T. gondii* to cross the BBB;

The research presented have identified several mRNA, miRNA and signalling pathways that were specifically altered in response to *T. gondii* infection of the hBMECs. These findings contribute to an improved understanding of the host-parasite interaction and have elucidated some of the mechanisms used by the parasite to cross the BBB. The results were obtained using an *in vitro* culture system and include progress towards validating the same findings *in vivo*. Future studies should focus on using gene editing technologies, such as CRISPR-CAS9 to study the role of specific mRNA or miRNAs in parasite infection biology.

Chapter 2 The Response of Human Brain Microvascular Endothelial Cells (hBMECs) to *Toxoplasma gondii* Infection

2.1 Abstract

Toxoplasma gondii can cause parasitic encephalitis, a life-threatening infection predominately found in immunocompromised individuals. *T. gondii* can invade the brain, but the mechanisms by which this parasite crosses the Blood-Brain-Barrier (BBB) to cause brain damage, are poorly understood. This study reports the structural and functional changes, associated with infection and replication of *T. gondii*, within human Brain Microvascular Endothelial cells (hBMECs) *in vitro*. Results from this study indicated that exposure of hBMECs to *T. gondii*, had a negative impact on the function and integrity of brain vascular endothelial cells, through compromised viability and increased monolayer permeability, as well as through deregulated expression of cytokine and TJ genes.

2.2 Introduction

Toxoplasma gondii is an obligate intracellular apicomplexan protozoan, which may infect at least one-third of the human population worldwide (Montoya and Liesenfeld, 2004; Weiss and Kim, 2013). Infection manifests as self-limiting flu-like symptoms, or even as asymptomatic in healthy individuals, and may result in the establishment of long-term latency. However, *T. gondii* can cause serious health consequences in cases of parasite reactivation in immunocompromised patients, or if primary infection occurs during pregnancy

(Elsheikha, 2008). *T. gondii* can invade, and proliferate within, all nucleated cells; and colonises multiple distinct organ system tissues inside all warm-blooded mammals. The brain is the most common site where the latent stage of *T. gondii* can be found (Carruthers and Suzuki, 2007). For *T. gondii* to infect the brain, the parasite must interact with, and cross, the Blood-Brain-Barrier (BBB), a cellular structure that regulates the entry of substances into the central nervous system (Elsheikha and Khan, 2010).

Events associated with *T. gondii* tropism for, and invasion of, the Central Nervous System (CNS), have been the focus of intense investigation in recent years. Experimental evidence indicates that *T. gondii* breaches the BBB (Lambert *et al.*, 2006; Lachenmaier *et al.*, 2011) paracellularly either by targeting TJ proteins (Elsheikha and Khan, 2010), by direct infection of endothelial cells (Däubener *et al.*, 2001) or inside leukocytes in a 'Trojan horse' manner. An *in vivo* study in mice has shown that the vascular endothelial cells serve as a replicative niche for the parasite which, after replication and bursting of endothelial cells, spreads to the adjacent brain cells (Konradt *et al.*, 2016). Despite this understanding, the mechanisms by which this crossing of the BBB occurs are still unresolved. Identifying factors that mediate the interaction of *T. gondii* with the endothelial cells of the BBB would provide a better understanding of the neuro-pathogenesis of infection and holds great promise for future development of novel therapeutics against toxoplasmosis.

In this study, the response of hBMECs to infection with *T. gondii*, as a simple 2D model of BBB was investigated. The hypothesis tested was that *T. gondii* infection compromises the functions of BBB endothelial cells to cross the BBB and infects the brain. To test this hypothesis, the phenotypic and functional changes that occur in hBMECs during the early stages of infection progression were investigated. The effect of *T. gondii* infection on viability, vitality, cell cycle, mitochondrial potential and DNA fragmentation of host cells were

characterised. Also, the integrity of TJs of hBMECs following tachyzoite infection was evaluated using a trans-endothelial electrical resistance (TEER) assay; and the alteration in hBMECs permeability following tachyzoite infection was assessed using a FITC-Dextran leakage assay. We also investigated the effect of infection on the expression of selected TJ and inflammatory genes, using real-time PCR. The obtained data indicate that *T. gondii* maintains host cells' functions and inhibits apoptosis to ensure its survival and replication within infected host cells. These results support earlier *in vivo* findings and show that hBMECs serve as a replicative niche and launching pad for breaching the BBB by *T. gondii* and spreading to the CNS. This study provided new insights into how *T. gondii* affects hBMECs while crossing the BBB, which may lead to new ways to counter the damage caused by this neurotropic parasite.

2.3 Materials and Methods

2.3.1 *Growth Media Formulation*

All work was carried out inside a BSC level II hood, under aseptic conditions. High glucose Gibco® Dulbecco's Modified Eagle Medium-DMEM media (Thermo Fisher Scientific, MA, USA), heat inactivated Gibco® Fetal Bovine Serum (HI-FBS), Gibco® MEM Non-essential amino acids (100X), Gibco® L-glutamine (200 mM), Gibco® trypsin-EDTA (0.25%) and Gibco® Antibiotic-Antimycotic (100X) were warmed in a 37°C water bath for 10-15 minutes. Once warmed, 50 mL HI-FBS (10%), 5 mL of Antibiotic-antimycotic (1%) and 5 mL of MEM Non-essential amino acid (1% or 1X) and 10 mL (2 mM or 2%) of L-glutamine, were added into freshly opened 500 mL DMEM media. Madin-Darby Canine Kidney (MDCK-ATCC® CCL-34™; ATCC, Middlesex, UK) cells were thawed from liquid nitrogen in around one minute using a 37°C water bath, and the outside of the cryogenic vial was sterilised with 70% ethanol.

Approximately 12 mL complete DMEM media were added into 75 cm^2 NUNC™ tissue culture flasks (Fisher Scientific, Leicestershire, UK). Cells within the vial were mixed gently using a serological pipette and transferred into a 75 cm^2 NUNC™ tissue culture flask filled with complete culture media. The cells were then incubated at 37°C with 5% CO_2. For the hBMECs, Gibco® RPMI medium (500 mL) was supplemented with 100 mL (20%) of Gibco® HI-FBS, 5 mL of Gibco® non-essential amino acids (1%), 5 mL of Gibco® Sodium pyruvate 100 mM (1%), 5 mL of Gibco® MEM Vitamin 100X (1%), 5 mL (1%) of Gibco® L-glutamine (200mM) and 5 mL of Gibco® Antibiotic-antimycotic 100X (1%) to make a complete media (cRPMI). Thawing steps for the hBMECs were the same as those used for thawing MDCK cells described above. For TEER measurement and hBMECs monolayer permeability by FITC-dextran experiments, hBMECs were grown in a Transwell system where hanging inserts (6.5 mm diameter, 0.33 cm^2 surface area, 5 µm pore size, polyethylene terephthalate) from Millicell® (Merck, Darmstadt, Germany) were positioned in a 24 well NUNC™ plate. For both experiments, 0.3 mL cRPMI media were pipetted into the inserts and another 1 mL of the same medium, were pipetted into the well outside the insert.

2.3.2 *Maintenance of Cell Culture*

If the flask was not confluent, when observed under an inverted microscope, the medium was removed with a serological pipette before adding 15 mL of fresh pre-warmed complete media and returned to the incubator. Culture medium was changed twice each week. When the cells were confluent, the culture medium was removed, and the cell monolayer was rinsed twice with cold 1X Gibco® PBS and then with 0.25% (w/v) Gibco® trypsin-EDTA solution, to remove all traces of serum that contains a trypsin inhibitor. Next, 2-3 mL of trypsin-EDTA solution was added to the flask and incubated for 2-3 minutes.

Cells were checked with an inverted microscope to monitor the detachment of cells. Next, 15 mL of complete growth medium were added, and cells were gently suspended. The cell suspension from the flask was then sub-cultured into three new culture flasks (1:3) and new media added to make up to 15 mL media/flask. Finally, the flasks were incubated at 37°C in 5% CO_2.

2.3.3 *Cell Counting*

Old culture medium from the culture flask was discarded. Then, the cell monolayer was rinsed twice with cold 1X Gibco® PBS, followed by 0.25% (w/v) Gibco® trypsin-EDTA solution to remove traces of serum that contains a trypsin inhibitor. Next, 2 mL of Gibco® trypsin-EDTA solution was added to the flask and incubated for 2-3 minutes. Cells were checked with an inverted microscope to ensure all cells had detached. Next, 6 to 8 mL of complete growth medium was added, and cells were mixed by repeated pipetting. Then, 100 µL of the cell suspension was mixed with 100 µL of Gibco® trypan blue stain solution 0.4%. The stained cell suspension was transferred to a haemocytometer (Paul Marienfeld GmbH & Co. KG, Lauda-Königshofen, Germany) using a micropipette. Finally, the haemocytometer chamber was viewed under the 10X objective of Leica DM 1L inverted microscope. Living cells appeared round and transparent, while dead cells were darker in colour. Living cells in the large, central gridded square (1 mm^2) were counted. Counted cells were then multiplied by 10^4 and then by 2 (the dilution factor of adding trypan blue) to estimate the number of cells per millilitre. All steps were repeated three separate times, with at least three technical replicates, and the average count was determined.

2.3.4 *Counting the Tachyzoites*

Flasks infected with *T. gondii* were observed using an inverted microscope until more than 90% destruction of the cell monolayer occurred. A cell scrapper was then used to detach the remaining cultured cells. Cells and medium were collected into a 50 mL centrifuge tube and centrifuged with Allegra X-22R (Beckman Coulter, California, USA) at 600x*g* for 5 minutes. The supernatant was transferred into a new 50 mL centrifuge tube and re-centrifuge at 1000x*g* for 10 minutes. The resulting pellet of tachyzoites was re-suspend in complete medium. About 100 µL of the collected tachyzoite were then mixed with 100 µL of Trypan blue stain solution 0.4%. The stained tachyzoites mixture was transferred to the haemocytometer using a micropipette (Eppendorf AG, Hamburg, Germany). Finally, the chamber was viewed under both 10X and 40X objectives of a Leica DM 1L inverted microscope (Leica Microsystems Ltd, Milton Keynes, UK). *T. gondii* tachyzoites appeared transparent/unstained while dead tachyzoites had a dark colour due to the integrity of the plasma membrane being compromised. Only the living parasites in the large, central gridded square (1 mm^2) were counted. The number of counted parasites was multiplied by 10^4 and then by 2, the dilution factor, to estimate the number of tachyzoites per millilitre. All steps were repeated three separate times, with three biological replicates, and the average count was calculated.

2.3.5 *Cell Seeding Optimisation*

Confluent hBMECs were harvested and counted using a haemocytometer as described above. Tissue culture inserts were seeded with hBMECs at 5×10^3, 10×10^3, 15×10^3 and 20×10^3 cells/insert. TEER readings were recorded at 24, 48, 72, 96, 120, 144, 168, 192 and 216 hours after seeding at three sides of the insert. Readings were recorded, and the resistance of each insert was

calculated using the formula described in section **2.3.14** (Measurement of TEER). Old media was replaced with new media at 96 and 168 hours post cell seeding.

2.3.6 *Cell Insert Count*

Because cells continue to grow after seeding, and to adjust the number of parasites added to cells (parasite: cell ratio, a multiplicity of infection [MOI]), the number of cells per well after 120 hours of seeding was determined. Cells were seeded as described above. After five days of seeding, cells were harvested using trypsin-EDTA and counted with a haemocytometer, as described above. To evaluate the effect of the prolonged culture of hBMECs within inserts, the number of cells in the inserts, and the TEER value was determined daily for nine days (216 hours). The media was changed twice - after 96 hours and 168 hours.

2.3.7 *Cell Viability Assays*

Two different viability assays were used to monitor the progression of *T. gondii* infection on hBMEC viability. Progress of infection determination leads to separation of stages in infection into early, middle and late stages. First, hBMECs were trypsinised, and 10^4 cells were seeded in NUNC™ 96 wells plate with 200 µL of cRPMI media. After 24 hours, media were changed, and *T. gondii* added into wells at MOI of 5. Two hours before the end of incubation period (3, 6, 12, 24, 48, 72 h.p.i), 10% Alamar blue (Thermo Scientific, Leicestershire, UK) was added to all the wells. At the end of incubation period, the fluorescence intensity of each well was read at 560 nm/590 nm (excitation/emission) using a Varioskan Flash (Thermo Scientific).

Then, the ChemoMetec viability assay (ChemoMetec A/S, Allerod, Denmark) was employed. Control and infected wells were treated with trypsin-EDTA for 2 minutes, followed by centrifugation at 500x*g*. Cells were re-suspended in PBS, and 190 µL of cell suspension was transferred into an Eppendorf tube. Next, 10 µL of Solution 5 containing acridine orange, propidium iodide and VB-48™ was added, and the mixture was re-suspended by pipetting. Then, 11 µL of the mixture was injected into the chambers of an A8 slide (ChemoMetec A/S, Allerod, Denmark). The NucleoView™ NC-3000™ Software (ChemoMetec A/S, Allerod, Denmark) was quickly employed, and the "Vitality Protocol" and the sample unit" A8 slide" options were selected before measurement with a NucleoCounter® NC-3000™ image cytometer (ChemoMetec A/S, Allerod, Denmark).

2.3.8 *T. gondii Infection Titration*

The effects of different multiplicities of infection (MOIs) on hBMECs' viability, monolayer integrity, monolayer permeability and the number of parasites crossing, were investigated. The effect of MOI on hBMECs' viability was determined, for hBMECs infected with MOI of 1, 3, 5 and 10 for 72 hours, using the Alamar blue assay. The protocol for Alamar blue essay was as described in section **2.3.7** above.

2.3.9 *Measurement of Cellular Thiols*

The vitality of hBMECs following *T. gondii* infection was evaluated using a Vitality Assay kit from Chemometec. In animal cells, thiols - such as the antioxidant glutathione (GSH) - are involved in many processes; including the quenching of free radicals, drug detoxification, cell signalling and proliferation. A decrease in the level of intracellular thiols is an early hallmark of apoptosis.

There is a correlation between cellular GSH depletion and the initiation and progression of apoptosis (Coppola and Ghibelli, 2000). When cellular GCH is depleted, the cytosol is shifted from a reducing to an oxidising environment, which may lead to further depletion of GSH. The Vitality Assay was performed to quantify the number of free thiols at the single-cell level. The stain VitaBright-48TM (VB-48™), a component of Solution 5, immediately reacts with thiols to form a fluorescent product. By quantifying the fluorescence, it was possible to determine the level of cellular thiols and determine cell health. A high level of fluorescence in a cell indicates that the cell has a high level of thiols, such as GSH, and is in a healthy state. Cellular fluorescence was quantified using a NucleoCounter® NC-3000™ image cytometer. The accompanying NucleoView® NC-3000™ software facilitates automated image acquisition, image analysis and data visualisation, and enables the quantification and gating of subpopulations.

2.3.10 *Mitochondrial Potential Assay*

Loss of mitochondrial membrane potential precedes apoptosis and chemical-hypoxia-induced necrosis (Kroemer, Galluzzi and Brenner, 2007). The mitochondrial potential assay enables the measurement of mitochondrial transmembrane potential (Δψm) using the cationic dye JC-1 (5,5,6,6-tetrachloro-1,1,3,3-tetraethylbenzimidazol-carbocyanine iodide). The lipophilic cationic dye JC-1 displays potential-dependent accumulation in the mitochondria; and provides a simple, fluorescent-based method for distinguishing between healthy and apoptotic cells. In healthy cells, the negative charge established by the intact mitochondrial membrane potential, facilitates the accumulation of JC-1 in the mitochondrial matrix. At high concentrations, JC-1 forms aggregate and becomes fluorescent red. In apoptotic cells, the mitochondrial potential collapses, and JC-1 localises to the

cytosol in its monomeric fluorescent green form. The hBMEC mitochondrial potential assay following *T. gondii* infection was performed using a mitochondrial potential assay kit from Chemometec.

Both control and infected cultures were treated with trypsin-EDTA for 2 minutes - followed by centrifugation of the detached cells at 500x*g*. Cells were washed twice with 1X PBS, and 12.5 µL of Solution 7 (final concentration: 2.5 µg/mL) were added to the cell sample, followed by 10 minutes of incubation at 37°C. After incubation, cells were washed twice with 1X PBS. The cell pellets were re-suspended in 0.25 mL Solution 8 by pipetting. Then, 11 µL of the cell suspension was loaded into a slide chamber (NC-Slide A8), for measurements of cellular fluorescence using the NucleoCounter NC-3000 cytometer.

Subsequent analyses of cellular stress were performed using NucleoView 2.1 software. The ratio of the intensity of red colour emitted from the J-aggregate to that of green colour emitted from the JC-1 monomer represents the relative values of the mitochondrial membrane potential in cells and is independent of mitochondrial mass. Two light-emitting diode light sources, with wavelengths of 475 nm and 530 nm, were used to excite JC-1 to generate green and red fluorescence. The green and red fluorescence emitted was detected independently using two emission filters, without overlap in bandpass (560 ± 35 nm for green fluorescence and 630 nm long pass for red fluorescence). Events of up to 5000 cells, from the images of single cells, were acquired, analysed; and displayed as quadrant plots - with red fluorescence on the Y axis and green fluorescence on the X-axis - using NucleoView NC-3000 software. After gating the boundary between upper polarised and lower depolarised cell populations, based on the distribution of a control sample, the percentage of cells in the lower right quadrant represents depolarised cells with low mitochondrial membrane potential.

2.3.11 *DNA Fragmentation Assay*

This assay evaluates the occurrence of late-stage apoptosis in hBMECs following *T. gondii* infection - as DNA fragmentation is the hallmark of late-stage apoptosis (He, Lu and Zhou, 2009). Both control and infected wells, were treated with Gibco® trypsin-EDTA for 2 minutes followed by centrifugation at 500x*g*. Cells were then washed once with 1X Gibco® PBS. The washed pellet was re-suspended with 1 mL 4% paraformaldehyde (Merck, Darmstadt, Germany) and incubated at 4°C for 24 hours. Cells were then washed twice with PBS, centrifuged at 500x*g*, re-suspended in 0.5 mL of Solution 3 and incubated at 37°C for a further 5 minutes. Finally, 11 µL of the cell suspension was added to the chamber of A8 slides. Immediately the NucleoView™ NC-3000™ Software was used, with both "DNA Fragmentation Assay" and the sample unit" A8 slide" options being selected before measurement. This assay is simple, rapid and cheap, but has some limitations as sub-G1 cells, cells with different chromatin structure, normal cells with lower DNA content that are in heterogeneous cell populations, or aneuploid populations, may also produce false-positive apoptotic cells. A further limitation is that this method may not detect apoptotic cells in their G2/M phase.

2.3.12 *Two-Step Cell Cycle Analysis*

The effect of *T. gondii* infection on hBMEC cell cycle was evaluated using a Two-Step Cell Cycle Assay kit from Chemometec. This assay for the NucleoCounter® NC-3000™ system enables the rapid quantification of the DNA content of mammalian cells - allowing the determination of the G0/G1, S and G2/M cell cycle phases. In general, any cell population includes cells in various stages of cell cycling: G1 /G0 phase (one set of paired chromosomes per cell), S phase (DNA synthesis with a variable amount of DNA), and G2/M phase (two

sets of paired chromosomes per cell, prior to cell division). DNA content can be measured using fluorescent, DNA-selective stains that exhibit emission signals proportional to the DNA mass.

Prior to analysis, 20 µL of Solution 12 was added to 980 µL of Solution 10 and mixed by pipetting. Then, control and infected wells were treated with trypsin-EDTA for 2 minutes, followed by centrifugation at 500x*g*. Cells were then washed once with PBS, and the cell pellet was re-suspended in 250 µL of Solution 10 supplemented with ten µg/mL DAPI. After the cells had been incubated at 37°C for 5 minutes, 11 µL of the mixture was loaded into the chamber of A8 slides. Immediately, the NucleoView™ NC-3000™ Software was engaged – with the "2-Step Cell Cycle Assay" and the sample unit" A8 slide" options being selected before measurement.

2.3.13 *EVOM Voltohmmeter Calibration*

To calibrate the voltohmmeter, the 'Mode Switch' was switched to 'R' (resistance/Ohms) then the 'Power' switch was turned on. The 'TEST R' button was then pressed, and the display showed the following reading:

Mode: 2000 Ω Reading: 1000 Ω ± 10 Ω (± 1%)

Mode: 20 KΩ Reading: 1 kΩ

The above steps were repeated three times. Next, the telephone-type plug at the end of the flexible electrode cable was inserted into the 'Electrode Port' on the meter. The electrode tips were then immersed in a vessel - containing an electrolyte solution similar to the experimental culture medium. Next, the 'Mode switch' was switched to 'R' followed by turning on the 'Power' switch. At this stage, when the meter is in the 'R' mode, and neither the 'Test R' nor 'Measure R' switch is set, the meter should display zero or very close to zero. If not, the 'Zero Ω' screw was adjusted with a small flat-head screwdriver

until the meter shows a reading of zero. Then, with the electrode still immersed in the electrolyte solution, the 'Measure R' switch is set. The reading should be less than 200 Ω and stable when the electrode is kept stationary. These steps were repeated three times.

2.3.14 *Measurement of TEER*

Here, the effect of *T. gondii* infection on hBMEC monolayer integrity was evaluated. Transendothelial electrical resistance (TEER) is a quantitative technique, used to measure the integrity of TJs in cell culture models of endothelial and epithelial monolayers (Srinivasan *et al.*, 2015). For resistance measurements, the EVOM Voltohmmeter (World Precision Instrument, Hitchin, UK) and STX2 (World Precision Instrument, Hitchin, UK) electrode can be used directly out of dry storage, without any preconditioning.

Firstly, the 'Mode Switch' was set to R, and the 'Power' switch turned on. Then, the electrodes were inserted into a well with the cell culture insert without cells, but with media that has been allowed to equilibrate at room temperature for 5 minutes. TEER readings were displayed and the results, after some steady ohms reading of the solution resistance, were recorded. The value of the blank added to the total resistance measured across a tissue culture membrane and was subtracted from the resistance reading of the well with cells, to obtain 'true resistance'. Next, the electrode was transferred into a new well with cells and media. TEER readings were recorded at 24, 48, 72, 96, 120, 144 and 168 hours after seeding in inserts. TEER values were calculated as ohms × cm^2. Briefly, the electrical resistance reading of the insert without cells was subtracted from the readings obtained from inserts with cells - and this value was then multiplied by the surface area of the insert (0.33 cm^2). Resistance is inversely proportional to the surface area, *i.e*. the larger the

membrane, the lower the resistance. The formula used for resistance calculation was:

R (total) - R (blank) = R (true tissue)

R (true tissue) x Surface Area (insert) = Ω cm^2

Millicell Hanging Insert Surface Area = 0.33 cm^2

Resistance Calculation : R (true tissue) x 0.33 cm^2 = _____ Ω cm^2

Uneven STX2 electrode lengths allow the longer electrode to touch the bottom of the well plate's outer chamber - containing the culture media while preventing the shorter electrode from reaching the bottom of the insert - where the cell membrane lays. Consistent positioning of the longer tip at the bottom of the dish for every reading, before steadily holding the electrode in a static condition, was done to increase the reproducibility of the measurements. The electrodes were also rinsed with culture media when moving from one insert to another. Detailed protocols of EVOM Voltohmmeter manual can be retrieved online at https://www.wpiinc.com/media/wysiwyg/pdf/EVOM-IM-021308.pdf (Accessed - 5 January 2017).

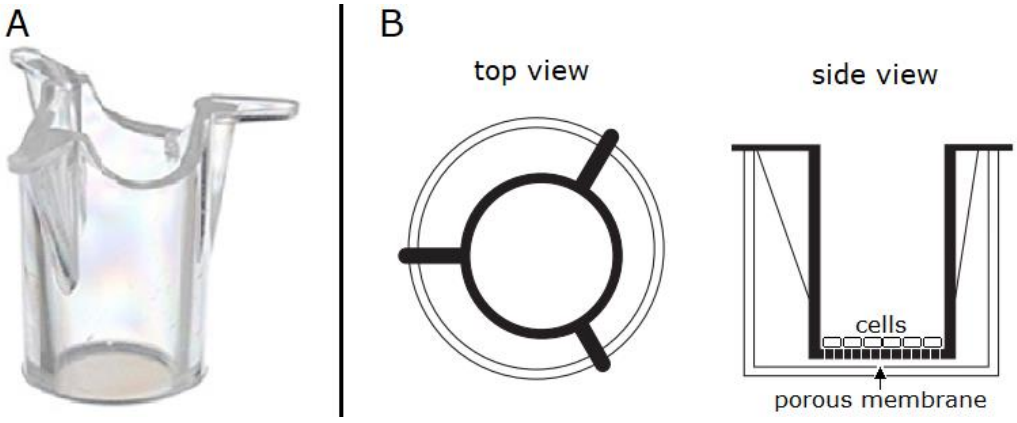


Figure 2-1 **A:** An image of an insert. **B:** Top and side views of a well in a Transwell culture system. For TEER measurement, the short electrode was placed inside the insert while the long electrode was placed at the bottom of the well

2.3.15 *HBMECs Monolayer Permeability*

The effect of *T. gondii* infection on the permeability of the hBMEC monolayer was evaluated, using the molecular tracer fluorescein isothiocyanate (FITC)-labeled dextran. Freshly purified *T. gondii* RH were administered to the inserts, positioned into 24 well culture plates apically, at an inoculation ratio (multiplicity of infection [MOI]) of 5:1 tachyzoite/endothelial cell, and the plate was incubated at 37°C for one hour. To measure the paracellular flux, the apical cell culture media in the upper chamber of the Transwell were replaced with 0.3 mL of culture medium containing FITC-dextran (1 mg/mL), whereas the basolateral reservoirs were filled with 1 mL culture medium alone. Culture medium containing FITC-dextran (1 mg/mL) was used as a positive control. After incubation for 3, 6, 24, 48, 72 and 96 hours, the culture media in the lower chamber, was collected and filtered through 0.22 µm filter to remove any debris. Then, 200 µL of the collected media were transferred into a 96 well culture plate (100 µL /well). The basolateral media was replenished with 200 µL fresh media added to each lower compartment. To determine the percent flux of FITC-dextran across the monolayer from upper chamber to lower chamber, fluorescence was measured in the basolateral media of the lower chambers of the transwell, using a fluorometer (Varioskan Flash, Thermo Fisher Scientific Inc., MA, USA) at an excitation wavelength of 485 nm, and an emission wavelength of 530 nm.

2.3.16 *Extracting total RNA using Qiagen RNeasy Kit*

The RNeasy® Plus Mini Kit (Qiagen®, Hilden, Germany) was used to extract and purify total RNA samples used in this study. With the RNeasy® procedure, all RNA molecules longer than 200 nucleotides are purified and most RNAs less than 200 nucleotides such as some ribosomal RNAs (rRNA) and

transfer RNAs (tRNA), which together comprise 15–20% of total RNA are selectively excluded. All pipetting was carried out with sterile and RNase free micropipette tips. Micropipette, gloves, working area were sprayed with RNase AWAY® to remove any RNase and DNA contamination. Also, all reagents from the kit were placed at room temperature 25°C for 30 minutes before starting the extraction procedure because reagents such as Buffer RLT and RW1 contain salt that could precipitate upon storage at 4°C. Extraction and purification procedure were exactly based on RNeasy® Mini Handbook (2012) downloaded from the following address https://www.qiagen.com/ch/resources/resourcedetail?id=14e7cf6e-521a-4cf7-8cbc-bf9f6fa33e24&lang=en. (Accessed – 8 January 2017)

Eluted RNA was separated into three different tubes to avoid repeated thawing and freesing of the sample which could affect the quality of the RNA with one tube for quality control analysis with a Nanodrop™ 8000 spectrophotometer (Thermo Fisher Scientific, Leicestershire, UK) and two tubes for PCR analysis. RNA was stored at -80°C.

2.3.17 *Total RNA Quality Analysis*

The quality of extracted RNA was determined primarily by measuring the absorbance at 260 nm and 280 nm using a NanoDrop™ 8000 spectrophotometer. Sample with an absorbance ratio value (A260/A280) of 1.8 to 2.0 were used for cDNA conversion.

2.3.18 *Converting RNA to cDNA*

RNA was converted to cDNA using Invitrogen™ SuperScript® III First-Strand Synthesis System for RT-PCR (Thermo Fisher Scientific, Leicestershire,

UK). The SuperScript® III First-Strand Synthesis System for RT-PCR is optimised to synthesise first-strand cDNA from purified poly(A)+ or total RNA. RNA targets from 100 bp to >12 kb can be detected with this system. The amount of starting material can vary from 1 pg – 5 µg of total RNA. SuperScript® III Reverse Transcriptase is a version of M-MLV RT that has been engineered to reduce RNase H activity and provide increased thermal stability. The enzyme was used to synthesise cDNA at a temperature range of 42–55°C, providing increased specificity, higher yields of cDNA, and more full-length product than other reverse transcriptases. As SuperScript® III RT is not significantly inhibited by ribosomal and transfer RNA, it may be used to synthesise the first-strand cDNA from a total RNA preparation. cDNA synthesis is performed using either total RNA or poly(A)+-selected RNA primed with oligo(dT), random primers, or a gene-specific primer.

After RT, it is common not to quantify the resulting cDNA by UV absorbance. Instead, the cDNA is assigned a concentration unit relative to the original concentration of RNA in the RT reaction. For example, if one loaded 10 µg of RNA into a 100 µL RT reaction, the designated concentration of the resulting cDNA would be 100 ng/µL; which means 1 µL of the sample contains the cDNA generated from 100 ng of RNA. In this experiment, 60 ng of total RNA was used with 30 µL reaction mixture for cDNA conversion resulting in an estimated 2 ng/µL cDNA concentration (60/30).

The following procedure is based on Invitrogen's protocol. The following RNA/primer mixture was prepared for each tube: total RNA 60 ng (maximum 11 µL), random hexamers (50 ng/µL) 1 µL, 10 mM dNTP mix 1 µL, nuclease-free water to 10 µL. Samples were incubated at 65°C for 5 minutes and then on ice for at least 1 minute. A reaction master mixture was prepared containing 2 µL 10x RT buffer, 4 µL 25 mM MgCl2, 2 µL 0.1M DTT, 1 µL RNAaseOUT and 1 µL SuperScript III RT (200 U/µL) for each reaction. The reaction mixture was

added to the RNA/primer mixture, mixed briefly, then left for 10 minutes at 25°C. Tubes were incubated 50°C for 50 minutes, heat inactivated at 85°C for 10 minutes and then chilled on ice for 2 minutes. Resultant cDNA was stored at -20°C until use for real-time PCR.

2.3.19 *Real time PCR using Roche Lightcycler 480 II and SYBR Green Mastermix*

The amount of cDNA in a reaction was set to be at 3 ng of converted RNA per 20 µL of reaction. The mixtures in a reaction are as follows; 10 µL SYBR Green Mix (Qiagen), 2 µL cDNA, 1 µL reverse primer (10 µM), 1 µL forward primer (10 µM) and 6 µL H_2O. The program steps are as follows; hot start incubation step (1 cycle) 95°C for 5 minutes followed by amplification steps (45 cycles) 95°C for 15 seconds, then 61°C for 30 seconds and then 72°C for 30 seconds and cooling period (1 cycle) at 40°C for 10 minutes.

The cycle number at which the fluorescence signal first exceeds the level of background fluorescence or the 'crossing point (CP) value' will be automatically set by the LightCycler software for each run. Aside from *T. gondii* DNA, No-template controls (NTC) and no-amplification controls (NAC) plus extracted total mRNA from infected samples were also included. A standard curve for calculating amplification efficiency and error was constructed by diluting target serially and analysing 6 concentrations in triplicate. The theoretical optimum amplification efficiency is 2. Amplification efficiency analysis was conducted for *T. gondii* DNA and both housekeeping genes.

2.3.20 *Primers*

Most of primer sequences for human genes were acquired from Primer Bank, a public resource for PCR primers where these primers are designed for gene expression detection or quantification by real-time PCR (https://pga.mgh.harvard.edu/primerbank) (Accessed – 20 February 2017). Primers name, GenBank accession, sequences, and PrimerBank ID/RTPrimerDB ID are listed in **Table** 2-1. Primers for inflammatory genes were obtained from published literature and RTPrimerDB, a public database for primer and probe sequences used in real-time PCR assays (http://www.rtprimerdb.org/) (Accessed – 23 February 2017).Meanwhile, primer for IL-6 was based on sequences published by Miller *et al.,* (2015)

Table 2-1 List of primers with their description, GenBank accession number, forward and reverse sequences, and their ID number from sourced databases. Primer sequences for IL-6 was based on published journal.

Human Gene Description	GenBank Accession	Primer Sequence (5' end to 3' end)	PrimerBank/ RTPrimerDB ID
ß-actin ACTB, mRNA (Housekeeping)	NM_001101	F: CATGTACGTTGCTATCCAGGC R: CTCCTTAATGTCACGCACGAT	4501885a1
hydroxymethylbilane synthase HMBS, mRNA (Housekeeping)	NM_001024382	F: AGCTTGCTCGCATACAGACG R: AGCTCCTTGGTAAACAGGCTT	66933008c1
occludin OCLN, mRNA	NM_001205254	F: ACAAGCGGTTTTATCCAGAGTC R: GTCATCCACAGGCGAAGTTAAT	327478413c1
tight junction protein 1/zona occludens 1 TJP1/ZO-1 mRNA	NM_003257	F: CAACATACAGTGACGCTTCACA R: CACTATTGACGTTTCCCCACTC	116875766c1
protein kinase, cAMP-dependent, catalytic alpha PRKACA, mRNA	NM_207518	F: AGCCCACTTGGATCAGTTTGA R: GTTCCCGGTCTCCTTGTGT	46909583c1
Tumor necrosis factor alpha, TNF-α mRNA	NM_000594	F: GGAGAAGGGTGACCGACTCA R: TGCCCAGACTCGGCAAAG	RTPrimerDB ID 3646
Interleukin-6, IL-6 mRNA	NM_000600	F: CCAGGAGCCCAGCTATGAAC R: CCCAGGGAGAAGGCAACTG	Miller *et al.*, (2015)
ATP-binding cassette, sub-family B (MDR/TAP) member 1 mRNA, ABCB1/P-GP	NM_000927	F: AAATTGGCTTGACAAGTTGTATATGG R: CACCAGCATCATGAGAGGAAGTC	RTPrimerDB ID 3512

2.3.21 *Statistical analysis*

Data are expressed as mean values ± standard errors (SE). Statistical analyses were performed with GraphPad Prism version 7 software (GraphPad Software, CA, USA). Data comparing more than two groups were analysed by one-way analysis of variance (ANOVA), or two-way ANOVA with Bonferroni multiple-comparison test. Data comparing two groups were analysed with the nonparametric Mann-Whitney test. A P value of < 0.05 was considered statistically significant. The level of significance was reported as: *, $P < 0.05$, ** $P < 0.01$, *** $P < 0.001$, and ****, $P < 0.0001$.

2.4 Results

2.4.1 *Optimisation of Cell Seeding and Multiplicity of Infection*

We aimed to determine the optimum cell seeding number that generate the highest hBMEC membrane resistance. As shown in **Figure** 2-2**,** the lowest reading, 10.64 ± 1.59 Ωcm^2 was measured at 48 hours from wells seeded with 5 x 10^3 cells; while the highest reading, 35.27 ± 4.28 Ωcm^2, was measured at 144 hours from wells seeded with 2 x 10^4 cells. Two cell seeding densities (10^4 and 2 x 10^4) resulted in the highest membrane resistance after 120 hours, 10^4 cells seeding generated 33.83 ± 8.37 Ωcm^2 resistance while 2 x 10^4 cells seeding generated 33.77 ± 9.73 Ωcm^2 resistance.

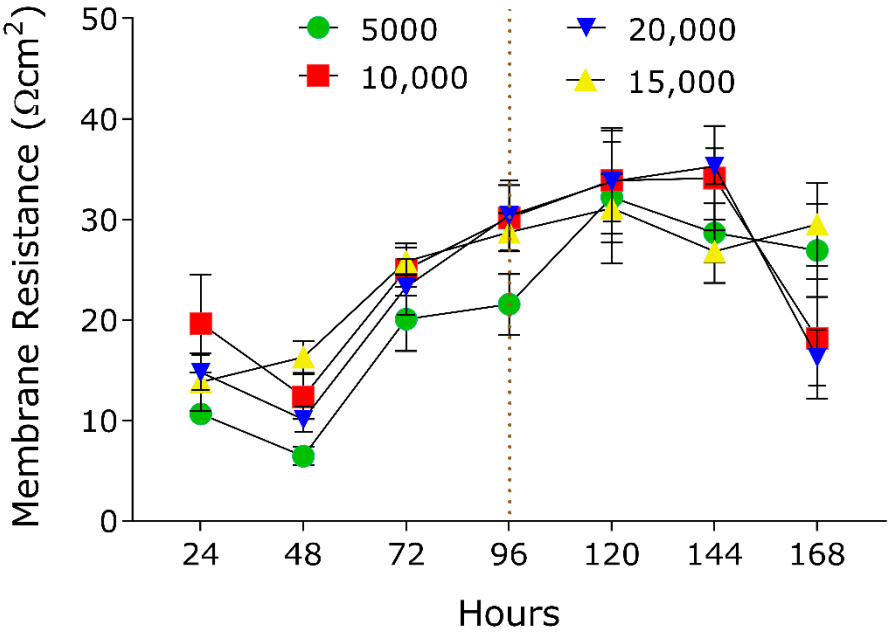


Figure 2-2 TEER value of hBMEC monolayer resistance in Ωcm^2 unit measured over 168 hours (7 days). The values represent averages from 4 inserts, where 3 TEER readings were recorded from 3 different sides of each insert. At 96 hours, the media in all inserts were changed with a fresh growth media. The resistance of all cell seeding densities gradually increased from 48 hours, peaking around 120 hours, and then declined after 120 hours until the end of the experiment.

A previous study, using the same cell type, obtained a maximal TEER value of 43.6 ± 3.89 Ωcm^2 after 3.19 days and at a seeding density of 4.5 × 10^4 cells/cm^2, or 14,850 cells per insert, with a 0.33 cm^2 surface (Eigenmann *et al.*, 2013). Both, this experiment and the previous study used inserts with 24 wells plate and a transparent PET membrane coated with collagen with a 3.0 µm pore size, but from different brands (Millicell *versus* Greiner Bio-one™). Based on the result in **Figure** 2-2 and those reported by Eigenmann *et al.*, (2013), 10^4 cells/well was chosen as the seeding density for all subsequent hBMECs resistance experiments.

We also performed a cell insert count, to determine the number of cells in the insert after 120 hours of 10^4 cell seeding. This step was important

to determine the multiplicity of infection (MOI) - the number of *T. gondii* tachyzoites per the number of host cells at the time of adding the parasite. The cell counts are presented in **Table** 2-2. The cells were counted from four insert cells inside four main corner squares. The average cell counts from seeding 10^4 cells for 120 hours was 175,625 cells, after 120 hours incubation.

Table 2-2 Counted hBMECs in Millicell Inserts (24 well 0.33 cm^2 surface area) after 120 hours at 10^4 cells seeding. The cells were counted from four inserts, where cells inside four main corner squares of two chambers were counted.

Seeding		**10,000**			
# of inserts		1	2	3	4
No of cells counted from two haemocytometer chambers	A	20	21	19	24
	B	30	28	30	24
	C	13	16	15	18
	D	12	7	1	3
Total		75	72	65	69
Average per quadrant		18.75	18	16.25	17.25
Standard deviation		8.30	8.83	11.98	9.91
Average per insert		175,625			
Total number of cells (suspended in 1 mL PBS after centrifugation) = Average per insert x 10^4		175,625			

2.4.2 *The Effect of Long-term Culture on Membrane Integrity*

To evaluate the effect of prolonged culture of hBMECs in inserts, the cells were grown in inserts for 216 hours (~ 9 days). The TEER value was measured daily. The media was changed twice during this experiment, after 96 hours and 168 hours. The results are presented in **Figure** 2-3.

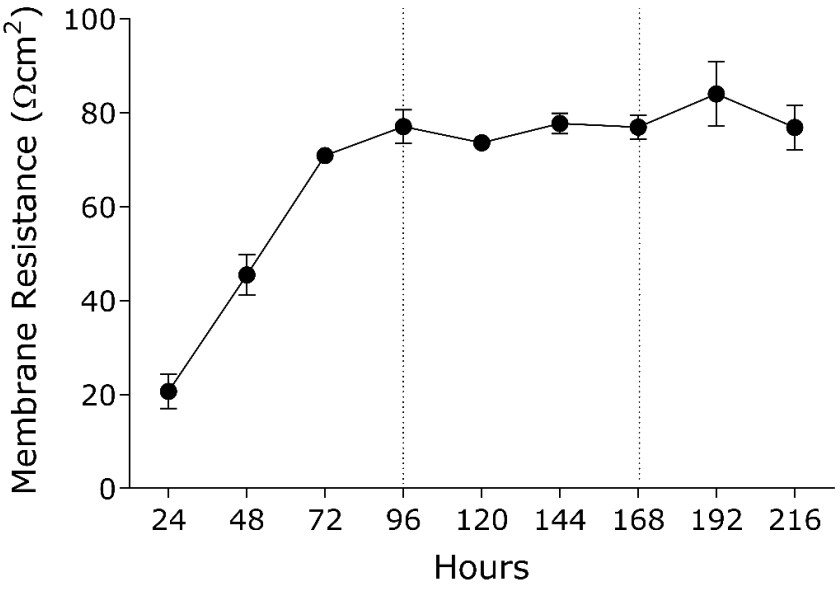


Figure 2-3 TEER value of hBMECs membrane resistance in Ωcm^2 unit measured over 216 hours (*i.e.* nine days). TEER values gradually increased from 24 hours, peaking at 96 hours, when it reached a plateau level until the end of the experiment. This result indicates that, if the media is changed every 96 hours (dotted line), the cells will maintain the membrane resistance. Media change re-supply the cells with fresh nutrients that were depleted in the old media, allowing the cells to remain viable. Data represent means of four inserts, where three TEER readings were recorded for each insert.

2.4.3 *Toxoplasma gondii Titration*

The effects of different MOIs on hBMECs' viability, monolayer integrity, monolayer permeability and the number of parasites crossing, were investigated. MOI of 01 refers to one parasite to one cell ratio while MOI of 03 refers to three parasites per cell ratio and so on. The effect of MOI on hBMECs' viability was determined using the Alamar blue assay for MOI of 1, 3, 5 and 10 for 72 hours. At 12 hours post infection (h.p.i), there was no significant change in cell viability when compared to control cells. However, from 24 h.p.i onwards, infection with MOI 3, 5 and 10 significantly reduced hBMECs' viability; while at MOI 1, significant changes started from 48 h.p.i (**Figure** 2-4).

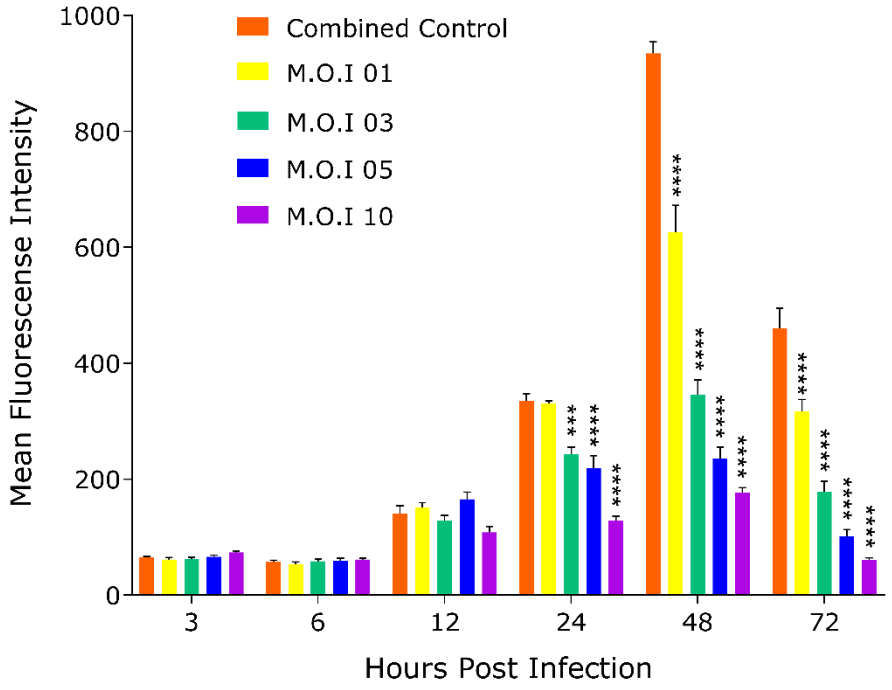


Figure 2-4 Temporal changes in hBMEC's viability. HBMECs were seeded at 10^4 cells/well and subjected to *T. gondii* infection at MOI of 1, 3, 5 and 10. Viability was assessed using the Alamar Blue Assay, as described in the materials and methods. From 24 h.p.i onwards, hBMECs' viability was significantly reduced by MOI 3, 5 and 10. Bars represent mean values ± SEM from 10 wells for control, and eight wells for infected. (***, $P < 0.001$; ****, $P < 0.0001$)

Figure 2-5 shows the effect of MOI on hBMECs monolayer integrity. All MOI caused a significant reduction in hBMEC's monolayer integrity. However this effect was more pronounced at MOI 3, 5 and 10.

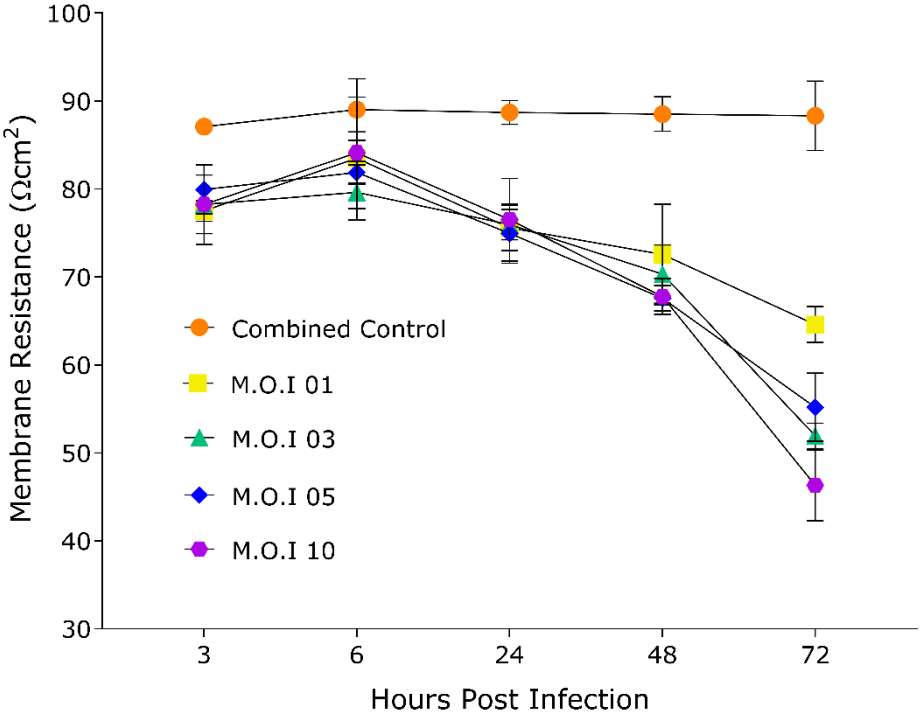


Figure 2-5 The effect of a multiplicity of infection on hBMECs' monolayer integrity. Pronounced reduction in hBMEC monolayer integrity can be seen in cells infected with MOI of 3, 5 and 10. Data shown are mean ± SEM from biological triplicates.

Figure 2-6 depicts the effect of MOI on hBMEC monolayer permeability over 72 h.p.i. There were slight differences between the control group and all MOIs, but no differences at any time points were significant (two-way ANOVA, $P < 0.05$). In this experiment, the control group leaked more FITC-dextran than the MOI groups up until 24 - where all MOI groups caught up which suggests that *T. gondii* infection seemed to reduce cell permeability.

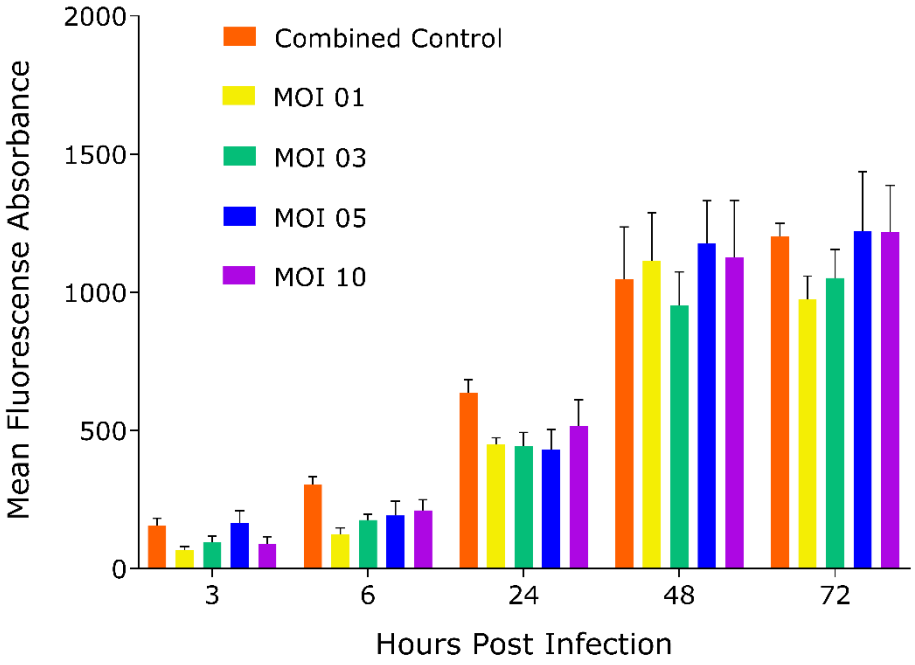


Figure 2-6 The effect of a multiplicity of infection on hBMECs' monolayer permeability. There were no significant differences in hBMEC monolayer permeability due to MOI, at any time point during the experiment ($P > 0.05$). Bars represent mean values from biological quadruplets ± SEM.

As *T. gondii* infection progressed, the number of parasites that managed to cross the hBMEC monolayer were counted and presented as a percentage of the number of crossed parasites over a total number of parasites inoculated (**Figure** 2-7). All MOI displayed sharp increases in percentage at 48 h.p.i, suggesting a major breach of hBMEC monolayer had occurred. The number of parasites counted increases as the number of MOI increases. However, in term of percentage (counted number of parasites in the bottom well/inoculated number of parasites in the hanging insert), MOI 05 infection resulted in more percentage than MOI 10 at 48 and 72 h.p.i.

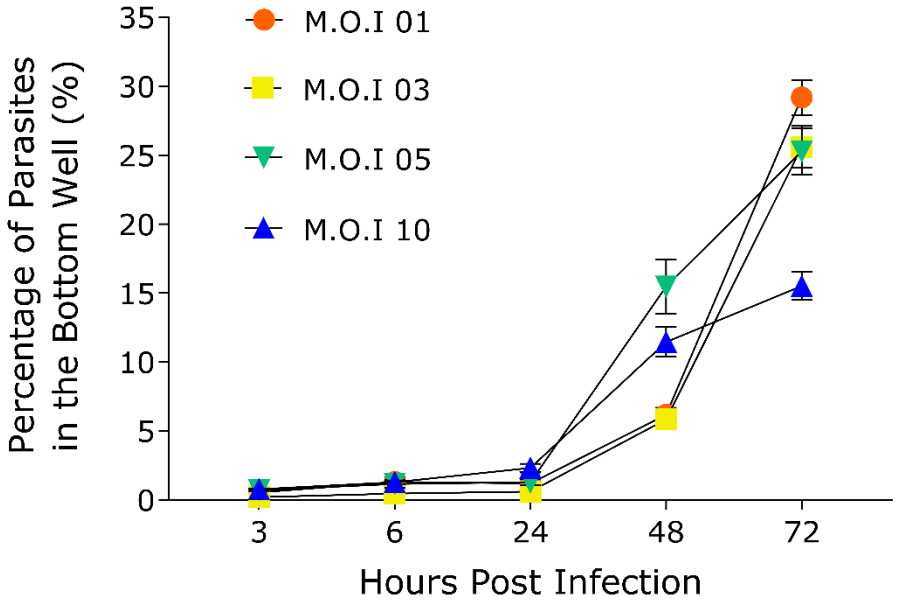


Figure 2-7 The number of *T. gondii* tachyzoites that passed through hBMECs' monolayer in the Transwell system. The percentage of parasites in the bottom well increased sharply at 48 h.p.i for all MOI, suggesting that a major breach of hBMECs monolayer occurred at 48 h.p.i. The highest percentage of crossing at 48 h.p.i was from MOI 05 (15.46 ± 3.41%); while at 72 h.p.i, MOI 01 had the highest percentage of crossing at 29.18 ± 2.22%. The results represent mean ± SEM from 4 wells.

2.4.4 *Characteristics of T. gondii Infection of hBMECs*

Monolayer Permeability Assay

The permeability of the hBMEC monolayer was evaluated by measuring the diffusion of fluorescein isothiocyanate (FITC)-dextran with molecular masses of 4 kDa (Sigma), from the apical to the basal medium compartments (**Figure** 2-8). The flux of FITC-dextran across hBMEC monolayers (indicative of paracellular permeability) was reduced, when monolayers were apically treated with *T. gondii* at MOI 5 from 3 hours to 24 hours. However, at 48 and 72 hours, more FITC-dextran leakage could be seen. No differences were statistically significant (two-way ANOVA, $P > 0.05$).

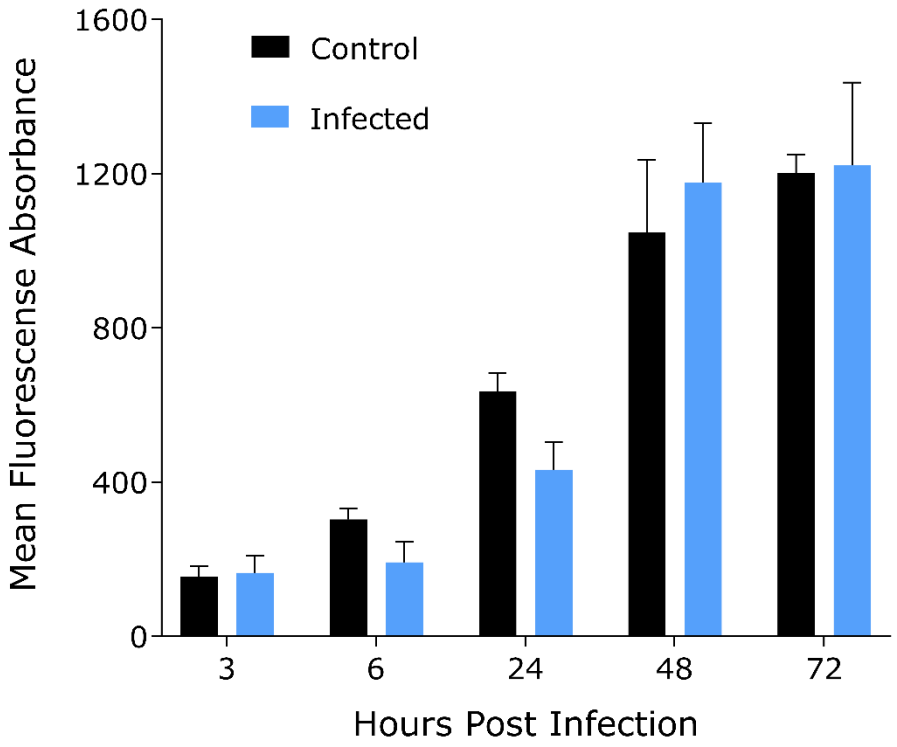


Figure 2-8 The effect of *T. gondii* infection on hBMECs' monolayer permeability. *T. gondii* infection reduced the permeability of hBMECs monolayers for over 24 hours until the parasite burst out of the cell at around 48 hours. Data were from quadruplets expressed as mean values ± SEM.

Membrane Integrity Assay

Monolayers of hBMECs in Transwell systems were infected with *T. gondii* tachyzoites at MOI of 5. TEER readings of all inserts were recorded for 72 hours and results are presented in **Figure** 2-9. Significant changes in hBMEC monolayer integrity could be detected after 24 h.p.i, and the monolayer integrity was significantly affected as infection progressed.

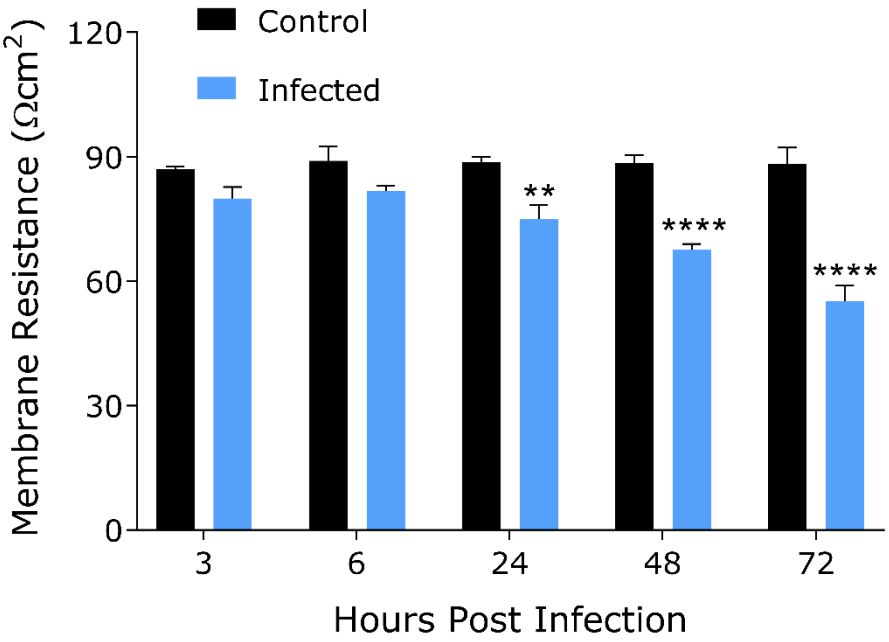
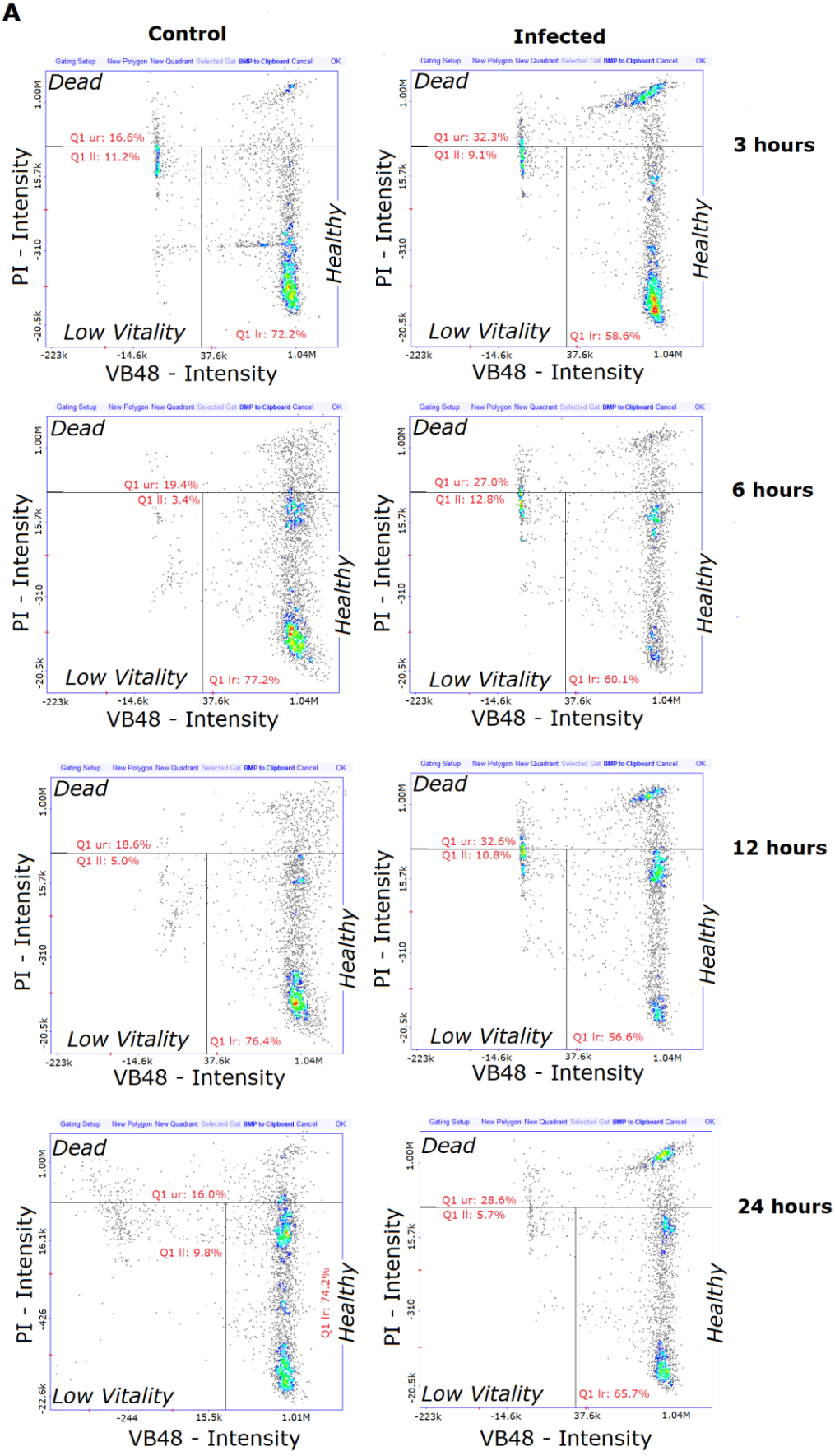


Figure 2-9 The effect of *T. gondii* infection on hBMECs' monolayer integrity. Monolayer integrity was significantly affected by *T. gondii* infection as early as 6 h.p.i and continued to be so as the infection progressed up to 72 hours. The results represent mean ± SEM from three wells for control and four wells for infected cells. (**, $P < 0.01$; ****, $P < 0.0001$)

Vitality Assay

NC-3000™ and VitaBright-48™ dye were employed to measure hBMECs' vitality, by determining the level of reduced thiols - that are involved in many cellular processes including neutralising of free radicals, drug detoxification, cell signalling and cell proliferation. **Figure** 2-10 shows the results from the cells' vitality assay, at 72 hours following *T. gondii* infection at MOI of 5.

A


Control
Infected
Dead
Healthy
Low Vitality
PI - Intensity
VB48 - Intensity
Q1 ur: 16.6%
Q1 ll: 11.2%
Q1 lr: 72.2%
Q1 ur: 32.3%
Q1 ll: 9.1%
Q1 lr: 58.6%
3 hours
Q1 ur: 19.4%
Q1 ll: 3.4%
Q1 lr: 77.2%
Q1 ur: 27.0%
Q1 ll: 12.8%
Q1 lr: 60.1%
6 hours
Q1 ur: 18.6%
Q1 ll: 5.0%
Q1 lr: 76.4%
Q1 ur: 32.6%
Q1 ll: 10.8%
Q1 lr: 56.6%
12 hours
Q1 ur: 16.0%
Q1 ll: 9.8%
Q1 lr: 74.2%
Q1 ur: 28.6%
Q1 ll: 5.7%
Q1 lr: 65.7%
24 hours

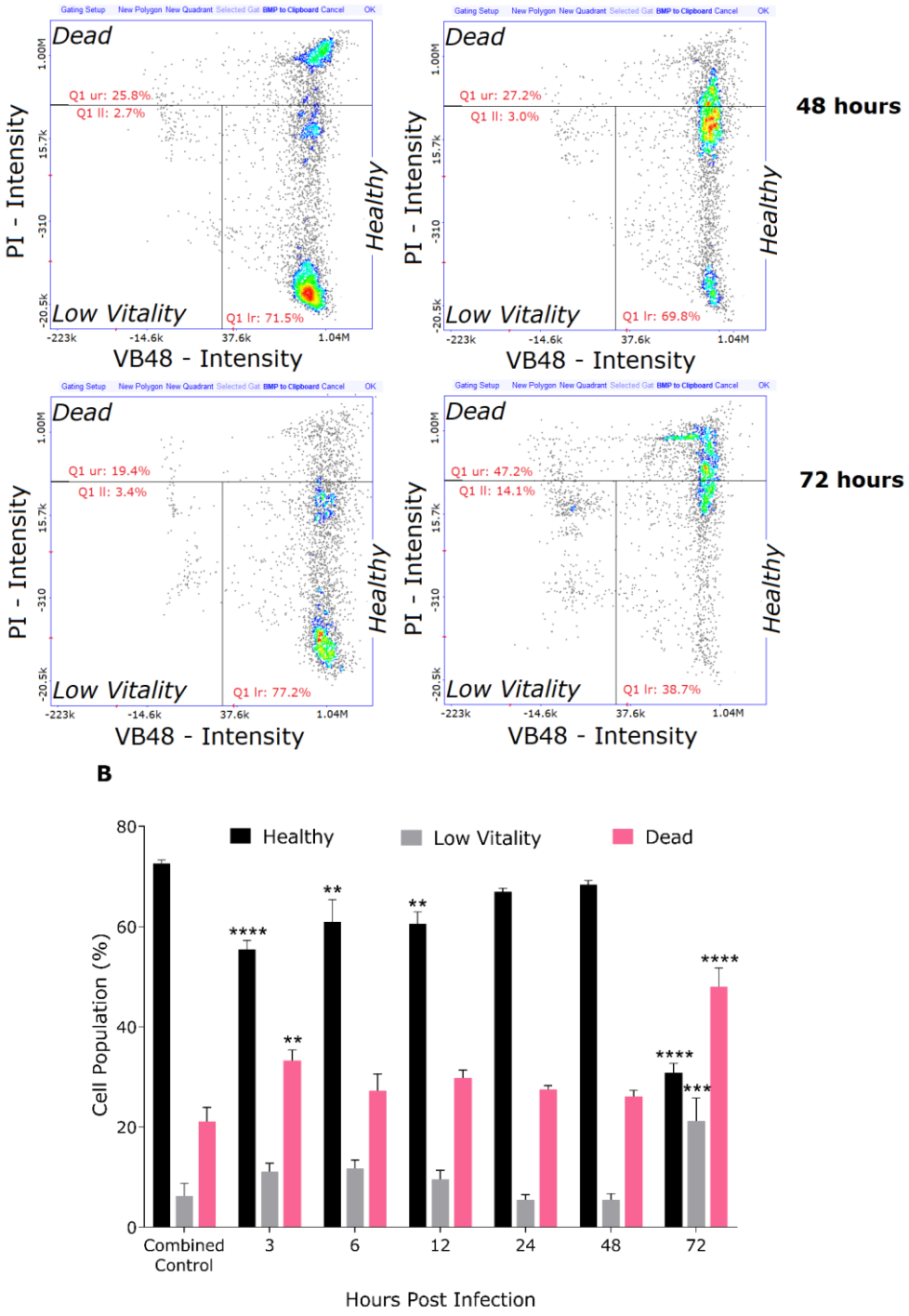
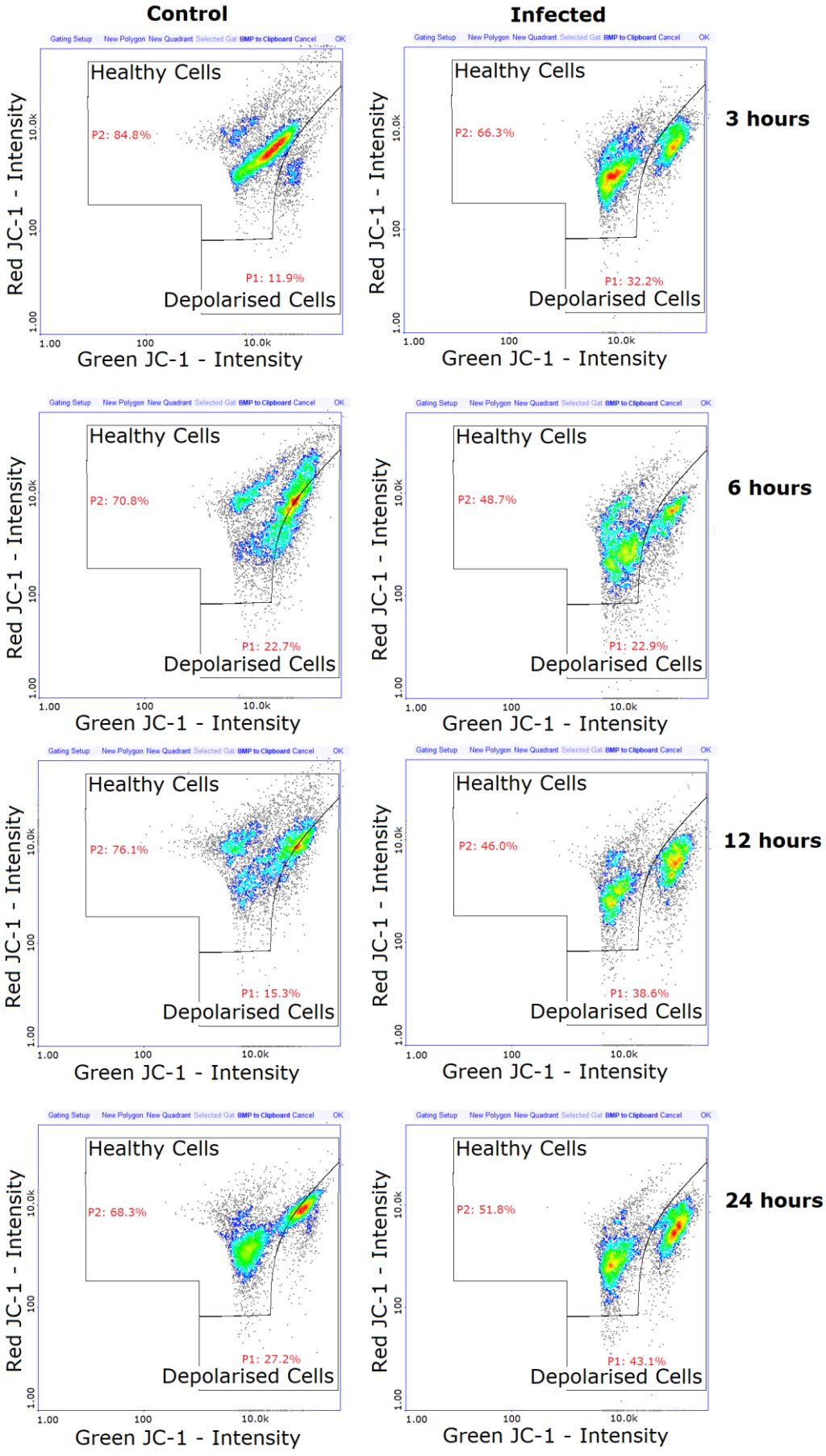


Figure 2-10 A: Scatter plots of uninfected hBMECs' vitality (left) and infected hBMECs' vitality (right) from 3 to 72 hours. B: Bar chart showing hBMECs' vitality population following *T. gondii* infection. Uninfected and infected hBMECs were stained with VB-48™, Acridine Orange (AO) and Propidium Iodide (PI) and analysed using the NucleoCounter® NC-3000™. After 3 h.p.i, hBMECs' vitality was reduced by about 12% but maintained around the same levels up until 48 h.p.i. At 72 h.p.i, the cells' vitality was reduced to half that of control cells. Data were from an average of triplicates while the error bars represent SEM. (**, $P < 0.001$, ***, $P < 0.001$; ****, $P < 0.0001$)

Mitochondrial Potential Assay

Loss of mitochondrial membrane potential is an event in early apoptosis and chemical-hypoxia-induced necrosis (Sakamuru, Attene-Ramos and Xia, 2016). In healthy cells, mitochondrial membrane potential is negatively charged; while in apoptotic or necrotic cells, the mitochondrial potential is absent. JC-1 is a positive green fluorescent dye attracted to negatively-charged mitochondrial membrane potential; leading to accumulation of JC-1 in the mitochondrial matrix forming aggregates of red fluorescent. Without the negative charge of mitochondrial potential, JC-1 localises to the cytosol in its monomeric green fluorescent form. **Figure** 2-10 depicts the effect of *T. gondii* infection on hBMEC mitochondrial potential over 72 hours. Compared to controls, mitochondrial potential of hBMECs were significantly affected at 12 (41.03 ± 5.8%), 24 (40.87 ± 5.76%), 48 (44.88 ± 4.750%) and 72 (46.64 ± 3.73%) h.p.i (one-way ANOVA, $P < 0.05$).

A


Control
Infected
3 hours
6 hours
12 hours
24 hours
Healthy Cells
P2: 84.8%
P1: 11.9%
Depolarised Cells
P2: 66.3%
P1: 32.2%
P2: 70.8%
P1: 22.7%
P2: 48.7%
P1: 22.9%
P2: 76.1%
P1: 15.3%
P2: 46.0%
P1: 38.6%
P2: 68.3%
P1: 27.2%
P2: 51.8%
P1: 43.1%
Red JC-1 - Intensity
Green JC-1 - Intensity
1.00
100
10.0k

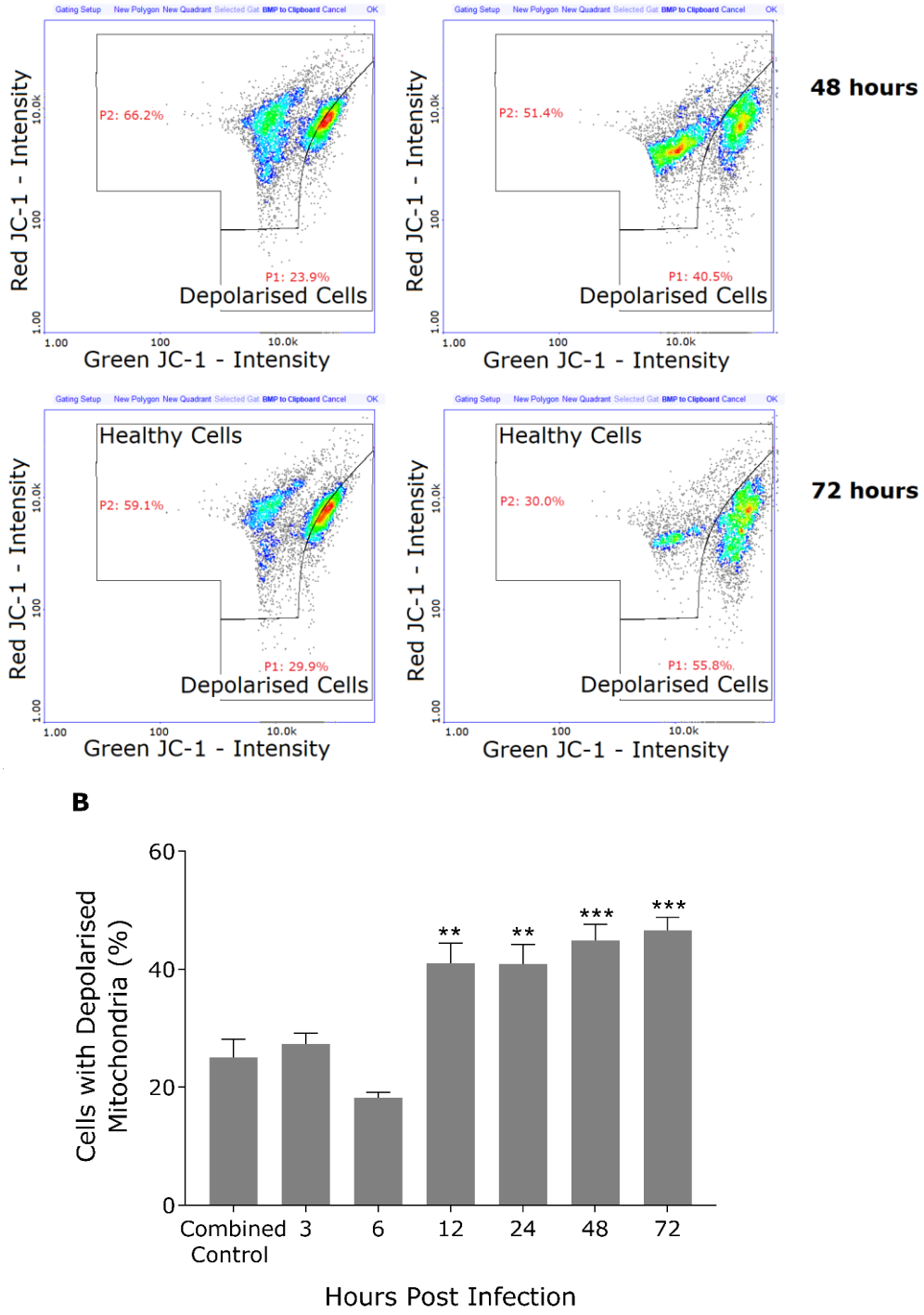
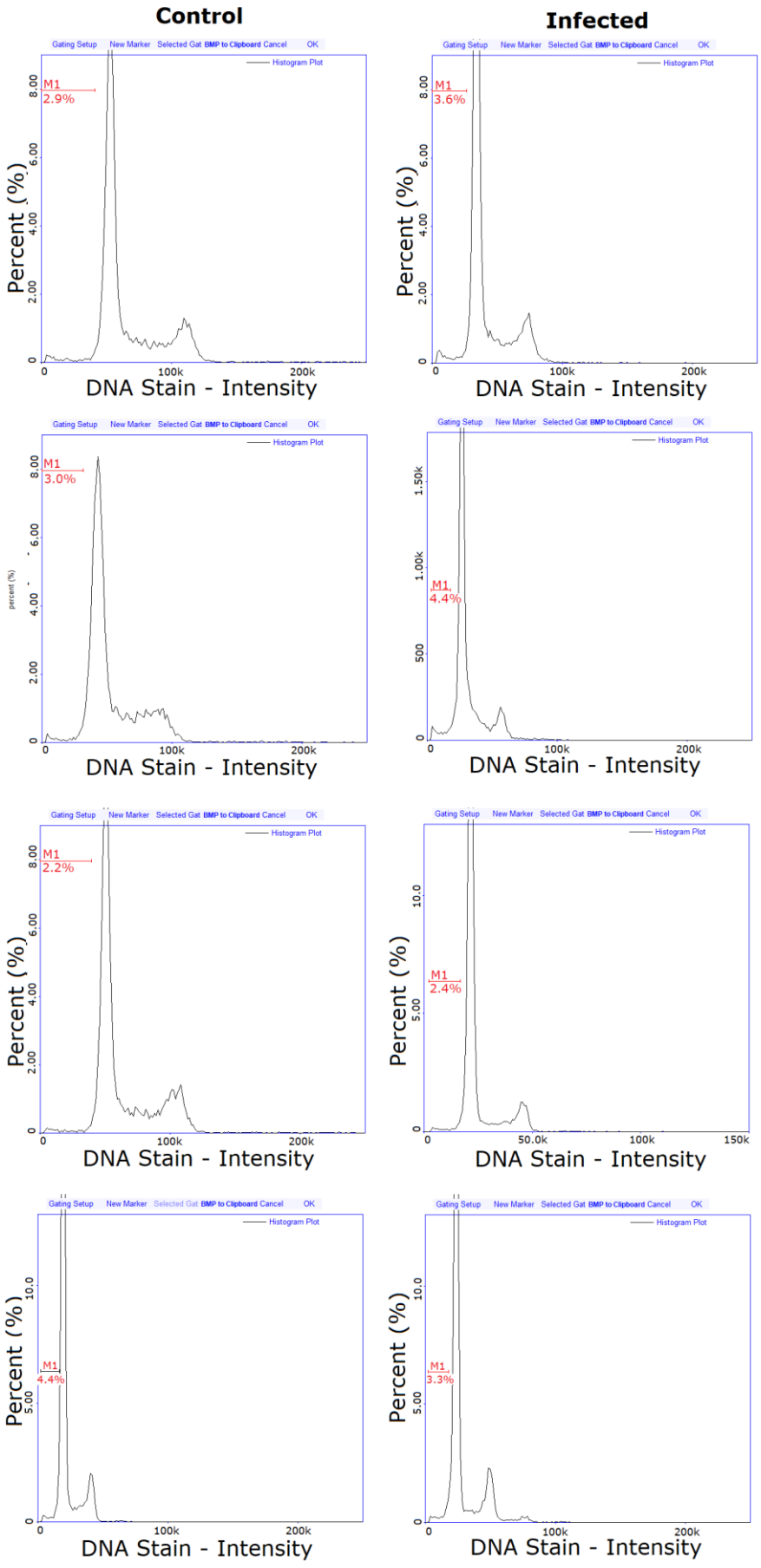


Figure 2-11 A: Scatter plots of uninfected hBMECs' mitochondrial potential (left) and infected hBMECs' mitochondrial potential (right), from 3 to 72 hours. B: Bar chart showing the mitochondrial potential state of hBMECs following *T. gondii* infection. Uninfected and infected hBMECs were stained with JC-1 and DAPI and analysed using the NucleoCounter® NC-3000™. Compared to control, mitochondrial potential of hBMECs were significantly affected at 12 (41.03 ± 5.8%), 24 (40.87 ± 5.76%), 48 (44.88 ± 4.750%) and 72 (46.64 ± 3.73%) h.p.i (one-way ANOVA, $P < 0.05$). Data were from the average of triplicates while the error bars represent SEM. (**, $P < 0.001$; ***, $P < 0.001$)

DNA Fragmentation Assay

During the later stages of apoptosis, double-strand breaks in the DNA result in fragmentation of DNA. This event can be detected with DAPI staining and NC-3000™ using DNA content analysis, to measure cells having less than one DNA equivalent (so-called sub-G1 cells). **Figure** 2-12 shows the effect of *T. gondii* infection on hBMEC DNA integrity. The bar chart shows that *T. gondii* infection did not affect DNA integrity of hBMECs, until 72 h.p.i when 13.49 ± 1.47% cells contain fragmented DNA.

A


Control
Infected
3 hours
6 hours
12 hours
24 hours
Histogram Plot
M1
2.9%
3.6%
3.0%
4.4%
2.2%
2.4%
3.3%
Percent (%)
DNA Stain - Intensity

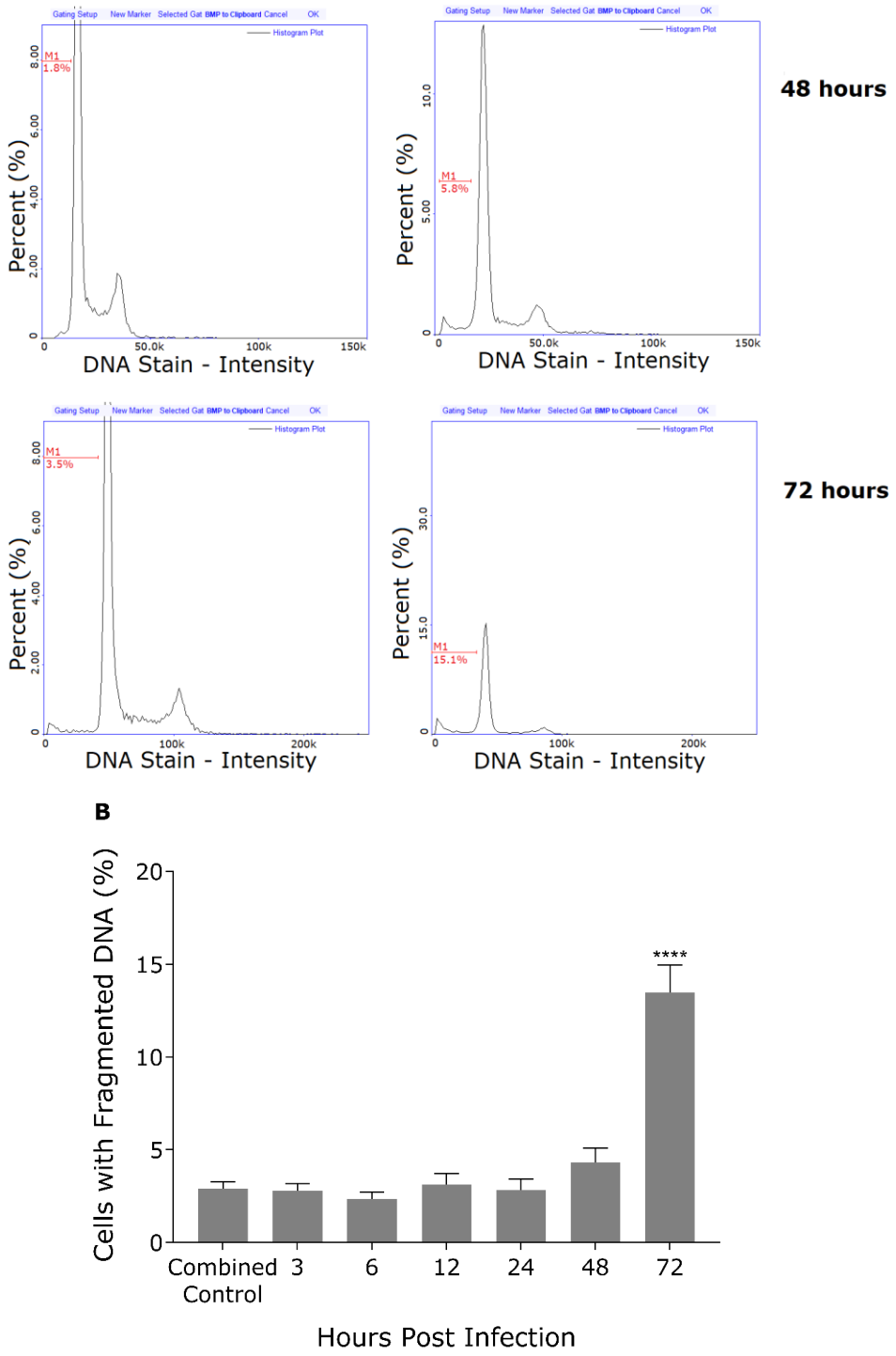
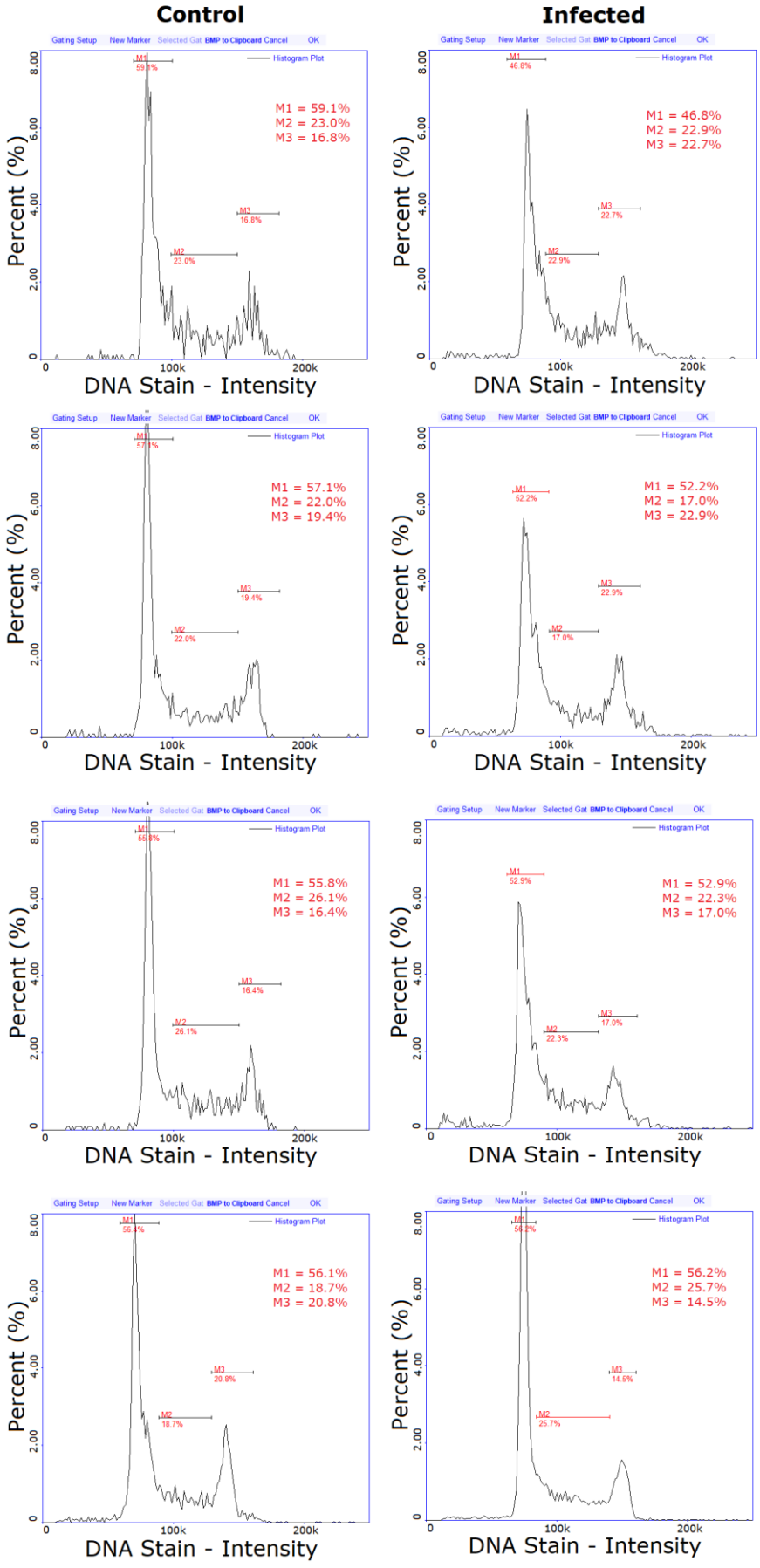


Figure 2-12 A: Histograms of uninfected hBMECs with fragmented DNA (left) and infected hBMECs with fragmented DNA (right), from 3 to 72 hours. B: Bar chart showing hBMECs with fragmented DNA following *T. gondii* infection. Uninfected and infected hBMECs were stained with DAPI, and cells with fragmented DNA (sub G0/G1 cells) were measured using the NucleoCounter® NC-3000™. The bar chart shows that the DNA integrity of hBMECs was not affected by *T. gondii* infection until 72 h.p.i when 13.49 ± 1.47 % of cells contain fragmented DNA. Data show the average of quadruplets while the error bars represent SEM. (****, P < 0.0001)

Cell Cycle Assay

The DNA content of hBMECs infected with *T. gondii* was evaluated using a DAPI stain and NC-3000™. DNA contents indicate the stage of the cell cycle where cells at the G2/M stage have double the DAPI dye intensity than those at the G0/G1 stage. **Figure** 2-13 depicts the effect of *T. gondii* infection on the host cell cycle. After 3 and 6 hours of infection, there were significant decreases ($P < 0.0001$ and $P < 0.05$, respectively) in the percentage of cells at G0/G1 stage, when compared to the control group; while at 72 h.p.i, there was a significant increase in the percentage of cells at the G0/G1 stage ($P < 0.01$). Meanwhile, at stage S, a significant increase was observed at 12 h.p.i ($P < 0.05$), but at 72 h.p.i there was a significant decrease in the percentage ($P < 0.01$). Generally, cell population at the G2/M stage was at the same level as the control from 3 to 48 hours. However, at 72 h.p.i there was a significant drop in numbers ($P < 0.01$)

A


Control
Infected
3 hours
6 hours
12 hours
24 hours
Histogram Plot
Percent (%)
DNA Stain - Intensity
M1 = 59.1%
M2 = 23.0%
M3 = 16.8%
M1 = 46.8%
M2 = 22.9%
M3 = 22.7%
M1 = 57.1%
M2 = 22.0%
M3 = 19.4%
M1 = 52.2%
M2 = 17.0%
M3 = 22.9%
M1 = 55.8%
M2 = 26.1%
M3 = 16.4%
M1 = 52.9%
M2 = 22.3%
M3 = 17.0%
M1 = 56.1%
M2 = 18.7%
M3 = 20.8%
M1 = 56.2%
M2 = 25.7%
M3 = 14.5%

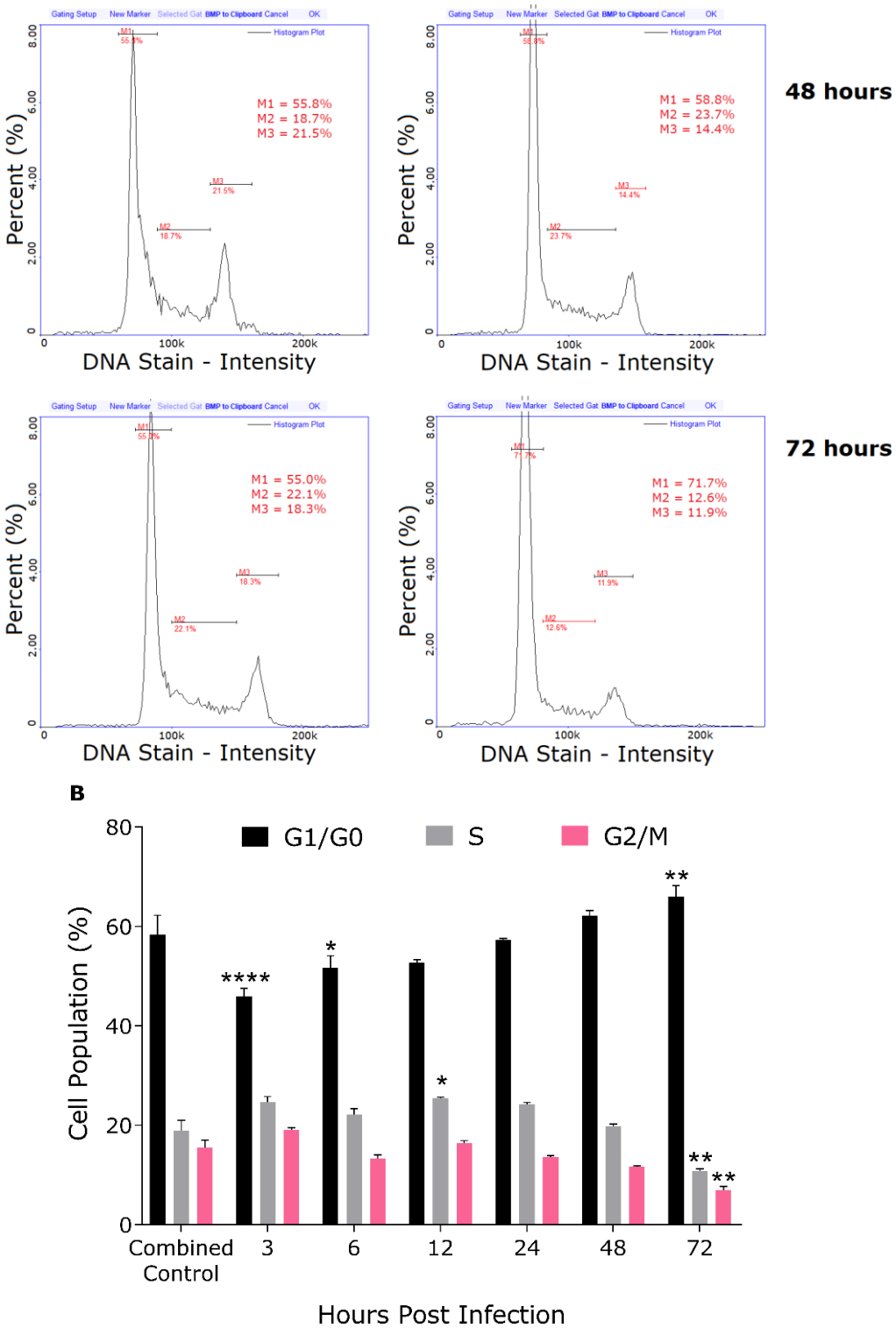


Figure 2-13 A: Histograms of uninfected hBMECs' cell cycle stage population (left) and infected hBMECs' cell cycle stage population (right) from 3 to 72 hours. B: Bar chart showing cell cycle stage population of hBMECs following *T. gondii* infection. Uninfected and infected hBMECs were stained with DAPI, and their DNA content was measured by the 2-Step cell cycle assay using the NucleoCounter® NC-3000™. The bar graph shows that, at 3 h.p.i, the percentage of cells at the G0/G1 stage dropped and then increased steadily until 72 hours. There were

more cells at S stage at 3, 6 and 12, and 24 h.p.i; while at 72 h.p.i, the cell number was significantly lower than in control ($P < 0.01$). A significant reduction in the cell population at G2/M stages occurred at 72 h.p.i. Data show the average of triplicates, while the error bars represent SEM. (*, $P < 0.05$; **, $P < 0.01$; ****, $P < 0.0001$)

2.4.5 *Tight Junction and Inflammatory Genes Expression following T. gondii Infection*

Real-time PCR Reaction Efficiency

Real-time PCR efficiency for all genes was calculated using the Pfaffl method (Pfaffl, 2001); and for each gene, three technical replicates were performed. The Pfaffl method assumes that both target and reference genes have the same amplification efficiency in test samples and calibrator samples. Careful handling and storage of samples and primers were essential for reproducible results. A perfect primer would have a primer efficiency of 2 in the Pfaffl method, where the amount of cDNA is doubled at each cycle. All primers used in this study had an efficiency ranging from 1.798 to 2.153 - as listed in **Table** 2-3.

Table 2-3 Calculation of primer pairs' efficiency using the Pfaffl method (Pfaffl 2001)

Gene	Primer Efficiency
Beta-actin	1.907
HMBS	1.954
ZO-1	1.952
Occludin	1.884
PRKCA	1.903
IL-6	1.798
P-GP	2.122
TNF-alpha	2.153

Housekeeping Genes Stability

Two housekeeping genes (beta-actin and HMBS) were analysed for their stability in both control and infected samples at 3, 6, 24, 48, and 72 h.p.i - to assess their suitability and quality for use in qPCR analyses of gene expression in hBMECs. The genes' stability was analysed using *BestKeeper*, software that determines the best-suited standards based on crossing points and the genes' primer efficiency (Pfaffl *et al*. 2004). The software is free and can be downloaded from this link http://bioinformatics.gene-quantification.info/bestkeeper.html (Accessed - 25 February 2017). The expression of the three housekeeping genes is provided (**Table** 2-4).

Table 2-4 Descriptive statistics of 2 housekeeping genes (3-72 hours)

	Beta-actin	**HMBS**
Number of Samples	22	23
Geometric Mean [CP]	16.63	26.24
Arithmetic Mean [CP]	16.66	26.26
Minimum [CP]	14.52	25.00
Maximum [CP]	18.06	27.76
Satandard Deviation [± CP]	0.84	0.97
Coefficient of Variance [% CP]	5.06	3.68

Note: CP = crossing point

Tight Junction and Inflammatory Genes Expression

Three TJ genes (Occludin, PRKCA and ZO-1) and two inflammatory cytokine genes (IL-6 and TNF-alpha) and a special protein, P-GP were selected to investigate the effect of infection on their expression. Five time points were chosen to reflect early (3 and 6 hours), middle (24 hours) and late stages (48 and 72 hours) of *T. gondii* infection. Beta-actin and hydroxymethyl-bilane synthase (HMBS) were chosen as the reference housekeeping genes, due to their stable expression in hBMECs in both

control and infected samples. Expression of genes in all samples was normalised to the expression of reference genes. A two-way ANOVA test was used to compare fold-changes in the expression of genes in both control and infected samples. **Figure** 2-14 shows the expression of all genes at 3, 6, 24, 48, and 72 h.p.i. At 3 h.p.i, all genes were down-regulated when compared to control, but only four genes (PRKCA, ZO-1, P-GP and TNF-alpha) were statistically significant ($P < 0.01$), whereas at 6 h.p.i, only TNF-alpha was up-regulated ($P < 0.0001$). At 24 h.p.i, only IL-6 was up-regulated ($P < 0.05$). At 48 hours, only IL-6 expression was significantly up-regulated ($P < 0.001$). At 72 h.p.i, only IL-6 was found to be significantly up-regulated.

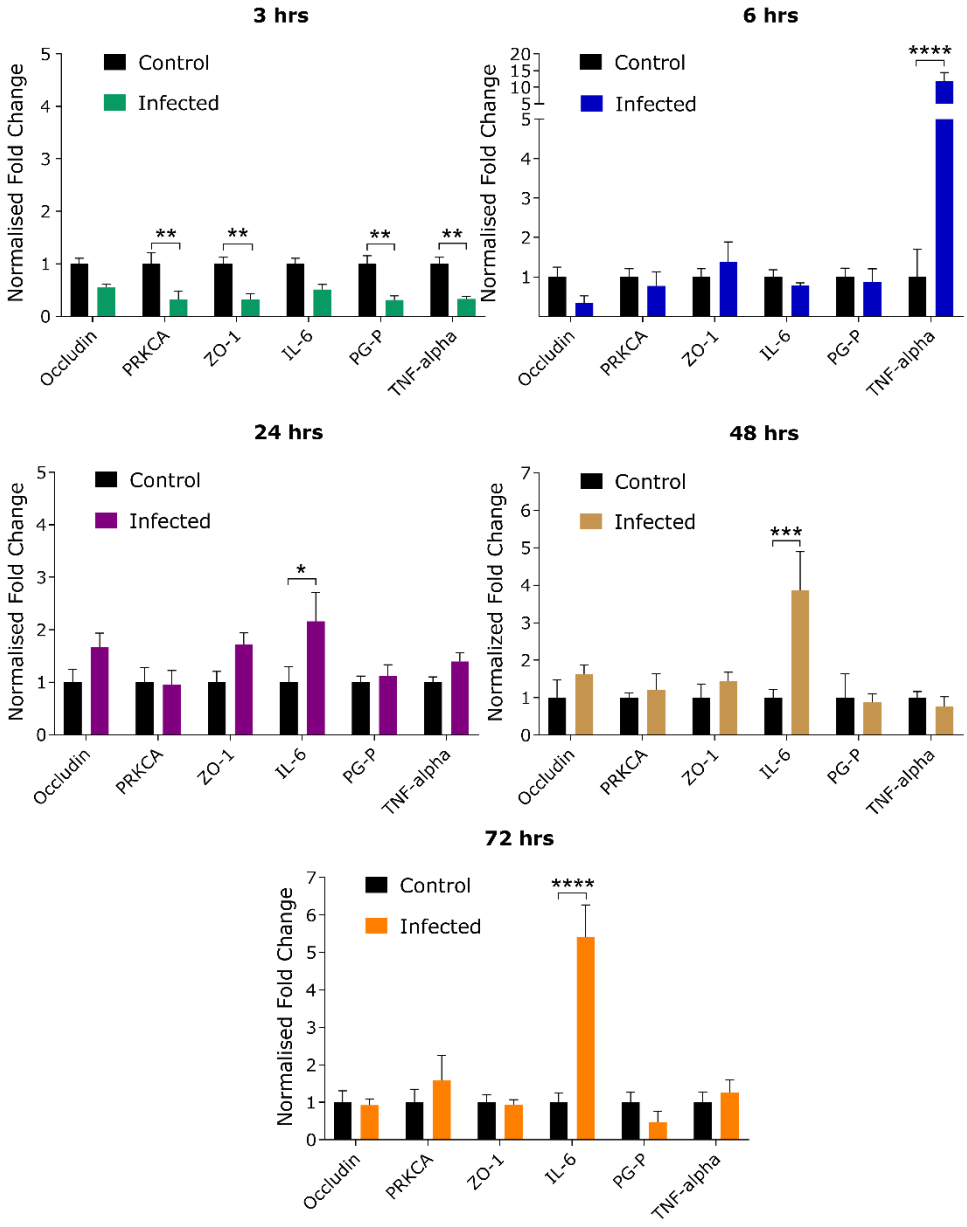


Figure 2-14 Normalised fold change of Occludin, PRKCA, ZO-1, IL-6, P-GP and TNF-alpha genes at 3, 6, 24, 48 and 72 h.p.i. Four genes (PRKCA, ZO-1, P-GP and TNF-alpha) were significantly down-regulated at 3 h.p.i, compared to control, whereas at 6 h.p.i, TNF-alpha gene was significantly up-regulated. At 24 h.p.i, all genes except PRKCA were up-regulated, but only IL-6 was found to be statistically significant. At 48 and 72 h.p.i, only IL-6 expression was statistically significant. Data were derived from three biological replicates, and the error bar represents SEM. (*, $P < 0.05$; **, $P < 0.01$; ***, $P < 0.001$; ****, $P < 0.0001$)

2.5 Discussion

In the first part of this study, temporal changes in the viability, vitality, cell cycle, mitochondrial potential and DNA fragmentation of hBMECs were cahracterised. Also, the trans-epithelial electrical resistance (TEER) and investigated alterations in hBMECs' permeability following *T. gondii* tachyzoite infection were determined. hBMECs maintained their ability to grow within the inserts for 216 hours, with culture media replenished every 3-4 days. The monolayer membrane resistance reached a plateau after 96 hours (4 days) of culture (**Figure** 2-3).

2.5.1 *Optimisation Experiments*

The number of cells seeded in the inserts was optimised, by measuring the TEER values of inserts over a period of 168 hours (**Figure** 2-2). A previous study, using the same cell type, obtained a maximal TEER value of 43.6 ± 3.89 Ωcm^2 - but after 3.19 days, and at a seeding density of 4.5×10^4 cells/cm^2 or 14,850 cells per 0.33cm^2 insert (Eigenmann *et al.*, 2013). Our experiment, together with the previous study, used inserts with 24-well plates, and a transparent PET membrane coated with collagen with 3.0µm pore size - but from different brands (Millicell vs Greiner Bio-one™). Based on results in **Figure** 2-2 and the study by Eigenmann *et al.*, (2013), it was decided that 10^4 cells/well is the most appropriate seeding density for use in subsequent experiments. Following changes to the electrode used in the TEER experiment from STX1 to STX2 electrode in the subsequent experiment, there were increases in overall peak reading of TEER values of hBMECs, in inserts seeded at 10^4 cells/well - as shown in **Figure** 2-3. The peak reading using STX1 ranged from 25-35 Ωcm^2 from 72 to 144 hours; whereas the peak reading using STX2 ranged from 63-77 Ωcm^2 during the

same period. Personal communication with the supplier did not reveal the underlying reason for this jump in TEER reading - even though the electrode was certified, and the reading was consistent across different independent experiments.

Optimisation of the number of parasites to add to cells in inserts seeded with 10^4 cells/well, was characterised by hBMEC viability monitoring using Alamar blue; monolayer integrity monitoring by TEER measurement; monolayer permeability assessment by FITC-dextran flux study and counting the number of *T. gondii* that managed to cross the hBMECs' monolayer. Multiplicity of infection (MOI) results - ranging from MOI 01 (one parasite to one cell ratio), 03, 05, and 10 - were compared. In the viability experiment, no significant changes were detected within 12 hours of infection for all groups, when compared to uninfected controls (**Figure** 2-4). Significant changes were detected at 24 h.p.i for MOI 03, 05 and 10; while at 48 and 72 h.p.i, all groups' viability were significantly affected. A significant reduction in the TEER value was also seen in all infected groups - however, the reductions were more pronounced in MOI 03, 05 and 10 (**Figure** 2-5). FITC-dextran assays revealed that less leakage was measured from all infected groups (when compared to controls) up to 24 h.p.i (**Figure** 2-6). At 48 and 72 h.p.i, FITC-dextran leakage was around the value of the control - possibly due to parasite egress, which may have damaged the hBMECs monolayer. The number of parasites that managed to cross the hBMEC monolayer was also counted for each infected group and the results presented as a percentage of a total number of parasites inoculated (**Figure** 2-7). MOI 05 was selected as the most suitable parasite infection dose for use in the subsequent experiment based on optimization experiment data because, at this ratio, consistent significant changes can be induced in hBMECs monolayer - across different types of experiment.

2.5.2 *Parasite Effects on Host Cell Viability and Vitality*

As an intracellular parasite, *T. gondii* must maintain the host cell's viability long enough for the parasite to complete its replication, and then egress and invade the neighbouring host cells. *T. gondii* maintained hBMEC viability for 24 h.p.i, whereas at 48 and 72 h.p.i there was a significant reduction in hBMECs' viability (**Figure** 2-4). The vitality of hBMECs following *T. gondii* infection was investigated using VitaBright-48™ dye and NC-3000™ Image Cytometer to measure the level of thiols in cells. A significant reduction was observed at 3, 6 and 12 and 72 h.p.i in infected cells, when compared to healthy cells (**Figure** 2-10). A cell with low vitality remained low throughout the first 48 h.p.i, then significantly increased at 72 h.p.i. A significant increase in the percentage of dead cells was measured at 72 h.p.i and, unexpectedly, at 3 h.p.i - though viability was reduced at 6 to 48 h.p.i. This suggests that *T. gondii* maintained hBMEC cell viability, at least 24 h.p.i and did not compromise cell vitality significantly until 72 h.p.i. This result concurs with findings reported in *T. gondii*-infected human foreskin fibroblast (HFF) cells, where cell viability was also maintained for 24 h.p.i (Molestina, El-guendy and Sinai, 2008).

2.5.3 *Effects on Host Cell Apoptosis*

The apoptotic response of *T. gondii*-infected host cells remains unknown, and differences reported in the literature suggest that the degree of the response varies with the host cell type, and with the infecting parasite strain. Several methods have been developed to study apoptosis in individual cells. One of the major problems in detecting apoptosis is that many features of apoptotic and necrotic processes overlap, therefore it may be necessary to use several independent assays before drawing a definitive conclusion.

The two best-characterised forms of host cell death during infection, are apoptosis and pyroptosis - both are modulated during infection. Apoptosis is one of the main types of programmed cell death, which occurs in multicellular organisms and is characterised by a series of signalling cascades that lead to a variety of morphological and biochemical changes; including membrane blebbing, cell shrinkage, alteration of membrane asymmetry and permeability, condensation of chromatin and nucleus, DNA fragmentation and formation of membrane-bound vesicles. Membrane blebbing results in the formation of apoptotic bodies that are taken up by phagocytic cells. In contrast, pyroptosis is dependent on the inflammasome activating caspase-1, leading to the release of interleukin-1 β (IL-1β) and IL-18, and membrane permeabilisation followed by cell swelling and osmotic lysis (Lamkanfi, Walle and Kanneganti, 2011).

An early apoptotic sign in hBMECs, following *T. gondii* infection, was monitored using a potential mitochondrial assay (**Figure** 2-11). Late apoptosis was monitored using a DNA fragmentation assay (**Figure** 2-12). Compared to uninfected control cells, the mitochondrial potential of hBMECs was significantly affected at 12 (41.03 ± 5.8%), 24 (40.87 ± 5.76%), 48 (44.88 ± 4.750%) and 72 (46.64 ± 3.73) h.p.i (one-way ANOVA, $P < 0.05$). The DNA fragmentation assays showed that *T. gondii* infection did not affect DNA integrity of hBMECs until 72 h.p.i. Though significance early apoptotic cells was detected at 12 to 72 h.p.i, DNA damage was not detected until 72 h.p.i. Blocking of apoptosis has been reported in *T. gondii* infected-HFF cells and macrophages, which was achieved through caspase and higher cytochrome *c* release blockade (Sinai *et al.*, 2004). These results suggest that the death of hBMECs did not occur through apoptosis, but more likely through pyroptosis.

2.5.4 *Effects on Host Cell Cycle*

The effect of *T. gondii* infection on hBMECs was monitored for 72 hours using the NC-3000™ Cell Cycle Assay (**Figure** 2-13). After 3 and 6 h.p.i, there was a significant drop in the percentage of cells at the G0/G1 stage, when compared to uninfected control cells - followed by a gradual increase up to 72 hours, where the increase was statistically significant. A significant increase in stage S cells was observed at 12 h.p.i, but at 72 h.p.i there was a significant decrease. There were minor changes to S and G2/M stages during infection until 72 h.p.i, when there was a significant decrease. This suggests that it took at least 6 h.p.i for *T. gondii* to manipulate hBMECs to remain or to revert to their G0/G1 stage. In contrast, in HFF cells *T. gondii* infection was reported to promote cells into S phase after 24 h.p.i (Molestina, El-guendy and Sinai, 2008).

2.5.5 *Effects on Host Cell Junction and Inflammatory Gene Expression*

The effects of *T. gondii* infection on host cell functions were investigated using a FITC-dextran assay (**Figure** 2-8), TEER (**Figure** 2-9) and RT-PCR (**Figure** 2-14). The flux of FITC-dextran across hBMEC monolayers (indicative of increased paracellular permeability) was low when monolayers were apically treated with *T. gondii* at MOI 5 from 3 hours to 24 hours (**Figure** 2-8). However, at 48 and 72 hours, more FITC-dextran leakage was measured when compared to control cell cultures. This may be due to egress of parasites from cells, destroying the monolayer barrier. No differences were statistically significant. Briceño *et al.*, (2016) reported that, in a Caco-2 cell line, *T. gondii* infection significantly decreased cell permeability after 24 h.p.i using FITC-dextran flux assay, even though

confocal microscopy revealed the uptake of FITC-dextran by endocytosis in infected cells to be lower than in uninfected cells. TEER values were also significantly lower in *T. gondii*-infected Caco-2 cells than in non-infected cells, at 20 and 24 h.p.i (Briceño *et al.*, 2016). Significant changes in hBMECs' monolayer integrity were detected after 24 h.p.i (**Figure** 2-9). This suggests that while *T. gondii* infection reduces hBMEC membrane integrity, hBMEC membrane permeability was not significantly affected. This could be due to an increase in hBMEC size following *T. gondii* infection. As the parasites enter the cell and form a parasitophorous vacuole, cell size/volume will increase which then limits FITC-dextran leakage through the TJs. TEER reflects the ionic conductance of the paracellular pathway in the cell monolayer, whereas the flux of non-electrolyte tracers indicates the paracellular water flow - as well as the pore size of the TJs (Srinivasan *et al.*, 2015). Our results suggest that *T. gondii* infection reduces ionic conductance and limits paracellular water flow through the hBMEC monolayer.

Brain endothelial cells challenged with *T. gondii*, displayed changes in TJ and cytokine gene expression - consistent with endothelial cell stress and compromised membrane integrity. *T. gondii* infection altered the expression of Occludin, PRCKA, ZO-1, IL-6, P-GP and TNF-alpha genes at 3 h.p.i where four of these genes (PRKCA, ZO-1, P-GP and TNF-alpha) were significantly upregulated (**Figure** 2-14). At 6 h.p.i, only TNF-alpha was significantly up-regulated in infected cells. At 24, 48 and 72 h.p.i, only expression of IL-6 was significantly elevated (**Figure** 2-14). The gene expression study and *T. gondii* counting (**Figure** 2-7) results suggest that it is unlikely that *T. gondii* tachyzoites cross hBMECs monolayer through modulating the expression of TJ genes. Interestingly, in the Caco-2 cell line, ZO-1 and Occludin expression were decreased significantly 24 hours after *T. gondii* infection (Briceño *et al.*, 2016).

In mice, IL-6 plays a protective role during early (~7 days) *T. gondii* infection (Jebbari *et al.*, 1998), as mice lacking IL-6 production were susceptible to severe encephalitis (Drogemuller *et al.*, 2008). In humans, IL-6 also plays an important role in the host response against *T. gondii* invasion, where it promotes NK cell activation and production of IFN-gamma (Gigley, 2016; Sher, Tosh and Jankovic, 2017). IL-6 up-regulation was reported in *T. gondii* infected human retinal pigment epithelial (HRPE) cells (Nagineni, Detrick and Hooks, 2000).

P-GP is a host membrane-bound efflux pump that actively transports host-derived cholesterol to the intracellular parasite and is important for parasite replication (Bottova *et al.*, 2009). P-GP gene was significantly down-regulated only at 3 h.p.i but not at other time points. Inhibition of host P-GP affects parasite replication but not parasite survival (Bottova *et al.*, 2009). The reason could be due to *T. gondii* itself encoding a similar protein, to P-GP protein substituting the need for host protein (Bottova *et al.*, 2010). Hence, these data concur with other findings that host P-GP protein is essential but not indispensable for parasite survival.

2.5.6 *Conclusion*

We have characterised *T. gondii* infection in hBMECs and revealed new insights into the underlying mechanisms involved in *T. gondii* penetration of the BBB. During the early stages of infection, *T. gondii* parasites-maintained host cells' viability, suppressed cell apoptosis by halting cells at the G0/G1 stage, induced up-regulation of the IL-6 gene, lowered the permeability of infected cells when compared to non-infected cells. Further understanding of the mechanisms that regulate these processes and underlie the ability of this pathogen to subvert normal cellular functions at this important biological interface may lead to the discovery of key factors/pathways involved in the neuro-pathogenesis of *T. gondii* infection - and may be targeted to design strategies to limit brain pathologies.

Chapter 3 Integrated Genome-wide mRNA and miRNA Expression Profiling of *Toxoplasma gondii*-Infected HBME Cells

3.1 Abstract

Cells infected with the intracellular protozoan parasite *T. gondii* undergo up-regulation of transcriptomic expression involving pro-inflammatory cytokines, cell cycle stoppage and protection from apoptosis. To examine the molecular basis of these and other changes, gene expression profiles of hBMECs infected with *Toxoplasma* were studied using next-generation sequencing (NGS) RNA sequencing (RNA-Seq) and small RNA sequencing followed by microarray and qRT-PCR analysis at 6, 24 and 48 hours post infection (h.p.i) representing early, middle and late stage of infection. The majority of genes were differentially expressed at 6 and 48 h.p.i while the least amount of changes occurs at 24 h.p.i. In general, results obtained confirmed previous findings that *T. gondii* infection halts cell cycle progression in infected cells and displays gene modulation seen in cancer cells. Unsurprisingly, the majority of pathways up-regulated were related to ATP synthesis and metabolism. Among all pathways affected by mRNAs and miRNAs, ATF4 activation, TP53 regulation, selenoamino acid metabolism and selenocysteine synthesis were selected as key pathways. This study also identified the increased expression of miR-7 family and miR-17-92 family members plays an important role in determining the fate of host cells in *T. gondii* infection. The study identified ribosomal proteins L36 and S12 as key players in *T. gondii* pathogenesis, with good potential as vaccine candidates. The results reveal several previously unidentified changes on the host cell

and contribute to the foundations of knowledge of the host-pathogen interaction.

3.2 Introduction

The previous chapter showed that at 6 and 48 h.p.i, there were significant biochemical and cellular changes in the host cells following *T. gondii* RH infection. These phenotypic changes must have been underpinned by molecular mechanisms driven by host cell response to the infection. Therefore, in this chapter, these changes were explored at the molecular level focusing on transcriptomic aspects, specifically mRNA and miRNA expression. While there have been several studies on mRNA transcriptomic changes in human cells infected with *T. gondii* (Chaussabel *et al.*, 2003; Radke *et al.*, 2005; Ander *et al.*, 2018) and miRNA transcriptomic changes in human cells infected with *T. gondii* (Zeiner *et al.*, 2010; Pope and Lässer, 2013; Xiao *et al.*, 2014), none of these studies have been conducted on hBMECs, which form a fundamental component of the BBB.

Herein, mRNA and miRNA transcriptomes produced by RNA sequencing (RNA-Seq) of hBMECs infected with *T. gondii* RH parasites at 6, 24 and 48 hours post infection (h.p.i) were characterised. Two hypotheses were tested:

Hypothesis 1: hBMECs infected with *T. gondii* RH exhibit a mRNA-miRNA expression profile that is different from that exhibited by healthy, uninfected cells.

Hypothesis 2: studying global gene expression during the time course of infection can identify specific biomarkers associated with *T. gondii* infection.

To test these inter-related hypotheses, next-generation sequencing (NGS) technology was used, validated with microarray technology and qRT-PCR. mRNA and miRNA sequencing were performed to capture the global expression profiles in addition to identifying novel genes, rare and lowly expressed genes, plus to facilitate the potential discovery of non-coding RNAs, which cannot be identified by using microarray technology. In addition to relative expression, absolute gene expression can also be obtained from NGS data, which is not available from microarray data. Using this integrated transcriptomics analysis based on different technologies allowed determination of whether there is a common transcriptomic signature, characteristic of *T. gondii* infection in hBMECs.

The results obtained from this study revealed new insight into genes that are differentially expressed in hBMECs in response to infection with *T. gondii* RH strain. Integrated mRNA/miRNA expression profiling and pathway analysis show multiple signalling pathways including, ATF4 activation, TP53 regulation, selenoamino acid metabolism and selenocysteine synthesis, as key pathways, potentially regulated during *T. gondii* infection. Among key up-regulated pathways are those pathways related to ATP synthesis and metabolism. Increased expression of miR-7 family and miR-17-92 family members, important miRNAs in determining the fate of host cells in *T. gondii* infection were identified from this study. In addition, our data suggested that ribosomal protein L36 and S12 are key players in *T. gondii* pathogenesis making them as possible vaccine candidates. This comprehensive characterisation of mRNA and miRNA transcriptomes in hBMECs provides insights on the regulation of mRNA and miRNA and creates valuable resources including gene variation and regulation in *T. gondii* infection, which are potentially useful for future mechanistic studies. Also, *T. gondii* infection-specific transcriptomic changes can be used as diagnostic and prognostic

biomarkers. Overall, the results reveal several previously unidentified changes on the host cell and contribute to the foundations of knowledge of the host-pathogen interaction.

3.3 Materials and Methods

3.3.1 *Cell Growth and Maintenance*

HBMECs were grown as described previously in section **2.32.3** (Chapter 2). Two biological replicates of control and *T. gondii* RH-infected samples at 6, 24 and 48 h.p.i were prepared for mRNA and miRNA sequencing experiments.

3.3.2 *Extracting total RNA and miRNA using Qiagen RNeasy Kit*

Total RNA was extracted using Qiagen RNeasy Plus Mini Kit (Qiagen, Hilden, Germany) and miRNA was extracted using Qiagen miRNeasy Mini Kit (Qiagen, Hilden, Germany). The extraction procedures for both kits were the same as the differences were in the spin column design and the buffer used in the first washing step. The protocols for extraction and total RNA quality analysis with Nanodrop™ 8000 spectrophotometer was as described previously in section **2.3.17** and **2.3.18** (Chapter 2). Eluted RNA was separated into 3 different tubes to avoid repeated thawing and freesing of the sample which could affect the quality of the RNA with two tubes for quality control analysis with Nanodrop 1000 (2 µL × 2 = 4 µL) and Illumina® Agilent 2100 Bioanalyser (5 µL × 2 = 10 µL) while the third one, for sequencing, is stored in -80°C. Samples with the absorbance ratio value (A260/A280) of 1.8 to 2.0 were considered acceptable for further analysis

with Illumina® Agilent® 2100 Bioanalyzer for mRNA and miRNA sequencing and cDNA conversion for qPCR analysis.

3.3.3 *RNA Quality Analysis: Illumina® Agilent® 2100 Bioanalyzer*

Agilent® RNA 6000 Nano kit (Agilent Technologies LDA UK Limited, Cheshire, UK) was used together with Agilent® 2100 Bioanalyser (Agilent Technologies LDA UK Limited, Cheshire, UK) to conduct quality and quantity analysis to the extracted total RNA samples to make sure the samples are of the highest quality and quantity for transcriptome sequencing. The Illumina HiSeq 4000 sequencer (Illumina EMEA, Cambridge, UK) requires the sample to have spectrophotometer absorbance 1.8 to 2.1, and RNA integrity number (RIN) 9 to 10 plus the concentration must be around ~200-250 ng/µl per sample. Analysis was performed exactly as manufacturer instructions which can be obtained at the following site https://www.agilent.com/cs/library/usermanuals/Public/G2938-90034_RNA6000Nano_KG.pdf (Accessed – 10 March 2017).

Successful run would contain three peaks where one peak represents marker peak while the other two are 18S and 28S ribosomal peaks as shown in **Figure** 3-1. The absence of one or both ribosomal peaks indicates poor sample preparation or poor sample pipetting technique.

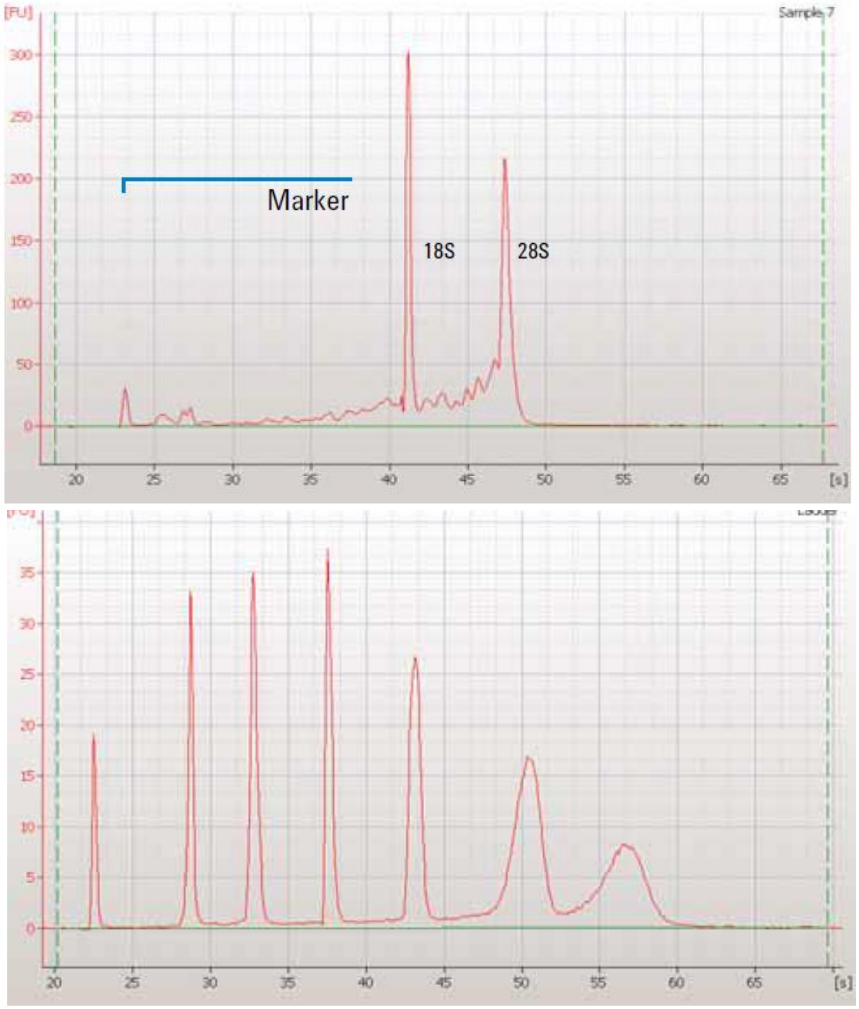


Figure 3-1 An electropherogram showing a successful sample total RNA run peaks complete with ladder electropherogram. A complete and well resolved RNA 6000 Nano ladder electropherogram, indicating a successful chip run, should resemble the bottom figure. It must feature one marker peak and 6 RNA peaks where all seven peaks are well resolved.

Messenger RNA sequencing was performed by Oxford Genomics Centre, The Wellcome Trust Centre for Human Genetics, University of Oxford, United Kingdom using Illumina HiSeq 4000 (Illumina EMEA, Cambridge, UK). Oxford Genomics Centre required >3 µg of total RNA containing mRNA prepared at ~200-250 ng/µl concentration in 15 µL of ultrapure water. The 260/280 OD reading of NanoDrop 8000 must be ~2 while quality analysis with Agilent 2100 Bioanalyser with RNA 6000 Nano kit

must have RIN number of 9-10. At each time points (6, 24, and 48 h.p.i), two controls and two infected samples were sent for mRNA sequencing. Bioanalyser 2100 total RNA quality reports of samples send for mRNA and microarray sequencing are available in **Appendix** 3-1 and **Appendix** 3-2 respectively.

3.3.4 *Messenger RNA: Library Preparation and Sequencing*

Messenger RNA libraries were prepared using Illumina's TruSeq Stranded mRNA HT Kit [RS-122-2103] (Illumina EMEA, Cambridge, UK). The full detail library preparation procedure can be accessed at https://support.illumina.com/content/dam/illumina-support/documents/documentation/chemistry_documentation/samplepreps_truseq/truseqstrandedmrna/truseq-stranded-mrna-sample-prep-guide-15031047-e.pdf (Accessed – 12 June 2017)**.** Briefly, 1 ug of samples were purified and fragmented followed by first and second strand cDNA synthesis. Then, 3' ends of the generated strands were ligated with adapters and sequencing libraries were prepared through PCR enrichment step using the custom primers (25 µM each) as follows:

- Multiplex PCR primer 1.0

5'-AATGATACGGCGACCACCGAGATCTACACTCTTTCCCTACACGACGCTCTTCCGATCT-3'

- Index primer

5'-CAAGCAGAAGACGGCATACGAGAT[INDEX]CAGTGACTGGAGTTCAGACGTGTGCTCTTCCGATCT-3'

Barcoding indices used the eight bases tags developed by WTCHG (Lamble *et al.*, 2013). Amplified libraries were analysed for size distribution using the Agilent Tapestation 2200 D1000 (Agilent Technologies LDA UK

Limited, Cheshire, UK). Libraries were quantified using Invitrogen™ Quant-iT™ PicoGreen™ Assay (Thermo Fisher Scientific, Leicestershire, UK) and relative volumes were pooled accordingly.

3.3.5 *Messenger RNA: Sequence Data and Differential Expression Analysis*

Sequencing was performed as 150 bp paired-end reads on Illumina's HiSeq4000 platform according to Illumina specifications. Raw sequences in FASTQ format were aligned to the human reference genome (GRCh37.EBVB95-8wt.ERCC) and the *T. gondii* reference genome ME49 (http://toxodb.org/common/downloads/release-13.0/TgondiiME49/fasta/data/) (Accessed – 15 December 2017) separately using HiSat2 program (Kim, Langmead and Salzberg, 2015). Reads mapping to each part of the genome were recorded in a sequence alignment map or SAM files. The SAMtools program (Li *et al.*, 2009) was used to convert SAM files into binary alignment/maps (BAM) files for storing alignment information. HTSeq-count (Anders, Pyl and Huber, 2015) was used to generate count files from BAM files for R Studio (R Studio, Boston, USA) with Bioconductor data analysis (Gentleman *et al.*, 2004; Huber *et al.*, 2015).

Appendix 3-3 represents the scripts used for data analysis by R Studio software (R Studio, Boston, USA) with Bioconductor packages (Gentleman *et al.*, 2004; Huber *et al.*, 2015) and the settings used for each process. In short, all required modules/packages (DESeq2, gplots, RColorBrewer) were downloaded and loaded into workspace terminal in R Studio. Then, our experimental design file (pdata.txt) was created to assign each mapped file to the specific treatment group (control or infected) and

time point (6, 24 or 48 hours). Each group was assigned to specific colour for drawing plots.

Next, *DESeqDataSetFromHTSeqCount* function from DESeq2 package (Love, Huber and Anders, 2014) was used to read counts before performing data normalisation based on the library size and scaling factor based on the median ratio. Following normalisation, data were subjected to quality control analysis through bar chart plots, PCA analysis, and sample correlation analysis. Differential expression was calculated through the use of negative binomial generalised linear models; the estimates of dispersion and logarithmic fold changes incorporate data-driven prior distributions (Love, Huber and Anders, 2014).

The control vs infected groups' comparison from mapping to human and *T. gondii* genome were generated separately. Comparison groups analysed were; control 6 hours *vs* infected 6 hours (Ctrl 6hrs *vs* Inf 6hrs), control 24 hours *vs* infected 24 hours (Ctrl 24 hrs *vs* Inf 24 hrs), control 48 hours *vs* infected 48 hours (Ctrl 48 hrs *vs* Inf 48 hrs). The cut-offs values were genes with $\log_2$ FC more than 1 (up-regulated) and less than -1 (down-regulated) and with adjusted *P*-values less than 0.01. Significant hits were highlighted through plotting heatmaps, volcano plots and listed in tables. A filtered gene list was considered for gene ontology analysis. Then PANTHER and Reactome web-based tools were used to determine the differentially expressed genes (DEGs) gene ontology and affected pathways.

3.3.6 *Microarray Experiment and Data Analysis*

Biological triplicates of control and *T. gondii* RH-infected samples at 6, 24, and 48 hours were prepared, extracted and their integrity was checked as previously described. All subsequent sample handling, labelling and microarray (GeneChip™ Human Gene 2.1 ST, Affymetrix) processing was performed at the Nottingham Arabidopsis Stock Centre (NASC). The RNA concentration and quality were assessed using the Agilent 2100 Bioanalyzer and the RNA 600 Nano Kit. Samples with a minimum RNA concentration of 100 ng/µL and RNA Integrity Number (RIN) ≥ 9 were used for gene expression analysis. Single-stranded complimentary DNA was prepared from 200 ng of total RNA as per the GeneChip™ WT PLUS Reagent Kit (Thermo Fisher Scientific, Leicestershire, USA). Total RNA was first converted to cDNA, followed by *in vivo* transcription to make cRNA. Single-stranded cDNA was synthesised, end labelled and hybridised for 16 h at 45°C to GeneChip™ Human Gene 2.1 ST arrays. All steps were performed by a GeneAtlas™ Personal Microarray system (Affymetrix UK, High Wycombe, UK).

The scripts used for data analysis by R Studio software (R Studio Inc, Boston, USA) and the settings used for each process are available in **Appendix** 3-4. Briefly, a data file, called 'pdata' was created to link each microarray data file with '.ga.cel' ending to one of the six experimental groups (Control 6 hours, Control 24 hours, Control 48 hours, Infected 6 hours, Infected 24 hours, Infected 48 hours). The libraries of modules (oligo, gplots, RColorBrewer, pvclust, colourspace, limma, gene filter, hugene21sttranscriptcluster.db) needed for quality control, differential genes expression and transcript cluster ID annotation were downloaded and uploaded into the workspace terminal. Next, Affymetrix microarray data files were uploaded together with 'pdata' file. Quality control analysis and

normalisation were performed using the robust multi-array average (RMA), which is the common normalisation method for microarray study (Irizarry *et al.*, 2003, 2012). RMA normalisation is sensitive for low expression values, consistent fold-change estimates, and excellent background adjustment compared to MAS 5.0 and dChip normalisation methods (Irizarry *et al.*, 2003, 2012). DEGs were considered significant if the adjusted *P*-value was < 0.05 and $\log_2$ FC ≥ 1 (up-regulated) or ≤ -1 (down-regulated). Contrast was made between control versus infected samples at each time point (Ctrl 6 hrs vs Inf 6 hrs, Ctrl 24 hrs *vs* Inf 24 hrs, Ctrl 48 hrs *vs* Inf 48 hrs). A filtered gene list was considered for gene ontology analysis.

3.3.7 *Gene Ontology (GO) with Protein Analysis Through Evolutionary Relationships Classification System (PANTHER) Analysis*

The interactions among genes expressed and between unexpressed genes and other genes can be elucidated using a computer or *in the silico* analysis which is defined as the process of elucidating associated pathways, molecular function, biological process, cellular components and protein products of a gene (Ashburner *et al.*, 2000). The bioinformatics database used to analyse gene identity and gene interaction is Protein Analysis Through Evolutionary Relationships Classification System (PANTHER) (http://www.pantherdb.org/). It is a unique resource that classifies genes by their functions, using published scientific experimental evidence and evolutionary relationships to predict function even in the absence of direct experimental evidence and is a part of the Gene Ontology Reference Genome Project (http://www.geneontology.org/).

PANTHER provides tools for gene expression analysis for data interpretation (Mi *et al.*, 2013, 2017). Multiple gene lists can be mapped to PANTHER molecular function, biological process and cellular component categories as well as to biological pathways. The gene expression data interpretation was conducted by comparing genes in a filtered list and statistically comparing the list to a reference list to look for under and over-represented functional categories. The detailed step by step method and the statistical test employed, were based on a published protocol (Mi *et al.*, 2013, 2017). In short, first, the filtered list of up-regulated or down-regulated genes with their GenBank symbols was entered or pasted into the designated workspace on the PANTHER homepage. Secondly, '*Homo sapiens*' was selected as the reference organism before selecting 'functional classification viewed in pie chart' option. The results were then downloaded as text files for analysis. For further analysis, the first and second steps were repeated then 'statistical overrepresentation test' option (PANTHER Overrepresentation Test Released 2017-12-05) was selected and the checkbox for 'use default settings' was ticked. Following that, from 'Annotation Data Set' drop-down menu (PANTHER annotation database version 13.1 released 2018-02-03), 'PANTHER GO-Slim Biological Process', 'PANTHER GO-Slim Molecular Function', and 'PANTHER GO-Slim Cellular Component' options were selected one by one, together with the 'Fisher's Exact with FDR multiple test correction' option from 'Test Type' options. Any functional annotations category with FDR < 0.05 was selected as significantly enriched and reported in this thesis.

3.3.8 *Reactome Pathway Analysis*

Pathway analysis was carried out at Reactome (https://reactome.org/) an open-source, curated and peer-reviewed pathway database. It provides intuitive bioinformatics tools for the visualisation, interpretation and analysis of pathway knowledge for research, genome analysis, modelling, systems biology and education. The Reactome Analysis Tool used (https://reactome.org/PathwayBrowser/#TOOL=AT) was the version v65 released on June 13, 2018. A detailed step by step protocol can be accessed at https://reactome.org/user/guide/analysis (Accessed - 14 June 2018).

The results consisted of several parameters, but the focus of this analysis was on four parameters. The first one was the pathway name and the second one was 'Entities found' where the matched submitted identifiers and their mapping to molecules in the pathway were displayed. The third parameter was the overlaid (average) $\log_2$ FC values which visualise the relative expression levels of a pathway. The last one was 'Entities FDR' which represent the over-representation analysis statistical (hypergeometric distribution) test that determines whether certain Reactome pathways are over-represented (enriched) in the submitted data. This test produces a probability score, which is corrected for false discovery rate (FDR) using the Benjamani-Hochberg method. Pathways with FDR < 0.01 were considered as significantly enriched.

3.3.9 *ToxoDB.org Gene Analysis*

Cut-off criteria from mapping to human and *T. gondii* reference genomes were set to have a baseMean value of ≥ 2000, adjusted *P*-value < 0.01 and $\log_2$ FC ≥ 5. Filtered transcript IDs were subjected to gene identity search, gene ontology and pathway analysis at ToxoDB.org (Gajria *et al.*, 2008). Briefly, at the 'My Strategies' tab, transcript IDs were entered into 'Gene ID input set' box. Then on the 'Analyze Results' tab, the Gene Ontology Enrichment tool was selected. Parameters set were as follows; *Organism: Toxoplasma gondii ME 49, Ontology: Cellular Component or Molecular Function or Biological Process, Evidence: Computed and Curated, Limit to GO Slim terms: No, P-Value Cutoff (0 - 1.0): 0.05.* Then, the 'Submit' button was clicked to complete the analysis. Similarly, on the 'Analyze Results' tab, 'Metabolic Pathway Enrichment' tool was selected, and the setting used were as follows; *Organism: Toxoplasma gondii ME 49, and Pathway Source: MetaCyc and KEGG, P-Value Cutoff: 0.05.* 'Submit' button was then clicked to complete the analysis. Pathway/cellular component/molecular function/biological process with more than three miRNAs were reported and discussed in this thesis.

3.3.10 *Small RNA: Library Preparation and Sequencing*

Small RNA sequencing was performed by DeepSeq, Centre for Genetics and Genomics, The University of Nottingham, United Kingdom using the NextSeq 500 platform (Illumina EMEA, Cambridge, UK). The quality of samples required by DeepSeq was the same as per Oxford Genomics Centre. Small RNA libraries were prepared using NEBnext Multiplex Small RNA Library Prep Set for Illumina [NEB, E7300S] (New England Biolabs UK Ltd. Herts, UK). Briefly, 1 ug of total RNA was used for 3' adapter ligation. 5' RNA

adapter was ligated following primer hybridisation to the 3' adapter. First strand synthesis was done to generate cDNA for adapter ligated sRNA. Sequencing libraries were prepared through PCR amplification of cDNA and subsequent purification using polyacrylamide gel electrophoresis. Libraries were quantified using Invitrogen™ Qubit™ dsDNA HS Assay Kit [Q32851] (Thermo Fisher Scientific. Leicestershire, UK) with Qubit 4 Fluorometer (Thermo Fisher Scientific. Leicestershire, UK) and KAPA Library Quantification Kits for next-generation sequencing qPCR [KK4824] (Kapa Biosystems, MA, USA).

3.3.11 *Small RNA: Sequence Data Analysis*

Small RNA libraries were then sequenced with the addition of 20% PhiX Control v3 library [FC-110-3001] (Illumina EMEA, Cambridge, UK), using 1 x 75 bp Illumina SBS chemistry NextSeq 500/550 High-Output v2 Kit [FC-404-2002] (Illumina EMEA, Cambridge, UK) on the NextSeq 500 platform. Small RNA data were analysed using a standalone web-based bioinformatic tool miRMaster (Fehlmann *et al.*, 2017) available at https://ccb-compute.cs.uni-saarland.de/mirmaster (Accessed - 5 May 2018). miRMaster use Bowtie for alignment to the human genome (hg38) and report mapping of reads to human miRbase (version 21). Since miRNA sequences are short, they are prone to false negative results hence conservative settings were selected for minimising the false negative effect.

There are six categories under 'Parameter Configuration' page which are 'Preprocessing', 'Genome Mapping', 'Precursor Excision', 'Filtering' and 'Merging and Global Signature Filtering' and 'Quantification'. NEB small RNA 3p adapter was selected at 'Preprocessing' category, and the minimum read length was set at 16 while other options under 'Preprocessing' category were

as in default setting. Under 'Filtering' category, the minimum length of potential miRNA was set at 16. For all other options in other categories, default settings were chosen for this analysis. The default settings are available at **Appendix** 3-5.

Meanwhile, mapping of small RNA sequencing data to *T. gondii* ME 49 reference genome was conducted using EuPathDB Galaxy Site, a free, interactive, web-based platform for large-scale data analysis (https://eupathdb.org/eupathdb/). Data quality control was analysed using FastQC Galaxy Tool Version 0.11.3 (Andrews, 2010) followed by file format conversion from fastq to fastqsanger quality format using FASTQ Groomer Galaxy Tool Version 1.0.4 (Blankenberg *et al.*, 2010). Then, adapter (Illumina's single end adapter – AGATCGGAAGAGCACACGTCTGAACTCC AGTCAC) and low-quality read trimming (Phred score < 20) was performed using Trim Galore! (Galaxy Tool Version CUTADAPT: 1.2; TRIM_GALORE: trim_galore_v0.3.3; FASTQC: default) Adaptive quality and adapter trimmer. Following that, Bowtie2 Galaxy Tool Version 2.1.0 (Langmead and Salzberg, 2012) and SAMTOOLS Galaxy Tool Version 1.2 (Li *et al.*, 2009) were employed for short-read alignment against TOXODB-29_TgondiiME49_Genome as the reference genome and file format processing respectively. Cufflinks Galaxy Tool Version 2.1.1 and Cuffdiff Galaxy Tool Version 2.1.1 were used to assemble transcripts, estimates their abundances (FPKM), tests for differential expression and regulation and find significant changes in transcript expression in RNA-Seq samples (Trapnell *et al.*, 2010). List of significantly differentially expressed miRNAs (*P*-value < 0.01 and $\log_2$ FC ≥ 1 or ≤ -1) was further analysed Diana Tools – mirPath v.3.

3.3.12 *Diana Tools – mirPath v.3*

DIANA-mirPath (http://snf-515788.vm.okeanos.grnet.gr/) is a miRNA pathway analysis, web-based tool with advanced statistics and advanced pipeline integration (Vlachos *et al.*, 2015). DIANA-mirPath can compile predicted miRNA targets utilising the DIANA-microT-CDS algorithm or even experimentally validated miRNA interactions derived from DIANA-TarBase. These compilations of interactions can be subsequently combined with sophisticated merging and meta-analysis algorithms. Following a search, the miRNA-target genes' interactions were presented with associated pathways, the number of miRNA and the number of target genes.

Four methods were offered for statistical analysis which are: priori-genes union, priori-genes intersection, posterior-pathways/categories union, and posteriori-pathways/categories intersection methods (Backes *et al.*, 2017; Vlachos and Hatzigeorgiou, 2017). The priori-genes union method compiles all target genes targeted by *at least one miRNA* as a union set then the set is used for statistical pathway enrichment analysis. Meanwhile, priori-genes intersection only compiles genes targeted by a defined number of miRNAs into a set, an intersection set, and the set is then used for statistical pathway enrichment analysis. For example, if the number defined is 5 microRNAs then only the genes targeted by a minimum of five miRNAs will be included in the set.

The posteriori method – pathways/categories union identifies all significantly targeted pathways targeted by at least one miRNA then performs enrichment analysis followed by calculation of the significance levels (*P*-value) between each miRNA and every pathway. Finally, the calculated *P*-values are merged using Fisher's meta-analysis method. The resultant *P*-value signifies the probability of a pathway being targeted by at

least one of the selected miRNAs. In contrast, posteriori method – pathways/categories intersection identifies only pathways significantly targeted by all selected microRNAs. In this study, consensus pathways from priori method – genes intersection (minimum three miRNAs per pathway) and posteriori method – pathway union were included in the results.

DIANA-miRPath v3.0 offers Fisher's Exact test with or without False Discovery Rate (FDR), EASE score and unbiased empirical distributions as statistical test options (Backes *et al.*, 2017; Vlachos and Hatzigeorgiou, 2017). Its meta-analysis algorithm enables the identification of pathways controlled by multiple miRNAs while promoting pathways which are targeted concurrently by multiple miRNAs. In this study, Fisher's Exact test with FDR was selected for all analysis.

3.3.13 *Converting RNA to cDNA*

RNA was converted to cDNA using Invitrogen™ SuperScript™ III First-Strand Synthesis System for RT-PCR (Thermo Fisher Scientific, Leicestershire, UK). The system is optimised to synthesise first-strand cDNA from purified poly(A)+ or total RNA. RNA targets from 100 bp to 12 kb can be detected with this system. The amount of starting material can vary from 1 pg – 5 µg of total RNA. SuperScript™ III Reverse Transcriptase enzyme is a version of M-MLV RT that has been engineered to reduce RNase H activity and provide increased thermal stability. The enzyme is used to synthesise cDNA at a temperature range of 42 – 55°C, providing increased specificity, higher yields of cDNA, and more full-length product than other reverse transcriptases. Because SuperScript™ III RT is not significantly inhibited by ribosomal and transfer RNA, it may be used to synthesise the first-strand

cDNA from a total RNA preparation. cDNA synthesis was performed using either total RNA or poly(A)+-selected RNA, primed with random primers.

After reverse transcription, it is common not to quantify the resulting cDNA by UV absorbance. Instead, the cDNA is assigned a concentration unit relative to the original concentration of RNA in the RT reaction. For example, if one loaded 10 µg (10,000 ng) of RNA into a 100 µL RT reaction, the designated concentration of the resulting cDNA would be 100 ng/µL (10,000 ng / 100 µL = 100 ng/µL); which means 1 µL of sample contains the cDNA generated from 100 ng of RNA. In this experiment, 60 ng of total RNA was used with 30 µL reaction mixture for cDNA conversion resulting in an estimated 2 ng/µL cDNA concentration (60/30).

The following procedure is based on Invitrogen's protocol. The following RNA/primer mixture was prepared for each tube: total RNA 60 ng (maximum 11 µL), random hexamers (50 ng/µL) 1 µL, 10 mM dNTP mix 1 µL, nuclease-free water to 10 µL. Samples were incubated at 65°C for 5 minutes and then on ice for at least one minute. The reaction master mixture was prepared for each reaction 2 µL 10X RT buffer, 4 µL 25 mM $MgCl_2$, 2 µL 0.1 M DTT, 1 µL RNAaseOUT and 1 µL SuperScript III RT (200 U/µL). The reaction mixture was added to the RNA/primer mixture, mixed briefly, and then placed at 25°C for 10 minutes. Then, tubes were incubated 50°C for 50 minutes, heat inactivated at 85°C for 10 minutes and then chill on ice for 2 minutes. The resulting cDNA was stored at -20°C until use for real-time PCR.

3.3.14 *Real-time PCR using Roche LightCycler® 480 II and SYBR Green Mastermix*

Real-time PCR *T. gondii* detection was based on the method published by Edvinsson *et al.*, (2006). They demonstrated that targeting the *Toxoplasma* 529 bp repeat element resulted in better accuracy and sensitivity in detecting *T. gondii* DNA compared to targeting the B1 gene. The amount of cDNA in a reaction was set to be at 3 ng of converted RNA per 20 µL of reaction. PCR was performed using Roche LightCycler® 480 Instrument II (Roche Diagnostics Ltd, Burgers Hill, UK) and SYBR green mastermix SensiFAST™ Probe No-ROX Kit (Bioline Reagents Limited, London, UK). The mixtures in a reaction were as follows; 10 µL SYBR Green Mix, 2 µL cDNA, 1 µL reverse primer (10 µM), 1 µL forward primer (10 µM) and 6 µL RNase/DNase free water. The program steps are as follows; hot start incubation step (1 cycle) 95°C for 5 minutes followed by amplification steps (45 cycles) 95°C for 15 seconds, then 60°C for 30 seconds and then 72°C for 30 seconds and cooling period (1 cycle) at 40°C for 10 minutes.

The cycle number at which the fluorescence signal first exceeds the level of background fluorescence or the 'crossing point (CP) value' will be automatically set by the LightCycler software for each run. Aside from *T. gondii* DNA, No-template controls (NTC) and no-amplification controls (NAC) plus extracted total mRNA from infected samples were also included. Amplification efficiency analysis for all genes were conducted as described in section **2.3.20** and **2.3.21** (Chapter 2).

3.3.15 *Primers*

As described in section **2.3.21** (Chapter 2), most primer sequences for human genes were acquired either from Primer Bank (X. Wang *et al.*, 2011), RTPrimerDB (Lefever *et al.*, 2009), GETPrime (David, Rougemont and Deplancke, 2017), or from published literature. Housekeeping genes (beta-actin and HMBS) and TJ genes (Occludin, PRKCA, and ZO-1) and P-GP primers sequences were as reported in section **2.3.21** (Chapter 2). The genes name, GenBank accession, sequences, and PrimerBank ID/RTPrimer DB ID/GETPrime ID/literature for other genes are listed in **Table** 3-1.

Table 3-1 List of genes analysed by qPCR and their respective primer pair sequences.

Human Gene Description	GenBank Accession	Primer Sequence (5' end to 3' end)	Source
CXCR4 C-X-C motif chemokine receptor 4	NM_001008540	F: GCCTTATCCTGCCTGGTATTGTC R: GCGAAGAAAGCCAGGATGAGGAT	RTPrimerDB ID 1792
heat shock protein 90 alpha family class A member 2, pseudogene, HSP90AA2P	M30627	F: GCAGAGAAAACTCTGTCTCG R: CCTGAGAGAATTCACTGTGAGC	Chen *et al.*, (2011)
interferon alpha-inducible protein 6 IFI6, mRNA	NM_003277	F: CTCTGCTGGTTCGCCAACAT R: CAGCTCGTACTTCTGCGACA	Primer Bank ID: 195947371c1
nuclear receptor subfamily 4 group A member 2, NR4A2	NM_006186	F: CAAGGAACCCAAGAGAGTGG R: TGTGTGCAAAGGGTACGAAG	RTPrimerDB ID 293
Tumor necrosis factor alpha, TNF-α mRNA	NM_000594	F: GGAGAAGGGTGACCGACTCA R: TGCCCAGACTCGGCAAAG	Bertrand *et al.*, (2009)
thioredoxin-interacting protein, TXNIP	NM_006472	F: TGGATGGCTCTCAAGACAG R: GGGATCCACCTCAGTATAAGTC	GETPrime ID 2018599
zinc finger protein 467, ZNF467	NM_001329856	F: CTCCCTGGGATTCTCTGTG R: AAGAGGACATCTGCTCCTG	GETPrime ID 1945884
zinc finger protein 451, ZNF 451	NM_001145520	F: GTTTGTCAGTGAAGGACCA R: TATAAGAGGTGCTAGGCTC	GETPPrime ID 2112691

3.3.16 *Statistical Analysis*

Data are expressed as mean values ± standard errors (SE). Statistical analyses were performed with GraphPad Prism version 7 software (GraphPad Software Inc, CA, USA). Data comparing more than two groups were analysed by one-way analysis of variance (ANOVA), or two-way ANOVA with Bonferroni multiple-comparison test. A P value of < 0.05 was considered statistically significant. The level of significance was reported as: *, $P < 0.05$, ** $P < 0.01$, *** $P < 0.001$, and ****, $P < 0.0001$.

3.4 Results

3.4.1 *Transcriptomes Based on mRNA Sequencing: Mapped to Human Reference Genome*

Bar Graph Pre- and Post-Normalisation

The normalisation method used in Deseq2 package was based on a method called size factor normalisation that is based on the hypothesis that most genes were not differentially expressed and their expression across all samples should have very similar counts (Anders and Huber, 2010). Given this, the median gene counts were used to estimate the size correction factor that should be applied to all read counts of a lane to fulfil the hypothesis. Dillies *et al.*, (2013) ran three real mRNA and miRNA sequencing datasets and identified only Deseq/Deseq2 size factor and trimmed mean of M-values (TMM) can control the false positive rate consistently across all samples without sacrificing the power to detect DEGs out of seven normalisation methods for miRNA and mRNA sequencing data analysis. The weakness of these two normalisation methods is the assumption that most genes are not

differentially expressed may not always be the reality. Size factor normalisation was applied to all 12 samples sequenced and the results were presented as bar plots in **Figure** 3-2. Normalisation reduced the total counts for 10 out of 12 samples, with the remaining two infected 48 hours samples, had increased total counts (**Figure** 3-2). This whichcan be potentially attributed to low sequencing depth, due to *T. gondii* infection causing destruction of cells.

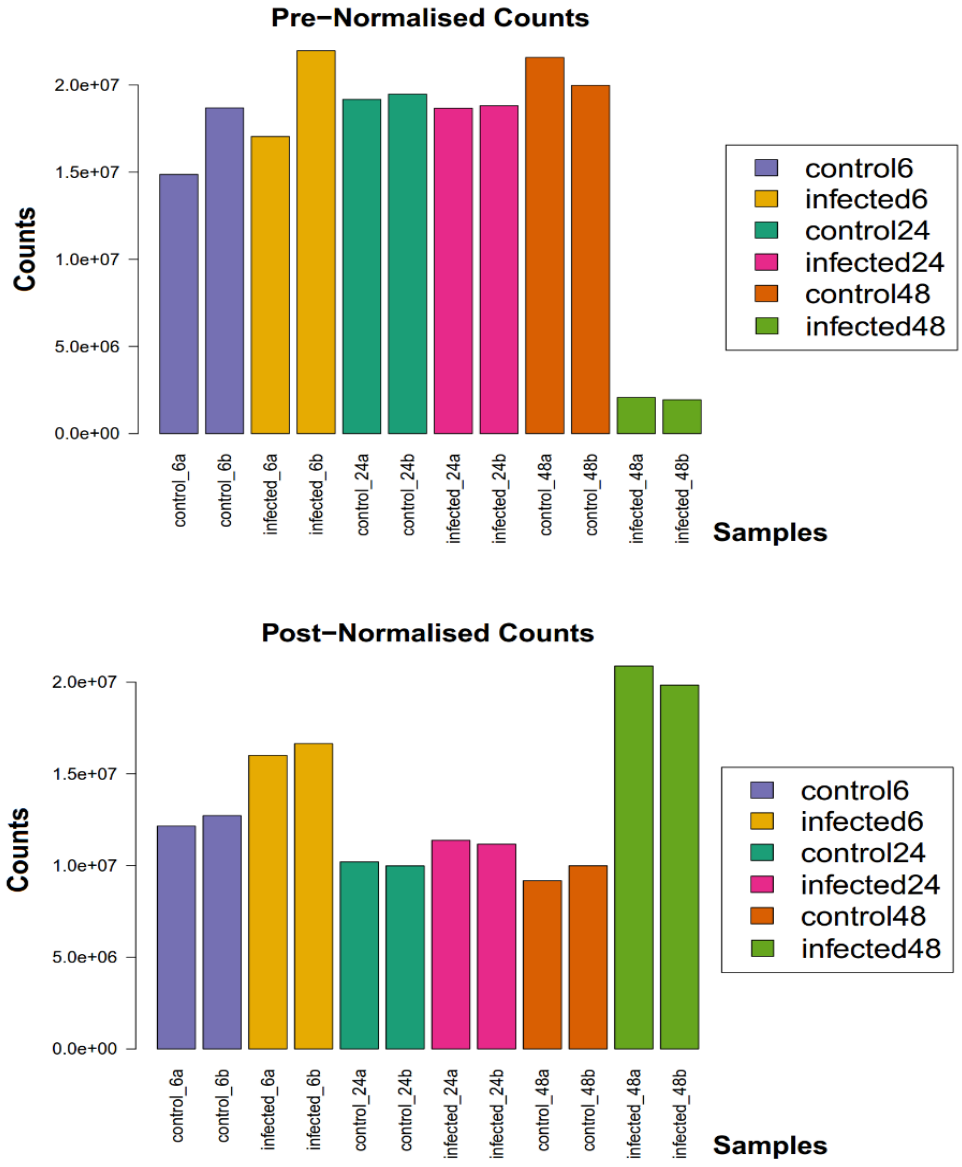


Figure 3-2 Pre and post-normalised counts of mRNA sequencing data after alignment to the human reference genome. The counts were normalised using the size factor normalisation method that normalises for sequencing depth and RNA composition (Anders and Huber, 2010).

Sample Correlation Heatmap

The sample to sample correlation allows comparison between samples at different time points. This can highlight similarities and differences and is commonly visualised using a heatmap. In heatmaps, the level of expression for each sample was represented as a coloured bar. Differences or similarities can be easily identified by aligning two samples and by comparing the colour of the same gene in different replicates. Dendrograms on the sides link closely correlated samples in each row or column to each other. Before any sequencing data were analysed for the transcriptional profile, data were pre-analysed in heatmaps as quality control measurements, for experimental reproducibility of the replicates of each time point. Sequencing data from the same time points should be positioned close to each other and have the similar colour tone. A sample correlation heatmap for mRNA sequencing is shown in **Figure** 3-3. In this heatmap, dark orange represents low correlation while bright pale yellow represents high correlation. From the figure, all samples at the same time points had the same colour tone except samples from control 48 hours and infected 48 hours, whereas control_48a and infected_48a have a slightly darker tone than control_48b and infected_48b respectively. The samples with the least correlation are control 6 hours versus infected 48 hours and control 48 hours versus infected 6 hours. This indicates that these two pairs have very different and unique expression profiles.

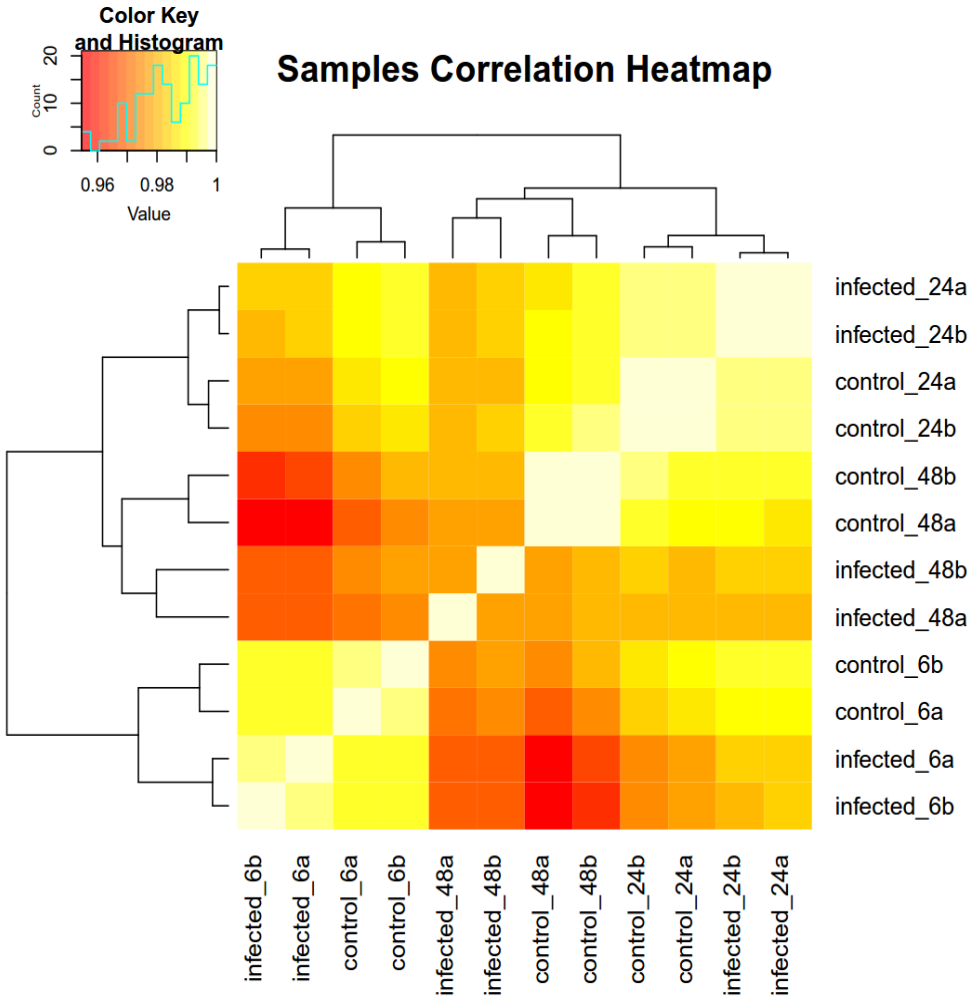


Figure 3-3 Correlation heatmap of all mRNA transcriptome expression profiles after mapping to the human reference genome. The heatmap showed a correlation between all samples sent for mRNA sequencing where shades of orange and yellow represented low and high correlation respectively, while dendrograms on the sides, closely links correlated samples in each row or column to each other. The heatmap showed three distinct clusters where control and infected samples at each time-point were clustered together.

Principal Component Analysis Plot

Principal component analysis (PCA) was used visualise data and to detect the variation between samples. PCA analysis was performed on all samples across all groups (**Figure** 3-4). The figure shows samples within each group were clustered together except for the 6 hours control samples. Positionwise, there was a clear distinction between control 6 hours, control 48 hours and infected 6 hours.

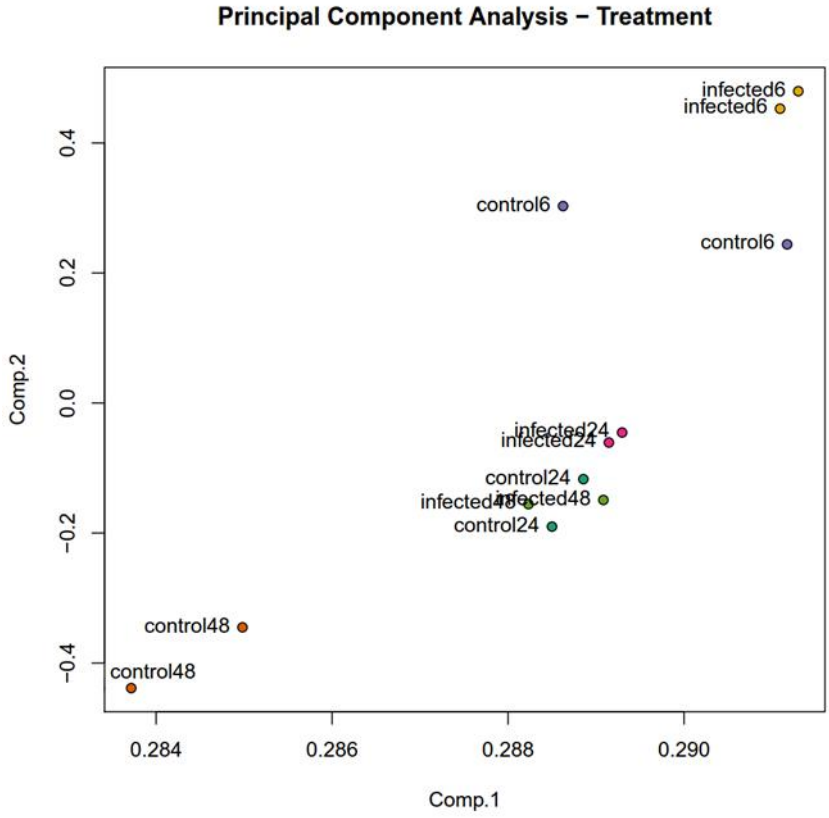


Figure 3-4 Principal component analysis (PCA) plot showing all samples transcriptome dataset variation. Samples within each group were in short distance to each except for control 6 samples. Four clusters were visible with three clusters were formed by control 6, infected 6 and control 48 hours groups separately while the last cluster were formed by combination of samples from control 24, infected 24 and infected 48 hours groups.

Volcano Plots

A volcano plot shows the relationship between *P*-values and $\log_2$ FC. In this plot, *P*-values were plotted on the y-axis while $\log_2$ FC was plotted on the x-axis. As such, the larger the fold change of a gene's expression, the more extreme its point will be from the 0 value of the x-axis. The more significant fold change, the smaller the P-value and thus the higher the -log10 (*P*-value). Each point or dot in the plot represents one gene. Thus, a gene with highly significant $\log_2$ FC will lie high in the plot. Features of interest are typically those which change significantly and by a certain magnitude. These are the points in the upper left and upper right parts of the volcano plot.

Figure 3-5 shows the relationship between *P*-values and $\log_2$ FC from all differently expressed genes of mRNA sequencing data. The accumulation of black dots on **Figure** 3-5 indicates that more genes were up-regulated than down-regulated at 6 h.p.i while there were more down-regulated genes at 24 and 48 h.p.i.

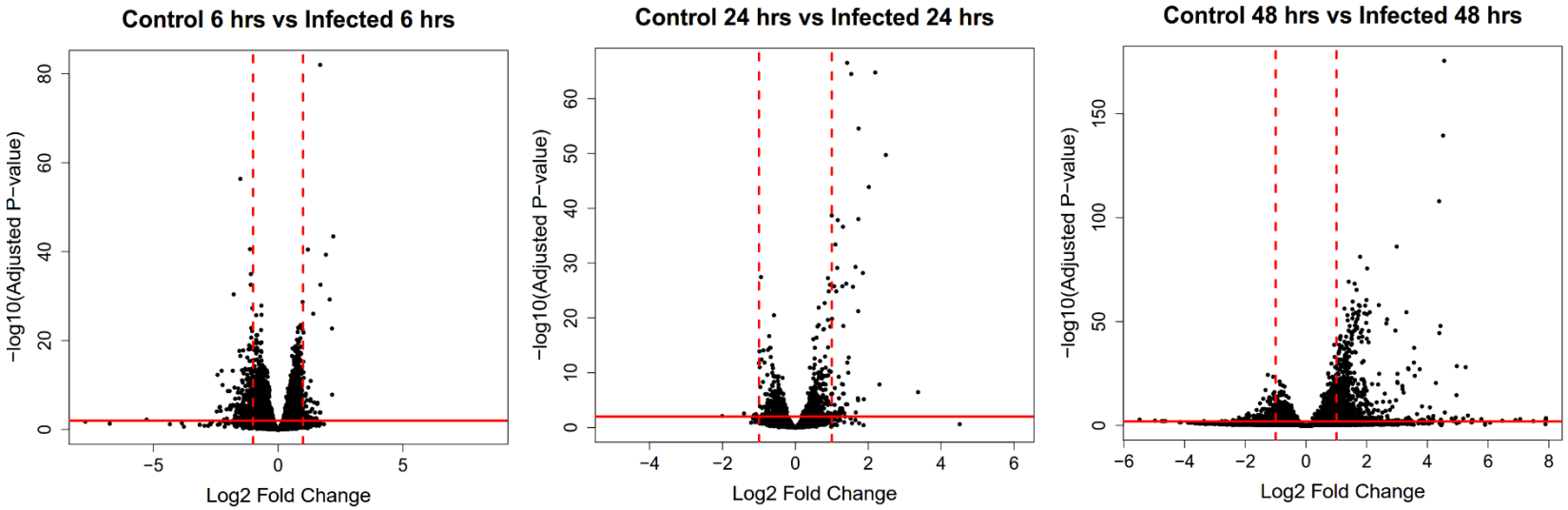


Figure 3-5 Volcano plots of DEGs (control *vs* infected) at 6, 24 and 48 h.p.i. The solid horizontal red line indicates *P*-value cut-off limit (0.01) while the dashed red line indicates $\log_2$ FC cut-off limit (1 and -1). The plots indicate that more genes were down-regulated than up-regulated at 6 h.p.i while there were more up-regulated genes at 24 and 48 h.p.i.

Venn Diagram

Venn diagrams, the gene lists from 6, 24 and 48 h.p.i were compared, all shown in **Figure** 3-6. The total number of genes expressed at each time point is shown in brackets. Common genes of different time points are shown in the central regions where their circles overlap. Of the 344 differently expressed genes at 6 hours, 5 were also expressed at 24 hours while another 22 genes were also expressed at 48 hours. Out of 65 DEGs at 24 hours, 22 genes were also expressed at 48 hours. At all time points, 14 genes were expressed; these are listed in **Table** 3-8**.**

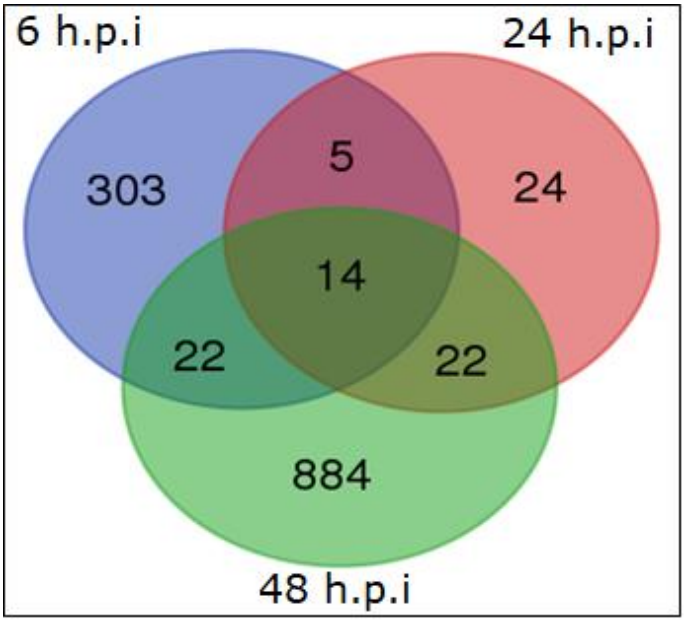


Figure 3-6 Venn diagram of DEGs at 6, 24 and 48 h.p.i from mRNA sequencing. Numbers in the overlapped area represent DEGs shared between groups.

Differentially Expressed Genes (DEGs) Gene Ontology

The term "Up-regulation" will be used from here on to describe a gene/set of genes/pathways was/were up-regulated in infected samples while "down-regulation" means those down-regulated in infected samples.

Control 6 hours vs Infected 6 hours

Cut-off values for DEGs at all time points are those with adjusted *P*-values < 0.01 and $\log_2$ FC ≥ 1 or ≤ -1. These strict selection criteria were chosen to reduce false positive results due to a low number of replicates. At 6 hours, 344 genes were differentially expressed. Of these, 287 were down-regulated while 57 were up-regulated. **Appendix** 3-6 contains a list of all significantly up-regulated and down-regulated genes. Among them, the three most highly down-regulated genes are RNA5-8SN1 (ENSG00000275215, 5.8S ribosomal RNA N1A), MYO18A (ENSG00000198744, myosin XVIIIA) and HSP90AA2 (ENSG00000196535, heat shock protein 90 alpha family class A member 2 pseudogene) with $\log_2$ FC of -5.268, -2.461, and -2.427 respectively. The three most up-regulated genes were CHAC1 (ENSG00000128965, ChaC glutathione specific gamma-glutamylcyclotransferase 1), MTCO3P12 (ENSG00000198744, mitochondrially encoded cytochrome c oxidase III pseudogene 12) and CISH (ENSG00000114737, cytokine-inducible SH2 containing protein) with $\log_2$ FC of 2.209, 2.166, and 2.159 respectively. The top 30 down-regulated and up-regulated genes are listed in **Table** 3-2 and **Table** 3-3 respectively.

Table 3-2 List of top 30 significantly down-regulated genes at 6 h.p.i. The filtered list resulted in 287 down-regulated genes, but only the top 30 genes are listed in this table sorted with the most highly significant gene at the top of the list. The full list is available in **Appendix** 3-6.

Ensembl Gene ID	Gene Symbol	Ensembl Gene Info	Log_2 FC
ENSG00000171159	TAF15	TATA-box binding protein associated factor 15	-1.782
ENSG00000142534	DCTN1	dynactin subunit 1	-1.817
ENSG00000105409	CDC42BPB	CDC42 binding protein kinase beta	-2.264
ENSG00000196535	HSP90AA2	heat shock protein 90 alpha family class A member 2, pseudogene	-2.427
ENSG00000162772	FAM196B	family with sequence similarity 196 member B	-2.224
ENSG00000168209	LEO1	LEO1 homolog, Paf1/RNA polymerase II complex component	-1.748
ENSG00000126705	BCL9L	B-cell CLL/lymphoma 9 like	-1.946
ENSG00000009307	FOXP4	forkhead box P4	-2.014
ENSG00000140264	RNF40	ring finger protein 40	-1.722
ENSG00000198752	SMARCC2	SWI/SNF related, matrix associated, actin dependent regulator of chromatin subfamily c member 2	-1.814
ENSG00000145592	PRR12	proline rich 12	-1.782
ENSG00000138758	SHANK1	SH3 and multiple ankyrin repeat domains 1	-1.902
ENSG00000204767	SMG6	SMG6, nonsense mediated mRNA decay factor	-1.731
ENSG00000237973	HSPG2	heparan sulfate proteoglycan 2	-2.328
ENSG00000114737	ATP1A3	ATPase Na+/K+ transporting subunit alpha 3	-2.351
ENSG00000204387	-	uncategorised long non-coding RNA	-1.878
ENSG00000157514	NLGN2	neuroligin 2	-1.937
ENSG00000247271	TLN1	talin 1	-2.062
ENSG00000198959	SHPRH	SNF2 histone linker PHD RING helicase	-1.912
ENSG00000224411	AHDC1	AT-hook DNA binding motif containing 1	-2.301
ENSG00000198744	MYO18A	myosin XVIIIA	-2.461
ENSG00000110713	RNF169	ring finger protein 169	-1.686
ENSG00000198561	SOGA1	suppressor of glucose, autophagy associated 1	-1.731
ENSG00000279348	ATN1	atrophin 1	-1.677
ENSG00000143013	ZNF710	zinc finger protein 710	-1.734
ENSG00000100219	LRP1	LDL receptor related protein 1	-2.055
ENSG00000275215	RNA5-8SN1	RNA, 5.8S ribosomal N1A	-5.268
ENSG00000142798	-	uncategorised long non-coding RNA	-2.168
ENSG00000170606	MED12	mediator complex subunit 12	-1.696
ENSG00000225972	-	poly(A) binding protein cytoplasmic 1 pseudogene 4	-1.716

Table 3-3 List of top 30 significantly up-regulated genes at 6 h.p.i. The filtered list resulted in 57 up-regulated genes but only the top 30 genes are listed in this table sorted with the most significant gene at the top of the list. The full list is available in **Appendix** 3-6.

Ensembl Gene ID	Gene Symbol	Ensembl Gene Info	Log_2 FC
ENSG00000168209	DDIT4	DNA damage inducible transcript 4	1.685
ENSG00000128965	CHAC1	ChaC glutathione specific gamma-glutamylcyclotransferase 1	2.209
ENSG00000101255	TRIB3	tribbles pseudokinase 3	1.192
ENSG00000162772	ATF3	activating transcription factor 3	1.915
ENSG00000157514	TSC22D3	TSC22 domain family member 3	1.697
ENSG00000237973	MTCO1P12	mitochondrially encoded cytochrome c oxidase I pseudogene 12	2.067
ENSG00000130766	SESN2	sestrin 2	1.406
ENSG00000114737	CISH	cytokine inducible SH2 containing protein	2.159
ENSG00000177600	RPLP2	ribosomal protein lateral stalk subunit P2	1.019
ENSG00000231414	-	uncategorised processed pseudogene	1.013
ENSG00000165175	MID1IP1	MID1 interacting protein 1	1.021
ENSG00000232388	SMIM26	small integral membrane protein 26	1.024
ENSG00000233016	SNHG7	small nucleolar RNA host gene 7	1.304
ENSG00000167550	RHEBL1	RHEB like 1	1.208
ENSG00000130513	GDF15	growth differentiation factor 15	1.111
ENSG00000198744	MTCO3P12	mitochondrially encoded cytochrome c oxidase III pseudogene 12	2.166
ENSG00000228253	ATP8	ATP synthase F0 subunit 8	1.080
ENSG00000264281	-	uncategorised processed pseudogene	1.099
ENSG00000175197	DDIT3	DNA damage inducible transcript 3	1.299
ENSG00000210196	MT-TP	mitochondrially encoded tRNA proline	1.151
ENSG00000155961	RAB39B	RAB39B, member RAS oncogene family	1.290
ENSG00000217716	RPS10P3	ribosomal protein S10 pseudogene 3	1.439
ENSG00000212664	-	uncategorised processed pseudogene	1.039
ENSG00000198840	ND3	NADH dehydrogenase, subunit 3 (complex I)	1.576
ENSG00000198727	CYTB	cytochrome b	1.564
ENSG00000198938	COX3	cytochrome c oxidase III	1.564
ENSG00000111678	C12orf57	chromosome 12 open reading frame 57	1.011
ENSG00000105327	BBC3	BCL2 binding component 3	1.129
ENSG00000198804	COX1	cytochrome c oxidase subunit I	1.364
ENSG00000198712	COX2	cytochrome c oxidase subunit II	1.287

PANTHER's gene ontology analysis results for molecular function, biological processes and cellular components for the significantly regulated genes are displayed in **Figure** 3-7, **Figure** 3-8 and **Figure** 3-9 respectively. From 287 Ensemble ID submitted, only 276 of the down-regulated genes were recognised by the database, while out of 57 significantly up-regulated

genes only 42 genes were recognised. In regards to molecular function, 187 hits were obtained from seven major functions (binding GO:0005488, 90 hits; catalytic activity GO:0003824, 60 hits; receptor activity GO:0004872, 10; signal transducer activity GO:0004871, six hits; structural molecule activity GO:0005198, nine hits; translation regulator activity GO:0045182, three hits; transporter activity GO:0005215, nine hits) from down-regulated genes list. Meanwhile, up-regulated genes were responsible for 29 molecular functions from four major functions (binding GO:0005488, nine hits; catalytic activity GO:0003824, 16 hits; signal transducer activity GO:0004871, one hit; transporter activity GO:0005215, three hits).

The PANTHER Overrepresentation Test for significantly down-regulated genes identified 16 highly enriched molecular functions, namely structural constituent of ribosome (GO:0003735), structural molecule activity (GO:0005198), RNA binding (GO:0003723), receptor activity (GO:0004872), signal transducer activity (GO:0004871), pyrophosphatase activity (GO:0016462), hydrogen ion transmembrane transporter activity (GO:0015078), G-protein coupled receptor activity (GO:0004930), catalytic activity (GO:0003824), microtubule binding (GO:0008017), cytoskeletal protein binding (GO:0008092), nucleic acid binding (GO:0003676), binding (GO:0005488), structural constituent of cytoskeleton (GO:0005200), and ion channel activity (GO:0005216). The same test for up-regulated genes returned two highly up-regulated functions namely hydrogen ion transmembrane transporter activity (GO:0015078) and oxidoreductase activity (GO:0016491).

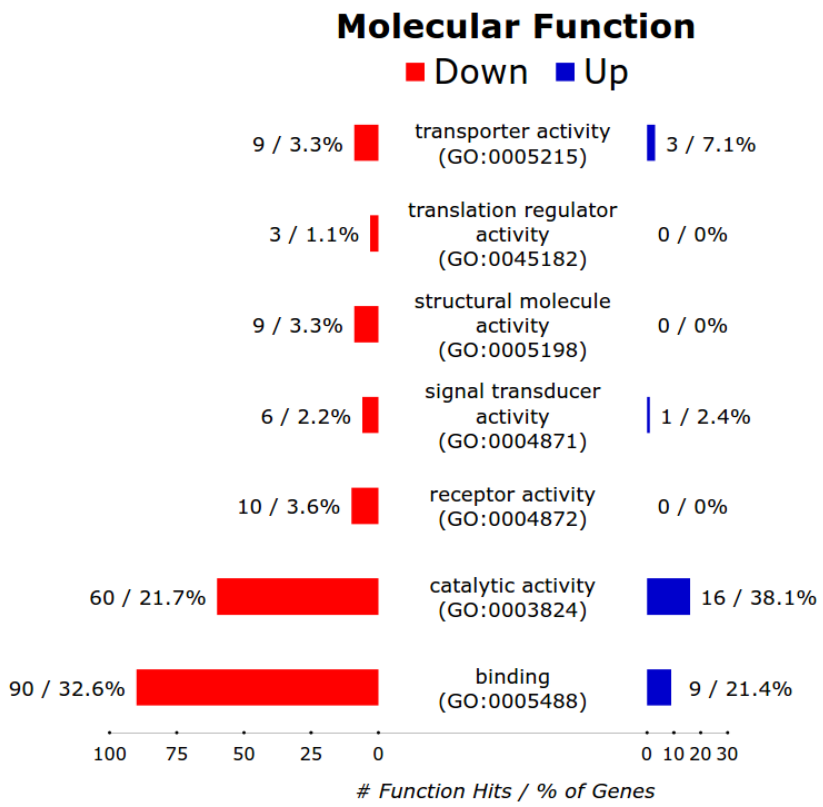


Figure 3-7 PANTHER GO-Slim molecular function ontology hits for significantly DEGs at 6 h.p.i. The down-regulated genes matched to 187 molecular functions from 7 major functions while up-regulated genes matched to 29 molecular functions from four major functions. The PANTHER's Overrepresentation Test (FDR < 0.05) then identified 16 significantly down-regulated and two significantly up-regulated functions.

Down-regulated genes matched to 421 biological processes from 12 major biological processes (biological adhesion GO:0022610, 11 hits; biological regulation GO:0065007, 35 hits; cellular component organisation or biogenesis GO:0071840, 33 hits; cellular process GO:0009987, 119 hits; developmental process GO:0032502, 33 hits; growth GO:0040007, one hit; immune system process GO:0002376, three hit; localisation GO:0051179, 36 hits; locomotion GO:0040011, six hits; metabolic process GO:0008152, 88 hits; multicellular organismal process GO:0032501, 22 hits; reproduction GO:0000003, three hits; response to stimulus GO:0050896, 31 hits) while up-regulated genes matched to 50 biological processes from 10 major

processes (cellular component organisation or biogenesis GO:0071840, one hit; cellular process GO:0009987, 16 hits; localisation GO:0051179, three hits; biological regulation GO:0065007, three hits; response to stimulus GO:0050896, four hits; developmental process GO:0032502, four hits; multicellular organismal process GO:0032501, one hit; biological adhesion GO:0022610, two hits; metabolic process GO:0008152, 14 hits; immune system process GO:0002376, two hits). The PANTHER Overrepresentation Test identified 43 significantly down-regulated biological processes (**Appendix** 3-7) and three significantly up-regulated biological processes (oxidative phosphorylation GO:0006119, respiratory electron transport chain GO:0022904, generation of precursor metabolites and energy GO:0006091).

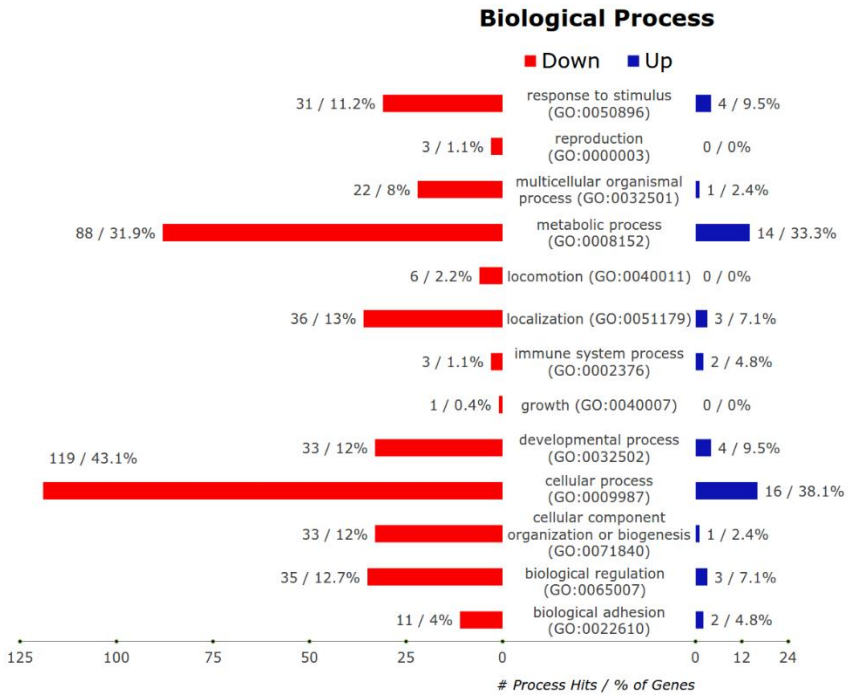


Figure 3-8 PANTHER GO-Slim biological processes ontology hits for significantly DEGs at 6 h.p.i. The down-regulated genes matched to 421 biological processes from 12 major processes while up-regulated genes matched to 50 biological processes from 10 major processes. The PANTHER Overrepresentation Test (FDR < 0.05) then identified 43 significantly down-regulated and three significantly up-regulated processes.

Down-regulated genes matched to 241 cellular components from eight major components (cell junction GO:0030054, three hits; cell part GO:0044464, 93 hits; extracellular matrix GO:0031012, six hits; extracellular region GO:0005576, eight hits; macromolecular complex GO:0032991, 35 hits; membrane GO:0016020, 20 hits; organelle GO:0043226, 73 hits; synapse GO:0045202, three hits) while up-regulated genes matched to 33 cellular components from five major components (cell part GO:0044464, 13 hits; extracellular matrix GO:0031012, one hit; macromolecular complex GO:0032991, eight hits; membrane GO:0016020, seven hits; organelle GO:0043226, four hits). The PANTHER Overrepresentation Test of down-regulated genes identified 17 significant locations (ribosome GO:0005840, ribonucleoprotein complex GO:0030529, intracellular GO:0005622, macromolecular complex GO:0032991, cell part GO:0044464, cytosol GO:0005829, organelle GO:0043226, cytoplasm GO:0005737, protein complex GO:0043234, nucleus GO:0005634, mitochondrial inner membrane GO:0005743, nuclear envelope GO:0005635, extracellular space GO:0005615, vesicle coat GO:0030120, nucleolus GO:0005730, cytoskeleton GO:0005856, extracellular region GO:0005576) and one significant location, mitochondrial inner membrane (GO:0005743) from up-regulated genes.

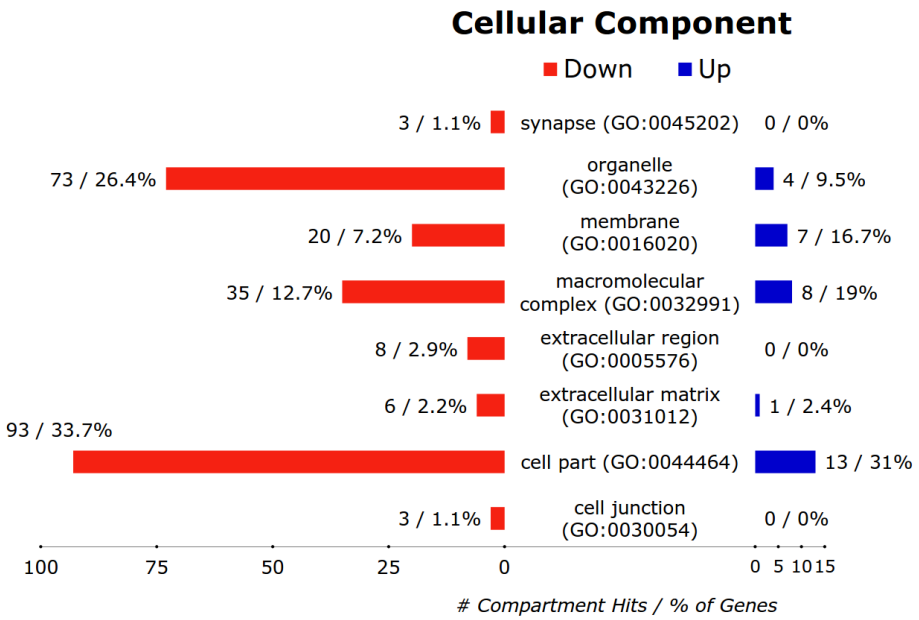


Figure 3-9 PANTHER GO-Slim cellular components ontology hits for significantly DEGs at 6 h.p.i. The down-regulated genes matched to 241 cellular components from 8 major components while up-regulated genes matched to 33 cellular components from 5 major components. The PANTHER Overrepresentation Test (FDR<0.05) then identified 17 and one significant locations from down and up-regulated genes respectively.

Control 24 hours vs Infected 24 hours

At 24 hours, 65 genes were differentially expressed. Of this number, seven were down-regulated, while 58 were up-regulated. The top 30 up-regulated genes and all down-regulated genes are listed in **Table** 3-5 and **Table** 3-4 respectively. Among them, the three most highly down-regulated genes are NOTCH3 (ENSG00000074181, notch 3), PPL (ENSG00000118898, periplakin), and CA11 (ENSG00000063180, carbonic anhydrase 11) with $\log_2$ FC of -2.009, -1.411, and -1.136 respectively. The three most up-regulated genes were MALAT1 (ENSG00000251562, metastasis-associated lung adenocarcinoma transcript 1 -non-protein coding), CHAC1 (ENSG00000128965, ChaC glutathione specific gamma-glutamylcyclotransferase 1), and GABRG1 (ENSG00000163285, gamma-

aminobutyric acid type A receptor gamma1 subunit) with log_2 FC of 3.365, 2.483, and 2.308 respectively.

Table 3-4 List of top 30 up-regulated genes at 24 h.p.i. The filtered list resulted in 58 up-regulated genes, but only the top 30 genes are listed in this table sorted with the most significant gene at the top of the list. The full list is available in **Appendix** 3-8.

Ensembl Gene ID	Gene Symbol	Ensembl Gene Info	log_2 FC
ENSG00000113739	STC2	stanniocalcin 2	1.420
ENSG00000118971	CCND2	cyclin D2	2.191
ENSG00000168209	DDIT4	DNA damage inducible transcript 4	1.531
ENSG00000135069	PSAT1	phosphoserine aminotransferase 1	1.734
ENSG00000128965	CHAC1	ChaC glutathione specific gamma-glutamylcyclotransferase 1	2.483
ENSG00000070669	ASNS	asparagine synthetase (glutamine-hydrolysing)	2.017
ENSG00000115902	SLC1A4	solute carrier family 1 member 4	1.728
ENSG00000101255	TRIB3	tribbles pseudokinase 3	1.162
ENSG00000092621	PHGDH	phosphoglycerate dehydrogenase	1.306
ENSG00000065911	MTHFD2	methylenetetrahydrofolate dehydrogenase (NADP+ dependent) 2, methenyltetrahydrofolate cyclohydrolase	1.097
ENSG00000100889	PCK2	phosphoenolpyruvate carboxykinase 2, mitochondrial	1.650
ENSG00000187840	EIF4EBP1	eukaryotic translation initiation factor 4E binding protein 1	1.148
ENSG00000162772	ATF3	activating transcription factor 3	1.851
ENSG00000130766	SESN2	sestrin 2	1.396
ENSG00000143013	LMO4	LIM domain only 4	1.062
ENSG00000151012	SLC7A11	solute carrier family 7 member 11	1.288
ENSG00000157514	TSC22D3	TSC22 domain family member 3	1.579
ENSG00000166123	GPT2	glutamic--pyruvic transaminase 2	1.122
ENSG00000116761	CTH	cystathionine gamma-lyase	1.723
ENSG00000146733	PSPH	phosphoserine phosphatase	1.004
ENSG00000268205	-	uncategorised LincRNA	1.315
ENSG00000136244	IL6	interleukin 6	1.462
ENSG00000196517	SLC6A9	solute carrier family 6 member 9	1.426
ENSG00000279184	-	uncategorised novel antisense	1.452
ENSG00000228253	ATP8	ATP synthase F0 subunit 8	1.190
ENSG00000074935	TUBE1	tubulin epsilon 1	1.278
ENSG00000136826	KLF4	Kruppel like factor 4	1.306
ENSG00000163285	GABRG1	gamma-aminobutyric acid type A receptor gamma1 subunit	2.308
ENSG00000130513	GDF15	growth differentiation factor 15	1.082
ENSG00000251562	MALAT1	metastasis associated lung adenocarcinoma transcript 1 (non-protein coding)	3.365

Table 3-5 List of all seven down-regulated genes at 24 h.p.i. The filtered list resulted in seven down-regulated genes listed in this table sorted with the most highly significant gene at the top of the list.

Ensembl Gene ID	Gene Symbol	Ensembl Gene Info	Log_2 FC
ENSG00000131389	SLC6A6	solute carrier family 6 member 6	-1.003
ENSG00000118898	PPL	periplakin	-1.411
ENSG00000112175	BMP5	bone morphogenetic protein 5	-1.084
ENSG00000183287	CCBE1	collagen and calcium binding EGF domains 1	-1.097
ENSG00000260401	-	uncharacterised sense overlapping gene	-1.131
ENSG00000063180	CA11	carbonic anhydrase 11	-1.136
ENSG00000074181	NOTCH3	notch 3	-2.009

The PANTHER gene ontology analysis results for molecular function, biological processes and cellular component for significantly regulated genes are displayed in **Figure** 3-10, **Figure** 3-11 and **Figure** 3-12 respectively. From seven down-regulated Ensemble ID submitted, six genes were recognised by the database while 48 genes were recognised from 58 up-regulated genes. In molecular function category, six hits were obtained from three major functions (binding GO:0005488, three hits; structural molecule activity GO:0005198, two hits; transporter activity GO:0005215, one hit) for down-regulated genes while up-regulated genes matched to 52 molecular functions from six major functions (binding GO:0005488, 18 hits; receptor activity GO:0004872, two hits; structural molecule activity GO:0005198, one hit; signal transducer activity GO:0004871, two hits; catalytic activity GO:0003824, 22 hits; transporter activity GO:0005215, seven hits). Due to a low number, the down-regulated list did not return any significance results from the PANTHER Overrepresentation Test. Meanwhile, the up-regulated genes list return four significant functions which are hydrogen ion transmembrane transporter activity (GO:0015078), cation transmembrane transporter activity (GO:0008324), oxidoreductase activity

(GO:0016491) and catalytic activity (GO:0003824) from PANTHER Overrepresentation Test.

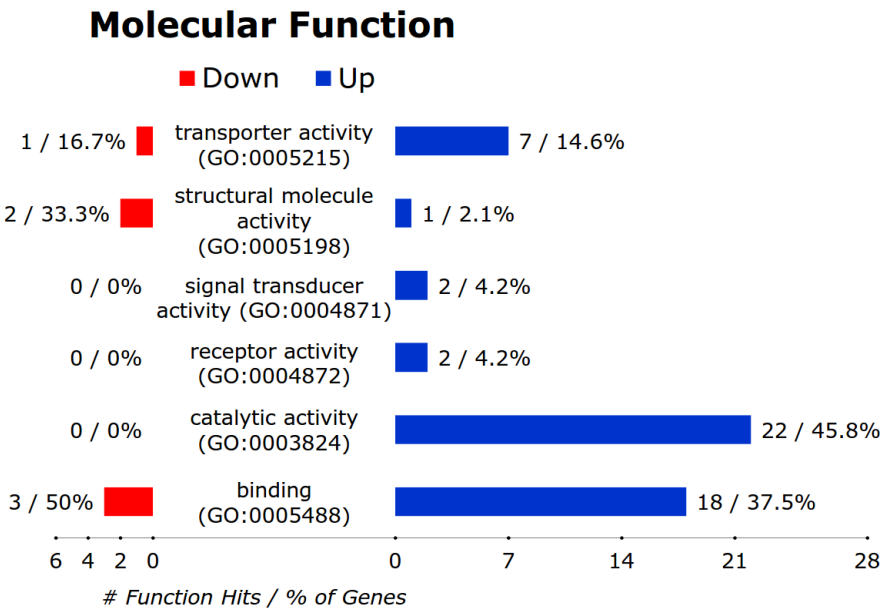


Figure 3-10 PANTHER GO-Slim molecular function ontology hits for significantly DEGs at 24 h.p.i. The down-regulated genes matched to 6 molecular functions from 3 major functions while up-regulated genes matched to 52 molecular functions from six major functions. The PANTHER Overrepresentation Test (FDR < 0.05) then identified four significantly up-regulated functions from the down-regulated list while no significant function was identified from the down-regulated list.

Significantly down-regulated genes matched to 10 biological processes from six major processes (stimulus GO:0050896, one hit; developmental process GO:0032502, two hits; cellular process GO:0009987, four hits; multicellular organismal process GO:0032501, one hit; metabolic process GO:0008152, one hit; biological regulation GO:0065007, one hit). Significantly up-regulated genes matched to 101 biological processes from 12 major processes (cellular component organisation or biogenesis GO:0071840, four hits; cellular process GO:0009987, 32 hits; localisation GO:0051179, four hits; reproduction GO:0000003, one hit; biological regulation GO:0065007, 10 hits; response to stimulus GO:0050896, eight hits; developmental process GO:0032502,

four hits; multicellular organismal process GO:0032501, four hits; biological adhesion GO:0022610, one hit; locomotion GO:0040011, one hit; metabolic process GO:0008152, 27 hits; immune system process GO:0002376, three hits). The PANTHER Overrepresentation Test identified eight significant biological processes which are cellular amino acid biosynthetic process (GO:0008652), oxidative phosphorylation (GO:0006119), cellular amino acid metabolic process (GO:0006520), biosynthetic process (GO:0009058), nitrogen compound metabolic process (GO:0006807), phosphate-containing compound metabolic process (GO:0006796), metabolic process (GO:0008152), and cellular process (GO:0009987) from down-regulated genes while no significant processes from up-regulated genes.

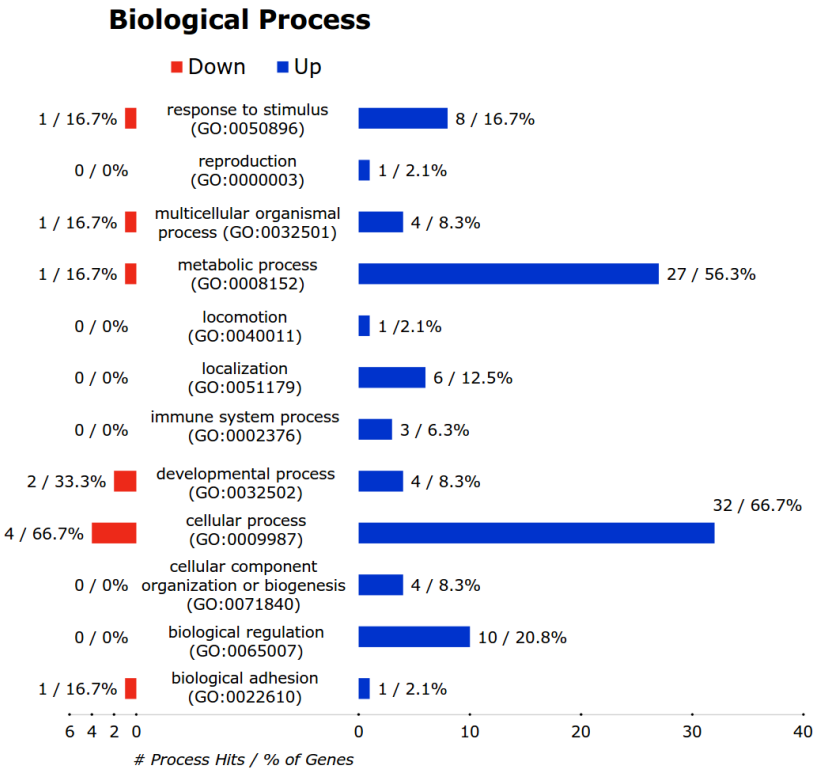


Figure 3-11 PANTHER GO-Slim biological processes ontology hits for significantly DEGs at 24 h.p.i. The down-regulated genes matched to 10 biological processes from 6 major processes while up-regulated genes matched to 101 biological processes from 12 major processes. The PANTHER Overrepresentation Test (FDR < 0.05) then identified 8 significant processes from up-regulated genes and none from down-regulated genes.

Down-regulated genes matched to four cellular components from three major components (cell part GO:0044464, one hit; extracellular matrix GO:0031012, one hit; extracellular region GO:0005576, two hits) while up-regulated genes matched to 48 cellular components from five major components (cell part GO:0044464, 22 hits; extracellular region GO:0005576, two hits; macromolecular complex GO:0032991, seven hits; membrane GO:0016020, seven hits; organelle GO:0043226, 10 hits). PANTHER Overrepresentation Test of up-regulated genes identified one significant location which is a mitochondrial inner membrane (GO:0005743) but no significant location from the list of down-regulated genes.

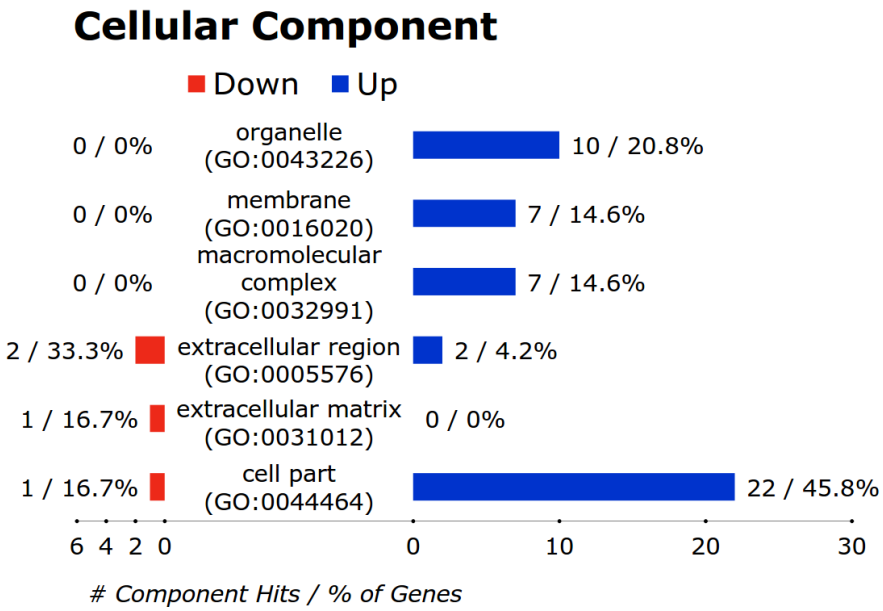


Figure 3-12 PANTHER GO-Slim cellular components ontology hits for significantly DEGs at 24 h.p.i. The down-regulated genes matched to 4 cellular components from 3 major components while up-regulated genes matched to 48 cellular components from 5 major components. The PANTHER Overrepresentation Test (FDR < 0.05) then identified 4 significant locations from up-regulated genes and none for down-regulated genes.

Control 48 hours vs Infected 48 hours

At 48 hours, 942 genes were differentially expressed where of this number 249 were down-regulated while 693 were up-regulated. The top 30 down-regulated and up-regulated genes were listed in **Table** 3-6 and **Table** 37 respectively. Among them, the three most highly down-regulated genes are COBLL1 (ENSG00000082438, cordon-bleu WH2 repeat protein-like 1), LCA5 (ENSG00000135338, LCA5, lebercilin), and TMCC2 (ENSG00000133069, transmembrane and coiled-coil domain family 2) with $\log_2$ FC of -5.482, -4.977, and -4.755 respectively. On another hand, the three most up-regulated genes were, uncharacterised sense intronic (ENSG00000225195, uncharacterised RNA gene), DEPDC1P2 (ENSG00000232486, DEP Domain Containing 1 Pseudogene 2), and KIRREL3-AS2 (ENSG00000254960, KIRREL3 antisense RNA 2) with $\log_2$ FC of 7.903, 7.897, and 7.893 respectively.

Table 3-6 List of top 30 down-regulated genes at 48 h.p.i. The filtered list resulted in 249 down-regulated genes, but only the top 30 genes are listed in this table sorted with the most significant gene at the top of the list. The full list is available in **Appendix** 3-9.

Ensembl Gene ID	Gene Symbol	Ensembl Gene Info	Log_2 FC
ENSG00000010292	NCAPD2	non-SMC condensin I complex subunit D2	-1.259
ENSG00000064666	CNN2	calponin 2	-1.084
ENSG00000183853	KIRREL1	kirre like nephrin family adhesion molecule 1	-1.336
ENSG00000125107	CNOT1	CCR4-NOT transcription complex subunit 1	-1.042
ENSG00000146918	NCAPG2	non-SMC condensin II complex subunit G2	-1.080
ENSG00000184640	SEPT9	septin 9	-1.041
ENSG00000112984	KIF20A	kinesin family member 20A	-1.199
ENSG00000160285	LSS	lanosterol synthase	-1.220
ENSG00000011426	ANLN	anillin actin-binding protein	-1.060
ENSG00000058668	ATP2B4	ATPase plasma membrane Ca2+ transporting 4	-1.166
ENSG00000140526	ABHD2	abhydrolase domain containing 2	-1.409
ENSG00000174231	PRPF8	pre-mRNA processing factor 8	-1.038
ENSG00000117115	PADI2	peptidyl arginine deiminase 2	-1.264
ENSG00000143641	GALNT2	polypeptide N-acetylgalactosaminyltransferase 2	-1.178
ENSG00000178921	PFAS	phosphoribosylformylglycinamidine synthase	-1.189
ENSG00000113368	LMNB1	lamin B1	-1.519
ENSG00000143799	PARP1	poly(ADP-ribose) polymerase 1	-1.006
ENSG00000198901	PRC1	protein regulator of cytokinesis 1	-1.184
ENSG00000160216	AGPAT3	1-acylglycerol-3-phosphate O-acyltransferase 3	-1.092
ENSG00000176619	LMNB2	lamin B2	-1.078
ENSG00000135476	ESPL1	extra spindle pole bodies like 1, separase	-1.430
ENSG00000125872	LRRN4	leucine rich repeat neuronal 4	-1.362
ENSG00000110048	OSBP	oxysterol binding protein	-1.141
ENSG00000136205	TNS3	tensin 3	-1.269
ENSG00000147130	ZMYM3	zinc finger MYM-type containing 3	-1.202
ENSG00000135862	LAMC1	laminin subunit gamma 1	-1.059
ENSG00000156970	BUB1B	BUB1 mitotic checkpoint serine/threonine kinase B	-1.628
ENSG00000106290	TAF6	TATA-box binding protein associated factor 6	-1.140
ENSG00000132842	AP3B1	adaptor related protein complex 3 beta 1 subunit	-1.016
ENSG00000109572	CLCN3	chloride voltage-gated channel 3	-1.081

Table 3-7 List of top 30 up-regulated genes at 48 h.p.i. The filtered list resulted in 693 up-regulated genes, but only the top 30 genes are listed in this table sorted with the most significant gene at the top of the list. The full list is available in **Appendix** 3-9.

Ensembl Gene ID	Gene Symbol	Ensembl Gene Info	log_2 FC
ENSG00000169429	CXCL8	C-X-C motif chemokine ligand 8	4.551
ENSG00000210082	MT-RNR2	mitochondrially encoded 16S RNA	4.515
ENSG00000136244	IL6	interleukin 6	4.384
ENSG00000118515	SGK1	serum/glucocorticoid regulated kinase 1	2.988
ENSG00000145592	RPL37	ribosomal protein L37	1.783
ENSG00000105825	TFPI2	tissue factor pathway inhibitor 2	2.011
ENSG00000142534	RPS11	ribosomal protein S11	1.404
ENSG00000169908	TM4SF1	transmembrane 4 L six family member 1	1.601
ENSG00000127920	GNG11	G protein subunit gamma 11	1.663
ENSG00000198918	RPL39	ribosomal protein L39]	1.990
ENSG00000197756	RPL37A	ribosomal protein L37a	1.537
ENSG00000164587	RPS14	ribosomal protein S14	1.738
ENSG00000108848	LUC7L3	LUC7 like 3 pre-mRNA splicing factor	2.396
ENSG00000234741	GAS5	growth arrest specific 5 (non-protein coding)	1.950
ENSG00000231500	RPS18	ribosomal protein S18	1.773
ENSG00000198034	RPS4X	ribosomal protein S4, X-linked	1.266
ENSG00000229117	RPL41	ribosomal protein L41	1.528
ENSG00000008988	RPS20	ribosomal protein S20	1.748
ENSG00000210196	MT-TP	mitochondrially encoded tRNA proline	3.305
ENSG00000117318	ID3	inhibitor of DNA binding 3, HLH protein	2.098
ENSG00000105193	RPS16	ribosomal protein S16	1.632
ENSG00000213741	RPS29	ribosomal protein S29	1.918
ENSG00000118181	RPS25	ribosomal protein S25	1.553
ENSG00000168209	DDIT4	DNA damage inducible transcript 4	2.010
ENSG00000133112	TPT1	tumor protein, translationally-controlled 1	1.725
ENSG00000137818	RPLP1	ribosomal protein lateral stalk subunit P1	1.365
ENSG00000182899	RPL35A	ribosomal protein L35a	1.529
ENSG00000071082	RPL31	ribosomal protein L31	1.694
ENSG00000228253	ATP8	ATP synthase F0 subunit 8	2.671
ENSG00000197958	RPL12	ribosomal protein L12	1.372

Among down-regulated genes, only 245 were recognised by the PANTHER database while for up-regulated genes the number is 492. In molecular function category, down-regulated genes matched to 150 functions from six major functions (binding GO:0005488, 68 hits; receptor activity GO:0004872, five hits; structural molecule activity GO:0005198, 11 hits; signal transducer activity GO:0004871, three hits; catalytic activity GO:0003824, 54 hits; transporter activity GO:0005215. nine hits) while up-

regulated genes matched to 343 functions from nine major functions (transporter activity GO:0005215, 27 hits; translation regulator activity GO:0045182, one hit; catalytic activity GO:0003824, 113 hit; channel regulator activity GO:0016247, one hit; receptor activity GO:0004872, seven hits; signal transducer activity GO:0004871, 11 hits; antioxidant activity GO:0016209, four hits; structural molecule activity GO:0005198, 57 hits; binding GO:0005488, 122 hits). The PANTHER molecular function ontology result is displayed in **Figure** 3-13. Surprisingly, there is no significant molecular function from the PANTHER Overrepresentation Test for down-regulated genes. A total nine significant functions were identified for the up-regulated genes (structural constituent of ribosome GO:0003735, hydrogen ion transmembrane transporter activity GO:0015078, structural molecule activity GO:0005198, cation transmembrane transporter activity GO:0008324, oxidoreductase activity GO:0016491, sequence-specific DNA binding RNA polymerase II gene ion factor activity GO:0000981, RNA binding GO:0003723, receptor activity GO:0004872).

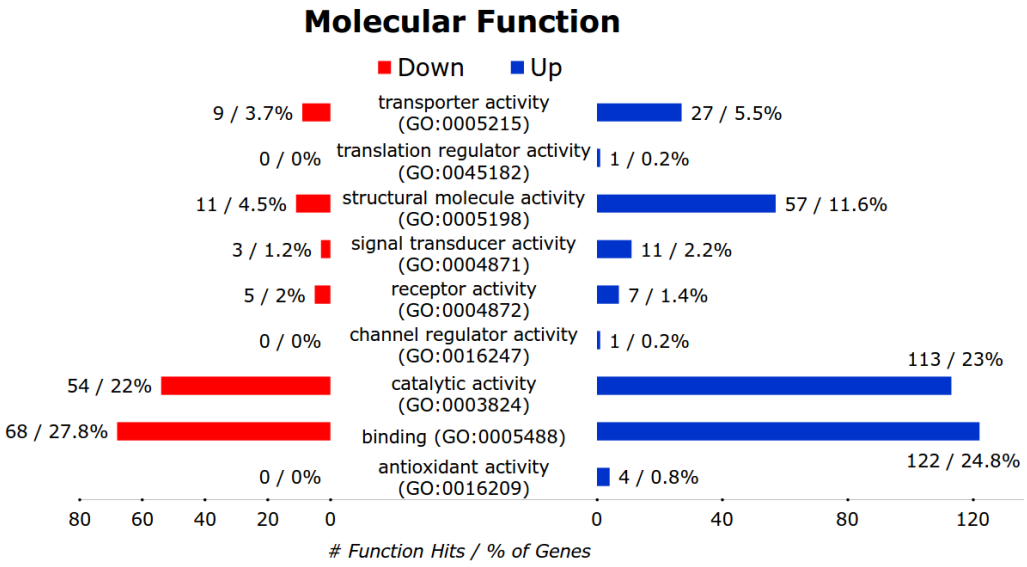


Figure 3-13 PANTHER GO-Slim molecular function ontology hits for significantly DEGs at 48 h.p.i. The down-regulated genes matched to 150 molecular functions from 6 major functions while up-regulated genes matched to 343 molecular functions from 9 major functions. No significant molecular function was identified by the PANTHER Overrepresentation Test (FDR < 0.05) for both conditions.

In the biological process category, down-regulated genes matched to 340 biological processes while up-regulated genes matched to 677 processes. The PANTHER Overrepresentation Test identified 11 processes from up-regulated list (oxidative phosphorylation GO:0006119, translation GO:0006412, respiratory electron transport chain GO:0022904, rRNA metabolic process GO:0016072, generation of precursor metabolites and energy GO:0006091, biosynthetic process GO:0009058, cellular component biogenesis GO:0044085, nitrogen compound metabolic process GO:0006807, metabolic process GO:0008152, single-multicellular organism process GO:0044707, multicellular organismal process GO:0032501) while no significant processes was identified from down-regulated list. The PANTHER biological process ontology result is displayed in **Figure** 3-14.

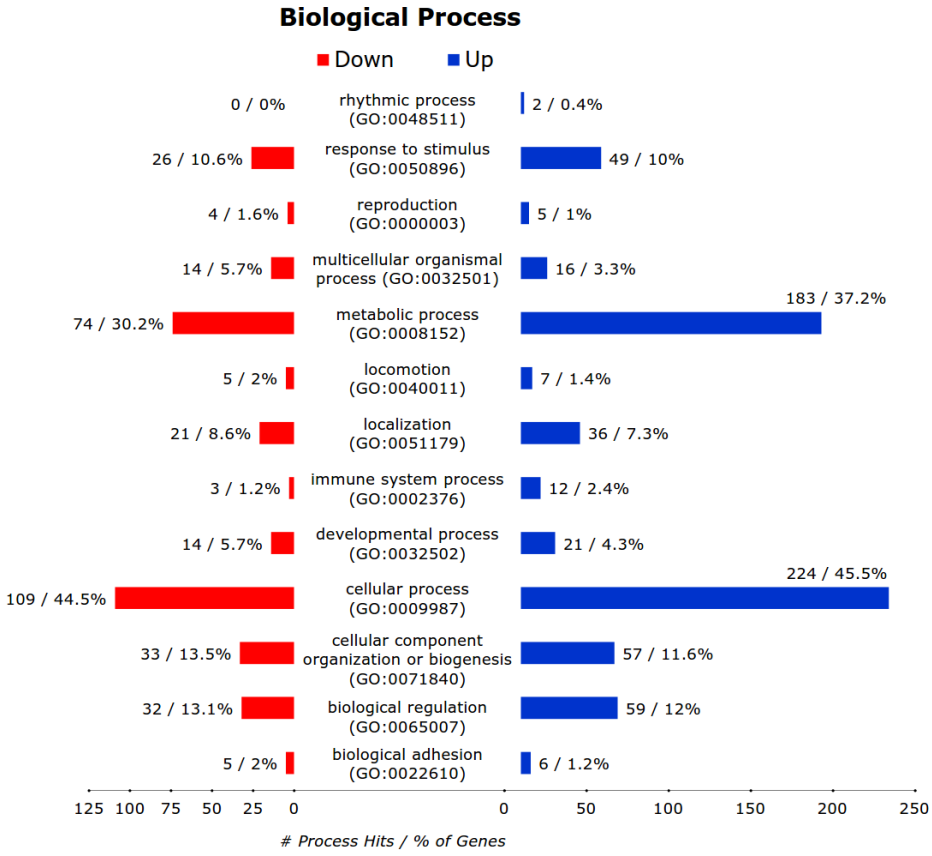


Figure 3-14 PANTHER GO-Slim biological processes ontology hits for significantly DEGs at 48 h.p.i. The down-regulated genes matched to 340 biological processes from 12 major processes while up-regulated genes matched to 677 biological processes from 13 major processes. The PANTHER Overrepresentation Test (FDR < 0.05) then identified 11 significant processes from up-regulated genes and none from down-regulated genes.

In the cellular component category, down-regulated genes matched to 222 cellular components from seven major components (synapse GO:0045202, one hit; membrane GO:0016020, 26 hits; macromolecular complex GO:0032991, 31 hits; extracellular matrix GO:0031012, four hits; cell part GO:0044464, 85 hits; organelle GO:0043226, 68 hits; extracellular region GO:0005576, seven hits) while up-regulated genes list matched to 616 components from eight major components (synapse GO:0045202, one hit; cell junction GO:0030054, one hit; membrane GO:0016020, 61 hits; macromolecular complex GO:0032991, 144 hits; extracellular matrix GO:0031012, two hits; cell part GO:0044464, 225 hits; organelle

GO:0043226, 168 hits; extracellular region GO:0005576, 14 hits). The PANTHER biological process ontology result is displayed in **Figure** 3-15. The PANTHER Overrepresentation Test identified three (nucleus GO:0005634, organelle GO:0043226, intracellular GO:0005622) and 15 (ribosome GO:0005840, proton-transporting ATP synthase complex GO:0045259, mitochondrial inner membrane GO:0005743, ribonucleoprotein complex GO:0030529, cytosol GO:0005829, macromolecular complex GO:0032991, mitochondrion GO:0005739, cytoplasm GO:0005737, protein complex GO:0043234, organelle GO:0043226, intracellular GO:0005622, cell part GO:0044464, nucleus GO:0005634, plasma membrane GO:0005886, cell projection GO:0042995) significant cellular components from down and up-regulated genes respectively.

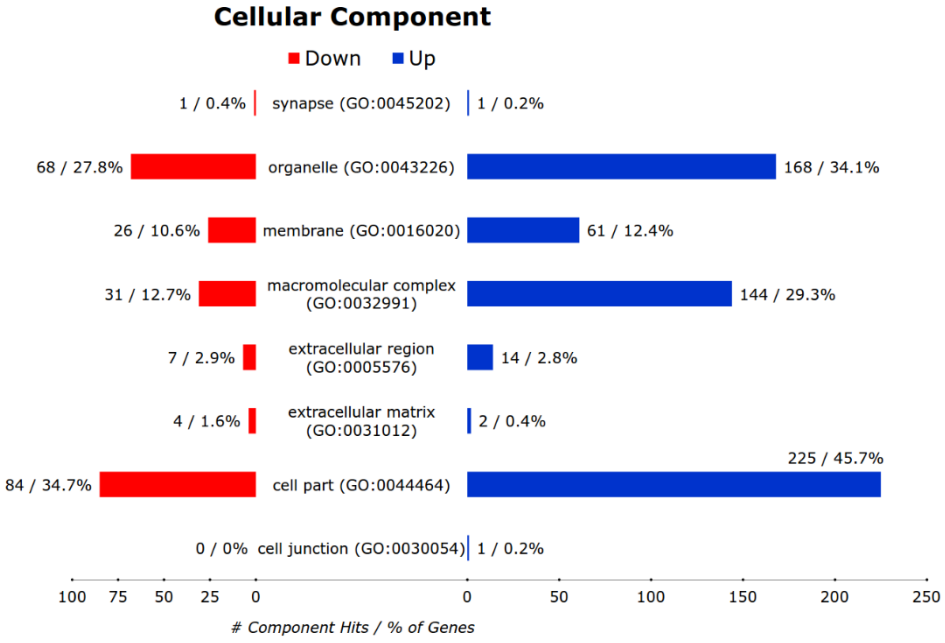


Figure 3-15 PANTHER GO-Slim cellular components ontology hits for significantly DEGs at 48 h.p.i. The down-regulated genes matched to 222 cellular components from 3 major components while up-regulated genes matched to 616 cellular components from 8 major components. The PANTHER Overrepresentation Test (FDR < 0.05) then identified 3 significant locations from down-regulated genes and 16 for up-regulated genes.

Comparison of DEGs between all three time points resulted in 14 genes, all of them up-regulated. The list of genes, their symbols and description, plus their $\log_2$ FC values at all time points are listed in **Table** 3-8. PANTHER database recognised 13 of these genes and matched them to 12 molecular functions from three major functions (binding GO:0005488, one hit; catalytic activity GO:0003824, 8 hits; transporter activity GO:0005215, 3 hits), 18 biological processes from six major processes (cellular process GO:0009987, seven hits; metabolic process GO:0008152, seven hits; response to stimulus GO:0050896, one hit; biological regulation GO:0065007, one hit; cellular component organisation or biogenesis GO:0071840, one hit; localisation GO:0051179, one hit) and 19 cellular components from four major components (membrane GO:0016020, six hits; macromolecular complex GO:0032991, four hits; cell part GO:0044464, seven hits; organelle GO:0043226, two hits). The PANTHER Overrepresentation Test then identified three significant molecular functions (hydrogen ion transmembrane transporter activity GO:0015078, cation transmembrane transporter activity GO:0008324, oxidoreductase activity GO:0016491), four significant biological processes (oxidative phosphorylation GO:0006119, respiratory electron transport chain GO:0022904, generation of precursor metabolites and energy GO:0006091, nitrogen compound metabolic process GO:0006807) and two significant components (mitochondrial inner membrane GO:0005743, membrane GO:0016020).

Table 3-8 List of the 14 DEGs shared between all time points.

Ensembl Gene ID	Gene Symbol	Ensembl Gene Info	Log_2 FC		
			6 hrs	24 hrs	48 hrs
ENSG00000128965	CHAC1	ChaC glutathione specific gamma-glutamylcyclotransferase 1	2.209	2.483	2.407
ENSG00000162772	ATF3	activating transcription factor 3	1.915	1.851	2.945
ENSG00000168209	DDIT4	DNA damage inducible transcript 4	1.685	1.531	2.010
ENSG00000198840	ND3	NADH dehydrogenase, subunit 3 (complex I)	1.576	1.064	4.426
ENSG00000198938	COX3	cytochrome c oxidase III	1.564	1.212	3.378
ENSG00000198727	CYTB	cytochrome b	1.564	1.423	3.554
ENSG00000198888	ND1	NADH dehydrogenase, subunit 1 (complex I)	1.476	1.342	3.177
ENSG00000198804	COX1	cytochrome c oxidase subunit I	1.364	1.282	2.080
ENSG00000155961	RAB39B	RAB39B, member RAS oncogene family	1.290	1.309	1.636
ENSG00000198712	COX2	cytochrome c oxidase subunit II	1.287	1.244	3.364
ENSG00000176907	TCIM	transcriptional and immune response regulator	1.186	1.720	2.537
ENSG00000198899	ATP6	ATP synthase F0 subunit 6	1.162	1.087	3.011
ENSG00000248527	MTATP6P1	mitochondrially encoded ATP synthase 6 pseudogene 1	1.149	1.098	3.005
ENSG00000228253	ATP8	ATP synthase F0 subunit 8	1.080	1.190	2.671

Pathway Analysis

The names of all DEGs and their $\log_2$ FC values at all three time points were submitted to Reactome analysis tools (https://reactome.org/PathwayBrowser/#TOOL=AT) to mine pathways affected by all those genes in human cells. The analysis was performed against Reactome version 65 on 14 of August 2018, and cut-off criteria are pathways with entities FDR < 0.01. For the 6 hours gene list, only 221 out of 344 ENSEMBL IDs were found in the Reactome database, where 843 pathways were hit by at least one of them. Only 47 pathways passed the cut-off, and the top 30 pathways are listed in **Table** 3-9 with the most significant pathway at the top. The number of entities or genes found per pathway ranges from 4 to 99. All pathways were down-regulated based on the average $\log_2$ FC of the matched genes (Range of $\log_2$ FC average: -0.192 ~ -1.308). The pathway with the lowest average $\log_2$ FC is R-HSA-8876384 (Listeria monocytogenes entry into host cells; average $\log_2$ FC = -1.308) while the pathway with the most entities found is R-HSA-392499 (Metabolism of proteins) with 99 hits.

Table 3-9 List of top 30 pathways affected by DEGs at 6 h.p.i (Entities FDR < 0.01) sorted with the most significant pathway at the top.

Pathway Identifier	Pathway Name	Entities Found / Total	Average Log_2 FC
R-HSA-975956	Nonsense Mediated Decay (NMD) independent of the Exon Junction Complex (EJC)	45 / 101	-1.204
R-HSA-72689	Formation of a pool of free 40S subunits	45 / 106	-1.204
R-HSA-192823	Viral mRNA Translation	45 / 114	-1.204
R-HSA-1799339	SRP-dependent cotranslational protein targeting to membrane	47 / 121	-1.203
R-HSA-72649	Translation initiation complex formation	24 / 63	-1.258
R-HSA-72706	GTP hydrolysis and joining of the 60S ribosomal subunit	46 / 122	-1.211
R-HSA-927802	Nonsense-Mediated Decay (NMD)	46 / 124	-1.205
R-HSA-975957	Nonsense Mediated Decay (NMD) enhanced by the Exon Junction Complex (EJC)	46 / 124	-1.205
R-HSA-72702	Ribosomal scanning and start codon recognition	24 / 66	-1.258
R-HSA-6791226	Major pathway of rRNA processing in the nucleolus and cytosol	47 / 189	-1.212
R-HSA-72662	Activation of the mRNA upon binding of the cap-binding complex and eIFs, and subsequent binding to 43S	24 / 67	-1.258
R-HSA-156902	Peptide chain elongation	45 / 99	-1.204
R-HSA-72737	Cap-dependent Translation Initiation	46 / 131	-1.211
R-HSA-72613	Eukaryotic Translation Initiation	46 / 131	-1.211
R-HSA-156827	L13a-mediated translational silencing of Ceruloplasmin expression	46 / 118	-1.211
R-HSA-72764	Eukaryotic Translation Termination	45 / 108	-1.204
R-HSA-8868773	rRNA processing in the nucleus and cytosol	47 / 207	-1.212
R-HSA-72766	Translation	53 / 340	-1.199
R-HSA-156842	Eukaryotic Translation Elongation	45 / 104	-1.204
R-HSA-72312	rRNA processing	48 / 245	-1.209
R-HSA-8953854	Metabolism of RNA	66 / 782	-1.223
R-HSA-72695	Formation of the ternary complex, and subsequently, the 43S complex	23 / 54	-1.248
R-HSA-9010553	Regulation of expression of SLITs and ROBOs	48 / 183	-1.202
R-HSA-2408557	Selenocysteine synthesis	45 / 116	-1.204
R-HSA-168273	Influenza Viral RNA Transcription and Replication	49 / 173	-1.233
R-HSA-5663205	Infectious disease	60 / 537	-1.230
R-HSA-168254	Influenza Infection	50 / 197	-1.230
R-HSA-2408522	Selenoamino acid metabolism	47 / 184	-1.207
R-HSA-168255	Influenza Life Cycle	49 / 189	-1.233
R-HSA-376176	Signalling by ROBO receptors	48 / 235	-1.202

At 24 h.p.i, only 41 out of 65 ENSEMBL ID in the sample were found in Reactome, where 150 pathways were hit by at least one of them. Among them, 8 passed the cut-off and are listed in **Table** 3-10. The number of entities or gene found per pathway ranges from 3 to 8 genes and all pathways were up-regulated based on the average log_2 FC of the matched genes (Range of log_2 FC average: 1.231 ~ 1.934). Pathways with the highest average log_2 FCs were R-HSA-380994 (ATF4 activates genes; average log_2 FC = 1.934) and R-HSA-381042 (PERK regulates gene expression; average log_2 FC = 1.934) while pathways with the most entities found were R-HSA-163200 (Respiratory electron transport, ATP synthesis by chemiosmotic coupling, and heat production by uncoupling proteins) and R-HSA-1428517 (The citric acid (TCA) cycle and respiratory electron transport) with 8 hits each.

Table 3-10 List of all eight pathways affected by DEGs at 24 h.p.i (Entities FDR < 0.01) sorted with the most significant pathway at the top.

Pathway Identifier	Pathway Name	Entities Found / Total	Average Log_2 FC
R-HSA-163200	Respiratory electron transport, ATP synthesis by chemiosmotic coupling, and heat production by uncoupling proteins.	8 / 146	1.231
R-HSA-5628897	TP53 Regulates Metabolic Genes	7 / 125	1.370
R-HSA-380994	ATF4 activates genes	4 / 32	1.934
R-HSA-611105	Respiratory electron transport	6 / 115	1.261
R-HSA-1428517	The citric acid (TCA) cycle and respiratory electron transport	8 / 229	1.231
R-HSA-381042	PERK regulates gene expression	4 / 38	1.934
R-HSA-70614	Amino acid synthesis and interconversion (transamination)	5 / 82	1.437
R-HSA-977347	Serine biosynthesis	3 / 26	1.348

At 48 h.p.i, 502 out of 942 identifiers in the sample were found in Reactome, where 1124 pathways were hit by at least one of them. Among them, 39 passed the cut-off and are listed in **Table** 3-11. The number of entities or gene found per pathway ranges from 17 to 101 genes, and all pathways were up-regulated based on the average log_2 FC of the matched genes (Range of log_2 FC average: 0.958 ~ 2.199). The pathway with the highest average log_2 FCs was R-HSA-6783783 (Interleukin-10 signalling; average log_2 FC = 2.199) while pathway with the most entities found was R-HSA-8953854 (Metabolism of RNA) with 101 hits.

Table 3-11 List of top 30 pathways affected by DEGs at 48 h.p.i (Entities FDR < 0.01) sorted with the most significant pathway at the top.

Pathway Identifier	Pathway Name	Entities Found / Total	Average Log_2 FC
R-HSA-975956	Nonsense Mediated Decay (NMD) independent of the Exon Junction Complex (EJC)	65 / 101	1.404
R-HSA-72689	Formation of a pool of free 40S subunits	65 / 106	1.404
R-HSA-1799339	SRP-dependent cotranslational protein targeting to membrane	69 / 121	1.406
R-HSA-192823	Viral mRNA Translation	65 / 114	1.404
R-HSA-156827	L13a-mediated translational silencing of Ceruloplasmin expression	65 / 118	1.404
R-HSA-927802	Nonsense-Mediated Decay (NMD)	67 / 124	1.325
R-HSA-975957	Nonsense Mediated Decay (NMD) enhanced by the Exon Junction Complex (EJC)	67 / 124	1.325
R-HSA-72706	GTP hydrolysis and joining of the 60S ribosomal subunit	65 / 122	1.404
R-HSA-6791226	Major pathway of rRNA processing in the nucleolus and cytosol	69 / 189	1.349
R-HSA-156902	Peptide chain elongation	65 / 99	1.404
R-HSA-156842	Eukaryotic Translation Elongation	66 / 104	1.406
R-HSA-72613	Eukaryotic Translation Initiation	65 / 131	1.404
R-HSA-72764	Eukaryotic Translation Termination	65 / 108	1.404
R-HSA-72737	Cap-dependent Translation Initiation	65 / 131	1.404
R-HSA-8868773	rRNA processing in the nucleus and cytosol	69 / 207	1.349
R-HSA-72766	Translation	82 / 340	1.346
R-HSA-72312	rRNA processing	69 / 245	1.349
R-HSA-72695	Formation of the ternary complex, and subsequently, the 43S complex	31 / 54	1.441
R-HSA-168273	Influenza Viral RNA Transcription and Replication	70 / 173	1.322
R-HSA-9010553	Regulation of expression of SLITs and ROBOs	69 / 183	1.386
R-HSA-2408557	Selenocysteine synthesis	65 / 116	1.404
R-HSA-2408522	Selenoamino acid metabolism	68 / 184	1.403
R-HSA-376176	Signalling by ROBO receptors	73 / 235	1.318
R-HSA-168255	Influenza Life Cycle	70 / 186	1.322
R-HSA-168254	Influenza Infection	71 / 197	1.322
R-HSA-72649	Translation initiation complex formation	31 / 63	1.441
R-HSA-72702	Ribosomal scanning and start codon recognition	31 / 66	1.441
R-HSA-72662	Activation of the mRNA upon binding of the cap-binding complex and eIFs, and subsequent binding to 43S	31 / 67	1.441
R-HSA-163200	Respiratory electron transport, ATP synthesis by chemiosmotic coupling, and heat production by uncoupling proteins.	42 / 146	1.703
R-HSA-611105	Respiratory electron transport	36 / 115	1.711

For all 14 genes expressed at all time points, 12 out of them were found in Reactome, where 28 pathways were hit by at least one of them while only 17 pathways passed the cut-off criteria (Entities FDR < 0.01). From this, it was narrowed down to five pathways (**Table** 3-12) by focusing on pathways with a minimum three identifiers.

Table 3-12 List of all five pathways affected by fourteen DEGs at all time points (Minimum three entities/pathway, entities FDR < 0.01) sorted with the most significant pathway at the top.

Pathway Identifier	Pathway Name	Entities Found / Total	Average Log_2 FC		
			6 hrs	24 hrs	48 hrs
R-HSA-163210	Respiratory electron transport, ATP synthesis by chemiosmotic coupling, and heat production by uncoupling proteins.	8 / 146	1.384	1.231	3.208
R-HSA-8949613	The citric acid (TCA) cycle and respiratory electron transport	8 / 229	1.384	1.231	3.208
R-HSA-380994	Respiratory electron transport	6 / 115	1.472	1.261	3.330
R-HSA-381042	TP53 Regulates Metabolic Genes	5 / 125	1.517	1.360	2.568
R-HSA-6799198	Transcriptional Regulation by TP53	5 / 486	1.517	1.360	2.568

3.4.2 *Transcriptomes Based on mRNA Sequencing: Mapped to T. gondii Reference Genome*

Pre and Post Normalisation Bar Graph

Normalisation greatly reduced the total counts for infected samples at infected_48a and infected_48b samples and slightly reduced the total counts of infected_6a, infected_6b, infected_24a and infected_24b (**Figure** 3-16). There were no counts from control samples at all time points as expected, due to the absence of *T. gondii* parasites.

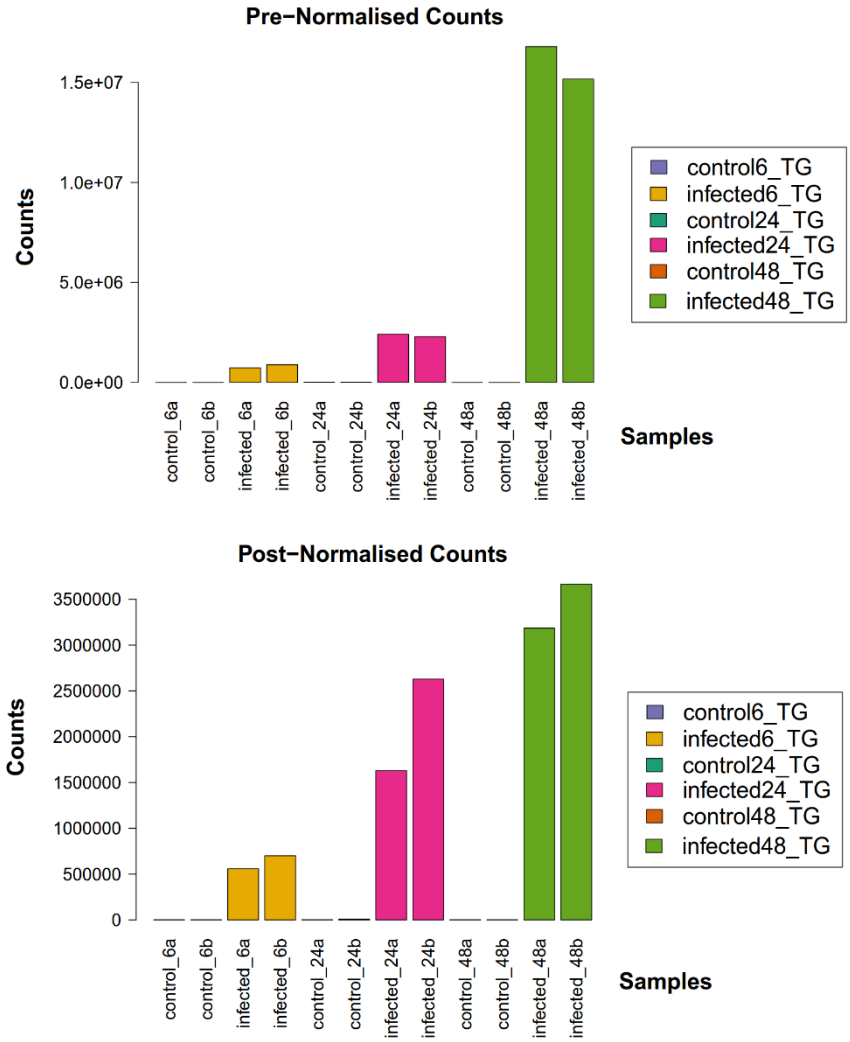


Figure 3-16 Pre and post-normalised counts of mRNA sequencing data after alignment to *T. gondii* ME49 reference genome. The counts were normalised using the size factor normalisation method that normalises for sequencing depth and RNA composition (Anders and Huber, 2010).

Sample Correlation Heatmap

Sample correlation heatmap for mRNA sequencing is shown in **Figure** 3-17. In this heatmap, light green represents low correlation while dark blue represents high correlation. From the figure, control 6 and 48 hours have the same colour tone (very light green) while control 24 hours samples have slightly darker green tone. The infected samples all have the blue tone, but

the tone gets darker as the time point increases from 6 to 48 h.p.i. The contrast between control samples and infected samples is obvious suggesting that the expression profiles between the two conditions were markedly different from each other.

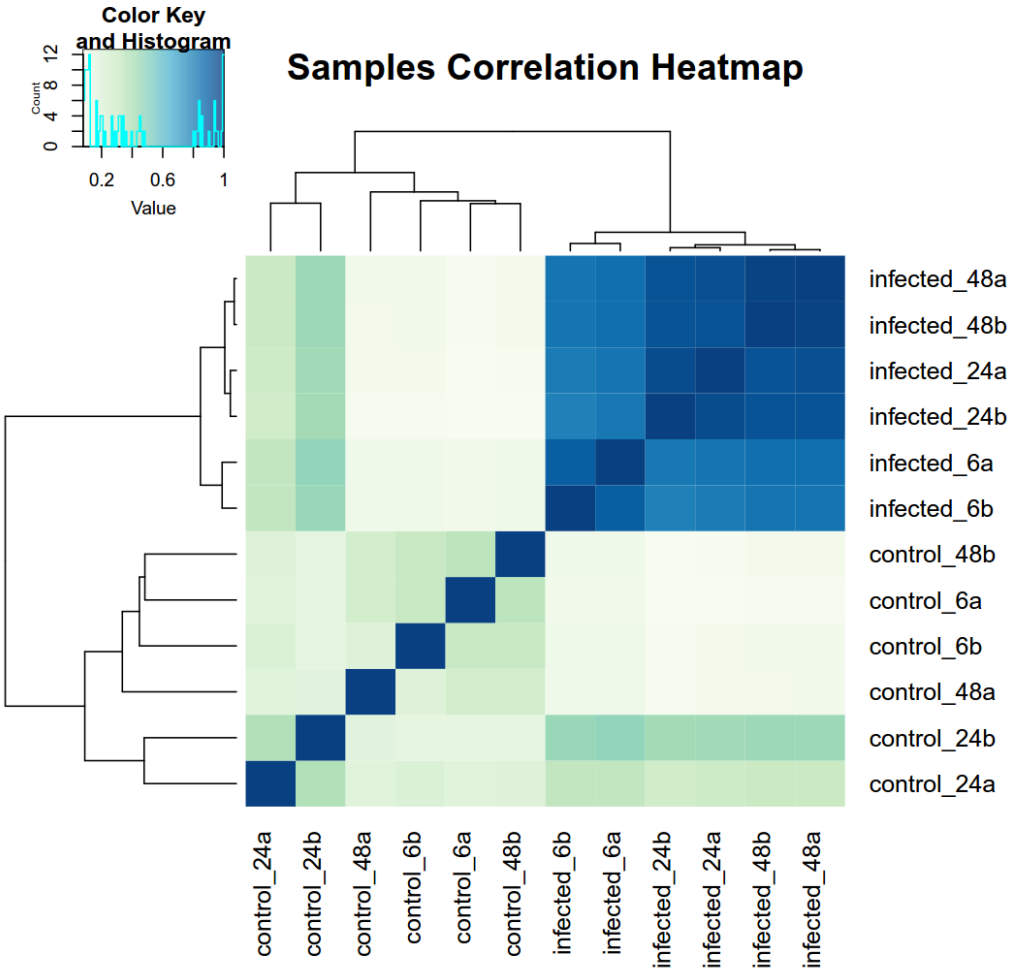


Figure 3-17 Correlation heatmap of all mRNA transcriptome expression profiles after mapping to *T. gondii* reference genome. The heatmap shows a correlation between all samples sent for mRNA sequencing where shades of dark blue and green represent high and low correlation respectively. Dendrograms on the side of the heatmap links closely correlated samples on each row or column to each other. Heatmap showed two distinct clusters where control and infected samples were separated into different clusters and had contrasting colour tones suggesting the expression profiles between control and infected samples were markedly different from each other.

Principal Component Analysis (PCA)

Principal component analysis (PCA) was used visualise data and to detect the variation between samples. PCA analysis was performed on all samples across all groups (**Figure** 3-18). The figure shows samples within each group were positioned close to each other suggesting similar expression profile while between groups, three clusters were form: 1) infected 48 and infected 24 hours, 2) infected 6 hours, and 3) control 6 and 48 hours. Control 24 samples were separated at two different positions suggesting different expression profiles after mapping to *T. gondii* reference genome.

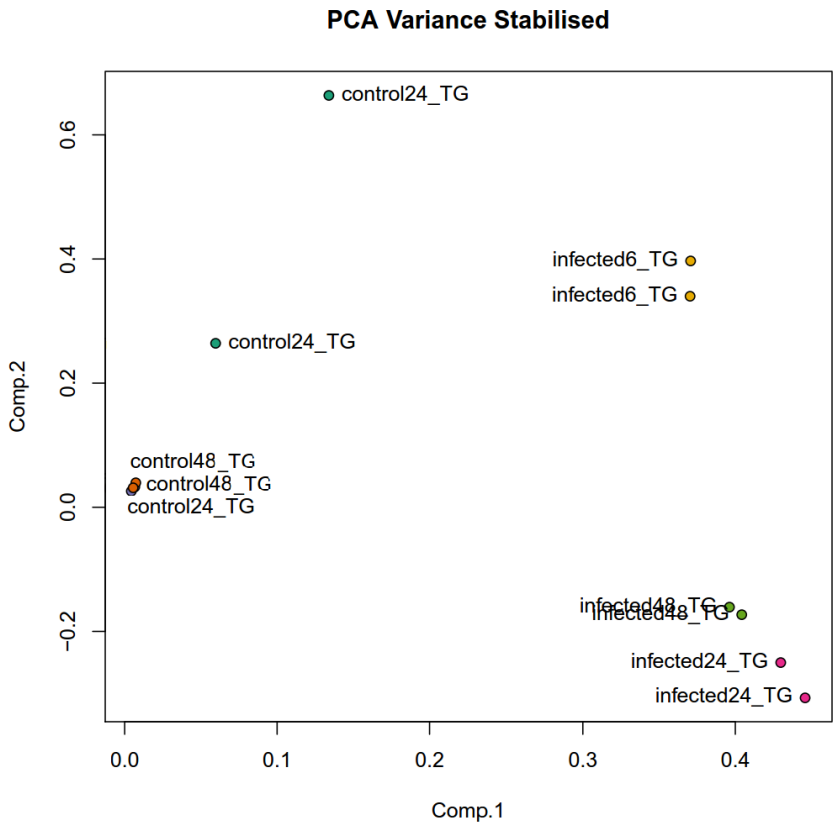


Figure 3-18 Principal component analysis (PCA) plot is showing all samples transcriptome dataset variation. The figure shows samples within each group were in short distance to each except for samples of control 24 hours group. Position wise, there were three clusters form where infected 24- and 48-hours samples in one cluster, control 6 hours and control 48 hours samples in another cluster, and infected 6 hours samples in the third cluster.

Venn Diagram

Overall, small RNA sequencing data matched to 4411, 6116, 6049 genes at 6,24 and 48 hours respectively. Using Venn diagrams, gene lists from 6, 24 and 48 h.p.i were compared in **Figure** 3-19. Common genes of different time points are shown in the central regions where their circles overlapped.

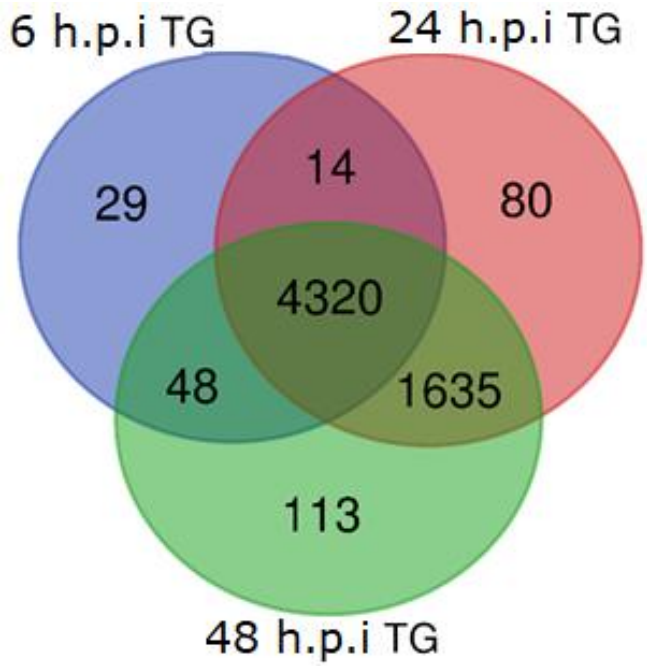


Figure 3-19 Venn diagram of DEGs at 6, 24 and 48 hours from transcriptome reads mapped to *T. gondii* genome. Numbers in the overlapped area represent DEGs shared between groups. The diagram showed that 4320 genes were differentially expressed at all time points.

Toxoplasma gondii Differentially Expressed Genes (DEGs)

After mapping to *T. gondii* reference genome and performing RNA-seq and differential expression data analysis, a very high number of genes were found to be significant as there are no controls that matched to *T. gondii* reference genome compared to counts from infected samples. Problems arise when calculating the $\log_2$ FC of genes (differential expression

analysis) since zero count of control samples will make all genes have infinity $\log_2$ FC (*n* counts of infected samples / zero count from control samples = infinity). DESeq2 solves this by providing a finite estimation of $\log_2$ FC based upon three criteria which are the dispersion/distribution of a given gene, how large the counts are for a given gene, and the distribution of log FCs for other genes which had finite $\log_2$ FC (Love, Huber and Anders, 2014). As there were only data from infected samples up-regulated, it was decided not to display volcano plots as they do not provide meaningful visual information.

DESeq2 estimated the values for all DEGs in the ranges from 0 to 16 $\log_2$ FC. Cut off values were set to genes with $\log_2$ FC ≥ 5, baseMean (average of the normalised count values) ≥ 2000, and significance level of $P < 0.01$. All three contrasts (Control 6 *vs* Infected 6, Control 24 *vs* Infected 24, and Control 48 *vs* Infected 48) produced the same 94 genes ID but with different $\log_2$ FC values. The full list is available at **Appendix** 3-10 (genes and $\log_2$ FC at all time points) and **Appendix** 3-11 (genes and product description) while **Table** 3-12 lists top 30 of them together with their gene name/symbol and description.

Table 3-13 List of 30 highly expressed *T. gondii* genes with ≥ 2000 baseMean counts, $\log_2$ FC ≥ 5 and *P*-value < 0.01 at 6, 24 and 48 h.p.i.

Gene ID	Gene Name or Symbol	Gene Product Description
TGME49_200360	null	hypothetical protein
TGME49_201390	null	hypothetical protein
TGME49_203310	GRA7	dense granule protein GRA7
TGME49_204020	RPL8	ribosomal protein RPL8
TGME49_204530	MIC11	microneme protein MIC11
TGME49_205340	RPS12	ribosomal protein RPS12
TGME49_205700	null	cyclophilin precursor
TGME49_207400	null	hypothetical protein
TGME49_208030	MIC4	microneme protein MIC4
TGME49_209030	ACT1	actin ACT1
TGME49_210408	null	HMG (high mobility group) box domain-containing protein
TGME49_210690	RPS6	ribosomal protein RPS6
TGME49_211680	null	protein disulfide isomerase
TGME49_212270	null	hypothetical protein
TGME49_212290	RPS19	ribosomal protein RPS19
TGME49_213280	SRS25	SAG-related sequence SRS25
TGME49_213350	RPS15	ribosomal protein RPS15
TGME49_213580	null	hypothetical protein
TGME49_214940	null	MIC2-associated protein M2AP
TGME49_215460	RPS24	ribosomal protein RPS24
TGME49_215470	RPL10A	ribosomal protein RPL10A
TGME49_215960	null	hypothetical protein
TGME49_217570	RPS27	ribosomal protein RPS27
TGME49_218260	null	histone H3.3
TGME49_218520	MIC6	microneme protein MIC6
TGME49_220400	ADF	actin depolymerising factor ADF
TGME49_220950	null	hypothetical protein
TGME49_225080	RPS18	ribosomal protein RPS18
TGME49_227280	GRA3	dense granule protein GRA3
TGME49_227360	RPL3	ribosomal protein RPL3

Note: Null = not available

All 94 genes then were subjected to gene ontology enrichment (molecular function, biological process, cellular component) analysis at ToxoDB.org (Gajria *et al.*, 2008). Gene ontology results are listed in **Table** 3-14.

Table 3-14 Gene ontology for all 94 miRNA up-regulated at 6, 24 and 48 h.p.i.

Molecular Function		
GO ID	**GO Term**	**Gene Matched / Background**
GO:0003779	actin binding	2 / 6
GO:0070566	adenylyltransferase activity	2 / 14
GO:0004345	glucose-6-phosphate dehydrogenase activity	1 / 2
GO:0043891	glyceraldehyde-3-phosphate dehydrogenase (NAD(P)+) (phosphorylating) activity	1 / 2
GO:0004365	glyceraldehyde-3-phosphate dehydrogenase (NAD+) (phosphorylating) activity	1 / 2
GO:0004457	lactate dehydrogenase activity	1 / 2
GO:0004459	L-lactate dehydrogenase activity	1 / 2
GO:0050661	NADP binding	2 / 14
GO:0004649	poly(ADP-ribose) glycohydrolase activity	1 / 2
GO:0043022	ribosome binding	1 / 2
GO:0003723	RNA binding	9 / 164
GO:0019843	rRNA binding	2 / 7
GO:0003735	structural constituent of ribosome	36 / 130
GO:0005198	structural molecule activity	36 / 143
GO:0004781	sulfate adenylyltransferase (ATP) activity	2 / 7
GO:0004779	sulfate adenylyltransferase activity	2 / 7
GO:0003746	translation elongation factor activity	3 / 13
GO:0008135	translation factor activity, RNA binding	4 / 41
Biological Process		
GO:0006412	translation	40 / 205
GO:0009058	biosynthetic process	40 / 481
GO:0034641	cellular nitrogen compound metabolic process	40 / 623
Cellular Component		
GO:0005623	cell	71 / 950
GO:0005840	ribosome	36 / 131
GO:0043226	organelle	53 / 559
GO:0005575	cellular component	72 / 1361
GO:0005737	cytoplasm	45 / 495
GO:0005622	intracellular	48 / 849
GO:0005576	extracellular region	12 / 46
GO:0005886	plasma membrane	6 / 42

All 94 genes then were also subjected to pathway analysis at ToxoDB.org (Gajria *et al.*, 2008). Pathway analysis returned 32 pathways listed in **Table** 3-15.

Table 3-15 List of pathways associated with 94 up-regulated *T. gondii* genes (*P*-value < 0.05).

Pathway ID (Database)	Pathway Name	Genes Matched / Background
P122-PWY (MetaCyc)	heterolactic fermentation	3 / 16
PWY-6901 (MetaCyc)	superpathway of glucose and xylose degradation	3 / 19
DISSULFRED-PWY (MetaCyc)	sulfate reduction IV (dissimilatory, to hydrogen sufide))	2 / 9
SULFMETII-PWY (MetaCyc)	sulfate reduction II (assimilatory)	2 / 9
PWY-5278 (MetaCyc)	sulfite oxidation III	2 / 9
PWY-5306 (MetaCyc)	superpathway of thiosulfate metabolism (*Desulfovibrio sulfodismutans*)	2 / 9
SO4ASSIM-PWY (MetaCyc)	sulfate reduction I (assimilatory)	2 / 9
PWY-5340 (MetaCyc)	sulfate activation for sulfonation	2 / 9
PWY-6932 (MetaCyc)	selenate reduction	2 / 9
PWY-6683 (MetaCyc)	sulfate reduction III (assimilatory)	2 / 9
P224-PWY (MetaCyc)	sulfate reduction V (dissimilatory, to thiosulfate)	2 / 9
PWY-5308 (MetaCyc)	superpathway of sulfur metabolism (*Desulfocapsa sulfoexigens*)	2 / 9
PWY-6676 (MetaCyc)	superpathway of sulfide oxidation (phototrophic sulfur bacteria)	2 / 10
PWY-821 (MetaCyc)	superpathway of sulfur amino acid biosynthesis (*Saccharomyces cerevisiae*)	2 / 12
PWY-5345 (MetaCyc)	superpathway of L-methionine biosynthesis (by sulfhydrylation)	2 / 13
SULFATE-CYS-PWY (MetaCyc)	superpathway of sulfate assimilation and cysteine biosynthesis	2 / 14
PWY-6395 (MetaCyc)	superpathway of seleno-compound metabolism	2 / 16
P124-PWY (MetaCyc)	Bifidobacterium shunt	2 / 17
ANAEROFRUCAT-PWY (MetaCyc)	homolactic fermentation	2 / 19
GLYCOLYSIS-E-D (MetaCyc)	superpathway of glycolysis and Entner-Doudoroff	2 / 19
P461-PWY (MetaCyc)	hexitol fermentation to lactate, formate, ethanol and acetate	2 / 19
ec00920 (KEGG)	Sulfur metabolism	2 / 21
PWY-7345 (MetaCyc)	superpathway of anaerobic sucrose degradation	2 / 22
PWY-5100 (MetaCyc)	pyruvate fermentation to acetate and lactate II	1 / 3
PWY-5481 (MetaCyc)	pyruvate fermentation to lactate	1 / 3
RUMP-PWY (MetaCyc)	formaldehyde oxidation I	1 / 3
ec00010 (KEGG)	Glycolysis / Gluconeogenesis	2 / 37
P41-PWY (MetaCyc)	pyruvate fermentation to acetate and lactate I	1 / 4
OXIDATIVEPENT-PWY (MetaCyc)	pentose phosphate pathway (oxidative branch) I	1 / 4

ec00450 (KEGG)	Selenocompound metabolism	2 / 51
PWY-7268 (MetaCyc)	NAD/NADP-NADH/NADPH cytosolic interconversion (yeast)	1 / 7
PENTOSE-P-PWY (MetaCyc)	pentose phosphate pathway	1 / 8

3.4.3 *Transcriptomes Based on miRNA: Mapped to Human Reference Genome*

The percentage of mapped reads to the human genome and miRbase database for control and infected groups are listed in **Table** 3-16 and **Table** 3-17.

Table 3-16 The percentage of sequenced reads mapped to the human genome.

Time	Treatment	Total Reads	Average Mapping %
6 h.p.i	Control	16890581	43.70 ± 2.71
	Infected	22939324	35.87 ± 0.81
24 h.p.i	Control	27641529	30.91 ± 12.63
	Infected	22364289	25.91 ± 12.48
48 h.p.i	Control	29105617	64.20 ± 0.61
	Infected	18359478	25.45 ± 5.84

Table 3-17 The percentage of sequenced reads mapped to the miRBase database.

Time	Treatment	Average Mapping on Precursor/ miRNA (%)	Average Mapping on miRNA only (%)
6 h.p.i	Control	23.67 ± 1.15	23.60 ± 1.15
	Infected	15.56 ± 0.34	15.49 ± 0.34
24 h.p.i	Control	23.69 ± 9.19	23.65 ± 9.19
	Infected	17.24 ± 8.02	17.20 ± 8.02
48 h.p.i	Control	60.69 ± 0.65	60.67 ± 0.65
	Infected	5.19 ± 1.49	5.15 ± 1.48

There are no miRNAs that passed the cut-off criteria at 24 h.p.i. In contrast, 36 miRNAs were differentially regulated at 6 hours with 31 of them

were down-regulated, and the rest were down-regulated. **Table** 3-18 and **Table** 3-19 list all up-regulated and down-regulated miRNAs at 6 h.p.i respectively. Some miRNAs are repeated in the list because they were derived from different precursors.

Table 3-18 List of all 31 up-regulated miRNAs at 6 hours sorted with the most significant on top. Filtering criteria were miRNAs with ≥ 1 log_2 FC and with adjusted *P*-value < 0.01. Out of these 31 miRNAs listed, 4 miRNAs (has-let-7a-3p, has-miR-19b-3p, has-miR-26a-5p, has-miR-30c-5p) were repeated twice while one miRNA (has-let-7a-5p) was repeated thrice because they have different precursors. Meanwhile, two precursors, hsa-let-7a-1 and hsa-let-7a-3, were the source of five miRNAs that were highly up-regulated. Therefore, a condensed list would result in 29 precursors producing 25 individually unique miRNAs.

Precursor	miRNA	Log_2 FC
hsa-let-7a-1	hsa-let-7a-3p	1.382
hsa-let-7a-3	hsa-let-7a-3p	1.376
hsa-let-7a-1	hsa-let-7a-5p	1.14
hsa-let-7a-3	hsa-let-7a-5p	1.14
hsa-let-7a-2	hsa-let-7a-5p	1.139
hsa-let-7d	hsa-let-7d-5p	1.054
hsa-let-7f-2	hsa-let-7f-2-3p	1.049
hsa-mir-125a	hsa-miR-125a-5p	1.149
hsa-mir-130b	hsa-miR-130b-5p	1.379
hsa-mir-140	hsa-miR-140-5p	1.078
hsa-mir-16-2	hsa-miR-16-2-3p	1.018
hsa-mir-19b-1	hsa-miR-19b-3p	1.135
hsa-mir-19b-2	hsa-miR-19b-3p	1.133
hsa-mir-20a	hsa-miR-20a-5p	1.04
hsa-mir-20b	hsa-miR-20b-5p	1.392
hsa-mir-221	hsa-miR-221-5p	1.105
hsa-mir-222	hsa-miR-222-3p	1.019
hsa-mir-26a-1	hsa-miR-26a-5p	1.027
hsa-mir-26a-2	hsa-miR-26a-5p	1.027
hsa-mir-26b	hsa-miR-26b-5p	1.28
hsa-mir-30c-1	hsa-miR-30c-5p	1.189
hsa-mir-30c-2	hsa-miR-30c-5p	1.189
hsa-mir-3691	hsa-miR-3691-5p	2.075
hsa-mir-374a	hsa-miR-374a-3p	1.248
hsa-mir-429	hsa-miR-429	1.108
hsa-mir-548am	hsa-miR-548am-3p	1.101
hsa-mir-660	hsa-miR-660-5p	1.287
hsa-mir-98	hsa-miR-98-5p	1.029
hsa-mir-19a	hsa-miR-19a-3p	1.483
hsa-mir-424	hsa-miR-424-3p	1.277
hsa-mir-454	hsa-miR-454-5p	1.192

Note: Greyed/ coloured boxes highlighted similar miRNA/ similar precursor.

Table 3-19 List of all five down-regulated miRNAs at 6 hours sorted with the lowest log_2 FC on top. Filtering criteria were miRNAs with ≤ -1 log_2 FC and with adjusted *P*-value < 0.01. All five miRNAs were derived from different precursors.

Precursor	miRNA	Log_2 FC
hsa-mir-204	hsa-miR-204-5p	-6.088
hsa-mir-375	hsa-miR-375	-2.945
hsa-mir-4788	hsa-miR-4788	-2.795
hsa-mir-1246	hsa-miR-1246	-1.421
hsa-mir-3976	hsa-miR-3976	-1.372

At 48 hours after infection, 531 miRNAs were up-regulated while 15 miRNAs were down-regulated. The top 30 up-regulated miRNAs are listed in **Table** 3-20 while all down-regulated miRNAs are listed in **Table** 3-21. In the up-regulated list, one miRNA was repeated 5 times (hsa-miR-941), 4 miRNAs were repeated 4 times (hsa-miR-3179, hsa-miR-548f-3p, hsa-miR-548i, hsa-miR-6724-5p), 5 miRNAs were repeated 3 times (hsa-let-7a-5p, hsa-miR-550a-3p, hsa-miR-5701, hsa-miR-7-5p, hsa-miR-9-5p), and 36 miRNAs were repeated twice as they were derived from different precursors. Meanwhile, 125 precursors were found to be the source of two different miRNAs. This essentially condenses the list to 469 individually unique miRNAs and 406 unique precursors. In the down-regulated list, one precursor hsa-miR-4485 produced two different miRNAs which are hsa-miR-4485-5p and has-miR-4485-3p where both were highly down-regulated at 48 hours.

Table 3-20 List of top 30 out of 531 up-regulated miRNAs at 48 hours. Filtering criteria were miRNAs with ≥ 1 log_2 FC and with adjusted *P*-value < 0.01. The full list is available in **Appendix** 3-12.

Precursor	miRNA	Log2 FC
hsa-mir-1277	hsa-miR-1277-5p	5.761
hsa-mir-561	hsa-miR-561-5p	5.335
hsa-mir-548u	hsa-miR-548u	5.087
hsa-mir-548e	hsa-miR-548e-3p	5.031
hsa-mir-191	hsa-miR-191-3p	5.023
hsa-mir-19a	hsa-miR-19a-3p	5.013
hsa-mir-3662	hsa-miR-3662	4.954
hsa-mir-4470	hsa-miR-4470	4.944
hsa-mir-3144	hsa-miR-3144-3p	4.899
hsa-mir-590	hsa-miR-590-3p	4.873
hsa-mir-374b	hsa-miR-374b-5p	4.873
hsa-mir-5582	hsa-miR-5582-3p	4.834
hsa-mir-148b	hsa-miR-148b-5p	4.825
hsa-mir-1306	hsa-miR-1306-5p	4.818
hsa-mir-500b	hsa-miR-500b-3p	4.811
hsa-mir-3613	hsa-miR-3613-5p	4.804
hsa-mir-301b	hsa-miR-301b-3p	4.79
hsa-mir-137	hsa-miR-137	4.607
hsa-mir-548ah	hsa-miR-548ah-3p	4.591
hsa-mir-3130-2	hsa-miR-3130-5p	4.585
hsa-mir-199b	hsa-miR-199b-5p	4.562
hsa-mir-4775	hsa-miR-4775	4.535
hsa-mir-5010	hsa-miR-5010-3p	4.53
hsa-mir-1261	hsa-miR-1261	4.523
hsa-mir-4755	hsa-miR-4755-5p	4.494
hsa-mir-1255a	hsa-miR-1255a	4.432
hsa-mir-99a	hsa-miR-99a-3p	4.427
hsa-mir-374a	hsa-miR-374a-3p	4.42
hsa-mir-548j	hsa-miR-548j-5p	4.364
hsa-mir-4677	hsa-miR-4677-3p	4.363

Table 3-21 List of all 15 down-regulated miRNAs at 48 hours. Filtering criteria were miRNAs with ≤ -1 log_2 FC and with adjusted *P*-value < 0.01. One precursor, hsa-miR-4485 produced two different miRNAs which are hsa-miR-4485-5p and has-miR-4485-3p where both were highly down-regulated at 48 hours.

Precursor	miRNA	log_2 FC
hsa-mir-4485	hsa-miR-4485-5p	-6.326
hsa-mir-4485	hsa-miR-4485-3p	-6.225
hsa-mir-4463	hsa-miR-4463	-6.035
hsa-mir-204	hsa-miR-204-5p	-5.017
hsa-mir-4284	hsa-miR-4284	-4.604
hsa-mir-6723	hsa-miR-6723-5p	-4.175
hsa-mir-1973	hsa-miR-1973	-3.045
hsa-mir-4449	hsa-miR-4449	-2.819
hsa-mir-1290	hsa-miR-1290	-2.653
hsa-mir-4461	hsa-miR-4461	-2.36
hsa-mir-375	hsa-miR-375	-2.063
hsa-mir-143	hsa-miR-143-3p	-1.936
hsa-mir-1246	hsa-miR-1246	-1.624
hsa-mir-4497	hsa-miR-4497	-1.617
hsa-mir-4792	hsa-miR-4792	-1.114

Note: Light blue box highlights the same precursor.

Figure 3-20 compares up-regulated miRNAs and precursors at 6 and 48 h.p.i. The result highlights 24 similar miRNAs and 28 similar precursors which are listed in **Table** 3-22.

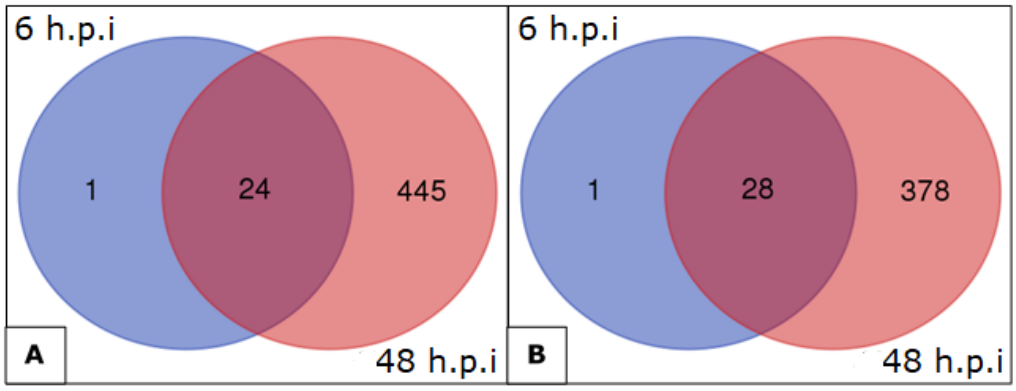


Figure 3-20 Venn diagram comparing up-regulated miRNAs (panel A) and precursors (panel B) at 6 and 48 h.p.i. The number of common miRNAs and precursors are shown in the central overlapping region. All 24 miRNAs shared between 6 and 48 hours are listed in **Table 3-22**.

Table 3-22 List of all 24 up-regulated plus three down-regulated miRNAs shared between 6 and 48 h.p.i. The list is sorted with the absolute difference on top.

Overlapping miRNAs	**Log_2 FC**		
	6 hrs	48 hrs	Absolute Difference
hsa-miR-19b-3p	1.135	5.127	3.992
hsa-miR-19a-3p	1.483	5.013	3.53
hsa-miR-140-5p	1.078	4.313	3.235
hsa-miR-429	1.108	4.333	3.225
hsa-miR-374a-3p	1.248	4.420	3.172
hsa-miR-130b-5p	1.379	4.544	3.165
hsa-miR-548am-3p	1.101	4.175	3.074
hsa-miR-16-2-3p	1.018	4.081	3.063
hsa-miR-454-5p	1.192	4.209	3.017
hsa-miR-221-5p	1.105	4.118	3.013
hsa-miR-26a-5p	1.027	3.870	2.843
hsa-let-7f-2-3p	1.049	3.840	2.791
hsa-miR-125a-5p	1.149	3.937	2.788
hsa-miR-20a-5p	1.04	3.796	2.756
hsa-miR-30c-5p	1.189	3.886	2.697
hsa-miR-424-3p	1.277	3.899	2.622
hsa-miR-660-5p	1.287	3.895	2.608
hsa-miR-20b-5p	1.392	3.997	2.605
hsa-let-7a-3p	1.382	3.978	2.596
hsa-miR-222-3p	1.019	3.569	2.55

hsa-miR-26b-5p	1.28	3.645	2.365
hsa-miR-98-5p	1.029	3.333	2.304
hsa-let-7d-5p	1.054	2.982	1.928
hsa-let-7a-5p	1.14	2.644	1.504
hsa-miR-204-5p	-6.088	-5.017	1.071
hsa-miR-375	-2.945	-2.063	0.882
hsa-miR-1246	-1.421	-1.624	0.203

Note: Greyed box highlighted shared down-regulated miRNAs.

Figure 3-21 compares down-regulated miRNAs and precursors at 6 and 48 h.p.i. The result highlights three similar miRNAs which are hsa-miR-1246, hsa-miR-204-5p, and hsa-miR-375 and three similar precursors which are hsa-mir-375, hsa-mir-1246, and hsa-mir-204.

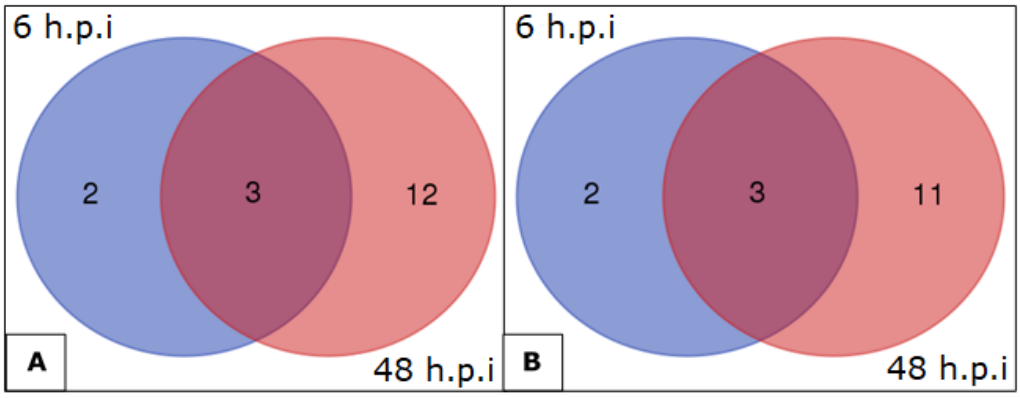


Figure 3-21 Venn diagram comparing down-regulated miRNAs (panel A) and precursors (panel B) at 6 and 48 h.p.i. The number of common miRNAs and precursors are shown in the central overlapping region.

DIANA – mirpath v.3 Analysis

DIANA-mirPath v.3 analysis of 25 unique up-regulated miRNAs from **Table** 3-18 using the genes intersection method (minimum three miRNAs / pathway) produced 58 related pathways (*P*-value < 0.05) while analysis by the pathway union method returned 25 related pathways (*P*-value < 0.05). **Table** 3-23 lists 23 pathways found in both lists.

Table 3-23 Consensus pathways from priori – genes intersection and posteriori – pathway/categories union methods associated with up-regulated miRNAs at 6 h.p.i. The list was sorted with the highest number of miRNAs matched from posteriori – pathway union method.

KEGG Pathway Name	No. of miRNA Matched	
	Genes Intersection	Pathway Union
Signalling pathways regulating pluripotency of stem cells (hsa04550)	25	11
TGF-beta signalling pathway (hsa04350)	18	9
Glycosaminoglycan biosynthesis - chondroitin sulfate / dermatan sulfate (hsa00532)	8	8
Axon guidance (hsa04360)	22	7
ECM-receptor interaction (hsa04512)	17	7
Proteoglycans in cancer (hsa05205)	24	7
FoxO signalling pathway (hsa04068)	24	6
Glutamatergic synapse (hsa04724)	24	6
Glycosphingolipid biosynthesis - lacto and neolacto series (hsa00601)	15	6
Wnt signalling pathway (hsa04310)	22	6
Prolactin signalling pathway (hsa04917)	23	5
Renal cell carcinoma (hsa05211)	24	5
Transcriptional misregulation in cancer (hsa05202)	24	5
Adherens junction (hsa04520)	20	4
Arrhythmogenic right ventricular cardiomyopathy (ARVC) (hsa05412)	21	4
Hippo signalling pathway (hsa04390)	19	4
mTOR signalling pathway (hsa04150)	24	4
ErbB signalling pathway (hsa04012)	22	3
Estrogen signalling pathway (hsa04915)	24	3
Glioma (hsa05214)	24	3
MAPK signalling pathway (hsa04010)	25	3
Rap1 signalling pathway (hsa04015)	25	3

Five miRNAs from the down-regulated genes at 6 h.p.i were associated with cell adhesion molecules/CAMs (hsa04514; three miRNAs), amphetamine addiction (hsa05031; three miRNAs) and nicotine addiction (hsa05033; three miRNAs) pathways from priori - genes intersection method. The posteriori - pathway union method matched to three different pathways which are biotin metabolism (hsa00780; one miRNA), estrogen signalling pathway (hsa04915; one miRNA) and fatty acid degradation (hsa00071; one miRNA) pathways though only one miRNA was

associated with each pathway. As such, the pathway union result was dismissed, and only the genes intersection result was discussed.

Of 469 unique miRNAs at 48 h.p.i, only the top 100 highly up-regulated miRNAs were analysed using DIANA-mirPath v.3 as that is the limit of the web tools. The genes intersection methods (minimum three miRNAs/pathway, *P*-value < 0.05) returns 64 associated KEGG pathways while the pathway union method returns 168 associated KEGG pathways (*P*-value < 0.05). Consensus pathways from these two methods consist of 64 pathways available in **Appendix** 3-13. The top thirty pathways are listed in **Table** 3-24.

The genes intersection method of down-regulated miRNAs list returns two associated KEGG pathways which are 'thyroid hormone signalling pathway' (hsa04919; five miRNAs) and 'lysine degradation' (hsa00310; five miRNAs). The pathways union method also returns the same number but different pathways which are 'cell adhesion molecules/CAMs' (hsa04514; three miRNAs) and 'ECM-receptor interaction' (hsa04512; two miRNAs).

Table 3-24 Consensus pathway from priori – genes intersection and posteriori – pathway/categories union methods associated with up-regulated miRNAs at 48 h.p.i. The list was sorted with the highest number of miRNAs matched from posteriori – pathway union method.

KEGG Pathway Name	No. of miRNA Matched	
	Genes Intersection	Pathway Union
TGF-beta signalling pathway (hsa04350)	30	81
Signalling pathways regulating pluripotency of stem cells (hsa04550)	28	90
Hippo signalling pathway (hsa04390)	27	88
Morphine addiction (hsa05032)	25	84
Proteoglycans in cancer (hsa05205)	24	89
Mucin type O-Glycan biosynthesis (hsa00512)	22	50
FoxO signalling pathway (hsa04068)	20	84
Glioma (hsa05214)	18	78
Axon guidance (hsa04360)	17	80
Lysine degradation (hsa00310)	17	72
Phosphatidylinositol signalling system (hsa04070)	17	73
Circadian rhythm (hsa04710)	16	68
Estrogen signalling pathway (hsa04915)	15	85
Adherens junction (hsa04520)	14	73
ErbB signalling pathway (hsa04012)	14	79
Gap junction (hsa04540)	14	84
Thyroid hormone signalling pathway (hsa04919)	14	81
GABAergic synapse (hsa04727)	13	80
Glutamatergic synapse (hsa04724)	13	86
Wnt signalling pathway (hsa04310)	12	88
Prolactin signalling pathway (hsa04917)	11	74
Ubiquitin mediated proteolysis (hsa04120)	11	88
Dorso-ventral axis formation (hsa04320)	10	63
Melanoma (hsa05218)	10	80
mTOR signalling pathway (hsa04150)	10	77
Ras signalling pathway (hsa04014)	10	92
Transcriptional misregulation in cancer (hsa05202)	10	86
Arrhythmogenic right ventricular cardiomyopathy (ARVC) (hsa05412)	9	68
cGMP-PKG signalling pathway (hsa04022)	9	87
Choline metabolism in cancer (hsa05231)	9	82

3.4.4 *Transcriptomes Based on miRNA: Mapped to T. gondii Reference Genome*

Small RNA sequencing produced 90,634,741 of total reads. Of these, only 16,472,250 were mapped to the *T. gondii* reference genome. The percentage of reads mapped to the *T. gondii* genome for control and infected groups are listed in **Table** 3-25.

Table 3-25 The percentage of sequenced reads mapped to the *T. gondii* genome.

Time	Treatment	Total Reads	Average Mapping %
6 h.p.i	Control	13,709,486	5.35 ± 0.99
	Infected	14,805,276	14.05 ± 1.60
24 h.p.i	Control	15,736,686	11.74 ± 4.48
	Infected	11,555,051	26.61 ± 2.19
48 h.p.i	Control	23,234,454	4.35 ± 0.08
	Infected	11,593,788	65.07 ± 14.68

There was no database cataloguing *T. gondii* miRNA that can be used to BLAST all mapped reads even at the ToxoDB.org database. Reads mapped annotated to the *T. gondii* genome were filtered by applying minimum cut-off FPKM values of ≥ 2000 (in infected samples) and *P*-values ≤ 0.01. At 6 h.p.i, 116 genes passed the selection criteria (**Appendix** 3-14). Among them, 58 are ribosomal RNA (18S, 1; 28S, 7; 5.8S, 50), one is ribosomal protein L36 and the rest, 57 are transfer-RNA (tRNA) for amino acids. Transfer RNA (tRNA) for glutamic acid (10), valine (8) and isoleucine (6) were the top three most abundant tRNA. The pathway analysis and gene ontology at ToxoDB.org did not return any significant results ($P < 0.05$).

Meanwhile, at 24 h.p.i, 138 genes passed the selection criteria (**Appendix** 3-15). Among them, 62 are ribosomal RNA (18S, 4; 28S, 6; 5.8S, 52), four ribosomal protein L36 and the rest, 62 are transfer-RNA (tRNA) for amino acids. Transfer RNA (tRNA) for glutamic acid (10), valine

(8) and aspartic acid (7) were the top three most abundant tRNA. The pathway analysis did not return any significant results ($P < 0.05$). Gene ontology returns 25 biological processes (**Table** 3-26), two molecular functions (structural constituent of ribosome GO:0003735, structural molecule activity GO:0005198) and 15 cellular components (**Table** 3-26). All of gene ontology results were based on only four genes which are TGME49_302055 (ribosomal protein S12), TGME49_300604 (ribosomal protein L36), TGME49_3006 (ribosomal protein L16, putative) and TGME49_300611 (ribosomal protein L14).

Table 3-26 Gene Ontology of 138 genes at 24 h.p.i.

GO ID	Biological Process	GO ID	Biological Process
GO:0043604	amide biosynthetic process	GO:0043170	macromolecule metabolic process
GO:0009058	biosynthetic process	GO:0008152	metabolic process
GO:0043603	cellular amide metabolic process	GO:0006807	nitrogen compound metabolic process
GO:0044249	cellular biosynthetic process	GO:1901576	organic substance biosynthetic process
GO:0034645	cellular macromolecule biosynthetic process	GO:0071704	organic substance metabolic process
GO:0044260	cellular macromolecule metabolic process	GO:1901566	organonitrogen compound biosynthetic process
GO:0044237	cellular metabolic process	GO:1901564	organonitrogen compound metabolic process
GO:0044271	cellular nitrogen compound biosynthetic process	GO:0043043	peptide biosynthetic process
GO:0034641	cellular nitrogen compound metabolic process	GO:0006518	peptide metabolic process
GO:0009987	cellular process	GO:0044238	primary metabolic process
GO:0044267	cellular protein metabolic process	GO:0019538	protein metabolic process
GO:0010467	gene expression	GO:0006412	translation
GO:0009059	macromolecule biosynthetic process		

GO ID	Cellular Compartment	GO ID	Cellular Compartment
GO:0005623	cell	GO:0043229	intracellular organelle
GO:0044464	cell part	GO:0044424	intracellular part
GO:0005575	cellular component	GO:0032991	macromolecular complex
GO:0005737	cytoplasm	GO:0043228	non-membrane-bounded organelle
GO:0044444	cytoplasmic part	GO:0043226	organelle
GO:0005622	intracellular	GO:0030529	ribonucleoprotein complex
GO:0043232	intracellular non-membrane-bounded organelle	GO:0005840	ribosome

At 48 h.p.i, 164 genes passed the selection criteria (**Appendix** 3-16). Among them, 81 are ribosomal RNA (18S, 4; 28S, 8; 5.8S, 69), two ribosomal protein L36 (TGME49_300604) and ribosomal protein S12 (TGME49_302055), 79 transfer-RNA (tRNA) for amino acids, one chaperone caseinolytic protease (TGME49_302000) and one unknown protein (TGME49_321685). The three most common tRNA are tRNA-Glu (glutamic acid, 9), tRNA-Val (valine, 7) and tRNA-Ile (isoleucine, 6). The pathway analysis did not return any significant results ($P < 0.05$). The gene ontology analysis returns 14 biological processes (**Table** 3-27), two molecular functions (structural constituent of ribosome GO:0003735, structural molecule activity GO:0005198) and nine cellular components (**Table** 3-27). All of gene ontology results were based on only two genes which are TGME49_300604 (ribosomal protein L36) and TGME49_302055 (ribosomal protein S12).

Table 3-27 Gene ontology of 164 genes at 48 h.p.i

GO ID	Biological Process
GO:0006412	translation
GO:0043043	peptide biosynthetic process
GO:0006518	peptide metabolic process
GO:0043604	amide biosynthetic process
GO:0043603	cellular amide metabolic process
GO:1901566	organonitrogen compound biosynthetic process
GO:0034645	cellular macromolecule biosynthetic process
GO:0009059	macromolecule biosynthetic process
GO:0044271	cellular nitrogen compound biosynthetic process
GO:0010467	gene expression
GO:1901564	organonitrogen compound metabolic process
GO:0044249	cellular biosynthetic process
GO:1901576	organic substance biosynthetic process
GO:0009058	biosynthetic process
GO ID	**Cellular Compartment**
GO:0005840	ribosome
GO:0030529	ribonucleoprotein complex
GO:0015935	small ribosomal subunit
GO:0043228	non-membrane-bounded organelle
GO:0043232	intracellular non-membrane-bounded organelle
GO:0044391	ribosomal subunit
GO:0044444	cytoplasmic part
GO:0032991	macromolecular complex
GO:0005737	cytoplasm

Genes matched to transcriptome data at 6, 24 and 48 h.p.i were compared using a Venn diagram (**Figure** 3-22). There were 86 similar genes differentially expressed at all time points.

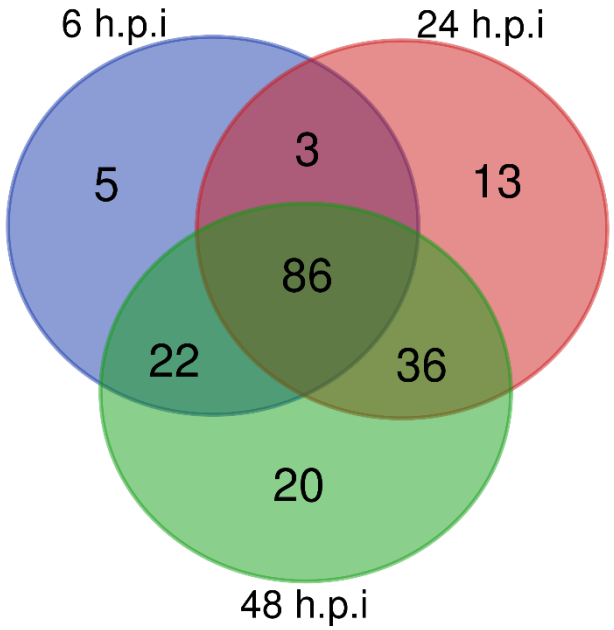


Figure 3-22 Venn Diagram of DEGs at 6, 24 and 48 h.p.i based on mapping to *T. gondii* reference genome. Comparison highlighted 86 genes differentially expressed at all time points

Among the 86 genes expressed at all time points (**Appendix** 3-17), 40 are ribosomal RNA (18S, 1; 28S, 3; 5.8S, 38), one ribosomal protein L36 (TGME49_300604), and 45 transfer-RNA (tRNA) for amino acids. The three most common tRNA are tRNA-Glu (glutamic acid, 9), tRNA-Val (valine, 7) and tRNA-Ile (isoleucine, 6). None of these genes are involved in pathways while molecular function and cellular component are only limited to ribosomal activity and ribosome complex. No biological process is associated with these groups of genes.

3.4.5 *Transcriptomes Based on Microarray Data*

Pre-and Post-Normalisation Box Plot

As shown in **Figure** 3-23, the distributions of all samples' median values were not uniform before normalisation which might lead to under or over-estimated expression when comparing between samples. As such normalisation is required and the common normalisation method for microarray study is robust multi-array average or RMA (Irizarry *et al.*, 2003). RMA normalisation was found to be sensitive for low expression values, consistent fold-change estimates, and excellent background adjustment compare to MAS 5.0 and dChip normalisation methods (Irizarry *et al.*, 2003). Following normalisation, the data become more uniform as can be seen from the median values of all samples (**Figure** 3-23).

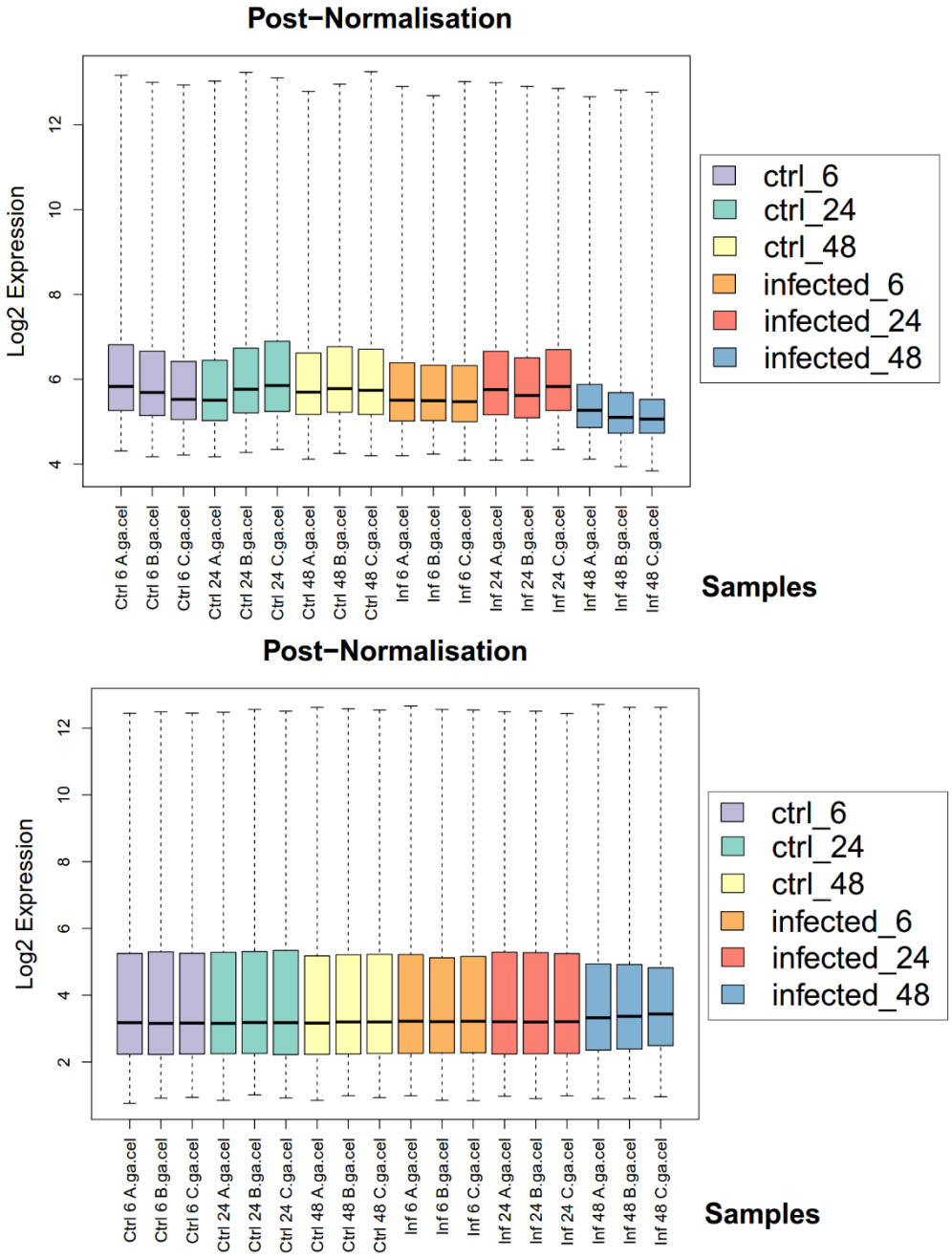


Figure 3-23 Box plots of expressed genes of all samples pre and post-normalisation of microarray samples. The samples were normalised using widely used robust multiarray average (RMA) method that considers background correction and variation between chipset (Irizarry *et al.*, 2003).

Sample Correlation Heatmap

In **Figure** 3-24 heatmap, light green represents low correlation while dark blue represents high correlation. Samples, either infected or control samples, within the same time points can be seen to have similar tone colour except for control samples at 48 hours and infected samples at 48 hours which have very low correlation based on the heatmap. This indicates that the expression profile of control samples is vastly different that infected samples at 48 hours.

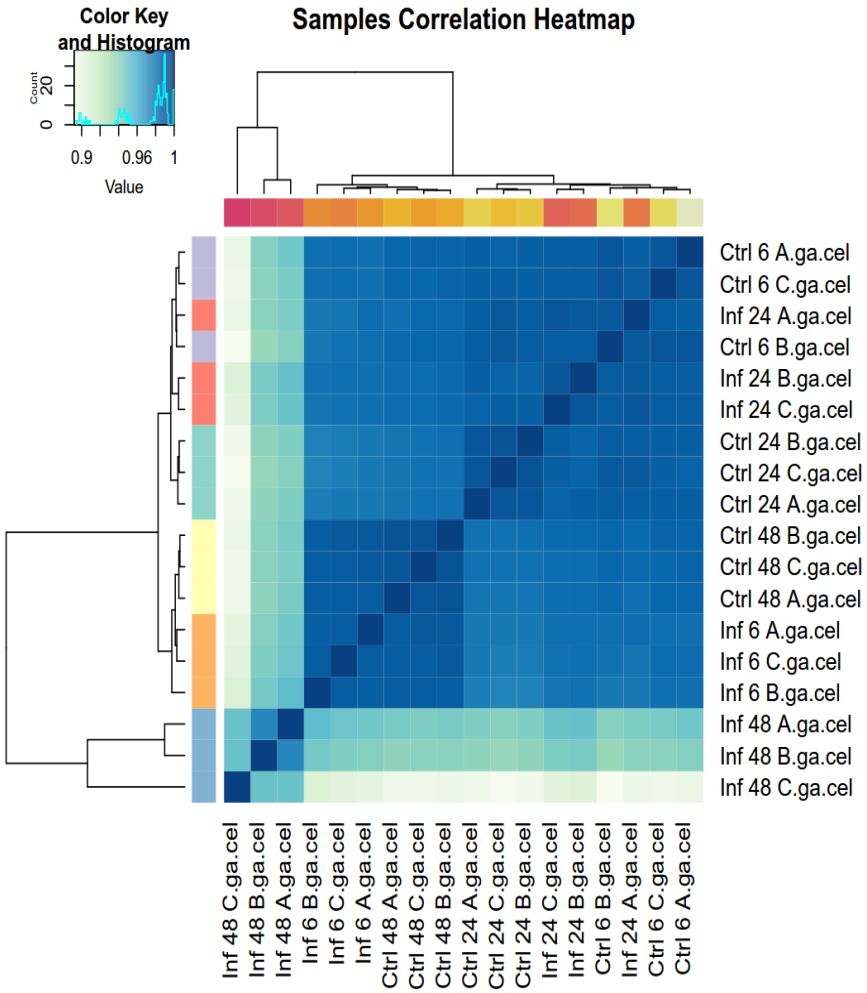


Figure 3-24 Correlation heatmap of all microarray sequencing samples. The heatmap shows a correlation between all samples sent for mRNA sequencing where shades of turquoise and blue represented low and high correlation respectively. Dendrograms on the side, links closely correlated samples in each row or column to each other.

Volcano Plots

Figure 3-25 shows the relationship between the *P*-values and the magnitude of $\log_2$ FC from control versus infected samples at 6, 24 and 48 h.p.i respectively. Cut-off criteria were $\log_2$ FC of 1 or -1 with *P*-value < 0.05.

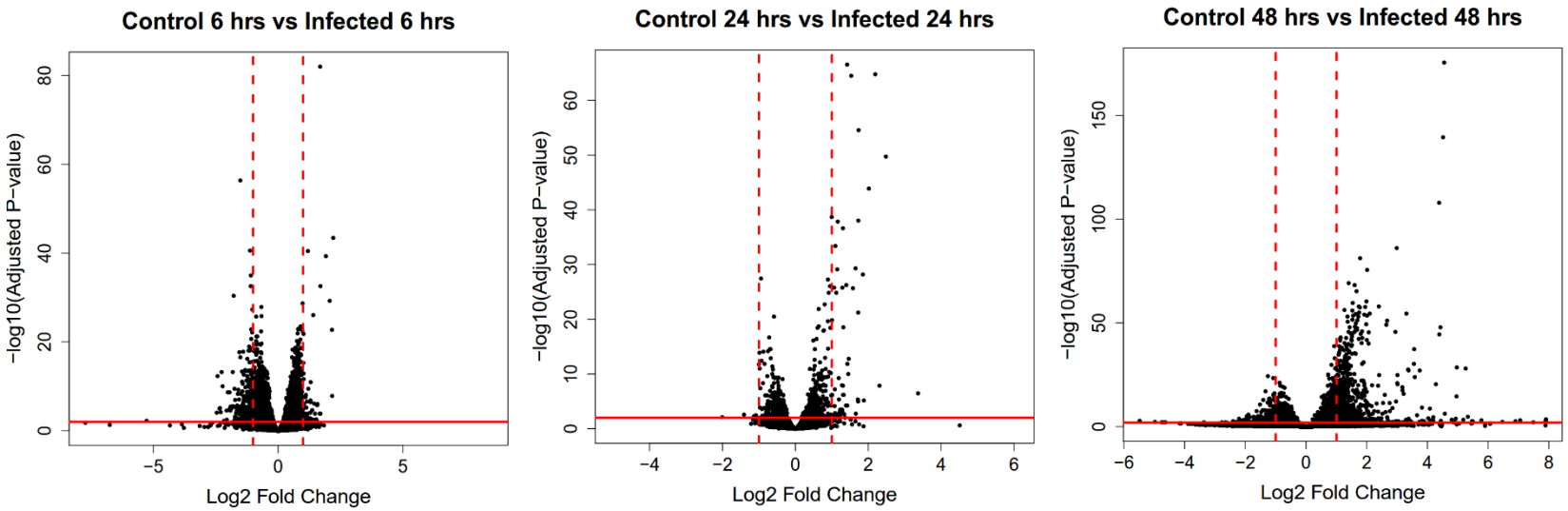


Figure 3-25 Volcano plot of DEGs (control *vs* infected) at 6, 24, and 48 h.p.i. The solid horizontal red line indicates *P*-value cut-off limit (0.05) while the dashed red line indicates $\log_2$ FC cut-off limit 1 and -1. Each black dot represents a gene. The pattern indicates that there were more down-regulated genes than up-regulated genes at 6 h.p.i, but there were more up-regulated genes than down-regulated genes at 24 and 48 h.p.i.

Venn Diagram

Figure 3-26 compares gene lists from 6, 24 and 48 h.p.i. The total number of genes expressed at each time point is shown in brackets. Common genes of different time points are shown in the central regions where their circles overlapped. Of the 383 differently expressed genes at six hours, 138 were also expressed at 48 hours, and four genes were also expressed at 24 hours. Out of 47 DEGs at 24 hours, 9 genes were also expressed at 48 hours. At all time points, only one gene was expressed which is PRTN3 or proteinase 3 that was down-regulated at 6 and 24 hours (log_2 FC: -1.334 and -1.337 respectively) but was up-regulated at 48 hours (log_2 FC: 3.197).

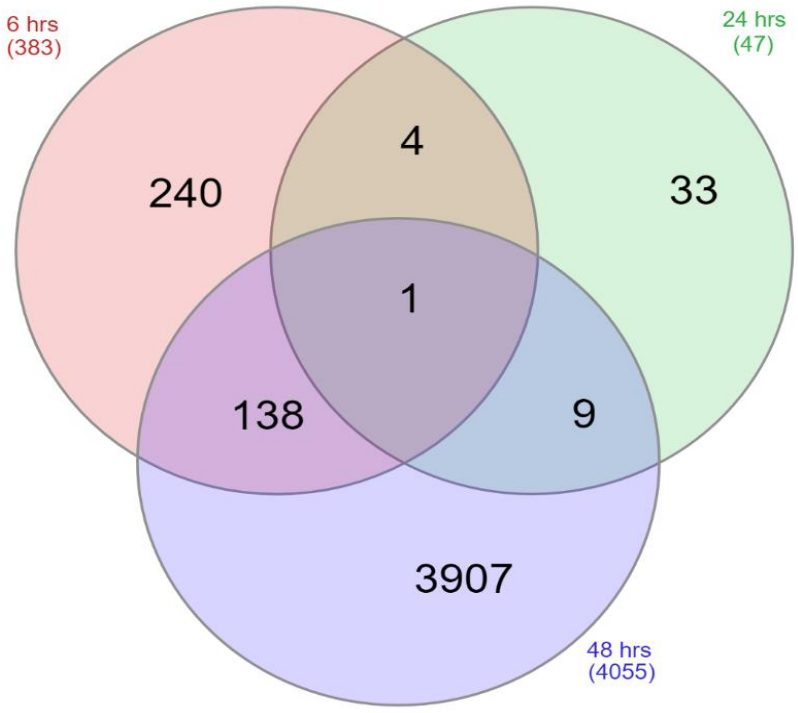


Figure 3-26 Venn diagram of DEGs at 6, 24, and 48 hours from a microarray experiment. The diagram highlighted one gene that was differentially expressed at all time points, which is PRTN3 or proteinase 3 that was down-regulated at 6 and 24 hours (log_2 FC: -1.334 and -1.337 respectively) but was up-regulated at 48 hours (log_2 FC: 3.197).

Differentially Expressed Genes (DEGs)

Cut-off values for DEGs at all time points are those with adjusted *P*-value < 0.05 and $\log_2$ FC ≥ 1 or ≤ -1. The higher cut off adjusted *P*-value for microarray experiment is due to there are three replicates at each time points compared to only two in mRNA and miRNA sequencing experiment. This microarray study also serves as a validation to mRNA sequencing study in addition to the qPCR experiment that also validate a small number of genes.

Control 6 hours vs Infected 6 hours

At 6 hours, 383 probe sets were differentially expressed where of this number 306 were down-regulated while 77 were up-regulated. Out of 306 down-regulated probe sets, only 285 mapped to known genes while out of 77 up-regulated probe sets, 71 mapped to known genes. The top 30 most significant down-regulated and up-regulated genes with annotation were listed in **Table** 3-28 and **Table** 3-29 respectively. Among them, the three most down-regulated genes are TXNIP (thioredoxin-interacting protein; $\log_2$ FC = -3.134), KIAA1107 (uncharacterised Protein KIAA1107, $\log_2$ FC = -2.879), and DBP (D-box binding PAR bZIP transcription factor, $\log_2$ FC = -2.631). The three top up-regulated genes are EFNB2 (ephrin B2, $\log_2$ FC = 1.880), CXCL8 (C-X-C motif chemokine ligand 8, $\log_2$ FC = 1.683), and ACTBL2 (actin, beta-like 2, $\log_2$ FC = 1.629).

Table 3-28 List of the top 30 down-regulated genes at 6 h.p.i. The filtered list result in 285 down-regulated genes, but only the top 30 most significant genes are listed in this table sorted with the most significant gene at the top. The full list is available in **Appendix** 3-18.

Gene Symbol	Gene Description	Log_2 FC
GRB7	growth factor receptor-bound protein 7	-2.350
DBP	D-box binding PAR bZIP transcription factor	-2.631
KLHL14	kelch-like family member 14	-2.279
CDC25C	cell division cycle 25C	-2.499
ETV1	ETS variant 1	-1.757
TP53INP1	tumour protein p53 inducible nuclear protein 1	-1.832
TXNIP	thioredoxin-interacting protein	-3.134
DHRS3	dehydrogenase/reductase 3	-1.536
KLHDC2	kelch domain containing 2	-1.621
NBR1	NBR1, autophagy cargo receptor	-1.287
CABYR	calcium binding tyrosine phosphorylation regulated	-1.796
H1F0	H1 histone family member 0	-1.463
DLGAP5	DLG associated protein 5	-1.498
KIAA1107	KIAA1107	-2.879
SMARCA2	SWI/SNF related, matrix associated, actin dependent regulator of chromatin, subfamily a, member 2	-1.505
DDB2	damage specific DNA binding protein 2	-1.461
PPL	periplakin	-2.033
BTBD8	BTB domain containing 8	-2.413
IQGAP3	IQ motif containing GTPase activating protein 3	-1.754
IGFBP1	insulin-like growth factor binding protein 1	-1.392
KIAA0586	KIAA0586	-1.140
WDR19	WD repeat domain 19	-1.411
ANP32E	acidic nuclear phosphoprotein 32 family member E	-1.044
HMMR	hyaluronan-mediated motility receptor	-2.023
KIF14	kinesin family member 14	-2.009
ERBB3	erb-b2 receptor tyrosine kinase 3	-1.481
JUP	junction plakoglobin	-1.353
UBALD2	UBA like domain containing 2	-2.112
TRANK1	tetratricopeptide repeat and ankyrin repeat containing 1	-1.920
EFNA4	ephrin A4	-1.447

Table 3-29 List of the top 30 up-regulated genes at 6 h.p.i. The filtered list resulted in 71 up-regulated genes but only the top 30 most significant genes are listed in this table sorted with the most significant gene at the top. The full list is available in **Appendix** 3-18.

Gene Symbol	Gene Description	Log_2 FC
EFNB2	ephrin B2	1.880
PPIF	peptidylprolyl isomerase F	1.201
HMOX1	heme oxygenase 1	1.121
GLIPR1	GLI pathogenesis-related 1	1.532
MARS2	methionyl-tRNA synthetase 2, mitochondrial	1.343
DAW1	dynein assembly factor with WD repeats 1	1.260
NIP7	NIP7, nucleolar pre-rRNA processing protein	1.097
ACTBL2	actin, beta-like 2	1.629
PXDC1	PX domain containing 1	1.280
SERPINB2	serpin family B member 2	1.385
URB2	URB2 ribosome biogenesis 2 homolog (S. cerevisiae)	1.196
GPAT3	glycerol-3-phosphate acyltransferase 3	1.156
RGS2	regulator of G-protein signalling 2	1.599
IFFO2	intermediate filament family orphan 2	1.098
IL6	interleukin 6	1.291
DUSP7	dual specificity phosphatase 7	1.082
HK2	hexokinase 2	1.067
SPHK1	sphingosine kinase 1	1.622
FOXD1	forkhead box D1	1.049
TAGLN	transgelin	1.147
CDC25A	cell division cycle 25A	1.384
MAT2A	methionine adenosyltransferase 2A	1.166
TNFAIP3	TNF alpha-induced protein 3	1.028
SOWAHC	Sosondowah ankyrin repeat domain family member C	1.031
KBTBD8	kelch repeat and BTB domain containing 8	1.321
NR4A3	nuclear receptor subfamily 4 group A member 3	1.279
CD3EAP	CD3e molecule associated protein	1.127
ADAMTS1	ADAM metallopeptidase with thrombospondin type 1 motif 1	1.024
PHLDA2	pleckstrin homology-like domain family A member 2	1.107
HOMER1	homer scaffolding protein 1	1.156

All 285 down-regulated and 71 up-regulated genes were recognised by PANTHER database. The down-regulated genes matched to 164 molecular functions from seven major functions (binding GO:0005488, 74 hits; receptor activity GO:0004872, six hits; structural molecule activity GO:0005198, eight hits; signal transducer activity GO:0004871, four hits;

channel regulator activity GO:0016247, one hit; catalytic activity GO:0003824, 63 hits; transporter activity GO:0005215, 8 hits) while up-regulated genes matched to 48 functions from six major functions (binding GO:0005488, 21 hits, receptor activity GO:0004872, two hits; structural molecule activity GO:0005198, two hits; signal transducer activity GO:0004871, three hits; catalytic activity GO:0003824, 18 hits; transporter activity GO:0005215, two hits). The PANTHER molecular function ontology results are displayed in **Figure** 3-27**.** No molecular functions passed the PANTHER Overrepresentation Test for both sets of DEGs.

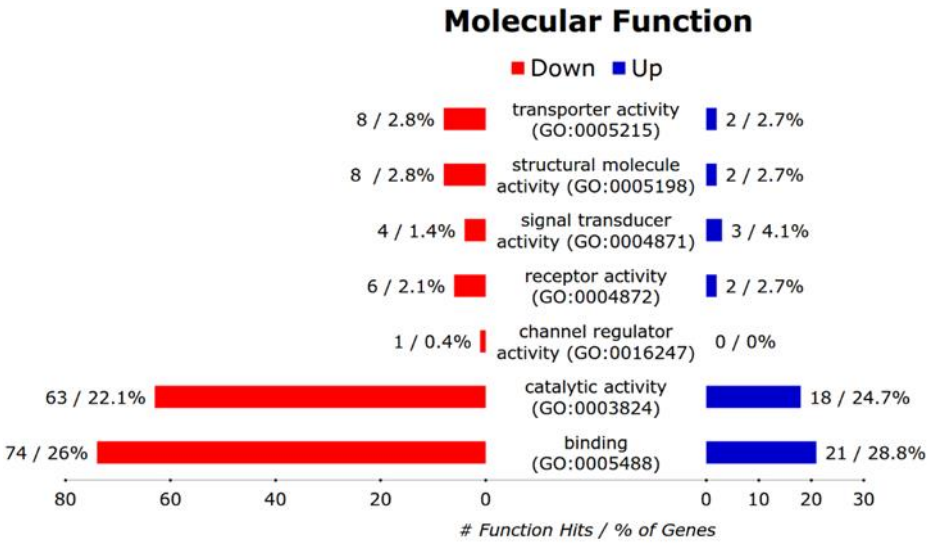


Figure 3-27 PANTHER GO-Slim molecular function ontology hits for significantly DEGs at 6 h.p.i. The down-regulated genes matched to 164 molecular functions from 7 major functions while the up-regulated genes matched to 48 molecular functions from six major functions. None of these functions passed the PANTHER Overrepresentation Test (FDR < 0.05).

In the biological process category, the down-regulated genes matched to 417 biological processes from 13 major processes (biological adhesion GO:0022610, three hits; biological regulation GO:0065007, 36 hits; cell killing GO:0001906, one hit; cellular component organisation or biogenesis GO:0071840, 44 hits; cellular process GO:0009987, 124 hits; developmental process GO:0032502, 19 hits; immune system process

GO:0002376, seven hits; localisation GO:0051179, 32 hits; locomotion GO:0040011, seven hits; metabolic process GO:0008152, 91 hits; multicellular organismal process GO:0032501, 14 hits; reproduction GO:0000003, nine hits; response to stimulus GO:0050896, 30 hits) while up-regulated genes matched to 115 major processes from 11 major processes (cellular component organisation or biogenesis GO:0071840, 11 hits; cellular process GO:0009987, 32 hits; localisation GO:0051179, seven hits; reproduction GO:0000003, two hits; biological regulation GO:0065007, 14 hits; response to stimulus GO:0050896, 11 hits; developmental process GO:0032502, six hits; multicellular organismal process GO:0032501, four hits; locomotion GO:0040011, two hits; metabolic process GO:0008152, 24 hits; immune system process GO:0002376, two hits). The PANTHER biological process ontology results are displayed in **Figure** 3-28**.** The PANTHER Overrepresentation Test identified five significantly down-regulated processes (chromosome segregation GO:0007059, mitosis GO:0007067, cellular component movement GO:0006928, cell cycle GO:0007049, cellular component organisation GO:0016043) and one significantly up-regulated process which is cell proliferation (GO:0008283).

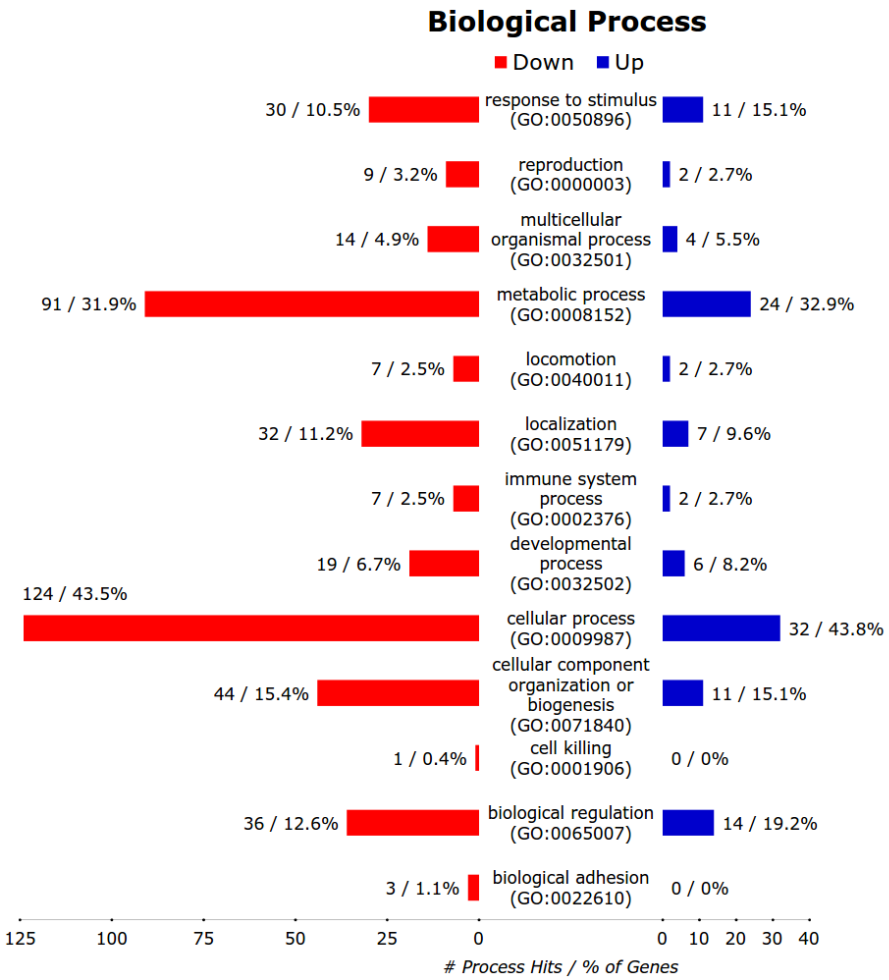


Figure 3-28 PANTHER GO-Slim biological process ontology hits for significantly DEGs at 6 h.p.i. The down-regulated genes matched to 417 molecular functions from 13 major processes while up-regulated genes matched to 115 biological processes from 11 major processes. The PANTHER Overrepresentation Test (FDR < 0.05) identified five down-regulated processes and one up-regulated process.

In the cellular component category, the down-regulated genes matched to 197 cellular components from seven major components (cell junction GO:0030054, two hits; cell part GO:0044464, 86 hits; extracellular matrix GO:0031012, one hits; extracellular region GO:0005576, four hits; macromolecular complex GO:0032991;, 28 hits; membrane GO:0016020, 17 hits; organelle GO:0043226, 59 hits). The up-regulated genes matched to 69 cellular components from six major components (cell part GO:0044464, 30 hits; extracellular region GO:0005576, two hits;

macromolecular complex GO:0032991, nine hits; membrane GO:0016020, eight hits; organelle GO:0043226, 19 hits; synapse GO:0045202, one hit). The PANTHER cellular component ontology results are displayed in **Figure** 3-29. The PANTHER Overrepresentation Test identified one significant cellular component (nucleolus GO:0005730) from down-regulated genes but none from a set of up-regulated genes.

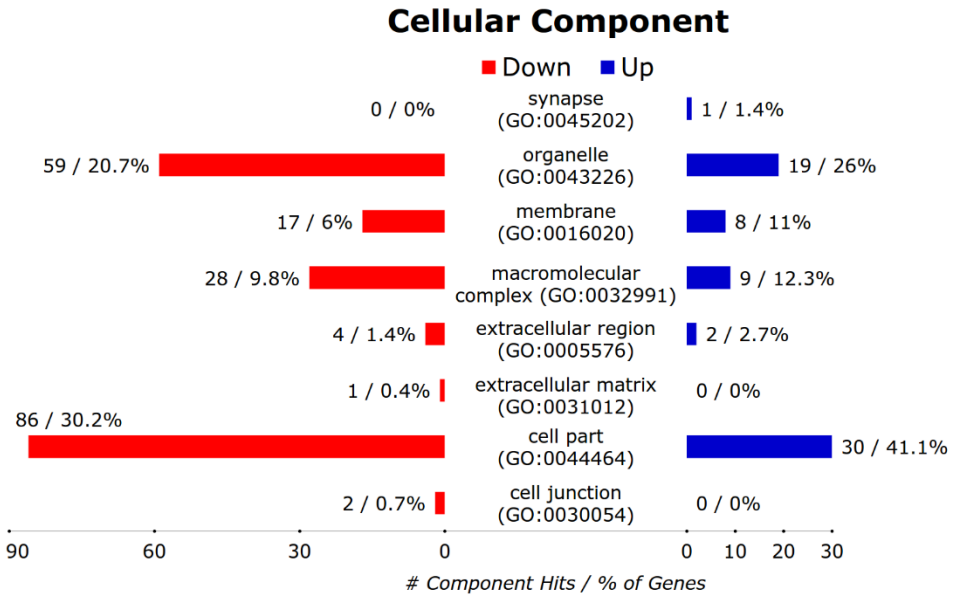


Figure 3-29 PANTHER GO-Slim cellular component ontology hits for significantly DEGs at 6 h.p.i. Down-regulated genes matched to 197 cellular components from seven major components while up-regulated genes matched to 69 cellular components from six major components. PANTHER Overrepresentation Test (FDR < 0.05) identified one down-regulated component from the set of down-regulated genes but no significant components from a set of up-regulated genes.

Control 24 hours vs Infected 24 hours

At 24 hours, 47 probe sets were differentially expressed where. Of this number, 26 were down-regulated while 21 were up-regulated. Out of 26 down-regulated probe sets, 24 matched to known genes while all 21 up-regulated probe sets matched to known genes. All 24 known down-regulated genes and all 21 up-regulated genes were listed in **Table** 3-30 and **Table**

3-31 respectively. Among them, the three most down-regulated genes are TXNIP (thioredoxin-interacting protein, log_2 FC = -1.576), GBP2 (guanylate binding protein 2, log_2 FC = -1.491) and ERP27 (endoplasmic reticulum protein 27, log_2 FC = -1.342). The three most up-regulated genes are IFIT1 (interferon-induced protein with tetratricopeptide repeats 1, log_2 FC = 2.515), IFI44L (interferon-induced protein 44 like, log_2 FC = 2.256), and IFI6 (interferon alpha-inducible protein 6, log_2 FC = 2.146).

Table 3-30 List of all 24 down-regulated genes at 24 h.p.i. The filtered list is sorted with the most significant gene at the top.

Gene Symbol	Gene Description	Log_2 FC
RGS9	regulator of G-protein signalling 9	-1.292
ASS1	argininosuccinate synthase 1	-1.139
NPR1	natriuretic peptide receptor 1	-1.260
PRKN	parkin RBR E3 ubiquitin protein ligase	-1.111
ZC3H6	zinc finger CCCH-type containing 6	-1.270
ZDHHC11	zinc finger DHHC-type containing 11	-1.337
GBP2	guanylate binding protein 2	-1.491
RASSF6	Ras association domain family member 6	-1.061
ERP27	endoplasmic reticulum protein 27	-1.342
TXNIP	thioredoxin-interacting protein	-1.576
EBF4	early B-cell factor 4	-1.057
PTP4A3	protein tyrosine phosphatase type IVA, member 3	-1.125
PLPPR3	phospholipid phosphatase related 3	-1.003
TSPAN2	tetraspanin 2	-1.091
ARRDC4	arrestin domain containing 4	-1.090
SLC25A27	solute carrier family 25 member 27	-1.071
CFHR3	complement factor H related 3	-1.027
KRTAP2-3	keratin associated protein 2-3	-1.114
PRTN3	proteinase 3	-1.337
TMEM74B	transmembrane protein 74B	-1.165
PAEP	progestagen associated endometrial protein	-1.117
NIPSNAP3B	nipsnap homolog 3B	-1.283
LOC105747689	uncharacterised LOC105747689	-1.091
ZNF404	zinc finger protein 404	-1.028

Table 3-31 List of all 21 up-regulated genes at 24 hours. The filtered list is sorted with the most significant gene at the top.

Gene Symbol	Gene Description	Log_2 FC
IFI44L	interferon induced protein 44 like	2.256
IFI6	interferon alpha inducible protein 6	2.146
IFI44	interferon induced protein 44	1.750
OAS1	2'-5'-oligoadenylate synthetase 1	1.262
IFIT1	interferon-induced protein with tetratricopeptide repeats 1	2.515
TMEM158	transmembrane protein 158 (gene/pseudogene)	1.143
OAS3	2'-5'-oligoadenylate synthetase 3	1.368
CYP1A1	cytochrome P450 family 1 subfamily A member 1	1.135
IFI27	interferon alpha inducible protein 27	1.114
MT1M	metallothionein 1M	1.572
OAS2	2'-5'-oligoadenylate synthetase 2	1.434
XAF1	XIAP associated factor 1	1.087
ANGPTL4	angiopoietin-like 4	1.632
SAMD9	sterile alpha motif domain containing 9	1.447
TUBA3C	tubulin alpha 3c	1.189
ISG15	ISG15 ubiquitin-like modifier	1.025
IFIT3	interferon-induced protein with tetratricopeptide repeats 3	1.140
IRF7	interferon regulatory factor 7	1.096
HIST1H3G	histone cluster 1 H3 family member g	1.123
PARP9	poly(ADP-ribose) polymerase family member 9	1.060
HIST1H4B	histone cluster 1 H4 family member b	1.147

All 24 down-regulated and 21 up-regulated genes were recognised by the PANTHER database. The down-regulated genes matched to 12 molecular functions from two major functions (binding GO:0005488, five hits; catalytic activity GO:0003824, 10 hits) while up-regulated genes matched to 14 functions from three major functions (binding GO:0005488, eight hits; structural molecule activity GO:0005198, one hit; catalytic activity GO:0003824, five hits). The PANTHER molecular function ontology results are displayed in **Figure** 3-30. The PANTHER Overrepresentation Test identified three significant functions (nucleotidyltransferase activity GO:0016779, nuclease activity GO:0004518, RNA binding GO:0003723) while from a set of

up-regulated genes, no significant function from the set of down-regulated genes.

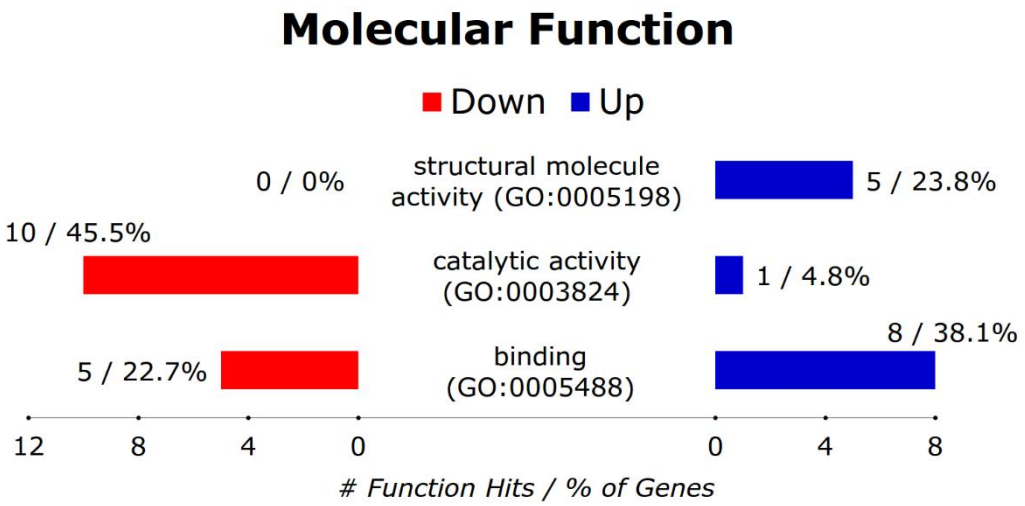


Figure 3-30 PANTHER GO-Slim molecular function ontology hits for significantly DEGs at 24 h.p.i. The down-regulated genes matched to 12 molecular functions from two major functions while the up-regulated genes matched to 14 functions from three major function. The PANTHER Overrepresentation Test (FDR < 0.05) identified three down-regulated function from the set of up-regulated genes but no significant function from the set of down-regulated genes.

Meanwhile, in the biological process category, the down-regulated genes matched to 37 biological processes from eight major processes (biological regulation GO:0065007, four hits; cellular component organisation or biogenesis GO:0071840, one hit; cellular process GO:0009987, 12 hits; developmental process GO:0032502, two hits; immune system process GO:0002376, one hit; localisation GO:0051179, three hits; metabolic process GO:0008152, nine hits; response to stimulus GO:0050896, five hits). The up-regulated genes matched to 25 processes from eight major processes (biological adhesion GO:0022610, one hit; biological regulation GO:0065007, five hits; cellular component organisation or biogenesis GO:0071840, one hit; cellular process GO:0009987, seven hits; developmental process GO:0032502, two hits; immune system process GO:0002376, two hits; metabolic process GO:0008152, four hits; response to stimulus GO:0050896, three hits). The

PANTHER biological process ontology results are displayed in **Figure** 3-31. The PANTHER Overrepresentation Test did not find any overrepresented processes from both sets of genes.

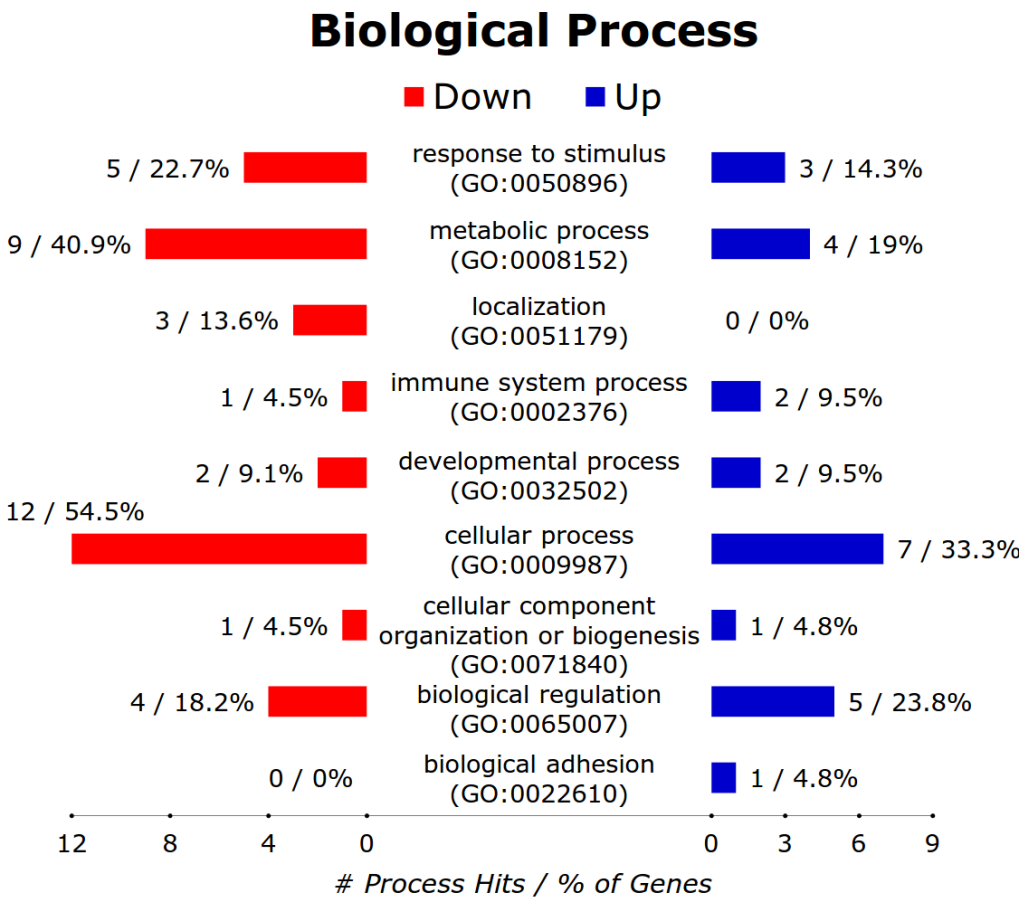


Figure 3-31 PANTHER GO-Slim biological process ontology hits for significantly DEGs at 24 h.p.i. The down-regulated genes matched to 37 biological processes from eight major processes while the up-regulated genes matched to 27 processes from eighth major processes. No processes passed the PANTHER Overrepresentation Test (FDR < 0.05).

In the cellular component category, the down-regulated genes matched to 20 cellular components from five major components (cell part GO:0044464, eight hits; extracellular region GO:0005576, one hit; macromolecular complex GO:0032991, two hits; membrane GO:0016020, three hits; organelle GO:0043226, six hits). The up-regulated genes matched to 21 cellular components from four major components (cell part GO:0044464, 11 hits;

extracellular region GO:0005576, one hit; macromolecular complex GO:0032991, one hit; organelle GO:0043226, eight hits). The PANTHER biological process ontology results are displayed in **Figure** 3-32.

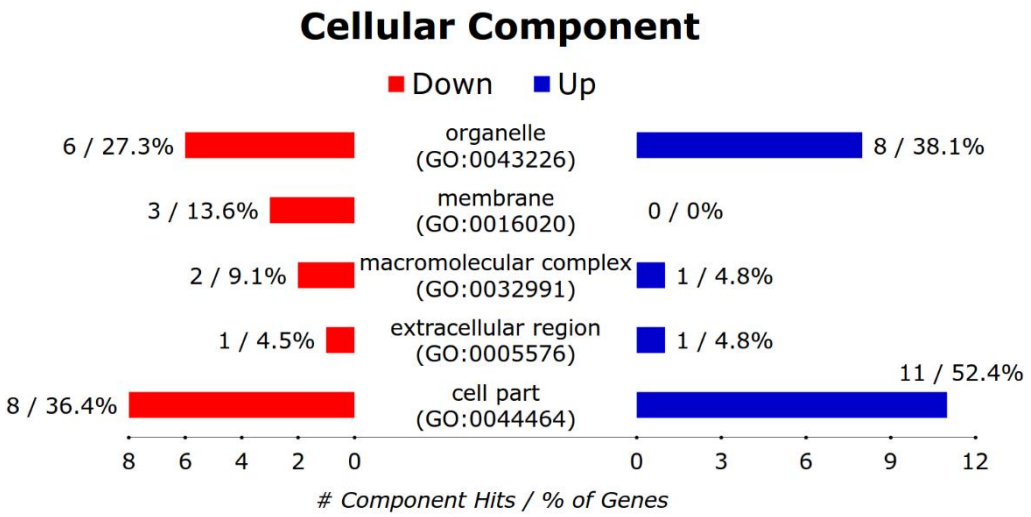


Figure 3-32 PANTHER GO-Slim cellular component ontology hits for significantly DEGs at 24 h.p.i. The down-regulated genes matched to 20 cellular components from five major components while the up-regulated genes matched to 21 cellular components from four major components. The PANTHER Overrepresentation Test (FDR < 0.05) identified one cellular component (cytosol GO:0005829) from the set of up-regulated genes but no overrepresented component from the set of down-regulated genes.

Control 48 hours vs Infected 48 hours

At 48 hours, 4055 probe sets were differentially expressed with 3653 were down-regulated while the rest 402 were up-regulated. Out of 3653, 3400 probe sets match to known genes while out of 402 down-regulated probe sets, 314 matched to known genes. Among them, the three most down-regulated genes are ZNF451 (zinc finger protein 451, $\log_2$ FC = -4.417), CDC6 (cell division cycle 6, $\log_2$ FC = -3.941), and SLC7A6 (solute carrier family 7 member 6, $\log_2$ FC = -3.859) while three top up-regulated genes are OR2T5 (olfactory receptor family 2 subfamily T member 5, $\log_2$ FC = 3.654), LOC441268 (uncharacterised LOC441268, $\log_2$ FC = 3.402), and DBP (D-box binding PAR bZIP transcription factor, $\log_2$ FC = 3.330). **Table** 3-23 and **Table** 3-33 listed

the top 30 most significant down-regulated and up-regulated genes respectively.

Table 3-32 List of the top 30 down-regulated genes at 48 h.p.i. The filtered list resulted in 3400 down-regulated genes with the top 30 most significant genes listed in this table sorted with the most significant gene at the top. The full list is available in **Appendix** 3-19.

Gene Symbol	Gene Description	Log_2 FC
SCFD2	sec1 family domain containing 2	-3.005
TTPAL	alpha-tocopherol transfer protein like	-3.312
GLIPR1	GLI pathogenesis-related 1	-3.679
CPA4	carboxypeptidase A4	-2.400
MTRF1L	mitochondrial translational release factor 1 like	-2.852
AGL	amylo-alpha-1, 6-glucosidase, 4-alpha-glucanotransferase	-2.808
HSPH1	heat shock protein family H (Hsp110) member 1	-2.250
MTRF1L	mitochondrial translational release factor 1 like	-2.661
POP1	POP1 homolog, ribonuclease P/MRP subunit	-3.439
TOP3A	topoisomerase (DNA) III alpha	-2.853
ABHD3	abhydrolase domain containing 3	-2.793
FOXD1	forkhead box D1	-2.821
CENPBD1	CENPB DNA-binding domain containing 1	-2.177
CDC6	cell division cycle 6	-3.941
B4GALT6	beta-1,4-galactosyltransferase 6	-3.693
EDEM3	ER degradation enhancing alpha-mannosidase like protein 3	-2.984
POLR3B	RNA polymerase III subunit B	-3.047
USP38	ubiquitin specific peptidase 38	-2.583
NAV3	neuron navigator 3	-2.496
ZWILCH	zwilch kinetochore protein	-2.685
C9orf64	chromosome 9 open reading frame 64	-2.139
MOCS3	molybdenum cofactor synthesis 3	-2.720
ZNF451	zinc finger protein 451	-4.417
DMXL1	Dmx like 1	-1.961
IFFO2	intermediate filament family orphan 2	-2.423
STK40	serine/threonine kinase 40	-1.947
URB2	URB2 ribosome biogenesis 2 homolog (S. cerevisiae)	-2.574
NABP1	nucleic acid binding protein 1	-2.917
COL12A1	collagen type XII alpha 1 chain	-2.240
INTS5	integrator complex subunit 5	-2.586

Table 3-33 List of the top 30 up-regulated genes at 48 h.p.i. The filtered list resulted in 314 up-regulated genes but only the top 30 most significant genes are listed in this table sorted with the most significant gene at the top. The full list is available in **Appendix** 3-19.

Gene Symbol	Gene Description	Log_2 FC
DBP	D-box binding PAR bZIP transcription factor	3.330
EDC4	enhancer of mRNA decapping 4	3.244
GDF15	growth differentiation factor 15	3.079
DHRS3	dehydrogenase/reductase 3	1.929
INSIG1	insulin induced gene 1	2.334
RNF225	ring finger protein 225	2.339
SLC44A2	solute carrier family 44 member 2	1.646
OR2T5	olfactory receptor family 2 subfamily T member 5	3.654
NR4A2	nuclear receptor subfamily 4 group A member 2	2.687
GRB7	growth factor receptor-bound protein 7	1.496
LOC441268	uncharacterised LOC441268	3.402
MXI1	MAX interactor 1, dimerisation protein	1.630
KLHL24	kelch-like family member 24	2.112
HMOX1	heme oxygenase 1	1.407
TLX3	T-cell leukaemia homeobox 3	1.746
PER1	period circadian clock 1	1.648
ZNF277	zinc finger protein 277	1.394
RPL22L1	ribosomal protein L22 like 1	1.735
SAT2	spermidine/spermine N1-acetyltransferase family member 2	1.394
CEBPD	CCAAT/enhancer binding protein delta	1.369
PPIP5K1	diphosphoinositol pentakisphosphate kinase 1	1.685
ELF3	E74 like ETS transcription factor 3	1.435
IFI44L	interferon induced protein 44 like	1.378
BHLHE40	basic helix-loop-helix family member e40	1.163
DDB2	damage specific DNA binding protein 2	1.387
MT1X	metallothionein 1X	1.126
ENO2	enolase 2	1.454
ZFAND5	zinc finger AN1-type containing 5	1.098
TUBA3C	tubulin alpha 3c	2.159
CLDN17	claudin 17	1.343

Of 3400 annotated down-regulated genes, 3302 were recognised by the PANTHER database whereas all 314 up-regulated genes were recognised by the database. The down-regulated genes matched to 2022 molecular functions from nine major functions (antioxidant activity GO:0016209, one hit; binding GO:0005488, 817 hits; catalytic activity GO:0003824, 878 hits; channel

regulator activity GO:0016247, two hits; receptor activity GO:0004872, 56 hits; signal transducer activity GO:0004871, 56 hits; structural molecule activity GO:0005198, 61 hits; translation regulator activity GO:0045182, 18 hits; transporter activity GO:0005215, 133 hits). The up-regulated genes matched to 212 functions from seven major functions (binding GO:0005488, 94 hits; catalytic activity GO:0003824, 47 hits; channel regulator activity GO:0016247, two hits; receptor activity GO:0004872, 22 hits; signal transducer activity GO:0004871, 20 hits; structural molecule activity GO:0005198, six hits; transporter activity GO:0005215, 21 hits). The PANTHER molecular function ontology results are displayed in **Figure** 3-33. The PANTHER Overrepresentation Test identified 38 significant functions (**Appendix** 3-20) from the set of down-regulated genes while four significant functions (sequence-specific DNA binding RNA polymerase II transcription factor activity GO:0000981, sequence-specific DNA binding transcription factor activity GO:0003700, receptor binding GO:0005102, DNA binding GO:0003677) were identified from the set of up-regulated genes.

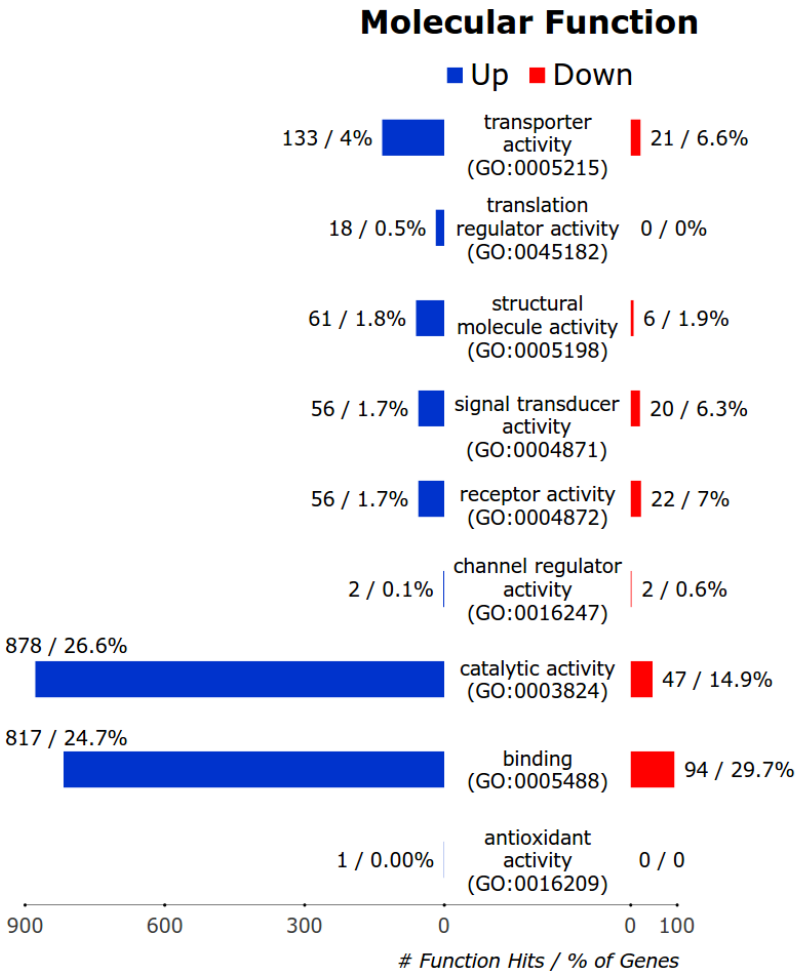


Figure 3-33 PANTHER GO-Slim molecular function ontology hits for significantly DEGs at 48 h.p.i. The down-regulated genes matched to 2022 molecular functions from nine major functions while the up-regulated genes matched to 312 functions from seven major function. The PANTHER Overrepresentation Test (FDR < 0.05) identified 38 down-regulated functions (**Appendix** 3-20) from the set of down-regulated genes and four significant functions from the set of up-regulated genes.

Meanwhile, in the biological process category, the down-regulated genes matched to 4576 biological processes from 15 major processes (biological adhesion GO:0022610, 40 hits; biological regulation GO:0065007, 361 hits; cell killing GO:0001906, two hits; cellular component organisation or biogenesis GO:0071840, 436 hits; cellular process GO:0009987, 1448 hits; developmental process GO:0032502, 168 hits; growth GO:0040007, two hits; immune system process GO:0002376, 47 hits; localisation GO:0051179, 356 hits; locomotion

GO:0040011, 28 hits; metabolic process GO:0008152, 1210 hits; multicellular organismal process GO:0032501, 126 hits; reproduction GO:0000003, 32 hits; response to stimulus GO:0050896, 318 hits; rhythmic process GO:0048511, two hits). The,up-regulated genes matched to 525 processes from 13 major processes (biological adhesion GO:0022610; two hits; biological regulation GO:0065007, 68 hits; cellular component organisation or biogenesis GO:0071840, 27 hits; cellular process GO:0009987, 132 hits; developmental process GO:0032502, 47 hits; immune system process GO:0002376, 17 hits; localisation GO:0051179, 26 hits; locomotion GO:0040011, nine hits; metabolic process GO:0008152, 91 hits; multicellular organismal process GO:0032501, 40 hits; reproduction GO:0000003, four hits; response to stimulus GO:0050896, 60 hits; rhythmic process GO:0048511, two hits). The PANTHER biological process ontology results are displayed in **Figure** 3-34. The PANTHER Overrepresentation Test (FDR < 0.05) identified 81 overrepresented processes (**Appendix** 3-21) from the down-regulated genes and three significant processes from the up-regulated genes (ectoderm development GO:0007398, developmental process GO:0032502, biological regulation (GO:0065007).

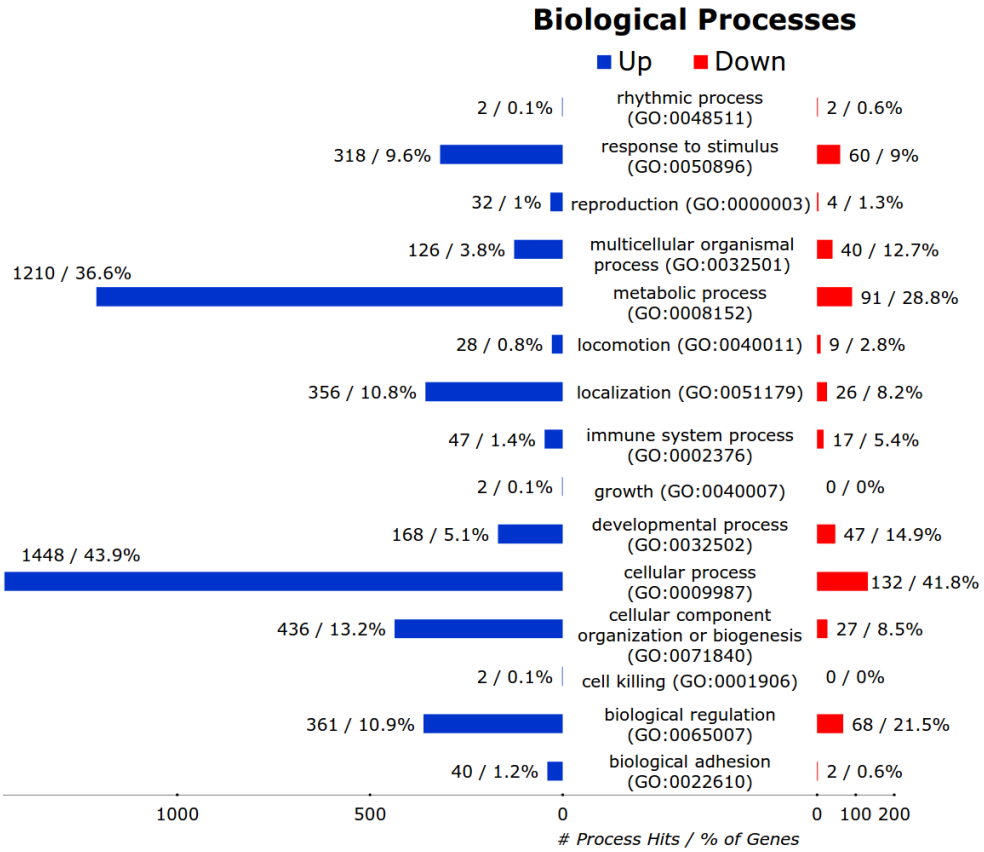


Figure 3-34 PANTHER GO-Slim biological process ontology hits for significantly DEGs at 48 h.p.i. The down-regulated genes matched to 4576 biological processes from 15 major processes while the up-regulated genes matched to 525 processes from 13 major processes. The PANTHER Overrepresentation Test (FDR < 0.05) identified 28 and three overrepresented processes from down and up-regulated genes respectively.

In the cellular component category, the down-regulated genes matched to 2805 cellular components from eight major components (cell junction GO:0030054, 22 hits; cell part GO:0044464, 1126 hits; extracellular matrix GO:0031012, nine hits; extracellular region GO:0005576, 39 hits; macromolecular complex GO:0032991, 455 hits; membrane GO:0016020, 297 hits; organelle GO:0043226, 844 hits; synapse GO:0045202, 13 hits). The up-regulated genes matched to 244 cellular components from 8 major components (cell junction GO:0030054, one hit; cell part GO:0044464, 75 hits; extracellular matrix GO:0031012, one hit; extracellular region GO:0005576, 17 hits; macromolecular complex GO:0032991, 22 hits; membrane GO:0016020, 44

hits; organelle GO:0043226, 50 hits; synapse GO:0045202, four hits). The PANTHER biological process ontology results are displayed in **Figure** 3-35. The PANTHER Overrepresentation Test identified 28 overrepresented components (**Appendix** 3-22) from the set of down-regulated genes but none from the set of up-regulated genes.

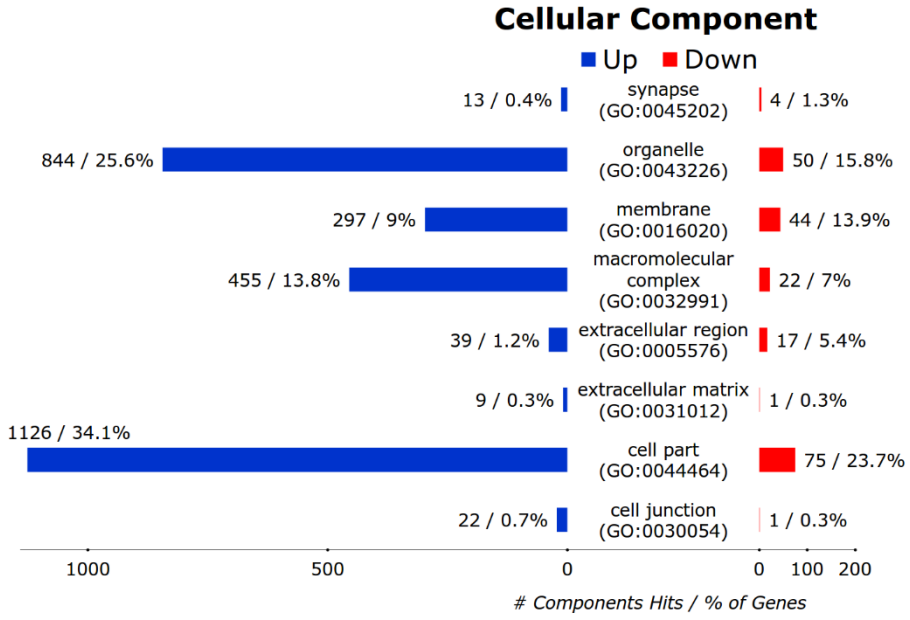


Figure 3-35 PANTHER GO-Slim cellular component ontology hits for significantly DEGs at 48 h.p.i. The down-regulated genes matched to 2805 cellular components from eight major components while the up-regulated genes matched to 214 cellular components from 8 major components. PANTHER Overrepresentation Test (FDR < 0.05) identified 28 cellular components (**Appendix** 3-22) from the set of down-regulated genes but no overrepresented component from the set of up-regulated genes.

Pathway Analysis

The analysis was performed against Reactome version 65 on 15 of August 2018, and cut-off criterium is pathways with entities FDR < 0.01. For 6 hours' gene list, 197 out of 352 gene symbols submitted were found in the Reactome database, where 664 pathways were hit by at least one of them.

Five pathways passed the cut-off criterium are listed in **Table** 3-34 with the most significant pathway at the top. The number of entities or gene found

per pathway ranges from seven to 35 genes. All pathways were down-regulated based on the average log_2 FC of the matched genes (Range of log_2 FC average: -0.836 ~ -1.310). The pathways with the lowest average log_2 FC were R-HSA-141444 (amplification of signal from unattached kinetochores *via* a MAD2 inhibitory signal) and R-HSA-141424 (amplification of signal from the kinetochores) with average log_2 FC -1.310 while the pathway with the most entities found was R-HSA-69278 (Cell Cycle, Mitotic) with 35 hits.

At 24 h.p.i, 29 out of 45 gene symbols were found in the Reactome database, where 240 pathways were hit by at least one of them. Among them, only five passed the cut-off criterium and are listed in **Table** 3-34 with the most significant pathway at the top. The number of entities or gene found per pathway ranges from 10 to 30 genes, and all pathways were up-regulated based on the average log_2 FC of the matched genes (Range of log_2 FC average: 0.734 ~ 1.154). The pathways with the highest average log_2 FCs were R-HSA-913531 (Interferon signaling) and R-HSA-909733 (Interferon alpha/beta signalling) with average log_2 FC 1.934 while the pathway with the most entities found was R-HSA-168256 (Immune System) with 30 hits.

At 48 h.p.i, 2122 out of 3605 identifiers in the sample were found in Reactome, where 1758 pathways were hit by at least one of them. However, none of them passed the cut-off criterium (Entities FDR < 0.01).

Table 3-34 List of the pathways affected by DEGs at 6 and 24 h.p.i (Entities FDR < 0.01) sorted with the most significant pathway at the top. No pathway passed the cut-off criterium at 48 h.p.i.

Pathway Identifier	Pathway Name	Entities Found / Total	Average Log_2 FC
	6 h.p.i		
R-HSA-156711	Polo-like kinase mediated events	7 / 23	-0.836
R-HSA-141444	Amplification of signal from unattached kinetochores *via* a MAD2 inhibitory signal	12 / 94	-1.318
R-HSA-141424	Amplification of signal from the kinetochores	12 / 94	-1.318
R-HSA-69278	Cell Cycle, Mitotic	35 / 569	-1.024
R-HSA-68877	Mitotic Prometaphase	18 / 206	-1.310
	24 h.p.i		
R-HSA-913531	Interferon Signaling	22 / 388	1.154
R-HSA-909733	Interferon alpha/beta signaling	22 / 184	1.154
R-HSA-1280215	Cytokine Signalling in the Immune system	25 / 1051	1.052
R-HSA-877300	Interferon gamma signalling	10 / 250	0.734
R-HSA-168256	Immune System	30 / 2638	0.748

3.4.6 *Validation of genes using RT-PCR*

Real-time PCR Reaction Efficiency – All Genes

Real-time PCR efficiency for all genes were calculated using the Pfaffl method (Pfaffl, 2001) and for each gene, 3 technical replicates were performed. All primers used in this study have efficiency close to this, ranging from 1.752 to 1.999 as listed in **Table** 3-35.

Table 3-35 Calculation of primer pairs efficiency using the Pfaffl method (Pfaffl, 2001)

Gene	Primer Efficiency
CXCR4	1.958
HSP90AAP	1.887
IFI-6	1.903
NR4A2	1.752
TXNIP	1.779
ZNF 451	1.942
ZNF 467	1.999

Other than mRNA sequencing and microarray experiment, the selected genes expression were also analysed using the standard approach, real-time reverse transcription PCR (RT-qPCR). This approach also was used to validate the same genes found to be upregulated in both mRNA sequencing and microarray experiment.

Analysis of mRNA Sequencing Data with RT-qPCR

Seven genes CXCR4, HSP90, IFI6, NR4A2, TXNIP, ZNF451, and ZNF467, were selected from mRNA and microarray studies for validation with RT-qPCR. Total RNA was extracted from a new batch of hBMECs cells infected with *T. gondii* RH at 6, 24 and 48 h.p.i then converted to cDNA after passing the quality checks. Following the qPCR step, data were analysed using the Pfaffl (2001) method. Data were presented in **Figure** 3-36. For easy comparison, the data from the RT-PCR experiment were converted into $\log_2$ form and presented in **Table** 3-36**.** Based on the table, RNA-seq unable to detect significant changes to the majority of the genes at 6 and 24 h.p.i. Generally, the nature of expression (up-regulated or down-regulated) were similar for most genes across all platforms.

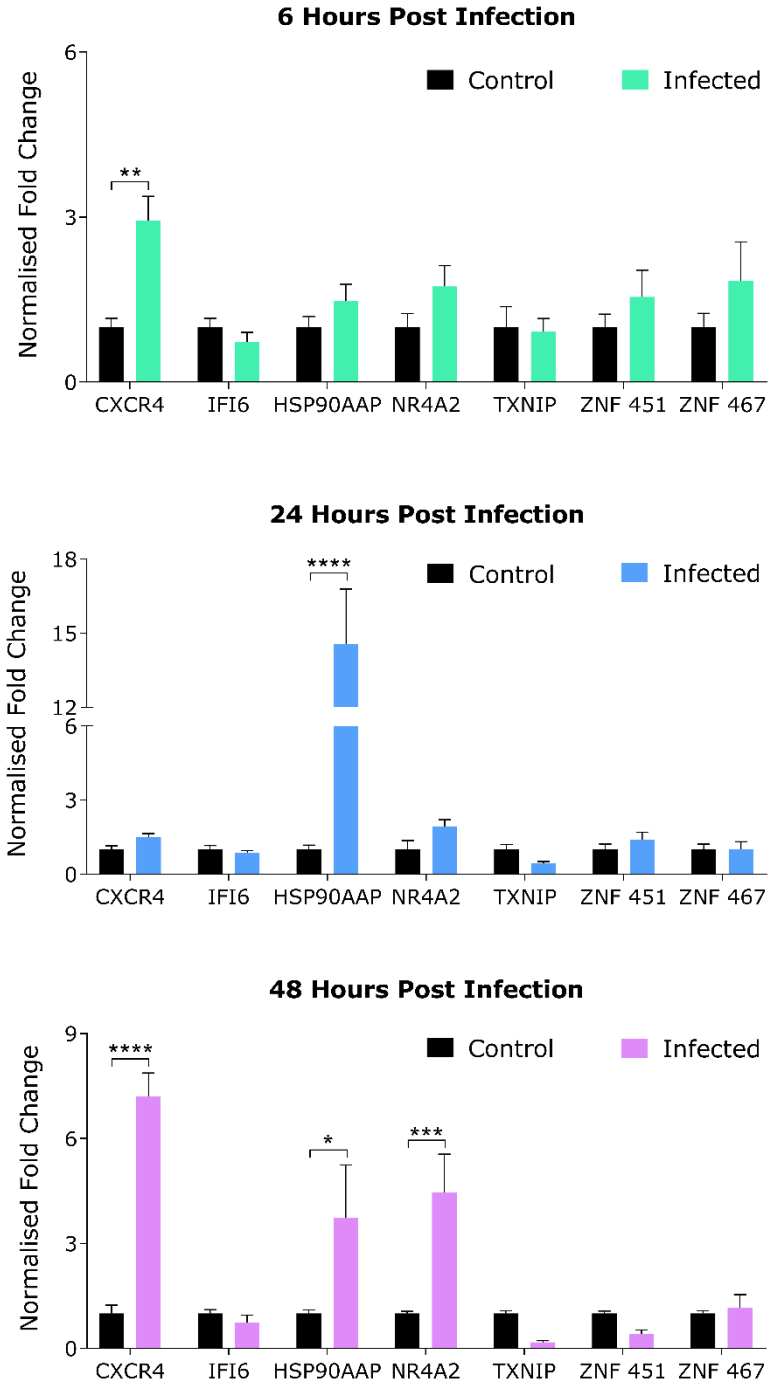


Figure 3-36 Normalised FC of CXCR4, IFI6, HSP90AAP, NR4A2, TXNIP, ZNF451, and ZNF467 genes at 6, 24 and 48 h.p.i at MOI of 5 by SYBR green RT-qPCR. Data were derived from three biological replicates, and the error bar represents SEM. CXCR4 was found to be significantly up-regulated at 6 h.p.i while HSP90AAP was found to be significantly up-regulated at 24 h.p.i. Three genes (CXCR4, HSP90AAP, and NR4A2) were found to be significantly up-regulated at 48 h.p.i.

Table 3-36 Validation of RNA-seq and microarray data by RT-PCR. All RT-PCR data have been converted to $\log_2$ from $\log_{10}$ for easy comparison to sequencing and microarray data. RNA-seq was unable to detect significant changes to the majority of selected genes at 6 and 24 h.p.i.

	6 h.p.i			24 h.p.i			48 h.p.i		
	RNA-seq	**Microarray**	**qPCR**	**RNA-seq**	**Microarray**	**qPCR**	**RNA-seq**	**Microarray**	**qPCR**
CXCR4	NA	NA	1.964	NA	NA	0.588	NA	1.675	2.849
HSP90AAP	-2.427	NA	0.973	NA	NA	3.864	-1.522	NA	1.900
IFI6	NA	NA	-0.731	NA	2.146	-0.201	-1.332	1.912	-0.455
NR4A2	NA	NA	1.204	NA	NA	0.956	NA	2.687	2.155
TXNIP	NA	-3.134	0.277	NA	-1.576	-1.138	-2.208	NA	-2.550
ZNF 451	NA	1.238	1.036	NA	NA	0.496	NA	-4.417	-1.282
ZNF 467	NA	-1.521	1.290	NA	NA	0.017	-2.067	NA	0.206

3.5 Discussion

In this chapter, the mRNA and miRNA transcriptome in the hBMEC model, which provides a global view of transcript regulation during *T. gondii* infection in an *in vitro* system, was characterised. The aim was to study temporal changes in the global expression of genes and miRNAs during the time course of *T. gondii* RH infection, with the hope of identifing specific biomarkers associated with parasite infection. Transcriptomes of *T. gondii* infected hBMECs cells have been sequenced using NGS sequencing technology (RNA-Seq), and transcriptome data were analysed using bioinformatics tools, revealing patterns of genes and gene interactions that may play important roles in *T. gondii* pathogenesis.

3.5.1 *Host Gene Expression Profile in T. gondii Infection*

Total RNA from control and infected cells at 6, 24 and 48 h.p.i were sequenced then mapped to the human reference genome in order to explore changes to the human transcriptome following *T. gondii* infection in hBMECs. Total RNA extracted from control and infected cells at the same three time points were also analysed using microarray technology. For RNA-seq where each group has only two samples, a strict cut-off of a *P*-value of < 0.01 was applied when analysing the DEGs from mRNA sequencing. In contrast, microarray has three samples per group thus less strict cut-off *P*-value of < 0.05 was applied when analysing its data. Filtered, differentially expressed mRNAs were analysed further for gene ontology and pathway analysis. Results from both technologies are combined and compared then discussed as follows.

6 h.p.i

At 6 h.p.i, mRNA sequencing identified 344 DEGs. Of this number 287 were down-regulated while 57 were up-regulated (**Appendix** 3-6). Correspondingly, 285 down-regulated genes and 71 up-regulated genes were identified from the microarray experiment (**Appendix** 3-18). There were only two genes found in both sets of up-regulated genes lists which are CHAC1 - ChaC glutathione specific gamma-glutamylcyclotransferase 1 (Log_2 FC - RNA-seq: 2.209, Microarray: 1.360) and CISH cytokine-inducible SH2 containing protein (Log_2 FC - RNA-seq: 2.159, Microarray: 1.176). CHAC1 plays a pro-apoptotic role in the unfolded protein response, and in the regulation of glutathione levels and oxidative balance in the cell. Increased expression was associated with increased breast and ovarian cancer recurrence (NCBI Gene - RefSeq, 2016). Meanwhile, CISH belongs to the cytokine-induced STAT inhibitor (CIS) protein family that are negative regulators of cytokine signalling through the JAK-STAT5 pathway (NCBI Gene - RefSeq, 2008).

Similarly, both sets of down-regulated genes lack similarity. Only six genes can be found on both lists, namely DOCK11 - dedicator of cytokinesis 11 (Log_2 FC - RNA-seq: 1.123, Microarray: 1.474), ITGB4 (Log_2 FC - RNA-seq: 1.288, Microarray: 1.085), KLF12 - Kruppel Like Factor 12 (Log_2 FC - RNA-seq: 1.171, Microarray: 1.448), NCAPD2 - non-SMC condensin I complex subunit D2 (Log_2 FC - RNA-seq: 1.041, Microarray: 1.402), NCAPG - non-SMC condensin I complex subunit G (Log_2 FC - RNA-seq: 1.094, Microarray: 1.097), NDC80 - NDC80, kinetochore complex component (Log_2 FC - RNA-seq: 1.078, Microarray: 1.676), and XPC - XPC complex subunit, DNA damage recognition and repair factor (Log_2 FC - RNA-seq: 1.669, Microarray: 1.010). XPC has DNA damage sensing ability and plays an important role in mitosis process and cancer prevention (Nemzow *et al.*, 2015) while NDC80 is required in

chromosome separation in mitosis process (Lin *et al.*, 2006). NCAPD2 converts interphase chromatin into mitotic-like condensed chromosomes (Olson *et al.*, 2011) while NCAPG is responsible for condensation and stabilisation of chromosomes (Murphy and Sarge, 2008). KLF12 plays an important role in suppressing cancer metastasis where it induces cell death by attachment (Godin-Heymann *et al.*, 2016). Down-regulation of KLF12 was associated with gastric cancer (Du *et al.*, 2016), ovarian cancer (Mak *et al.*, 2017) and breast cancer (Guan *et al.*, 2016). ITGB4 is part of a complex that controls cell adhesion, migration and proliferation where high levels of ITGB4 was associated with poor cancer prognosis (Stewart *et al.*, 2016; Bierie *et al.*, 2017). DOCK11 binds to Cdc42 which then activates a variety of functions like cell morphology, migration, adhesion, and growth (Etienne-Manneville, 2004; Sinha and Yang, 2008).

Nevertheless, when looking at GO of these two sets of genes both have a similar category of molecular function, biological process and cellular compartments. In the molecular function ontology, the majority of up and down-regulated genes from both sets matched to catalytic activity (GO:0003824) and binding (GO:0005488) functions (**Figure** 3-7, **Figure** 3-27) while for biological process ontology the two main categories are cellular process (GO:0009987) and metabolic process (GO:0008152) for both up and down-regulated genes (**Figure** 3-8, **Figure** 3-28). Two main cellular components for both sets of genes are cell part (GO:0044464) and organelle (GO:0043226) for both up and down-regulated genes (**Figure** 3-9, **Figure** 3-29). From RNA-seq data, the PANTHER Overrepresentation test identified 16 significant molecular functions (microarray – zero), 43 significant biological processes (microarray – five) and 17 significant cellular components (microarray – zero) were down-regulated. In contrast, only two significant molecular functions (microarray – zero), three significant biological processes

(microarray – one) and one significant cellular component (microarray – one) were up-regulated. The only overlapped GO result is a biological process (cellular component organisation GO:0016043) from both sets of down-regulated lists which was defined as a process that results in the assembly, arrangement of constituent parts, or disassembly of a cellular component (PANTHER Classification System, 2019).

Reactome identified 47 pathways from the RNA-seq DEGs list while the gene list from the microarray experiment identified five significant pathways (Entities FDR < 0.01). However, none of the pathway's names overlap each other even though all pathways from both lists were down-regulated. Since there were more down-regulated genes than up-regulated genes, the average $\log_2$ FC values for all pathways are skewed towards negative values. All five pathways (R-HSA-156711 Polo-like kinase-mediated events; R-HSA-141444 Amplification of signal from unattached kinetochores *via* a MAD2 inhibitory signal; R-HSA-141424 Amplification of signal from the kinetochores; R-HSA-69278 Cell Cycle Mitotic; R-HSA-68877 Mitotic Prometaphase) from microarray data have negative values and were related to cell-cycle supporting data from the previous chapter that *T. gondii* halts cell cycle process. Meanwhile all pathways from RNA-seq data were negative in values and the majority of them were related to processing of RNA, metabolism of RNA, protein and amino acids. Among them, a noteworthy pathway is R-HSA-164940 (Nef-mediated downregulation of MHC class I complex cell surface expression). This pathway was down-regulated in HIV-1 infected cells and protect infected cells from cytotoxic T-lymphocyte recognition (Blagoveshchenskaya *et al.*, 2002). MHC class I and II antigen presenting pathway was also down-regulated in *T. gondii* infected murine macrophages, so as to avert immune response (Lüder *et al.*, 1998, 2001).

24 h.p.i

At 24 h.p.i, mRNA sequencing identified 65 genes DEGs, where of this number seven were down-regulated while 58 were up-regulated (**Appendix** 3-8). In addition, 24 down-regulated genes and 21 up-regulated genes were identified from the microarray experiment. None of the genes in these two sets overlap each other.

Gene ontology of these two sets of genes indicates both have similar categories of molecular function, biological process and cellular compartments. In the molecular function ontology, the majority of genes from both sets matched to the binding (GO:0005488 - both) function plus catalytic activity (GO:0003824 – RNA-seq), and structural molecule activity (GO:0005198 - microarray) for up-regulated genes (**Figure** 3-10, **Figure** 3-30) while for down-regulated genes binding (GO:0005488 - both) function plus catalytic activity (GO:0003824 – microarray), and structural molecule activity (GO:0005198 – RNA-seq) were the main categories. For biological process ontology, up-regulated genes from both sets matched to cellular process (GO:0009987) and metabolic process (GO:0008152) processes while down-regulated genes matched to cellular process (GO:0009987 - both), metabolic process (GO:0008152 - microarray) and developmental process (GO:0032502 – RNA-seq) (**Figure** 3-11, **Figure** 3-31). Two main cellular components for up and down-regulated genes from both sets and down-regulated genes are cell part (GO:0044464) and organelle (GO:0043226) (**Figure** 3-12, **Figure** 3-32). From the RNA-seq data, the PANTHER Overrepresentation test identified zero significant molecular functions (microarray – zero), eight significant biological processes (microarray – zero) and zero significant cellular components (microarray – zero) were down-regulated. In contrast only four significant molecular functions (microarray – three), zero significant biological processes

(microarray – zero) and one significant cellular component (microarray – one) were up-regulated. There is no similarity between GO results from both sets of experiments.

Reactome identified eight significant pathways from the RNA-seq DEGs list, while the gene list from the microarray experiment identified five significant pathways (Entities FDR < 0.01). There is no similarity between identified pathways from both sets of experiments. As the majority of DEGs from RNA-seq data were up-regulated, all pathways identified by the database were up-regulated. Three of the pathways are involved in energy metabolism (R-HSA-163200 – 'Respiratory electron transport, ATP synthesis by chemiosmotic coupling, and heat production by uncoupling proteins', R-HSA-1428517 - The citric acid (TCA) cycle and respiratory electron transport, R-HSA-611105 – Respiratory electron transport), three are upstream regulatory pathways (R-HSA-380994 – ATF4 activates genes, R-HSA-381042 – PERK regulates gene expression, R-HSA-5628897 – TP53 Regulates Metabolic Genes) and two on amino acids synthesis (R-HSA-70614 – Amino acid synthesis and interconversion, R-HSA-977347 – Serine biosynthesis). Amino acids are important for *T. gondii* development and serine was predicted to be among several metabolic needs of *T. gondii* (Tymoshenko *et al.*, 2015). Host up-regulation of the amino acid synthesis and metabolism pathways, plus energy metabolism were likely to have been directed by the parasite for their survival. R-HSA-380994 (ATF4 activates genes) and R-HSA-381042 (PERK regulates gene expression) both were involved in cell cycle arrest which has been reported in *T. gondii* infected cells (Molestina, El-guendy and Sinai, 2008; Szatanek *et al.*, 2012). Meanwhile, R-HSA-5628897 (TP53 Regulates Metabolic Genes) can also cause cell cycle arrest but is predominantly involved in the metabolism of carbohydrates, nucleotides and amino acids, protein synthesis and aerobic respiration (Puzio-Kuter, 2011; Napoli and Flores, 2016).

All five pathways from microarray data also have positive average log_2 FC values. All of them (R-HSA-913531 Interferon Signalling, R-HSA-909733 Interferon alpha/beta signalling, R-HSA-1280215 Cytokine Signalling in Immune system, R-HSA-877300 Interferon gamma signalling, R-HSA-168256 Immune System) were related to immune response which differed to the pathways from RNA-seq data and indicate the host-parasite interplay to survive.

48 h.p.i

At 48 h.p.i, mRNA sequencing identified 942 genes DEGs where of this number 249 were down-regulated while 693 were up-regulated (**Appendix** 3-9). In addition, 314 down-regulated genes and 3400 up-regulated genes were identified from the microarray experiment (**Appendix** 3-19). Only four down-regulated genes were found on both lists which are TRIM15, GPRC5B, GRB7, and LRCOL1. TRIM15 regulates cell migration, focal adhesion and down-regulation was associated with limiting virus release from cells (Uchil *et al.*, 2008, 2014). Increased GPRC5B was associated with reduced insulin secretion and beta-cell viability (Soni *et al.*, 2013). GRB7 regulation of cell migration, proliferation and tumorigenesis (Chu *et al.*, 2009) while little is known about LRCOL1 function.

Among the up-regulated genes, 110 genes can be found on both lists. Gene ontology of these two sets of genes indicates both have similar categories of molecular function, biological process and cellular compartments. In the molecular function ontology, the majority of genes from both sets matched to binding (GO:0005488 - both) function plus catalytic activity (GO:0003824 – RNA-seq), and structural molecule activity (GO:0005198 - microarray) for up-regulated genes (**Figure** 3-10, **Figure** 3-30) while for down-regulated genes

binding (GO:0005488 - both) function plus catalytic activity (GO:0003824 – microarray), and structural molecule activity (GO:0005198 – RNA-seq) were the main categories. For the biological process ontology, the up-regulated genes from both sets matched to cellular process (GO:0009987) and metabolic process (GO:0008152) processes while the down-regulated genes matched to cellular process (GO:0009987 - both), metabolic process (GO:0008152 - microarray) and developmental process (GO:0032502 – RNA-seq) (**Figure** 3-11, **Figure** 3-31). The two main cellular components for up and down-regulated genes from both sets and down-regulated genes are cell part (GO:0044464) and organelle (GO:0043226) (**Figure** 3-12, **Figure** 3-32).

From the RNA-seq data, the PANTHER Overrepresentation test identified zero significant molecular functions (microarray – 38), zero significant biological processes (microarray – 81) and three significant cellular components (microarray – 28) were down-regulated. In contrast only 11 significant molecular functions (microarray – three), nine significant biological processes (microarray – four) and 16 significant cellular components (microarray – zero) were up-regulated. Overlapping occurs at cellular components ontology where both down-regulated genes lists listed nucleus (GO:0005634), organelle (GO:0043226) and intracellular (GO:0005622) as significant cellular components. In addition, both up-regulated genes lists are associated with sequence-specific DNA binding RNA polymerase II transcription factor activity (GO:0000981) as significant molecular function.

Reactome identified 39 pathways from RNA-seq DEGs list while no pathway passed the selection criterium (Entities FDR < 0.01) from microarray experiment. The majority of these pathways (21) were related to mRNA translation and protein processing and there are four pathways related to immune response to infectious disease like R-HSA-6783783 (Interleukin-10

signalling). Another four pathways are related to metabolism RNA and destruction of RNA through non-sense mediated decay (NMD) pathway. Three pathways are related to developmental biology, three pathways in energy production and metabolism, two upstream regulatory pathways (R-HSA-380994 - ATF4 activates genes, R-HSA-381042 - PERK regulates gene expression) with multiple downstream effects and finally two pathways related to selenium synthesis and metabolism (R-HSA-2408522 - Selenoamino acid metabolism, R-HSA-2408557 - Selenocysteine synthesis).

The 14 up-regulated genes (**Table** 3-8) shared between all time points post infection from RNA-seq data were associated with five pathways, 'respiratory electron transport, ATP synthesis by chemiosmotic coupling, and heat production by uncoupling proteins' (R-HSA-163210), 'respiratory electron transport' (R-HSA-380994), 'the citric acid (TCA) cycle and respiratory electron transport' (R-HSA-8949613), 'TP53 regulates metabolic genes' (R-HSA-381042), and 'transcriptional Regulation by TP53' (R-HSA-6799198). The first three pathways are key pathway for energy production while the latter two are pathways where p53 is one of the key genes involved in gene transcription regulating cell metabolism, metabolism of carbohydrates, nucleotides and amino acids, protein synthesis and aerobic respiration (Puzio-Kuter, 2011). Because *T. gondii* infection was associated with recruitment of host mitochondria to parasitophorous vehicle (Pernas *et al.*, 2014), it is very likely that after recruitment, *T. gondii* controlled host mitochondria and p53 protein to cooperate in its pathogenesis by up-regulation of all five pathways. Meanwhile, only one gene was shared between all time points from microarray data which is PRTN3 or proteinase 3. PRTN3 was up-regulated in PK13 cells (porcine kidney epithelial cell) at 1, 2, 3, 4, 6 h.p.i but not at 24, 48 and 72 h.p.i (Okomo-Adhiambo, Beattie and Rink, 2006). Meanwhile, neutrophil-derived-PRTN3 was reported to enhance endothelial cells junctional integrity

(Kuckleburg and Newman, 2013) and at the same time can attract other neutrophils and facilitate seslective crossing of endothelial barrier (Kuckleburg *et al.*, 2012). Thus, it is possible that hBMEC up-regulate PRTN3 to strengthen the barrier and attract neutrophil to site of infection.

3.5.2 *Expression Profile of T. gondii Genes During Infection*

As total RNA extracted from infected cells would also contain mRNA from *T. gondii* itself, sequenced mRNAs were mapped to *T. gondii* reference genome in order to asses the expression profile of *T. gondii* genes. RNA-seq data matched to 4411, 6116, 6049 genes at 6,24 and 48 hours respectively following mapping to the *T. gondii* ME49 reference genome. Among them, 4320 were expressed at all time points. The shared gene list has been filtered to 94 (**Appendix** 3-11) for all time points by selecting genes with baseMean expression of > 2000, *P*-value < 0.01 and $\log_2$ FC ≥ 1 in order to narrow the list down to essential genes with potential as targets for vaccination. This approach was based on the thinking that high baseMean expression value (also means high counts) correspond to high mRNA and high protein expression, which in forth indicate their importance in *T. gondii* pathogenesis.

Among these 94 genes, 41 of them are ribosomal proteins, 10 are dense granule proteins (GRA1~8, GRA12, GRA14), nine are hypothetical proteins with unknown functions, seven microneme proteins (MIC1, MIC3~6, MIC10, MIC11), four are surface antigens (SRS25, SAG1, SAG2A, SRS51) while the rest were proteins involved in transcription initiation, energy metabolism, cytoskeleton formation and other unknown functions. During *T. gondii* invasion, microneme proteins are released, first to help with attachment and internalisation (Huynh *et al.*, 2003), then rhoptries proteins are released, followed by dense granular proteins (Nam, 2009). Secreted rhoptries proteins and dense granular proteins

either remain soluble in the lumen or they become part of parasitophouruos vacuole membrane or network structure within the vacuole for intracellular survival and replication (Mercier *et al.*, 2002; Nam, 2009).

While there were several micronemes and dense granule genes highly up-regulated in this study, only one rhoptry gene ROP1 was found to be highly expressed at all time points indicating its importance in *T. gondii* pathogenesis. Partial protection was achieved when mice immunised with recombinant ROP1 rpotein was challenged with *T. gondii* RH infection (Sonaimuthu *et al.*, 2016). Two noteworthy highly expressed *T. gondii* genes are TGME49_211680 (protein disulfide isomerase) and TGME49_293690 (PRF - profilin). These two genes are key components to parasite motility (Skillman *et al.*, 2012) and can elicit an immune response (Kucera *et al.*, 2010). A DNA vaccine encoding PRF was reported to invoke a strong immune response, reducing brain cysts ~40% compared to unvaccinated mice (Gao *et al.*, 2018).

Another noteworthy gene is effector protein 14-3-3, which can induce migration of parasitised microglial and dendritic cells, suggesting it crucial role in parasite dissemination (Weidner *et al.*, 2016). Knockout of 14-3-3 gene leads to non-viable *T. gondii* and it was fairly effective as a vaccine candidate (Meng *et al.*, 2012; Weidner *et al.*, 2016).

Only a small number of genes were responsible for pathway ontology among all 94 genes (**Table** 3-15). TGME49_232350 (LDH1 - lactate dehydrogenase LDH1), TGME49_289690 (GAPDH1 - glyceraldehyde-3-phosphate dehydrogenase) and TGME49_294200 (glucose-6-phosphate 1-dehydrogenase) were key genes in 10 of the pathways which are related to glycolysis, gluconeogenesis, sugar degradation and pyruvate fermentation. These three genes were among 10 key enzymes/proteins in glycolysis which are important for pyruvate generation for energy production in the form of ATP

(adenosine triphosphate). Host glycolysis proteins was reported to be up-regulated in *T. gondii* infected HFF cells (Blader, Manger and Boothroyd, 2001). Our result suggests that up-regulation of host glycolysis proteins is not a significant step, as *T. gondii* itself can produce its own proteins for glycolysis.

Meanwhile, TGME49_286420 (EF-1-ALPHA - elongation factor 1-alpha, putative) and TGME49_294800 (EF-1-ALPHA - elongation factor 1-alpha, putative) were responsible for 18 pathways which are related to sulfur and selenocompound metabolism. EF-1-ALPHA role in *T. gondii* pathogenesis is still vague but was hypothesised to be responsible for cell invasion and key compound metabolism (Wang *et al.*, 2017). Several *T. gondii* proteins like *T. gondii*-glutathione reductase protein are selenium-dependent (Hassan *et al.*, 2014) and thus EF-1-ALPHA is required for selenium scavenging. In addition, selenium is beneficial to the host where it has anti-oxidant properties and has been reported to help fight *T. gondii* infection in mice (McCarthy and Davis, 2003). Thus, depleting the host selenium reservoir can ensure successful infection. EF-1-ALPHA was the target for a monoclonal antibody vaccine and was reported to increased mice survival from *T. gondii* infection (Wang *et al.*, 2017). Currently, there is lack of data on sulfur metabolism in *T. gondii* pathogenesis. Sulfur metabolism was not listed as one of the essential metabolic needs for *T. gondii* replication based on computational approach (Elsheikha *et al.*, 2014; Tymoshenko *et al.*, 2015).

Three cytoskeleton related *T. gondii* genes, namely TGME49_209030 (ACT1 - actin ACT1), TGME49_220400 (ADF - actin depolymerising factor ADF) and TGME49_316400 (TUBA1 - alpha tubulin TUBA1) were also highly expressed at all time points by the parasite. ADF and ACT1 have been reported to be important but not essential in parasite movement, especially during entry into and egress from host cells, from individual knockout of each gene (Mehta

and Sibley, 2011; Drewry and Sibley, 2015). Meanwhile, the role of TUBA1 is still an enigma. Targeting ADF, ACT1 and TUBA1 collectively as knockout candidates, could result in better restriction of parasite invasiveness.

3.5.3 *Host Small RNA Expression Profile in T. gondii Infection*

At 6 h.p.i, 36 miRNAs passed the criteria with 31 of them were up-regulated. No miRNA passed the criteria at 24 h.p.i while at 48 h.p.i, 531 miRNAs were up-regulated while 15 miRNAs were down-regulated. Among up-regulated and down-regulated miRNAs at 6 and 48 h.p.i, 24 and three miRNAs were expressed at both time points respectively.

6 h.p.i

Among 28 precursor miRNAs, two of them (hsa-mir-19a and hsa-mir-20a) were also significantly up-regulated in human PBMC infected with TgCtwh3 (China strain) at 6, 12 and 24 h.p.i and 12 and 24 h.p.i respectively (Cai *et al.*, 2014). Toxoplasma infection in HFF cells were also found to specifically increases levels of host miR-17, miR-18, miR-19, miR-20 and miR-25 family members at 6, 12 and 24 h.p.i (Zeiner *et al.*, 2010). In this study, only members from miR-19 (hsa-miR-19a-3p, hsa-miR-19b-3p) and miR-20 (hsa-miR-20a-5p, hsa-miR-20b-5p) were up-regulated.

Also, 23 pathways were identified to be up-regulated while another three were down-regulated. Down-regulated pathways are cell adhesion molecules/CAMs (hsa04514; 3 miRNAs), amphetamine addiction (hsa05031; 3 miRNAs) and nicotine addiction (hsa05033; 3 miRNAs). All three pathways were associated with the same three miRNAs which are hsa-miR-375, hsa-miR-1246 and hsa-miR-3976. The result agrees with biological process ontology of RNA-

seq and microarray data where biological adhesion (GO:0022610) process was down-regulated at 6 h.p.i. Meanwhile, a meta-analysis study found there is no strong evidence to support the relationship between addiction and *T. gondii* infection in humans (Sutterland *et al.*, 2015) which agrees with data from this study.

Among the 23 pathways identified, four pathways (glioma hsa05214, proteoglycans in cancer hsa05205, renal cell carcinoma hsa05211, transcriptional misregulation in cancer hsa05202) were directly related to cancer diseases. While there is no strong evidence that *T. gondii* cause cancer, there is strong resemblances between transcriptomes from infected cells and cancer cells from various studies (Ngô *et al.*, 2017). Parasite linkage to cancer was also supported by experiments where injection of attenuated, non-replicating parasite into cancerous mice increased their long-term survival chances (Baird *et al.*, 2013; Sanders, Fox and Bzik, 2015; Ngô *et al.*, 2017). Another cancer linked pathway up-regulated in this study is the WNT signalling pathway (Clevers and Nusse, 2012). Human brain infected with *T. gondii* was found to up-regulate 14 genes from Wnt/Ca+pathway, including six frizzled class receptor genes FZD2, FZD3, FZD4, FZD5, FZD8, and FZD9 (Ngô *et al.*, 2017).

24 h.p.i

There are no miRNAs that passed the cut-off criteria at 24 h.p.i from *T. gondii* infected hBMECs in this study even though other studies found several miRNAs to be significantly differentially expressed at the same time points (Zeiner *et al.*, 2010; Cai *et al.*, 2014).

48 h.p.i

A literature search did not find any other study on miRNAs from *T. gondii* infected human cells at 48 h.p.i. As such, this study is the first to describe changes in miRNAs expression at 48 h.p.i following *T. gondii* infection. Several noteworthy miRNAs were up-regulated in this study and among them is has-miR-132 (hsa-miR-132-3p: 2.343, hsa-miR-132-5p: 3.478). These miRNAs are classified as modulators of both neuronal and immune processes or 'neurimmiR' (Soreq and Wolf, 2011). Up-regulation of this miRNA was also reported in *T. gondii* infected human neuroepithelioma and was shown to affect dopamine signalling pathway (Xiao *et al.*, 2014). Other noteworthy miRNAs are miRNAs encoded by miR-17–92 gene cluster that affects apoptosis and G1/S cell cycle development by targeting multiple components of each pathway (Zeiner *et al.*, 2010). A part of this cluster is hsa-miR-20a-5p that was expressed at 6 and 48 h.p.i (log_2 FC – 6 hrs: 1.04 48 hrs: 3.796). Inhibition of this miRNA in *T. gondii* infected human macrophages, promotes the cell to undergo apoptosis (Rezaei *et al.*, 2018). Interestingly, the miR-17-92 family miRNAs' expression were not affected when HFF cells were infected with *Neospora*, a closely related parasite to Toxoplasma (Zeiner *et al.*, 2010). This cluster of miRNAs plus hsa-mir-125b-2 (hsa-miR-125b-2-3p: 3.253, hsa-miR-125b-5p: 3.373) are involved in anti-apoptosis in response to *T. gondii* infection (Cai *et al.*, 2013, 2014). Two more inflammatory response regulators and mediators hsa-miR-146a-5p (log_2 FC = 3.154) and hsa-miR-155-5p (log_2 FC = 2.950) were also highly up-regulated. miR-146a up-regulation was induced by *T. gondii* ROP16 and silencing this miRNA leads to higher IFN-gamma production and better mice survival rate (Cannella *et al.*, 2014). Interestingly, miR-146a can also be found in the exosome in blood from infected mice suggesting this miRNAs was utilised to systemically reduce immune response (Cannella *et al.*, 2014). Meanwhile, miR-155 is one of key immunomodulators commonly found in cancer cells (Vigorito

et al., 2013). Collectively all of miRNAs mentioned above can be used as biomarkers for *T. gondii* persistent and latency infection.

Down-regulated miRNAs were associated with 'thyroid hormone signalling pathway' (hsa04919, 5 miRNAs), 'lysine degradation' (hsa00310, 5 miRNAs) and 'cell adhesion molecules/CAMs' (hsa04514, 3 miRNAs). The role of thyroid hormones in toxoplasmosis is unclear but impaired thyroid function was reported in murine toxoplasmosis (Stahl and Kaneda, 1998) and a slight reduction in serum thyroid stimulating hormone was identified in pregnant women (Kaňková *et al.*, 2014). Lysine is required for *T. gondii* motility (Heaslip *et al.*, 2011) and down-regulation of the 'lysine degradation' pathway could be the result of *T. gondii* manipulation of the host cell in order to preserve a lysine reservoir, especially at 48 h.p.i when newly form tachyzoites are matured and ready to exit the cells. In an identical fashion to the response at 6 h.p.i, the CAMs pathway was also down-regulated at 48 h.p.i. While *T. gondii* infection caused up-regulation of cell adhesion molecules like ICAM-1 and VCAM-1 (Lambert *et al.*, 2009; Harker *et al.*, 2013) in leukocytes, a different effect can be seen in this study, as cell adhesion molecule related gene and miRNAs were down-regulated. Among the top 30 highly similar sequences between predicted *T. gondii* miRNA and human miRNAs (Saçar, Bağci and Allmer, 2014), seven of them (hsa-miR-1277-5p, hsa-miR-185-5p, hsa-miR-18a-3p, hsa-miR-210-3p, hsa-miR-3173-5p, hsa-miR-328-3p, hsa-miR-7706) were up-regulated at 48 h.p.i but not at 6 h.p.i. These human miRNAs sequences have 88-100% similarity to predicted *T. gondii* miRNA sequences.

The condensed the list of up-regulated miRNAs contains 469 individually unique miRNAs and 406 individually unique precursors. The top 100 of them (based on $\log_2$ FC) were analysed using DIANA-mirPath version 3. These genes were associated with 64 pathways where among them 19 were also found to

be up-regulated at 6 h.p.i. Among 64 pathways, 12 were directly related to cancer while cancer-related pathways like WNT and p53 signalling pathways were also up-regulated. This result adds further evidence linking *T. gondii* infection to cancer diseases. Interestingly, the 'lysine degradation' (hsa00310) pathway was also found to be up-regulated with more miRNAs linked to this pathway (pathway union method - 17 miRNAs; genes intersection method - 72 miRNAs) compared to five miRNAs from the down-regulated miRNAs list. Modulation of several up-stream signalling pathways were also implicated: PI3K-Akt, MAPK, FoxO, AMPK, Wnt, HIF-1, TGF-beta and p53 signalling, pathways that are responsible for variety of processes including signalling, protein metabolism, developmental biology, apoptosis, cell growth, cell differentiation, energy production and the cell cycle are observed in this study.

3.5.4 *T. gondii Small RNA Expression Profile During Infection*

Classical RNA molecules are messenger RNA (mRNA), ribosomal RNA (rRNA) and transfer RNA (tRNA) while small RNAs are defined as 18-30 nucleotides of non-coding RNA, divided into three groups namely small interfering RNAs (siRNAs), microRNAs (miRNAs) and Piwi-associated RNAs (piRNAs) (Großhans and Filipowicz, 2008; Zhang, 2009). It was predicted that *T. gondii* RH strain contains 117,315 small RNAs while *T. gondii* ME49 strain contains 67,623 small RNAs (J. Wang *et al.*, 2012). Among small RNAs of *T. gondii* ME49, 336 of them are miRNAs while for *T. gondii* RH, 201 of them are miRNAs (J. Wang *et al.*, 2012). Unfortunately, there is no specific database cataloguing *T. gondii* miRNA that can be used to BLAST all mapped reads even at ToxoDB.org. As such this study unable to provide data on differentially expressed *T. gondii* siRNAs, miRNAs and piRNAs. In addition, latest analysis on *T. gondii* genome only manages to confirm limited amounts of three types of

noncoding RNA which are 181 copies of tRNA, 18 copies of rRNA and 4 copies of miRNA (Lau *et al.*, 2016). Reads mapped and annotated to *T. gondii* genome were filtered by applying minimum cut-off FPKM values of ≥ 2000 (in infected samples) and *P*-values ≤ 0.01. At 6 h.p.i, 116 genes passed the selection criteria (**Appendix** 3-14) which are 58 ribosomal RNA (18S, one; 28S, seven; 5.8S, 50), one ribosomal protein L36 and 57 transfer-RNA (tRNA) for amino acids. Transfer RNA (tRNA) for glutamic acid (10), valine (eight) and isoleucine (six) were the top three most abundant tRNAs. Pathway analysis and gene ontology at ToxoDB.org did not return any significant results ($P < 0.05$).

Meanwhile at 24 h.p.i, 138 genes passed the selection criteria (**Appendix** 3-15) which are 62 ribosomal RNA (18S, four; 28S, six; 5.8S. 52), four ribosomal protein L36 and 62 tRNA for amino acids. Transfer RNA (tRNA) for glutamic acid (10), valine (eight) and aspartic acid (seven) were the top three most abundant tRNA. Pathway analysis did not return any significant results ($P < 0.05$). Gene ontology returns 25 biological processes (**Table** 3-26), two molecular functions (structural constituent of ribosome GO:0003735, structural molecule activity GO:0005198) and 15 cellular components (**Table** 3-26). All of gene ontology results were based on only four genes which are TGME49_302055 (ribosomal protein S12), TGME49_300604 (ribosomal protein L36), TGME49_3006 (ribosomal protein L16, putative) and TGME49_300611 (ribosomal protein L14).

At 48 h.p.i, 164 genes passed the selection criteria (**Appendix** 3-16) which are 81 ribosomal RNA (18S, four; 28S, eight; 5.8S, 69), two ribosomal protein L36 (TGME49_300604) and ribosomal protein S12 (TGME49_302055), 79 tRNA for amino acids, one chaperone caseinolytic protease (TGME49_302000) and one unknown protein (TGME49_321685). The three most common tRNA are for glutamic acid (nine), valine (seven) and isoleucine

(six). Pathway analysis did not return any significant results ($P < 0.05$). Gene ontology returns 14 biological processes (**Table** 3-27), two molecular functions (structural constituent of ribosome GO:0003735, structural molecule activity GO:0005198) and nine cellular components (**Table** 3-27). All of gene ontology results were based on only two genes which are TGME49_300604 (ribosomal protein L36) and TGME49_302055 (ribosomal protein S12).

Ribosomal protein L36 and S12 were up-regulated at 6, 24 and 48 h.p.i indicating the importance role in *T. gondii* pathogenesis. RPL36 function is unknown while RPS12 function also has not been characterised though based on similarity to other proteins on UniProt website (Uniprot.org, 2019), RPS12 may play an important role in ensuring translational accuracy together with S4 and S5.

3.5.5 *Sequencing Data Validation with qPCR*

Seven genes CXCR4, HSP90, IFI6, NR4A2, TXNIP, ZNF451, and ZNF467 were selected from mRNA and microarray studies for validation with RT-qPCR (**Table** 3-36). Selection of genes were done randomly as there is lack of similarity between RNA-seq and microarray data.

Overall, four genes expression (CXCR4, NR4A2, TXNIP, ZNF 451) from microarray and RNA-seq studies showed similar results to the PCR study while another three genes (HSP90AAP, IFI6, ZNF 467) produce contrasting expression results from the PCR study. CXCR4 and NR4A2 up-regulation at 48 h.p.i by microarray technology, was validated to be up-regulated by PCR study. HSP90 which was down-regulated at 6 and 48 h.p.i by RNA-seq study was found to be slightly up-regulated at 6 h.p.i and highly up-regulated at 48 h.p.i by PCR study. IFI6, up-regulated at 24 and 48 h.p.i by microarray study, was found to

be down-regulated at both time points by the PCR study. TNXIP, down-regulated at all time points by microarray and RNA-seq studies was found to be slightly up-regulated at 6 h.p.i but was validated to be down-regulated at 24 and 48 h.p.i by the PCR study. ZNF451 up-regulation at 6 h.p.i and down-regulation at 48 h.p.i by microarray study matched with the results from the PCR study. In contrast, ZNF467 down-regulation at 6 h.p.i and 48 h.p.i by microarray and RNA-seq studies respectively was found to be highly up-regulated at 6 h.p.i and slightly up-regulated at 48 h.p.i by PCR study.

3.5.6 *Conclusion*

In general, this study confirmed previous findings that *T. gondii* infection halts cell cycle progression at genes level in infected cells and modulates the expression of genes and pathways seen in cancer cells. Thus, the hypothesis that hBMECs infected with *T. gondii* RH exhibit an mRNA-miRNA expression profile that is different from that exhibited by healthy, uninfected, cells was accepted. The majority of the up-regulated pathways were related to ATP synthesis and metabolism. Integrated mRNA/miRNA expression profiling and pathway analysis show multiple signalling pathways including, ATF4 activation, TP53 regulation, selenoamino acid metabolism and selenocysteine synthesis as key pathways potentially regulated during *T. gondii* infection. Small RNA study led to the identification of the increased expression of miR-7, miR-19, miR-20 families and expression of the miR-17-92 family plays important role in determining the fate of host cells in *T. gondii* infection. Also, ribosomal proteins L36 and S12 were identified as key players in *T. gondii* pathogenesis and have good potential as vaccine candidates. Overall, the results reveal several previously unidentified changes in the host cell and contribute to fundamental knowledge of the host-pathogen interaction.

Chapter 4 Chapter 4 Cytotoxic and Anti-*Toxoplasma gondii* Activities of Monensin (a WNT Signalling Inhibitor)

4.1 Abstract

Central to the progression of cerebral toxoplasmosis is the interaction of *Toxoplasma gondii* with the blood-brain barrier (BBB) endothelium. In the present work, this study tested the hypothesis that inhibition of WNT signalling by the monovalent ionophore monensin reduces the growth of *T. gondii* infecting human brain microvascular endothelial cells (hBMECs) or microglial cells. The anti-parasitic effects of monensin (a WNT Signalling Inhibitor) on the *in vitro* growth of *T. gondii* tachyzoites was identified using two separate methods (Sulforhodamine B staining and microscopic parasite count). Also, the cytotoxic effect of monensin on key functions of hBMECs, including viability, mitochondrial potential, DNA fragmentation, cell cycle, and the integrity of the cell monolayer were investigated. In addition, the transcriptome of hBMECs infected with *T. gondii* and infected with *T. gondii* plus monensin treatment were examined. Monensin significantly ($P < 0.05$) inhibited *T. gondii* growth at 0.1 μM concentration, with limited cytotoxicity to hBMECs or microglial cells. The effects of *T. gondii* on the integrity of the BBB were assessed by the transendothelial electrical resistance (TEER) assay in an *in vitro* human BBB model. The results revealed several changes in hBMECs' function, which may contribute to the adverse effects observed following treatment with monensin. *T. gondii* infection significantly decreased hBMECs' TEER resistance, which was rescued when cells were treated with monensin, probably attributed to the anti-parasitic activity of monensin. Interestingly, treatment of hBMECs with

monensin did not significantly down-regulate WNT signalling pathway even though *T. gondii* infection inhibition was achieved and cell growth was restored. These findings indicate that the WNT signalling pathway did not play an important role in *T. gondii* infection in hBMECs and the potential use of monensin as treatment for *T. gondii* infection at BBB interface.

4.2 Introduction

Toxoplasma gondii is an apicomplexan protozoan parasite with a strict intracellular and neurotropic affinity. The disease associated with *T. gondii* infection, toxoplasmosis, can lead to severe central nervous system (CNS) pathologies and reproductive abnormalities (Montoya and Liesenfeld, 2004; Elsheikha, 2008). Although infection is usually asymptomatic in healthy humans, infection can be fatal in immunocompromised individuals and in unborn foetuses, because the parasite can spread transplacentally from pregnant mother to fetus (Tenter, Heckeroth and Weiss, 2000). Besides the lack of a vaccine, current treatment options for toxoplasmosis are limited and responses to commonly used medicines are often unsatisfactory (Leport *et al.*, 1988). There is a clear need for new and more potent anti-*T. gondii* therapeutics to reduce the clinical impact of toxoplasmosis. Ideal therapeutic agents prevent parasite growth, without inhibiting the proliferation or perturbing the homeostasis of host cells. However, in general, although available agents display potent anti-*T. gondii* properties, many are cytotoxic to mammalian cells (Schmidt *et al.*, 2005).

The blood-brain barrier (BBB) is the site of critical interaction between neuro-pathogens and the mammalian CNS (Feustel, Meissner and Liesenfeld, 2012). Microvascular cerebral endothelium, a fundamental constituent of the BBB plays important roles in maintaining a barrier to protect against brain

invasion by neuropathogenic microorganisms and in regulating the immune response to CNS infection that has breached this barrier. During *T. gondii* infection, different signalling transduction pathways control the expression of a wide range of genes that orchestrate molecular and cellular events to eliminate the invading parasite and regulate the associated inflammation (Jia, B. *et al.*, 2013). One of these pathways is the WNT pathway, which is considered as an important regulatory axis in the immune system. The expression of genes involved in this pathway were increased in *T. gondii*-infected mice (Jia, B. *et al.*, 2013). Intracellular pathogens have been shown to manipulate the host WNT pathway or exploit this pathway to facilitate their entry into the cell and establish infection, such as *Chlamydia trachmatis* (Kessler *et al.*, 2012) and influenza virus (Shapira *et al.*, 2009), among others.

Small molecule inhibitors of the WNT pathway are becoming more prominent in the pharmaceutical industry (Clevers and Nusse, 2012), and are increasingly being used to target cancer cells and intracellular pathogens (Kapoor *et al.*, 2013). Natural polyether ionophores, such as monensin, have been objects of great interest, because of their antimicrobial activities (Rutkowski and Brzezinski, 2013). Monensin has been extensively used in veterinary applications as a growth promoter (Callaway, Edrington and Rychlik, 2003) and to treat coccidiosis and cryptosporidiosis (Teichmann *et al.*, 2012; Rutkowski and Brzezinski, 2013). Also, monensin was proposed as an anticancer agent (Tumova *et al.*, 2014; Deng *et al.*, 2015). Monensin, secreted by the bacteria *Streptomyces cinnamonensis*, has been shown to modulate WNT signalling by antagonising β-catenin and the lipoprotein receptor-related protein, LRP, a WNT co-receptor (Tumova *et al.*, 2014). Investigation into how manipulation of the WNT pathway by monensin can impair the growth of *T. gondii* could be greatly beneficial in the development of new anti-*T. gondii* therapeutics.

In this study, the hypotheses were that (1) inhibition of the WNT signalling pathway by monensin can reduce the growth of *T. gondii* infecting human brain microvascular endothelial cells (hBMECs) or human microglial cells and (2) by suppression of the growth of *T. gondii using* monensin, impairment of the BBB integrity can be restored. The aim of the present work was to investigate the effect of monensin on the *in vitro* growth of *T. gondii* tachyzoites and on the proliferation of hBMECs and microglial cells.

4.3 Materials and Methods

4.3.1 *Chemicals*

Monensin was purchased as a sodium salt powder from Alfa Aesar (Ward Hill, USA) and 1.73 mg of it was dissolved in 250 μl of absolute methanol. The 10 mM of stock solution was diluted with complete culture medium to prepare five working concentrations 0.01 μM, 0.1 μM, 1 μM, 10 μM and 100 μM that were stored at 4°C until use. Sulforhodamine B (SRB) was purchased from Sigma-Aldrich (SIGMA-ALDRICH®/Merck KGaA, Darmstadt, Germany) and a solution of 0.4% (w/v) SRB dissolved in 1% acetic acid (Fisher Scientific, Leicestershire, UK) was prepared and stored, protected from light, at 4°C. Kits for Cell Viability, Mitochondrial Potential, Cell Cycle, and DNA fragmentation NC-3000™ assays were obtained from ChemoMetec A/S, Allerod, Denmark.

4.3.2 *Cell Lines*

Human brain microvascular endothelial cells (hBMECs) were used at passage 9 and were maintained in modified Gibco® Roswell Park Memorial Institute (RPMI) 1640 media (Thermo Fisher Scientific, MA, USA) containing 20% Gibco® Heat Inactivated Fetal Bovine Serum (HI-FBS), 1% Gibco® Non-

essential amino-acids (100X), 1% Gibco® Sodium pyruvate (100 mM), 1% Gibco® MEM Vitamins (100X), 1% L-glutamine (200 mM) and 1% Antibiotic-antimycotic solution 100X. Human microglial cells were used at passage 11 and were grown in modified Gibco® Dulbecco's Modified Eagle Medium (DMEM; Thermo Fisher Scientific, MA, USA) containing 5% Gibco® HI-FBS and 1% Gibco® Antibiotic-antimycotic solution. Both cell lines were passaged twice a week and grown in T75 (75 cm^2) NUNC™ tissue culture flasks (Fisher Scientific, Leicestershire, UK) for two weeks before being used in the experiment. All cultures were maintained in a cell culture incubator at 37°C with 5% atmospheric CO_2.

4.3.3 *Parasite Strain and Culture Conditions*

Tachyzoites of *T. gondii* RH strain were cultured in NUNC™ T-75 tissue culture flasks containing hBMECs using the same culture conditions described above. The tachyzoites were harvested after they completed their growth and exited host cells in about three days. Then, they were separated from host cell debris *via* centrifugation at 500x*g* for five minutes. Based on the cell line used in the subsequent experiments, the number of tachyzoites was adjusted with the respective medium (RPMI for hBMECs or DMEM for microglial cells) to achieve a multiplicity of infection (M.O.I) of five (5 tachyzoites: 1 cell) for each cell line.

4.3.4 *Efficacy of Monensin on the In vitro Growth of T. gondii*

Two approaches (parasite count in 24-well plates and Sulforhodamine B (SRB) assay in 96-well plates) were used to investigate the effects of inhibition of the WNT signalling pathway by monensin on the intracellular growth of *T. gondii.*

4.3.5 *Parasite Count*

Microglial and hBMEC cultures were seeded on Nunclon™ Delta Surface 24-well culture plates (Thermo Fisher Scientific, MA, USA) at seeding densities of 5 x 10^4 cells and 10^5 cells per well, respectively. Cultures of both cell types were infected with *T. gondii* tachyzoites at MOI of five. Three hours post-infection (h.p.i); the culture medium in each well was discarded and replaced with 1 mL of media supplemented with one of the five working concentrations of monensin (0.01 μM, 0.1 μM, 1 μM, 10 μM and 100 μM). Growth of cell cultures was monitored daily by microscopic observation using a Zeiss Axiovert 25 inverted microscope (Leica Microsystems, Milton Keynes, UK) with a 10X objective lens. When the parasites had completed their development and began to exit the cells at about five days after infection (~3 days for control), the absolute number of tachyzoites in each well was counted. To achieve this, the remaining media in the wells was topped up with Gibco® Phosphate Buffered Saline (PBS) with pipetting to loosen the tachyzoites and to produce a homogenous parasite suspension. A small amount (50 μl) of the suspension from each well was used to count tachyzoites using a standard haemocytometer counting assay.

4.3.6 *Colorimetric SRB Assay*

The Sulforhodamine B assay involves the measurement of cellular protein content using a plate reader to measure absorbance after cells have been fixed and stained with SRB dye. The absorbance is directly proportional to the number of cells and thus indirectly measures the rate of cell growth. Cells were cultured in Corning® Costar® 96-well plates (SIGMA-ALDRICH®/Merck KGaA, Darmstadt, Germany). Each well was seeded with 5×10^3 microglial cells or 10^4 hBMECs in 100 µL of the respective medium and then grown to confluency (typically 1 day). Tachyzoites used to infect each well were able to invade the host cells within three hours. Then, the medium was discarded to remove any extracellular tachyzoites and 100 µL of media containing one of each of the following concentrations of monensin 0.01 µM, 0.1 µM, 1 µM, 10 µM, and 100 µM was added to each well. Wells that received medium without monensin (untreated) served as controls. After five days in incubation, the SRB assay staining was performed according to Vichai and Kirtikara (2006). Ice-cold 100 µM of 10% trichloroacetic acid solution - TCA (Fisher Scientific, Leicestershire, UK) was added to each well. The plates were then kept at 4°C for one hour. Afterwards, the solution was discarded from the wells followed by thorough washing with distilled water. Next, 25 µL of SRB dye was added to each well and incubated for 15 minutes at ambient temperature. The plates were wrapped with foil to protect the dye from the light. The wells were then washed with 1% acetic acid to remove any unattached stain, followed by addition of 100 µL of 10 mM Tris base solution (SIGMA-ALDRICH®/Merck KGaA, Darmstadt, Germany) to the wells. Finally, the plates were set on a plate shaker at 35 rotations per minute for 5 minutes. The plates were shaken gently for three to five seconds before the absorbance was measured at 492 nm using a plate reader (LT-4000 Microplate Reader, LabTech International Ltd, UK).

4.3.7 *Effects of Monensin on Host Cell Viability*

To investigate the effects of monensin on host cell viability, hBMECs and microglial were chosen as two representative cell lines. Cells were grown in 96-well tissue culture plates and treated with monensin at a serial concentration that ranged from 0 μM to 100 μM for five days. To assess the effects of these concentrations, the haemocytometer cell count method and the SRB assay were performed, as described above, but without addition of *T. gondii*. This experiment was important to isolate the direct anti-parasitic effects of monensin from nonspecific cytotoxic effects against the host cells, which might have also affected the parasite growth. The percentage of cell growth inhibition was calculated as follows: Growth inhibition (%): (Control − Sample/Control) × 100.

4.3.8 *Monensin Cytoxicity using Nucleic Acid Double Staining*

In this and subsequent experiments, 0.1 μM monensin was used because it was the lowest concentration at which an anti-*T. gondii* effect was shown without causing significant cell toxicity. We selected 24 hours as the duration of the drug exposure because the effect of monensin on the parasite declines 24 hours after treatment (Lavine and Arrizabalaga, 2011, 2012). HBMECs were treated with 0.1 μM monensin or mock-treated with medium only. After 24 hours, cells were trypsinised and centrifuged at 500*xg* and the cell pellet was suspended in 0.5 mL PBS. About 60 μL of cell suspension was loaded into the Via1-Cassette™ (ChemoMetec A/S, Allerod, Denmark), which contained dual-fluorescent stains, acridine orange (AO) and DAPI. AO permeates both live and dead cells and stains all nucleated cells to generate green fluorescence. DAPI (4’,6-diamidino-2-phenylindole) enters non-viable cells with compromised membrane and stains all dead nucleated cells to

generate blue fluorescence. The Via1-Cassette™ was placed in the NucleoCounter® NC-3000™ and the cell count and viability were determined following the manufacturer's instructions. The total cell population was stained with acridine orange and appeared green in the acquired image, while non-viable cells were detected through DAPI staining since they did not possess an intact cell membrane, appearing as blue cells.

4.3.9 *Mitochondrial Potential, DNA Fragmentation, Cell Cycle Analyses*

In this experiment, hBMECs were treated with 0.1 μM monensin or mock-treated with medium only. After 24 hours cells were harvested by trypsinisation, centrifuged at 500x*g* and the cell pellet was suspended in 0.5 mL PBS, loaded into Via1-Cassette and counted using a NucleoCounter® NC-3000™ cytometer as described above. After that cells were either fixed with 4% formaldehyde or stained with specific dyes depending on the analysis. Mitochondrial potential, DNA fragmentation and cell cycle analyses were performed as described in section **2.3.10**, **2.3.11** and **2.3.12** respectively.

4.3.10 *Effect of Monensin on BBB Integrity*

In order to determine if and to what extent integrity of hBMECs is affected by exposure to 0.1 μM monensin in the presence or absence of *T. gondii* infection, transendothelial electrical resistance (TEER) was measured. A 0.5 μM PET-inserts (24-well Millicell® Cell Culture Inserts, Millipore (UK) Limited, Switzerland) were fitted to wells of the 24-well culture plates. Then, 10^4 cells in 100 μL of RPMI medium were added to each insert and 100μl of the medium was added to the bottom of the well. The plate was incubated for one hour; then the medium was discarded and replaced with 1.3 mL fresh media in

the bottom of each well. Also, 300 µL fresh media were added onto the cell monolayer in the inserts.

Three days after seeding the cells, media in the inserts and wells were discarded and replaced with fresh media. Six days after seeding, one of the plates was infected with *T. gondii* by removing old media and adding tachyzoites at MOI of 5, in fresh medium, to the inserts. The plate was incubated for one hour and then monensin-supplemented RPMI media or fresh RPMI was added in the same volumes used for media change. TEER was measured in each insert daily over a week post infection (wpi). TEER was measured using an Evom voltohmmeter with the Endohm 12 and STX2 electrodes (World Precision Instruments, Inc., Sarasota, FL). The electrodes were placed into the insert membrane and bottom of each well. TEER values were measured three times from each well, while changing the position of the electrodes slightly each time in order to obtain the overall average of the insert resistance. A background resistance was established by placing the electrodes into inserts with a blank medium only, without cells. This value was used to calculate the TEER value of each well using the equation ($TEER_{(cells)} = (TEER_{(total)} - TEER_{(blank)})\ culture\ area$). The culture area of the insert was 0.33 cm^2. The TEER value was expected to increase with increased resistance of the hBMEC monolayer.

4.3.11 *Microarray Data Analysis*

The aim of this experiment was to isolate the effect of 0.1 µM monensin on the differential expression of genes involved in WNT signalling. We used cDNA microarrays to detect changes in mRNA expression in four experimental groups. (1) uninfected, un-treated hBMECs grown in RPMI media - *Control*; (2) hBMECs treated with 0.1 uM monensin for 24 hours – *Monensin_only*; (3) *T. gondii*-infected hBMECs treated with 0.1 uM monensin RPMI media after three

hours of infection and incubated for further 24 hours – *TG_Monensin*; and (4) *T. gondii* infected hBMECs in RPMI media incubated for 24 hours – *TG_only*.

Total RNA was isolated using RNeasy Mini Kit (Qiagen, Manchester, UK) and eluted with nuclease-free water. RNA was stored at −80°C for one week prior to microarray analysis. All subsequent sample handling, labelling, and GeneChip (GeneChip Human Gene 1.0 ST arrays, Affymetrix) processing were performed at the transcriptomics service at Nottingham Arabidopsis Stock Centre (NASC). The RNA concentration and quality were assessed using the Agilent 2100 Bioanalyzer (Agilent Technologies Inc., Palo Alto, CA) and the RNA 6000 Nano kit (Caliper Life Sciences, Mountain View, CA) prior to the microarray analysis. Samples with a minimum RNA concentration of 100 ng/µL and RNA integrity number (RIN) value more than 8 were used for gene expression analysis.

Single-stranded complimentary DNA was prepared from 200 ng of total RNA as per the Ambion® WT Expression Kit (Thermo Fisher Scientific, Paisley, UK) for Affymetrix GeneChip Whole Transcript WT Expression Arrays (Affymetrix, Wycombe, UK). Total RNA was first converted to cDNA, followed by *in vitro* transcription to make cDNA. Single-stranded cDNA was synthesised, end labelled and hybridised, for 16 hrs at 45°C, to Human Gene 1.0 ST arrays (Affymetrix, Wycombe, UK). All liquid handling steps were performed by a GeneChip Fluidics Station 450 and GeneChips were scanned with the GeneChip Scanner 3000 7G (Affymetrix, Wycombe, UK) using Command Console v3.2.4. The scripts used for data analysis by R Studio software (R Studio Inc, Boston, USA) and the settings opted for each process are available in **Appendix** 4-1. Briefly, a data file, called 'pdatamon' was created to link each microarray data file with '.ga.cel' ending to one of the four experimental groups (Control, Monensin_only, TG_Monensin or TG_only). The libraries of modules (oligo,

gplots, RColorBrewer, pvclust, colourspace, limma, gene filter, hugene21sttranscriptcluster.db) needed for quality control, differential gene expression and transcript cluster ID annotation were downloaded and uploaded into the workspace. Next, Affymetrix microarray data files were uploaded together with 'pdatamon' file. Quality control analysis and normalisation were performed using the robust multi-array average (RMA), which is the common normalisation method for microarray study (Irizarry *et al.*, 2003, 2012). RMA normalisation is sensitive for low expression values, consistent fold-change estimates, and excellent background adjustment compared to MAS 5.0 and dChip normalisation methods (Irizarry *et al.*, 2003, 2012). DEGs were considered significant if adjusted *P*-value was <0.05 and $\log_2$ FC ≥ 1 (up-regulated) or ≤ -1 (down-regulated). Contrast was made between Control versus Monensin_only, Control versus TG_only and Control *vs* TG_Monensin. The filtered gene list was considered for gene ontology analysis.

4.3.12 *Gene Ontology (GO) with Protein Analysis Through Evolutionary Relationships Classification System (PANTHER) Analysis*

Gene ontology analysis was performed as reported in section **3.3.7** (Chapter 3).

4.3.13 *Reactome Pathway Analysis*

Reactome's pathway analysis was performed as reported in section **3.3.8** (Chapter 3).

4.3.14 *Statistical Analysis*

Results were expressed as means ± SEMs. Statistical analysis was performed using a Student's t-test (two independent groups), one-way ANOVA (multiple groups, one independent factor) or two-way ANOVA (multiple groups, two independent factors) followed by a Bonferroni-Holm post hoc test using GraphPad Prism 7 (GraphPad Software, USA). Differences were considered significant at a *P* value of < 0.05. The level of significance was reported as: *, $P < 0.05$, ** $P < 0.01$, *** $P < 0.001$, and ****, $P < 0.0001$.

4.4 Results

4.4.1 *Cytotoxicity of Monensin*

Host cell viability in the presence of monensin was determined using microscopic count (**Figure** 4-1), NC-3000™ viability assay (**Figure** 4-2) and SRB assay (**Figure** 4-4). The cell numbers of treated cells were significantly decreased ($P < 0.01$; one-way ANOVA), indicating that monensin had an inhibitory effect on cell growth in both cell lines (**Figure** 4-4).

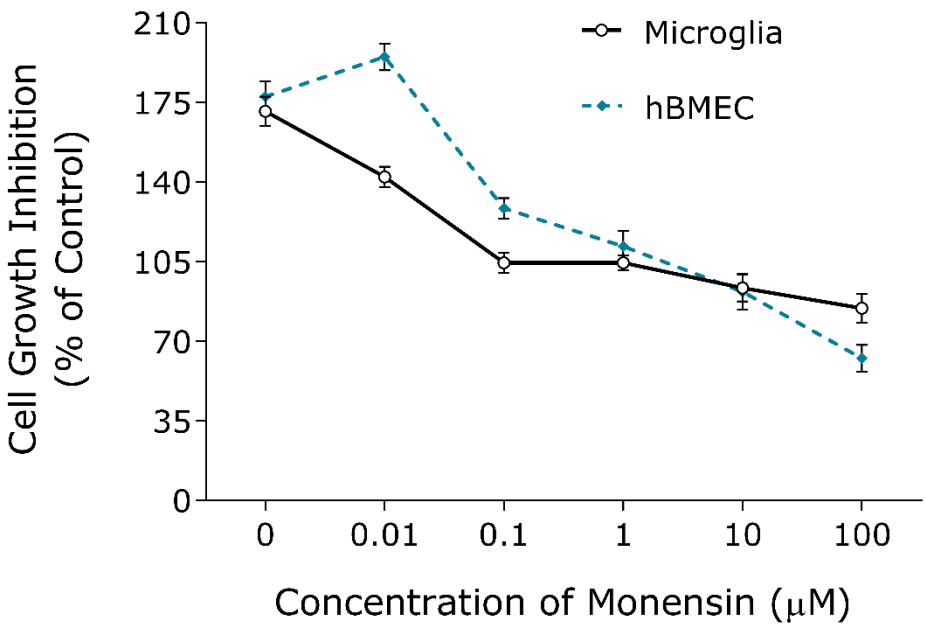


Figure 4-1 Cytotoxic effect of monensin on hBMECs and microglial cells. The assessment was performed using hemocytometer cell count. Results are presented as a percentage of growth inhibition compared with the control cells (untreated microglial/hBME cells). The graph shows that as monensin concentration increases, the number of counted cells decreases. Data represent mean values (± SEM) of triplicate measurements from three independent experiments.

We also examined the effect of 0.1 μM monensin toxicity on hBMECs viability using a NucleoCounter® NC-3000™ system (**Figure** 4-2). Viability percent of hBMECs treated with 0.1 μM was 74.74 ± 1.2%, which was lower, and significantly decreased compared to cells exposed to culture media + 1% methanol (89.36 ± 2.2%), culture media alone (87.41 ± 0.9%), and 0.01 μM monensin (86.58 ± 3.8%). However, only 0.78 ± 0.2% of cells were stained with DAPI.

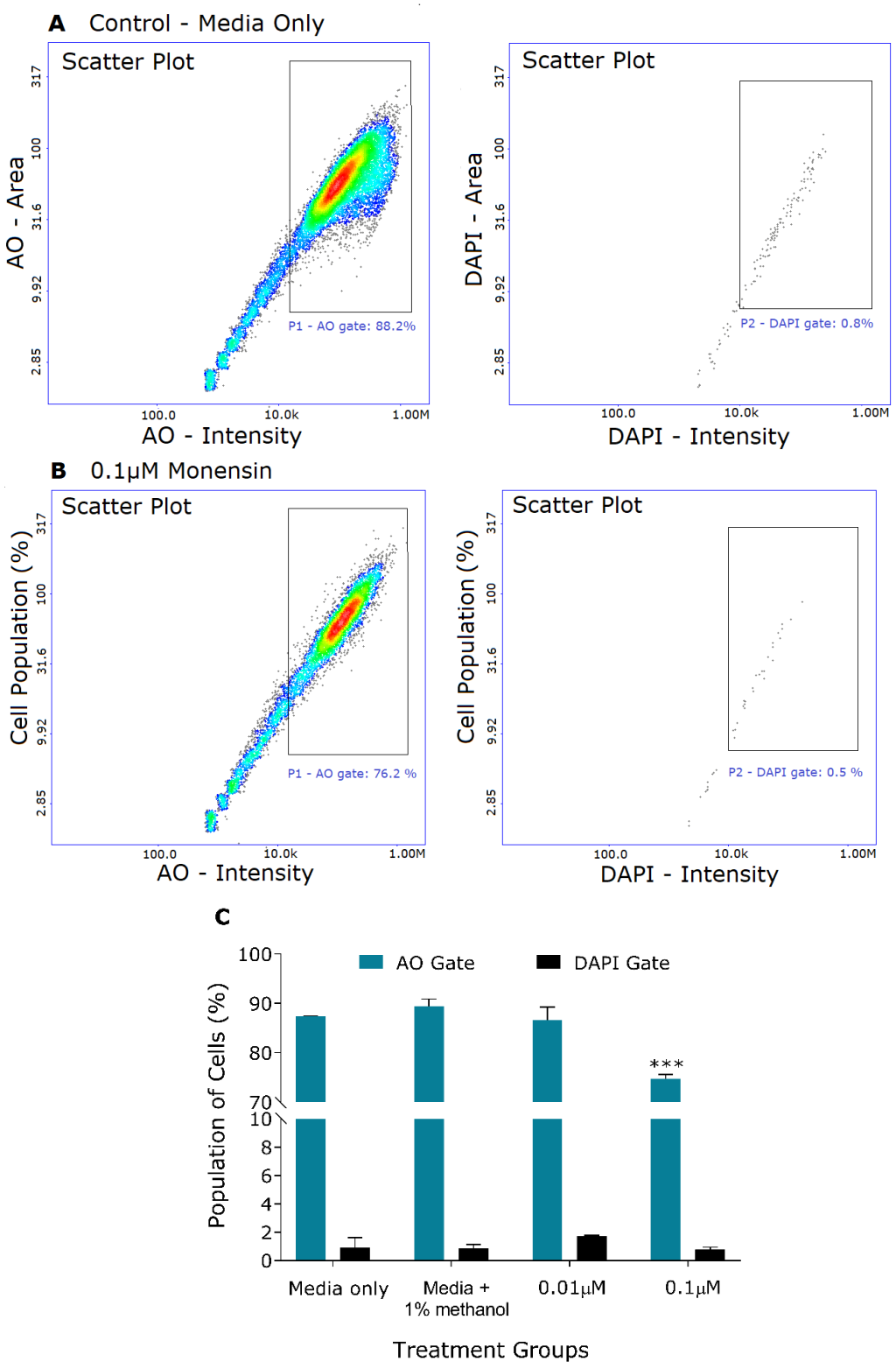

A Control - Media Only
Scatter Plot
AO - Area
AO - Intensity
P1 - AO gate: 88.2%
Scatter Plot
DAPI - Area
DAPI - Intensity
P2 - DAPI gate: 0.8%
B 0.1µM Monensin
Scatter Plot
Cell Population (%)
AO - Intensity
P1 - AO gate: 76.2 %
Scatter Plot
Cell Population (%)
DAPI - Intensity
P2 - DAPI gate: 0.5 %
C
AO Gate
DAPI Gate
Population of Cells (%)
***
Media only
Media + 1% methanol
0.01µM
0.1µM
Treatment Groups

Figure 4-2 The effects of 24 hours treatment with 0.01 µM and 0.1 µM monensin on hBMEC's viability. A and **B** are representative of scatter plots and histogram of control and 0.1 µM-treated samples, respectively generated from Via1-Cassette™ using "Viability and Cell Count" protocol from NucleoCounter® NC-3000™. **C** A summary of the results. Significance difference was observed when comparing AO gate reading of 0.1 µM monensin group to the other 3 groups (two-way ANOVA, $P < 0.05$). Methanol, the vehicle used to dilute monensin did not affect hBMEC's viability. Data represent mean values (± SEM) of triplicate samples.

When analysing the SRB assay results of non-infected cells (**Figure** 4-4), both cell lines showed no significant change in cell density between 0 µM and 100 µM concentrations of monensin using ANOVA, even though a decrease in absorbance was observed. However, when a t-test was performed on the data from 0.1 µM and 100 µM concentrations, there was a significant decrease in cell density ($P = 0.04$ and $P = 0.03$ for hBMECs and microglial cells, respectively) indicating that treatment with high concentrations of monensin does affect cell density and therefore, IS cytotoxic.

4.4.2 *The Antiparasitic Effect of Monensin*

When tachyzoite counts were carried out to measure the effects of monensin on the *in vitro* growth of *T. gondii* more than 90% and 70% inhibition of *T. gondii* was achieved at 1 µM monensin concentration in hBMECs and microglial cells, respectively. Monensin appeared to be more effective in inhibiting *T. gondii* growth in hBMECs. For microglial cells, monensin had a lower EC50 (effective concentration resulting in 50% parasite inhibition) than for hBMECs. The inhibitory effect, however, was greater on hBMEC infected cultures from 0.1 µM to 100 µM. These data showed a significant decrease ($P < 0.01$) in the number of counted tachyzoites in proportional to the increase in the concentration of monensin as determined by ANOVA. The most effective dose for both cell lines was 0.1 µM because there was no significant difference

between the effect obtained by 0.1 μM and higher concentrations on the reduction in tachyzoite counts (**Figure** 4-3).

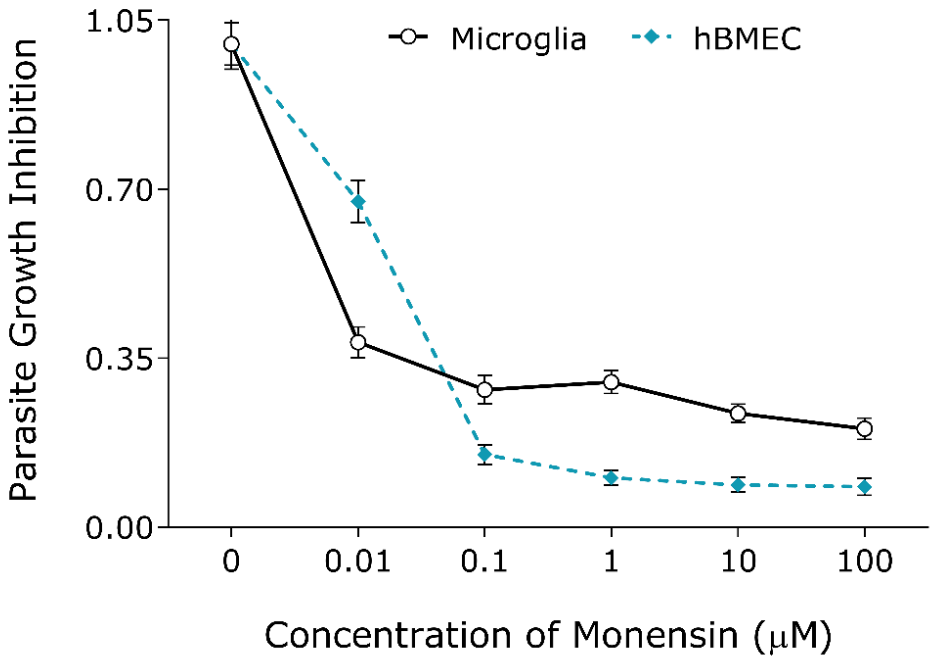


Figure 4-3 *Toxoplasma gondii* tachyzoite growth inhibition in microglial and hBMEC cultures is dependent on monensin concentration. The growth of the parasite was generally inhibited (compared to parasite growth in cells without monensin treatment) as the concentration of monensin increases, but at 0.1 μM the inhibition plateaus (reached its maximum). Tachyzoite counts were performed at 6 different concentrations. Data represent mean values (± SEM) of triplicate determinations from two independent experiments for each cell line.

The results obtained from SRB measurements of infected hBMECs treated with monensin revealed that host cell density significantly decreased ($P < 0.05$) within the entire range of the tested concentrations (0 μM to 100 μM). This suggests either monensin was cytotoxic to host cells or that infection damages the cells. However, when the same SRB assay was performed on infected microglial cells there was no significance difference, suggesting that monensin had either inhibited *T. gondii* infection, but limited damage due to infection has occurred, restricting cell growth or that cell growth had been

inhibited by the cytotoxic effects of monensin (**Figure** 4-4). We performed t-tests to draw comparisons on the effect of each concentration of monensin between infected and non-infected cultures of each cell line. None of the data showed any significant differences except the 10 µM treated-hBMEC cultures and 100 µM treated-microglial cultures. This suggests that *T. gondii* had not caused much reduction in cell density between cell lines suggesting that monensin has inhibited the parasite.

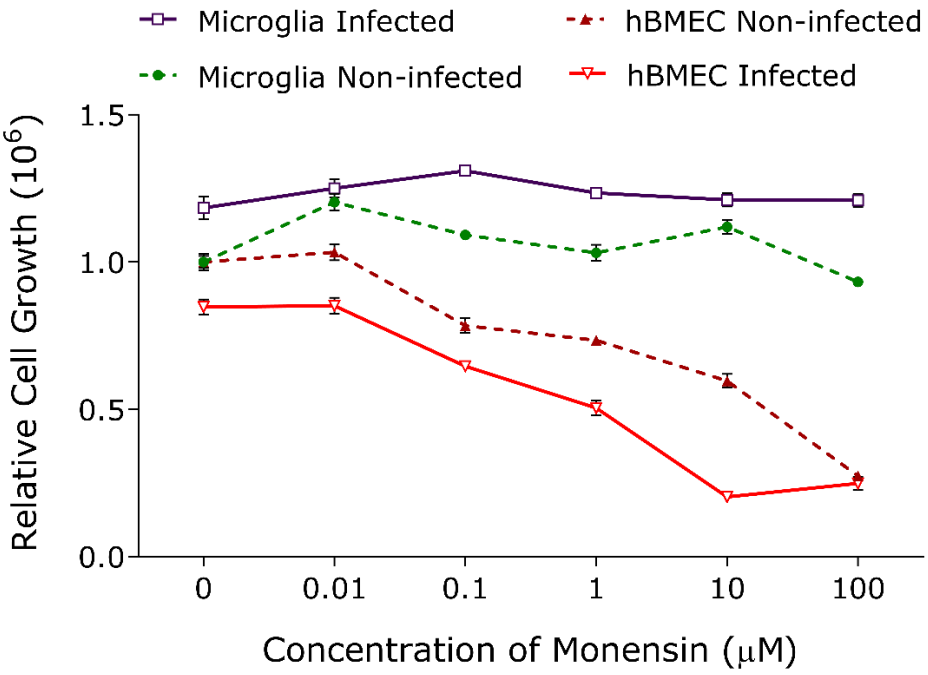
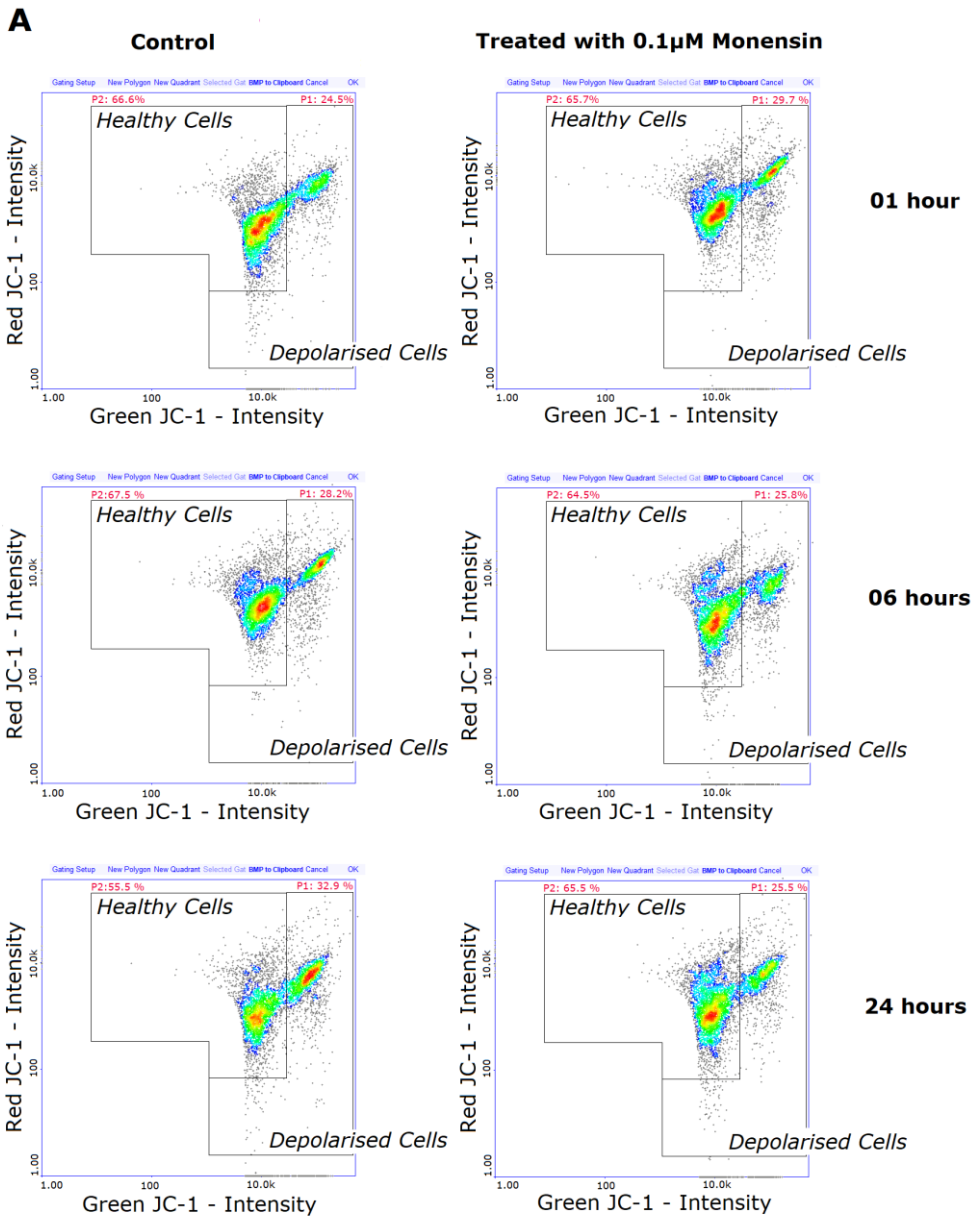


Figure 4-4 Microglial and hBMEC cultures showed different sensitivity to monensin concentration. Relative growth of each cell line was assessed by SRB assay. The relative absorbance values of infected and treated cells were compared to uninfected and untreated (control) cells. A significant, decrease in cell number was observed in infected and uninfected hBMECs with increasing monensin concentration compared to microglial cell cultures. Data represent mean values (± SEM) of five replicates from three independent experiments for each cell line.

4.4.3 *Effects on Mitochondrial Potential, DNA Fragmentation and Cell Cycle Assays*

The mitochondrial transmembrane potential (ΔΨm) was measured using the fluorescence image cytometer NucleoCounter® NC-3000™ (ChemoMetec A/S, Allerod, Denmark). After one hour of 0.1 μM treatment, there was an increase in the mitochondrial potential in treated cells compared to control, suggesting an increase in cell energetics following monensin exposure (**Figure** 4-5). However, the mitochondrial potential started to decline at six hours post-treatment UNtill the end of the experiment (24 hours post-treatment). Statistically, no significant difference was observed between one, six and 24 hours against a control group (one-way ANOVA, $P < 0.05$).


A
Control
Treated with 0.1µM Monensin
Healthy Cells
Depolarised Cells
P2: 66.6%
P1: 24.5%
P2: 65.7%
P1: 29.7 %
P2:67.5 %
P1: 28.2%
P2: 64.5%
P1: 25.8%
P2:55.5 %
P1: 32.9 %
P2: 65.5 %
P1: 25.5 %
Red JC-1 - Intensity
Green JC-1 - Intensity
1.00
100
10.0k
01 hour
06 hours
24 hours

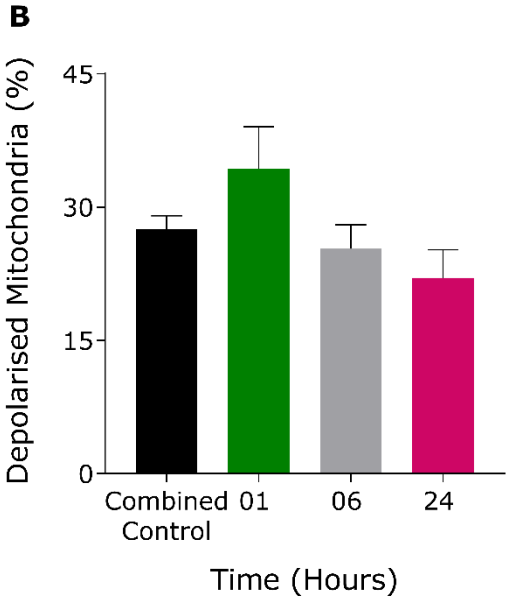

B
Depolarised Mitochondria (%)
45
30
15
0
Combined Control
01
06
24
Time (Hours)

Figure 4-5 The effects of 24 hours treatment with 0.1 μM monensin on hBMEC's mitochondrial potential. A represents scatter plots of control and 0.1 μM monensin-treated cells at 1, 6 and 24 hours post-treatment respectively. All results were summarised in bar charts in **B**. Cells were stained with JC-1 and DAPI dyes then analysed using the "Mitochondrial Potential Assay" where cell's mitochondrial potential was measured using NucleoCounter® NC-3000™. A slight increase in mitochondria polarisation was observed one hour after 0.1 μM monensin exposure, but the percentage then drops to slightly lower than control group percentage at 6 and 24 hours. No significant difference was observed between 1, 6 and 24 hours against a control group (one-way ANOVA, $P < 0.05$). Data represent mean values (±SEM) of triplicate samples.

Next, the DNA fragmentation in order to assess late apoptosis was investigated. DNA fragmentation 3.2 ± 1.1% was detected in the control, untreated cells was not significantly different from those recorded in hBMECs treated with 0.1 μM monensin: 4.7 ± 1.1%, 5.5 ± 1.6% and 5.05 ± 0.9% at one, six and 24 hours after treatment, respectively (**Figure** 4-6).

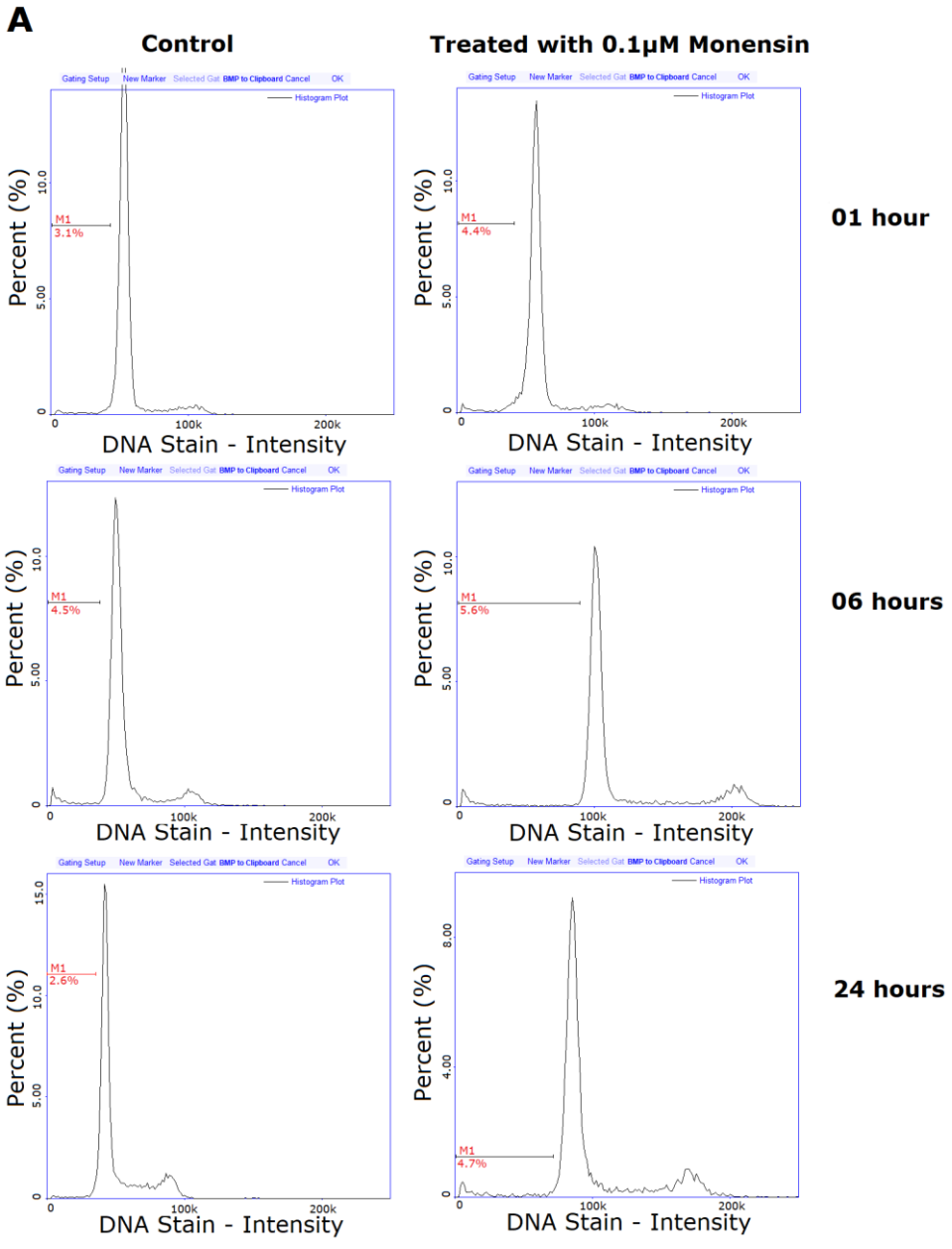
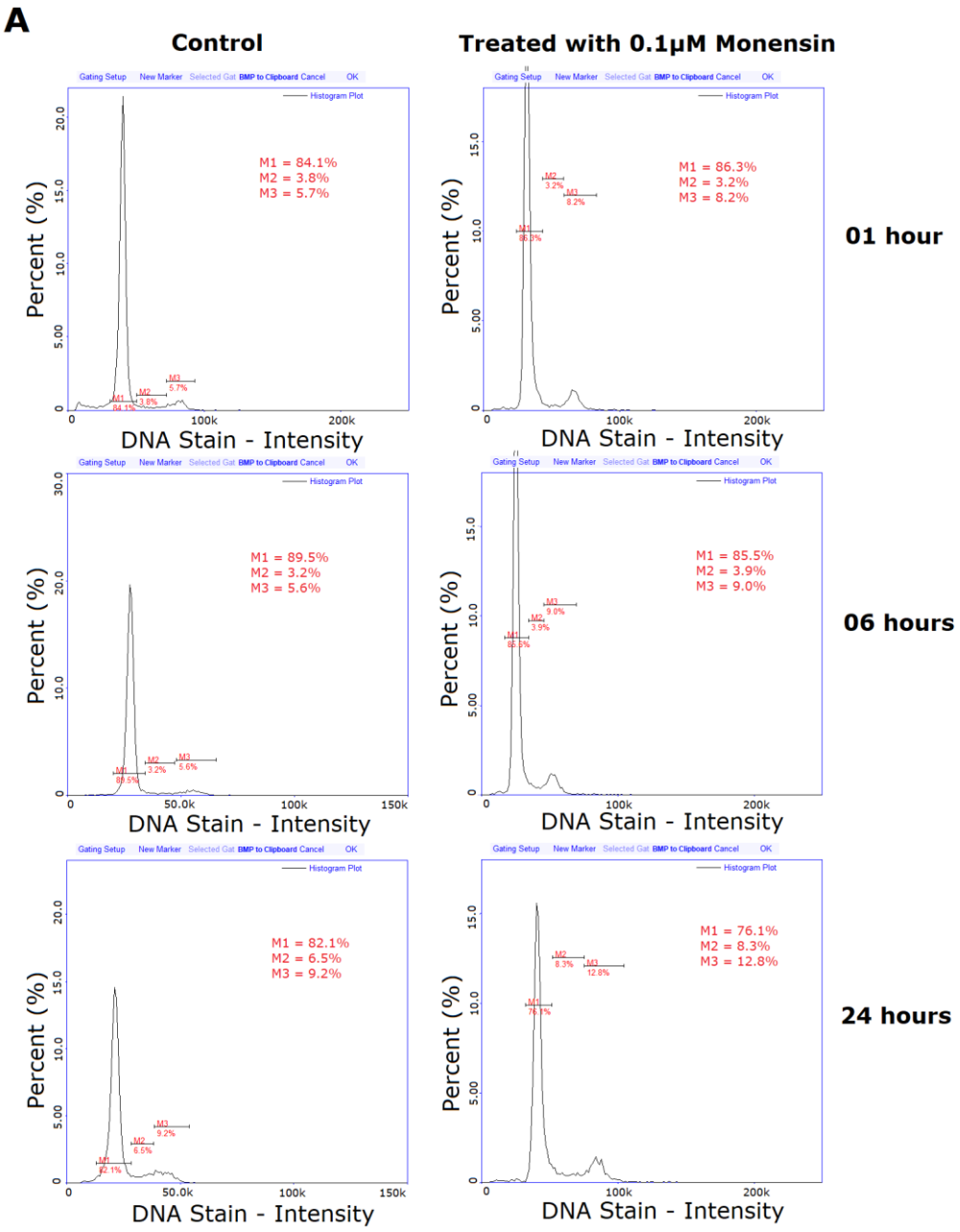

A
Control
Treated with 0.1µM Monensin
01 hour
06 hours
24 hours
Percent (%)
DNA Stain - Intensity
M1
3.1%
4.4%
4.5%
5.6%
2.6%
4.7%
B
DNA Fragmentation (%)
Combined Control
01
06
24
Time (Hours)

Figure 4-6 The effects of 24 hours treatment with 0.1 μM monensin on hBMECs DNA fragmentation. A represents histogram of control and 0.1 μM monensin at one, six and 24 hours post treatment respectively. All results were summarised in bar charts in **B**. Cells were stained with DAPI then analysed using "DNA Fragmentation Assay" protocol where cells with less than one DNA equivalent (sub-G1) cells were quantified by NucleoCounter® NC-3000™ system. In late apoptosis, double strands DNA are degraded by calcium- and magnesium-dependent nucleases causing fragmentation. No significance difference was observed during 24 hours of treatment with 0.1 μM monensin (one-way ANOVA, $P < 0.05$). Data represent mean values (±SEM) of triplicate samples.

There were slight changes in the cell cycle population at 24 hours compared to one and six hours post treatment (**Figure** 4-7). However, the changes were not statistically significant (Two-way ANOVA, $P < 0.05$).


A
Control
Treated with 0.1µM Monensin
01 hour
06 hours
24 hours
Percent (%)
DNA Stain - Intensity
M1 = 84.1%
M2 = 3.8%
M3 = 5.7%
M1 = 86.3%
M2 = 3.2%
M3 = 8.2%
M1 = 89.5%
M2 = 3.2%
M3 = 5.6%
M1 = 85.5%
M2 = 3.9%
M3 = 9.0%
M1 = 82.1%
M2 = 6.5%
M3 = 9.2%
M1 = 76.1%
M2 = 8.3%
M3 = 12.8%

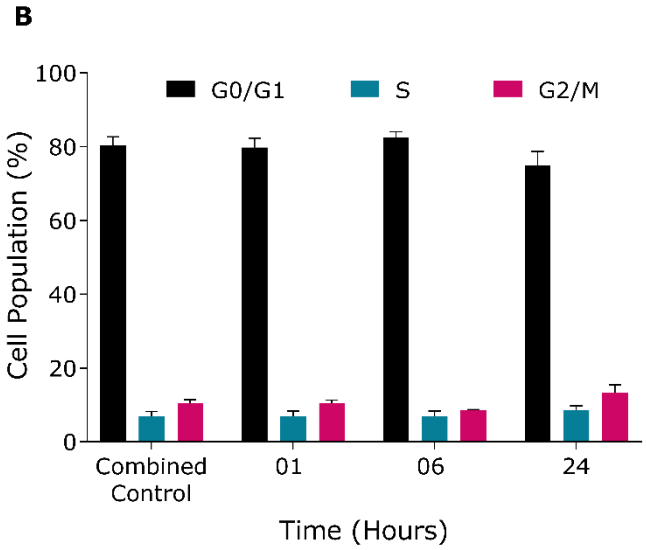

B
G0/G1
S
G2/M
Cell Population (%)
Combined Control
01
06
24
Time (Hours)

Figure 4-7 The effects of 24 hours treatment with 0.1 µM monensin on hBMECs G0/G1, S and G2/M cell cycle stages. A represents histogram of control and 0.1 µM monensin at one, six and 24 hours post treatment respectively. All results were summarised in bar charts in **B**. Cells were stained with DAPI then analyzed using "Fixed Cell Cycle - DAPI Assay" protocol where cellular fluorescence of DAPI-stained cells was quantified by NucleoCounter® NC-3000™ system. A statistical test comparing each cell cycle stage at different time points to the control group did not reveal any significance difference (two-way ANOVA, $P < 0.05$) across 24 hours of treatment compared to control. Data represent mean values (± SEM) of quadruplets determinations.

4.4.4 *Assessment of hBMEC Monolayer Integrity*

We determined how hMBECs' integrity was affected by *T. gondii* infection and/or modulated by WNT inhibition *via* exposure to 0.1 µM monensin. The effect of monensin on the TEER of infected and uninfected hMBECs was monitored over a week. At one day post infection, there was no significant ($P \geq 0.05$; t-tests) difference between *T. gondii*-infected cells treated with 0.1 µM compared to infected untreated, probably because it takes about a day for infection to establish. However, from day 2 after infection there was a significant decrease in hBMECs' TEER between 0.1 µM monensin-treated and untreated samples. Interestingly, infected and treated cells did not show any significant difference throughout the entire experiment, suggesting that cell integrity was maintained by monensin treatment, possibly *via* inhibiting the damage inflicted by the parasite growth (**Figure** 4-8). The infected and untreated groups showed the largest percentage reduction in TEER readings compared to the negative control ($P < 0.01$), suggesting that *T. gondii* infection compromised host cell integrity. The infected, treated cells showed a slight, but non-significant decrease in hBMEC's resistance at day 7, however, infected and untreated cells showed a gradual decrease until day 7. The TEER readings of uninfected cells (untreated or 0.1 µM-treated) were analysed daily. Using *t*-test, it was found that hBMECs' resistance did not change significantly from day to day between the two groups as the integrity of the cells changed gradually

over the week. However, as shown in **Figure** 4-8, cell integrity generally stable over the time period for control, infected+treated and monensin only groups. Treated cells (infected and uninfected) did not exhibit decreased resistance, however untreated (infected only) did. There was a 38.2% decrease in the resistance of infected+untreated cells compared to infected+treated cells relative to the control cells. These results suggest that monensin had inhibited the parasite, hence; fewer parasites invaded and damaged cells leading to better cell integrity than infected+untreated cells.

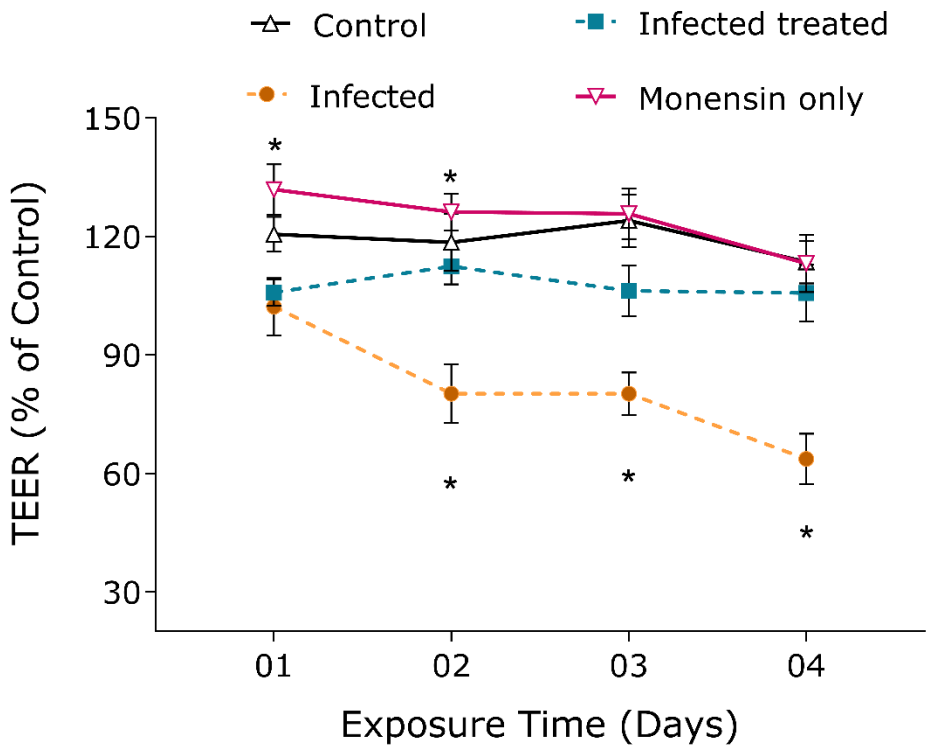


Figure 4-8 The effect of 0.1 μM monensin treatment on transendothelial electrical resistance (TEER) of the hBMECs monolayer. Cells grown on the membrane of transwell inserts, a simplified blood-brain barrier model, were treated with 0.1 μM monensin and the effect on monolayer TEER was measured over four days. Comparison between control (no infection and no monensin treatment) and monensin only reveals significant difference at day one and day two where TEER values of monensin treated cells were higher than control (Multiple Student *t*-tests; *, $P < 0.05$). Infected and monensin treated monolayer maintained TEER value over four days compared to infected, but in non-treated monolayer gradual decrease of TEER values was observed. Significance difference was observed at two, three and four days (Multiple Student *t*-tests; *, $P < 0.05$)**.** The data shown represent the means of six replicates from two separate experiments and the error bars indicate SEM.

4.4.5 *Microarray Quality Control and Normalisation*

Pre and Post Normalisation Box Plot

The overall distributions between samples indicate that normalisation was required before the samples are compared. As shown in the pre-normalisation box plots (**Figure** 4-9), the distributions of all sample median values were not uniformed before normalisation which might lead to under or over-estimated expression when comparing between samples. Therefore, normalisation was required and the common normalisation method for microarray study, robust multi-array average or RMA (Irizarry *et al.*, 2003, 2012) was performed. Following normalisation, the data become more uniform as can be seen from the median values of all samples (**Figure** 4-9).

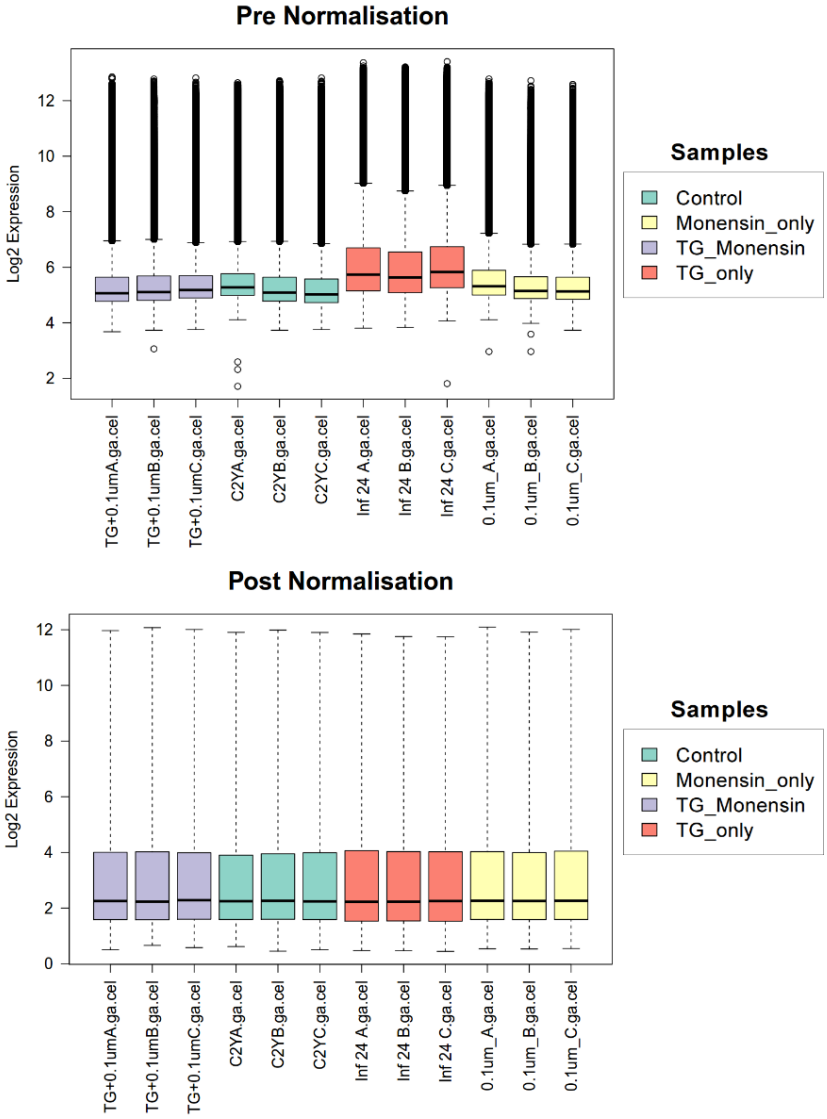


Figure 4-9 Box plots of pre (top) and post-normalisation (bottom) for all samples. The samples were normalised using the widely used robust multiarray average (RMA) method that considers background correction and variation between chipset (Irizarry *et al.*, 2003, 2012). Normalisation improves overall distribution between samples for the accurate sample to sample comparison.

Sample Correlation Heatmap

In **Figure** 4-10 heatmaps, shades of light green represent low correlation while shades of dark blue represent high correlation. The heatmap shows a correlation between the transcriptome expression profiles of all 12 samples through a branch of clustering tree also known as dendrogram. Based on the dendrogram, four experimental groups of 12 samples expression profiles were clustered into five distinct clusters. Three clusters correspond to three groups of samples from Control_only, TG_only and Monensin_only groups where samples within each of this group had similar expression profiles. Unexpectedly, three samples from TG_Monensin group were separated into two clusters with TG+0.1μM_A and TG+0.1μM_B in one cluster while TG+0.1μM_C in another cluster. TG_Monensin group expression profile was more similar to Monensin_only group expression profile rather than TG_only group expression profile as indicated by the dendrogram. Dendrogram also indicated that TG_only group had different expression profile than Control_only, TG_only and TG_Monensin groups expression profiles.

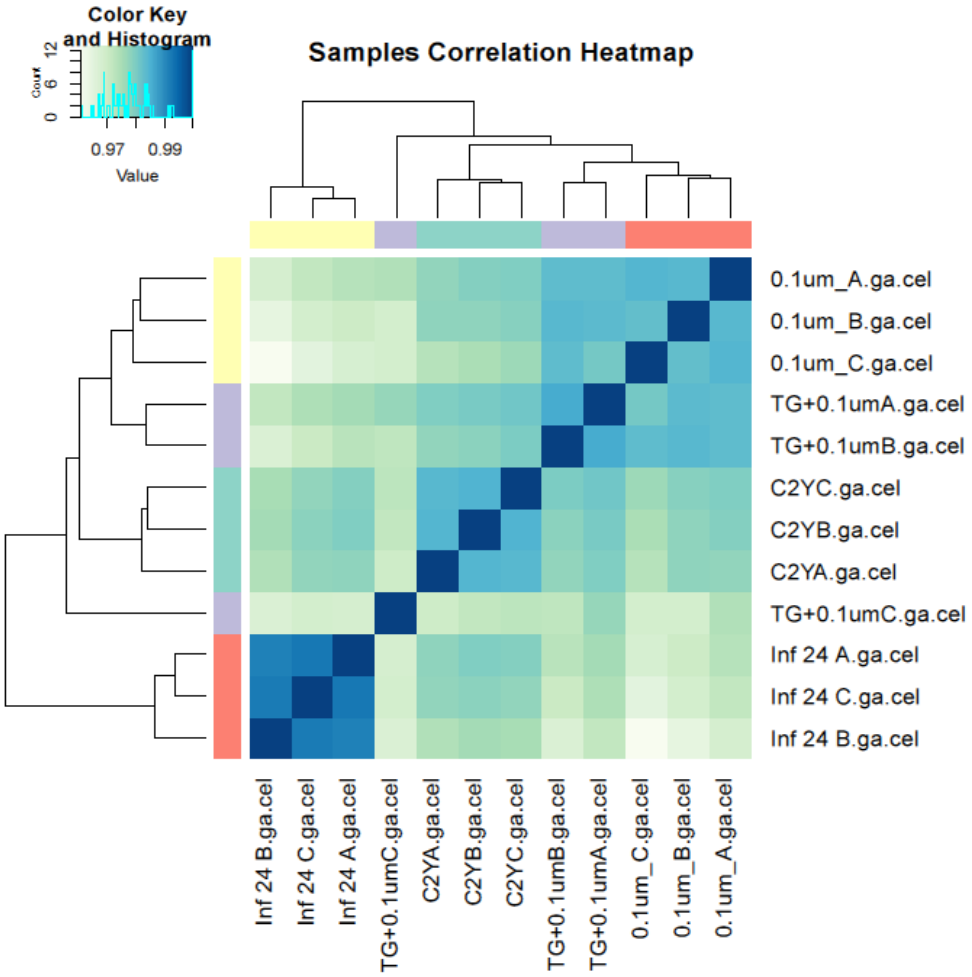


Figure 4-10 Correlation heatmap for all 12 microarray transcriptome expression profiles. The heatmap shows a correlation between all 12 samples used in microarray analysis where shades of light green and dark blue represent low and high correlation respectively. Dendrogram on the sides links closely correlated samples in each row or column to each other. Based on the dendrogram, four groups of the 12 sample expression profiles were clustered into five distinct clusters. Three clusters correspond to three experimental groups of samples (Control_only, TG_only and Monensin_only), whereas samples within each of this group had similar expression profiles. Unexpectedly, three samples from TG_Monensin group were separated into two clusters with TG+0.1μM_A and TG+0.1μM_B in one cluster, and TG+0.1μM_C in another cluster. TG_Monensin group expression profile is more similar to Monensin_only group expression profile rather than TG_only group expression profile as shown in the dendrogram. Dendrogram also indicates that TG_only group has a different expression profile than Control_only, TG_only and TG_Monensin groups expression profiles.

Principal Component Analysis (PCA)

Principal component analysis (PCA) was used visualise data and to detect the variation between samples. PCA analysisis was performed on all samples across all four groups (**Figure** 4-10). The figure shows similar findings to the heatmap, where samples within each group were very similar to each other and TG_only group samples were different from the other three groups. As observed in **Figure** 4-10, TG_Monensin group and Monensin_only group samples were closely clustered together except for TG+0.1µM_C.

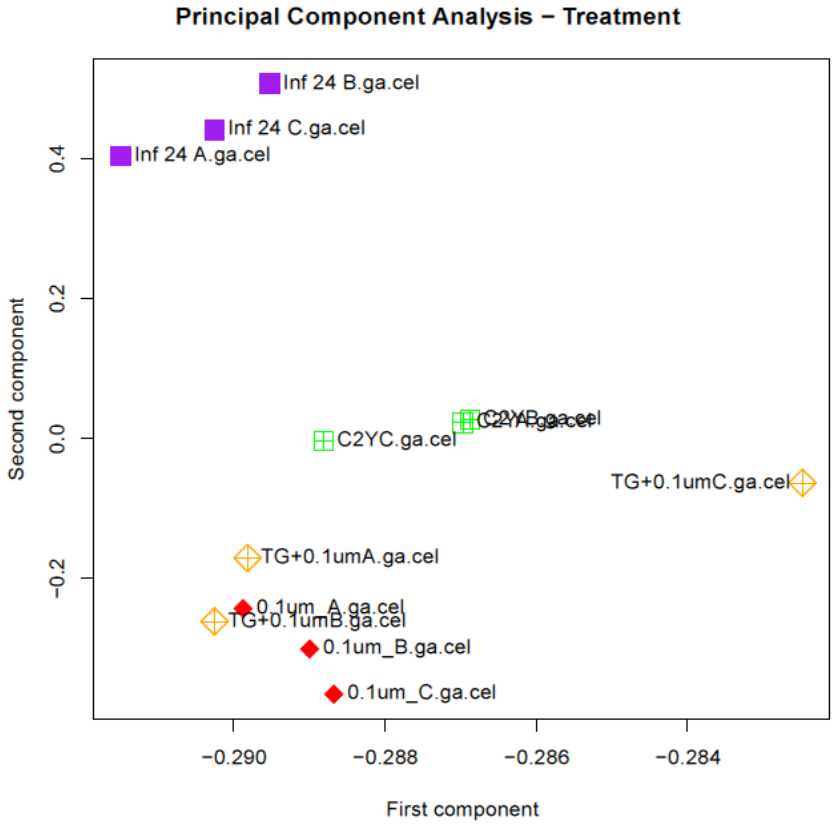


Figure 4-11 Principal component analysis (PCA) plot is showing all samples transcriptome dataset variation. The plot shows similar findings to the heatmap (**Figure** 4-10) where samples within each group were very similar to each other and the dataset of TG_only group samples was different from the other three groups. Also, as observed in **Figure** 4-10 TG_Monensin group and Monensin_only group samples datasets were clustered together except for one sample, TG+0.1µM_C.

4.4.6 *Venn Diagrams*

Overall view of the expression profiles between three groups of treatment is displayed as a Venn diagram (**Figure** 4-12). The diagram highlights shared and unique DEGs between the three sample groups. Among the three groups, TG_only had more total DEGs compared to the other two groups.

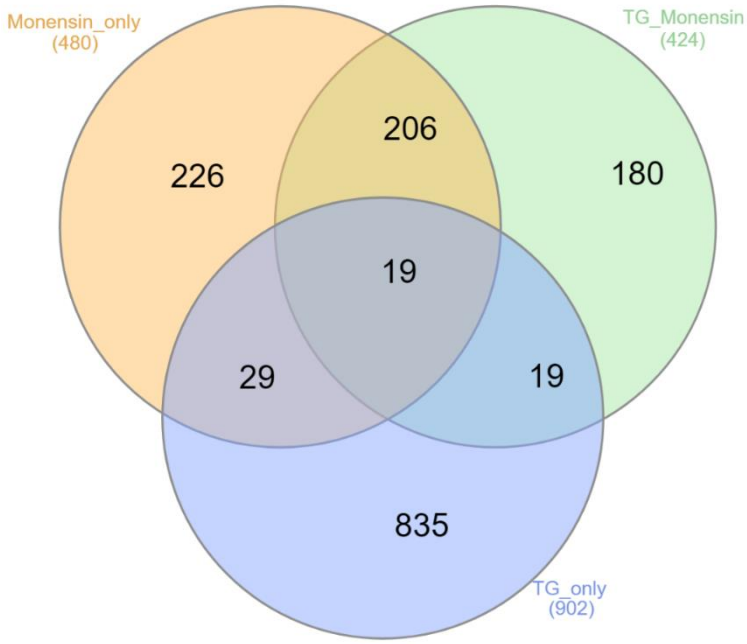


Figure 4-12 Venn diagram comparing expression profiles of Control *vs* TG_only, Control *vs* Monensin_only and Control *vs* TG_Monensin. Numbers in the overlapped area represent DEGs shared between groups. The area in the middle represents DEGs shared between the three groups where there are 19 genes.

4.4.7 *Patterns of Altered Gene Expression: Control vs Monensin_only*

Here, the transcriptional response of *T. gondii* infection and/or host cells to monensin was scrutinised. To obtain a detailed overview of the mechanistic action of monensin, single time point (24 hrs) transcriptome profiling of uninfected and untreated cells (Control - C2YA; C2YB; C2YC), uninfected cells

and treated with monensin (Monensin_only – 0.1μM_A; 0.1μM_B; 0.1μM_C), cells infected with *T. gondii* only (TG_only – Inf 24 A; Inf 24 B; Inf 24 C), and *T. gondii*-infected hBMECs that were treated with monensin after three hours of infection (TG_Monensin – TG+0.1μMA; TG+0.1μMB; TG+0.1μMC) were performed at the IC_{50} of 0.1 μM monensin. The 0.1 μM concentration was selected for the array experiments to avoid the growth defects/inhibition of hBMECs that would have occurred at higher concentrations. Previous data found that 0.1 μM concentration was just sufficient to trigger the transcriptional response.

Volcano Plot

Figure 4-13 depicts the overall expression profile of hBMECs treated with 0.1 μM monensin (Monensin_only) for 24 hours, insignificance versus $\log_2$ FC scatter plot (also known as volcano plot). Overall, the treatment caused more up-regulation of genes than down-regulation and hence more up-regulated genes passed the cut-off values ($P < 0.05$ indicated by the horizontal red line, $\log_2$ FC ≤ -1 or ≥ 1 indicated by vertical long dash red line) than down-regulated genes.

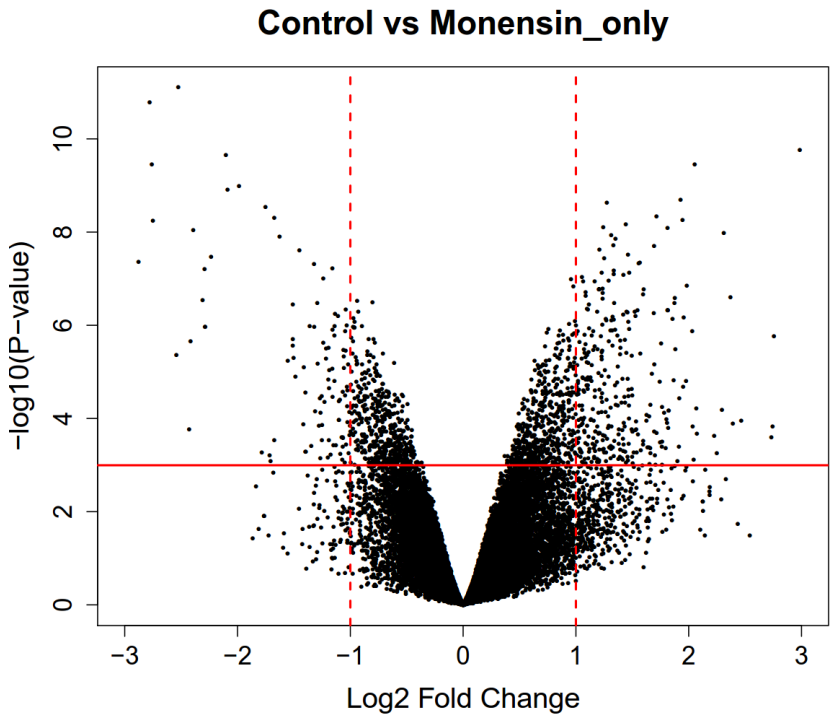


Figure 4-13 Volcano plot showing the expression profile of hBMECs after treatment with 0.1 µM monensin (Monensin_only). The red horizontal line represents significance cut-off value of $P < 0.05$ while vertical long dash red line represents $\log_2$ FC cut-off value of ≤ -1 or ≥ 1. Generally, treatment with monensin causes more genes up-regulation than down-regulation and hence more up-regulated genes passed both cut-off values than down-regulated genes.

Top 30 Most Significantly Differentiated Genes Heatmap

The heatmap is showing a correlation between samples based on to top 30 most significant DEGs after 24 hours treatment with 0.1 µM monensin (**Figure** 4-10). The rows represent expressed genes while the columns represent 12 samples. Based column dendrogram, 12 samples expression profiles were clustered into four distinct clusters corresponding to four experimental groups. Four clusters then formed two major clusters where Control_only and TG_only were grouped in one cluster whereas the other two groups were clustered in another cluster. Among the top 30 most DEGs, 12 of were without annotation because they are either uncharacterised genes or

uncharacterised non-coding RNA genes. These genes were assigned as 'NA' (not available). All 30 genes are listed in **Table** 4-1 together with their name, gene symbol, gene description, and log_2 FC values.

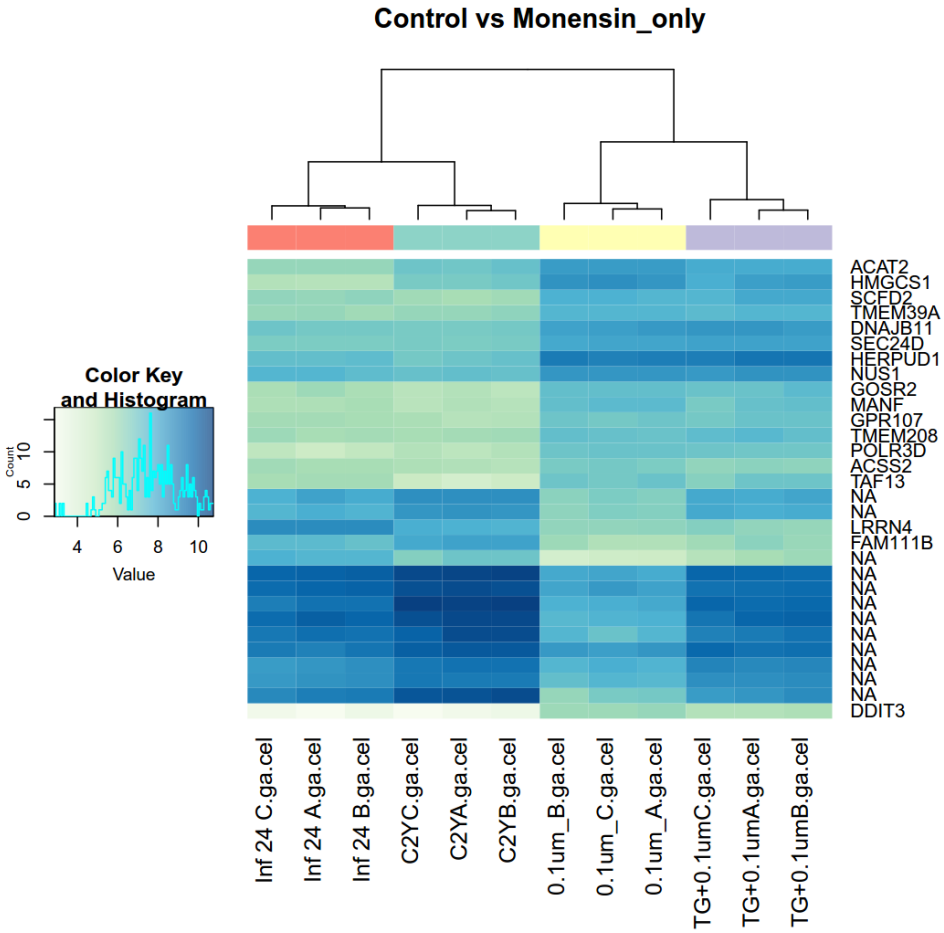


Figure 4-14 Correlation heatmap of the top 30 most significant DEGs following 24 hours treatment with 0.1 μM monensin. The rows represent expressed genes and the columns represent 12 samples. Column dendrogram shows a high correlation between samples in each group for all groups. Unlike in **Figure** 4-9**,** TG+0.1μM_C shows similar expression profile to other samples in the same group and to samples in 0.1 μM monensin treated group. Also, there were 12 significant genes without annotation labelled as NA.

The top 30 most significant DEGs induced by 24 hours treatment with 0.1 μM monensin and their name, gene symbol, gene description, and log_2 FC values are listed in **Table** 4-1. The most highly significantly down-regulated genes with annotation was 'family with sequence similarity 111 member B' -

FAM111B with log_2 FC -2.393 while the most highly significantly up-regulated gene with annotation was 'DNA damage-inducible gene 3' - DDIT3 with log_2 FC 2.984. Overall, the total number of genes that passed the selection criteria was 480 genes, 112 of them were down-regulated and 368 were up-regulated. **Appendix** 4-2 lists all filtered up-regulated and down-regulated genes.

Table 4-1 List of the top 30 significant DEGs induced by 24 hours treatment with 0.1 μM monensin (Monensin_only) with the most highly significant at the top.

Gene Cluster ID	Gene Symbol	Gene Description	Log_2 FC
17100663	NA	NA	-2.527
17100655	NA	NA	-2.780
17100695	NA	NA	-2.104
16766578	DDIT3	DNA damage inducible transcript 3	2.984
17100675	NA	NA	-2.761
16819325	HERPUD1	homocysteine inducible ER protein with ubiquitin-like domain 1	2.052
17100685	NA	NA	-3.600
17126276	NA	NA	-1.988
17126264	NA	NA	-2.090
16835125	GOSR2	golgi SNAP receptor complex member 2	1.927
16979256	SEC24D	SEC24 homolog D, COPII coat complex component	1.273
17100693	NA	NA	-1.753
16679936	NA	NA	-1.675
17066561	POLR3D	RNA polymerase III subunit D	1.713
17100679	NA	NA	-2.751
16941167	MANF	mesencephalic astrocyte derived neurotrophic factor	1.944
16949292	DNAJB11	DnaJ heat shock protein family (Hsp40) member B11	1.441
17014309	ACAT2	acetyl-CoA acetyltransferase 2	1.241
16975954	SCFD2	sec1 family domain containing 2	1.811
16725041	FAM111B	family with sequence similarity 111 member B	-2.393
16690511	TAF13	TATA-box binding protein associated factor 13	2.310
16912975	ACSS2	acyl-CoA synthetase short-chain family member 2	1.312
17100691	NA	NA	-1.628
16957771	TMEM39A	transmembrane protein 39A	1.350
16820076	TMEM208	transmembrane protein 208	1.331
16995890	HMGCS1	3-hydroxy-3-methylglutaryl-CoA synthase 1	1.692
17012079	NUS1	NUS1 dehydrodolichyl diphosphate synthase subunit	1.207
16917054	LRRN4	leucine rich repeat neuronal 4	-1.453
17090161	GPR107	G protein-coupled receptor 107	1.461
16983742	NA	NA	-2.235

Note: NA – Not available

Top 30 Differentially Regulated Genes

Among 480 DEGs, 244 were without annotation (NA) while 236 were annotated. Focusing on those with annotation, 171 were up-regulated while 65 were down-regulated. Top 30 up-regulated and down-regulated genes are listed in **Table** 4-2 and **Table** 4-3 respectively.

Table 4-2 List of top 30 up-regulated genes sorted with the highest log_2 FC at the top.

Gene Cluster ID	Gene Symbol	Gene Description	Log_2 FC
16766578	DDIT3	DNA damage inducible transcript 3	2.984
16690511	TAF13	TATA-box binding protein associated factor 13	2.310
16819325	HERPUD1	homocysteine inducible ER protein with ubiquitin-like domain 1	2.052
16864907	ERVV-2	endogenous retrovirus group V member 2, envelope	2.030
16774188	COG6	component of oligomeric Golgi complex 6	1.982
16898890	MCEE	methylmalonyl-CoA epimerase	1.954
16800301	PDIA3	protein disulfide isomerase family A member 3	1.950
16941167	MANF	mesencephalic astrocyte derived neurotrophic factor	1.944
16835125	GOSR2	golgi SNAP receptor complex member 2	1.927
16868827	YIPF2	Yip1 domain family member 2	1.876
16673104	HSD17B7	hydroxysteroid 17-beta dehydrogenase 7	1.865
16659133	NPPA-AS1	NPPA antisense RNA 1	1.855
16975954	SCFD2	sec1 family domain containing 2	1.811
17103946	GPR173	G protein-coupled receptor 173	1.754
17066561	POLR3D	RNA polymerase III subunit D	1.713
16995890	HMGCS1	3-hydroxy-3-methylglutaryl-CoA synthase 1	1.692
16900053	EIF2AK3	eukaryotic translation initiation factor 2 alpha kinase 3	1.689
17000518	HSPA9	heat shock protein family A (Hsp70) member 9	1.649
16704055	HSD17B7P2	hydroxysteroid 17-beta dehydrogenase 7 pseudogene 2	1.600
16772733	GOLGA3	golgin A3	1.595
16700872	LYST	lysosomal trafficking regulator	1.574
16927633	SDF2L1	stromal cell-derived factor 2 like 1	1.570
16950686	SEC13	SEC13 homolog, nuclear pore and COPII coat complex component	1.565
16708161	ENTPD7	ectonucleoside triphosphate diphosphohydrolase 7	1.556
16659102	CLCN6	chloride voltage-gated channel 6	1.545
16941052	CYB561D2	cytochrome b561 family member D2	1.532

16848079	WIPI1	WD repeat domain, phosphoinositide interacting 1	1.527
16829139	MVD	mevalonate diphosphate decarboxylase	1.520
16842576	IFT20	intraflagellar transport 20	1.494
16774551	COG3	component of oligomeric Golgi complex 3	1.471

Table 4-3 List of top 30 down-regulated genes sorted with the lowest log_2 FC at the top.

Gene Cluster ID	Gene Symbol	Gene Description	Log_2 FC
16798216	SNORD116-24	small nucleolar RNA, C/D box 116-24	-2.543
16725041	FAM111B	family with sequence similarity 111 member B	-2.393
17093722	RMRP	RNA component of mitochondrial RNA processing endoribonuclease	-1.716
17122086	LINC01224	long intergenic non-protein coding RNA 1224	-1.555
17079293	CCNE2	cyclin E2	-1.511
16714747	RTKN2	rhotekin 2	-1.511
17016499	HIST1H1B	histone cluster 1 H1 family member b	-1.511
16986913	VCAN	versican	-1.504
17080595	DSCC1	DNA replication and sister chromatid cohesion 1	-1.488
16917054	LRRN4	leucine rich repeat neuronal 4	-1.453
16671514	MIR4258	microRNA 4258	-1.418
16732891	NRGN	neurogranin	-1.413
17121990	ZNF730	zinc finger protein 730	-1.399
16736638	E2F8	E2F transcription factor 8	-1.399
17004903	EDN1	endothelin 1	-1.361
17020019	MCM3	minichromosome maintenance complex component 3	-1.323
16919769	NCOA5	nuclear receptor coactivator 5	-1.321
17016490	HIST1H2AJ	histone cluster 1 H2A family member j	-1.313
17093724	ARHGEF39	Rho guanine nucleotide exchange factor 39	-1.294
16815090	CCNF	cyclin F	-1.291
16868035	CTXN1	cortexin 1	-1.271
16764791	KRT80	keratin 80	-1.255
16822084	VPS9D1-AS1	VPS9D1 antisense RNA 1	-1.253
16922584	CHAF1B	chromatin assembly factor 1 subunit B	-1.241
16989636	KIF20A	kinesin family member 20A	-1.241
16869588	ASF1B	anti-silencing function 1B histone chaperone	-1.230
16847432	BRIP1	BRCA1 interacting protein C-terminal helicase 1	-1.216
17074781	FAM86B2	family with sequence similarity 86 member B2	-1.196
16714504	ZWINT	ZW10 interacting kinetochore protein	-1.194
17009482	CENPQ	centromere protein Q	-1.190

4.4.8 *Patterns of Altered Genes Expression: Control vs TG_only*

Volcano Plot

Figure 4-15 depicts the overall expression profile of hBMECs infected with *T. gondii* (TG_only) for 24 hours in significance versus $\log_2$ FC volcano plot. Overall, there are more genes up-regulated than down-regulated and hence more up-regulated genes passed the cut-off values ($P < 0.05$ indicated by the horizontal red line, $\log_2$ FC ≤ -1 or ≥ 1 indicated by vertical long dash red line) than down-regulated genes.

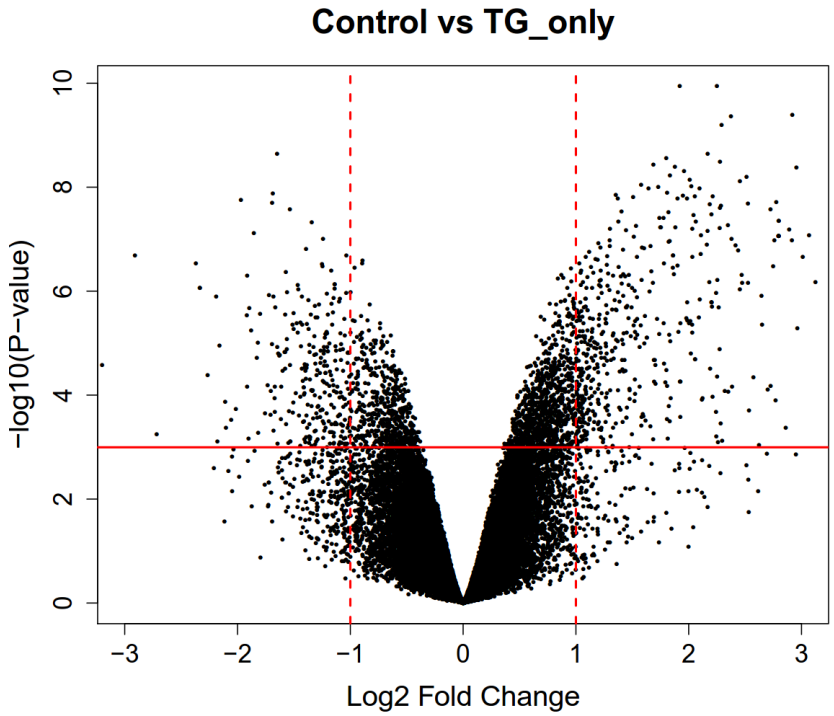


Figure 4-1 Volcano plot showing the expression profile of hBMEC after being infected with *T. gondii* for 24 hours (TG_only). Generally, there are more genes up-regulated than down-regulated and hence more up-regulated genes passed both cut-off values compared to down-regulated genes.

Top 30 Most Significant Genes Heatmap

Figure 4-16 depicts the heatmap showing a correlation between samples based on to top 30 most significant DEGs from 24 hours *T. gondii*

infection. Based column dendrogram, all 12 samples were clustered into four distinct clusters correspond to four experimental groups. These four clusters then form two major clades with one consisting of Control_only, Monensin_only and TG_Monensin samples and another clade with TG_only samples highlighting the unique expression profile of TG_only samples. Among the 30 most significance genes, four of them did not have gene symbol annotation and were assigned as NA.

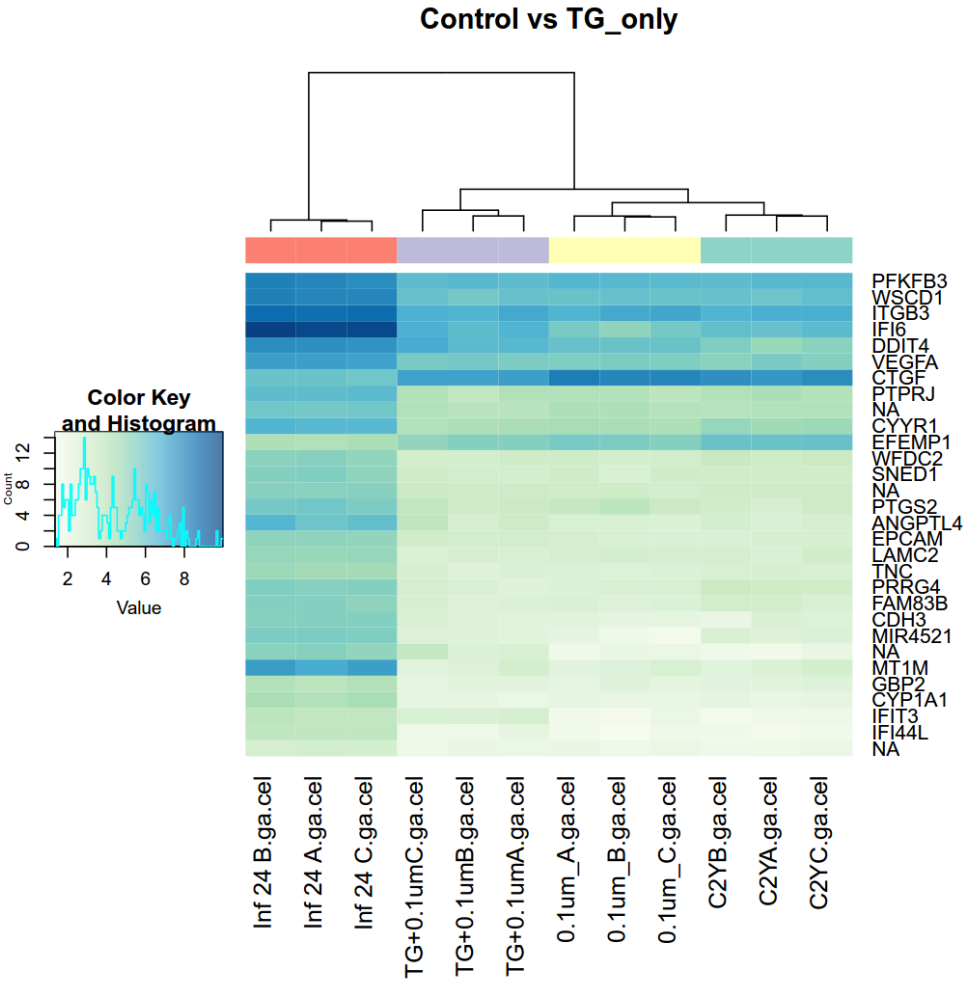


Figure 4-2 Correlation heatmap of the top 30 most significant DEGs from 24 hours of *T. gondii* infection (TG_only). Based column dendrogram, all 12 samples were clustered into four distinct clusters correspond to four experimental groups. These four clusters then form two major clades with one consisting of Control_only, Monensin_only and TG_Monensin samples and TG_only samples in another clade highlighting the different expression profile of TG_only samples. Among them, four of them were either uncharacterised genes or uncharacterised non-coding RNA genes without any symbol and were labelled as NA (not available).

The top 30 most significant DEGs from TG_only samples and their gene cluster ID, gene symbol, gene description, and $\log_2$ FC values are listed in **Table** 4-4. Among them, the most highly significant up-regulated gene with annotation is connective tissue growth factor or CTGF with $\log_2$ FC 1.650. Meanwhile, the most highly significant down-regulated gene with annotation is metallothionein 1M or MT1M with $\log_2$ FC -4.414. Overall, the total number of genes that passed selection criteria is 902 genes with 353 of them were up-regulated while the rest, 549 were down-regulated. **Appendix** 4-3 lists all filtered up-regulated and down-regulated genes.

Table 4-4 List of top 30 most significant DEGs from 24 hours of *T. gondii* infection (TG_only) with the most highly significant at the top.

Gene Cluster ID	Gene Symbol	Gene Description	Log_2 FC
16713762	NA	NA	1.919
16879863	EPCAM	epithelial cell adhesion molecule	2.249
16811684	CYP1A1	cytochrome P450 family 1 subfamily A member 1	2.373
17119058	MIR4521	microRNA 4521	2.917
16684080	IFI6	interferon alpha inducible protein 6	3.544
16819224	MT1M	metallothionein 1M	4.414
17009760	FAM83B	family with sequence similarity 83 member B	2.290
17023646	CTGF	connective tissue growth factor	-1.650
16707184	IFIT3	interferon-induced protein with tetratricopeptide repeats 3	2.167
16857886	ANGPTL4	angiopoietin-like 4	3.262
17009093	VEGFA	vascular endothelial growth factor A	1.800
16666485	IFI44L	interferon induced protein 44 like	2.276
16924592	CYYR1	cysteine and tyrosine-rich 1	1.685
16830158	WSCD1	WSC domain containing 1	1.877
16820463	CDH3	cadherin 3	2.954
16835158	ITGB3	integrin subunit beta 3	1.958
17097661	TNC	tenascin C	1.833
16697370	PTGS2	prostaglandin-endoperoxide synthase 2	2.512
17023469	NA	NA	3.432
16723318	PRRG4	proline rich and Gla domain 4	2.008
16705961	DDIT4	DNA damage inducible transcript 4	2.453
16702175	PFKFB3	6-phosphofructo-2-kinase/fructose-2,6-biphosphatase 3	1.577
16724633	PTPRJ	protein tyrosine phosphatase, receptor type J	2.022
16800242	NA	NA	1.643
16914264	WFDC2	WAP four-disulfide core domain 2	1.729
16893349	SNED1	sushi, nidogen and EGF like domains 1	2.095
16897834	EFEMP1	EGF containing fibulin extracellular matrix protein 1	-1.688
17105005	NA	NA	1.352
16672390	IFI16	interferon gamma inducible protein 16	1.370
16931815	SHANK3	SH3 and multiple ankyrin repeat domains 3	1.506

Note: NA – Not available

Top 30 Differentially Expressed Genes

Among 902 differentially regulated genes, 454 were without annotation (NA) while the rest 448 were annotated. Focusing on annotated genes, 345 of

them were up-regulated while 103 were down-regulated. Top 30 up-regulated and down-regulated genes are listed in **Table** 4-5 and **Table** 4-6.

Table 4-5 List of top 30 up-regulated genes following 24 hours *T. gondii* infection sorted with the highest log_2 FC values at the top.

Gene Cluster ID	Gene Symbol	Gene Description	Log_2 FC
16819224	MT1M	metallothionein 1M	4.414
16684080	IFI6	interferon alpha inducible protein 6	3.544
16717520	SNORA12	small nucleolar RNA, H/ACA box 12	3.406
16857886	ANGPTL4	angiopoietin-like 4	3.262
16728284	LOC105369371	uncharacterised LOC105369371	3.066
16798132	SNORD116-1	small nucleolar RNA, C/D box 116-1	3.010
16820463	CDH3	cadherin 3	2.954
17119058	MIR4521	microRNA 4521	2.917
16834091	IGFBP4	insulin-like growth factor binding protein 4	2.890
16843241	MYO1D	myosin ID	2.775
16720085	IFITM1	interferon induced transmembrane protein 1	2.724
16830837	SCARNA21	small Cajal body-specific RNA 21	2.534
16850216	SECTM1	secreted and transmembrane 1	2.524
16697370	PTGS2	prostaglandin-endoperoxide synthase 2	2.512
16705961	DDIT4	DNA damage inducible transcript 4	2.453
17046586	SNORA22	small nucleolar RNA, H/ACA box 22	2.383
16707196	IFIT1	interferon-induced protein with tetratricopeptide repeats 1	2.379
16811684	CYP1A1	cytochrome P450 family 1 subfamily A member 1	2.373
16962316	LIPH	lipase H	2.347
17009760	FAM83B	family with sequence similarity 83 member B	2.290
16815925	SNX29	sorting nexin 29	2.285
16666485	IFI44L	interferon induced protein 44 like	2.276
16879721	EPAS1	endothelial PAS domain protein 1	2.276
16666509	IFI44	interferon induced protein 44	2.274
16912362	ID1	inhibitor of DNA binding 1, HLH protein	2.253
16879863	EPCAM	epithelial cell adhesion molecule	2.249
16854301	ANKRD29	ankyrin repeat domain 29	2.212
17059771	SAMD9	sterile alpha motif domain containing 9	2.200
16968735	HERC6	HECT and RLD domain containing E3 ubiquitin protein ligase family member 6	2.182
17061099	RASA4	RAS p21 protein activator 4	2.181

Table 4-6 List of top 30 down-regulated genes following 24 hours *T. gondii* infection sorted with the lowest log_2 FC value at the top.

Gene Cluster ID	Gene Symbol	Gene Description	Log_2 FC
17062941	MIR29A	microRNA 29a	-3.201
16702257	LINC00707	long intergenic non-protein coding RNA 707	-2.370
16686273	RNU5D-1	RNA, U5D small nuclear 1	-2.161
16686271	RNU5F-1	RNA, U5F small nuclear 1	-2.050
16844585	KRTAP2-3	keratin associated protein 2-3	-1.971
16708260	OLMALINC	oligodendrocyte maturation-associated long intergenic non-coding RNA	-1.856
17117888	ZEB2	zinc finger E-box binding homeobox 2	-1.850
16745503	BLID	BH3-like motif containing, cell death inducer	-1.830
16683268	LINC01355	long intergenic non-protein coding RNA 1355	-1.734
16970188	LOC645513	septin 7 pseudogene	-1.706
16809748	MNS1	meiosis specific nuclear structural 1	-1.694
16897834	EFEMP1	EGF containing fibulin extracellular matrix protein 1	-1.688
16909524	SNORD82	small nucleolar RNA, C/D box 82	-1.682
16677898	LOC100287497	septin 7 pseudogene	-1.672
17122654	CYTOR	cytoskeleton regulator RNA	-1.666
17023646	CTGF	connective tissue growth factor	-1.650
16900293	ANKRD36C	ankyrin repeat domain 36C	-1.649
16745507	MIRLET7A2	microRNA let-7a-2	-1.626
17020480	GUSBP4	glucuronidase, beta pseudogene 4	-1.616
16697660	MIR181B1	microRNA 181b-1	-1.578
16900286	LINC00342	long intergenic non-protein coding RNA 342	-1.545
17051553	CPA4	carboxypeptidase A4	-1.537
17124806	LINC-PINT	long intergenic non-protein coding RNA, p53 induced transcript	-1.536
17109714	SCARNA9L	small Cajal body-specific RNA 9-like	-1.507
16836624	MIR21	microRNA 21	-1.476
17062945	LINC-PINT	long intergenic non-protein coding RNA, p53 induced transcript	-1.467
17122664	CYTOR	cytoskeleton regulator RNA	-1.462
17087768	NIPSNAP3B	nipsnap homolog 3B	-1.422
17124904	LINC-PINT	long intergenic non-protein coding RNA, p53 induced transcript	-1.407
17072622	LOC101927657	uncharacterised LOC101927657	-1.406

4.4.9 *Patterns of Altered Genes Expression: Control vs TG_Monensin*

Volcano Plot

Figure 4-17 depicts the overall expression profile of hBMECs infected with *T. gondii* then treated with 0.1 µM monensin (TG_Monensin) for 24 hours insignificance versus $\log_2$ FC volcano plot. Overall, there are more genes down-regulation than up-regulation leading to more down-regulated genes that passed the cut-off values ($P < 0.05$ indicated by the horizontal red line, $\log_2$ FC ≤ -1 or ≥ 1 indicated by vertical long dash red line) than up-regulated genes.

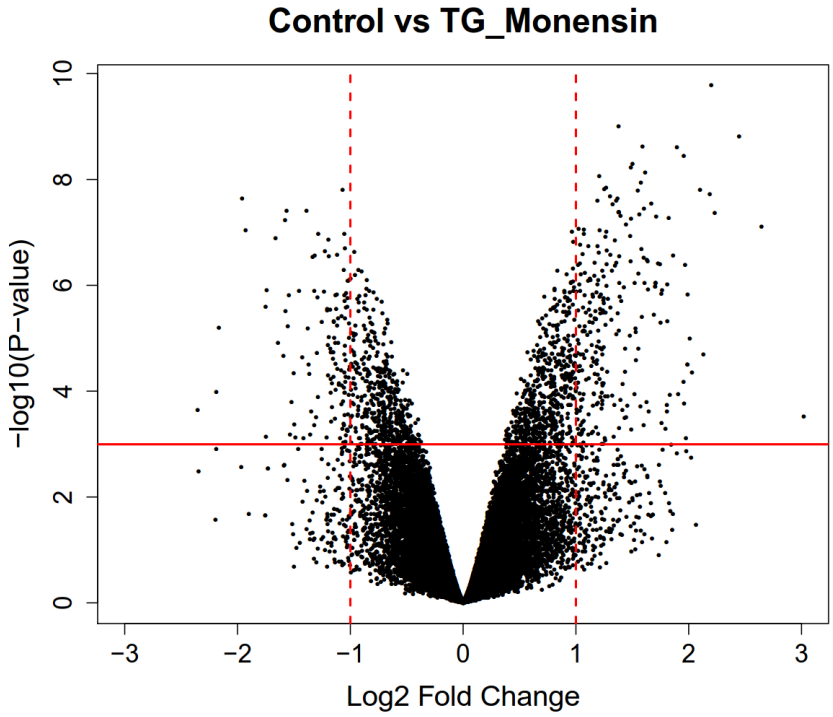


Figure 4-3 Volcano plot showing the expression profile of hBMECs infected with *T. gondii* then treated with 0.1 µM monensin (TG_Monensin). Generally, there are more genes up-regulation than down-regulation leading to more up-regulated genes that passed both cut-off values compared to down-regulated genes.

Top 30 Most Significant Genes Heatmap

Figure 4-18 depicts the heatmap showing a correlation between samples based on to the top 30 most significant DEGs in hBMECs infected with *T. gondii* and treated with 0.1 µM monensin (TG_Monensin). Based on column dendrogram, the 12 samples expression profiles were clustered into four distinct clusters corresponding to four experimental groups. These four clusters then join to form two clades with Control and TG_only samples in one clade while Monensin_only and TG_Monensin samples in the other clade.

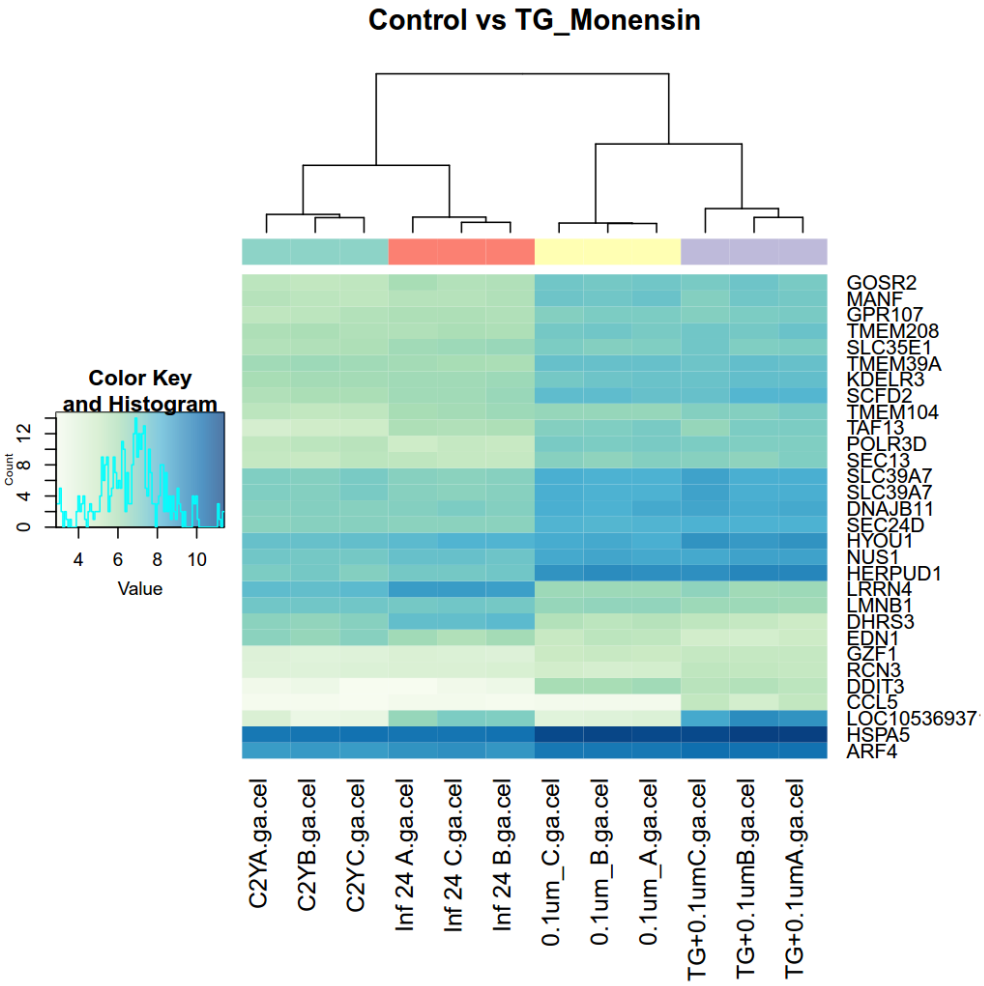


Figure 4-4 Correlation heatmap of the top 30 most significant DEGs from hBMECs infected with *T. gondii* then treated with 0.1 µM monensin (TG_Monensin). Based on column dendrogram, the 12 samples expression profiles were clustered into four distinct clusters corresponding to four experimental groups. These four clusters then join to form two clades with Control and TG_only samples in one clade while Monensin_only and TG_Monensin samples in the other clade.

The top 30 most significant DEGs in hBMECs infected with *T. gondii* and treated with 0.1 μM monensin (TG_Monensin) and their name, gene symbol, gene description and log_2 FC values are listed in **Table** 4-7. Among these, the most highly significant up-upregulated genes with annotation were endothelin 1 or EDN1 with log_2 FC 1.960. Meanwhile, the most highly significant down-regulated gene with annotation was uncharacterised LOC105369371 or LOC105369371 with log_2 FC -5.135. Overall, the total number of genes that passed the selection criteria was 424 genes, of these 134 were up-regulated and 290 were down-regulated. **Appendix** 4-4 lists all filtered up-regulated and down-regulated genes.

Table 4-7 List of the top 30 most significant DEGs in hBMECs infected with *T. gondii* and treated with 0.1 μM monensin (TG_Monensin) with the most highly significant at the top.

Gene Cluster ID	Gene Symbol	Gene Description	Log_2 FC
16819325	HERPUD1	homocysteine inducible ER protein with ubiquitin-like domain 1	2.199
16728284	LOC105369371	uncharacterised LOC105369371	5.135
16979256	SEC24D	SEC24 homolog D, COPII coat complex component	1.377
16766578	DDIT3	DNA damage inducible transcript 3	2.446
16949292	DNAJB11	DnaJ heat shock protein family (Hsp40) member B11	1.589
16835125	GOSR2	golgi SNAP receptor complex member 2	1.894
16975954	SCFD2	sec1 family domain containing 2	1.955
16930066	KDELR3	KDEL endoplasmic reticulum protein retention receptor 3	1.500
16820076	TMEM208	transmembrane protein 208	1.486
16837646	TMEM104	transmembrane protein 104	1.613
16955442	ARF4	ADP ribosylation factor 4	1.205
16988703	LMNB1	lamin B1	-1.070
16864181	RCN3	reticulocalbin 3	1.250
17012079	NUS1	NUS1 dehydrodolichyl diphosphate synthase subunit	1.266
17090161	GPR107	G protein-coupled receptor 107	1.548
17066561	POLR3D	RNA polymerase III subunit D	1.575
16843511	CCL5	C-C motif chemokine ligand 5	2.099
16690511	TAF13	TATA-box binding protein associated factor 13	2.186
16957771	TMEM39A	transmembrane protein 39A	1.301
17004903	EDN1	endothelin 1	-1.960
16745186	HYOU1	hypoxia up-regulated 1	1.367
16912057	GZF1	GDNF inducible zinc finger protein 1	1.190
17098411	HSPA5	heat shock protein family A (Hsp70) member 5	1.356
16870047	SLC35E1	solute carrier family 35 member E1	1.324
16941167	MANF	mesencephalic astrocyte derived neurotrophic factor	1.667
16681827	DHRS3	dehydrogenase/reductase 3	-1.566
16917054	LRRN4	leucine rich repeat neuronal 4	-1.390
17007377	SLC39A7	solute carrier family 39 member 7	1.378
17028426	SLC39A7	solute carrier family 39 member 7	1.378
17031238	SLC39A7	solute carrier family 39 member 7	1.378

Top 30 Differentially Expressed Genes

Among 424 differentially regulated genes, 114 were without annotation (NA) while the rest 310 were annotated. Focusing on annotated genes, 201 of them were up-regulated while 109 were down-regulated. Top 30 up-regulated and down-regulated genes are listed in **Table** 4-8 and **Table** 4-9.

Table 4-8 List of top 30 up-regulated genes from 24 hours treatment with 0.1 uM monensin and *T. gondii* infection sorted with the highest log_2 FC values at the top.

Gene Cluster ID	Gene Symbol	Gene Description	Log_2 FC
16728284	LOC105369371	uncharacterised LOC105369371	5.135
16766578	DDIT3	DNA damage inducible transcript 3	2.446
16868827	YIPF2	Yip1 domain family member 2	2.229
16819325	HERPUD1	homocysteine inducible ER protein with ubiquitin-like domain 1	2.199
16690511	TAF13	TATA-box binding protein associated factor 13	2.186
16843511	CCL5	C-C motif chemokine ligand 5	2.099
16941052	CYB561D2	cytochrome b561 family member D2	2.008
17120058	PDE4DIP	phosphodiesterase 4D interacting protein	1.989
16927633	SDF2L1	stromal cell-derived factor 2 like 1	1.967
16975954	SCFD2	sec1 family domain containing 2	1.955
16835125	GOSR2	golgi SNAP receptor complex member 2	1.894
16774188	COG6	component of oligomeric Golgi complex 6	1.860
16772733	GOLGA3	golgin A3	1.822
16659133	NPPA-AS1	NPPA antisense RNA 1	1.763
16863287	FOSB	FosB proto-oncogene, AP-1 transcription factor subunit	1.756
16900053	EIF2AK3	eukaryotic translation initiation factor 2 alpha kinase 3	1.744
16960844	VEPH1	ventricular zone expressed PH domain containing 1	1.727
16775856	DNAJC3	DnaJ heat shock protein family (Hsp40) member C3	1.710
17103946	GPR173	G protein-coupled receptor 173	1.690
16941167	MANF	mesencephalic astrocyte derived neurotrophic factor	1.667
16769481	ALDH1L2	aldehyde dehydrogenase 1 family member L2	1.638
16934476	APOL2	apolipoprotein L2	1.635
16848079	WIPI1	WD repeat domain, phosphoinositide interacting 1	1.628
16996176	MIR449A	microRNA 449a	1.625
16837646	TMEM104	transmembrane protein 104	1.613
16861647	KCNK6	potassium two-pore domain channel subfamily K member 6	1.607
16950686	SEC13	SEC13 homolog, nuclear pore and COPII coat complex component	1.602
16829139	MVD	mevalonate diphosphate decarboxylase	1.600
16949292	DNAJB11	DnaJ heat shock protein family (Hsp40) member B11	1.589
16774112	UFM1	ubiquitin-fold modifier 1	1.579

Table 4-9 List of top 30 down-regulated genes from 24 hours treatment with 0.1 uM monensin and *T. gondii* infection sorted with the lowest log_2 FC values at the top.

Gene Cluster ID	Gene Symbol	Gene Description	Log_2 FC
17004903	EDN1	endothelin 1	-1.960
16725041	FAM111B	family with sequence similarity 111 member B	-1.929
17080595	DSCC1	DNA replication and sister chromatid cohesion 1	-1.752
16714747	RTKN2	rhotekin 2	-1.664
16997676	MTRNR2L2	MT-RNR2 like 2	-1.642
17016400	HIST1H3F	histone cluster 1 H3 family member f	-1.594
16800355	WDR76	WD repeat domain 76	-1.580
16986913	VCAN	versican	-1.576
16681827	DHRS3	dehydrogenase/reductase 3	-1.566
17122086	LINC01224	long intergenic non-protein coding RNA 1224	-1.556
17016499	HIST1H1B	histone cluster 1 H1 family member b	-1.546
16739636	SNHG1	small nucleolar RNA host gene 1	-1.503
16716124	CERNA2	competing endogenous lncRNA 2 for microRNA let-7b	-1.498
16877473	GEN1	GEN1, Holliday junction 5' flap endonuclease	-1.488
17016403	HIST1H3G	histone cluster 1 H3 family member g	-1.463
16932821	YPEL1	yippee-like 1	-1.456
16736638	E2F8	E2F transcription factor 8	-1.428
16798216	SNORD116-24	small nucleolar RNA, C/D box 116-24	-1.417
16917054	LRRN4	leucine rich repeat neuronal 4	-1.390
17079293	CCNE2	cyclin E2	-1.379
17072622	LOC101927657	uncharacterised LOC101927657	-1.371
16707695	HELLS	helicase, lymphoid-specific	-1.365
17121990	ZNF730	zinc finger protein 730	-1.357
16679411	EXO1	exonuclease 1	-1.336
17016363	HIST1H3B	histone cluster 1 H3 family member b	-1.321
16922584	CHAF1B	chromatin assembly factor 1 subunit B	-1.321
17093724	ARHGEF39	Rho guanine nucleotide exchange factor 39	-1.317
17016366	HIST1H2AB	histone cluster 1 H2A family member b	-1.305
16965346	NCAPG	non-SMC condensin I complex subunit G	-1.298
16847432	BRIP1	BRCA1 interacting protein C-terminal helicase 1	-1.293

4.4.10 *Gene Ontology (GO) and Pathway Analysis*

Here, the cumulative effect of altered transcriptional changes in hBMECs in response to treatment with 0.1 μM monensin (Monensin_only), *T. gondii* infection (TG_only), and *T. gondii* infection in hBMECs treated with 0.1 μM monensin (TG_Monensin) were investigated. For this analysis, only genes with gene symbol were considered for analysis. Out of 112 down-regulated genes only 65 (58.03%) were annotated whereas only 171 out of 368 (46.47%) up-regulated genes were annotated from Control *vs* Monensin_only filtered list. From Control *vs* TG_only filtered list, 103 out of 353 (29.18%) down-regulated genes were annotated while 345 out of 549 (62.84%) up-regulated genes were annotated. From Control *vs* TG_Monensin filtered list, 109 out of 134 (81.34%) down-regulated genes were annotated while 201 out of 290 (69.31%) up-regulated genes were annotated.

Control vs Monensin _only

Of the 65 annotated down-regulated genes, only 54 were recognised by PANTHER database and the hits for three GO term categories (biological process, molecular function, cellular compartment) are presented in **Figure** 4-19, **Figure** 4-20 and **Figure** 4-21 respectively. Overall, 54 annotated genes matched 11 GO terms of biological processes and 96 sub-categories which are cellular process (GO:0009987, 27 hits), metabolic process (GO:0008152, 26 hits), cellular component organisation or biogenesis (GO:0071840, 12 hits), biological regulation (GO:0065007, 11 hits), response to stimulus (GO:0050896, five hits), developmental process (GO:0032502, three hits), multicellular organismal process (GO:0032501, three hits), localisation (GO:0051179, two hits), reproduction (GO:0000003, one hit), rhythmic

process (GO:0048511, one hit), and locomotion (GO:0040011, one hit). In PANTHER Overrepresentation Test with default setting (Fisher's Exact with FDR multiple test correction) for PANTHER GO-Slim Biological Process, 11 out of 92 biological processes were remarkably enriched (FDR < 0.05) which are DNA metabolic process (GO:0006259), cell cycle (GO:0007049), regulation of cell cycle (GO:0051726), mitosis (GO:0007067), nucleobase-containing compound metabolic process (GO:0006139), DNA replication (GO:0006260), chromosome segregation (GO:0007059), organelle organisation (GO:0006996), cell proliferation (GO:0008283), chromatin organisation (GO:0006325), and metabolic process (GO:0008152). Meanwhile, annotated down-regulated genes also matched to four major molecular function terms further divided into 41 sub-categories which are binding (GO:0005488; 25 hits), catalytic activity (GO:0003824, 14 hits), receptor activity (GO:0004872, one hit) and structural molecule activity (GO:0005198, one hit). PANTHER Overrepresentation Test then identified DNA helicase activity (GO:0003678), helicase activity (GO:0004386), kinase regulator activity (GO:0019207), nucleic acid binding (GO:0003676) and binding (GO:0005488) as overrepresented molecular functions. In cellular component ontology, annotated down-regulated genes matched to six major cellular components further divided into 56 sub-categories which are cell part (GO:0044464, 21 hits), organelle (GO:0043226, 19 hits), macromolecular complex (GO:0032991, 10 hits), membrane (GO:0016020, two hits), extracellular matrix (GO:0031012, two hits) and extracellular region (GO:0005576, 2 hits). The PANTHER Overrepresentation Test then identified nucleus (GO:0005634) as the only overrepresented cellular component.

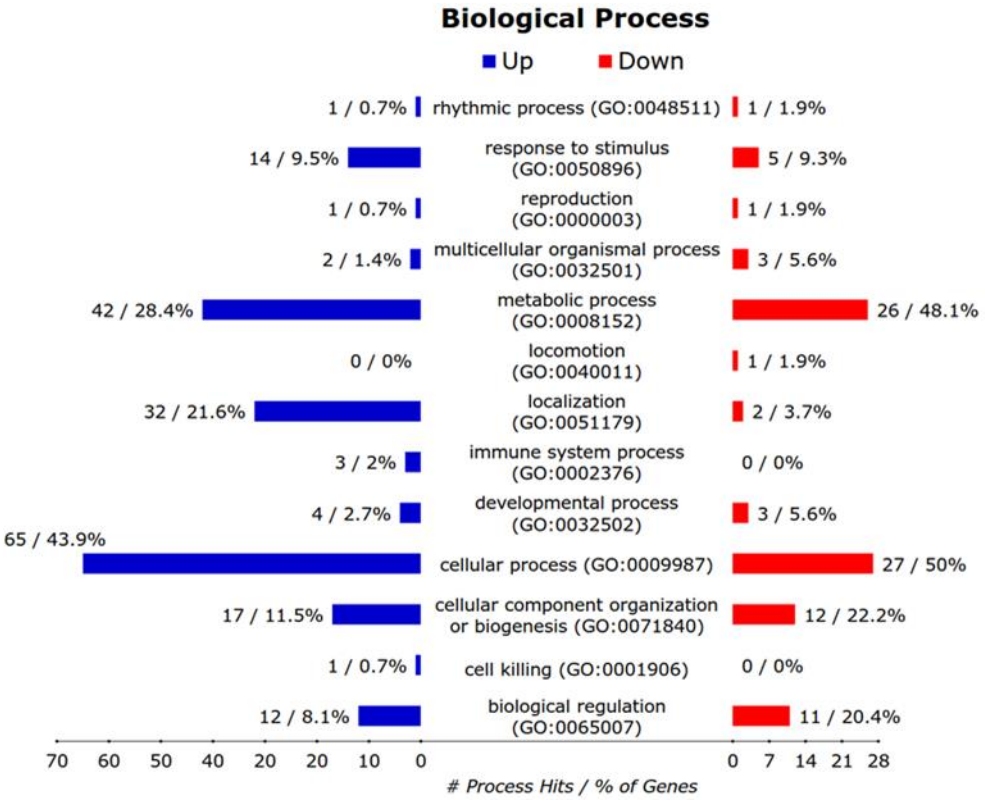


Figure 4-5 PANTHER GO-Slim biological process ontology hits for significantly DEGs due to treatment with 0.1 µM monensin for 24 hours (Monensin_only). The down-regulated genes matched to 92 processes from 11 major processes while the up-regulated genes matched to 194 processes from 12 major processes. The PANTHER Overrepresentation Test (FDR < 0.05) then identified 11 and 10 overrepresented processes from down and up-regulated genes respectively.

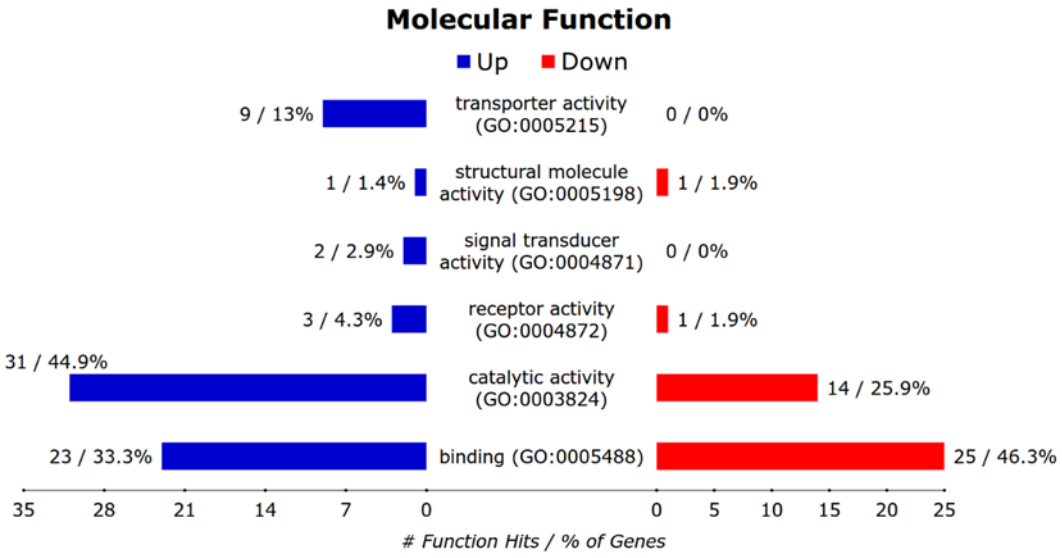


Figure 4-6 PANTHER GO-Slim molecular function ontology hits for significantly DEGs due to treatment with 0.1 µM monensin for 24 hours (Monensin_only). The down-regulated genes matched to 41 functions from four major functions while up-regulated genes matched to 69 functions from six major functions. The PANTHER Overrepresentation Test (FDR < 0.05) then identified five and one overrepresented molecular functions for down and up-regulated genes respectively.

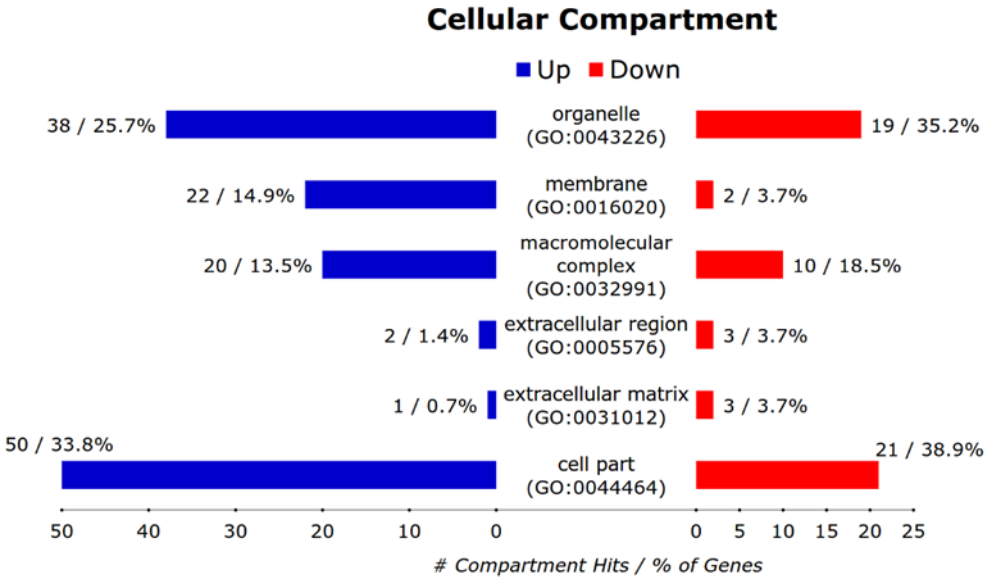


Figure 4-7 PANTHER GO-Slim cellular component ontology hits for significantly DEGs due to treatment with 0.1 µM monensin for 24 hours (Monensin_only). The down-regulated genes matched to 56 cellular components from six major components while up-regulated genes matched to 133 cellular components from six major components. The PANTHER Overrepresentation Test (FDR < 0.05) then identified one and six significant locations from down and up-regulated genes respectively.

Of the 171 annotated up-regulated genes only 148 were recognised by PANTHER database and the hits for three GO term categories (biological process, molecular function, cellular compartment) are presented in **Figure** 4-19, **Figure** 4-20 and **Figure** 4-21 above respectively. Overall, these genes matched to 194 biological processes from 12 major categories (cellular process GO:0009987, 65 hits; metabolic process GO:0008152, 42 hits; localisation GO:0051179, 32 hits; cellular component organisation or biogenesis GO:0071840, 17 hits; response to stimulus GO:0050896, 14 hits; biological regulation GO:0065007, 12 hits; developmental process GO:0032502, four hits; immune system process GO:0002376, three hits, multicellular organismal process GO:0032501, two hits; reproduction GO:0000003, one hit; rhythmic process GO:0048511, one hit; cell killing GO:0001906, one hit), 69 molecular function from six major categories (catalytic activity GO:0003824, 31 hits; binding GO:0005488, 23 hits; transporter activity GO:0005215, nine hits; receptor activity GO:0004872, three hits; signal transducer activity GO:0004871, two hits; structural molecule activity GO:0005198, one hit) and 133 cellular components also from six major categories (cell part GO:0044464, 50 hits; organelle GO:0043226, 38 hits; membrane GO:0016020, 22 hits; macromolecular complex GO:0032991, 20 hits; extracellular region GO:0005576, two hits; extracellular matrix GO:0031012, one hit). The PANTHER Overrepresentation Test (FDR < 0.05) identified significantly enriched 10 biological process terms (steroid metabolic process GO:0008202, protein targeting GO:0006605, protein transport GO:0015031, vesicle-mediated transport GO:0016192, intracellular protein transport GO:0006886, protein localisation GO:0008104, transport GO:0006810, localisation GO:0051179, single-multicellular organism process GO:0044707, multicellular organismal process GO:0032501), one molecular function (SNAP receptor activity GO:0005484) and six cellular components (vesicle coat GO:0030120, SNARE

complex GO:0031201, Golgi apparatus GO:0005794, cytoplasmic membrane-bounded vesicle GO:0016023, endoplasmic reticulum GO:0005783, cytoplasm GO:0005737).

All 236 differentially regulated annotated genes filtered list (log_2 FC ≤ -1 or ≥ 1; adjusted *P*-value $P < 0.05$) were submitted to Reactome Pathways Analysis tool (https://reactome.org/PathwayBrowser/#TOOL=AT) together with their log_2 FC values. Out of these, only 132 were recognised by the Reactome database and considered for pathway analysis. All 23 pathways linked with the submitted genes with FDR < 0.05 are listed in **Table** 4-10 sorted with the lowest FDR values at the top. The table includes Reactome pathway identifiers, pathway name, the number of matched genes plus the pathway expression representation which were calculated from the average log_2 FC of matched genes. Overall, 17 pathways were up-regulated while another six were down-regulated. The most highly up-regulated pathway is 'PERK regulates gene expression' (R-HSA-381042) with average log_2 FC of 2.165 while the most down-regulated pathway is 'G0 and Early G1' (R-HSA-1538133) with average log_2 FC of -1.179.

Table 4-10 List of all 23 Reactome pathways affected by 24 hours treatment with 0.1 µM monensin (Monensin_only) with FDR < 0.05 sorted with the lowest FDR values at the top. Overall, 17 pathways were down-regulated while another three were up-regulated.

Pathway identifier	Pathway name	Entities Found / Total	Average Log_2 FC
R-HSA-381119	Unfolded Protein Response (UPR)	31 / 160	1.440
R-HSA-381070	IRE1alpha activates chaperones	24 / 110	1.273
R-HSA-381038	XBP1(S) activates chaperone genes	21 / 106	1.293
R-HSA-1655829	Regulation of cholesterol biosynthesis by SREBP (SREBF)	19 / 86	1.279
R-HSA-2426168	Activation of gene expression by SREBF (SREBP)	16 / 70	1.295
R-HSA-199977	ER to Golgi Anterograde Transport	17 / 163	1.318
R-HSA-8957322	Metabolism of steroids	24 / 321	1.302
R-HSA-446203	Asparagine N-linked glycosylation	26 / 420	1.301
R-HSA-381183	ATF6 (ATF6-alpha) activates chaperone genes	6 /15	1.766
R-HSA-381033	ATF6 (ATF6-alpha) activates chaperones	6 / 17	1.766
R-HSA-6807878	COPI-mediated anterograde transport	12 / 106	1.316
R-HSA-948021	Transport to the Golgi and subsequent modification	17 / 218	1.318
R-HSA-191273	Cholesterol biosynthesis	10 / 72	1.373
R-HSA-392499	Metabolism of proteins	75 / 2432	0.969
R-HSA-204005	COPII-mediated vesicle transport	9 / 76	1.381
R-HSA-6811442	Intra-Golgi and retrograde Golgi-to-ER traffic	14 / 217	1.127
R-HSA-176974	Unwinding of DNA	4 / 12	-1.121
R-HSA-381042	PERK regulates gene expression	6 / 38	2.165
R-HSA-1362300	Transcription of E2F targets under negative control by p107 (RBL1) and p130 (RBL2) in complex with HDAC1	4 / 20	-1.096
R-HSA-1538133	G0 and Early G1	5 / 38	-1.179
R-HSA-1640170	Cell Cycle	25 / 681	-0.763
R-HSA-6811438	Intra-Golgi traffic	5 / 48	1.558
R-HSA-5693554	Resolution of D-loop Structures through Synthesis-Dependent Strand Annealing (SDSA)	4 / 30	-1.129

Note: Greyed rows indicate down-regulated pathways.

In addition to the pathways above, some genes were also matched to the WNT signalling pathways but were not included in **Table** 4-11 above since the FDR values were above 0.05. **Table** 4-11 lists pathways related to WNT signalling plus their pathway's identifiers, the number of matched genes, FDR values and pathway expression representation by an average of log_2 FC.

Table 4-11 List of WNT signalling related pathways with the matched genes, average log_2 FC and FDR values.

Pathway Identifier	Pathway Name	Entities Found / Total	Average Log_2 FC	FDR values
R-HSA-201681	TCF dependent signalling in response to WNT	2 / 216	1.232	0.918
Matched Genes	HIST1H2AJ; HIST1H3F			
R-HSA-195721	Signalling by WNT	2 / 330	1.232	0.987
Matched Genes	HIST1H2AJ; HIST1H3F			

Control vs TG _only

Of 103 annotated down-regulated genes, only 38 were recognised by PANTHER database and the hits for all GO annotations (biological process, molecular function, cellular component) and their major categories were presented in **Figure** 4-22, **Figure** 4-23 and **Figure** 4-24. Overall, these up-regulated genes matched to 51 biological processes from nine major categories (cellular process GO:0009987, 14 hits; metabolic process GO:0008152, 14 hits; localisation GO:0051179, five hits; biological regulation GO:0065007, five hits; response to stimulus GO:0050896, four hits; cellular component organisation or biogenesis GO:0071840, three hits; multicellular organismal process GO:0032501, three hits; developmental process GO:0032502, two hits; biological adhesion GO:0022610, one hit), 27 molecular functions from five major categories (binding GO:0005488, 12 hits; catalytic activity GO:0003824, nine hits; transporter activity GO:0005215, three hits; signal transducer activity GO:0004871, two hits; receptor activity GO:0004872, one hit) and 28

cellular compartments from seven major categories (cell part GO:0044464, 11 hits; organelle GO:0043226, seven hits; macromolecular complex GO:0032991, four hits; membrane GO:0016020, two hits; extracellular region GO:0005576, two hits; synapse GO:0045202, one hit, extracellular matrix GO:0031012, one hit). Further analysis with the PANTHER Overrepresentation Test unfortunately found no significantly enriched biological processes, molecular function or cellular compartment (FDR < 0.05).

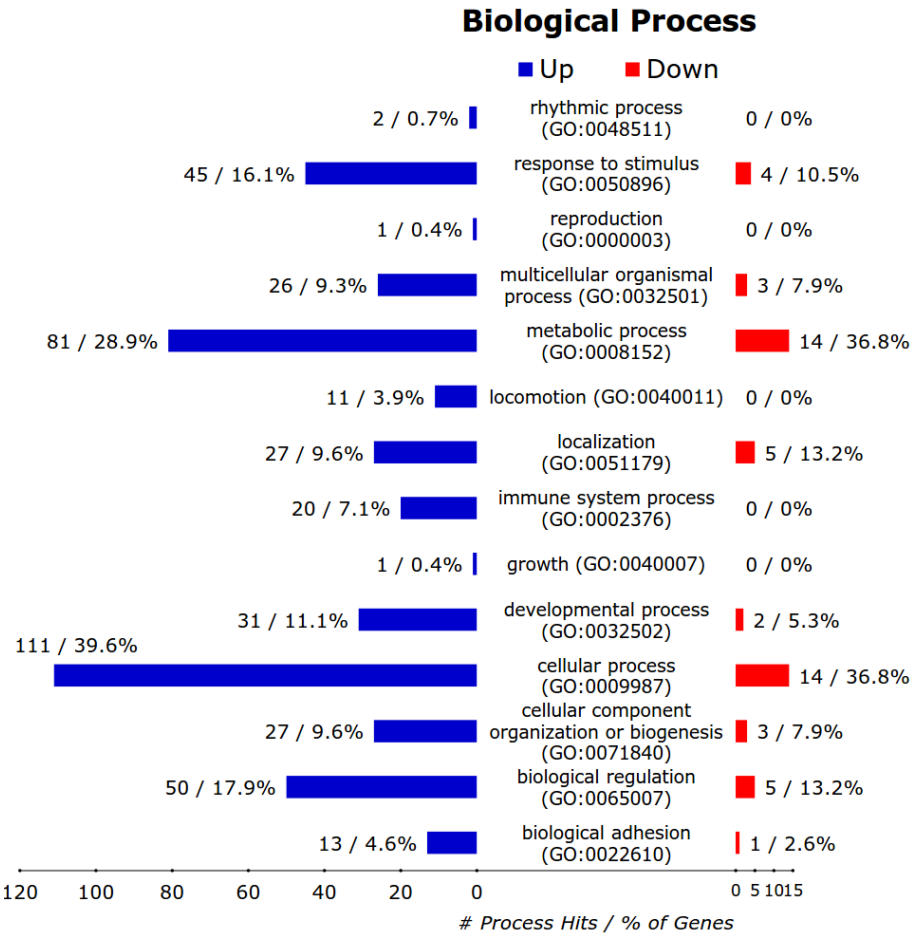


Figure 4-8 PANTHER GO-Slim biological process ontology hits for significantly DEGs due to *T. gondii* infection (TG_only). The down-regulated genes matched to 51 processes from nine major processes while the up-regulated genes matched to 446 processes from 14 major processes. The PANTHER Overrepresentation Test (FDR < 0.05) then identified two overrepresented processes from down but none for up-regulated genes.

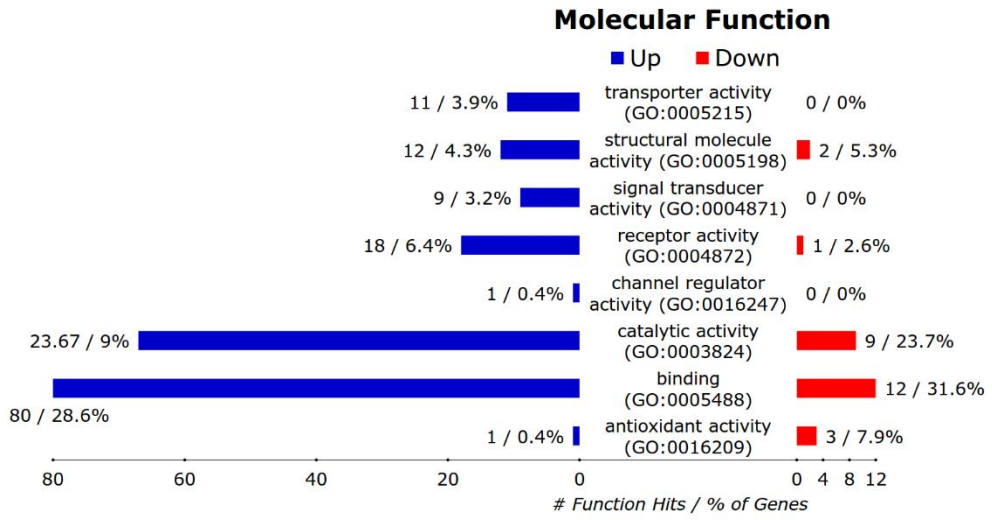


Figure 4-9 PANTHER GO-Slim molecular function ontology hits for significantly DEGs due to *T. gondii* infection (TG_only). The down-regulated genes matched to 27 functions from five major functions while the up-regulated genes matched to 199 functions from eight major functions. No overrepresented function from the PANTHER Overrepresentation Test (FDR < 0.05) for both sets of genes.

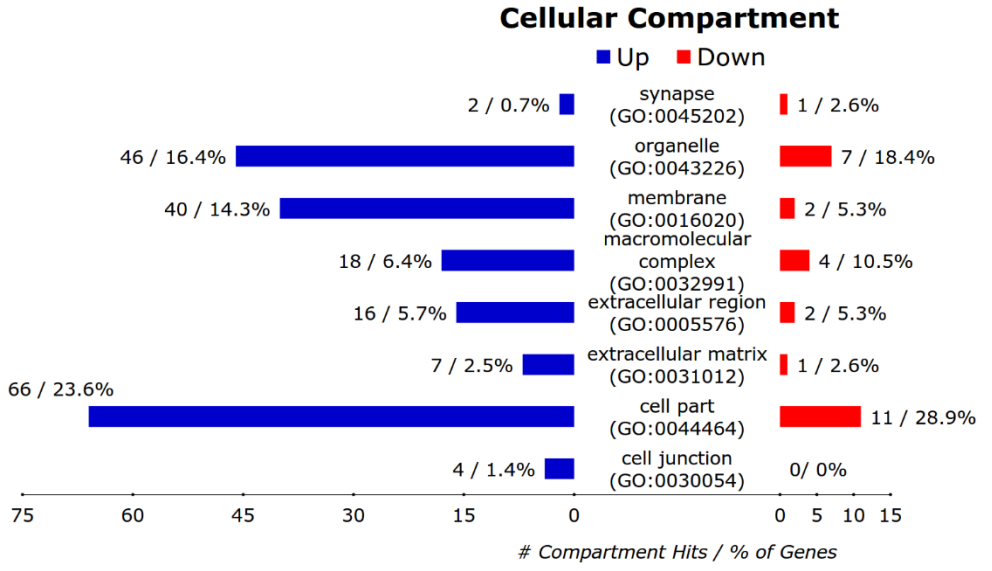


Figure 4-10 PANTHER GO-Slim cellular component ontology hits for significantly DEGs due to *T. gondii* infection (TG_only). The down-regulated genes matched to 28 cellular components from seven major components while the up-regulated genes matched to 199 cellular components from eight major components. No overrepresented component from the PANTHER Overrepresentation Test (FDR < 0.05) for both sets of genes.

Of 345 annotated down-regulated genes, only 280 were recognised by the PANTHER database and the hits for all GO annotations (biological process, molecular function, cellular component) and their major categories were presented in **Figure** 4-22, **Figure** 4-23 and **Figure** 4-24. Overall, these up-regulated genes matched to 446 biological processes from 14 major categories (biological adhesion GO:0022610, 13 hits; biological regulation GO:0065007, 50 hits; cellular component organisation or biogenesis GO:0071840, 27 hits; cellular process GO:0009987, 111 hits; developmental process GO:0032502, 31 hits; growth GO:0040007, one hit; immune system process GO:0002376, 20 hits; localisation GO:0051179, 27 hits; locomotion GO:0040011, 11 hits; metabolic process GO:0008152, 81 hits; multicellular organismal process GO:0032501, 26 hits; reproduction GO:0000003, one hit; response to stimulus GO:0050896, 45 hits; rhythmic process GO:0048511, two hits), 199 molecular functions from eight major categories (antioxidant activity GO:0016209, one hit; binding GO:0005488, 80 hits; catalytic activity GO:0003824, 67 hits; channel regulator activity GO:0016247, one hit; receptor activity GO:0004872, 18 hits; signal transducer activity GO:0004871, nine hits; structural molecule activity GO:0005198, 12 hits; transporter activity GO:0005215, 11 hits) and 199 cellular compartments from eight major categories (cell junction GO:0030054, four hits; cell part GO:0044464. 66 hits; extracellular matrix GO:0031012, seven hits; extracellular region GO:0005576, 16 hits; macromolecular complex GO:0032991, 18 hits; membrane GO:0016020, 40 hits; organelle GO:0043226, 46 hits; synapse GO:0045202, two hits) biological processes to be significantly enriched but there are no significantly enriched molecular function or cellular compartment (FDR < 0.05).

All 448 differentially regulated genes with a symbol from the filtered list ($\log_2$ FC ≤ -1 or ≥ 1; adjusted *P* value *P* < 0.05) were submitted to Reactome's 'Pathways Analysis' tool together with their $\log_2$ FC values. Out of these, only

232 were recognised by the Reactome database and considered for pathway analysis. Pathways linked with the submitted genes with FDR < 0.05 are listed in **Table** 4-12 sorted with the lowest FDR values at the top. Surprisingly, even though there were more genes submitted compared to Monensin_only, only four pathways passed the corrected overrepresentation probability test (FDR < 0.05). Overall, all four pathways were up-regulated with the most highly up-regulated pathway being 'Interferon alpha/beta signalling' (R-HSA-909733) with average $\log_2$ FC of 1.570.

Table 4-12 List of all four Reactome pathways affected by 24 hours infection with *T. gondii* (TG_only) with FDR < 0.05 sorted with the lowest FDR values at the top. Overall, all four pathways were down-regulated with the most highly down-regulated pathway is interferon alpha/beta signalling (R-HSA-909733) with average $\log_2$ FC of 1.611.

Pathway Identifier	Pathway Name	Entities Found / Total	Average Log_2 FC
R-HSA-909733	Interferon alpha/beta signalling	38 / 184	1.611
R-HSA-913531	Interferon Signalling	50 / 388	1.532
R-HSA-1280215	Cytokine Signalling in the Immune system	72 / 1051	1.535
R-HSA-877300	Interferon gamma signalling	23 / 250	1.359

In addition to the pathways above, some genes were also matched to the WNT signalling pathways but were not included in **Table** 4-12 above since the FDR values were above 0.05. **Table** 4-13 lists pathways related to the WNT signalling plus their pathway's identifiers, the number of matched genes, FDR values, and pathway expression representation by an average of $\log_2$ FC.

Table 4-13 List of WNT signalling related pathways with the matched genes, average log_2 FC and FDR values.

Pathway Identifier	Pathway Name	Entities Found / Total	Average Log_2 FC	FDR values
R-HSA-195721	Signalling by WNT	7 / 330	1.303	0.937
Matched Genes	HIST1H4B; FZD7; HIST1H2BG; HIST2H3D; PLCB1; GNG11; HIST1H2AB			
R-HSA-201681	TCF dependent signalling in response to WNT	4 / 216	1.279	0.939
Matched Genes	HIST1H4B; HIST1H2BG; HIST2H3D; HIST1H2AB			
R-HSA-3858494	Beta-catenin independent WNT signalling	3 / 165	1.335	0.923
Matched Genes	FZD7; PLCB1; GNG11			

Control vs TG_Monensin

Of 109 annotated down-regulated genes, only 101 were recognised by the PANTHER database and the hits for all GO annotations (biological process, molecular function, cellular component) and their major categories were presented in **Figure** 4-25, **Figure** 4-26 and **Figure** 4-27 respectively. Overall, these down-regulated genes matched to 156 biological processes from 10 major categories (biological adhesion GO:0022610, one hit; biological regulation GO:0065007, 17 hits; cellular component organisation or biogenesis GO:0071840, 22 hits; cellular process GO:0009987, 48 hits; developmental process GO:0032502, two hits; localisation GO:0051179, five hits; metabolic process GO:0008152, 48 hits; multicellular organismal process GO:0032501, one hit; reproduction GO:0000003, three hits; response to stimulus GO:0050896, nine hits), 68 molecular function from three major categories (binding GO:0005488, 43 hits; catalytic activity GO:0003824, 24 hits; structural molecule activity GO:0005198, one hit), and 106 cellular components from six major categories (cell part GO:0044464, 43 hits; extracellular matrix GO:0031012, one hit; extracellular region GO:0005576, two hits; macromolecular complex GO:0032991, 16 hits; membrane GO:0016020, two hits; organelle GO:0043226, 42 hits).

Further analysis with the PANTHER Overrepresentation Test (FDR < 0.05) found 25 significantly enriched biological processes (**Table** 4-14), nine significantly enriched molecular functions (DNA binding GO:0003677, nucleic acid binding GO:0003676, DNA helicase activity GO:0003678, helicase activity GO:0004386, binding GO:0005488, single-stranded DNA binding GO:0003697, microtubule binding GO:0008017, microtubule motor activity GO:0003777, motor activity GO:0003774) and 12 significantly enriched cellular components (chromosome GO:0005694, nucleus GO:0005634, nuclear chromosome GO:0000228, organelle GO:0043226, protein-DNA complex GO:0032993, nucleoplasm GO:0005654, intracellular GO:0005622, cell part GO:0044464, microtubule GO:0005874, plasma membrane GO:0005886, membrane GO:0016020, cytoskeleton GO:0005856).

Table 4-14 List of all 25 significantly enriched biological processes from 101 annotated up-regulated genes sorted with the most significant at the top (PANTHER Overrepresentation Test with Fisher's Exact with multiple correction test, FDR < 0.05).

PANTHER GO-Slim Biological Process	No of Matched Gene	FDR
DNA metabolic process (GO:0006259)	23	5.44E-16
nucleobase-containing compound metabolic process (GO:0006139)	38	0.000000104
cell cycle (GO:0007049)	19	0.000000122
chromosome segregation (GO:0007059)	9	0.000000151
mitosis (GO:0007067)	11	0.0000011
DNA repair (GO:0006281)	9	0.00000688
organelle organisation (GO:0006996)	21	0.0000104
regulation of cell cycle (GO:0051726)	9	0.0000123
DNA replication (GO:0006260)	8	0.0000344
nitrogen compound metabolic process (GO:0006807)	30	0.0000427
chromatin organisation (GO:0006325)	9	0.000187
metabolic process (GO:0008152)	48	0.000635
primary metabolic process (GO:0044238)	41	0.00118
DNA recombination (GO:0006310)	4	0.00259
cellular component organisation (GO:0016043)	22	0.00308
cell communication (GO:0007154)	2	0.00369
cellular component organisation or biogenesis (GO:0071840)	22	0.00555
regulation of gene expression, epigenetic (GO:0040029)	4	0.00623
chromatin assembly (GO:0031497)	3	0.0146
signal transduction (GO:0007165)	2	0.0147
meiosis (GO:0007126)	3	0.0433
multicellular organismal process (GO:0032501)	1	0.0459
single-multicellular organism process (GO:0044707)	1	0.0469
cell surface receptor signalling pathway (GO:0007166)	0	0.0485
cell proliferation (GO:0008283)	3	0.0487

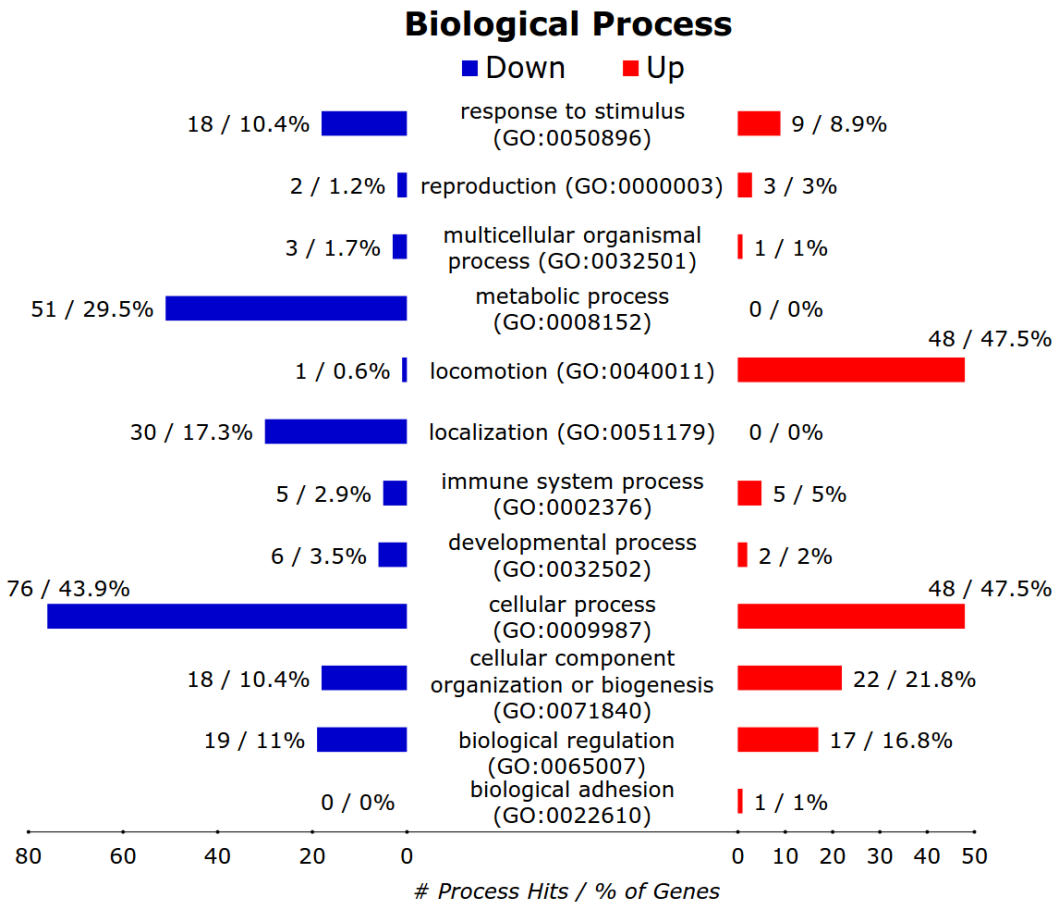


Figure 4-11 PANTHER GO-Slim biological process ontology hits for significantly DEGs due to *T. gondii* infection and treatment with monensin (TG_Monensin). The down-regulated genes matched to 156 processes from 10 major processes while the up-regulated genes matched to 229 processes from 11 major processes. The PANTHER Overrepresentation Test (FDR < 0.05) then identified 25 and nine overrepresented processes from down and up-regulated genes respectively.

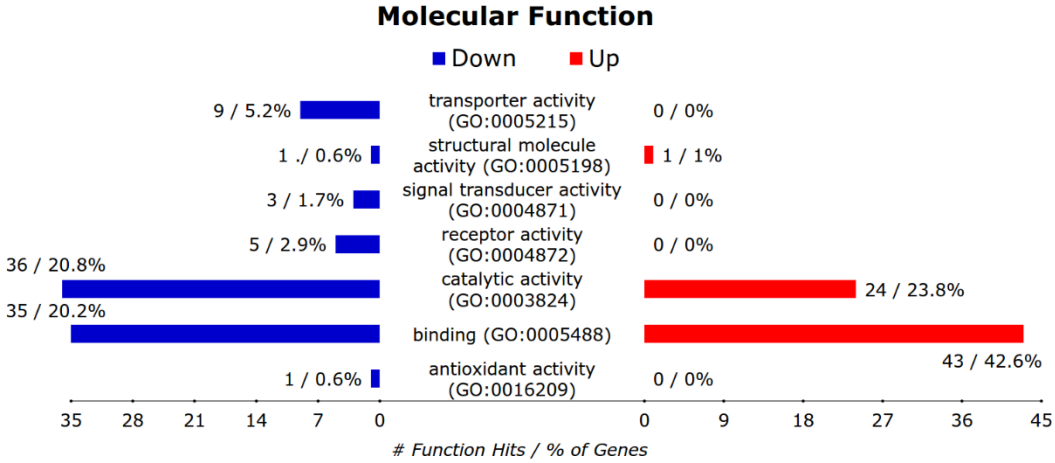


Figure 4-12 PANTHER GO-Slim molecular function ontology hits for significantly DEGs due to *T. gondii* infection and treatment with monensin (TG_Monensin). The down-regulated genes matched to 68 functions from three major functions while the up-regulated genes matched to 90 functions from seven major functions. The PANTHER Overrepresentation Test (FDR < 0.05) identified nine for down-regulated genes but none for up-regulated genes.

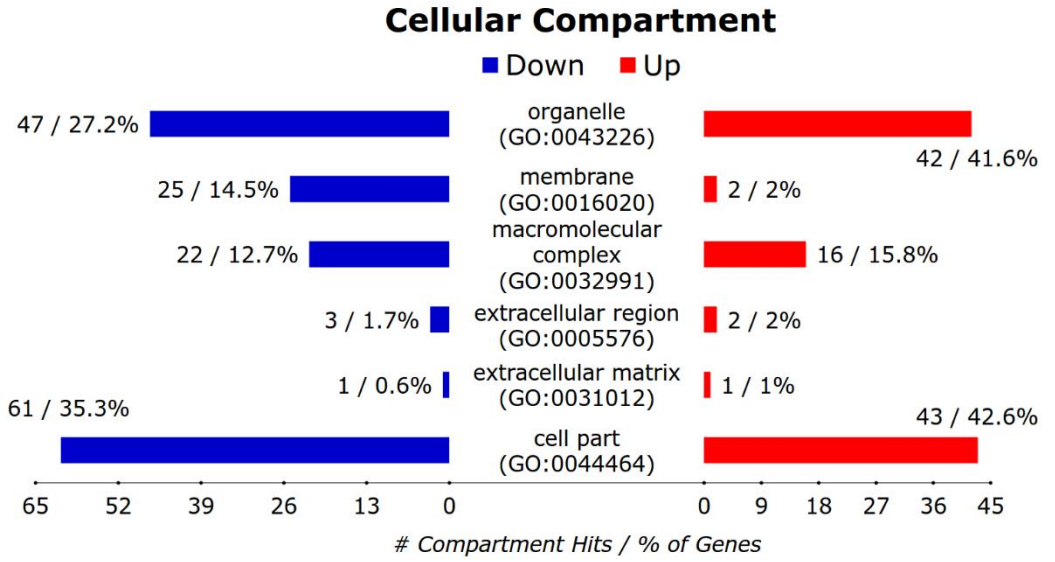


Figure 4-13 PANTHER GO-Slim cellular component ontology hits for significantly DEGs due to *T. gondii* infection and treatment with monensin (TG_Monensin). The down-regulated genes matched to 106 cellular components from six major components while the up-regulated genes matched to 159 cellular components from six major components. The PANTHER Overrepresentation Test (FDR < 0.05) identified 12 and nine overrepresented components for down-regulated and up-regulated genes respectively.

Of 201 annotated up-regulated genes, only 173 were recognised by PANTHER database and the hits for all GO annotations (biological process, molecular function, cellular component) and their major categories were presented as a pie chart in **Figure** 4-25, **Figure** 4-26 and **Figure** 4-27 above respectively. Overall, these up-regulated genes matched to 229 biological processes from 11 major categories (biological regulation GO:0065007, 19 hits; cellular component organisation or biogenesis GO:0071840, 18 hits; cellular process GO:0009987, 76 hits; developmental process GO:0032502, six hits; immune system process GO:0002376, five hits; localisation GO:0051179, 30 hits; locomotion GO:0040011, one hit; metabolic process GO:0008152, 51 hits; multicellular organismal process GO:0032501, three hits; reproduction GO:0000003, two hits; response to stimulus GO:0050896, 18 hits), 90 molecular functions from seven major categories (antioxidant activity GO:0016209, one hit; binding GO:0005488, 35 hits; catalytic activity GO:0003824, 36 hits; receptor activity GO:0004872, five hits; signal transducer activity GO:0004871, three hits; structural molecule activity GO:0005198, one hit; transporter activity GO:0005215, nine hits), and 159 cellular components from six major categories (cell part GO:0044464, 61 hits; extracellular matrix GO:0031012, one hit; extracellular region GO:0005576, three hits; macromolecular complex GO:0032991, 22 hits; membrane GO:0016020, 25 hits; organelle GO:0043226, 47 hits). Further analysis with the PANTHER Overrepresentation Test (FDR < 0.05) found nine significantly enriched biological processes (protein glycosylation GO:0006486, vesicle-mediated transport GO:0016192, protein transport GO:0015031, protein localisation GO:0008104, intracellular protein transport GO:0006886, transport GO:0006810, localisation GO:0051179, single-multicellular organism process GO:0044707, multicellular organismal process GO:0032501) and nine significantly enriched cellular components (vesicle coat GO:0030120, SNARE

complex GO:0031201, Golgi apparatus GO:0005794, cytoplasmic membrane-bounded vesicle GO:0016023, endoplasmic reticulum GO:0005783, nuclear outer membrane-endoplasmic reticulum membrane network GO:0042175, cytoplasm GO:0005737, organelle GO:0043226, intracellular GO:0005622) but no significantly enriched molecular functions.

All 310 differentially regulated genes with a symbol from the filtered list (log_2 FC ≤ -1 or ≥ 1; adjusted *P*-value < 0.05) were submitted to Reactome pathways analysis tool together with their log_2 FC values. Out of these, only 180 were recognised by the Reactome database and considered for pathway analysis. Pathways linked with the submitted genes with FDR < 0.05 are listed in **Table** 4-15 sorted with the lowest FDR values at the top. Overall, the most up-regulated pathway is 'PERK regulates gene expression' (R-HSA-381042) with average log_2 FC of 2.065 while the most down-regulated pathway is 'Resolution of D-loop Structures through Holliday Junction Intermediates' (R-HSA-5693568) and 'Resolution of D-Loop Structures' (R-HSA-5693537) both with average log_2 FC of -1.239.

Table 4-15 List of top 30 out of 55 Reactome pathways affected by 24 hours *T. gondii* infection and treatment with 0.1 μM monensin (TG_Monensin) sorted with the lowest FRD values at the top. Among 310 gene symbols submitted, only 180 were recognised by the Reactome database and considered for analysis. **Appendix** 4-5 lists all 55 Reactome pathways.

Pathway Identifier	Pathway Name	No. of Matched Genes	Average Log_2 FC
R-HSA-381038	XBP1(S) activates chaperone genes	27 / 106	1.399
R-HSA-381070	IRE1alpha activates chaperones	30 / 110	1.373
R-HSA-381119	Unfolded Protein Response (UPR)	38 / 160	1.469
R-HSA-69278	Cell Cycle, Mitotic	43 / 569	-1.000
R-HSA-1640170	Cell Cycle	47 / 681	-1.017
R-HSA-1538133	G0 and Early G1	10 / 38	-1.091
R-HSA-446203	Asparagine N-linked glycosylation	31 / 420	1.307
R-HSA-199977	ER to Golgi Anterograde Transport	18 / 163	1.343
R-HSA-453279	Mitotic G1-G1/S phases	17 / 173	-1.091
R-HSA-69620	Cell Cycle Checkpoints	22 / 279	-1.017
R-HSA-381183	ATF6 (ATF6-alpha) activates chaperone genes	6 / 15	1.612
R-HSA-6811442	Intra-Golgi and retrograde Golgi-to-ER traffic	19 / 217	0.809
R-HSA-6807878	COPI-mediated anterograde transport	13 / 106	1.362
R-HSA-381033	ATF6 (ATF6-alpha) activates chaperones	6 / 17	1.612
R-HSA-392499	Metabolism of proteins	92 / 2432	0.796
R-HSA-948021	Transport to the Golgi and subsequent modification	18 / 218	1.343
R-HSA-1362300	Transcription of E2F targets under negative control by p107 (RBL1) and p130 (RBL2) in complex with HDAC1	6 / 20	-1.054
R-HSA-6811434	COPI-dependent Golgi-to-ER retrograde traffic	12 / 106	0.447
R-HSA-141424	Amplification of signal from the kinetochores	11 / 94	-0.858
R-HSA-141444	Amplification of signal from unattached kinetochores *via* a MAD2 inhibitory signal	11 / 94	-0.858
R-HSA-69618	Mitotic Spindle Checkpoint	11 / 110	-0.858
R-HSA-68886	M Phase	23 / 389	-0.912
R-HSA-2500257	Resolution of Sister Chromatid Cohesion	12 / 133	-0.872
R-HSA-5693568	Resolution of D-loop Structures through Holliday Junction Intermediates	6 / 36	-1.239
R-HSA-8856688	Golgi-to-ER retrograde transport	12 / 147	0.447
R-HSA-5693537	Resolution of D-Loop Structures	6 / 37	-1.239
R-HSA-381042	PERK regulates gene expression	6 / 38	2.065
R-HSA-69206	G1/S Transition	12 / 150	-1.103

R-HSA-1362277	Transcription of E2F targets under negative control by DREAM complex	5 / 25	-1.070
R-HSA-774815	Nucleosome assembly	7 / 54	-1.108

In addition to the pathways above, some genes were also matched to the WNT signalling pathways but were not included in **Table** 4-15 above since the FDR values were above 0.05. **Table** 4-16 lists pathways related to WNT signalling plus their pathway's identifiers, the number of matched genes, FDR values, and pathway expression representation by an average of log_2 FC.

Table 4-16 List of WNT signalling related pathways with the matched genes, average log_2 FC and FDR values affected by 198 DEGs.

Pathway Identifier	Pathway Name	Entities Found / Total	Average Log_2 FC	FDR values
R-HSA-195721	Signalling by WNT	5 / 330	-1.207	0.911
Matched Genes	HIST1H2BM; HIST1H2AJ; HIST1H3F; HIST1H3G; HIST1H2BE; HIST1H3B; HIST1H2AB			
R-HSA-201681	TCF dependent signalling in response to WNT	5 / 216	-1.207	0.617
Matched Genes	HIST1H2BM; HIST1H2AJ; HIST1H3F; HIST1H3G; HIST1H2BE; HIST1H3B; HIST1H2AB			

Note: HIST1H2BM/HIST1H2BE and HIST1H3B/HIST1H3F are duplicated genes related by duplication.

4.5 Discussion

For cerebral toxoplasmosis to be established, *T. gondii* must cross the BBB, which consists mainly of cerebral vascular endothelial cells. The effect of *T. gondii* on the BBB was investigated using an *in vitro* 2D model using hBMECs and was compared with human microglial cell cultures. The main aim of this study was to investigate the effect of WNT inhibition by monensin on the growth of *T. gondii in vitro*. These observations suggest that monensin significantly decreased ($P < 0.01$) the growth of *T. gondii* tachyzoites. The efficacy of parasite inhibition increased as the concentration of the compound increased (*i.e*. dose-dependent). Of note, the 0.1 µM concentration of monensin was effective in inhibiting *T. gondii* growth. This finding fits within the range of the effective concentration reported by Kapoor *et al*. (2013) against the virus human cytomegalovirus (HCMV) at 0.01 µM and 0.1 µM concentration.

T. gondii growth inhibition was evidenced by the significant reduction in the number of tachyzoites and the lack of significant difference in cell density levels (shown by the SRB assay results) between infected and non-infected cultures at low levels of monensin. The relative similarity in the cell density, between infected and control cultures, suggests that the number of treated cells did not decrease, probably due to inhibition of infection by monensin. It is also possible that the inhibition of *T. gondii* growth is mediated by the aberrant WNT signalling caused by monensin treatment (Tumova *et al*. 2014). Monensin has been shown to be effective against *T. gondii* (Lavine and Arrizabalaga, 2011, 2012). The exact mechanism of anti- *T. gondii* activity of monensin is unknown, however osmotic swelling of the parasite (Couzinet *et al.*, 2000), presumably due to the inability to regulate ionic homeostasis as a result of Na+influx (Wang *et al.*, 2006), interference with vesicular traffic (Tartakoff, 1983), arresting the parasite in the late S phase of the cell cycle (Lavine and Arrizabalaga, 2011),

or inducing nutrient stress in *T. gondii*, leading to TgMSH-1-mediated autophagy in the parasite (Lavine and Arrizabalaga, 2012) have all been suggested to contribute to the parasite death. In addition, pre-treatment of hBMEC with monensin at concentrations of five to 50 mg/mL (~7.22-72.2 μM, considering a monensin molecular weight of 692.86) for one hour was found to inhibit the susceptibility of hBMEC to *Citrobacter freundii* (gram-negative bacteria) and *Brucella abortus* (gram-negative bacteria) invasion or survival in a dose-dependent manner (Badger, Stins and Kim, 1999; Miraglia *et al.*, 2018). Pre-treatment with monensin, increased the pH of intracellular vacuoles, which then effectively inhibited bacteria or any parasite internalisation (Badger, Stins and Kim, 1999). As such, monensin has multiple infection inhibitory effects on the parasite and also on the host cells.

A second aim of the study was to determine the cytotoxicity of monensin on hBMECs. Since *in vitro* inhibition of *T. gondii* growth did not show a significant difference between 0.1 μM and higher concentration, this study examined whether 0.1 μM would cause any adverse impact on the host cell functions. In contrast to previous reports that showed non-toxic effects of monensin on human foreskin fibroblasts (HFFs) (Lavine and Arrizabalaga, 2011; Kapoor *et al.*, 2013) or human colon ileocecal (HCT-8) cells (Teichmann *et al.*, 2012), these results revealed some level of cytotoxicity in treated microglial and hBMECs (**Figure** 4-2 and **Figure** 4-3), probably due to the sensitivity of brain cells compared to HFFs or HCT-8 cells. Monensin can have cytopathological effects on mammalian cells, including lysosomal pH (Grinde, 1983), vesicle transport (Tartakoff, 1983) and mitochondrial damage (Souza *et al.*, 2005), which can occur at drug concentrations similar to the highest concentrations used in this study. However, even though staining with acridine orange stain showed significant drop in cell viability (**Figure** 4-4), a transient increase at one hour for mitochondrial potential (**Figure** 4-5) and a statistically

insignificant increase in cell's DNA fragmentation (**Figure** 4-6) indicate no significant toxicity effect of 0.1 µM monensin on hBMECs. This suggests that while there was a mild cytotoxic effect of monensin, the effect was tolerable by the cells and the toxicity can be reversible because no permanent damage was detected in the mitochondria and DNA. While there was no other study that shows the reversible effect of monensin on host cells, the reversible effect of monensin on *T. gondii* was demonstrated by Couzinet *et al.*, (2000) and Lavine and Arrizabalaga (2011, 2012). Monensin's ability to reduce cell density could in fact reduce the growth of *T. gondii*, because fewer cells would leave low intercellular space for the parasites to grow. This indicates that the obtained results for *T. gondii* inhibition may be lower, if monensin did not cause any cell toxicity.

Further, this determined the effect of *T. gondii* with and without monensin on the integrity of cerebrovascular endothelial cell monolayer and microglial cell cultures. *T. gondii* was reported to cause minimal damage to individual cell integrity to facilitate a paracellular migration route across the BBB (Barragan and Sibley, 2003). Our findings showed that *T. gondii* infection could compromise the integrity of BBB endothelial cells compared to uninfected cells ($P < 0.05$; **Figure** 4-8). Cellular barrier function is mediated through intercellular tight junction (TJ) protein complexes, which can be dysregulated following *T. gondii* infection to promote barrier permeability and parasite crossing (Dalton *et al.*, 2006). Alteration in the TJ function may occur either through direct effects of *T. gondii* infection on the host cell cytoskeleton (Weidner *et al.*, 2013) or *via* the indirect action of *T. gondii*-induced proinflammatory cytokines, which can enhance the opening of TJ that would allow leukocytes to migrate across the endothelial barrier into inflamed cerebral tissue (Vries *et al.*, 1997; Elsheikha and Khan, 2010). It is important to study how *T. gondii* affects leukocytes' ability to migrate across the BBB, as it is

known that the parasite invades these cells and uses them as a Trojan-horse to migrate across the BBB (Lambert *et al.*, 2009). If monensin is effective in inhibiting *T. gondii* before it can invade leukocytes, the parasite should not be able to disseminate to CNS tissue. *T. gondii*-infected and treated cells seemed to maintain their resistance, presumably due to the inhibitory effect of monensin on *T. gondii* thereby protecting cells from cytoskeletal rearrangement associated with parasite invasion and growth, which compromises TJ and, BBB integrity. Of interest, uninfected and treated cells showed slightly lower resistance than untreated cells at seven days after treatment, possibly due to the increasingly inhospitable conditions over the time period of the experiment, such as the competition for nutrients, a build-up of waste products or a lack of space. This observation concurs with the haemocytometer cell count results, which demonstrated that monensin is cytotoxic especially at higher concentrations.

Microarray analysis was performed to test the hypothesis that treatment with 0.1 µM monensin down-regulates the WNT signalling pathway, which in turn inhibits *T. gondii* infection and enhances hBMECs survival. The DEGs from four groups (control, treatment with 0.1 µM monensin, infected with *T. gondii*, and infected with *T. gondii* then treated with monensin) were analysed for enriched PANTHER-GO Slim GO terms and enriched Reactome pathways. The microarray quality control checks indicated that experiments had acceptable quality. Variations within samples were minimal (**Figure** 4-9 and **Figure** 4-11) and variations between samples were made comparable by RMA normalisation (**Figure** 4-9).

Reactome pathway enrichment analyses on transcriptome from hBMECs treated with 0.1 µM monensin (Control *vs* Monensin_only) revealed that monensin treatment reduced steroids, cholesterol and protein biosynthesis and

their transport between endoplasmic reticulum (ER) and Golgi apparatus in the cells related pathways (**Table** 4-4). However, at the same time monensin treatment also up-regulated pathways related to cell cycle and DNA replication in the nucleus. The result concurs with the cell cycle assay where after 24 hours of treatment with 0.1 uM monensin there was a slight increase in S and G2/M cell population percentage although the increment was not significant (two-way ANOVA, $P < 0.05$). This growth promoting effect disagrees with the effect of monensin treatment on human ovarian cancer cells (Deng *et al.*, 2015) and human colorectal cancer (Tumova *et al.*, 2014) where cell proliferation, migration and cell cycle progression were suppressed. This suggests that monensin affects a different type of cells differently. Unexpectedly, WNT signalling and WNT related pathways were not significantly affected by treatment with 0.1 μM monensin as all WNT related genes, such as Frizzled receptors, beta-catenin, protein kinase C (PKC) expression were not affected after treatment or if affected the changes were minimal and were not significant ($P < 0.05$; **Table** 4-5). The same also applies to Control *vs* TG_only and Control *vs* TG_Monensin transcriptomes (**Table** 4-7 and **Table** 4-10 respectively). This finding suggests that monensin treatment did not affect WNT signalling pathway in hBMECs and that inhibition of *T. gondii* infection in hBMECs following monensin treatment was not achieved through direct blocking of the WNT signalling pathway. This study did however identified changes in expression of genes related to other signal pathways such as cell cycle control and apoptosis. This suggests pleiotropic effects of monensin on multiple biological processes. Parasite inhibition could have been achieved through combined efforts by directly killing the parasite and inhibition of transport between organelles within cells limiting nutrients transport into parasitophorous vacuole.

Meanwhile, transcriptome analysis from hBMECs infected with *T. gondii* for 24 hours (Control *vs* TG_only) revealed significantly reduced interferon-

alpha/beta and gamma signalling related pathways (**Table** 4-6). This finding is consistent with previous transcriptome studies in murine macrophages (Lüder *et al.*, 2003) and human fibroblast cells (Kim, Fouts and Boothroyd, 2007) substantiating the deregulation of the immune response following *T. gondii* infection of hBMEC. The transcriptome of hBMECs treated with monensin after *T. gondii* infection (Control *vs* TG-Monensin) revealed similar patterns to Control *vs* Monensin_only transcriptome, where pathways related to steroids, cholesterol, protein biosynthesis and their transport between endoplasmic reticulum (ER) and Golgi apparatus were down-regulated but at the same time pathways related to cell cycle and DNA replication activities in the nucleus were up-regulated. However, there were more significantly up-regulated cell cycle, cell division and DNA replication-related pathways (39 pathways) compared to only three significantly up-regulated from Control *vs* Monensin_only transcriptome data. This transcriptome data (Control *vs* TG_Monensin) in combination with *T. gondii* counting data (**Figure** 4-1) demonstrate the potential effectiveness of monensin in treating *T. gondii* infection in hBMECs *in vitro* without causing permanent damage to host cells.

4.5.1 *Conclusion*

In conclusion, the ionophore compound monensin, an inhibitor of the host cell WNT signalling pathway, showed significant anti-*T. gondii* activity against the tachyzoite stage of this parasite grown in cerebral endothelial cell and microglial cell cultures. These findings indicate that inhibition of *T. gondii* infection in hBMECs was not directly achieved through blocking WNT signalling and WNT signalling pathway did not play an important role in *T. gondii* infection. Also, monensin had more lethal effect against the parasite compared to its mild and reversible toxic effect on host cells. Furthermore, a correlation between *T.*

gondii infection and compromisation of the hBMECs' integrity was detected, which was restored by treatment with 0.1 μM monensin. The implications of monensin treatment and *T. gondii* infection on barrier function and parasite neuropathogenesis deserve further investigation. More studies are required to elucidate how monensin inhibits *T. gondii* infection in hBMECs. Future work might consider the validation of microarray experiments by q-RT-PCR on the same biological sample and parasite variant. Additionally, future work should include experiments on the protein level to assess whether differential gene regulation is accompanied by a parallel change of the encoded protein.

Chapter 5 Assessment of Quorum Sensing Molecules Roles in *Toxoplasma gondii* Infection

5.1 Abstract

Quorum-sensing signalling molecule *N*-(3-oxododecanoyl)-L-homoserine lactone (3-Oxo) and 2-heptyl-3-hydroxy-4(1H)-quinolone (PQS) are quorum sensing molecules produced by *Pseudomonas aeruginosa* (Pesci *et al.*, 1999; Mayer *et al.*, 2011). One of them, 3-Oxo was reported to disrupt epithelial barrier integrity in Caco-2 cells by the degradation of the tight junction while there is no report on whether PQS can do the same (Vikström, Tafazoli and Magnusson, 2006). Co-infection of *T. gondii* and *P. aeruginosa* while uncommon, has been reported in at least two cases in French Guiana (Carme *et al.*, 2002; Demar *et al.*, 2012) and Peru (Nunura *et al.*, 2010). However, there have been no previous studies that specifically, and directly, assessed the impact of co- or pre-infection with *P. aeruginosa* on *T. gondii* infection at the BBB interface. Therefore, in this study, the hypothesis is that quorum sensing molecules compromise the integrity of the BBB based on the assumption that quorum sensing molecules derived from *P. aeruginosa* open the tight junctions of the BBB and so enhance *T. gondii* infection by facilitating *T. gondii*'s passage across the BBB and hence its ability to cause brain infection. The effects of 3-Oxo and PQS at a low and high concentration with and without *T. gondii* infection on hBMECs were characterised and provided new insights into the underlying mechanisms involved in 3-Oxo and PQS modulation of the hBMEC monolayer. 3-Oxo and PQS increased hBMEC monolayer permeability and integrity through PRKCA gene up-regulation, slowly induced cell apoptosis and

halted cell proliferation at the G0/G1 stage. Overall, these results did not support the hypothesis that QS molecules from *P. aeruginosa* facilitate *T. gondii* crossing of BBB into the brain. Further understanding of the mechanisms that regulate these processes and underlie the effect of QS molecules on the BBB may lead to the discovery of key factors/pathways involved in supporting the BBB capability to limit brain invasion.

5.2 Introduction

An infectious disease is generally described as the outcome of infection by a single species of pathogen. However, this definition is too simplistic to describe the variety of disease outcomes that could happen naturally due to coinfections. Neuro-pathogens offer an excellent venue for shedding light on alternative infectious outcomes that can emerge due to coinfections. Bacterial pathogens and their individual components have long been fascinating tools with regard to studying host cell physiology. The use of two pathogens simultaneously takes this one step further.

The intracellular apicomplexan protozoan parasite *Toxoplasma gondii* (*T. gondii*) is the causative agent of toxoplasmosis, which is characterised by flu-like symptoms in immune-competent individuals. However, *T. gondii* can cause life-threatening conditions in immune-compromised persons and pregnant women. The parasite has a remarkable ability to rapidly disseminate *via* the bloodstream to tissue sites distant from the site of initial infection. It can cross the blood-brain, blood-retinal and blood-placental barriers. In a process that is still poorly understood, *T. gondii* is believed to traverse the blood-brain barrier (BBB) in order to establish access to the CNS. In response to infection, cells of innate immunity including macrophages and natural killer (NK) cells are the

first to infiltrate CNS following infection. They, then secrete IFN-gamma and IL-12 that attract and activate $CD4^+$ and $CD8^+$ T-cells, astrocytes and microglial cells to produce more IFN-gamma and IL-12 that are essential to clear parasites most likely by autophagy and nitric oxide (NO) mediated mechanisms (Peterson *et al.*, 1995; Suzuki *et al.*, 2005; Middleton *et al.*, 2009).

The *Pseudomonas aeruginosa* (*P. aeruginosa)* quorum-sensing signalling molecule *N*-(3-oxododecanoyl)-L-homoserine lactone (3-Oxo) is a bacterial virulence factor that can induce proinflammatory cytokine production in different cell types in addition to suppressing the function of key immune responses responsible for bacterial clearance (Mayer *et al.*, 2011). It is also capable of inducing apoptosis in certain cell types, such as mammary epithelial cells and Caco-2 cells (Li *et al.*, 2004; Taguchi *et al.*, 2014). Additionally, 3-Oxo-C12-HSL disrupts epithelial barrier integrity in Caco-2 cells by the degradation of tight junctions (Vikström, Tafazoli and Magnusson, 2006). Thus far, there is no report on whether this molecule affects BBB membrane integrity.

The 2-Heptyl-3-hydroxy-4(1H)-quinolone (PQS) is another quorum sensing molecule produced by *P. aeruginosa* (Pesci *et al.*, 1999). Both 3-Oxo and PQS suppresses T-cell proliferation, but only 3-Oxo was able to suppress human peripheral blood mononuclear cell proliferation (hPBMC) and IL-2 release (Hooi *et al.*, 2004). It is still not known whether PQS can affect hBMEC viability and/or BBB integrity. There are already known similarities between the abilities of both the protozoan *T. gondii* and bacterium *P. aeruginosa* to cross the BBB. However, there had been no previous studies that specifically, and directly, assessed the impact of co- or pre-infection with *P. aeruginosa* on *T. gondii* infection at the BBB interface. Co-infection of *T. gondii* and *P. aeruginosa* while uncommon, has been reported in at least two cases in French Guiana (Carme *et al.*, 2002; Demar *et al.*, 2012) and Peru (Nunura *et al.*, 2010).

Therefore, in this study the hypothesis that quorum sensing molecules can compromise the integrity of the BBB was tested. This hypothesis is based on the assumption that quorum sensing molecules derived from *P. aeruginosa* open the tight junctions (TJs) of the BBB and so enhance *T. gondii* infection by facilitating *T. gondii*'s passage across the BBB and hence its ability to cause brain infection. This hypothesis may have some clinical relevance. If co-infection with bacteria and *T. gondii* was found to exert any effect on cerebral toxoplasmosis in HIV patients, for example, where quorum sensing molecules from bacteria could open TJs at the BBB allowing *T. gondii* to cross more easily. To test this hypothesis three aims have been identified:

i. To assess alteration in hBMEC permeability following treatment with 3-Oxo or PQS using FITC-Dextran flux assay.
ii. To evaluate the integrity of the TJs of hBMEC cells following treatment with 3-Oxo or PQS by using trans-endothelial electrical resistance (TEER) assay.
iii. To investigate the effect of 3-Oxo and PQS on hBMEC viability, mitochondrial potential, DNA fragmentation, cell cycle and TJ genes expression.

5.3 Material and Methods

All work was carried out in a BSC level II hood and all aseptic techniques and protective clothing were observed. HBMECs culturing (passaging, counting) and parasite culturing (maintenance, passaging, counting) were performed as mentioned previously in chapter 2 in the material and methods section.

5.3.1 *Preparation of 3-Oxo and PQS Solutions*

N-(3-Oxo-dodecanoyl) homoserine lactone (3-Oxo) and 2-Heptyl-3-hydroxy-4(1H)-quinolone (PQS) were purchased from Sigma Aldrich/Merck (Darmstadt, Germany). To make 10X Working Solutions (1 mM), 0.00148695 g of 3-Oxo was dissolved with 5 mL of DMSO (Sigma Aldrich/Merck, Darmstadt, Germany). Then, 0.012967 g of PQS was dissolved with 5 mL of DMSO. Both solutions were vortexed and mixed thoroughly before being aliquoted into small 1 - 2 mL tubes for storage at -20ºC. For the assay, 1 - 2 mL tubes of 1 mM were thawed and diluted with complete RPMI media in order to make 10, 20 and 100 µM concentrations.

5.3.2 *HBMEC Monolayer Permeability Assessment by FITC-Dextran Flux Assay*

Here, this study evaluated whether 3-Oxo and PQS can open up and increase the permeability of hBMEC's monolayer. The cell monolayer in the inserts was treated with quorum sensing molecules at 10, 20 and 100 µM concentrations for two, three, four, six and 24 hours. Preparation of FITC-dextran working solution (1 mg/mL) and evaluation of hBMEC monolayer

permeability by FITC-Dextran flux assay were performed as previously described in section **2.3.16** (Chapter 2).

5.3.3 *HBMEC Monolayer Integrity Assessment by TEER Measurement*

The effect of treatment with 3-Oxo or PQS on hBMEC's monolayer integrity was evaluated. EVOM Voltohmeter calibration for TEER measurement, TEER measurement and TEER calculation formula were performed as described previously in section **2.3.15** (Chapter 2).

5.3.4 *Cell Viability Assay by Alamar Blue*

Initial assessment of the effect of 3-Oxo and PQS on hBMEC's viability was determined using Alamar blue assay perfomed as described in section **2.3.7** (Chapter 2).

5.3.5 *The Effect of 3-Oxo and PQS on hBMEC Cells Mitochondrial Potential, DNA Fragmentation and Cell Cycle.*

The effects of treatment with 3-Oxo and PQS on hBMEC mitochondrial potential, DNA fragmentation and cell cycle were performed using NC-3000™ Advanced Image Cytometer (Chemometec A/S, Allerod, Denmark) as previously described in section **2.3.10**, **2.3.11** and **2.3.12** respectively (Chapter 2).

5.3.6 *Tight Junction Genes Expression Study*

Here, the effect of 3-Oxo and PQS on the expression of TJ genes was investigated. Confluent five-days old hBMEC monolayer in 6 well plate was treated with 3-Oxo or PQS for three, six and 24 hours at 10 and 100 µM concentrations before total RNA extraction. The protocol for extraction of total RNA using Qiagen RNeasy kit, total RNA quality analysis, converting RNA to cDNA, the cycling conditions for real-time PCR using Roche Lightcycler 480 II and SYBR Green Mastermix plus the primers used were the same as mentioned in section **2.3.17**, **2.3.18**, **2.3.19**, **2.3.20** and **2.3.21** (Chapter 2).

5.3.7 *Effect of Quorum Sensing Molecules on T. gondii Infection*

The effect of the presence of 3-Oxo and PQS on *T. gondii* infection on hBMECs monolayer was investigated. Confluent five-day old hBMEC monolayers in the inserts were treated for one hour with 10 or 100 µM 3-Oxo or PQS, prior to *T. gondii* tachyzoites at MOI of 5 were added. The pre-treatment was done to equilibrate all cells in the hBMECs monolayer to the presence of quorum sensing molecules and DMSO prior to *T. gondii* introduction. Then, 1 mL complete RPMI media was added in the lower chamber of the inserts. Then, TEER measurement and calculation, and FITC-Dextran flux assay were performed at 3, 6, 24- and 48-hours using methods previously described in Chapter 2 in the material and methods section.

Similarly, for the TJ genes expression study, confluent five-day old hBMECs in six well plates were treated for one hour with 10 or 100 µM 3-Oxo or PQS then *T. gondii* tachyzoites at a MOI of five were added. At three, six, 24 h.p.i, total RNA extraction using Qiagen RNeasy kit, total RNA quality analysis, converting RNA to cDNA, the programming for real-time PCR using Roche

Lightcycler 480 II and SYBR Green Mastermix plus the primers used were the same as mentioned in section **2.3.17**, **2.3.18**, **2.3.19**, **2.3.20** and **2.3.21** (Chapter 2).

5.3.8 *Statistical analysis*

Data are expressed as mean values ± standard errors (SE). Statistical analysis was performed using GraphPad Prism version 7 software (GraphPad Software, CA, USA). Data comparing more than two groups were analysed by one-way analysis of variance (ANOVA) or two-way ANOVA with Bonferroni multiple-comparison test. Data comparing two groups were analysed with the nonparametric Mann-Whitney test. A *P* value of < 0.05 was considered statistically significant.

5.4 Results

5.4.1 *Cytotoxic Effects of PQS and 3-Oxo*

We tested whether PQS and 3-Oxo can modulate TJs in hBMECs. But, before testing the effect of the QS molecules on TJs of hBMECs, the cytotoxicity of 3-Oxo and PQS was examined for 24 hours using Alamar blue assay. The viability of hBMECs treated with PQS and 3-Oxo at three different concentrations (10, 20 and 100 μM) was not significantly different from the viability of control, untreated cells or cells treated with 0.1% DMSO, suggesting that none of these QS molecules was toxic to the hBMECs over a 24-hour period (**Figure** 5-1).

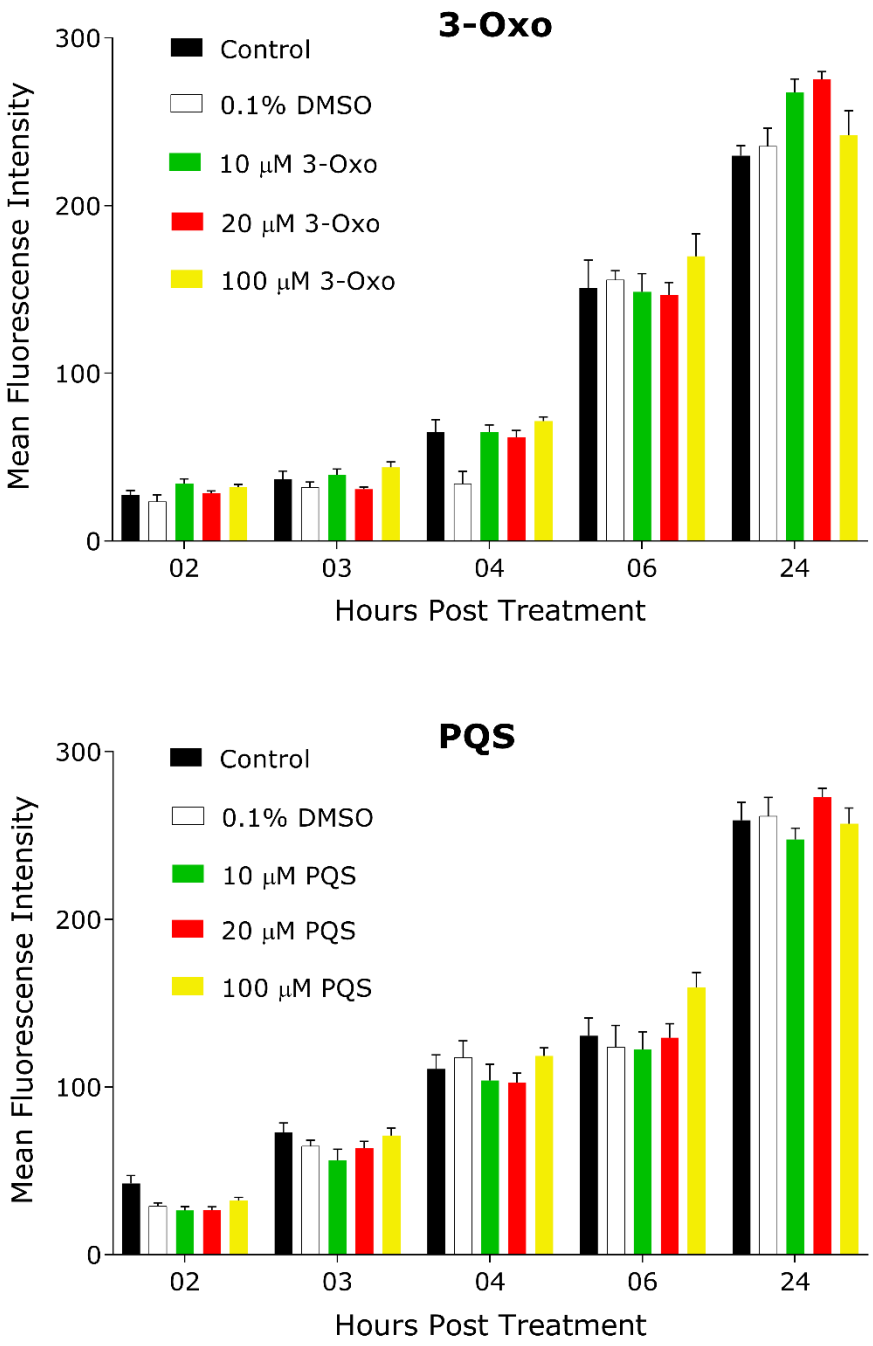


Figure 5-1 The effect of 3-Oxo and PQS treatment on hBMECs cell viability assessed using Alamar blue assay. There were no significant differences between control and any of the treated groups suggesting that none of the two quorum sensing molecules was toxic to hBMECs over 24 hours of treatment. Data are expressed as mean value ± SEM and represent the average from at least four replicates.

5.4.2 *Monolayer Permeability Assay*

The permeability of the hBMEC monolayer was evaluated by measuring the diffusion of fluorescein isothiocyanate (FITC)-dextran with molecular mass of 4 kDa (Sigma), from the apical to the basal medium compartments. The flux of FITC-dextran across hBMEC monolayers (indicative of paracellular permeability) was reduced with treatment of 100 μM 3-Oxo and PQS at and was significantly reduced after treatment with 3-Oxo and PQS at 10 μM concentration (**Figure** 5-2)**.**

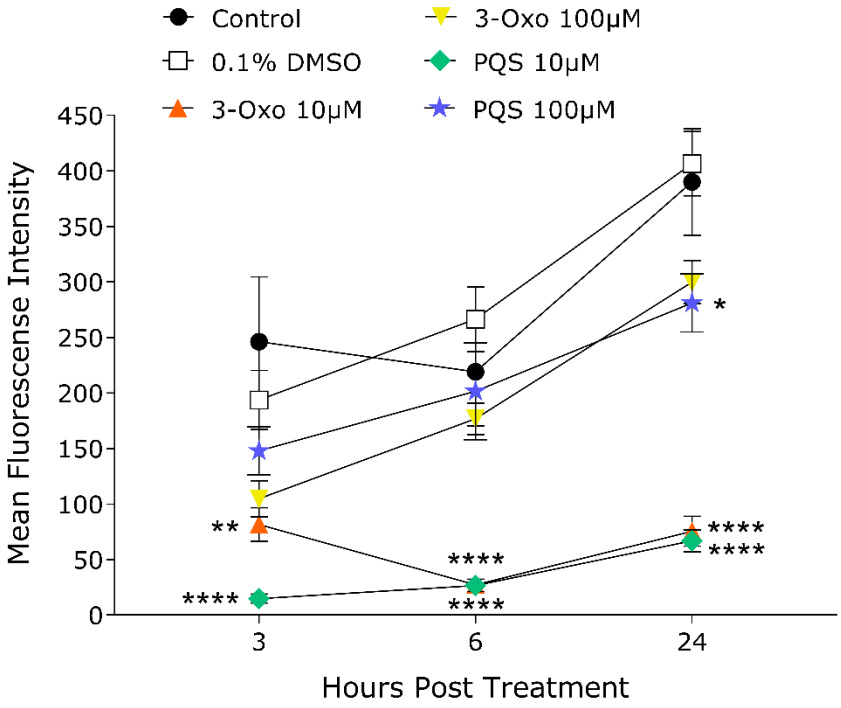


Figure 5-2 The effect of quorum sensing molecules on hBMEC monolayer permeability. The effect of 3-Oxo and PQS at 10 μM and 100 μM concentration on the hBMEC monolayer permeability was measured by FITC-dextran fluorescence intensity over 24 hours. In general, 3-Oxo and PQS molecules reduced hBMEC permeability and the reduction in permeability was significant at 10 μM concentration. Data were derived from four biological replicates and the error bar represents SEM.

5.4.3 *Membrane Integrity Assay*

The effect of QS molecules on hBMEC monolayer integrity is displayed in **Figure** 5-3. In general, QS treatment of hBMECs increased cell monolayer integrity compared to untreated cell monolayer where the increase in TEER values was statistically significant at 24 hours post-treatment for all treated groups compared with the control group (two-way ANOVA, $P < 0.05$). Also, treatment with PQS increased the monolayer integrity more than treatment with 3-Oxo.

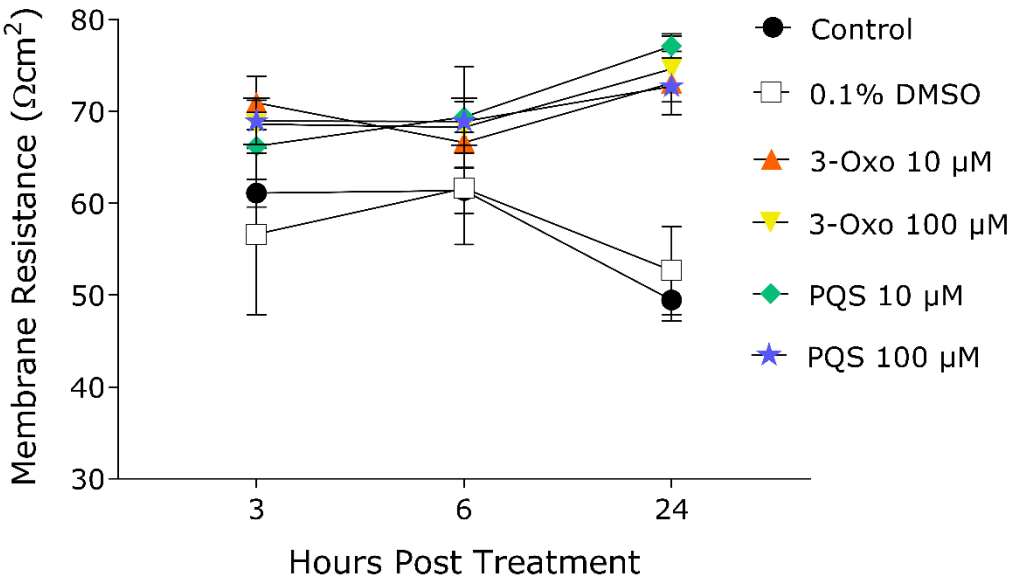


Figure 5-3 The effect of quorum sensing molecules on hBMEC monolayer integrity. The effect of 3-Oxo and PQS QS molecules at 10 uM and 100 uM concentrations on hBMEC monolayer integrity was measured by TEER Assay. Overall TEER values of control and 0.1% DMSO groups were lower than the values of QS-treated groups. Furthermore, at 24 hours post-treatment the differences were statistically significant for all treated groups compared with the control group (two-way ANOVA, $P < 0.05$). Data were derived from four biological replicates and the error bar represents SEM.

5.4.4 *Mitochondrial Potential Assay*

The effect of 3-Oxo and PQS at 10 µM and 100 µM on hBMEC mitochondrial potential, which indicates an early sign of apoptosis, was investigated using NC-3000™. As shown in **Figure** 5-4**,** the effect of treatment with two QS molecules treatment on hBMEC mitochondrial potential over 24 hours was observed. Compared to the control, the mitochondrial potential of hBMECs was significantly affected by treatment with PQS at 100 µM at all time points, whereas 3-Oxo significantly affected the cells at 3 and 6 hours, but not at 24 hours post-treatment at the same concentration. At 10 µM concentration, a significant increase in mitochondrial potential was detected at 6 hours after treatment with PQS and 3 hours post-treatment with 3-Oxo (one-way ANOVA, $P<0.05$).

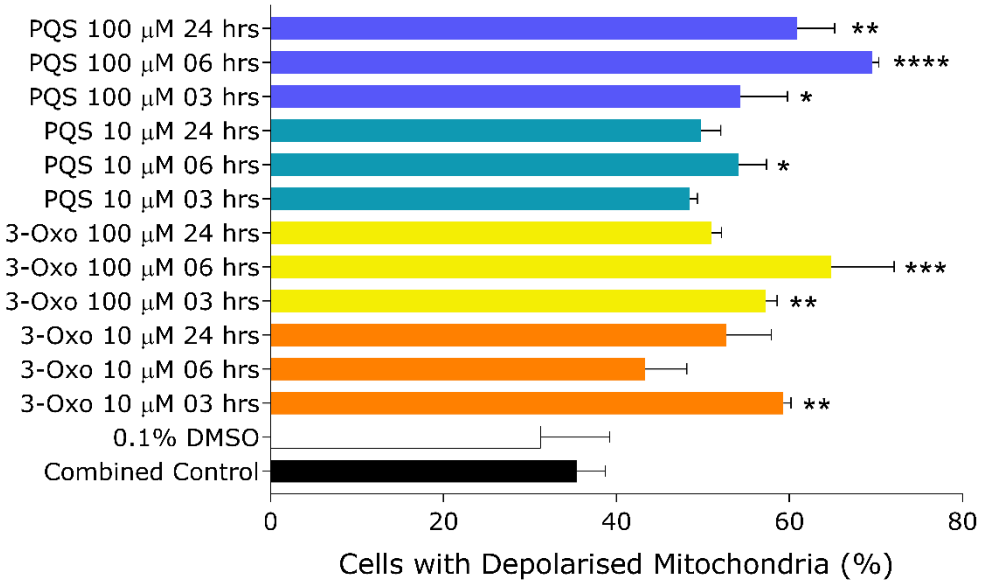


Figure 5-4 The effect of 3-Oxo and PQS at 10 µM and 100 µM on hBMECs mitochondrial potential. This bar chart shows that treatment with each QS molecule increased hBMEC mitochondrial potential, suggesting an early sign of apoptosis. PQS at 100 µM significantly increased hBMEC mitochondrial potential at all time points, whereas 3-Oxo significantly affected the cells at three and six hours, but not at 24 hours post-treatment at the same concentration. At 10 µM concentration, significant increase in mitochondrial potential was measured at 6 hours after treatment with PQS and three hours post-treatment with 3-Oxo (one-way ANOVA, $P < 0.05$). Data were derived from four biological replicates and the error bar represents SEM.

5.4.5 *DNA Fragmentation*

The effect of 3-Oxo and PQS treatment at two concentrations on hBMECs DNA integrity was examined. **Figure** 5-5 shows that both QS molecules at both concentrations caused fragmentation of the DNA of hBMECs significantly after 24 hours of treatment.

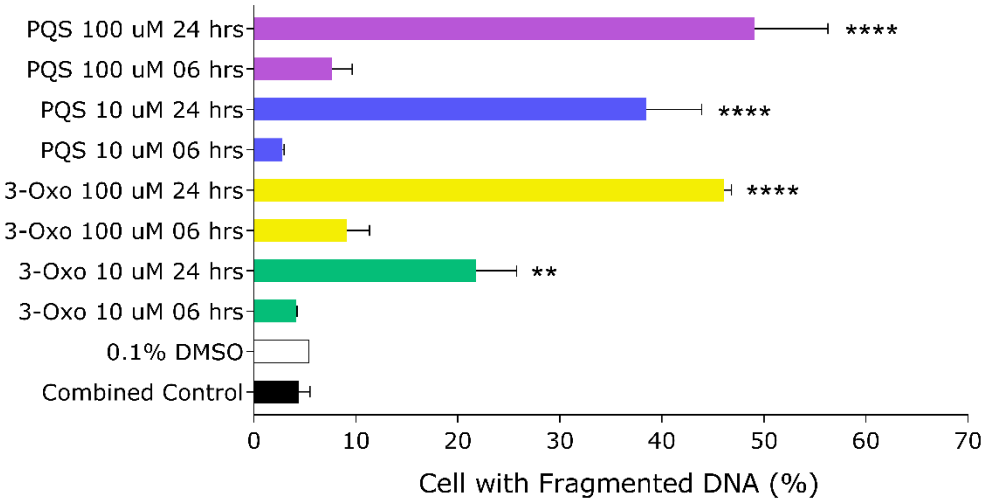


Figure 5-5 DNA fragmentation in hBMECs following treatment with quorum sensing molecules. This bar chart shows that the DNA integrity of hBMECs was significantly affected by treatment with both QS molecules at both concentrations after 24 hours of treatment. Data represent the average of quadruplets and the error bars represent SEM. (**, $P < 0.01$; ****, $P < 0.0001$)

5.4.6 *Cell Cycle Assay*

Figure 5-6 depicts the effect of 3-Oxo and PQS treatment at two concentrations on hBMEC cell cycle. After six hours of treatment, there was a significant increase in the percentage of cells at the G0/G1 stage, and a significant decrease in cells at S stage and G2/M stage compared to control group for both QS molecules at both concentrations. Meanwhile at 24 hours post-treatment, there was a significant decrease in the percentage of cells at

the G2/M stage, whereas there were no significant changes in the G0/G1 and S stage.

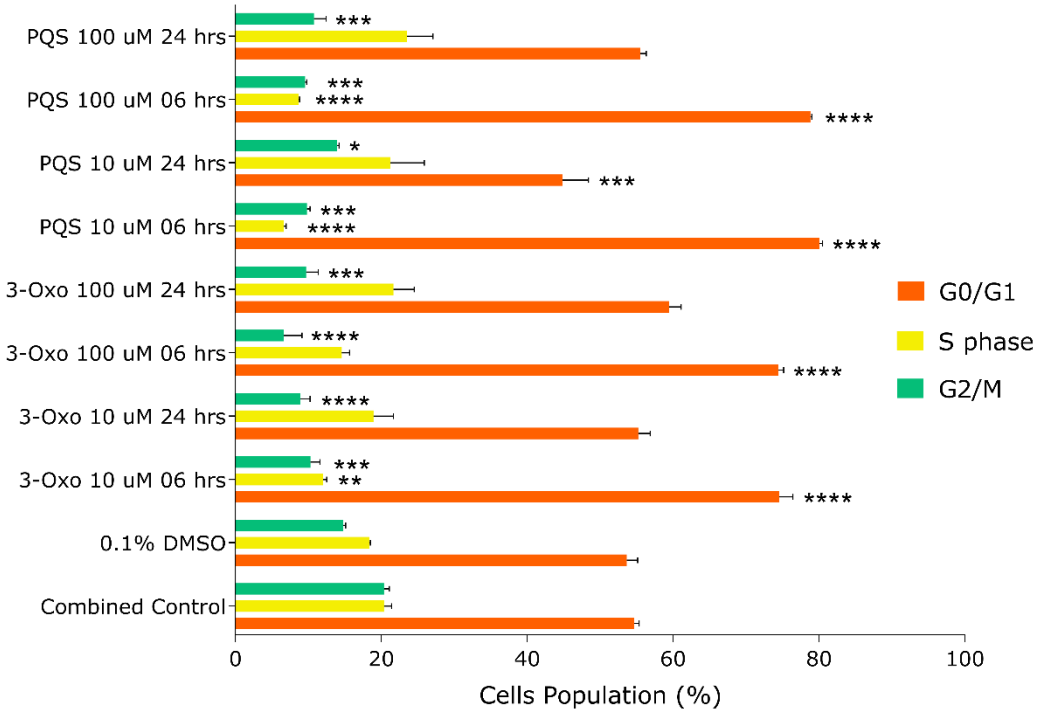


Figure 5-6 Cell cycle assay following treatment with quorum sensing molecules on hBMECs. After 6 hours of treatment, there was a significant increase in the percentage of cells at the G1/G0 stage, and a significant decrease in cells at S stage and G2/M stage compared to control group for both QS molecules at both concentrations. Meanwhile, at 24 hours post-treatment, there was a significant decrease in the percentage of cells at the G2/M stage but no significant changes in the G0/G1 and S stage percentages. Data are the average of triplicates and the error bars represent SEM. (*, $P < 0.05$; **, $P < 0.01$; ***, $P < 0.001$; ****, $P < 0.0001$)

5.4.7 *Tight Junction Genes Expression*

Three TJ genes (Occludin, PRKCA and ZO-1) were selected to establish the effect of 10 µM and 100 µM QS molecules on the expression of these genes at three, six and 24 hours after treatment. Beta-actin and HMBS were selected as reference housekeeping genes due to their stable expression in hBMECs in control and infected samples. Expression of genes in all samples was normalised to the expression of the reference genes and two-way ANOVA test was used to

compare FC in the expression of control and treated samples. **Figure** 5-7 shows the expression of all genes at three, six and 24 hours post treatment with 3-Oxo QS molecule. Overall, 3-Oxo significantly affected PRKCA gene expression at both concentrations where at 10 μM significant increase in FC was observed at three- and six-hours post-treatment, but not at 24 hours post-treatment. At 100 μM, 3-Oxo was found to significantly increase the expression of PRKCA at all time points. At both concentrations, 3-Oxo did not affect ZO-1 expression at all, but seem to increase Occludin gene expression relatively, but not significantly.

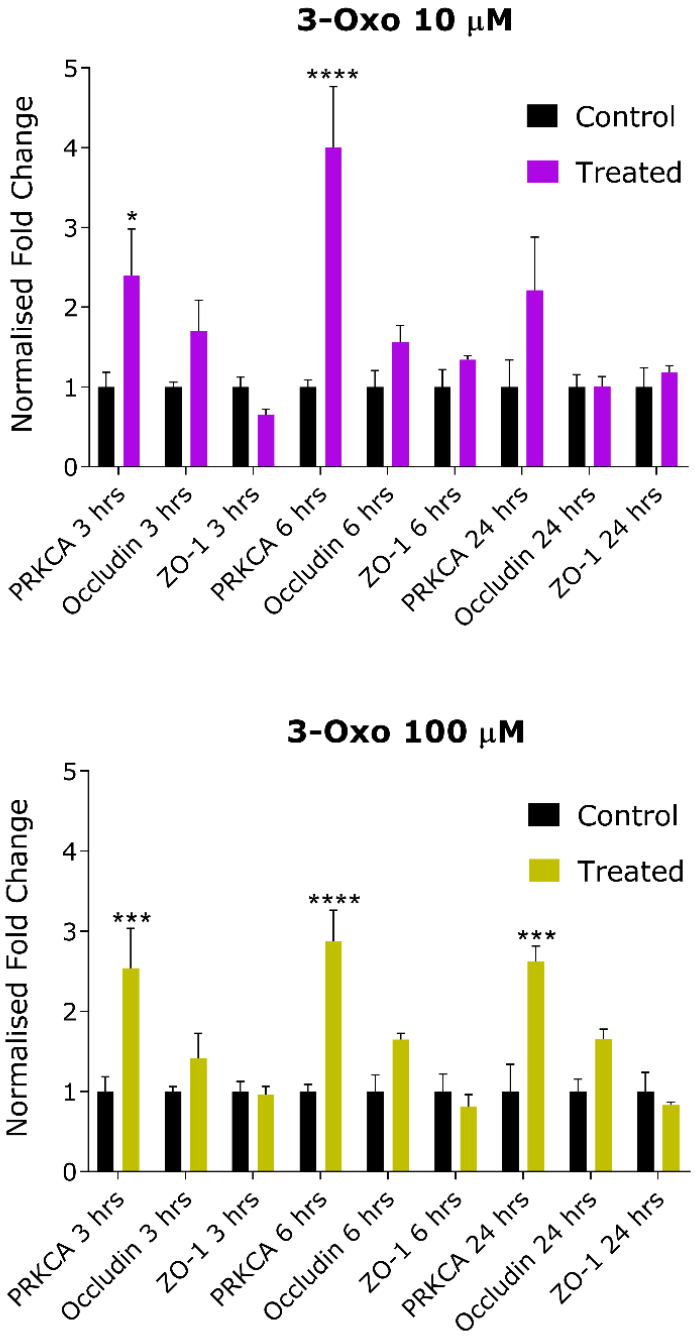


Figure 5-7 The effect of 10 and 100 μM 3-Oxo on TJ genes expression in hBMECs. This figure shows relative genes expression of TJ-related genes following treatment with 10 and 100 μM 3-Oxo for 24 hours. Of the three studied genes, PRKCA expression was the most significantly affected by 10 μM 3-Oxo from 3 hours (2.40 ± 0.58) peaking at 6 hours (4.01 ± 0.76), before dropping back at 24 hours (2.21 ± 0.67). The similar pattern can also be observed from treatment with 100 μM 3-Oxo where PRKCA expression was up-regulated at all 3 time points (3 hrs: 2.45 ± 0.50, 6 hrs: 2.88 ± 0.39, 24 hrs: 2.62 ± 0.19). Data represent biological triplicates and the error bar represents SEM. (*, $P < 0.05$; (***, $P < 0.001$; ****, $P < 0.0001$)

Meanwhile, PQS at 10 µM and 100 µM caused a slight increase in PRKCA expression and a slight decrease in ZO-1 and Occludin expression at all time points. The changes, however, were not statistically significant (**Figure** 5-8)

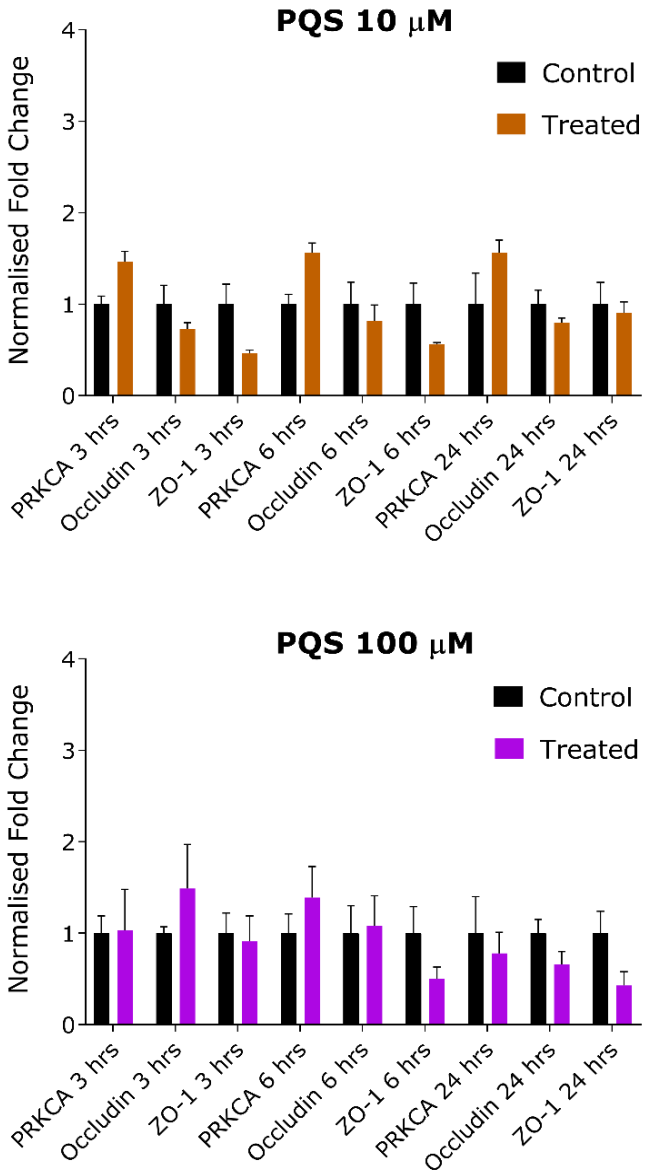


Figure 5-8 The effect of 10 and 100 µM PQS on TJ genes expression in hBMECs. This figure shows relative genes expression of TJ-related genes following treatment with 10 and 100 µM PQS for 24 hours. Of the three studied genes, PRKCA expression was slightly up-regulated, whereas the expression of ZO-1 and Occludin genes was slightly down-regulated by the molecule when treated with 10 µM PQS. However, none of the changes was statistically significant. Treatment with 100 µM PQS caused slight changes in FC of the three genes, but none of the changes was statistically significant. Data represent three biological replicates and the error bar represents SEM.

5.4.8 *The Effect of Quorum Sensing Molecules on T. gondii Infection on hBMECs*

The flux of FITC-dextran across hBMEC monolayers (indicative of paracellular permeability) following treatment with QS molecules at 10 uM and 100 uM concentrations and *T. gondii* infection are shown in **Figure** 5-9. This figure shows that QS molecules decrease hBMEC monolayer permeability for 24 hours even in the presence of *T. gondii* infection.

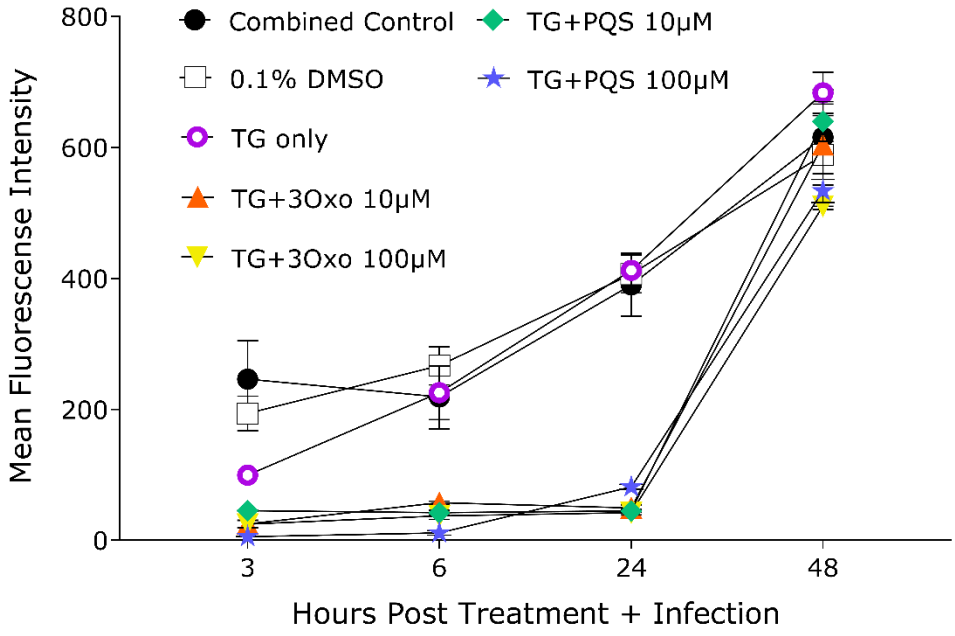


Figure 5-9 The effect of treatment with quorum sensing molecules and *T. gondii* infection on hBMEC monolayer permeability. The bar chart shows the effect of *T. gondii* infection with and without the presence of QS molecules on hBMEC monolayer permeability measured by FITC-dextran fluorescence intensity. Based on the figure, QS molecules plus *T. gondii* infection do significantly decrease monolayer membrane permeability compared to negative control (FITC-dextran only) and positive control (*T. gondii* only) over 24 hours. However, after 48 hours, there were no significant differences in the amount of leaked FITC-dextran. Data were derived from four biological replicates and the error bar represents SEM.

The effect of QS molecules and *T. gondii* infection on hBMECs monolayer integrity was also investigated by measuring TEER values of the hBMECs monolayer. The result is shown in **Figure** 5-10. In general, TEER value of control and 0.1% DMSO were stable in 48 hours, but in the infected groups the values dropped at 24 and 48 hours. However, none of the differences was statistically significant (Two-way ANOVA, $P > 0.05$).

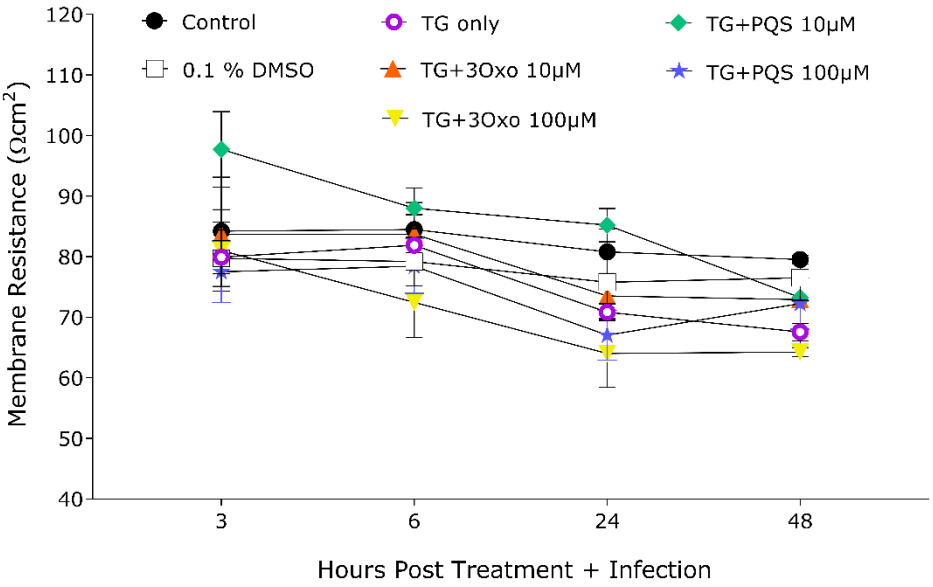


Figure 5-10 The effect of quorum sensing treatment on hBMECs monolayer and *T. gondii* infection on hBMEC monolayer integrity. A decrease of TEER values was observed over time for all groups with control and 0.1% DMSO decreased by small margin while the treated and infected groups decreased by bigger margin. Data were derived from four biological replicates and the error bar represents SEM.

The combined effect of QS molecules and *T. gondii* infection on TJ genes expression were investigated for 24 hours. **Figure** 5-11 and **Figure** 5-12 present the expression of TJ genes following treatment with QS molecules and *T. gondii* infection. **Figure** 5-11 shows the relative expression of TJ genes following treatment with 10 μM 3-Oxo and *T. gondii* infection for 24 hours. PRKCA gene was significantly up-regulated at three and 24 h.p.i and treatment (1.53 ± 0.12 and 1.65 ± 0.17, respectively). Meanwhile, the combined effect

of 100 µM 3-Oxo and *T. gondii* infection caused a significant reduction in Occludin (0.48 ± 0.06) and ZO-1 (0.42 ± 0.03) fold change at 3 h.p.i and treatment (**Figure** 5-11).

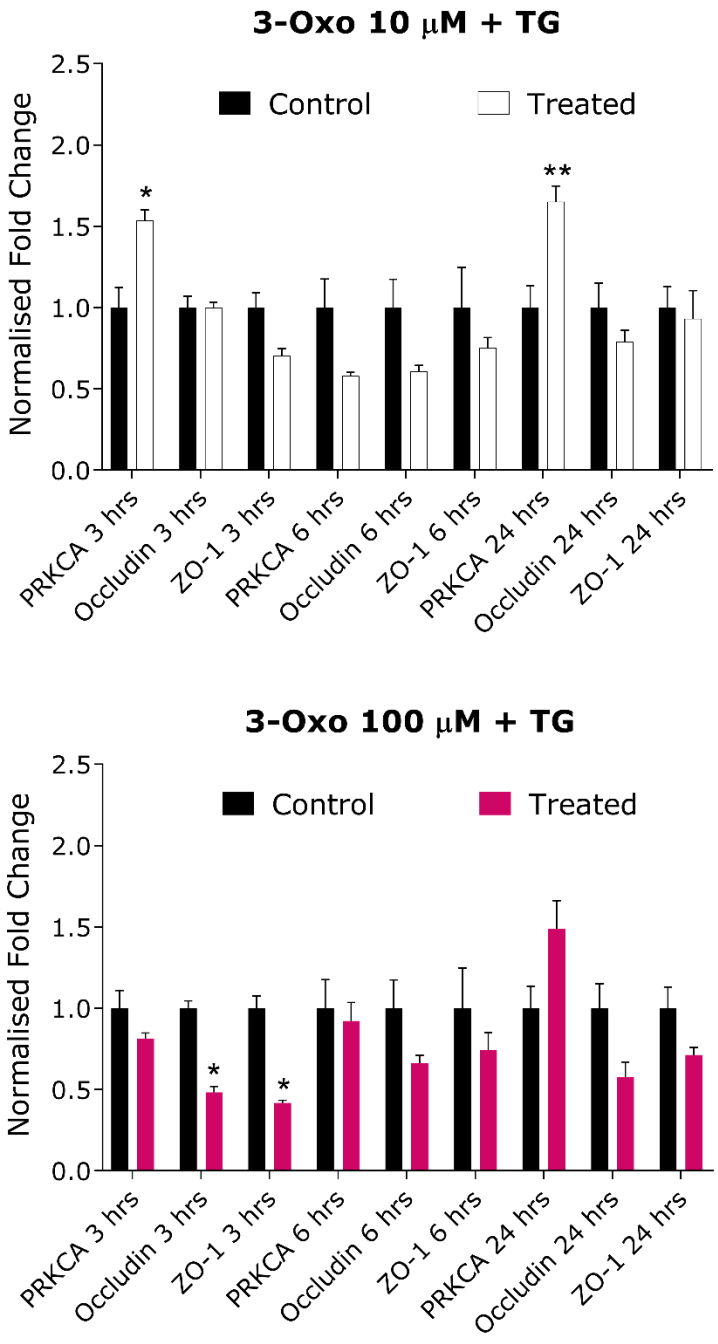


Figure 5-11 The combined effect of 3-Oxo at 10 and 100 µM concentration and *T. gondii* infection on TJ genes expression in hBMECs. This figure shows relative expression of TJ genes following treatment with 10 and 100 µM 3-Oxo and *T. gondii* infection for 24 hours. PRKCA gene was significantly up-regulated at three and 24 h.p.i and treatment (1.53 ± 0.12

and 1.65 ± 0.1, respectively) at 10 µM concentration. Also, there was a slight down-regulation in fold change of ZO-1 and Occludin genes at three- and six-hours post-treatment, but none of the changes was significant. Meanwhile, the combined effect of 100 µM 3-Oxo and *T. gondii* infection caused a significant reduction in Occludin (0.48 ± 0.06) and ZO-1 (0.42 ± 0.03) expression at 3 h.p.i and treatment. There was an increase of PRKCA expression at 24 h.p.i and treatment similar to the effect of treatment with 10 µM, but the increase was not statistically significant. Data represent biological replicates and the error bar represents SEM. (*, $P < 0.05$)

Figure 5-12 shows relative expression of TJ genes following treatment with 10 and 100 µM PQS and *T. gondii* infection for 24 hours. Here, 10 µM PQS caused up-regulation of PRKCA gene significantly at 3three hours (1.87 ± 0.10) while at 6 hours, ZO-1 was significantly down-regulated (0.47 ± 0.02). Down-regulation of ZO-1 also occurred at three and 24 h.p.i and treatment, but they were not significant. Meanwhile, PRKCA gene was significantly up-regulated at three hours (1.83 ± 0.07) and 24 hours (1.91 ± 0.15) while at six hours it was significantly down-regulated (0.51 ± 0.03) by 100 µM PQS. Down-regulation of ZO-1 occurs at three, six and 24 h.p.i and treatment, but only at 6 hours it was significant (0.47 ± 0.05).

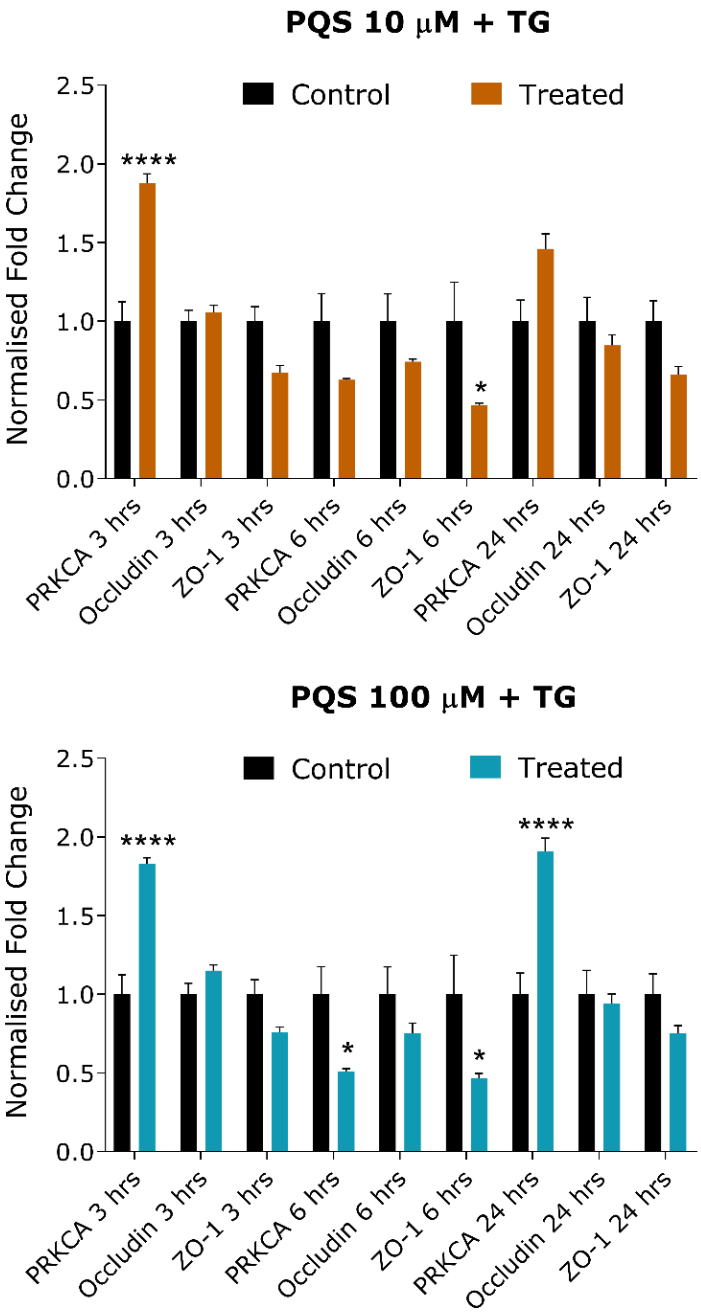


Figure 5-12 The combined effect of PQS and *T. gondii* infection on TJ genes expression in hBMECs. This figure shows relative expression of TJ genes following treatment with 10 and 100 μM PQS and *T. gondii* infection for 24 hours. PRKCA gene was significantly differentially regulated up-regulated at three hours (1.87 ± 0.10), whereas at six hours, ZO-1 was significantly down-regulated (0.47 ± 0.02) from treatment with 10 μM PQS. Meanwhile, 100 μM PQS plus *T. gondii* infection induced PRKCA gene up-regulation significantly at three hours (1.83 ± 0.07) and 24 hours (1.91 ± 0.15) whereas at six hours it was significantly down-regulated (0.51 ± 0.03). Down-regulation of ZO-1 occurred at three, six and 24 hours, but only at six hours the down-regulation was significant (0.47 ± 0.05). Data represent biological replicates and the error bar represents SEM. (*, $P < 0.05$; ****, $P < 0.0001$)

5.5 Discussion

In this study, the effect of 3-Oxo and PQS on the viability, cell cycle, mitochondrial potential, DNA fragmentation of hBMECs, and alteration of the hBMEC integrity and permeability, in the presence and absence of *T. gondii* infection were examined. This study is the first to characterise the effect of 3-Oxo or PQS on hBMECs and in association with *T. gondii* infection.

5.5.1 *Effects of QS Molecules on hBMEC viability and Cell Cycle*

It was reported by Vikström, Tafazoli and Magnusson (2006) and Eum *et al.*, (2014) that QS treatment has a reversible effect where after, 24 hours post treatment no junction-opening effect can be significantly detected. Thus, it was decided to consider 24 hours as the end time point of the experiment except for the hBMEC monolayer permeability and integrity assays with combined QS treatment and *T. gondii* infection, where the end time point was extended to 48 hours in order to allow time to monitor the the progress of the *T. gondii* infection. The cytotoxicity of 3-Oxo and PQS was assessed using Alamar blue for 24 hours and the results showed that there was no significant reduction in hBMEC viability following treatment at 10, 20 or 100 μM concentration within 24 hours of treatment (**Figure** 5-1). Since there was no significant difference between 10 and 20 μM of both QS molecules on hBMEC viability, it was decided to investigate the effect of QS molecules using 10 and 100 μM as a low and high concentration.

Since it was reported that 3-Oxo is capable of inducing apoptosis in certain cell types, such as mammary epithelial cells and Caco-2 cells (Li *et al.*, 2004), early apoptosis and late apoptosis analysis on hBMECs treated with each of the two QS molecules at 10 and 100 μM concentrations were performed.

Using the Alamar blue assay, this study did not observe any indication that either 3-Oxo or PQS was toxic to hBMECs. This is not surprising since Tateda *et al.*, (2003) reported that different cells have different sensitivity to 3-Oxo, where this molecule induced significant loss of viability in mouse neutrophils and U-937 (human macrophage) and P388D1 cells (mouse macrophage), but not in CCL-185 (human lung epithelial) and HEp-2 (human epithelial) cells over 24 hours of treatment at 50 μM concentration. However, an increased percentage of cells in early apoptosis stage was observed following treatment with both QS molecules at both concentrations by the mitochondrial potential assay, where roughly 60% of hBMECs were detected at early apoptosis 24 hours post-treatment (**Figure** 5-4). Late apoptosis was also measured at 6 and 24 hours post-treatment by DNA fragmentation assay where both QS molecules at both concentrations were found to increase the percentage of cells with fragmented DNA at 24 hours post-treatment ranging from 21.77 ± 4.02% for 10 μM 3-Oxo at 24 hours to 49.09 ± 7.20% for 100 μM PQS (**Figure** 5-5).

Interestingly, apoptosis was observed while hBMEC monolayer barrier function was not affected, suggesting a dual effect of 3-Oxo and PQS on hBMECs. This could also explain the contrasting results between Alamar blue and mitochondrial potential plus DNA fragmentation assay, where cell energetics/metabolism as indicated by the reduction of reducing resazurin (blue colour) into resorufin (red colour) was not affected while the apoptosis process was underway. Induction of apoptosis by 3-Oxo and PQS was probably a slow process that will take at least 48 hours to complete where disruption of barrier function can only be observed after that period.

The effect of 3-Oxo and PQS at 10 and 100 μM on hBMEC cycling was analysed at 6- and 24-hours post-treatment. The result indicates that generally all treated groups resulted in significant increase in the percentage of cells at

G0/G1 stage ranging from 74-78% of total cell population after six hours of treatment (control = 54.67 ± 1.31%) and slight decrease in the cells at S stage and significant decrease of cells at G2/M stages at both time points (**Figure** 5-6). The G0/G1 percentage then returns to the control level after 24 hours of treatment, which in the range of 53-59% of total cells population. This suggests that 3-Oxo and PQS favour cells at G0/G1 and S stages to remain in that stages, while causing cells at the G2/M stage to proceed to the G0/G1 stage. Our result concurs with a report on U937, a human monocyte cell line and human colonic goblet LS174T cell line where 3-Oxo was shown to block 62% and 78% of the cells at the G0/G1 stage after 12 hours and four hours of treatment, respectively (Bortolotti *et al.*, 2015; Tao *et al.*, 2018).

5.5.2 *Effects of QS Molecules on hBMEC Permeability and Integrity*

In order to elucidate the effects of 3-Oxo and PQS on the hBMEC monolayer, this study performed FITC-dextran flux assay and TEER experiment at a low (10 μM) and high concentration (100 μM) at three, six, and 24 hours post-treatment. Flux assay revealed surprising results because rather than increasing monolayer permeability, 3-Oxo and PQS significantly reduced monolayer permeability at a low concentration over 24 hours post-treatment (**Figure** 5-2). HBMEC monolayer permeability following treatment with 100 μM of 3-Oxo or PQS was also lower than the control over 24 hours period although these were not statistically significant. When the QS treatment was administered together with *T. gondii* infection at MOI of 5, the same effect was observed, but only until 24 hours post treatment because at 48 h.p.i, no significant reduction in hBMEC monolayer was observed compared to control cells, probably because cell monolayer was then destroyed by infection (**Figure** 5-9). The observed decrease in monolayer permeability could be due to a

combination effect of QS molecules plus *T. gondii* infection or due to *T. gondii* infection only, as observed in Chapter 2, and at 3 and 6 h.p.i in **Figure** 5-9**.** *Toxoplasma gondii* infection does result in lower permeability due to cell size increase as the parasites form parasitophorous vacuole and multiply.

Results of the TEER measurement also concur with the flux assay data where, 3-Oxo and PQS at both concentrations generated higher TEER values compared to control, suggesting that both QS molecules at both concentrations increased hBMEC monolayer integrity (**Figure** 5-3). When treatment with both QS molecules was administered together with *T. gondii* infection, there was a reduction in TEER values from 3 to 48 hours post-treatment and infection similar to TEER values from *T. gondii* infection only (**Figure** 5-10). This result suggests that the observed increased monolayer integrity associated with treatment with QS molecules can be compromised by *T. gondii* infection. This is because *T. gondii* parasites establish themselves in the cells, they take control of the cell's machinery rendering the effect of quorum sensing molecules negligible.

Expression analysis of three TJ genes (Occludin, PRKCA and ZO-1) was carried out in order to investigate how 3-Oxo and PQS increased hBMEC monolayer barrier permeability and integrity, and the effect of treatment with either QS molecules in conjunction with *T. gondii* infection at three, six and 24 hours. 10 µM 3-Oxo increased PRKCA gene expression at all time points and caused slight increase in Occludin expression at three and six hours post treatment but did not significantly affect ZO-1 expression at all time points while at 100 µM significant increase PRKCA expression and a slight increase in *Occludin* expression was observed at all time points with ZO-1 expression remained relatively unchanged at all time points (**Figure** 5-7). 10 µM PQS caused slight increase in PRKCA expression and slight decrease in Occludin and

ZO-1 gene expression at all time points, while 100 µM slightly increased PRKCA and Occludin gene expression at three and six hours and slightly decreased all genes at 24 hours post-treatment (**Figure** 5-8). The combined effect of 10 µM 3-Oxo and *T. gondii* infection induced significant increase in the expression of PRKCA gene at 3 and 24 hours post-treatment and infection, and slightly decreased Occludin and ZO-1 gene expression at all time points (**Figure** 5-11). A different trend was observed following treatment with 100 µM 3-Oxo and *T. gondii* infection where a decrease in Occludin and ZO-1 expression was observed at all time points whereas decrease in PRKCA expression was observed at three and six hours, but there was slight increase at 24 hours post-treatment and infection (**Figure** 5-11). 10 and 100 µM PQS in conjunction with *T. gondii* infection induced a similar trend, where there were an increase in PRKCA expression at 3 and 24 hours post-treatment and infection, but there was a slight decrease in Occludin and ZO-1 gene expression at all time points (**Figure** 5-12).

3-Oxo disrupts epithelial barrier integrity of Caco-2 cells through the degradation of TJ (Vikström, Tafazoli and Magnusson, 2006), specifically through decreasing the levels of Occludin and Tricellulin expression and increasing the levels of MMP-2 and MMP-3 expression (Eum *et al.*, 2014). However, this effect of 3-Oxo was not observed in this study. Other than different cell lines, the difference could also be attributed to the use of higher concentrations of 3-Oxo (200 and 400 µM) on 12-mm diameter inserts (Eum *et al.*, 2014) *versus* 6.5mm used in this study. Eum *et al.*, (2014) also did not find any significant effect of 3-Oxo on Caco-2 cells at 100 µM, though measurement was obtained with a larger insert diameter. Meanwhile, Vikström, Tafazoli and Magnusson, (2006) used 200 µM 3-Oxo on inserts of similar size to the one used in this study. Our results that showed improvement in barrier integrity and permeability were also consistent with the results obtained from gene

expression analysis of three TJ genes (*Occludin*, *PRKCA* and *ZO*-1), where a significant increase in *PRKCA* expression and a slight increase in *Occludin* expression were observed within 24 hours of treatment with 3-Oxo at 10 and 100 μM, whereas a slight increase in *PRKCA* expression was also observed following treatment with PQS at both concentrations. Both 3-Oxo and PQS also slightly reduced *ZO-1* expression. *PRKCA* is essential for endothelial cell growth, migration, adhesion, and vessel formation (Nakashima, 2002; Wang, 2002).

5.5.3 *Conclusion*

The effect of 3-Oxo and PQS at a low and high concentration with and without *T. gondii* infection on hBMECs were characterised and provided new insights into the underlying mechanisms involved in 3-Oxo and PQS modulation of the hBMEC monolayer. 3-Oxo and PQS increased hBMEC monolayer permeability and integrity through PRKCA gene up-regulation, slowly induced cell apoptosis and halted cell proliferation at the G0/G1 stage. Overall, these results did not support the hypothesis that QS molecules from *P. aeruginosa* facilitate *T. gondii* crossing of BBB into the brain. Further understanding of the mechanisms that regulate these processes and underlie the effect of QS molecules on the BBB may lead to the discovery of key factors/pathways involved in supporting the BBB capability to limit brain invasion.

Chapter 6 General Discussion

6.1 Introduction

In the second chapter of this study, the response of hBMECs to infection with *T. gondii* was investigated, as a simple 2D model by investigating the phenotypic and functional changes that occur in hBMECs during the early stages of infection progression. The effect of *T. gondii* infection on viability, vitality, the cell cycle, mitochondrial potential and DNA fragmentation of host cells were also characterised. Then, the integrity of TJs of hBMECs following tachyzoite infection was evaluated using a trans-endothelial electrical resistance (TEER) assay; and the alteration in hBMEC's permeability following tachyzoite infection was assessed using a FITC-Dextran leakage assay. The effect of infection on the expression of the selected TJ and inflammatory genes was also investigated using real-time PCR. The results show that hBMECs serve as a replicative niche and launching pad for breaching the BBB by *T. gondii* and spreading through the CNS.

In the third chapter, the result from the second chapter that has shown that at 6 and 48 h.p.i, there were significant biochemical and cellular changes in the host cells following *T. gondii* RH infection was explored further. Since these phenotypic changes must have been underpinned by molecular mechanisms driven by host cell response to the infection, these changes at molecular level focusing on transcriptomic aspects, specifically mRNA and miRNA expression was explored. While there have been several studies on mRNA transcriptomic changes in human cells infected with *T. gondii* (Chaussabel *et al.*, 2003; Radke *et al.*, 2005; Ander *et al.*, 2018) and miRNA transcriptomic changes in human cells infected with *T. gondii* (Zeiner *et al.*,

2010; Pope and Lässer, 2013; Xiao *et al.*, 2014), none of these studies have been conducted on hBMECs, which form a fundamental component of the BBB. mRNA and miRNA transcriptomes of hBMECs infected with *T. gondii* RH parasites at 6, 24 and 48 h.p.i. by RNA sequencing (RNA-Seq) were characterised followed by expression analysis with microarray technology and validation with qRT-PCR. mRNA and miRNA sequencing were performed so that global expression profiling can be determined, in addition to identifying novel genes, rare and lowly expressed genes, plus the potential discovery of non-coding RNAs, which cannot be obtained by using microarray technology. In addition to relative expression, absolute gene expression can also be obtained from RNA-Seq data, which is not available from microarray data. Using this integrated transcriptomics analysis based on different technologies allowed the determination of whether there is a common transcriptomic signature characteristic of *T. gondii* infection effect on hBMECs.

In general, this study confirmed previous findings that *T. gondii* infection halts cell cycle progression and displays modulation of cancer-like genes in infected cells. Thus, the hypothesis that, hBMECs infected with *T. gondii* RH exhibit mRNA-miRNA expression profile that is different from that exhibited by healthy, uninfected, cells was accepted. Unsurprisingly, the majority of pathways up-regulated were related to ATP synthesis and metabolism. Integrated mRNA/miRNA expression profiling and pathway analysis show multiple signalling pathways including, ATF4 activation, TP53 regulation, selenoamino acid metabolism and selenocysteine synthesis, as key pathways potentially regulated during *T. gondii* infection. Small RNA study led to the identification of the increased expression of miR-7 family and miR-17-92 family, such expression plays an important role in determining the fate of host cells in *T. gondii* infection. Also, ribosomal protein L36 and S12 were identified as key players in *T. gondii* pathogenesis and have good potential as vaccine

candidates. Overall, these results reveal several previously unidentified changes on the host cell and contribute to foundation knowledge of the host-pathogen interaction.

In the fourth chapter, the effect of inhibition of the WNT pathway on *T. gondii* RH infection on hBMECs was explored. WNT pathway was up-regulated in *T. gondii*-infected mice (B. Jia *et al.*, 2013) and in hBMECs at 6 and 48 h.p.i derived from miRNAs sequencing data analysis presented in the third chapter. Intracellular pathogens have been shown to manipulate the host WNT pathway or exploit this pathway to facilitate their entry into the cell and establish infection, such as *Chlamydia trachmatis* (Kessler *et al.*, 2012) and influenza virus (Shapira *et al.*, 2009), among others. Monensin has been extensively used in veterinary applications as a growth promoter (Callaway, Edrington and Rychlik, 2003) and to treat coccidiosis and cryptosporidiosis (Teichmann *et al.*, 2012; Rutkowski and Brzezinski, 2013). Monensin, secreted by the bacteria *Streptomyces cinnamonensis*, has been shown to modulate the WNT signalling by antagonising the β-catenin and lipoprotein receptor-related protein, LRP, a WNT co-receptor (Tumova *et al.*, 2014). In addition, the WNT pathway was found to be up-regulated in *T. gondii* infection in brain cells (Ngô *et al.*, 2017). The investigation into how the manipulation of the WNT pathway by monensin can impair the growth of *T. gondii* could be greatly beneficial in the development of new anti-*T. gondii* therapeutics. Therefore, the effect of monensin on the *in vitro* growth of *T. gondii* RH tachyzoites and on the proliferation of hBMECs and microglial cells was investigated. This study found that monensin showed high anti-*T. gondii* activity, inhibited the growth of the parasites with a nanomolar concentration, and with limited but reversible cytotoxic influence on the host cells.

In the fifth chapter, the impact of co- or pre-infection with *P. aeruginosa* on *T. gondii* infection at the BBB interface using quorum sensing molecules produced by the bacteria was assessed. Co-infection of *T. gondii* and *P. aeruginosa* while uncommon, have been reported in at least two cases in French Guiana (Carme *et al.*, 2002; Demar *et al.*, 2012) and Peru (Nunura *et al.*, 2010). Quorum-sensing signalling molecules N-(3-oxododecanoyl)-L-homoserine lactone (3-Oxo) and 2-Heptyl-3-hydroxy-4(1H)-quinolone (PQS) are secreted by *P. aeruginosa* (Pesci *et al.*, 1999; Mayer *et al.*, 2011). One of them, 3-Oxo was reported to disrupt epithelial barrier integrity in Caco-2 cells by the degradation of TJ while there is no report on whether PQS can do the same (Vikström, Tafazoli and Magnusson, 2006). In this chapter, the effect of 3-Oxo and PQS at a low and high concentration with and without *T. gondii* RH infection on hBMECs were characterised and provided new insights into the underlying mechanisms involved in 3-Oxo and PQS modulation of the hBMEC monolayer. 3-Oxo and PQS increased hBMEC monolayer permeability and integrity through PRKCA gene up-regulation, slowly induced cell apoptosis and halted cell proliferation at the G0/G1 stage. Overall, these results did not support the hypothesis that QS molecules from *P. aeruginosa* facilitate *T. gondii* RH crossing of BBB into the brain. Further understanding of the mechanisms that regulate these processes and underlie the effect of QS molecules on the BBB may lead to the discovery of key factors/pathways involved in supporting the BBB capability to limit brain invasion.

6.2 Phenotypic and Functional Changes in hBMECs following *T. gondii* Infection

It takes around 30 seconds for *T. gondii* to enter a cell following a contact (Håkansson *et al.*, 1999) and once entered the parasite will incorporate its protein into part of human cell membrane to form its own parasitophorous vacuole (PV) membrane before twisting to mechanically close the membrane and pinch off into the cell (David Sibley, 2011; Pavlou *et al.*, 2018). Inside the PV in the cell, each parasite will take around six hours to complete from a new daughter tachyzoite by endodyogenies process (Nishi *et al.*, 2008). In other words, a number of tachyzoites in the cell will double every six hours. As an intracellular parasite, *T. gondii* must maintain the host cell's viability long enough for the parasite to complete its replication, and then egress and invade the neighbouring host cells. In chapter two, study has shown that *T. gondii* maintained hBMEC viability for 24 h.p.i, whereas at 48 and 72 h.p.i there was a significant reduction in hBMECs' viability (**Figure** 2-4). This suggests that *T. gondii* maintained hBMEC cell viability, at least 24 h.p.i and did not compromise cell vitality significantly until 72 h.p.i. This result concurs with findings reported in *T. gondii*-infected human foreskin fibroblast (HFF) cells, where cell viability was also maintained for 24 h.p.i (Molestina, El-guendy and Sinai, 2008).

The vitality, *i.e* the cells' energy levels, of hBMECs following *T. gondii* infection was investigated using VitaBright-48™ dye and NC-3000™ Image Cytometer resulted in significant reduction of host vitality at three, six and 12 and 72 h.p.i in infected cells, when compared to healthy cells (**Figure** 2-10). Cells with low vitality remained low in percentage throughout the first 12 h.p.i, then significantly increased at 72 h.p.i. Based on transcriptomics data, two genes, CHAC1 (ChaC glutathione specific gamma-glutamylcyclotransferase 1)

and ATF3 (activating transcription factor 3) were highly expressed at all time points. These two genes are pro-apoptotic proteins that act through the ATF4-ATF3-CHOP cascade (Mungrue *et al.*, 2009) together with DDIT3 and TRIB3 which were also found to be up-regulated at 6 h.p.i by RNA-seq. In addition, CHAC1 also specifically degrades glutathione in cells (Kumar *et al.*, 2012). The result suggests that expression of these genes was induced by hBMECs in order to reduce cell vitality and initiate apoptosis. However, our data showed that apoptosis was not achieved as apoptotic cells and cells with low vitality remain low in numbers within 48 h.p.i. Blocking of apoptosis has been reported in *T. gondii* infected-HFF cells and macrophages, which was achieved through caspase and higher cytochrome-c release blockade (Sinai *et al.*, 2004). Coincidently, at BCL2A1, a gene capable of reducing the release of pro-apoptotic cytochrome-c from mitochondria and block caspase activation (Vogler, 2011) was up-regulated at 6 h.p.i from microarray data. These results suggest that the death of hBMECs did not occur through apoptosis, but likely through pyroptosis. How infected hBMECs manage to negate apoptosis even with a high expression of pro-apoptotic genes early during infection is unknown and should be a subject for future research.

An early apoptotic sign in hBMECs, following *T. gondii* infection, was monitored using a mitochondrial potential assay (**Figure** 2-11). Late apoptosis was monitored using a DNA fragmentation assay (**Figure** 2-12). Though early apoptotic sign was measured at 12 to 72 h.p.i, DNA damage was not detected until 72 h.p.i. The DNA fragmentation assays showed that *T. gondii* infection did not affect DNA integrity of hBMECs until 72 h.p.i. A possible explanation to increase of the percentage of the cell with depolarised cells is due to three genes (CYTB, ATP6, ATP8) that were highly up-regulated at 6, 24 and 48 h.p.i based on RNA-seq data. These genes contribute to proton gradient generation on the mitochondrial membrane for ATP synthesis (Legros *et al.*, 2001; Davies

et al., 2011). Since protons are positively charged, the JC-1 dye will not accumulate in the mitochondria' matrix as it is only attracted to the negatively charged membrane. This contributes to possibly false positive result and suggest that membrane potential measurement is not a good measure for early apoptosis in *T. gondii* infected cells.

The effect of *T. gondii* infection on hBMECs was monitored for 72 hours using the NC-3000™ Cell Cycle Assay. The data suggest that it took at least 6 h.p.i for *T. gondii* to manipulate hBMECs to remain or to revert to their G0/G1 stage. In contrast, in HFF cells *T. gondii* infection was reported to promote cells into S phase after 24 h.p.i (Molestina, El-guendy and Sinai, 2008). Though cell cycle experiment indicates that cells remain in the G0/G1 stage, some of the genes that promote G1 to S stage were up-regulated in this study. The genes are CCNE1 (microarray), CCNE2 (microarray) and TCIM (RNA-seq). In conjunction with the study in HFF infected cells, these data indicate that *T. gondii* infection does induce host cells into S phase, but the induction may not necessarily promote host cell into S stage as different cell type may resist to changes.

6.3 Effects on Host Cell Junction and Inflammatory Gene Expression

The effects of *T. gondii* infection on host cell functions, were investigated using a FITC-dextran assay (**Figure** 2-8), TEER (**Figure** 2-9) and RT-PCR (**Figure** 2-14). The flux of FITC-dextran across hBMEC monolayers (indicative of increased paracellular permeability) was low, when monolayers were apically treated with *T. gondii* at MOI five from three hours to 24 hours (**Figure** 2-8). However, at 48 and 72 hours, more FITC-dextran leakage was measured when

compared to control cell cultures. This may be due to egress of parasites from cells, destroying the monolayer barrier. No differences were statistically significant. Briceño *et al.*, (2016) reported that, in a Caco-2 cell line, *T. gondii* infection significantly decreased cell permeability after 24 h.p.i using FITC-dextran flux assay, even though confocal microscopy revealed the uptake of FITC-dextran by endocytosis in infected cells to be lower than in uninfected cells. Significant changes in hBMECs' monolayer integrity were detected after 24 h.p.i (**Figure** 2-9). TEER values were also significantly lower in *T. gondii*-infected Caco-2 cells, than in non-infected cells, at 20 and 24 h.p.i (Briceño *et al.*, 2016). This suggests that while *T. gondii* infection reduces hBMEC membrane integrity, hBMEC membrane permeability was not significantly affected. This could be due to an increase in hBMEC size following *T. gondii* infection, as the parasites enter the cell and form a parasitophorous vacuole, and the increase in cell size/volume limits FITC-dextran leakage through the TJs. TEER reflects the ionic conductance of the paracellular pathway in the cell monolayer, whereas the flux of non-electrolyte tracers indicates the paracellular water flow - as well as the pore size of the TJs (Srinivasan *et al.*, 2015). These results suggest that, *T. gondii* infection reduces ionic conductance, and limits paracellular water flow through the hBMEC monolayer.

Brain endothelial cells challenged with *T. gondii*, displayed changes in TJ and cytokine gene expression - consistent with endothelial cell stress and compromised membrane integrity. *T. gondii* infection altered the expression of Occludin, PRCKA, ZO-1, IL-6, P-GP and TNF-alpha genes at 3 h.p.i where four of these genes (PRKCA, ZO-1, P-GP and TNF-alpha) were significantly upregulated (**Figure** 2-14). At 6 h.p.i, only TNF-alpha was significantly up-regulated in infected cells. At 24, 48 and 72 h.p.i, only expression of IL-6 was significantly elevated (**Figure** 2-14). The gene expression study and *T. gondii* counting (**Figure** 2-7) results, suggest that it is unlikely that *T. gondii*

tachyzoites cross hBMECs monolayer through modulating the expression of TJ genes. Interestingly, in the Caco-2 cell line, ZO-1 and Occludin expression was decreased significantly 24 hours after *T. gondii* infection (Briceño *et al.*, 2016). In humans, IL-6 also plays an important role in the host response against *T. gondii* invasion, where it promotes NK cell activation and production of IFN-gamma (Gigley, 2016; Sher, Tosh and Jankovic, 2017). IL-6 up-regulation was reported in *T. gondii* infected human retinal pigment epithelial (HRPE) cells (Nagineni, Detrick and Hooks, 2000). Among these six genes (IL-6, Occludin, P-GP, PRKCA, TNF-alpha, ZO-1) analysed by qPCR in chapter two, only two genes, PRKCA and IL-6 were found to be differentially expressed. A contrasting result was observed between different technologies where for the PRKCA gene no significant changes were seen by qPCR study at 48 h.p.i while microarray found the gene to be up-regulated at the same time point. Meanwhile, no significant changes of IL-6 were observed by PCR at 6 h.p.i while microarray and RNA-seq studies found the gene to be up-regulated and no significant changes respectively. At 24 h.p.i, IL-6 was highly up-regulated by PCR and RNA-seq studies while no significant changes were observed from microarray studies. At 48 h.p.i, IL-6 was found to be highly up-regulated while both microarray and RNA-seq studies found it to be highly down-regulated. These contrasting results highlight high variation between biological samples and the importance of using multiple studies to observe variation in biological samples.

6.4 HBMECs Immune Response to *T. gondii* Infection

One of the most critical functions of the innate immune response to *T. gondii* is the ability to sense the pathogen and produce the cytokine IL-12, which stimulates natural killer (NK) cells and T cells to produce the cytokine IFN-γ (Dupont, Christian and Hunter, 2012; Yarovinsky, 2014). Another key cytokine is TNF-alpha, produced by several cell populations in response to *T. gondii* or *T. gondii* antigens including neutrophils, DCs, macrophages, microglial, and T cells (Yarovinsky, 2014; Coombes and Hunter, 2015). TNF-alpha together with IFN-γ promotes anti-parasitic mechanisms in macrophages, as well as non-hematopoietic cells through the production of nitric oxide (Yarovinsky, 2014; Coombes and Hunter, 2015). The balance of immune response in *T. gondii* infection is juggled by IL-10 limiting inflammation (Coombes and Hunter, 2015).

At 6 h.p.i, IL-15, IL-16 and CXCL8 were up-regulated by hBMECs. IL-15 is an anti-apoptosis protein that promotes proliferation of T, B and natural killer cells connecting innate and adaptive immune response (Patidar, Yadav and Dalai, 2016). However, at the same time CD274 molecule gene (previously known as PD-L1 or programmed cell death 1 ligand 1) and PDCD1LG2 were also up-regulated. These proteins inhibit cytokine and T-cells activation and was implicated in tumour survival (Freeman *et al.*, 2000; Brown *et al.*, 2003; Burr *et al.*, 2017). In addition, TNF-alpha was also found to be highly expressed at 6 h.p.i but not at 3 h.p.i (**Figure** 2-14) by RT-PCR.

Then at 24 h.p.i, a plethora of immune induction genes (IFI27, IFI44, IFI44L, IFI6, IFIT1, IFIT3, IRF7, ISG15, OAS1, OAS2, OAS3, PARP9) and anti-apoptosis genes (ANGPTL4, SAMD9, XAF1) were up-regulated as identified by

microarray data. In addition, RT-PCR detected significantly up-regulated IL-6 and slightly up-regulated TNF-alpha at this time point similar to published data in infected HFF cells (Blader, Manger and Boothroyd, 2001). At 6 and 24 h.p.i, a possible reason for low key immune response is the upregulation of TSC22D3 (TSC22 domain family member 3; log2 FC 6 h.p.i = 1.697, 24 h.p.i = 1.579) gene. This gene is an anti-inflammatory and an anti-apoptosis gene (André *et al.*, 2016; Lee *et al.*, 2016) which could contribute to low key immune response in hBMECs.

At 48 h.p.i, 12 (RNA-seq) and 47 (microarray) of DEGs were immune-related genes. In addition, IL-6 was significantly up-regulated while TNF-alpha was slightly down-regulated at this time point. TNF-alpha expression was suppressed at 3, 24, 48 and 72 h.p.i as identified by RT-PCR indicating that the cytokine is crucial to parasite clearing. However, treating infected cells with TNF-alpha alone will not help parasite clearing but if combined with IFN-gamma, the combination will inhibit 75-80% of replication (Halonen, Chiu and Weiss, 1998).

6.5 Key Pathways in *T. gondii* Invasion of hBMECs

MRNA sequencing discovered five key pathways which are R-HSA-5628897 (TP53 Regulates Metabolic Genes), R-HSA-3700989 (Transcriptional Regulation by TP53), R-HSA-380994 (ATF4 activates genes), R-HSA-2408522 (Selenoamino acid metabolism) and R-HSA-2408557 (Selenocysteine synthesis). When RNA-seq data were matched to the *T. gondii* reference genome, two protein coding genes, TGME49_286420 (EF-1-ALPHA = elongation factor 1-alpha, putative) and TGME49_294800 (EF-1-ALPHA = elongation factor 1-alpha, putative) were found to be highly up-regulated and were matched to

Selenocompound metabolism (ec00450__PK__KEGG) selenate reduction (PWY-6932__PK__MetaCyc) and superpathway of seleno-compound metabolism (PWY-6395__PK__MetaCyc) pathways. The genes were recorded in different chromosomes indicating their significance to *T. gondii* virulence and survival judging from the strategy used by another protozoan *Plasmodium falciparum* (Ribacke *et al.*, 2007). Another indicator of these two genes' importance is that they are also implicated in superpathway of sulfur amino acid biosynthesis (PWY-821__PK__MetaCyc) and superpathway of L-methionine biosynthesis by sulfhydrylation (PWY-5345__PK__MetaCyc), two pathways related to sulfur-containing amino acids synthesis. Sulfur-containing amino acids (methionine, cysteine, homocysteine, and taurine) are indispensable in protozoans and have been suggested as a practical target for drug development and prophylactic agents against diseases caused by protozoan parasites (Nozaki, Ali and Tokoro, 2005; Maresi *et al.*, 2018).

The only pathway consensus between RNA-seq data and miRNAs data is 'Axon guidance' (KEGG: hsa04360; REACTOME: R-HSA-422475) which is the process of neurons extending axon towards a stimulus from the environment through cytoskeleton changes. The significance of this pathway in *T. gondii* pathogenesis is unknown.

TP53, part of p53 regulatory pathways, was implicated as a mediator of apoptosis and cell cycle arrest in human neuroblastoma cells through rhoptry protein 16 (Chang *et al.*, 2015). Thus, the two TP53 related pathways could be manipulated by the parasite to halt apoptosis and cell cycle in hBMECs. The central gene of this pathway based on these data is DDIT4, which was found to be up-regulated at all time points. In contrast, 'ATF4 activates genes' pathway was implicated in the apoptosis-inducing pathway with the ATF4 gene, up-regulated at 6, 24 and 48 h.p.i, as the key player. As mentioned earlier, ATF4-

ATF3-DDIT3 and TRIB3 were all pro-apoptotic proteins that act through ATF4-ATF3-CHOP cascade (Mungrue *et al*., 2009). Thus, this study identifies the interplay between host-pathogen in infected hBMECs that can be targeted in future research to promote host survival.

6.6 Potential Use of Monensin as Anti-*T. gondii* Treatment at BBB

We investigated the effect of WNT inhibition by monensin on the growth of *T. gondii in vitro*. Our observations suggest that monensin significantly decreased ($P < 0.01$) the growth of *T. gondii* tachyzoites. The efficacy of parasite inhibition increased as the concentration of the compound increased (*i.e*. it was dose-dependent). Of note, the 0.1 µM concentration of monensin was effective in inhibiting *T. gondii* growth. This finding fits within the range of the effective concentration reported by Kapoor *et al.*, (2013) against the virus human cytomegalovirus (HCMV) at 0.01 µM and 0.1 µM concentration. WNT pathways were found to be up-regulated in *T. gondii* infection in brain cells (Ngô *et al.*, 2017). In contrast, in this study, genome-wide gene expression investigation through RNA-seq and microarray technologies did not find up-regulation of WNT signalling related genes in *T. gondii* infected hBMECs. Instead the relationship is inverse where *T. gondii* infection down-regulates genes involves in WNT signalling pathway. Our result concurs with recently published finding where ROP18 of the parasite was found to be responsible for WNT signalling pathway inhibition in neural stem cells (Zhang *et al.*, 2017). However, data from small RNA sequencing study found that miRNAs are associated with positive regulation, as WNT signalling pathways were up-regulated at six and 48 h.p.i. This finding also agrees with miRNA profiling study in mouse spleen where they also found the WNT pathway among 12 enriched pathways resulted

from *T. gondii* infection (He *et al.*, 2016). Other miRNA sequencing studies on *T. gondii* infected primary human foreskin fibroblasts (Zeiner *et al.*, 2010), human macrophage (Cai *et al.*, 2014) and human neuro-like cell (Xiao *et al.*, 2014) did not report on the effect of infection on WNT signalling pathways as their reports focused on specific miRNAs. Re-analysing their data would add confidence to the current finding.

Pre-treatment of cells with monensin was found to increased the pH of intracellular vacuoles effectively inhibit *Citrobacter freundii* (gram-negative bacteria) and *Brucella abortus* (gram-negative bacteria) invasion and internalisation (Badger, Stins and Kim, 1999; Miraglia *et al.*, 2018). Meanwhile, this study plus a previous study found that *T. gondii* growth was inhibited by monensin, a Wnt signalling inhibitor (Lavine and Arrizabalaga, 2011, 2012). While previous reports showed non-toxic effect of monensin on human foreskin fibroblasts (HFFs) (Lavine and Arrizabalaga, 2011; Kapoor *et al.*, 2013) or human colon ileocecal (HCT-8) cells (Teichmann *et al.*, 2012), while our results revealed some level of cytotoxicity in treated microglial and hBMECs (**Figure** 4-2 and **Figure** 4-3), probably due to the sensitivity of brain cells compared to HFFs or HCT-8 cells. Our data suggest that while there was a mild cytotoxic effect of monensin, the effect was tolerable by the cells and the toxicity appears to be reversible because no permanent damage was detected in the mitochondria and DNA. While there was no other study that shows the reversible effect of monensin on host cells, the reversible effect of monensin on *T. gondii* was demonstrated by Couzinet *et al.*, (2000) and Lavine and Arrizabalaga, (2011, 2012).

Microarray analysis was performed on four groups; control, treatment with 0.1 µM monensin, infected with *T. gondii*, and infected with *T. gondii* then treated with monensin then analysed for enriched PANTHER-GO Slim GO terms

and enriched Reactome pathways. Reactome pathway enrichment analyses on transcriptome from hBMECs treated with 0.1 μM monensin (Control *vs* Monensin_only) revealed that monensin treatment reduced steroids, cholesterol and protein biosynthesis and their transport between endoplasmic reticulum (ER) and Golgi apparatus in the cells related pathways (**Table** 4-4). However, at the same time monensin treatment also up-regulated pathways related to cell cycle and DNA replication in the nucleus. The result concurs with the cell cycle assay where after 24 hours of treatment with 0.1 uM monensin there was a slight increase in the percentage of S and G2/M cell populations thought the increment was not significant (two-way ANOVA, $P < 0.05$). This growth promoting effect disagrees with the effect of monensin treatment on human ovarian cancer cells (Deng *et al.*, 2015) and human colorectal cancer (Tumova *et al.*, 2014) where cell proliferation, migration and cell cycle progression were suppressed. This suggests that monensin effect is specific to cell type. Unexpectedly, WNT signalling and WNT related pathways were not significantly affected by treatment with 0.1 μM monensin, as all WNT related genes, such as Frizzled receptors, beta-catenin, protein kinase C (PKC) expression were not affected after treatment or if affected the changes were minimal and were not significant ($P < 0.05$; **Table** 4-5). The same also applies to Control *vs* TG_only and Control *vs* TG_Monensin transcriptomes (**Table** 4-7 and **Table** 4-10). This finding suggests that monensin treatment did not affect the WNT signalling pathway in hBMECs and that inhibition of *T. gondii* infection in hBMECs following monensin treatment was not achieved through direct blocking of the WNT signalling pathway. In the meantime, this study identified genes related to other signal pathways such as cell cycle control and apoptosis that were affected. This suggests pleiotropic effects of monensin on multiple biological processes.

Transcriptome of hBMECs treated with monensin after *T. gondii* infection (Control *vs* TG-Monensin) revealed similar pattern to Control *vs* Monensin_only transcriptome, where pathways related to steroids, cholesterol, protein biosynthesis and their transport between endoplasmic reticulum (ER) and Golgi apparatus were down-regulated but at the same time pathways related to cell cycle and DNA replication activities in the nucleus were up-regulated. However, there were more significantly up-regulated cell cycle, cell division and DNA replication-related pathways (39 pathways) compared to only three significantly up-regulated from Control *vs* Monensin_only transcriptome data. This transcriptome data (Control *vs* TG_Monensin) in combination with *T. gondii* counting data (**Figure** 4-1) demonstrate the potential effectiveness of monensin in treating *T. gondii* infection in hBMECs in vitro without causing permanent damage to host cells.

Overall, microarray data supports the notion that parasite inhibition could have been achieved through concerted efforts by directly killing the parasite and inhibition of transport between organelles within cells limiting nutrient transport into parasitophorous vacuole. The implications of monensin treatment and *T. gondii* infection on barrier function and parasite neuropathogenesis deserve further investigation as this study has identified the potential of its usage in treating *T. gondii* at a simple BBB model.

6.7 Quorum Sensing Molecules Reduce hBMECs Permeability Possibly by Inducing PRKCA Expression

We performed FITC-dextran flux assay and TEER experiment at a low (10 μM) and high concentration (100 μM) at 3, 6, and 24 hours post-treatment on hBMEC monolayer to study the effects of 3-Oxo and PQS. Flux assay revealed surprising results, where 3-Oxo and PQS significantly reduced monolayer permeability at a low concentration over 24 hours post-treatment (**Figure** 5-2). HBMEC monolayer permeability following treatment with 100 μM of 3-Oxo or PQS was also lower than the control over 24 hours period although these were not statistically significant. When the QS treatment was administered together with *T. gondii* infection at MOI of 5, the same effect was observed, but only until 24 hours post treatment because at 48 h.p.i, no significant reduction in hBMEC monolayer was observed compared to control cells, probably because cell monolayer was then destroyed by infection (**Figure** 5-9). The observed decrease in monolayer permeability could be due to a combination effect of QS molecules plus *T. gondii* infection or due to *T. gondii* infection only as observed in Chapter 2, and at 3 and 6 h.p.i in **Figure** 5-9. *Toxoplasma gondii* infection does result in lower permeability due to cell size increase as the parasites form parasitophorous vacuole and multiply.

Results of the TEER measurement also concur with the flux assay data where, 3-Oxo and PQS at both concentrations generated higher TEER values compared to control, suggesting that both QS molecules at both concentrations increased hBMEC monolayer integrity (**Figure** 5-3). When treatment with either QS molecules was administered together with *T. gondii* infection, there was a reduction in TEER values from 3 to 48 hours post-treatment and infection

similar to TEER values from *T. gondii* infection only (**Figure** 5-10). This result suggests that the observed increased monolayer integrity associated with treatment with QS molecules can be compromised by *T. gondii* infection. This is because when *T. gondii* parasites establish themselves in the cells they take control of the cell's machinery rendering the effect of quorum sensing molecules negligible.

Expression analysis of three TJ genes (Occludin, PRKCA and ZO-1) was carried out in order to investigate how 3-Oxo and PQS affect hBMEC monolayer barrier permeability and integrity, and the effect of treatment with both QS molecules in conjunction with *T. gondii* infection at 3, 6 and 24 hours. 10 μM 3-Oxo increased PRKCA gene expression at all time points and caused slight increase in Occludin expression at 3 and 6 hours post-treatment, but did not significantly affect ZO-1 expression at any time point while at 100 μM significant increase PRKCA expression and a slight increase in Occludin expression was observed at all time points with ZO-1 expression remained relatively unchanged at all time points (**Figure** 5-7). 10 μM PQS caused a slight increase in PRKCA expression and a slight decrease in Occludin and ZO-1 gene expression at all time points, while 100 μM slightly increased PRKCA and Occludin gene expression at 3 and 6 hours and slightly decreased all genes at 24 hours post-treatment (**Figure** 5-8). The combined effect of 10 μM 3-Oxo and *T. gondii* infection induced significant increase in the expression of PRKCA gene at 3- and 24-hours post-treatment and infection, and slightly decreased Occludin and ZO-1 gene expression at all time points (**Figure** 5-11). A different trend was observed following treatment with 100 μM 3-Oxo and *T. gondii* infection where a decrease in Occludin and ZO-1 expression was observed at all time points whereas a decrease in PRKCA expression was observed at 3 and 6 hours, but there was slight increase at 24 hours post-treatment and infection (**Figure** 5-11). 10 and 100 μM PQS in conjunction with *T. gondii* infection induced a similar

trend, where there were an increase in PRKCA expression at 3 and 24 hours post-treatment and infection, but there was a slight decrease in Occludin and ZO-1 gene expression at all time points (**Figure** 5-12).

3-Oxo disrupts epithelial barrier integrity of Caco-2 cells through the degradation of TJ (Vikström, Tafazoli and Magnusson, 2006), specifically through decreasing the levels of Occludin and Tricellulin expression and increasing the levels of MMP-2 and MMP-3 expression (Eum *et al.*, 2014). However, this effect of 3-Oxo was not observed in our study. Other than different cell lines, the difference could also be attributed to the use of higher concentrations of 3-Oxo (200 and 400 μM) on 12-mm diameter inserts (Eum *et al.*, 2014) versus 6.5 mm used in this study. Eum *et al.*, (2014) also did not find any significant effect of 3-Oxo on Caco-2 cells at 100 μM, although measurement was obtained with a larger insert diameter. Meanwhile, Vikström, Tafazoli and Magnusson, (2006) used 200 μM 3-Oxo on inserts of similar size to those used in this study. Our results that showed improvement in barrier integrity and permeability were also consistent with the results obtained from gene expression analysis of three TJ genes (Occludin, PRKCA and ZO-1), where a significant increase in PRKCA expression and a slight increase in Occludin expresssion were observed within 24 hours of treatment with 3-Oxo at 10 and 100 μM, whereas a slight increase in PRKCA expression was also observed following treatment with PQS at both concentrations. In contrast, both 3-Oxo and PQS also slightly reduced ZO-1 expression. PRKCA is essential for endothelial cell growth, migration, adhesion, and vessel formation (Nakashima, 2002; A. Wang, 2002). Thus, our data suggest that PRKCA is the key gene in reducing hBMECs monolayer permeability.

6.8 Quorum Sensing Molecules Induce Apoptosis and Halt Cell Cycle Stage Progression in hBMECs

We studied the effect of two QS molecules from *P. aeruginosa*, 3-Oxo and PQS, on the viability, cell cycle, mitochondrial potential, DNA fragmentation of hBMECs, and alteration of the hBMEC integrity and permeability, in the presence and absence of *T. gondii* infection. This study is the first to characterise the effect of 3-Oxo or PQS on hBMECs and in association with *T. gondii* infection. This study was formulated to highlight the possible compounding effect of co-infection of *T. gondii* and *P. aeruginosa* and the potential use of QS molecules to open up BBB barrier for treatment purposes. Effects of QS molecules were observed within 24 hours as reports identified that QS treatment has a reversible effect such that after 24 hours post-treatment no junction-opening effect can be significantly detected (Vikström, Tafazoli and Magnusson, 2006; Eum *et al.*, 2014). However, for QS treatment plus *T. gondii* infection, the end time point was extended to 48 hours in order to allow time to monitor the progress of *T. gondii* infection. Initial cytotoxicity analysis of 3-Oxo and PQS showed that there was no significant reduction in hBMEC viability following treatment at 10, 20 or 100 μM concentration within 24 hours of treatment (**Figure** 5-1), leading to decision to investigate the effect of QS molecules at 10 and 100 μM as a low and high concentration.

Since 3-Oxo was reported to induce apoptosis in certain cell types, such as mammary epithelial cells and Caco-2 cells (Li *et al.*, 2004), early apoptosis and late apoptosis analysis on hBMECs treated with each of the two QS molecules at 10 and 100 μM concentrations were performed. Using Alamar blue assay, this study did not observe any indication that either 3-Oxo or PQS was

toxic to hBMECs. This is not surprising since (Tateda *et al.*, 2003) reported that different cells have different sensitivity to 3-Oxo, where this molecule induced significant loss of viability in mouse neutrophils and U-937 (human macrophage) and P388D1 cells (mouse macrophage), but not in CCL-185 (human lung epithelial) and HEp-2 (human epithelial) cells over 24 hours of treatment at 50 μM concentration. However, an increased percentage of cells in early apoptosis stage was observed following treatment with each of the QS molecules at both concentrations by mitochondrial potential assay, where roughly 60% of hBMECs were detected at early apoptosis 24 hours post-treatment (**Figure** 5-4). Late apoptosis was also measured at 6 and 24 hours post-treatment by DNA fragmentation assay where both QS molecules at both concentrations were found to increase the percentage of cells with fragmented DNA at 24 hours post-treatment ranging from 21.77 ± 4.02% for 10 μM 3-Oxo at 24 hours to 49.09 ± 7.20% for 100 μM PQS (**Figure** 5-5). Interestingly, apoptosis was observed while hBMEC monolayer barrier function was not affected suggesting a dual effect of 3-Oxo and PQS on hBMECs. This could also explain the contrasting results between Alamar blue and mitochondrial potential plus DNA fragmentation assays, where cell energetics/metabolism as indicated by the reduction of reducing resazurin (blue colour) into resorufin (red colour) was not affected while the apoptosis process was underway. Induction of apoptosis by 3-Oxo and PQS is probably a slow process that will take at least 48 hours to complete where disruption of barrier function can only be observed after that period.

6.9 Limitations of Study

One of limitations of this study was that the majority of the work done has been at the gene level. Gene expression does not always equal protein expression. Hence, for future work, confirmation of this study's findings at the protein level is recommended. Another limitation of this thesis was the BBB model used in the investigation, which is a simple 2D cell culture model compared to the complex structure of the BBB, which is composed of three different cells types, namely endothelial cells, microglial and astrocytes. Culturing three different cells at the same time is very challenging, requires expensive set up and has not been well established. Thus, the simple model of BBB used in this thesis is a reasonable way to explore interaction between BBB, *T. gondii* parasite, monensin and quorum sensing molecules. We are cognizant that our research represents interaction interface at *in vitro* level. Thus, more studies are required before extending our conclusion to *in vivo* level.

In the cell's permeability study, FITC-dextran was used a tracer for permeability measurement. However, the technique did not exclusively reflect the properties of the paracellular pathway, but rather was a combination of the paracellular and transcellular routes. An increase in FITC-dextran permeability could be due to either increased paracellular diffusion and/or increased rates of fluid-phase transcytosis. Similarly, in cell's integrity study, TEER measurement did not exclusively reflect paracellular resistance, but a combination of transcellular and paracellular resistance. As such, caution should be excercised before drawing a definitive conclusion.

Cells viability study using Alamar blue did not detect any cyttoxic effect of QS molecules, but mitochondrial potential and DNA fragmentation assays were able to detect signs of early apoptosis and late apoptosis. This shows the

limitation of Alamar blue assay in detecting toxic effect of substances on cells and should not be used as the only viability/toxicity study on cells.

6.10 Future Work and Conclusion

This thesis uncovers several gaps in knowledge about *T. gondii* pathogenesis in host cells. Notable among these is the lack of a curated database of *T. gondii* miRNAs available for bioinformatics analysis. This gap stems from lack of study confirming the predicted miRNAs generated from analysis of *T. gondii* genome. As such, more studies should address this gap by conducting more small RNA sequencing experiment with more samples in order to increase the sequencing depth. In addition, re-analysing published data on small RNA-seq data from cells infected with the same type of *T. gondii* by eliminating host sequences then predicting miRNA from unmatched sequences would create a foundation to accurately validate the parasite's miRNAs repertoire. This work however requires collaboration with highly skilled bioinformaticians.

Another gap is related to confirming the hypothesis that *T. gondii* regulates host cells by injecting miRNAs with the highly similar sequence to human miRNAs. Initial work by Saçar *et al*. (2014) has shown that the top 30 predicted *T. gondii* miRNAs hairpins have 88-100% similarity to human miRNAs. Choosing several *T. gondii* miRNAs with the highly similar sequences to human miRNAs but that can still be differentiated by qRT-PCR, then analysis of their expression would be one way to address this hypothesis. Similarly, meta-analysis study on data of published small RNA-seq studies of *T. gondii* infected cells would be an alternative way to address the hypothesis.

The third gap is the lack of a method to culture *T. gondii* without the presence of host cells. As an intracellular parasite, *T. gondii* needed a host cell to proliferate. However, a culture purely made of *T. gondii* parasite without a host cell (axenic condition) would allow studies on the parasites' nutritional needs, biochemical and molecular properties, and sensitivity to antimicrobial agents. This was based on the successful development of an axenic culture of *Plasmodium* spp., (Trager, Zung and Tershakovec, 1990; Schuster, 2002) that contribute hugely to successful anti-malaria drug development. Furthermore, this study has reported several *T. gondii* hypothethical proteins being highly expressed at all time points such as RPL36 and RPS12, but not all of them have been clearly characterised. Characterising these proteins would increase current understanding of *T. gondii* pathogenesis.

In conclusion, alteration in the BBB function by *T. gondii* infection of hBMECs was characterised where new insights into the underlying mechanisms involved in *T. gondii* penetration of the BBB at a transcriptomic level was presented. In addition, this study has discovered key miRNAs plus key *T. gondii* genes involved in *T. gondii* pathogenesis. Our study reports several new findings, which add to the understanding of the mechanisms that regulate and underlie the ability of this pathogen to subvert normal cellular functions at this important biological interface. This thesis also showed the significant anti-*T. gondii* activity of monensin against the tachyzoite stage of this parasite, grown in cerebral endothelial cell and microglial cell cultures and at the same time discovered that Wnt signalling pathway is not up-regulated in *T. gondii*-infected cells, suggesting that this pathway is not essential in the parasite pathogenesis. Additionally, this thesis has characterised the effect of 3-Oxo and PQS at a low and high concentration with and without *T. gondii* infection on hBMECs and provided new insights into the underlying mechanisms involved in 3-Oxo and PQS modulation of the hBMEC monolayer. Quorum sensing molecules data do

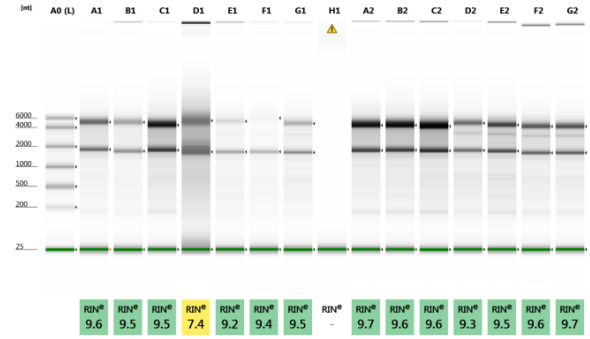
not support the hypothesis that QS molecules from *P. aeruginosa* facilitate *T. gondii* crossing of BBB into the brain. Finally, the hypothesis that *T. gondii* infection with hBMECs induces molecular alterations in gene expression, which can be used as biomarkers or biosignatures specific to infection, was accepted because this thesis discovered several genes and miRNAs, which were altered by infection. Overall, this thesis has achieved all specific aims set at the beginning of this study.

Chapter 7 Appendices

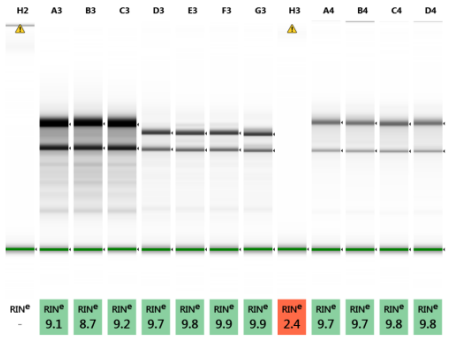
Appendix 3-1: Illumina Bioalayser 2100 total RNA quality results for mRNA sequencing (1/2)

Filename: 2017-02-01-p170043-p170044-BRTape-SQC-AEW.RNA

Gel Image



Default image (Contrast 100%), Image is Scaled to view larger Molecular Weight range



Default image (Contrast 100%), Image is Scaled to view larger Molecular Weight range

Sample Info

Well	RINe	28S/18S (Area)	Conc. [ng/µl]	Sample Description	Alert	Observations
A0	-	-	97.5	Electronic Ladder		Ladder
A1	9.6	1.4	88.5	ELS4403A1-P170044		
B1	9.5	1.1	59.7	ELS4403A2		
C1	9.5	1.8	182	ELS4403A3		
D1	7.4	1.7	131	ELS4403A4		
E1	9.2	0.7	43.8	ELS4403A5		
F1	9.4	0.3	27.8	ELS4403A6		
G1	9.5	1.0	57.2	ELS4403A7		
H1	-	-	4.95	Blank	⚠	RNA concentration outside recommended range for RINe
A2	9.7	2.0	174	ELS4403A8		
B2	9.6	2.1	193	ELS4403A9		
C2	9.6	2.2	233	ELS4403A10		
D2	9.3	1.3	101	ELS4403A11		
E2	9.5	1.6	144	ELS4403A12		
F2	9.6	1.5	111	ELS4403A13		
G2	9.7	1.5	113	ELS4403A14		

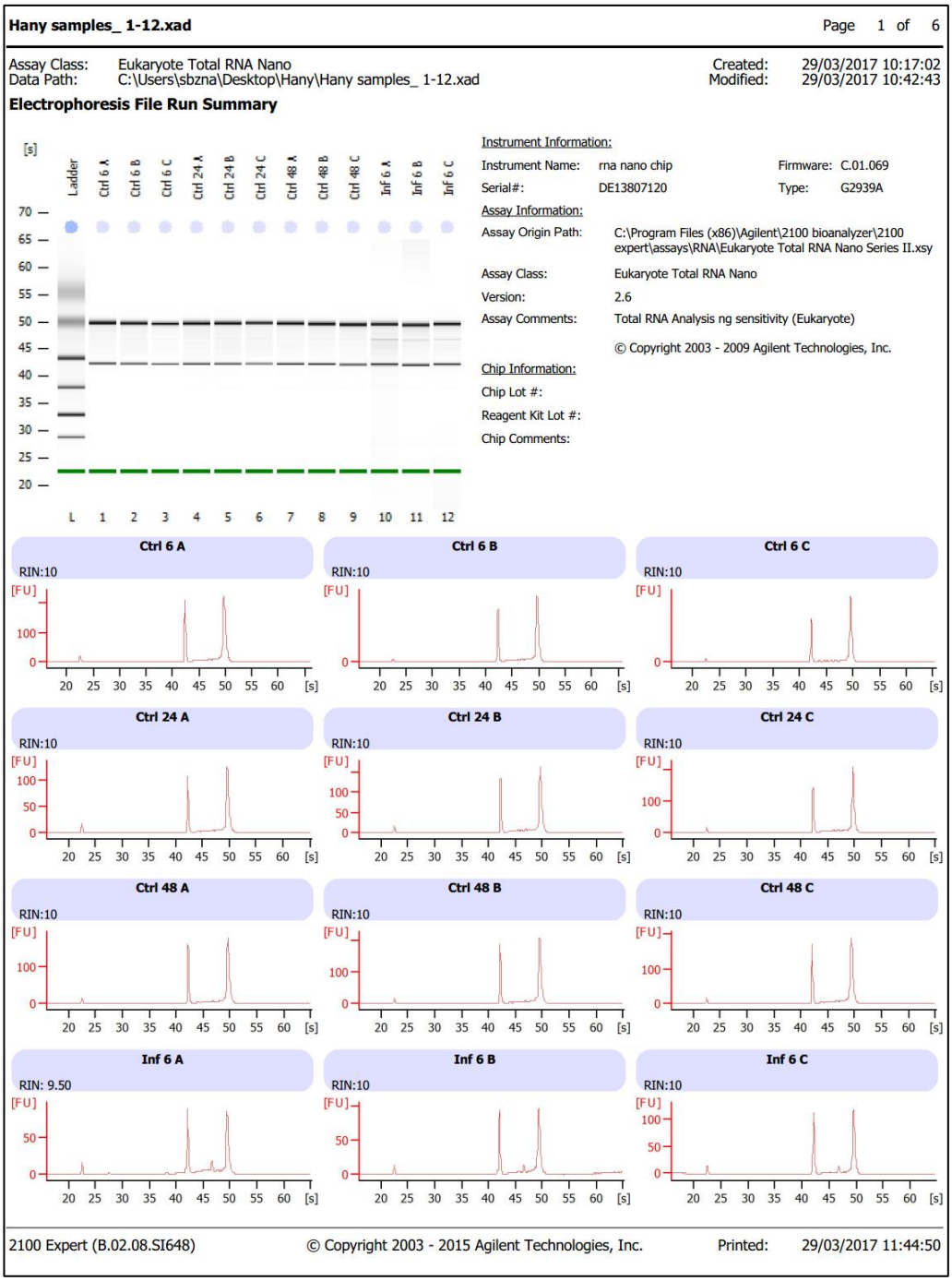
 © Agilent Technologies, Inc. 2015

Appendix 3-1: Illumina Bioalayser 2100 total RNA quality results for mRNA sequencing (2/2)

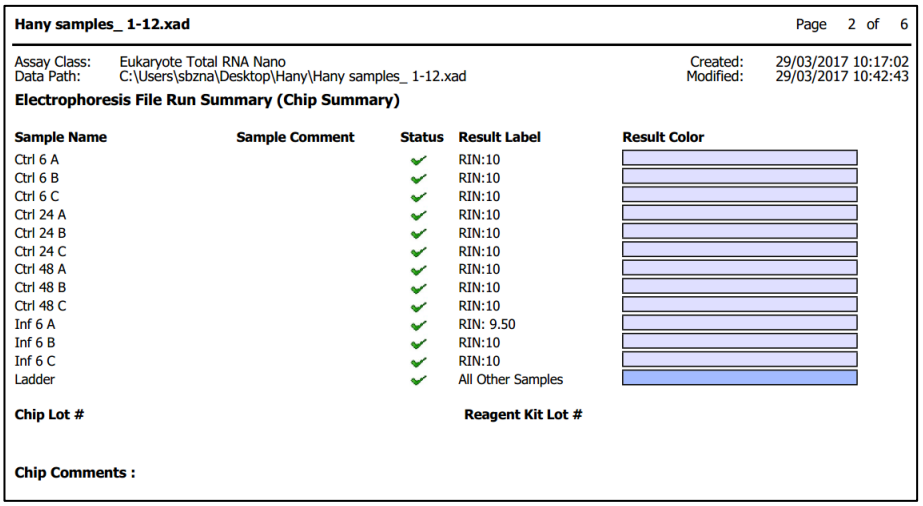
H2	-	-	9.46	Blank	⚠	RNA concentration outside recommended range for RINe
A3	9.1	2.4	325	ELS4403A15		
B3	8.7	2.1	308	ELS4403A16		
C3	9.2	2.3	312	ELS4403A17		
D3	9.7	1.5	85.7	ELS4403A18		
E3	9.8	1.6	80.6	ELS4403A19		
F3	9.9	1.7	77.2	ELS4403A20		
G3	9.9	1.7	81.9	ELS4403A21		
H3	2.4	-	3.46	Blank	⚠	RNA concentration outside recommended range for RINe
A4	9.7	2.9	62.0	RAM4460A1-P170043		
B4	9.7	2.8	63.5	RAM4460A2		
C4	9.8	2.9	66.5	RAM4460A3		
D4	9.8	3.2	63.2	RAM4460A4		

 © Agilent Technologies, Inc. 2015

Appendix 3-2: Illumina Bioalayser 2100 total RNA quality results for microarray sequencing (1/3)



Appendix 3-2: Illumina Bioalayser 2100 total RNA quality results for microarray sequencing (2/3)



Hany samples_ 1-12.xad Page 2 of 6

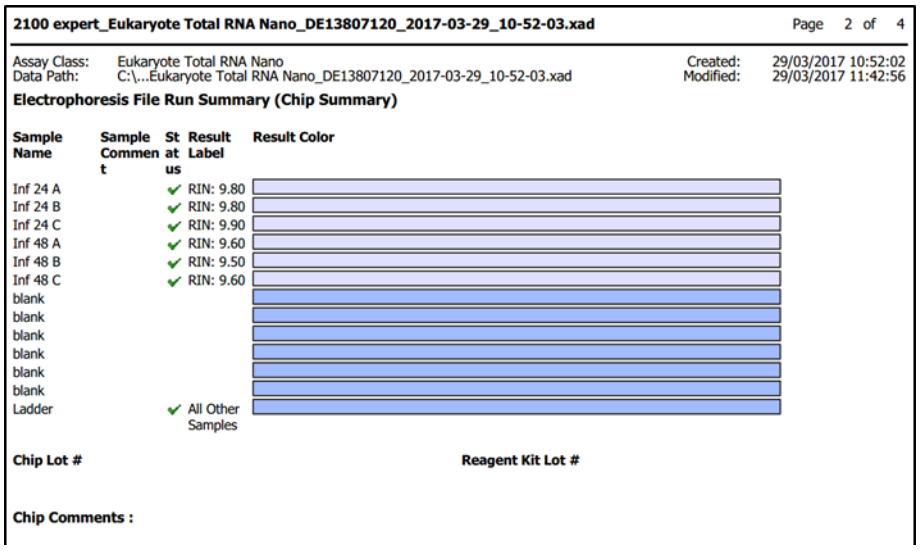
Assay Class: Eukaryote Total RNA Nano
Data Path: C:\Users\sbzna\Desktop\Hany\Hany samples_ 1-12.xad
Created: 29/03/2017 10:17:02
Modified: 29/03/2017 10:42:43

Electrophoresis File Run Summary (Chip Summary)

Sample Name	Sample Comment	Status	Result Label	Result Color
Ctrl 6 A		✓	RIN:10	
Ctrl 6 B		✓	RIN:10	
Ctrl 6 C		✓	RIN:10	
Ctrl 24 A		✓	RIN:10	
Ctrl 24 B		✓	RIN:10	
Ctrl 24 C		✓	RIN:10	
Ctrl 48 A		✓	RIN:10	
Ctrl 48 B		✓	RIN:10	
Ctrl 48 C		✓	RIN:10	
Inf 6 A		✓	RIN: 9.50	
Inf 6 B		✓	RIN:10	
Inf 6 C		✓	RIN:10	
Ladder		✓	All Other Samples	

Chip Lot # **Reagent Kit Lot #**

Chip Comments :



2100 expert_Eukaryote Total RNA Nano_DE13807120_2017-03-29_10-52-03.xad Page 2 of 4

Assay Class: Eukaryote Total RNA Nano
Data Path: C:\...Eukaryote Total RNA Nano_DE13807120_2017-03-29_10-52-03.xad
Created: 29/03/2017 10:52:02
Modified: 29/03/2017 11:42:56

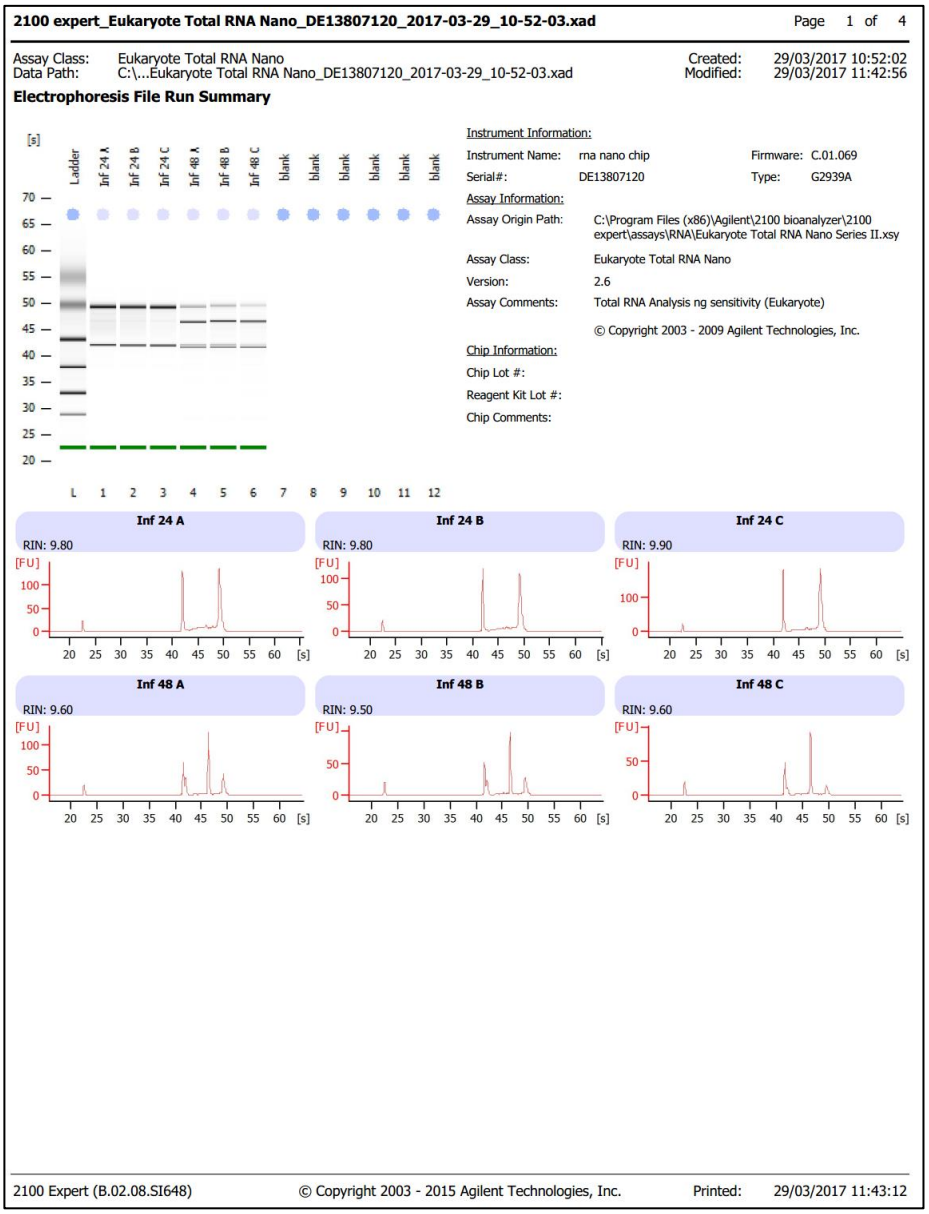
Electrophoresis File Run Summary (Chip Summary)

Sample Name	Sample Comment	Status	Result Label	Result Color
Inf 24 A		✓	RIN: 9.80	
Inf 24 B		✓	RIN: 9.80	
Inf 24 C		✓	RIN: 9.90	
Inf 48 A		✓	RIN: 9.60	
Inf 48 B		✓	RIN: 9.50	
Inf 48 C		✓	RIN: 9.60	
blank				
blank				
blank				
blank				
blank				
blank				
Ladder		✓	All Other Samples	

Chip Lot # **Reagent Kit Lot #**

Chip Comments :

Appendix 3-2: Illumina Bioalayser 2100 total RNA quality results for microarray sequencing (3/3)



Appendix 3-3: R Studio analysis script for mRNA sequencing data analysis

```
---
title: "mRNA RNAseq"
author: "Harun Mohammed"
date: "29 Nov 2017"
output: pdf_document
---

## R Markdown

```{r setup, include=FALSE}
#knitr::opts_chunk$set(echo = TRUE)
echo = FALSE` - to prevent printing of the R code that generated the plot.
```

Set directory
```{r}
setwd("C:/Users/Mohammad Harun/Desktop/chapter 3")
getwd()
```
Affymetrix Analysis of Infected cells
This experiment involves the comparison of infected vs control samples at three time points (6, 24each with 2 replicates for each group.
The experimental design is as follows:
sample|filename|time|treatment | group
control_6a|hisat.WTCHG_356243_281186.5538.gene.counts|6
|control|control6
control_6b|hisat.WTCHG_356243_282174.5538.gene.counts|6
|control|control6
infected_6a| hisat.WTCHG_356243_283162.5538.gene.counts|6
|infected |infected6
infected_6b| hisat.WTCHG_356243_284150.5538.gene.counts|6
|infected |infected6
control_24a| hisat.WTCHG_356243_285138.5538.gene.counts | 24
|control|control24
control_24b|hisat.WTCHG_356243_286126.16092.gene.counts|24|control|co
ntrol24
infected_24a|hisat.WTCHG_356243_287114.16092.gene.counts|24|infected
  |infected24
infected_24b|hisat.WTCHG_356243_288102.16092.gene.counts|
24|infected|infected24
control_48a| hisat.WTCHG_356243_202184.5538.gene.counts
|48|control|control48
control_48b|hisat.WTCHG_356243_203172.5538.gene.counts|48|control|cont
rol48
infected_48a|hisat.WTCHG_356243_204160.5538.gene.counts|48|infected|in
fected48
infected_48b|hisat.WTCHG_356243_205148.5538.gene.counts|48|infected|in
fected48

Initial Setup
```

First we load some modules to start the analysis.
```{r}
#install.packages("GOplot")
#library(GOplot)
library("DESeq2")
library("gplots")
library("RColorBrewer")
#library(limma)
```

Making colour palette 100 colours for nice heatmaps from green to blue
```{r}
hmcol = colorRampPalette(brewer.pal(9, "RdPu"))(100)
```

Reading in Annotation and Count Data
Read the file pdata.txt and the containing gene names(gene_names.txt)
Create a vector containing group name for each sample
Make a vector of colours that correspond to each condition for nicer plots and also colours corresponding to each group
```{r}
pdata=read.table("pdata.txt", header = TRUE)
group=as.vector(pdata$group)
names=read.table("genenames.txt", header=FALSE, row.names = 1)
groupcols=brewer.pal(n=length(unique(group))+2, name="Dark2")
names(groupcols)= unique(group)
typecols=rainbow(44)[names$V4]
#names(typecols)=rownames(names)
```

Next read the actual raw counts derived from HTSeq.
The DESeq2 function has an option 'DESeqDataSetFromHTSeqCount' that reads in counts from HTSeq output files.
Need to provide it with a directory and an appropriate pdata.txt file
```{r}
ddsHTSeq <- DESeqDataSetFromHTSeqCount(sampleTable = pdata, directory = ".", design = ~ group)
# Restrict to protein coding and lincRNA ?
#ddsHTSeq=ddsHTSeq[(names[rownames(ddsHTSeq),"V4"] == "protein_coding") | (names[rownames(ddsHTSeq),"V4"] == "lincRNA"),]
colData(ddsHTSeq)$group <- factor(colData(ddsHTSeq)$group,levels=levels(pdata$group))
```
Data Normalisation
```{r}
# Data Normalisation
dds <- ddsHTSeq
dds <- dds[ rowSums(counts(dds)) > 1, ]
dds <- estimateSizeFactors(ddsHTSeq)
# Data Dispersion
dds <- estimateDispersions(dds)
# New Neg. Binomial test
dds <- nbinomWaldTest(dds)
counts_table=counts(dds,normalised=TRUE)
```

Look at DESeq2 Dispersion plot

```{r}
#win.graph()
pdf(file="dispersion plots.pdf", width = 8, height = 7)
plotDispEsts(dds,main="Dispersion Plot")
```

Post-Normalisation QC

```{r}
#win.graph()
pdf(file="post normalisaton bar plots.pdf", width = 8, height = 7)
par(oma = c(2, 2, 0, 0))
#par(mfrow=c(3,1))
#barplot(colSums(counts(dds, normalised=F)), col=groupcols[as.factor(group)], las=2,cex.names=1.2,main="Pre-Normalised Counts Samples", cex = 1.2, cex.main = 1.8)
#boxplot(counts(dds,normalised=FALSE), col=groupcols[as.factor(group)], las=2,cex.names=1.2,main="Pre-Normalised Counts", cex = 1.2, cex.main = 1.8)
#boxplot(counts(dds,normalised=TRUE), col=groupcols[as.factor(group)], las=2,cex.names=1.2,main="Pre-Normalised Counts", cex = 1.2, cex.main = 1.8)
plot(1, type="n", axes=F, xlab="", ylab="")
legend("center",levels(as.factor(group)),fill=groupcols, cex = 2)
barplot(colSums(counts(dds, normalised=T)), col=groupcols[as.factor(group)], las=2,cex.names=1.2,cex = 1.2, main="Post-Normalised Counts", margins = c(5,20), cex.main = 1.8)
#dev.off()
```

Stabilising the Variance (VST) instead of log2

Regularised log transformation and variance stabilising transformation, these function are usesful to visualise the data. See the DESeq2 manual for more information.

```{r}
vsd <- varianceStabilisingTransformation(dds)
vstMat <- assay(vsd)
counts_table=data.frame(counts_table,vstMat)
```

Sample to Sample Correlation

```{r}
#win.graph()
pdf(file= "sample to sample correlation XX.pdf")
heatmap.2(cor(assay(vsd)),trace="none",margin = c(9,7), main="Samples Correlation Heatmap",cexRow=1.2,cexCol=1.2, keysize = 1.3, dendrogram = c("both"))
```

#Sample to Sample PCA

Sample PCA

```{r}
#win.graph()
pdf(file= "sample to sample correlation pca2 XX.pdf")
pca <- princomp(assay(vsd))
```

```
plot(pca$loadings, main="Principal Component Analysis - Treatment", col="black", bg=groupcols[pdata$group], pch=21, cex=1)
text(pca$loadings, group, pos=2, cex=1)
```

#Statistical Analysis
Now we will perform the statistical tests.
control6 vs infected6
For the test we are looking for how many genes are significantly changed with an Absolute Log2 Fold Change of at least 1 and an Adjusted P-Value of less than 0.01. Lets see how many genes we find.
```{r}
res6X <- results(dds, contrast=c("group","infected6","control6"))
res6X=res6X[order(res6X$padj),]
res6X
hits6X=(rownames(res6X[((res6X$padj <= 0.01) & (abs(res6X$log2FoldChange) >= 1) & (!is.na(res6X$padj))),]))

res6X
write.table(res6X, "res6X.txt", quote = FALSE, sep = "\t", row.names = TRUE)
write.table(hits6X, "hits6X.txt", quote = FALSE, sep = "\t", row.names = TRUE)

res24X <- results(dds, contrast=c("group","infected24","control24"))
res24X=res24X[order(res24X$padj),]
res24X
hits24X=(rownames(res24X[((res24X$padj <= 0.01) & (abs(res24X$log2FoldChange) >= 1) & (!is.na(res24X$padj))),]))
res24X

write.table(res24X, "res24X.txt", quote = FALSE, sep = "\t", row.names = TRUE)
write.table(hits24X, "hits24X.txt", quote = FALSE, sep = "\t", row.names = TRUE)

res48X <- results(dds, contrast=c("group","infected48","control48"))
res48X=res48X[order(res48X$padj),]
res48X
hits48X=(rownames(res48X[((res48X$padj <= 0.01) & (abs(res48X$log2FoldChange) >= 1) & (!is.na(res48X$padj))),]))
res48X
write.table(res48X, "res48X.txt", quote = FALSE, sep = "\t", row.names = TRUE)
write.table(hits48X, "hits48X.txt", quote = FALSE, sep = "\t", row.names = TRUE)
```

#Analysis of Sample Median Data
Sometimes it is useful to compute the median of each sample so we can make some different plots (e.g. pairwise plots).
```{r}
control6_median=apply(vstMat[,1:2],1,median)
infected6_median=apply(vstMat[,3:4],1,median)
#win.graph()
plot(control6_median,infected6_median,pch=19,main=paste("Control 6 vs Infected 6 XX"),col="darkblue",cex=1)
```

```
points(control6_median[hits6X],infected6_median[hits6X],pch=19,col=typecols[hits6X],cex=1)
text(control6_median[hits6X],infected6_median[hits6X],cex=1,pos=4,labels=names[hits6X,"V2"])
abline(a=0,b=1,lty=2,col="red",lwd=2,cex=1)
control24_median=apply(vstMat[,5:6],1,median)
infected24_median=apply(vstMat[,7:8],1,median)

#win.graph()
plot(control24_median,infected24_median,pch=19,main=paste("Control 24 vs Infected 24 XX"),col="darkblue",cex=1)
points(control24_median[hits24X],infected24_median[hits24X],pch=19,col=typecols[hits24X],cex=1)
text(control24_median[hits24X],infected24_median[hits24X],cex=1,pos=4,labels=names[hits24X,"V2"])
abline(a=0,b=1,lty=2,col="red",lwd=2,cex=1)

control48_median=apply(vstMat[,9:10],1,median)
infected48_median=apply(vstMat[,11:12],1,median)

#win.graph()
plot(control48_median,infected48_median,pch=19,main=paste("Control 48 vs Infected 48 XX"),col="darkblue",cex=1)
points(control48_median[hits48X],infected48_median[hits48X],pch=19,col=typecols[hits48X],cex=1)
text(control48_median[hits48X],infected48_median[hits48X],cex=1,pos=4,labels=names[hits48X,"V2"])
abline(a=0,b=1,lty=2,col="red",lwd=2,cex=1)

```

```{r}
pdf(file= "VSD pca2 XX.pdf")
heatmap.2(cor(assay(vsd)),trace="none",main="Sample Correlation Variance Stabilised",col=hmcol,cexRow=0.6,cexCol=0.6)
pca <- princomp(assay(vsd))
plot(pca$loadings, main="PCA Variance Stabilised", col="black", bg=groupcols[pdata$group], pch=21, cex=1)
text(pca$loadings, group, pos=3, cex=0.8)

#X11()
#plot(ctr_median,m210_median,pch=19,main=paste("ctrl vs m210 Biotype"),col="darkblue",cex=0.4)
#points(ctr_median[hits],m210_median[hits],pch=19,col=typecols[hits],cex=0.4)
#points(ctr_median,m210_median,pch=19,col=typecols,cex=0.2)
#text(ctr_median[hits],m210_median[hits],cex=0.4,pos=4,labels=names[hits,"V2"])
#abline(a=0,b=1,lty=2,col="red",lwd=2,cex=0.4)
#legend("topleft",levels(unique(names$V4)),cex=0.4,bty="n",fill=rainbow(44))
```

Post-Statistical QC

Now we will construct a Volcano Plot to highlight each gene's Significance versus its Fold Change. Genes which do not change much usually have poor P-Values

so the plot has low significance around zero and hence looks like a volcano. Some genes may have high fold changes but poor significance, in these cases, usually the foldchanges observed do not replicate well from sample to sample.
Volcano Plot of Significance and Fold Change

```{r}
#win.graph()
pdf(file = "volcano plots c v inf final2 XX.pdf")
plot(res6X$log2FoldChange,-log(res6X$padj,10),ylab="-log10(Adjusted P-value)",xlab="Log2 Fold Change",main=paste("Control 6 hrs vs Infected 6 hrs"),pch=19, cex.main=1.8, cex.names=1.4, cex.axis=1.4, cex = 0.6, cex.lab=1.6)
#text(res6[hits6,]$log2FoldChange,-log(res6[hits6,]$padj,10),labels=names[rownames(res6[hits6,]),"V2"],pos=4, cex=1.3)
points(res6X[hits6X,"log2FoldChange"],-log(res6X[hits6X,"padj"],10),pch=19,cex=1,col=typecols[hits6X])
#legend("topright","Up in Infected\nDown in Control",cex=1)
#legend("topleft","Down in Infected\nUp in Control",cex=1)
abline(h=-log10(0.01),lty=1, lwd = 3,col="red" )
abline(v=-1,lty=2, lwd = 3,col="red")
abline(v=1,lty=2, lwd = 3,col="red" )
#win.graph()
plot(res24X$log2FoldChange,-log(res24X$padj,10),ylab="-log10(Adjusted P-value)",xlab="Log2 Fold Change",main=paste("Control 24 hrs vs Infected 24 hrs"),pch=19,cex.main=1.8, cex.names=1.4, cex.axis=1.4, cex = 0.6, cex.lab=1.6)
#text(res24[hits24,]$log2FoldChange,-log(res24[hits24,]$padj,10),labels=names[rownames(res24[hits24,]),"V2"],pos=4,cex=1.3)
points(res24X[hits24X,"log2FoldChange"],-log(res24X[hits24X,"padj"],10),pch=19,cex=1,col=typecols[hits24X])
#legend("topright","Up in Infected\nDown in Control",cex=1)
#legend("topleft","Down in Infected\nUp in Control",cex=1)
abline(h=-log10(0.01),lty=1, lwd = 3, col="red")
abline(v=-1,lty=2, lwd = 3,col="red")
abline(v=1,lty=2,lwd = 3, col="red")

#win.graph()
plot(res48X$log2FoldChange,-log(res48X$padj,10),ylab="-log10(Adjusted P-value)",xlab="Log2 Fold Change",main=paste("Control 48 hrs vs Infected 48 hrs"),pch=19,cex.main=1.8, cex.names=1.4, cex.axis=1.4, cex = 0.6, cex.lab=1.6)
#text(res48[hits48,]$log2FoldChange,-log(res48[hits48,]$padj,10),labels=names[rownames(res48[hits48,]),"V2"],pos=4,cex=1.3)
points(res48X[hits48X,"log2FoldChange"],-log(res48X[hits48X,"padj"],10),pch=19,cex=1,col=typecols[hits48X])
#legend("topright","Up in Infected\nDown in Control",cex=1)
#legend("topleft","Down in Infected\nUp in Control",cex=1)
abline(h=-log10(0.01),lty=1, lwd = 3, col="red")
abline(v=-1,lty=2,lwd = 3, col="red")
abline(v=1,lty=2, lwd = 3, col="red")

plot(res48X$log2FoldChange,-log(res48X$padj,10),xlab="-log10(Adjusted P-value)",main=paste("Control 48 hrs vs Infected 48
```

```
hrs"),pch=19,cex.main=1.8, cex.names=1.4, cex.axis=1.4, cex = 0.6, cex.lab=1.6)
```

#Heatmap of Signficant Hits
We now compute a heatmap of the most significant hits.
```{r}
#6
pdf(file="significant heatmap6hrs mrna seq XXX.pdf", width = 8, height = 50)
heatmap.2(vstMat[hits6X,],trace="none",col=hmcol,labRow=names[hits6X,"V2"],cexRow=1,cexCol=2,las=2,Colv=FALSE,dendrogram="row",
main="Heatmap Significant Hits 6 hrs",RowSideColors = typecols[hits6X],
margins = c(12,5),
keysize = 2)
#key.par=list(mgp=c(1, 0.5, 0),
#mar=c(1, 1, 1, 0))
#print(heatmap.2)

#24
heatmap.2(vstMat[hits24X,],trace="none",col=hmcol,labRow=names[hits24X,"V2"],cexRow=1,cexCol=1,las=2,Colv=FALSE,dendrogram="row",
main="Heatmap Significant Hits 24 hrs",RowSideColors = typecols[hits24X])
print(heatmap.2)

#48
heatmap.2(vstMat[hits48X,],trace="none",col=hmcol,labRow=names[hits48X,"V2"],cexRow=1,cexCol=1,las=2,Colv=FALSE,dendrogram="row",
main="Heatmap Significant Hits 48 hrs",RowSideColors = typecols[hits48X])
print(heatmap.2)
```

Output Final Results
Let's write the results out to a txt table file called FullCountsandStats.txt*

```{r}
#6
fullresults=merge(names,counts_table,by.x=0,by.y=0)
fullresults=merge(fullresults,as.matrix(res6X),by.x=1,by.y=0)
fullresults=fullresults[order(fullresults$log2FoldChange),]
write.table(fullresults,"FullCountsandStats6.txt",sep="\t")

#24
fullresults=merge(names,counts_table,by.x=0,by.y=0)
fullresults=merge(fullresults,as.matrix(res24X),by.x=1,by.y=0)
fullresults=fullresults[order(fullresults$log2FoldChange),]
write.table(fullresults,"FullCountsandStats24.txt",sep="\t")

#48
fullresults=merge(names,counts_table,by.x=0,by.y=0)
fullresults=merge(fullresults,as.matrix(res48X),by.x=1,by.y=0)
fullresults=fullresults[order(fullresults$log2FoldChange),]
write.table(fullresults,"FullCountsandStats48.txt",sep="\t")
```

Appendix 3-4: R Studio analysis script for microarray data analysis

````
---
title: "Affymetrix Analysis"
author: "Harun Mohammed"
date: "30 Nov 2017"
output: pdf_document
---
```{r setup, include=FALSE}
knitr::opts_chunk$set(echo = FALSE)
```
`echo = FALSE` - to prevent printing of the R code that generated the plot.

# Set directory
```{r}
setwd("D:/microarray data")
getwd()
```

# Affymetrix Analysis of infected cells
This experiment involves the comparison of infected vs control samples at three time points each with three replicates.
The experimental design is as follows:
filename|time|treatment|group
--------|----|---------|-----
Ctrl|6|A.ga.cel|6|ctrl|ctrl_6
Ctrl|6|B.ga.cel|6|ctrl|ctrl_6
Ctrl|6|C.ga.cel|6|ctrl|ctrl_6
Ctrl|24|A.ga.cel|24|ctrl|ctrl_24
Ctrl|24|B.ga.cel|24|ctrl|ctrl_24
Ctrl|24|C.ga.cel|24|ctrl|ctrl_24
Ctrl|48|A.ga.cel|48|ctrl|ctrl_48
Ctrl|48|B.ga.cel|48|ctrl|ctrl_48
Ctrl|48|C.ga.cel|48|ctrl|ctrl_48
Inf|6|A.ga.cel|6|infected|infected_6
Inf|6|B.ga.cel|6|infected|infected_6
Inf|6|C.ga.cel|6|infected|infected_6
Inf|24|A.ga.cel|24|infected|infected_24
Inf|24|B.ga.cel|24|infected|infected_24
Inf|24|C.ga.cel|24|infected|infected_24
Inf|48|A.ga.cel|48|infected|infected_48
Inf|48|B.ga.cel|48|infected|infected_48
Inf|48|C.ga.cel|48|infected|infected_48

## Initial Setup
First we load some modules to start the analysis.

```{r}
library(oligo)
#library(ggplot2)
library(gplots)
library(RColorBrewer)
#library(pvclust)
library(colorspace)
library(limma)
````
````

```
#library(genefilter)
#library(pd.hugene.2.1.st)
library(hugene21sttranscriptcluster.db)
```

Setup Color Palettes, load pdata file
We will make individual colour palettes for group and sample types, and a heatmap colour palette.
We will load the experimental description (pdata.txt) file.
```{r}
hmcol = colorRampPalette(brewer.pal(9, "GnBu"))(100)
setwd("D:/microarray data")
pdata=read.table("pdata.txt",header=TRUE)
pdataPCA=read.table("pdataPCA.txt",header=TRUE)
pdata$group = as.factor(paste(pdata$treatment,pdata$time,sep="_"))
pdata

# Make colour palette by timepoint
time_colours = rev(heat_hcl(n=length((pdata$time))))
names(time_colours)=pdata$time

# Make colour palette by treatment
treat_colours =
brewer.pal(length(unique(pdata$treatment))+1,"Set3")[as.factor(pdata$treat
ment)]
names(treat_colours)=pdata$treatment

# Colours for each group (treatment and time)
group_colours =
brewer.pal(length(unique(pdata$group)),"Set3")[as.factor(pdata$group)]
names(group_colours)=pdata$group
```

Affymetrix Loading and Normalisation
Load the CEL files and summarised the unnormalised raw expression data using oligo package
Normalised the expression using Robust multi-array average normalisation (RMA)
```{r}
geneCELs = as.character(pdata$filename)

# Prenormalised object-> all expression all probes
affyGeneFS <- read.celfiles(geneCELs)

# Post normalised RMA -> core expression by gene
geneCore <- rma(affyGeneFS, target = "core")
```

Quality Control
Raw expression level accross samples before and after normalisation
```{r}
#x11()
#par(mfrow=c(2,1))
#pdf(file= "Pre-Normalisation2.pdf", height=7, width=8)
#pdf(file= "Legend boxplot.pdf")
#par(oma = c(2.5, 1, 0, 0))
```

```
#boxplot(affyGeneFS,target="core",las=3,cex.axis=1.12,main="Pre-
Normalisation",col=group_colours, ylab="Log2 Expression",
#        cex.lab = 1.5, cex.main=1.8)
#xlab="Samples"

#par(fig = c(0, 1, 0, 1), oma = c(0, 0, 0, 0), mar = c(1, 0, 0, 0), new = TRUE)
#plot(0, 0, type = "n", bty = "n", xaxt = "n", yaxt = "n")
#text(0, 0, labels = "Samples", cex = 1.1)

#legend("bottom",
levels(pdata$group),fill=group_colours[levels(pdata$group)], xpd = TRUE,
     #horiz = TRUE,
     #inset = c(0, 0),
     #bty = "n", cex = 2)get
#par(fig=c(0, 1, 0, 1), oma=c(0, 0, 0, 0), mar=c(0, 0, 0, 0), new=TRUE)
#par(xpd=TRUE, margin (t = 1, r= 10, b = 5, l = 1, unit = "pt"))
#legend("bottom",
levels(pdata$group),fill=group_colours[levels(pdata$group)],cex=0.9)
#pdf(file= "Post-Normalisation.pdf", height= 7, width = 8)
#par(oma = c(2.5, 1, 0, 0))
#pdf(file= "samples legend Normalisation.pdf", height= 7, width = 8)
#ar(mfrow=c(2,1))
#boxplot(geneCore,              las=3,cex.axis=1.12,main="Post-Normalisation
Samples",col=group_colours, ylab="Log2 Expression",
#      cex.lab = 1.5, cex.main=1.8)
#legend(2,levels(pdata$group),fill=group_colours[levels(pdata$group)],   cex
= 1.7)
#legend("bottom",horiz=TRUE,
levels(pdata$group),fill=group_colours[levels(pdata$group)],cex=0.9)
```

Heatmap to view sample to sample correlation

```{r}
#x11()
pdf(file= "sample correlation pop.pdf")
#pdf(file= "key heatmap sample correlation.pdf")
heatmap.2(cor(exprs(geneCore)),col=hmcol,trace="none",margin=c(10,10),c
exRow=1.5,cexCol=1.5,ColSideColors=time_colours,RowSideColors=group_c
olours, keysize = 1.2, dendrogram = c("both"), main="Samples Correlation
Heatmap", cex.main=2
       #lhei = c(6,15))
```

Draw PCA plots for exploring the effect of Time, Treatment and Group

```{r}
#x11()
#par(mfrow=c(3,1))
pdf(file= "pca time.pdf")
pca <- princomp(exprs(geneCore))
#plot(pca$loadings, main="Principal Component Analysis - Time",
  #  col=time_colours,
  #  pch = c( 9, 9, 9, 9, 12, 12, 12, 12, 15, 15, 15, 15, 18, 18, 18, 18),
  #  cex=3)
#text(pca$loadings, as.character(pdata$filename), pos=2, cex=1)
#par(xpd= T, mar = c(0,0,0,7))
plot(pca$loadings,
```

```
    main = "Principal Component Analysis - Time",
    xlab = "First component",
    ylab = "Second component",
    col = c( "orange", "orange", "orange",
           "green", "green", "green",
           "purple", "purple", "purple",
           "black", "black", "black",
           "blue", "blue", "blue",
           "red", "red", "red")[pdata[, 1]],
    pch = c( 15, 15, 15, 17, 17, 17, 19, 19, 19, 3, 3, 3, 25, 25, 25, 23, 23,
23)[pdata[, 1]],
    cex = 2
  # ylim (-1,NA), xlim(-0.28,NA)          )
#text(pca$loadings, as.character(pdataPCA$filename), pos=1, cex=1)
legend("bottomright", cex = 1.1,
      as.character(pdataPCA$filename),
      col = c( "orange", "orange", "orange",
           "green", "green", "green",
           "purple", "purple", "purple",
           "black", "black", "black",
           "blue", "blue", "blue",
           "red", "red", "red")[pdata[, 1]],
    pch = c( 15, 15, 15, 17, 17, 17, 19, 19, 19, 3, 3, 3, 25, 25, 25, 23, 23,
23)[pdata[, 1]]     )
      #lwd = 1,
      #lty = 1

#c("Ctrl 6 A.ga.cel", "Ctrl 6 B.ga.cel", "Ctrl 6 C.ga.cel",
#"Ctrl 24 A.ga.cel", "Ctrl 24 B.ga.cel", "Ctrl 24 C.ga.cel",
#"Ctrl 48 A.ga.cel", "Ctrl 48 B.ga.cel", "Ctrl 48 C.ga.cel",
#"Inf 6 A.ga.cel", "Inf 6 B.ga.cel", "Inf 6 C.ga.cel",
#"Inf 24 A.ga.cel", "Inf 24 B.ga.cel", "Inf 24 C.ga.cel",
#"Inf 48 A.ga.cel", "Inf 48 B.ga.cel". "Inf 48 C.ga.cel"),
#pch = c( 9, 9, 9, 9, 12, 12, 12, 12, 15, 15, 15, 15, 18, 18, 18, 18)
#)

#pca <- princomp(exprs(geneCore))
#plot(pca$loadings, main="PCA Treatment", col=treat_colours,    pch=19,
cex=2)
#text(pca$loadings, as.character(pdata$filename), pos=3, cex=1)

#pca <- princomp(exprs(geneCore))
#plot(pca$loadings, main="PCA Group", col=group_colours,  pch=19, cex=2)
#text(pca$loadings, as.character(pdata$filename), pos=3, cex=1)

#Notice particularly par(xpd = T, mar = par()$mar + c(0,0,0,7)) which allows
us to display stuff outside the plotting area. The default value for xpd which is
NA means that the plot will cover the whole image. When specifying xpd = T,
the plotting will be clipped to the figure region. We then extend the margins on
our graph to give us space to display our legends with mar = par()$mar +
c(0,0,0,7). Finally, we restore mar to its default value: par(mar=c(5, 4, 4, 2)
+ 0.1)
```
Extract Annotation Information for each probe from Annotation package
```{r}
probes = rownames(expression)
```

```
genesymbols = unlist(mget(probes,hugene21sttranscriptclusterSYMBOL,ifnotfound=NA))
genedescs = unlist(mget(probes,hugene21sttranscriptclusterGENENAME,ifnotfound=NA))

featureData(geneCore) <- getNetAffx(geneCore, "transcript")

lincrnas=grep("gene_biotype:lincRNA",pData(featureData(geneCore))[, "mrnaassignment"])
protein_coding=grep("gene_biotype:protein_coding",pData(featureData(geneCore))[, "mrnaassignment"])
non_coding=grep("gene_biotype:non_coding",pData(featureData(geneCore))[, "mrnaassignment"])

# Restrict to protein coding ?
expression=exprs(geneCore)[protein_coding,]
```

Perform Statitstical Test
T-test with groups as a factor
times as a factor = times <- as.facor(pdata$time)

```{r}
groups <- as.factor(pdata$group)
design <- cbind(model.matrix(~0+groups))
colnames(design) = levels(groups)
design
```

Contrast
Create a differential expression control versus infected at each time point (horizontal comparison)
```{r}
# horizontal 6 hrs
c1 = "ctrl_6-infected_6"
# horizontal 24 hrs
c2 = "ctrl_24-infected_24"
# horizontal 48 hrs
c3 = "ctrl_48-infected_48"
# vertical 6 hrs
c4 = "infected_6-infected_24"
# vertical 24 hrs
c5 = "infected_6-infected_48"
# vertical 48 hrs
c6 = "infected_24-infected_48"
contrast.matrix <- makeContrasts(c1,c2,c3,c4,c5,c6, levels=design)
contrast.matrix
```

Fit the linear Model - run the t-test
```{r}
fit <- lmFit(expression, design)
fit2 <- eBayes(contrasts.fit(fit, contrast.matrix))
```

Transfer the Annotation Data to the fit2 object

```{r}
fit2$genes$Symbol = genesymbols[as.character(rownames(fit2))]
fit2$genes$Description = genedescs[as.character(rownames(fit2))]
```

Set threshold for significance and fold change
```{r}
p_value_cutoff=0.05
lfc_cutoff=1
```

Volcanoplot of significance versus fold-change
```{r}
pdf(file = "volcanoplot.pdf", height=7, width=8)
# ctrl 6 vs infected 6


#plot(res$log2FoldChange,-log(res$padj,10),ylab="-log10(Adjusted
P)",xlab="Log2 FoldChange",main=paste("Volcano Plot Ctrl v
miR210_oe"),pch=19,cex=0.2)
#text(res[hits,]$log2FoldChange,-
log(res[hits,]$padj,10),labels=names[rownames(res[hits,]),"V2"],pos=3,cex=
0.4)
#points(res[hits,"log2FoldChange"],-
log(res[hits,"padj"],10),pch=19,cex=0.4,col=typecols[hits])
#legend("topleft","Up in 210\nDown in Ctrl",cex=0.5)
#legend("topright","Down in 210\nUp in Ctrl",cex=0.5)
#abline(h=-log10(0.05),lty=3)
#abline(v=-1,lty=3)
#abline(v=1,lty=3)

#x11()
volcanoplot(fit2,coef=1,highlight=5,names=fit2$genes$Symbol,xlim=c(-
3,3),main="Control 6 hrs vs Infected 6 hrs", cex.main=1.8, cex.names=1.4,
cex.axis=1.4, cex = 0.5, cex.lab=1.6)
abline(h=-log(p_value_cutoff,exp(1)),col="red",lty=1, lwd = 2)
abline(v=-(lfc_cutoff),col="red",lty=2, lwd = 2)
abline(v=(lfc_cutoff),col="red",lty=2, lwd = 2)

# ctrl 24 vs infected 24
#x11()
volcanoplot(fit2,coef=2,highlight=5,names=fit2$genes$Symbol,xlim=c(-
3,3),main="Control 24 hrs vs Infected 24 hrs", cex.main=1.8, cex.names=1.4,
cex.axis=1.4, cex = 0.5, cex.lab=1.6)
abline(h=-log(p_value_cutoff,exp(1)),col="red",lty=1, lwd = 2)
abline(v=-(lfc_cutoff),col="red",lty=2,lwd = 2 )
abline(v=(lfc_cutoff),col="red",lty=2, lwd = 2)

# ctrl 48 vs infected 48
#x11()
volcanoplot(fit2,coef=3,highlight=5,names=fit2$genes$Symbol,xlim=c(-
4,4),main="Control 48 hrs vs Infected 48 hrs",cex.main=1.8, cex.names=1.4,
cex.axis=1.4, cex = 0.5, cex.lab=1.7)
abline(h=-log(p_value_cutoff,exp(1)),col="red",lty=1,lwd = 2 )
abline(v=-(lfc_cutoff),col="red",lty=2, lwd = 2)
abline(v=(lfc_cutoff),col="red",lty=2, lwd = 2)
```

```
# infected 6 v 24
#x11()
volcanoplot(fit2,coef=4,highlight=5,names=fit2$genes$Symbol,xlim=c(-3.5,3.5),main="Infected 6 hrs v Infected 24 hrs", xlab = "-log10(P-value)", cex.lab=1.7)
#abline(h=-log(p_value_cutoff,exp(1)),col="red",lty=1)
#abline(v=-(lfc_cutoff),col="red",lty=2)
#abline(v=(lfc_cutoff),col="red",lty=2)

# infected 6 v 48
#x11()
#volcanoplot(fit2,coef=5,highlight=5,names=fit2$genes$Symbol,xlim=c(-3.9,3.9),main="Infected 6 hrs v Infected 48 hrs")
#abline(h=-log(p_value_cutoff,exp(1)),col="red",lty=1)
#abline(v=-(lfc_cutoff),col="red",lty=2)
#abline(v=(lfc_cutoff),col="red",lty=2)

# infected 24 v 48
#x11()
#volcanoplot(fit2,coef=6,highlight=5,names=fit2$genes$Symbol,xlim=c(-5,5),main="Infected 24 hrs v Infected 48 hrs")
#abline(h=-log(p_value_cutoff,exp(1)),col="red",lty=1)
#abline(v=-(lfc_cutoff),col="red",lty=2)
#abline(v=(lfc_cutoff),col="red",lty=2)
```

Venn diagrams of significant hits.p-0.05

```{r}
result <- decideTests(fit2, p.value=p_value_cutoff, lfc=lfc_cutoff, adjust="BH")
#x11()
#par(mfrow=c(2,1))
pdf(file= "ven diagram microarray.pdf")
vennDiagram(result[,1:3], include=c("up","down"), circle.col=1:4, main="Venn Diagram: Control vs Infected",names=c("6 hrs","24 hrs","48 hrs"))

vennDiagram(result[,4:6], include=c("up","down"), circle.col=2:4, main="Venn Diagram: Infected vs Infected",names=c("6/24 hrs","6/48 hrs","24/48 hrs"))
```

List of significant hits for heatmap p-=0,05, 1 to 6

```{r}
stats = topTable(fit2,coef=1,number=10000000)
significant1 = rownames(stats[(stats[,"adj.P.Val"] < p_value_cutoff) & (abs(stats[,"logFC"]) > lfc_cutoff),])
stats = topTable(fit2,coef=2,number=10000000)
significant2 = rownames(stats[(stats[,"adj.P.Val"] < p_value_cutoff) & (abs(stats[,"logFC"]) > lfc_cutoff),])

stats = topTable(fit2,coef=3,number=10000000)
significant3 = rownames(stats[(stats[,"adj.P.Val"] < p_value_cutoff) & (abs(stats[,"logFC"]) > lfc_cutoff),])
total_significant_by_infection=unique(c(significant1,significant2,significant3))
```

```
stats = topTable(fit2,coef=4,number=10000000)
significant4 = rownames(stats[(stats[,"adj.P.Val"] < p_value_cutoff) & (abs(stats[,"logFC"]) > lfc_cutoff),])
stats = topTable(fit2,coef=5,number=10000000)
significant5 = rownames(stats[(stats[,"adj.P.Val"] < p_value_cutoff) & (abs(stats[,"logFC"]) > lfc_cutoff),])
stats = topTable(fit2,coef=6,number=10000000)
significant6 = rownames(stats[(stats[,"adj.P.Val"] < p_value_cutoff) & (abs(stats[,"logFC"]) > lfc_cutoff),])
total_significant_by_time=unique(c(significant4,significant5,significant6))
```

List of significant hits for heatmap p-=0,01, 1 to 3 -> only for mRNA seq

```
p_value_cutoff=0.01
lfc_cutoff=1
stats = topTable(fit2,coef=1,number=10000000)
significant1 = rownames(stats[(stats[,"adj.P.Val"] < p_value_cutoff) & (abs(stats[,"logFC"]) > lfc_cutoff),])
stats = topTable(fit2,coef=2,number=10000000)
significant2 = rownames(stats[(stats[,"adj.P.Val"] < p_value_cutoff) & (abs(stats[,"logFC"]) > lfc_cutoff),])
stats = topTable(fit2,coef=3,number=10000000)
significant3 = rownames(stats[(stats[,"adj.P.Val"] < p_value_cutoff) & (abs(stats[,"logFC"]) > lfc_cutoff),])
total_significant=unique(c(significant1,significant2,significant3))
```

List of DEG at all hrs

```{r}
list=merge((exprs(geneCore)),topTable(fit2,coef=1,number=1000000000000),by.x=0,by.y=0)
list=list[order(list$logFC),]
write.table(list,paste(c1,".results.txt",sep=""),sep="\t",quote=F)

list=merge((exprs(geneCore)),topTable(fit2,coef=2,number=1000000000000),by.x=0,by.y=0)
list=list[order(list$logFC),]
write.table(list,paste(c2,".results.txt",sep=""),sep="\t",quote=F)

list=merge((exprs(geneCore)),topTable(fit2,coef=3,number=1000000000000),by.x=0,by.y=0)
list=list[order(list$logFC),]
write.table(list,paste(c3,".results.txt",sep=""),sep="\t",quote=F)

list=merge((exprs(geneCore)),topTable(fit2,coef=4,number=1000000000000),by.x=0,by.y=0)
list=list[order(list$logFC),]
write.table(list,paste(c4,".results.txt",sep=""),sep="\t",quote=F)

list=merge((exprs(geneCore)),topTable(fit2,coef=5,number=1000000000000),by.x=0,by.y=0)
list=list[order(list$logFC),]
write.table(list,paste(c5,".results.txt",sep=""),sep="\t",quote=F)

list=merge((exprs(geneCore)),topTable(fit2,coef=6,number=1000000000000),by.x=0,by.y=0)
list=list[order(list$logFC),]
```

```
write.table(list,paste(c6,".results.txt",sep=""),sep="\t",quote=F)
```

All significant genes heat map - too many genes
```{r}
heatmap.2(exprs(geneCore)[significant1,],trace="none",col=hmcol,ColSideCo
lors = group_colours,main="Sig. List 1")
heatmap.2(exprs(geneCore)[significant2,],trace="none",col=hmcol,ColSideCo
lors = group_colours,main="Sig. List 2")
heatmap.2(exprs(geneCore)[significant3,],trace="none",col=hmcol,ColSideCo
lors = group_colours,main="Sig. List 3")
heatmap.2(exprs(geneCore)[significant4,],trace="none",col=hmcol,ColSideCo
lors = group_colours,main="Sig. List 4")
heatmap.2(exprs(geneCore)[significant5,],trace="none",col=hmcol,ColSideCo
lors = group_colours,main="Sig. List 5")
heatmap.2(exprs(geneCore)[significant6,],trace="none",col=hmcol,ColSideCo
lors = group_colours,main="Sig. List 6")
```

top 30 most significant genes heatmap
```{r}
#win.graph()
#x11()
#png(filename = "Control 6 hrs vs Infected 6 hrs",    # create PNG for the heat
map
# width = 600,        # 5 x 300 pixels
# height = 600,
# bg = "white",  # background
#res = 6,           # 300 pixels per inch
# pointsize = 9)       # smaller font size
#dev.off()
pdf(file= "heatmap c6 vinf6.pdf")
heatmap.2(exprs(geneCore)[significant1[1:min(30,length(significant1))],],tra
ce="none",scale="none",col=hmcol,ColSideColors =
group_colours,main="Control 6 hrs vs Infected 6 hrs",
labRow=fit2[significant1,]$genes$Symbol,
        margins=c(9.8,6.8),
        cexRow = 1.4, cexCol = 1.5)

#win.graph()
pdf(file= "heatmap c24 v inf24.pdf")
heatmap.2(exprs(geneCore)[significant2[1:min(30,length(significant2))],],tra
ce="none",col=hmcol,ColSideColors = group_colours,main="Control 24 hrs vs
Infected 24 hrs", labRow=fit2[significant2,]$genes$Symbol,
        margins=c(9.8,6.8),
        cexRow = 1.4, cexCol = 1.5)

#win.graph()
pdf(file= "heatmap c48 v inf48.pdf")
heatmap.2(exprs(geneCore)[significant3[1:min(30,length(significant3))],],tra
ce="none",col=hmcol,ColSideColors = group_colours,main="Control 48 hrs vs
Infected 48 hrs", labRow=fit2[significant3,]$genes$Symbol,
          margins=c(9.8,6.8),
        cexRow = 1.4, cexCol = 1.5)

#win.graph()
```

```
pdf(file= "heatmap Infected 6 v inf24.pdf")
heatmap.2(exprs(geneCore)[significant4[1:min(30,length(significant4))],],tra
ce="none",col=hmcol,ColSideColors = group_colours,main="Infected 6 hrs vs
Infected 24 hrs", labRow=fit2[significant4,]$genes$Symbol,
        margins=c(9.8,6.8),
        cexRow = 1.4, cexCol = 1.5)

#win.graph()
heatmap.2(exprs(geneCore)[significant5[1:min(30,length(significant5))],],tra
ce="none",col=hmcol,ColSideColors = group_colours,main="Infected 6 hrs vs
Infected 48 hrs", labRow=fit2[significant5,]$genes$Symbol,
        margins=c(9.8,6.8),
        cexRow = 1.4, cexCol = 1.5)

#win.graph()
heatmap.2(exprs(geneCore)[significant6[1:min(30,length(significant6))],],tra
ce="none",col=hmcol,ColSideColors = group_colours,main="Infected 24 hrs vs
Infected 48 hrs", labRow=fit2[significant6,]$genes$Symbol,
        margins=c(9.8,6.8),
        cexRow = 1.4, cexCol = 1.5)
```

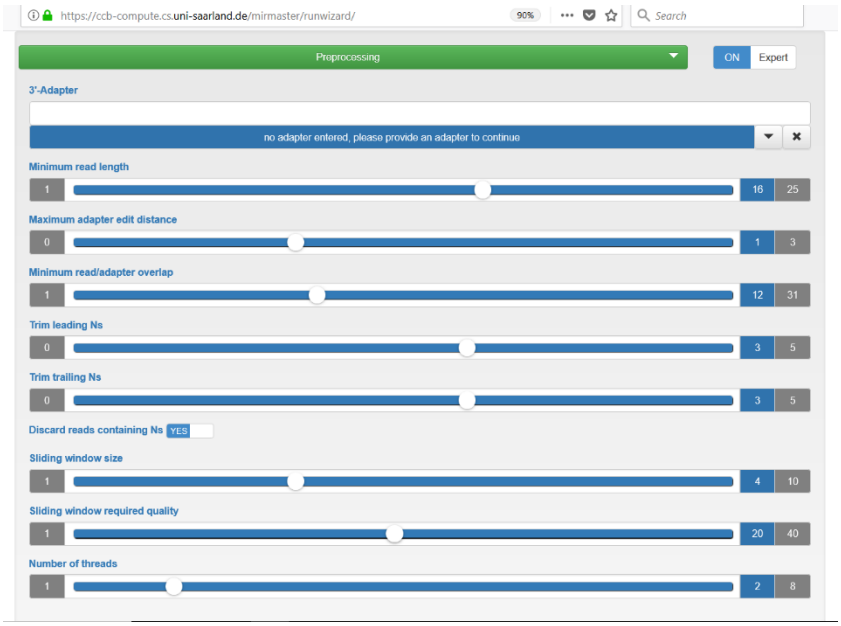
Writing data to a file

```{r}
write.table(exprs(geneCore),"expression_normalised.txt",sep="\t")
#write.table(filtered, "expression_filtered.txt", sep="/t")
exprestion=exprs(geneCore)
```

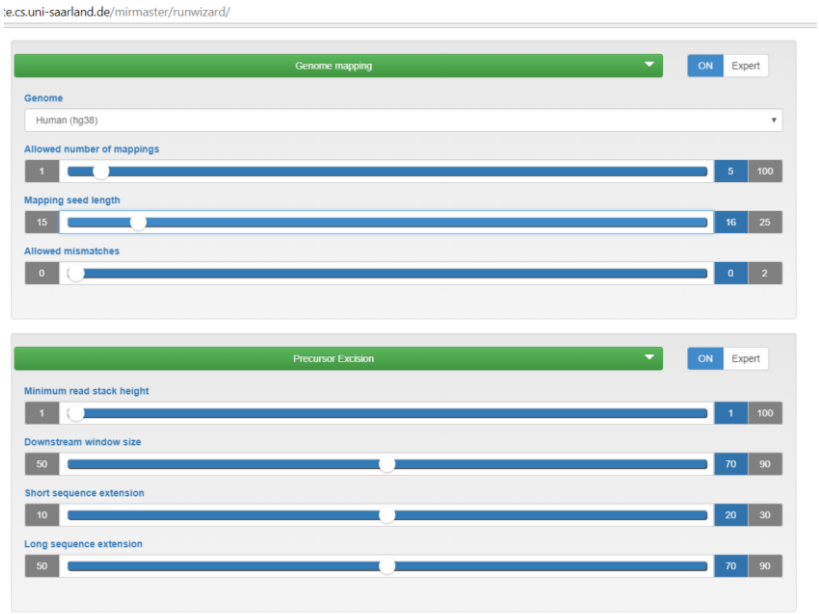
```{r}
final=as.data.frame(exprestion)
final$Symbol=genesymbols[rownames(expression)]
final$Desc=genedescs[rownames(expression)]
write.table(final, "biolayout_table.txt",sep="/t")
```

Appendix 3-5: miRMaster setting (1/2)

Processing

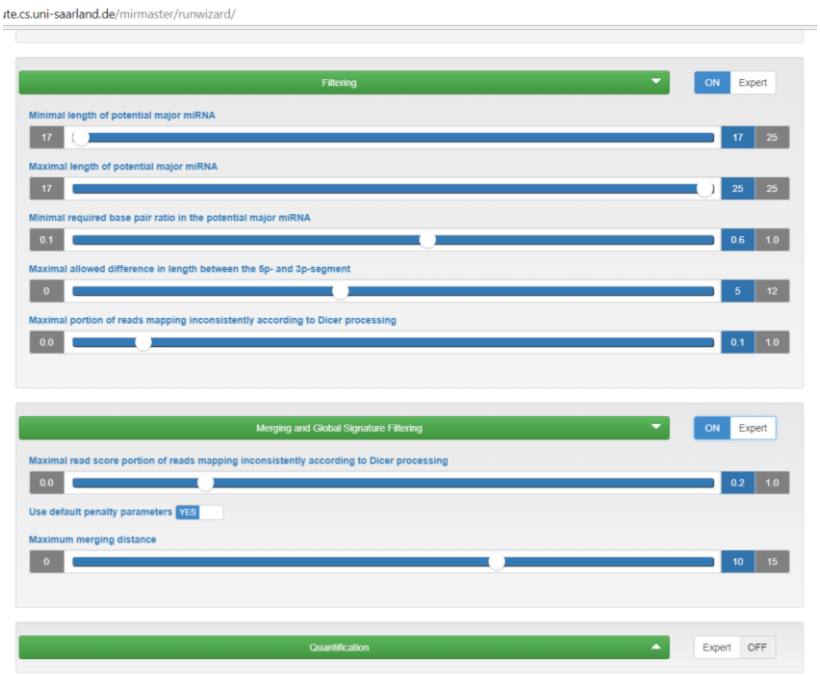


Genome mapping and precursor excision



Appendix 3-5: miRMaster setting (2/2)

Filtering + merging and global signature filtering



Quantification



Appendix 3-6: Full list of DEGs (287 down-regulated and 57 up-regulated) at 6 h.p.i of mRNA sequencing.

#in Excel file

Appendix 3-7: PANTHER Overrepresentation Test identified 43 significantly down-regulated biological processes (mRNA sequencing at 6 h.p.i)

No.	PANTHER GO-Slim Biological Process
1	biological regulation (GO:0065007)
2	biosynthetic process (GO:0009058)
3	catabolic process (GO:0009056)
4	cellular component biogenesis (GO:0044085)
5	cellular component organisation (GO:0016043)
6	cellular component organisation or biogenesis (GO:0071840)
7	cellular process (GO:0009987)
8	DNA metabolic process (GO:0006259)
9	DNA replication (GO:0006260)
10	generation of precursor metabolites and energy (GO:0006091)
11	immune response (GO:0006955)
12	intracellular protein transport (GO:0006886)
13	localisation (GO:0051179)
14	metabolic process (GO:0008152)
15	mRNA processing (GO:0006397)
16	mRNA splicing, *via* spliceosome (GO:0000398)
17	multicellular organismal process (GO:0032501)
18	neurological system process (GO:0050877)
19	nitrogen compound metabolic process (GO:0006807)
20	nuclear transport (GO:0051169)
21	nucleobase-containing compound metabolic process (GO:0006139)
22	organelle organisation (GO:0006996)
23	oxidative phosphorylation (GO:0006119)
24	phosphate-containing compound metabolic process (GO:0006796)
25	primary metabolic process (GO:0044238)
26	protein lipidation (GO:0006497)
27	protein localisation (GO:0008104)

28	protein metabolic process (GO:0019538)
29	protein targeting (GO:0006605)
30	protein transport (GO:0015031)
31	regulation of translation (GO:0006417)
32	respiratory electron transport chain (GO:0022904)
33	RNA metabolic process (GO:0016070)
34	RNA splicing, *via* transesterification reactions (GO:0000375)
35	rRNA metabolic process (GO:0016072)
36	sensory perception (GO:0007600)
37	sensory perception of chemical stimulus (GO:0007606)
38	sensory perception of smell (GO:0007608)
39	single-multicellular organism process (GO:0044707)
40	system process (GO:0003008)
41	translation (GO:0006412)
42	transport (GO:0006810)
43	Unclassified (UNCLASSIFIED)

Appendix 3-8: Full list of 58 up-regulated genes at 24 h.p.i of mRNA sequencing.

#in Excel file

Appendix 3-9: Full list of DEGs (249 down-regulated and 693 up-regulated) at 48 h.p.i of mRNA sequencing.

#in Excel file

Appendix 3-10: List of log_2 FC from 94 *T. gondii* genes highly up-regulated at 6, 24 and 48 h.p.i.

Gene ID	Log_2 FC		
	6 hours	24 hours	48 hours
TGME49_200360-t26_1	10.292	7.419	14.719
TGME49_201390-t26_1	13.684	8.074	13.968
TGME49_203310-t26_1	12.040	8.750	15.501
TGME49_204020-t26_1	13.970	9.018	12.463
TGME49_204530-t26_1	12.275	7.980	12.875
TGME49_205340-t26_1	13.920	8.292	14.045
TGME49_205700-t26_1	13.558	8.417	12.517
TGME49_207400-t26_1	10.144	7.715	14.762
TGME49_208030-t26_1	10.058	9.038	14.205
TGME49_209030-t26_1	12.388	8.530	12.605
TGME49_210408-t26_1	10.135	8.840	13.662
TGME49_210690-t26_1	13.211	9.084	13.762
TGME49_211680-t26_1	12.705	8.450	13.911
TGME49_212270-t26_1	10.563	7.596	12.105
TGME49_212290-t26_1	13.341	9.209	13.588
TGME49_213280-t26_1	12.805	7.800	13.597
TGME49_213350-t26_1	13.696	9.061	13.593
TGME49_213580-t26_1	12.992	8.799	12.032
TGME49_214940-t26_1	13.162	8.166	12.978
TGME49_215460-t26_1	13.665	8.458	14.016
TGME49_215470-t26_1	13.338	8.960	13.599
TGME49_215960-t26_1	10.721	7.943	14.702
TGME49_217570-t26_1	13.941	9.488	14.478
TGME49_218260-t26_1	12.995	8.600	12.801
TGME49_218520-t26_1	11.348	8.475	14.322
TGME49_220400-t26_1	11.358	9.120	14.291
TGME49_220950-t26_1	10.993	8.554	14.634
TGME49_225080-t26_1	13.856	9.071	13.923
TGME49_227280-t26_1	13.238	8.332	14.433
TGME49_227360-t26_1	12.737	8.936	13.252
TGME49_227620-t26_1	13.052	8.311	14.287
TGME49_229670-t26_1	13.244	8.638	12.163
TGME49_230160-t26_1	10.544	11.011	14.672
TGME49_231140-t26_1	12.040	9.486	13.775
TGME49_232350-t26_1	10.581	9.340	11.777
TGME49_232710-t26_1	12.809	8.886	14.256
TGME49_233460-t26_1	11.403	8.591	14.318
TGME49_234450-t26_1	12.320	8.980	12.255
TGME49_238250-t26_1	13.566	10.126	13.629
TGME49_239100-t26_1	13.878	9.194	14.222
TGME49_239330-t26_1	13.693	8.599	13.959

TGME49_239740-t26_1	10.821	8.412	13.153
TGME49_239760-t26_1	11.907	8.978	13.972
TGME49_242330-t26_1	13.726	8.880	13.950
TGME49_242340-t26_1	13.684	9.150	13.590
TGME49_245460-t26_1	13.423	9.420	11.612
TGME49_245680-t26_1	13.350	9.460	13.579
TGME49_248390-t26_1	13.259	8.623	13.795
TGME49_248480-t26_1	13.486	8.494	12.107
TGME49_249250-t26_1	13.296	8.885	13.703
TGME49_249850-t26_1	10.979	9.068	13.707
TGME49_250710-t26_1	12.976	8.773	15.634
TGME49_250770-t26_1	13.574	9.488	14.276
TGME49_251810-t26_1	13.405	9.031	13.282
TGME49_254720-t26_1	12.588	9.609	14.286
TGME49_255260-t26_1	10.462	8.730	13.554
TGME49_261740-t26_1	11.687	8.610	13.906
TGME49_262690-t26_1	13.422	8.601	12.421
TGME49_263040-t26_1	13.780	9.166	12.473
TGME49_263090-t26_1	11.417	8.332	13.840
TGME49_266070-t26_1	11.249	9.856	13.767
TGME49_267400-t26_1	13.553	9.336	12.502
TGME49_270250-t26_1	13.696	8.824	14.451
TGME49_270380-t26_1	13.480	9.245	12.306
TGME49_271050-t26_1	11.267	8.769	14.962
TGME49_273760-t26_1	12.503	8.482	11.665
TGME49_275440-t26_1	11.593	8.848	15.715
TGME49_277080-t26_1	12.000	8.523	16.020
TGME49_280380-t26_1	12.585	9.603	14.091
TGME49_284560-t26_1	13.283	8.831	13.517
TGME49_286090-t26_1	13.027	7.690	11.667
TGME49_286420-t26_1	11.708	9.033	13.857
TGME49_286450-t26_1	14.078	8.048	13.860
TGME49_288650-t26_1	11.746	8.745	15.037
TGME49_288720-t26_1	13.403	8.808	13.521
TGME49_289530-t26_1	12.967	8.940	13.689
TGME49_289690-t26_1	14.277	8.674	15.088
TGME49_289750-t26_1	13.532	9.225	13.730
TGME49_291890-t26_1	10.356	8.484	15.138
TGME49_292130-t26_1	13.184	8.214	12.046
TGME49_293690-t26_1	12.315	8.750	13.929
TGME49_294200-t26_1	12.643	7.789	12.810
TGME49_294800-t26_1	12.292	8.550	14.598
TGME49_300000-t26_1	13.426	9.276	13.637
TGME49_305520-t26_1	14.216	8.613	14.071
TGME49_308840-t26_1	12.302	8.558	14.454
TGME49_309590-t26_1	11.809	8.840	13.969
TGME49_309810-t26_1	14.105	9.111	14.332

TGME49_309820-t26_1	13.495	8.639	13.746
TGME49_310490-t26_1	13.520	9.020	14.099
TGME49_310780-t26_1	13.410	8.694	13.445
TGME49_316400-t26_1	12.265	8.322	14.309
TGME49_319560-t26_1	12.236	8.690	13.253
TGME49_320050-t26_1	13.074	8.127	13.926

Appendix 3-11: List of 94 up-regulated *T. gondii* transcripts with their gene name/symbol and description.

Gene ID	Gene Name or Symbol	Transcript Product Description
TGME49_200360	null	hypothetical protein
TGME49_201390	null	hypothetical protein
TGME49_203310	GRA7	dense granule protein GRA7
TGME49_204020	RPL8	ribosomal protein RPL8
TGME49_204530	MIC11	microneme protein MIC11
TGME49_205340	RPS12	ribosomal protein RPS12
TGME49_205700	null	cyclophilin precursor
TGME49_207400	null	hypothetical protein
TGME49_208030	MIC4	microneme protein MIC4
TGME49_209030	ACT1	actin ACT1
TGME49_210408	null	HMG (high mobility group) box domain-containing protein
TGME49_210690	RPS6	ribosomal protein RPS6
TGME49_211680	null	protein disulfide isomerase
TGME49_212270	null	hypothetical protein
TGME49_212290	RPS19	ribosomal protein RPS19
TGME49_213280	SRS25	SAG-related sequence SRS25
TGME49_213350	RPS15	ribosomal protein RPS15
TGME49_213580	null	hypothetical protein
TGME49_214940	null	MIC2-associated protein M2AP
TGME49_215460	RPS24	ribosomal protein RPS24
TGME49_215470	RPL10A	ribosomal protein RPL10A
TGME49_215960	null	hypothetical protein
TGME49_217570	RPS27	ribosomal protein RPS27
TGME49_218260	null	histone H3.3
TGME49_218520	MIC6	microneme protein MIC6
TGME49_220400	ADF	actin depolymerising factor ADF
TGME49_220950	null	hypothetical protein
TGME49_225080	RPS18	ribosomal protein RPS18
TGME49_227280	GRA3	dense granule protein GRA3
TGME49_227360	RPL3	ribosomal protein RPL3
TGME49_227620	GRA2	dense granule protein GRA2

TGME49_229670	RPS23	ribosomal protein RPS23
TGME49_230160	null	hypothetical protein
TGME49_231140	RPS25	ribosomal protein RPS25
TGME49_232350	LDH1	lactate dehydrogenase LDH1
TGME49_232710	RPS3A	ribosomal protein RPS3A
TGME49_233460	SAG1	SAG-related sequence SRS29B
TGME49_234450	RPS15A	ribosomal protein RPS15A
TGME49_238250	RPL36	ribosomal protein RPL36
TGME49_239100	RPS7	ribosomal protein RPS7
TGME49_239330	RPL37	ribosomal protein RPL37
TGME49_239740	GRA14	dense granule protein GRA14
TGME49_239760	RPL22	ribosomal protein RPL22
TGME49_242330	RPS5	ribosomal protein RPS5
TGME49_242340	RPS29	ribosomal protein RPS29
TGME49_245460	RPS8	ribosomal protein RPS8
TGME49_245680	RPL21	ribosomal protein RPL21
TGME49_248390	RPL26	ribosomal protein RPL26
TGME49_248480	RPS9	ribosomal protein RPS9
TGME49_249250	RPL35A	ribosomal protein RPL35A
TGME49_249850	GAP40	GAP40 protein
TGME49_250710	MIC10	microneme protein MIC10
TGME49_250770	null	eukaryotic initiation factor-4A, putative
TGME49_251810	null	translation initiation factor eIF-5A, putative
TGME49_254720	GRA8	dense granule protein GRA8
TGME49_255260	null	apical membrane antigen AMA1
TGME49_261740	null	hypothetical protein
TGME49_262690	RPL27	ribosomal protein RPL27
TGME49_263040	RPS16	ribosomal protein RPS16
TGME49_263090	null	14-3-3 protein
TGME49_266070	RPL31	ribosomal protein RPL31
TGME49_267400	RPL32	ribosomal protein RPL32
TGME49_270250	GRA1	dense granule protein GRA1
TGME49_270380	RPS13	ribosomal protein RPS13
TGME49_271050	SAG2A	SAG-related sequence SRS34A
TGME49_273760	HSP70	heat shock protein HSP70
TGME49_275440	GRA6	dense granule protein GRA6
TGME49_277080	MIC5	microneme protein MIC5
TGME49_280380	null	poly(ADP-ribose) glycohydrolase
TGME49_284560	RPL9	ribosomal protein RPL9
TGME49_286090	null	translation initiation factor SUI1, putative
TGME49_286420	null	elongation factor 1-alpha (EF-1-ALPHA), putative
TGME49_286450	GRA5	dense granule protein GRA5
TGME49_288650	GRA12	dense granule protein GRA12
TGME49_288720	RPL10	ribosomal protein RPL10
TGME49_289530	RPL19	ribosomal protein RPL19

TGME49_289690	GAPDH1	glyceraldehyde-3-phosphate dehydrogenase GAPDH1
TGME49_289750	RPL40	ribosomal-ubiquitin protein RPL40
TGME49_291890	MIC1	microneme protein MIC1
TGME49_292130	RPL13A	ribosomal protein RPL13A
TGME49_293690	PRF	profilin PRF
TGME49_294200	null	glucose-6-phosphate 1-dehydrogenase
TGME49_294800	null	elongation factor 1-alpha (EF-1-ALPHA), putative
TGME49_300000	RPL18	ribosomal protein RPL18
TGME49_305520	RPS2	ribosomal protein RPS2
TGME49_308840	SRS51	SAG-related sequence SRS51
TGME49_309590	ROP1	rhoptry protein ROP1
TGME49_309810	RPP2	ribosomal protein RPP2
TGME49_309820	RPL11	ribosomal protein RPL11
TGME49_310490	RPL27A	ribosomal protein RPL27A
TGME49_310780	GRA4	dense granule protein GRA4
TGME49_316400	TUBA1	alpha tubulin TUBA1
TGME49_319560	MIC3	microneme protein MIC3
TGME49_320050	RPL5	ribosomal protein RPL5

Appendix 3-12: Full list of 531 up-regulated miRNAs at 48 h.p.i from miRNA sequencing.

#in Excel file

Appendix 3-13: Full list of 64 consensus pathways from of DIANA-mirPath v.3 analysis of top 100 up-regulated miRNA at 48 h.p.i

KEGG Pathway Name	No. of miRNA Matched	
	Genes Intersection	Pathway Union
TGF-beta signalling pathway	30	81
Signalling pathways regulating pluripotency of stem cells	28	90
Hippo signalling pathway	27	88
Morphine addiction	25	84
Proteoglycans in cancer	24	89
Mucin type O-Glycan biosynthesis	22	50
FoxO signalling pathway	20	84
Glioma	18	78
Axon guidance	17	80
Phosphatidylinositol signalling system	17	73
Lysine degradation	17	72
Circadian rhythm	16	68
Estrogen signalling pathway	15	85
Gap junction	14	84
Thyroid hormone signalling pathway	14	81
ErbB signalling pathway	14	79
Adherens junction	14	73
Glutamatergic synapse	13	86
GABAergic synapse	13	80
Wnt signalling pathway	12	88
Ubiquitin mediated proteolysis	11	88
Prolactin signalling pathway	11	74
Ras signalling pathway	10	92
Transcriptional misregulation in cancer	10	86
Melanoma	10	80
mTOR signalling pathway	10	77
Dorso-ventral axis formation	10	63
Pathways in cancer	9	94
cGMP-PKG signalling pathway	9	87
Prostate cancer	9	84
Choline metabolism in cancer	9	82
Renal cell carcinoma	9	79
Arrhythmogenic right ventricular cardiomyopathy (ARVC)	9	68
Glycosaminoglycan biosynthesis - heparan sulfate / heparin	9	45
PI3K-Akt signalling pathway	8	93
Focal adhesion	8	86
N-Glycan biosynthesis	8	61
Prion diseases	8	52

Cell cycle	7	86
AMPK signalling pathway	7	85
Circadian entrainment	7	85
p53 signalling pathway	7	71
Inositol phosphate metabolism	7	64
Rap1 signalling pathway	6	90
Oxytocin signalling pathway	6	89
Pancreatic cancer	6	82
Chronic myeloid leukemia	6	78
Non-small cell lung cancer	6	74
Bacterial invasion of epithelial cells	6	72
Retrograde endocannabinoid signalling	5	86
Adrenergic signalling in cardiomyocytes	5	84
Long-term potentiation	5	81
Colorectal cancer	5	73
Endometrial cancer	5	71
cAMP signalling pathway	4	91
MAPK signalling pathway	4	90
Regulation of actin cytoskeleton	4	88
Neurotrophin signalling pathway	3	86
Endocytosis	3	85
GnRH signalling pathway	3	82
Melanogenesis	2	85
mRNA surveillance pathway	1	76
T cell receptor signalling pathway	1	74
Propanoate metabolism	1	33

Appendix 3-14: Full list of genes matched to *T. gondii* genome from small RNA sequencing data at 6 h.p.i. Genes were filtered by applying minimum cut-off FPKM values of ≥ 2000 (in infected samples) and *P*-values ≤ 0.01. 116 genes passed these criteria.

#in Excel file

Appendix 3-15: Full list of genes matched to *T. gondii* genome from small RNA sequencing data at 24 h.p.i. Genes were filtered by applying minimum cut-off FPKM values of ≥ 2000 (in infected samples) and *P*-values ≤ 0.01. 138 genes passed these criteria.

#in Excel file

Appendix 3-16: Full list of genes matched to *T. gondii* genome from small RNA sequencing data at 48 h.p.i. Genes were filtered by applying minimum cut-off FPKM values of ≥ 2000 (in infected samples) and *P*-values ≤ 0.01. 164 genes passed these criteria.

#in Excel file

Appendix 3-17: Full list of 86 genes matched to *T. gondii* genome from small RNA sequencing data at 6, 24 and 48 h.p.i. 86 genes passed these criteria.

#in Excel file

Appendix 3-18: Full list of DEGs (285 down-regulated and 71 up-regulated) at 6 h.p.i of microarray experiment.

#in Excel file

Appendix 3-19: Full list of DEGs (3400 down-regulated and 314 up-regulated) at 48 h.p.i of microarray experiment.

#in Excel file

Appendix 3-20: Full list of 38 significant molecular functions from PANTHER Overrepresentation Test (FDR < 0.05) from set of down-regulate genes at 48 h.p.i (microarray)

No	PANTHER GO-Slim Molecular Function
1	RNA helicase activity (GO:0003724)
2	exodeoxyribonuclease activity (GO:0004529)
3	helicase activity (GO:0004386)
4	DNA helicase activity (GO:0003678)
5	RNA methyltransferase activity (GO:0008173)
6	single-stranded DNA binding (GO:0003697)
7	methyltransferase activity (GO:0008168)
8	ubiquitin-protein ligase activity (GO:0004842)
9	mRNA binding (GO:0003729)
10	transferase activity, transferring acyl groups (GO:0016746)
11	chromatin binding (GO:0003682)
12	nuclease activity (GO:0004518)
13	RNA binding (GO:0003723)
14	transferase activity (GO:0016740)
15	protein kinase activity (GO:0004672)
16	kinase activity (GO:0016301)
17	ligase activity (GO:0016874)
18	nucleic acid binding (GO:0003676)
19	pyrophosphatase activity (GO:0016462)
20	enzyme regulator activity (GO:0030234)
21	DNA binding (GO:0003677)
22	catalytic activity (GO:0003824)
23	hydrolase activity (GO:0016787)
24	transmembrane transporter activity (GO:0022857)
25	oxidoreductase activity (GO:0016491)
26	receptor binding (GO:0005102)
27	signal transducer activity (GO:0004871)
28	cytokine activity (GO:0005125)
29	adenylate cyclase activity (GO:0004016)
30	cation channel activity (GO:0005261)
31	receptor activity (GO:0004872)
32	G-protein coupled receptor activity (GO:0004930)
33	ion channel activity (GO:0005216)
34	voltage-gated ion channel activity (GO:0005244)
35	voltage-gated potassium channel activity (GO:0005249)
36	ligand-gated ion channel activity (GO:0015276)
37	antigen binding (GO:0003823)
38	anion channel activity (GO:0005253)

Appendix 3-21: List of 81 overrepresented biological processes from PANTHER Overrepresentation Test (FDR < 0.05 from down-regulated genes at 48 h.p.i (microarray)

#in Excel file

Appendix 3-22: List of 28 overrepresented cellular components from PANTHER Overrepresentation Test (FDR < 0.05) from down-regulated genes at 48 h.p.i (microarray)

No	PANTHER GO-Slim Cellular Component
1	cell part (GO:0044464)
2	cell projection (GO:0042995)
3	chromosome (GO:0005694)
4	cytoplasm (GO:0005737)
5	endoplasmic reticulum (GO:0005783)
6	endosome (GO:0005768)
7	extracellular matrix (GO:0031012)
8	extracellular region (GO:0005576)
9	extracellular space (GO:0005615)
10	Golgi apparatus (GO:0005794)
11	immunoglobulin complex (GO:0019814)
12	integral to membrane (GO:0016021)
13	intracellular (GO:0005622)
14	macromolecular complex (GO:0032991)
15	membrane (GO:0016020)
16	neuron projection (GO:0043005)
17	nuclear chromosome (GO:0000228)
18	nuclear envelope (GO:0005635)
19	nuclear outer membrane-endoplasmic reticulum membrane network (GO:0042175)
20	nucleolus (GO:0005730)
21	nucleoplasm (GO:0005654)
22	nucleus (GO:0005634)
23	organelle (GO:0043226)
24	plasma membrane (GO:0005886)
25	protein complex (GO:0043234)
26	proteinaceous extracellular matrix (GO:0005578)
27	protein-DNA complex (GO:0032993)
28	ribonucleoprotein complex (GO:0030529)

Appendix 4-1: R Studio analysis script for microarray data analysis (monensin experiment)

cex.---

title: "Affymetrix Analysis"

author: "Harun Mohammed"

date: "30 Nov 2017"

output: pdf_document

```{r setup, include=FALSE}

#knitr::opts_chunk$set(echo = FALSE)

```

`echo = FALSE` - to prevent printing of the R code that generated the plot.

Set directory

```{r}

setwd("D:/monensin microarray")

getwd()

```

Affymetrix Analysis of infected cells

This experiment involves the comparison of control vs infected vs 0.1um monensin treated vs TG+0.1um monensin treated samples at 24 hours post trreatment/infected each with three replicates. The experimental design is as follows:

filename	time	treatment	group
TG5+0.1um_2YA.ga.cel	24	infected treated	tg_mon
TG5+0.1um_2YB.ga.cel	24	infected treated	tg_mon
TG5+0.1um_2YC.ga.cel	24	infected treated	tg_mon
Ctrl 24 A.ga.cel	24	ctrl	ctrl_mon
Ctrl 24 B.ga.cel	24	ctrl	ctrl_mon

Ctrl 24 C.ga.cel	24	ctrl	ctrl_mon
Inf 24 A.ga.cel	24	infected only	inf_mon
Inf 24 B.ga.cel	24	infected only	inf_mon
Inf 24 C.ga.cel	24	infected only	inf_mon
0.1um_2YA.ga.cel	24	treated only	mon_only
0.1um_2YB.ga.cel	24	treated only	mon_only
0.1um_2YC.ga.cel	24	treated only	mon_only

Initial Setup

First we load some modules to start the analysis.

```{r}
library(oligo)
library(gplots)
library(RColorBrewer)
library(pvclust)
library(colorspace)
library(limma)
library(genefilter)
library(hugene21sttranscriptcluster.db)
```

Setup Color Palettes, load pdata file

We will make individual colour palettes for group and sample types, and a heatmap colour palette. We will load the experimental description (pdata.txt) file.

```{r}
hmcol = colorRampPalette(brewer.pal(9, "GnBu"))(100)
pdatamon=read.table("pdatamon.txt",header=TRUE)
pdatamonPCA=read.table("pdatamonPCA.txt",header=TRUE)
pdatamon$group = as.factor(paste(pdatamon$treatment,pdatamon$group,sep="_"))

# Make colour palette by timepoint
```

#time_colours = rev(heat_hcl(n=length((pdatamon$time))))

#names(time_colours)=pdatamon$time

Make colour palette by treatment

treat_colours = brewer.pal(length(unique(pdatamon$treatment))+1,"Set3")[as.factor(pdatamon$treatment)]

names(treat_colours)=pdatamon$treatment

Colours for each group (treatment and time)

group_colours = brewer.pal(length(unique(pdatamon$group)),"Set3")[as.factor(pdatamon$group)]

names(group_colours)=pdatamon$group

```

## Affymetrix Loading and Normalisation

Load the CEL files and summarised the unnormalised raw expression data using oligo package

Normalised the expression using Robust multi-array average normalisation (RMA)

```{r}

geneCELs = as.character(pdatamon$filename)

# Prenormalised object-> all expression all probes

affyGeneFS <- read.celfiles(geneCELs)

# Post normalised RMA -> core expression by gene

geneCore <- rma(affyGeneFS, target = "core")

```

Quality Control

Raw expression level accross samples before and after normalisation

```{r}

```
#window()

#pdf (file = "Pre Normalisation Monensin.pdf", height=7, width=8)

#par(mfrow=c(2,1))

tiff(filename = "Pre Normalisation.tif", width = 1200, height = 1200)

par(oma = c(4.3, 0.5, 0, 0), xpd=TRUE)

boxplot(log2(exprs(affyGeneFS)),las=2,cex.axis=1.2,main="Pre Normalisation",col=group_colours, ylab="Log2 Expression", cex.lab=1.2, cex.main=1.8)

#boxplot(geneCore,las=2,cex.axis=1.2,main="Post Normalisation Samples",col=group_colours, ylab="Log2 Expression", cex.lab=1.2, cex.main=1.8)

#par(mfrow=c(2,1))

#par(fig = c(0, 1, 0, 1), oma = c(0, 0, 0, 0), mar = c(1, 0, 0, 0), new = TRUE)

#plot(0, 0, type = "n", bty = "n", xaxt = "n", yaxt = "n")

#legend("bottom",levels(pdatamon$group),fill=group_colours[levels(pdatamon$group)],cex=1.6)
```

Heatmap to view sample to sample correlation

```{r}

#x11()

pdf(file= "sample correlation heatmap monen.pdf")

#pdf(file= "key heatmap sample correlation.pdf")

heatmap.2(cor(exprs(geneCore)),col=hmcol,trace="none",margin=c(12,12),cexRow=1.5,cexCol=1.5,ColSideColors=treat_colours,RowSideColors=group_colours, keysize = 1.2, dendrogram = c("both"), main="Samples Correlation Heatmap", cex.main=2

      #lhei = c(6,15))
```

Draw PCA plots for exploring the effect of Time, Treatment and Group

```{r}

#x11()

#par(mfrow=c(3,1))

pdf(file= "pca treatment monen.pdf")
```

```
pca <- princomp(exprs(geneCore))

plot(pca$loadings, main="Principal Component Analysis - Treatment",

     xlab = "First component",

     ylab = "Second component",

     pch = c( 9, 9, 9, 12, 12, 12, 15, 15, 15, 18, 18, 18),

    col=c("orange", "orange", "orange",

           "green", "green", "green",

            "purple", "purple", "purple",

         "red", "red", "red"), cex = 2)

 text(pca$loadings, as.character(pdatamon$filename), pos=2, cex=1)
```

```
# Extract Annotation Information for each probe from Annotation package

# Fetch Annotation information for each probe from annotation package

```{r}

probes = rownames(expression)

genesymbols = unlist(mget(probes,hugene21sttranscriptclusterSYMBOL,ifnotfound=NA))

genedescs = unlist(mget(probes,hugene21sttranscriptclusterGENENAME,ifnotfound=NA))

featureData(geneCore) <- getNetAffx(geneCore, "transcript")

lincrnas=grep("gene_biotype:lincRNA",pData(featureData(geneCore))[, "mrnaassignment"])

protein_coding=grep("gene_biotype:protein_coding",pData(featureData(geneCore))[, "mrnaassignment"])

non_coding=grep("gene_biotype:non_coding",pData(featureData(geneCore))[, "mrnaassignment"])

expression=exprs(geneCore)

# Restrict to protein coding ?

#expression=exprs(geneCore)[protein_coding,]

```

Perform Statitstical Test
```

T-test with groups as a factor

times as a factor = times <- as.facor(pdata$time)

```{r}

group <- as.factor(pdatamon$group)

design <- cbind(model.matrix(~0+group))

colnames(design) = levels(group)

design

```


Contrast

Create a differential expression control versus infected at each time point (horizontal comparison)

```{r}

# horizontal Control v TG_only

c1 = "infected_only_TG_only-ctrl_Control"

# horizontal Control v Monensin_only

c2 = "treated_only_Monensin_only-ctrl_Control"

# horizontal Control v TG_Monensin

c3 = "infected_treated_TG_Monensin-ctrl_Control"

# vertical Monensin_only v TG_Monensin

c4 = "treated_only_Monensin_only-infected_treated_TG_Monensin"

# vertical TG_only v TG_Monensin

c5 = "infected_only_TG_only-infected_treated_TG_Monensin"

contrast.matrix <- makeContrasts(c1,c2,c3,c4,c5, levels=design)

contrast.matrix

```


Fit the linear Model - run the t-test

```{r}

fit <- lmFit(expression, design)

fit2 <- eBayes(contrasts.fit(fit, contrast.matrix))
```

```

# Transfer the Annotation Data to the fit2 object

```{r}
fit2$genes$Symbol = genesymbols[as.character(rownames(fit2))]
fit2$genes$Description = genedescs[as.character(rownames(fit2))]
```

Set threshold for significance and fold change

```{r}
p_value_cutoff=0.05
lfc_cutoff=1
```

Volcanoplot of significance versus fold-change

```{r}
pdf(file = "volcanoplot no highlight.pdf", height=7, width=8)

# horizontal = Control v TG_only c1
#x11()
volcanoplot(fit2,coef=1,highlight=0,names=fit2$genes$Symbol,xlim=c(-3,3),main="Control vs TG_only", cex.main=1.8,
          cex.names=1.4, cex.axis=1.4, cex = 0.5, cex.lab=1.6)
abline(h=-log(p_value_cutoff,exp(1)),col="red",lty=1, lwd = 2)
abline(v=-(lfc_cutoff),col="red",lty=2, lwd = 2)
abline(v=(lfc_cutoff),col="red",lty=2, lwd = 2)

# horizontal = Control v Monensin_only c2
#x11()
volcanoplot(fit2,coef=2,highlight=0,names=fit2$genes$Symbol,xlim=c(-3,3),main="Control vs Monensin_only", cex.main=1.8,
           cex.names=1.4, cex.axis=1.4, cex = 0.5, cex.lab=1.6)
```
```

```
abline(h=-log(p_value_cutoff,exp(1)),col="red",lty=1, lwd = 2)

abline(v=-(lfc_cutoff),col="red",lty=2,lwd = 2 )

abline(v=(lfc_cutoff),col="red",lty=2, lwd = 2)


# horizontal = Control v TG_Monensin c3

#x11()

volcanoplot(fit2,coef=3,highlight=0,names=fit2$genes$Symbol,xlim=c(-
3,3),main="Control vs TG_Monensin",cex.main=1.8,

        cex.names=1.4, cex.axis=1.4, cex = 0.5, cex.lab=1.6)

abline(h=-log(p_value_cutoff,exp(1)),col="red",lty=1,lwd = 2 )

abline(v=-(lfc_cutoff),col="red",lty=2, lwd = 2)

abline(v=(lfc_cutoff),col="red",lty=2, lwd = 2)



# vertical = Monensin_only v TG_Monensin c4

#x11()

volcanoplot(fit2,coef=4,highlight=0,names=fit2$genes$Symbol,xlim=c(-
3,3),main="Monensin_only vs TG_Monensin",cex.main=1.8,

        cex.names=1.4, cex.axis=1.4, cex = 0.5, cex.lab=1.6)

abline(h=-log(p_value_cutoff,exp(1)),col="red",lty=1,lwd = 2 )

abline(v=-(lfc_cutoff),col="red",lty=2, lwd = 2)

abline(v=(lfc_cutoff),col="red",lty=2, lwd = 2)


# vertical = TG_only v TG_Monensin c5

#x11()

volcanoplot(fit2,coef=5,highlight=0,names=fit2$genes$Symbol,xlim=c(-
3,3),main="TG_only vs TG_Monensin",cex.main=1.8,

        cex.names=1.4, cex.axis=1.4, cex = 0.5, cex.lab=1.6)

abline(h=-log(p_value_cutoff,exp(1)),col="red",lty=1,lwd = 2 )

abline(v=-(lfc_cutoff),col="red",lty=2, lwd = 2)

abline(v=(lfc_cutoff),col="red",lty=2, lwd = 2)

```

Venn diagrams of significant hits.p-0.05

```{r}

result <- decideTests(fit2, p.value=p_value_cutoff, lfc=lfc_cutoff, adjust="BH")

#x11()

#par(mfrow=c(2,1))

pdf(file= "ven diagram microarray test.pdf")

vennDiagram(result[,1:3], include=c("up","down"), circle.col=1:4, main="Control:TG_only vs Control:Monensin_only vs Control:TG_Monensin",names=c("TG_only","Monensin_only","TG_Monensin"), mar=rep(1,4))

vennDiagram(result[,4:5], include=c("up","down"), circle.col=2:4, main="Venn Diagram - Monensin_only vs TG_only : TG_Monensin",names=c("TG_only","TG_Monensin"))

```


List of significant hits for heatmap p-=0,05, 1 to 5

```{r}

stats = topTable(fit2,coef=1,number=10000000)

significant1 = rownames(stats[(stats[,"adj.P.Val"] < p_value_cutoff) & (abs(stats[,"logFC"]) > lfc_cutoff),])

stats = topTable(fit2,coef=2,number=10000000)

significant2 = rownames(stats[(stats[,"adj.P.Val"] < p_value_cutoff) & (abs(stats[,"logFC"]) > lfc_cutoff),])

stats = topTable(fit2,coef=3,number=10000000)

significant3 = rownames(stats[(stats[,"adj.P.Val"] < p_value_cutoff) & (abs(stats[,"logFC"]) > lfc_cutoff),])

total_significant_by_treatment=unique(c(significant1,significant2,significant3))

stats = topTable(fit2,coef=4,number=10000000)

significant4 = rownames(stats[(stats[,"adj.P.Val"] < p_value_cutoff) & (abs(stats[,"logFC"]) > lfc_cutoff),])

stats = topTable(fit2,coef=5,number=10000000)

significant5 = rownames(stats[(stats[,"adj.P.Val"] < p_value_cutoff) & (abs(stats[,"logFC"]) > lfc_cutoff),])

total_significant_by_infection=unique(c(significant4,significant5))
```

```

# List of significant hits for heatmap p-=0,01, 1 to 3 -> only for mRNA seq

p_value_cutoff=0.01

lfc_cutoff=1

stats = topTable(fit2,coef=1,number=10000000)

significant1 = rownames(stats[(stats[,"adj.P.Val"] < p_value_cutoff) & (abs(stats[,"logFC"]) > lfc_cutoff),])

stats = topTable(fit2,coef=2,number=10000000)

significant2 = rownames(stats[(stats[,"adj.P.Val"] < p_value_cutoff) & (abs(stats[,"logFC"]) > lfc_cutoff),])

stats = topTable(fit2,coef=3,number=10000000)

significant3 = rownames(stats[(stats[,"adj.P.Val"] < p_value_cutoff) & (abs(stats[,"logFC"]) > lfc_cutoff),])

total_significant=unique(c(significant1,significant2,significant3))


# List of DEG at all hrs

```{r}

list=merge((exprs(geneCore)),topTable(fit2,coef=1,number=1000000000000),by.x=0,by.y=0)

list=list[order(list$logFC),]

write.table(list,paste(c1,".results.txt",sep=""),sep="\t",quote=F)

list=merge((exprs(geneCore)),topTable(fit2,coef=2,number=1000000000000),by.x=0,by.y=0)

list=list[order(list$logFC),]

write.table(list,paste(c2,".results.txt",sep=""),sep="\t",quote=F)

list=merge((exprs(geneCore)),topTable(fit2,coef=3,number=1000000000000),by.x=0,by.y=0)

list=list[order(list$logFC),]

write.table(list,paste(c3,".results.txt",sep=""),sep="\t",quote=F)

list=merge((exprs(geneCore)),topTable(fit2,coef=4,number=1000000000000),by.x=0,by.y=0)

list=list[order(list$logFC),]

write.table(list,paste(c4,".results.txt",sep=""),sep="\t",quote=F)
```
```

```
list=merge((exprs(geneCore)),topTable(fit2,coef=5,number=1000000000000),by.x=0,by.y=0)

list=list[order(list$logFC),]

write.table(list,paste(c5,".results.txt",sep=""),sep="\t",quote=F)
```

All significant genes heat map - too many genes

```{r}
heatmap.2(exprs(geneCore)[significant1,],trace="none",col=hmcol,ColSideColors = group_colours,main="Sig. List 1")

heatmap.2(exprs(geneCore)[significant2,],trace="none",col=hmcol,ColSideColors = group_colours,main="Sig. List 2")

heatmap.2(exprs(geneCore)[significant3,],trace="none",col=hmcol,ColSideColors = group_colours,main="Sig. List 3")

heatmap.2(exprs(geneCore)[significant4,],trace="none",col=hmcol,ColSideColors = group_colours,main="Sig. List 4")

heatmap.2(exprs(geneCore)[significant5,],trace="none",col=hmcol,ColSideColors = group_colours,main="Sig. List 5")
```

top 30 most significant genes heatmap

```{r}
pdf(file= "heatmap monensin colmn only 15.pdf")

# horizontal Control v TG_only

#c1 = "Control-TG_only"

#win.graph()

heatmap.2(exprs(geneCore)[significant1[1:min(15,length(significant1))],],trace="none",scale="none",col=hmcol,ColSideColors = group_colours,main="Control vs TG_only", labRow=fit2[significant1,]$genes$Symbol,

        margins=c(11.9,6.8),

        cexRow = 1.3, cexCol = 1.5,

        dendrogram = "col")

# horizontal Control v Monensin_only

#c2 = "Control-Monensin_only"
```

```
#win.graph()

heatmap.2(exprs(geneCore)[significant2[1:min(15,length(significant2))],],trace="none",col=hmcol,ColSideColors = group_colours,main="Control vs Monensin_only", labRow=fit2[significant2,]$genes$Symbol,

        margins=c(11.9,6.8),

        cexRow = 1.3, cexCol = 1.5,

        dendrogram = "col")

# horizontal Control v TG_Monensin

#c3 = "Control-TG_Monensin"

#win.graph()

heatmap.2(exprs(geneCore)[significant3[1:min(15,length(significant3))],],trace="none",col=hmcol,ColSideColors = group_colours,main="Control vs TG_Monensin", labRow=fit2[significant3,]$genes$Symbol,

          margins=c(11.9,8),

        cexRow = 1.3, cexCol = 1.5,

        dendrogram = "col")

# vertical Monensin_only v TG_Monensin

#c4 = "Monensin_only-TG_Monensin"

#win.graph()

heatmap.2(exprs(geneCore)[significant4[1:min(15,length(significant4))],],trace="none",col=hmcol,ColSideColors = group_colours,main="Monensin_only vs TG_Monensin", labRow=fit2[significant4,]$genes$Symbol,

        margins=c(11.9,8),

        cexRow = 1.3, cexCol = 1.5,

        dendrogram = "col")

# vertical TG_only v TG_Monensin

#c5 = "TG_only-TG_Monensin"

#win.graph()

heatmap.2(exprs(geneCore)[significant5[1:min(15,length(significant5))],],trace="none",col=hmcol,ColSideColors = group_colours,main="TG_only vs TG_Monensin", labRow=fit2[significant5,]$genes$Symbol,

        margins=c(11.9,6.8),

        cexRow = 1.3, cexCol = 1.5,

        dendrogram = "col")
```

```

# Writing data to a file

```{r}
write.table(exprs(geneCore),"expression_normalised.txt",sep="\t")
#write.table(filtered, "expression_filtered.txt", sep="/t")
exprestion=exprs(geneCore)
```

```{r}
final=as.data.frame(exprestion)
final$Symbol=genesymbols[rownames(expression)]
final$Desc=genedescs[rownames(expression)]
write.table(final, "biolayout_table.txt",sep="/t")
```

Appendix 4-2: R Full list of DEGs (65 down-regulated and 171 up-regulated) of monensin microarray experiment (Control vs Monensin_only)

#in Excel file

Appendix 4-3: Full list of DEGs (103 down-regulated and 345 up-regulated) of monensin microarray experiment (Control vs TG_only)

#in Excel file
```

Appendix 4-4: Full list of DEGs (109 down-regulated and 201 up-regulated) of monensin microarray experiment (Control vs TG_Monensin)

#in Excel file

Appendix 4-5: Full list of 55 pathways from monensin microarray experiment (Control vs TG_Monensin)

No	Pathway identifier	Pathway name	Entities found	Control vs TG_Monensin
1	R-HSA-381042	PERK regulates gene expression	6	-2.06472888
2	R-HSA-381183	ATF6 (ATF6-alpha) activates chaperone genes	6	-1.611905849
3	R-HSA-381033	ATF6 (ATF6-alpha) activates chaperones	6	-1.611905849
4	R-HSA-381119	Unfolded Protein Response (UPR)	38	-1.469203779
5	R-HSA-381038	XBP1(S) activates chaperone genes	27	-1.399052182
6	R-HSA-381070	IRE1alpha activates chaperones	30	-1.373276346
7	R-HSA-204005	COPII-mediated vesicle transport	8	-1.366793722
8	R-HSA-6807878	COPI-mediated anterograde transport	13	-1.361826374
9	R-HSA-199977	ER to Golgi Anterograde Transport	18	-1.343396004
10	R-HSA-948021	Transport to the Golgi and subsequent modification	18	-1.343396004
11	R-HSA-1655829	Regulation of cholesterol biosynthesis by SREBP (SREBF)	8	-1.319450748
12	R-HSA-446203	Asparagine N-linked glycosylation	31	-1.306684586
13	R-HSA-6811442	Intra-Golgi and retrograde Golgi-to-ER traffic	19	-0.808854056
14	R-HSA-392499	Metabolism of proteins	92	-0.795809917
15	R-HSA-6811434	COPI-dependent Golgi-to-ER retrograde traffic	12	-0.446829203
16	R-HSA-8856688	Golgi-to-ER retrograde transport	12	-0.446829203
17	R-HSA-8936459	RUNX1 regulates genes involved in megakaryocyte differentiation and platelet function	7	0.555662327

18	R-HSA-141444	Amplification of signal from unattached kinetochores *via* a MAD2 inhibitory signal	11	0.858579674
19	R-HSA-141424	Amplification of signal from the kinetochores	11	0.858579674
20	R-HSA-69618	Mitotic Spindle Checkpoint	11	0.858579674
21	R-HSA-5663220	RHO GTPases Activate Formins	11	0.858579674
22	R-HSA-2500257	Resolution of Sister Chromatid Cohesion	12	0.871618102
23	R-HSA-68886	M Phase	23	0.911591974
24	R-HSA-68877	Mitotic Prometaphase	14	0.915094795
25	R-HSA-69278	Cell Cycle, Mitotic	43	0.999554652
26	R-HSA-69620	Cell Cycle Checkpoints	22	1.016659164
27	R-HSA-1640170	Cell Cycle	47	1.017133692
28	R-HSA-539107	Activation of E2F1 target genes at G1/S	6	1.046724667
29	R-HSA-69205	G1/S-Specific Transcription	6	1.046724667
30	R-HSA-1362300	Transcription of E2F targets under negative control by p107 (RBL1) and p130 (RBL2) in complex with HDAC1	6	1.054287899
31	R-HSA-1362277	Transcription of E2F targets under negative control by DREAM complex	5	1.069683888
32	R-HSA-453279	Mitotic G1-G1/S phases	17	1.090684474
33	R-HSA-1538133	G0 and Early G1	10	1.091034081
34	R-HSA-69206	G1/S Transition	12	1.103086444
35	R-HSA-73886	Chromosome Maintenance	8	1.10313788
36	R-HSA-5689901	Metalloprotease DUBs	5	1.107795106
37	R-HSA-606279	Deposition of new CENPA-containing nucleosomes at the centromere	7	1.10850424
38	R-HSA-774815	Nucleosome assembly	7	1.10850424
39	R-HSA-69473	G2/M DNA damage checkpoint	7	1.154194904
40	R-HSA-5693607	Processing of DNA double-strand break ends	8	1.156336924
41	R-HSA-176974	Unwinding of DNA	3	1.175108946
42	R-HSA-2299718	Condensation of Prophase Chromosomes	6	1.175355499
43	R-HSA-3214815	HDACs deacetylate histones	7	1.185636937
44	R-HSA-5693567	HDR through Homologous Recombination (HRR) or Single Strand Annealing (SSA)	10	1.185959999

45	R-HSA-5693538	Homology-Directed Repair	10	1.185959999
46	R-HSA-912446	Meiotic recombination	6	1.186165279
47	R-HSA-5693579	Homologous DNA Pairing and Strand Exchange	5	1.189054574
48	R-HSA-5693554	Resolution of D-loop Structures through Synthesis-Dependent Strand Annealing (SDSA)	5	1.189054574
49	R-HSA-2559586	DNA Damage/Telomere Stress Induced Senescence	8	1.20558496
50	R-HSA-5334118	DNA methylation	5	1.207418437
51	R-HSA-212300	PRC2 methylates histones and DNA	5	1.207418437
52	R-HSA-73728	RNA Polymerase I Promoter Opening	5	1.207418437
53	R-HSA-427359	SIRT1 negatively regulates rRNA expression	5	1.207418437
54	R-HSA-5693537	Resolution of D-Loop Structures	6	1.238889681
55	R-HSA-5693568	Resolution of D-loop Structures through Holliday Junction Intermediates	6	1.238889681

Chapter 8 References

Aalto, A. and Pasquinelli, A. (2012). Small non-coding RNAs mount a silent revolution in gene expression. *Current Opinion in Cell Biology*, 24(3), pp.333-340.

Abbott, N. (2002). Astrocyte-endothelial interactions and blood-brain barrier permeability. *Journal of Anatomy*, 200(5), pp.523-534.

Advisory committee on the microbiological safety of food (2012). *Risk Profile in Relation to Toxoplasma in the Food Chain*. UK Food Standard Agency. Available at: http://www.food.gov.uk/sites/default/files/multimedia/pdfs/committee/acmsfrtaxopasm.pdf [Last accessed 10 Mar. 2019].

Agilent RNA 6000 Nano Kit Guide. (2013). 3rd ed. [ebook] Agilent Technologies. Available at: https://www.agilent.com/cs/library/usermanuals/Public/G293890034_RNA6000Nano_KG.pdf [Accessed 10 March 2017].

Ander, S., Rudzki, E., Arora, N., Sadovsky, Y., Coyne, C. and Boyle, J. (2018). Human placental syncytiotrophoblasts restrict *Toxoplasma gondii* attachment and replication and respond to infection by producing immunomodulatory chemokines. *mBio*, 9(1).

Anders, S. and Huber, W. (2010). Differential expression analysis for sequence count data. *Genome Biology*, 11(10), p.R106.

Anders, S., Pyl, P. and Huber, W. (2014). HTSeq--a Python framework to work with high-throughput sequencing data. *Bioinformatics*, 31(2), pp.166-169.

André, F., Corazao-Rozas, P., Idziorek, T., Quesnel, B., Kluza, J. and Marchetti, P. (2016). GILZ overexpression attenuates endoplasmic reticulum stress-mediated cell death via the activation of mitochondrial oxidative

phosphorylation. *Biochemical and Biophysical Research Communications*, 478(2), pp.513-520.

Andrew, S. (2019). *Babraham Bioinformatics - FastQC A Quality Control tool for High Throughput Sequence Data*. [online] Bioinformatics.babraham.ac.uk. Available at: http://www.bioinformatics.babraham.ac.uk/projects/fastqc/ [Last accessed 10 Mar. 2019].

Ashburner, M., Ball, C., Blake, J., Botstein, D., Butler, H., Cherry, J., Davis, A., Dolinski, K., Dwight, S., Eppig, J., Harris, M., Hill, D., Issel-Tarver, L., Kasarskis, A., Lewis, S., Matese, J., Richardson, J., Ringwald, M., Rubin, G. and Sherlock, G. (2000). Gene Ontology: tool for the unification of biology. *Nature Genetics*, 25(1), pp.25-29.

Atluri, V., Hidalgo, M., Samikkannu, T., Kurapati, K., Jayant, R., Sagar, V. and Nair, M. (2015). Effect of human immunodeficiency virus on blood-brain barrier integrity and function: an update. *Frontiers in Cellular Neuroscience*, 9

Backes, C., Kehl, T., Stöckel, D., Fehlmann, T., Schneider, L., Meese, E., Lenhof, H. and Keller, A. (2016). miRPathDB: a new dictionary on microRNAs and target pathways. *Nucleic Acids Research*, 45(D1), pp. D90-D96.

Badger, J. L., Stins, M. F., & Kim, K. S. (1999). Citrobacter freundii invades and replicates in human brain microvascular endothelial cells. *Infection and immunity*, *67*(8), 4208-15.

Baird, J., Fox, B., Sanders, K., Lizotte, P., Cubillos-Ruiz, J., Scarlett, U., Rutkowski, M., Conejo-Garcia, J., Fiering, S. and Bzik, D. (2013). Avirulent *Toxoplasma gondii* generates therapeutic antitumor immunity by reversing immunosuppression in the ovarian cancer microenvironment. *Cancer Research*, 73(13), pp.3842-3851.

Barragan, A. and David Sibley, L. (2003). Migration of *Toxoplasma gondii* across biological barriers. *Trends in Microbiology*, 11(9), pp.426-430.

Behnke, M., Khan, A., Lauron, E., Jimah, J., Wang, Q., Tolia, N. and Sibley, L. (2015). Rhoptry proteins ROP5 and ROP18 are major murine virulence factors in genetically divergent South American strains of *Toxoplasma gondii*. *PLOS Genetics*, 11(8), p.e1005434.

Belluco, S., Mancin, M., Conficoni, D., Simonato, G., Pietrobelli, M. and Ricci, A. (2016). Investigating the determinants of *Toxoplasma gondii* prevalence in meat: A systematic review and meta-regression. *PLOS ONE*, 11(4), p.e0153856.

Bertrand, M., Doiron, K., Labbé, K., Korneluk, R., Barker, P. and Saleh, M. (2009). Cellular inhibitors of apoptosis cIAP1 and cIAP2 are required for innate immunity signaling by the pattern recognition receptors NOD1 and NOD2. *Immunity*, 30(6), pp.789-801.

Bierie, B., Pierce, S., Kroeger, C., Stover, D., Pattabiraman, D., Thiru, P., Liu Donaher, J., Reinhardt, F., Chaffer, C., Keckesova, Z. and Weinberg, R. (2017). Integrin-β4 identifies cancer stem cell-enriched populations of partially mesenchymal carcinoma cells. *Proceedings of the National Academy of Sciences*, 114(12), pp. E2337-E2346.

Blader, I., Manger, I. and Boothroyd, J. (2001). Microarray analysis reveals previously unknown changes in *Toxoplasma gondii*-infected human cells. *Journal of Biological Chemistry*, 276(26), pp.24223-24231.

Blagoveshchenskaya, A., Thomas, L., Feliciangeli, S., Hung, C. and Thomas, G. (2002). HIV-1 Nef downregulates MHC-I by a PACS-1- and PI3K-regulated ARF6 endocytic pathway. *Cell*, 111(6), pp.853-866.

Blankenberg, D., Gordon, A., Von Kuster, G., Coraor, N., Taylor, J. and Nekrutenko, A. (2010). Manipulation of FASTQ data with Galaxy. *Bioinformatics*, 26(14), pp.1783-1785.

Bortolotti, D., LeMaoult, J., Trapella, C., Di Luca, D., Carosella, E. and Rizzo, R. (2015). *Pseudomonas aeruginosa* quorum sensing molecule N-(3-Oxododecanoyl)-l-Homoserine-Lactone induces HLA-G expression in human immune cells. *Infection and Immunity*, 83(10), pp.3918-3925.

Bottova, I., Hehl, A., Štefanić, S., Fabriàs, G., Casas, J., Schraner, E., Pieters, J. and Sonda, S. (2009). Host cell P-glycoprotein is essential for cholesterol uptake and replication of *Toxoplasma gondii*. *Journal of Biological Chemistry*, 284(26), pp.17438-17448.

Bottova, I., Sauder, U., Olivieri, V., Hehl, A. and Sonda, S. (2010). The P-glycoprotein inhibitor GF120918 modulates Ca2+-dependent processes and lipid metabolism in *Toxoplasma gondii*. *PLoS ONE*, 5(4), p.e10062.

Brasil, T., Freire-de-Lima, C., Morrot, A. and Vetö Arnholdt, A. (2017). Host-*Toxoplasma gondii* coadaptation leads to fine tuning of the immune response. *Frontiers in Immunology*, 8.

Briceño, M., Nascimento, L., Nogueira, N., Barenco, P., Ferro, E., Rezende-Oliveira, K., Goulart, L., Alves, P., Barbosa, B., Lima, W. and Silva, N. (2016). *Toxoplasma gondii* infection promotes epithelial barrier dysfunction of Caco-2 cells. *Journal of Histochemistry & Cytochemistry*, 64(8), pp.459-469.

Brown, J., Dorfman, D., Ma, F., Sullivan, E., Munoz, O., Wood, C., Greenfield, E. and Freeman, G. (2003). Blockade of programmed death-1 ligands on dendritic cells enhances T-cell activation and cytokine production. *The Journal of Immunology*, 170(3), pp.1257-1266.

Burr, M., Sparbier, C., Chan, Y., Williamson, J., Woods, K., Beavis, P., Lam, E., Henderson, M., Bell, C., Stolzenburg, S., Gilan, O., Bloor, S., Noori, T., Morgens, D., Bassik, M., Neeson, P., Behren, A., Darcy, P., Dawson, S., Voskoboinik, I., Trapani, J., Cebon, J., Lehner, P. and Dawson, M. (2017). CMTM6 maintains the expression of PD-L1 and regulates anti-tumour immunity. *Nature*, 549(7670), pp.101-105.

Buttmann, M., Lorenz, A., Weishaupt, A. and Rieckmann, P. (2007). Atorvastatin partially prevents an inflammatory barrier breakdown of cultured human brain endothelial cells at a pharmacologically relevant concentration. *Journal of Neurochemistry*, 102(4), pp.1001-1008.

Cabezas, R., Ã□vila, M., Gonzalez, J., El-BachÃi, R., BÃiez, E., GarcÃa-Segura, L., Jurado Coronel, J., Capani, F., Cardona-Gomez, G. and Barreto, G. (2014). Astrocytic modulation of blood brain barrier: perspectives on Parkinson's disease. *Frontiers in Cellular Neuroscience*, 8.

Cai, Y., Chen, H., Jin, L., You, Y. and Shen, J. (2013). STAT3-dependent transactivation of miRNA genes following *Toxoplasma gondii* infection in macrophage. *Parasites & Vectors*, 6(1), p.356.

Cai, Y., Chen, H., Mo, X., Tang, Y., Xu, X., Zhang, A., Lun, Z., Lu, F., Wang, Y. and Shen, J. (2014). *Toxoplasma gondii* inhibits apoptosis via a novel STAT3-miR-17–92-Bim pathway in macrophages. *Cellular Signalling*, 26(6), pp.1204-1212.

Callaway, T., Edrington, T., Rychlik, J., Genovese, K., Poole, T., Jung, Y., Bischoff, K., Anderson, R. and Nisbet, D. (2003). Ionophores: their use as ruminant growth promotants and impact on food safety. *Curr Issues Intest Microbiol.* 4(2), pp. 43-51.

Cannella, D., Brenier-Pinchart, M., Braun, L., van Rooyen, J., Bougdour, A., Bastien, O., Behnke, M., Curt, R., Curt, A., Saeij, J., Sibley, L., Pelloux, H. and Hakimi, M. (2014). miR-146a and miR-155 delineate a microRNA fingerprint associated with Toxoplasma persistence in the host brain. *Cell Reports*, 6(5), pp.928-937.

Carme, B., Bissuel, F., Ajzenberg, D., Bouyne, R., Aznar, C., Demar, M., Bichat, S., Louvel, D., Bourbigot, A., Peneau, C., Neron, P. and Darde, M. (2002). Severe acquired Toxoplasmosis in immunocompetent adult patients in French Guiana. *Journal of Clinical Microbiology*, 40(11), pp.4037-4044.

Carmen, J., Hardi, L. and Sinai, A. (2006). *Toxoplasma gondii* inhibits ultraviolet light-induced apoptosis through multiple interactions with the mitochondrion-dependent programmed cell death pathway. *Cellular Microbiology*, 8(2), pp.301-315.

Carruthers, V. and Suzuki, Y. (2007). Effects of *Toxoplasma gondii* infection on the brain. *Schizophrenia Bulletin*, 33(3), pp.745-751.

Ccb-compute.cs.uni-saarland.de. (2019). *miRMaster Webservice*. [online] Available at: https://ccb-compute.cs.uni-saarland.de/mirmaster [Accessed 5 May 2018].

Chang, S., Shan, X., Li, X., Fan, W., Zhang, S., Zhang, J., Jiang, N., Ma, D. and Mao, Z. (2015). *Toxoplasma gondii* rhoptry protein ROP16 mediates partially SH-SY5Y cells apoptosis and cell cycle arrest by directing Ser15/37 phosphorylation of p53. *International Journal of Biological Sciences*, 11(10), pp.1215-1225.

Chapman, H., Jeffers, T. and Williams, R. (2010). Forty years of monensin for the control of coccidiosis in poultry. *Poultry Science*, 89(9), pp.1788-1801.

Charvat, R. and Arrizabalaga, G. (2016). Oxidative stress generated during monensin treatment contributes to altered *Toxoplasma gondii* mitochondrial function. *Scientific Reports*, 6(1).

Chaussabel, D. (2003). Unique gene expression profiles of human macrophages and dendritic cells to phylogenetically distinct parasites. *Blood*, 102(2), pp.672-681.

Chen, W., Lee, C., Hsu, Y., Chen, C. and Huang, T. (2011). Identification of heat shock protein 90α as an IMH-2 epitope-associated protein and correlation of its mRNA overexpression with colorectal cancer metastasis and poor prognosis. *International Journal of Colorectal Disease*, 26(8), pp.1009-1017.

Chiang, H., Hung, C., Lee, C., Chen, H., Chen, M., Sheng, W., Hsieh, S., Sun, H., Ho, C. and Yu, C. (2011). Admissions to intensive care unit of HIV-infected patients in the era of highly active antiretroviral therapy: etiology and prognostic factors. *Critical Care*, 15(4), p.R202.

Chu, P., Huang, L., Hsu, C., Liang, C., Guan, J., Hung, T. and Shen, T. (2009). Tyrosine phosphorylation of growth factor receptor-bound protein-7 by focal adhesion kinase in the regulation of cell migration, proliferation, and tumorigenesis. *Journal of Biological Chemistry*, 284(30), pp.20215-20226.

Clevers, H. and Nusse, R. (2012). Wnt/β-catenin signaling and disease. *Cell*, 149(6), pp.1192-1205.

Coombes, J. and Hunter, C. (2015). Immunity to *Toxoplasma gondii*- into the 21st century. *Parasite Immunology*, 37(3), pp.105-107.

Coppens, Isabelle & Asai, T & Tomavo, Stanislas. (2013). 'Biochemistry and metabolism of *Toxoplasma gondii*. Carbohydrates, lipids and nucleotides' in

Weiss, L. and Kim, K. (eds.) *Toxoplasma gondii: The Model Apicomplexan - Perspectives and Methods.* Second Edition. pp. 257-295.

Coppola, S. and Ghibelli, L. (2000). GSH extrusion and the mitochondrial pathway of apoptotic signalling. *Biochemical Society Transactions*, 28(2), pp.56-61.

Courret, N. (2006). CD11c- and CD11b-expressing mouse leukocytes transport single *Toxoplasma gondii* tachyzoites to the brain. *Blood*, 107(1), pp.309-316.

Couzinet, S., Dubremetz, J., Buzoni-Gatel, D., Jeminet, G. and Prensier, G. (2000). In vitro activity of the polyether ionophorous antibiotic monensin against the cyst form of *Toxoplasma gondii*. *Parasitology*, 121(4), pp.359-365.

Croken, M., Ma, Y., Markillie, L., Taylor, R., Orr, G., Weiss, L. and Kim, K. (2014). Distinct strains of *Toxoplasma gondii* feature divergent transcriptomes regardless of developmental stage. *PLoS ONE*, 9(11), p.e111297.

D£, J., F£, L., M£, J. and McLeod, R. (2011). Oral oocyst-induced mouse model of toxoplasmosis: effect of infection with *Toxoplasma gondii* strains of different genotypes, dose, and mouse strains (transgenic, out-bred, in-bred) on pathogenesis and mortality. *Parasitology*, 139(01), pp.1-13.

Da Gama, L., Ribeiro-Gomes, F., Guimarães, U. and Arnholdt, A. (2004). Reduction in adhesiveness to extracellular matrix components, modulation of adhesion molecules and in vivo migration of murine macrophages infected with *Toxoplasma gondii*. *Microbes and Infection*, 6(14), pp.1287-1296.

Dalton, J., Cruickshank, S., Egan, C., Mears, R., Newton, D., Andrew, E., Lawrence, B., Howell, G., Else, K., Gubbels, M., Striepen, B., Smith, J., White, S. and Carding, S. (2006). Intraepithelial γδ+ lymphocytes maintain the

integrity of intestinal epithelial tight junctions in response to infection. *Gastroenterology*, 131(3), pp.818-829.

Dardé, M.-L. (2004) 'Genetic analysis of the diversity in *Toxoplasma gondii*.', *Ann Ist Super Sanita*, 40(1), pp. 57–63.

Daubener, W., Spors, B., Hucke, C., Adam, R., Stins, M., Kim, K. and Schroten, H. (2001). Restriction of *Toxoplasma gondii* growth in human brain microvascular endothelial cells by activation of indoleamine 2,3-dioxygenase. *Infection and Immunity*, 69(10), pp.6527-6531.

David Sibley, L. (2011). Invasion and intracellular survival by protozoan parasites. *Immunological Reviews*, 240(1), pp.72-91.

David, F., Rougemont, J. and Deplancke, B. (2016). GETPrime 2.0: gene- and transcript-specific qPCR primers for 13 species including polymorphisms. *Nucleic Acids Research*, 45(D1), pp. D56-D60.

Davies, K., Strauss, M., Daum, B., Kief, J., Osiewacz, H., Rycovska, A., Zickermann, V. and Kuhlbrandt, W. (2011). Macromolecular organization of ATP synthase and complex I in whole mitochondria. *Proceedings of the National Academy of Sciences*, 108(34), pp.14121-14126.

de Vries, H.E., 1997. The blood-brain barrier in neuroinflammatory diseases. Pharmacological reviews 49, 143–55.

Deli, M. A. (2007) 'Blood-brain barrier models', in Lajtha, A. (ed) *Handbook of neurochemistry and molecular neurobiology*. New York: Springer, pp. 29-56

Dellacasa-Lindberg, I., Hitziger, N. and Barragan, A. (2008). Localized recrudescence of *Toxoplasma gondii* infections in the central nervous system of immunocompromised mice assessed by in vivo bioluminescence imaging. *BMC Proceedings*, 2(S1).

Demar, M., Hommel, D., Djossou, F., Peneau, C., Boukhari, R., Louvel, D., Bourbigot, A., Nasser, V., Ajzenberg, D., Darde, M. and Carme, B. (2012). Acute toxoplasmoses in immunocompetent patients hospitalized in an intensive care unit in French Guiana. *Clinical Microbiology and Infection*, 18(7), pp.E221-E231.

Deng, Y., Zhang, J., Wang, Z., Yan, Z., Qiao, M., Ye, J., Wei, Q., Wang, J., Wang, X., Zhao, L., Lu, S., Tang, S., Mohammed, M., Liu, H., Fan, J., Zhang, F., Zou, Y., Liao, J., Qi, H., Haydon, R., Luu, H., He, T. and Tang, L. (2015). Antibiotic monensin synergizes with EGFR inhibitors and oxaliplatin to suppress the proliferation of human ovarian cancer cells. *Scientific Reports*, 5(1).

DIANA tools. (2015). *DIANA TOOLS - mirPath v.3*. [online] Available at: http://snf-515788.vm.okeanos.grnet.gr/ [Last accessed 11 Mar. 2019].

Dillies, M., Rau, A., Aubert, J., Hennequet-Antier, C., Jeanmougin, M., Servant, N., Keime, C., Marot, G., Castel, D., Estelle, J., Guernec, G., Jagla, B., Jouneau, L., Laloe, D., Le Gall, C., Schaeffer, B., Le Crom, S., Guedj, M. and Jaffrezic, F. (2012). A comprehensive evaluation of normalization methods for Illumina high-throughput RNA sequencing data analysis. *Briefings in Bioinformatics*, 14(6), pp. 671-683.

dos Santos, T., Portes, J., Damasceno-Sá, J., Caldas, L., de Souza, W., DaMatta, R. and Seabra, S. (2011). Phosphatidylserine exposure by *Toxoplasma gondii* is fundamental to balance the immune response granting survival of the parasite and of the host. *PLoS ONE*, 6(11), p.e27867.

Drewry, L. and Sibley, L. (2015). Toxoplasma actin is required for efficient host cell invasion. *mBio*, 6(3).

Drogemuller, K., Helmuth, U., Brunn, A., Sakowicz-Burkiewicz, M., Gutmann, D., Mueller, W., Deckert, M. and Schluter, D. (2008). Astrocyte gp130

expression is critical for the control of Toxoplasma encephalitis. *The Journal of Immunology*, 181(4), pp.2683-2693.

Du, Y., Chen, Y., Wang, F. and Gu, L. (2016). miR-137 plays tumor suppressor roles in gastric cancer cell lines by targeting KLF12 and MYO1C. *Tumor Biology*, 37(10), pp.13557-13569.

Dubey, J., Lindsay, D. and Speer, C. (1998). Structures of *Toxoplasma gondii* tachyzoites, bradyzoites, and sporozoites and biology and development of tissue cysts. *Clinical Microbiology Reviews*, 11(2), pp.267-299.

Dubey, J., Zarnke, R., Thomas, N., Wong, S., Bonn, W., Briggs, M., Davis, J., Ewing, R., Mense, M., Kwok, O., Romand, S. and Thulliez, P. (2003). *Toxoplasma gondii*, Neospora caninum, *Sarcocystis neurona,* and *Sarcocystis canis*-like infections in marine mammals. *Veterinary Parasitology*, 116(4), pp.275-296.

Dupont, C., Christian, D. and Hunter, C. (2012). Immune response and immunopathology during toxoplasmosis. *Seminars in Immunopathology*, 34(6), pp.793-813.

Edvinsson, B., Lappalainen, M. and Evengård, B. (2006). Real-time PCR targeting a 529-bp repeat element for diagnosis of toxoplasmosis. *Clinical Microbiology and Infection*, 12(2), pp.131-136.

Eigenmann, D., Jähne, E., Smieško, M., Hamburger, M. and Oufir, M. (2016). Validation of an immortalized human (hBMEC) in vitro blood-brain barrier model. *Analytical and Bioanalytical Chemistry*, 408(8), pp.2095-2107.

Eigenmann, D., Xue, G., Kim, K., Moses, A., Hamburger, M. and Oufir, M. (2013). Comparative study of four immortalized human brain capillary endothelial cell lines, hCMEC/D3, hBMEC, TY10, and BB19, and optimization of

culture conditions, for an in vitro blood–brain barrier model for drug permeability studies. *Fluids and Barriers of the CNS*, 10(1), p.33.

Elsheikha, H. (2008). Congenital toxoplasmosis: Priorities for further health promotion action. *Public Health*, 122(4), pp.335-353.

Elsheikha, H. and Khan, N. (2010). Protozoa traversal of the blood–brain barrier to invade the central nervous system. *FEMS Microbiology Reviews*, 34(4), pp.532-553.

Elsheikha, H., Alkurashi, M., Kong, K. and Zhu, X. (2014). Metabolic footprinting of extracellular metabolites of brain endothelium infected with Neospora caninum in vitro. *BMC Research Notes*, 7(1).

eport, C., Raffi, F., Matheron, S., Katlama, C., Regnier, B., Saimot, A., Marche, C., Vedrenne, C. and Vilde, J. (1988). Treatment of central nervous system toxoplasmosis with pyrimethamine/sulfadiazine combination in 35 patients with the acquired immunodeficiency syndrome. *The American Journal of Medicine*, 84(1), pp.94-100.

Etienne-Manneville, S. (2004). Cdc42 - the centre of polarity. *Journal of Cell Science*, 117(8), pp.1291-1300.

Eum, S., Jaraki, D., Bertrand, L., András, I. and Toborek, M. (2014). Disruption of epithelial barrier by quorum-sensing N-3-(oxododecanoyl)-homoserine lactone is mediated by matrix metalloproteinases. *American Journal of Physiology-Gastrointestinal and Liver Physiology*, 306(11), pp.G992-G1001.

Eupathdb.org. (2019). *EuPathDB: The Eukaryotic Pathogen Genomics Resource*. [online] Available at: https://eupathdb.org/eupathdb/ [Last accessed 11 Mar. 2019].

EVOM & EVOMX Epithelial Voltohmmeters Instruction Manual. (2008). [ebook] World Precision Instruments Inc. Available at: https://www.wpiinc.com/media/wysiwyg/pdf/EVOM-IM-021308.pdf [Accessed 5 January 2017].

Fehlmann, T., Backes, C., Kahraman, M., Haas, J., Ludwig, N., Posch, A., Würstle, M., Hübenthal, M., Franke, A., Meder, B., Meese, E. and Keller, A. (2017). Web-based NGS data analysis using miRMaster: a large-scale meta-analysis of human miRNAs. *Nucleic Acids Research*, 45(15), pp.8731-8744.

Feustel, S., Meissner, M. and Liesenfeld, O. (2012). *Toxoplasma gondii* and the blood-brain barrier. *Virulence*, 3(2), pp.182-192.

Flegr, J., Klapilová, K. and Kaňková, Š. (2014). Toxoplasmosis can be a sexually transmitted infection with serious clinical consequences. Not all routes of infection are created equal. *Medical Hypotheses*, 83(3), pp.286-289.

Fletcher, N., Wilson, G., Murray, J., Hu, K., Lewis, A., Reynolds, G., Stamataki, Z., Meredith, L., Rowe, I., Luo, G., Lopez–Ramirez, M., Baumert, T., Weksler, B., Couraud, P., Kim, K., Romero, I., Jopling, C., Morgello, S., Balfe, P. and McKeating, J. (2012). Hepatitis C virus infects the endothelial cells of the blood-brain barrier. *Gastroenterology*, 142(3), pp.634-643.e6.

Focus on ovine abortions. (2017). *Veterinary Record*, 180(10), pp.246-247.

Forman, D., West, N., Francis, J. and Guy, E. (2009). The sero-prevalence of *Toxoplasma gondii* in British marine mammals. *Memórias do Instituto Oswaldo Cruz*, 104(2), pp.296-298.

Förster, C. (2008). Tight junctions and the modulation of barrier function in disease. *Histochemistry and Cell Biology*, 130(1), pp.55-70.

Fouts, A. and Boothroyd, J. (2007). Infection with *Toxoplasma gondii* bradyzoites has a diminished impact on host transcript levels relative to tachyzoite infection. *Infection and Immunity*, 75(6), pp.3209-3209.

Freeman, G., Long, A., Iwai, Y., Bourque, K., Chernova, T., Nishimura, H., Fitz, L., Malenkovich, N., Okazaki, T., Byrne, M., Horton, H., Fouser, L., Carter, L., Ling, V., Bowman, M., Carreno, B., Collins, M., Wood, C. and Honjo, T. (2000). Engagement of the Pd-1 immunoinhibitory receptor by a novel B7 family member leads to negative regulation of lymphocyte activation. *The Journal of Experimental Medicine*, 192(7), pp.1027-1034.

Furtado, J., Winthrop, K., Butler, N. and Smith, J. (2012). Ocular toxoplasmosis I: parasitology, epidemiology and public health. *Clinical & Experimental Ophthalmology*, 41(1), pp.82-94.

Furuse, M., Fujita, K., Hiiragi, T., Fujimoto, K. and Tsukita, S. (1998). Claudin-1 and -2: Novel integral membrane proteins localizing at tight junctions with no sequence similarity to occludin. *The Journal of Cell Biology*, 141(7), pp.1539-1550.

Fux, B., Nawas, J., Khan, A., Gill, D., Su, C. and Sibley, L. (2007). *Toxoplasma gondii* strains defective in oral transmission are also defective in developmental stage differentiation. *Infection and Immunity*, 75(5), pp.2580-2590.

Gajria, B., Bahl, A., Brestelli, J., Dommer, J., Fischer, S., Gao, X., Heiges, M., Iodice, J., Kissinger, J., Mackey, A., Pinney, D., Roos, D., Stoeckert, C., Wang, H. and Brunk, B. (2007). ToxoDB: an integrated *Toxoplasma gondii* database resource. *Nucleic Acids Research*, 36(Database), pp. D553-D556.

Gallego-Delgado, J., Basu-Roy, U., Ty, M., Alique, M., Fernandez-Arias, C., Movila, A., Gomes, P., Weinstock, A., Xu, W., Edagha, I., Wassmer, S., Walther, T., Ruiz-Ortega, M. and Rodriguez, A. (2016). Angiotensin receptors and β-

catenin regulate brain endothelial integrity in malaria. *Journal of Clinical Investigation*, 126(10), pp.4016-4029.

Gao, Q., Zhang, N., Zhang, F., Wang, M., Hu, L. and Zhu, X. (2018). Immune response and protective effect against chronic *Toxoplasma gondii* infection induced by vaccination with a DNA vaccine encoding profilin. *BMC Infectious Diseases*, 18(1).

Gene Ontology Resource. (2019). *The Gene Ontology Resource*. [online] Available at: http://geneontology.org/ [Last accessed 11 Mar. 2019].

Gentleman, R. C., Carey, V. J., Bates, D. M., Bolstad, B., Dettling, M., Dudoit, S., Ellis, B., Gautier, L., Ge, Y., Gentry, J., Hornik, K., Hothorn, T., Huber, W., Iacus, S., Irizarry, R., Leisch, F., Li, C., Maechler, M., Rossini, A. J., Sawitzki, G., Smith, C., Smyth, G., Tierney, L., Yang, J. Y., … Zhang, J. (2004). Bioconductor: open software development for computational biology and bioinformatics. *Genome biology*, *5*(10), pp. R80.

Gigley, J. (2016). The diverse role of NK Cells in immunity to *Toxoplasma gondii* infection. *PLOS Pathogens*, 12(2), p.e1005396.

Gilbert, R. (2006). Newborn screening for congenital toxoplasmosis: feasible, but benefits are not established. *Archives of Disease in Childhood*, 91(8), pp.629-631.

Gingo, M., George, M., Kessinger, C., Lucht, L., Rissler, B., Weinman, R., Slivka, W., McMahon, D., Wenzel, S., Sciurba, F. and Morris, A. (2010). Pulmonary function abnormalities in HIV-infected patients during the current antiretroviral therapy era. *American Journal of Respiratory and Critical Care Medicine*, 182(6), pp.790-796.

Godin-Heymann, N., Brabetz, S., Murillo, M., Saponaro, M., Santos, C., Lobley, A., East, P., Chakravarty, P., Matthews, N., Kelly, G., Jordan, S., Castellano, E. and Downward, J. (2015). Tumour-suppression function of KLF12 through regulation of anoikis. *Oncogene*, 35(25), pp.3324-3334.

Goebel, S., Gross, U., Lüder C. G. (2001). Inhibition of host cell apoptosis by *Toxoplasma gondii* is accompanied by reduced activation of the caspase cascade and alterations of poly (ADP-ribose) polymerase expression. *Journal of Cell Science*, 114(Pt 19), pp. 3495–3505.

Grainger, C., Greenwell, L., Lockley, D., Martin, G. and Forbes, B. (2006). Culture of Calu-3 cells at the air interface provides a representative model of the airway epithelial barrier. *Pharmaceutical Research*, 23(7), pp.1482-1490.

Greene, C. and Campbell, M. (2016). Tight junction modulation of the blood brain barrier: CNS delivery of small molecules. *Tissue Barriers*, 4(1), p.e1138017.

Greiffenberg, L., Goebel, W., Kim, K., Daniels, J. and Kuhn, M. (2000). Interaction of Listeria monocytogenes with Human Brain Microvascular Endothelial Cells: An Electron Microscopic Study. *Infection and Immunity*, 68(6), pp.3275-3279.

Grinde, B. (1983). Effect of carboxylic ionophores on lysosomal protein degradation in rat hepatocytes. *Experimental Cell Research*, 149(1), pp.27-35.

Großhans, H. and Filipowicz, W. (2008). The expanding world of small RNAs. *Nature*, 451(7177), pp.414-416.

Guan, B., Li, Q., Shen, L., Rao, Q., Wang, Y., Zhu, Y., Zhou, X. and Li, X. (2016). MicroRNA-205 directly targets Krüppel-like factor 12 and is involved in

invasion and apoptosis in basal-like breast carcinoma. *International Journal of Oncology*, 49(2), pp.720-734.

Günzel, D. and Yu, A. (2013). Claudins and the modulation of tight junction permeability. *Physiological Reviews*, 93(2), pp.525-569.

Håkansson, S., Morisaki, H., Heuser, J. and Sibley, L. (1999). Time-lapse video microscopy of gliding motility in *Toxoplasma gondii* reveals a novel, biphasic mechanism of cell locomotion. *Molecular Biology of the Cell*, 10(11), pp.3539-3547.

Halonen, S. K., Chiu, F., & Weiss, L. M. (1998). Effect of cytokines on growth of *Toxoplasma gondii* in murine astrocytes. *Infection and immunity*, *66*(10), pp. 4989-93.

Halsby, K., Guy, E., Said, B., Francis, J., O'connor, C., Kirkbride, H. and Morgan, D. (2013). Enhanced surveillance for toxoplasmosis in England and Wales, 2008–2012. *Epidemiology and Infection*, 142(08), pp.1653-1660.

Harker, K., Ueno, N. and Lodoen, M. (2015). *Toxoplasma gondii* dissemination: a parasite's journey through the infected host. *Parasite Immunology*, 37(3), pp.141-149.

Harker, K., Ueno, N., Wang, T., Bonhomme, C., Liu, W. and Lodoen, M. (2013). *Toxoplasma gondii* modulates the dynamics of human monocyte adhesion to vascular endothelium under fluidic shear stress. *Journal of Leukocyte Biology*, 93(5), pp.789-800.

Hassan, I., Wang, S., Xu, L., Yan, R., Song, X. and Li, X. (2014). Immunoglobulin and cytokine changes induced following immunization with a DNA vaccine encoding *Toxoplasma gondii* selenium-dependent glutathione reductase protein. *Experimental Parasitology*, 146, pp.1-10.

He, B., Lu, N. and Zhou, Z. (2009). Cellular and nuclear degradation during apoptosis. *Current Opinion in Cell Biology*, 21(6), pp.900-912.

He, J., Ma, J., Wang, J., Xu, M. and Zhu, X. (2016). Analysis of miRNA expression profiling in mouse spleen affected by acute *Toxoplasma gondii* infection. *Infection, Genetics and Evolution*, 37, pp.137-142.

Heaslip, A., Nishi, M., Stein, B. and Hu, K. (2011). The motility of a human parasite, *Toxoplasma gondii*, is regulated by a novel lysine methyltransferase. *PLoS Pathogens*, 7(9), p.e1002201.

Holland, G. (2003). Ocular toxoplasmosis: a global reassessment. *American Journal of Ophthalmology*, 136(6), pp.973-988.

Hooi, D., Bycroft, B., Chhabra, S., Williams, P. and Pritchard, D. (2004). Differential immune modulatory activity of *Pseudomonas aeruginosa* quorum-sensing signal molecules. *Infection and Immunity*, 72(11), pp.6463-6470.

Huang, S. and Jong, A. (2001). Cellular mechanisms of microbial proteins contributing to invasion of the blood-brain barrier. MicroReview. *Cellular Microbiology*, 3(5), pp.277-287.

Huber, W., Carey, V., Gentleman, R., Anders, S., Carlson, M., Carvalho, B., Bravo, H., Davis, S., Gatto, L., Girke, T., Gottardo, R., Hahne, F., Hansen, K., Irizarry, R., Lawrence, M., Love, M., MacDonald, J., Obenchain, V., Oleś, A., Pagès, H., Reyes, A., Shannon, P., Smyth, G., Tenenbaum, D., Waldron, L. and Morgan, M. (2015). Orchestrating high-throughput genomic analysis with Bioconductor. *Nature Methods*, 12(2), pp.115-121.

Hunter, C. and Sibley, L. (2012). Modulation of innate immunity by *Toxoplasma gondii* virulence effectors. *Nature Reviews Microbiology*, 10(11), pp.766-778.

Huynh, M. (2003). Rapid invasion of host cells by Toxoplasma requires secretion of the MIC2-M2AP adhesive protein complex. *The EMBO Journal*, 22(9), pp.2082-2090.

Iovino, F., Orihuela, C., Moorlag, H., Molema, G. and Bijlsma, J. (2013). Interactions between blood-borne Streptococcus pneumoniae and the blood-brain barrier preceding meningitis. *PLoS ONE*, 8(7), p.e68408.

Irizarry, R. (2003). Exploration, normalization, and summaries of high-density oligonucleotide array probe level data. *Biostatistics*, 4(2), pp.249-264.

Irizarry, R. (2003). Summaries of Affymetrix GeneChip probe level data. *Nucleic Acids Research*, 31(4), pp.15e-15.

Irizarry, R.A., Hobbs, B., ... Speed, T.P., 2012. Exploration, normalization, and summaries of high-density oligonucleotide array probe level data, in *Selected Works of Terry Speed*. New York: Springer, pp. 601–616.

Jebbari, H., & Roberts, C. W., Ferguson, D. J., Bluethmann, H., Alexander, J. (1998). A protective role for IL-6 during early infection with *Toxoplasma gondii*. *Parasite immunology*. 20(5), pp. 231–239.

Jensen, K., Camejo, A., Melo, M., Cordeiro, C., Julien, L., Grotenbreg, G., Frickel, E., Ploegh, H., Young, L. and Saeij, J. (2015). *Toxoplasma gondii* superinfection and virulence during secondary infection correlate with the exact ROP5/ROP18 allelic combination. *mBio*, 6(2).

Jia, B., Lu, H., Liu, Q., Yin, J., Jiang, N. and Chen, Q. (2013). Genome-wide comparative analysis revealed significant transcriptome changes in mice after *Toxoplasma gondii* infection. *Parasites & Vectors*, 6(1), p.161.

Jia, W., Martin, T., Zhang, G.-B., Jiang, W. (2013). Junctional adhesion molecules in cerebral endothelial tight junction and brain metastasis. *Anticancer research*. 33, pp. 2353-9.

Jong, A., Stins, M., Huang, S., Chen, S. and Kim, K. (2001). Traversal of Candida albicans across human blood-brain barrier in vitro. *Infection and Immunity*, 69(7), pp.4536-4544.

Kaňková, Š., Procházková, L., Flegr, J., Calda, P., Springer, D. and Potluková, E. (2014). Effects of latent toxoplasmosis on autoimmune thyroid diseases in pregnancy. *PLoS ONE*, 9(10), p.e110878.

Kapoor, A., He, R., Venkatadri, R., Forman, M. and Arav-Boger, R. (2013). Wnt modulating agents inhibit human Cytomegalovirus replication. *Antimicrobial Agents and Chemotherapy*, 57(6), pp.2761-2767.

Keller, P., Schaumburg, F., Fischer, S., HÃ¤cker, G., GroÃŸ, U. and LÃ¼der, C. (2006). Direct inhibition of cytochromec-induced caspase activation in vitro by *Toxoplasma gondii* reveals novel mechanisms of interference with host cell apoptosis. *FEMS Microbiology Letters*, 258(2), pp.312-319.

Kessler, M., Zielecki, J., Thieck, O., Mollenkopf, H., Fotopoulou, C. and Meyer, T. (2012). *Chlamydia trachomatis* disturbs epithelial tissue homeostasis in fallopian tubes via paracrine Wnt signaling. *The American Journal of Pathology*, 180(1), pp.186-198.

Kim, D., Langmead, B. and Salzberg, S. (2015). HISAT: a fast-spliced aligner with low memory requirements. *Nature Methods*, 12(4), pp.357-360.

Kim, K. (2002). Strategy of *Escherichia coli* for crossing the blood-brain barrier. *The Journal of Infectious Diseases*, 186(s2), pp. S220-S224.

Kim, K. (2012). Current concepts on the pathogenesis of *Escherichia coli* meningitis. *Current Opinion in Infectious Diseases*, 25(3), pp.273-278.

Kim, K. and Weiss, L. (2004). *Toxoplasma gondii*: the model apicomplexan. *International Journal for Parasitology*, 34(3), pp.423-432.

Kim, S., Fouts, A. and Boothroyd, J. (2007). *Toxoplasma gondii* dysregulates IFN-inducible gene expression in human fibroblasts: Insights from a genome-wide transcriptional profiling. *The Journal of Immunology*, 178(8), pp.5154-5165.

Kongsaengdao, S., Samintarapanya, K., Oranratnachai, K., Prapakarn, W. and Apichartpiyakul, C. (2007). Randomized controlled trial of pyrimethamine plus sulfadiazine versus trimethoprim plus sulfamethoxazole for treatment of Toxoplasmic Encephalitis in AIDS patients. *Journal of the International Association of Physicians in AIDS Care*, 7(1), pp.11-16.

Konradt, C., Ueno, N., Christian, D., Delong, J., Pritchard, G., Herz, J., Bzik, D., Koshy, A., McGavern, D., Lodoen, M. and Hunter, C. (2016). Endothelial cells are a replicative niche for entry of *Toxoplasma gondii* to the central nervous system. *Nature Microbiology*, 1(3), p.16001.

Kreft, M., Jerman, U., Lasič, E., Hevir-Kene, N., Rižner, T., Peternel, L. and Kristan, K. (2015). The characterization of the human cell line Calu-3 under different culture conditions and its use as an optimized in vitro model to investigate bronchial epithelial function. *European Journal of Pharmaceutical Sciences*, 69, pp.1-9.

Kroemer, G., Galluzzi, L. and Brenner, C. (2007). Mitochondrial membrane permeabilization in cell death. *Physiological Reviews*, 87(1), pp.99-163.

Kucera, K., Koblansky, A., Saunders, L., Frederick, K., De La Cruz, E., Ghosh, S. and Modis, Y. (2010). Structure-based analysis of *Toxoplasma gondii* profilin: A parasite-specific motif is required for recognition by toll-like receptor 11. *Journal of Molecular Biology*, 403(4), pp.616-629.

Kuckleburg, C. and Newman, P. (2013). Neutrophil proteinase 3 acts on protease-activated receptor-2 to enhance vascular endothelial cell barrier function. *Arteriosclerosis, Thrombosis, and Vascular Biology*, 33(2), pp.275-284.

Kuckleburg, C., Tilkens, S., Santoso, S. and Newman, P. (2012). Proteinase 3 contributes to transendothelial migration of NB1-positive neutrophils. *The Journal of Immunology*, 188(5), pp.2419-2426.

Kumar, A., Tikoo, S., Maity, S., Sengupta, S., Sengupta, S., Kaur, A. and Kumar Bachhawat, A. (2012). Mammalian proapoptotic factor ChaC1 and its homologues function as γ-glutamyl cyclotransferases acting specifically on glutathione. *EMBO reports*, 13(12), pp.1095-1101.

Lachenmaier, S., Deli, M., Meissner, M. and Liesenfeld, O. (2011). Intracellular transport of *Toxoplasma gondii* through the blood–brain barrier. *Journal of Neuroimmunology*, 232(1-2), pp.119-130.

Lambert, H., Hitziger, N., Dellacasa, I., Svensson, M. and Barragan, A. (2006). Induction of dendritic cell migration upon *Toxoplasma gondii* infection potentiates parasite dissemination. *Cellular Microbiology*, 8(10), pp.1611-1623.

Lambert, H., Vutova, P., Adams, W., Lore, K. and Barragan, A. (2009). The *Toxoplasma gondii*-Shuttling Function of Dendritic Cells Is Linked to the Parasite Genotype. *Infection and Immunity*, 77(4), pp.1679-1688.

Lamble, S., Batty, E., Attar, M., Buck, D., Bowden, R., Lunter, G., Crook, D., El-Fahmawi, B. and Piazza, P. (2013). Improved workflows for high throughput library preparation using the transposome-based nextera system. *BMC Biotechnology*, 13(1).

Lamkanfi, M., Walle, L. and Kanneganti, T. (2011). Deregulated inflammasome signaling in disease. *Immunological Reviews*, 243(1), pp.163-173.

Langmead, B. and Salzberg, S. (2012). Fast gapped-read alignment with Bowtie 2. *Nature Methods*, 9(4), pp.357-359.

Lau, Y., Lee, W., Gudimella, R., Zhang, G., Ching, X., Razali, R., Aziz, F., Anwar, A. and Fong, M. (2016). Deciphering the draft genome of *Toxoplasma gondii* RH strain. *PLOS ONE*, 11(6), p.e0157901.

Lavine, M. and Arrizabalaga, G. (2010). The antibiotic monensin causes cell cycle disruption of *Toxoplasma gondii* mediated through the DNA repair enzyme TgMSH-1. *Antimicrobial Agents and Chemotherapy*, 55(2), pp.745-755.

Lavine, M. and Arrizabalaga, G. (2012). Analysis of monensin sensitivity in *Toxoplasma gondii* reveals autophagy as a mechanism for drug induced death. *PLoS ONE*, 7(7), p.e42107.

Lee, M., Yang, R., Karastergiou, K., Smith, S., Chang, J., Gong, D. and Fried, S. (2016). Low expression of the GILZ may contribute to adipose inflammation and altered adipokine production in human obesity. *Journal of Lipid Research*, 57(7), pp.1256-1263.

Lefever, S., Vandesompele, J., Speleman, F. and Pattyn, F. (2009). RTPrimerDB: the portal for real-time PCR primers and probes. *Nucleic Acids Research*, 37(Database), pp. D942-D945.

Legros, F., Chatzoglou, E., Frachon, P., Ogier de Baulny, H., Laforêt, P., Jardel, C., Godinot, C. and Lombès, A. (2001). Functional characterization of novel mutations in the human cytochrome b gene. *European Journal of Human Genetics*, 9(7), pp.510-518.

Li, H., Handsaker, B., Wysoker, A., Fennell, T., Ruan, J., Homer, N., Marth, G., Abecasis, G. and Durbin, R. (2009). The sequence alignment/map format and SAMtools. *Bioinformatics*, 25(16), pp.2078-2079.

Li, L., Hooi, D., Chhabra, S., Pritchard, D. and Shaw, P. (2004). Bacterial N-acylhomoserine lactone-induced apoptosis in breast carcinoma cells correlated with down-modulation of STAT3. *Oncogene*, 23(28), pp.4894-4902.

Lin, Y., Chen, Y., Wu, G. and Lee, W. (2006). Hec1 sequentially recruits Zwint-1 and ZW10 to kinetochores for faithful chromosome segregation and spindle checkpoint control. *Oncogene*, 25(52), pp.6901-6914.

Love, M., Huber, W. and Anders, S. (2014). Moderated estimation of fold change and dispersion for RNA-seq data with DESeq2. *Genome Biology*, 15(12).

Lüder, C., Lang, C., Giraldo-Velasquez, M., Algner, M., Gerdes, J. and Gross, U. (2003). *Toxoplasma gondii* inhibits MHC class II expression in neural antigen-presenting cells by down-regulating the class II transactivator CIITA. *Journal of Neuroimmunology*, 134(1-2), pp.12-24.

Lüder, C., Walter, W., Beuerle, B., Maeurer, M. and Gross, U. (2001). *Toxoplasma gondii* down-regulates MHC class II gene expression and antigen presentation by murine macrophages via interference with nuclear translocation of STAT1α. *European Journal of Immunology*, 31(5), pp.1475-1484.

Lüder, C., Walter, W., Beuerle, B., Maeurer, M. and Gross, U. (2001). *Toxoplasma gondii* down-regulates MHC class II gene expression and antigen presentation by murine macrophages via interference with nuclear translocation of STAT1α. *European Journal of Immunology*, 31(5), pp.1475-1484.

Luissint, A., Artus, C., Glacial, F., Ganeshamoorthy, K. and Couraud, P. (2012). Tight junctions at the blood brain barrier: physiological architecture and disease-associated dysregulation. *Fluids and Barriers of the CNS*, 9(1), p.23.

Mak, C., Yung, M., Hui, L., Leung, L., Liang, R., Chen, K., Liu, S., Qin, Y., Leung, T., Lee, K., Chan, K., Ngan, H. and Chan, D. (2017). MicroRNA-141 enhances anoikis resistance in metastatic progression of ovarian cancer through targeting KLF12/Sp1/survivin axis. *Molecular Cancer*, 16(1).

Maresi, E., Janson, G., Fruncillo, S., Paiardini, A., Vallone, R., Dominici, P. and Astegno, A. (2018). Functional characterization and structure-guided mutational analysis of the transsulfuration enzyme cystathionine γ-Lyase from *Toxoplasma gondii*. *International Journal of Molecular Sciences*, 19(7), p.2111.

Matter, K. and Balda, M. (2003). Functional analysis of tight junctions. *Methods*, 30(3), pp.228-234.

Mayer, M., Sheridan, J., Blohmke, C., Turvey, S. and Hancock, R. (2011). The Pseudomonas aeruginosa autoinducer 3O-C12 homoserine lactone provokes hyperinflammatory responses from cystic fibrosis airway epithelial cells. *PLoS ONE*, 6(1), p.e16246.

McCarthy, S. and Davis, C. (2003). Prooxidant diet provides protection during murine infection with *Toxoplasma gondii*. *Journal of Parasitology*, 89(5), pp.886-894.

Mehta, S. and Sibley, L. (2011). Actin depolymerizing factor controls actin turnover and gliding motility in *Toxoplasma gondii*. *Molecular Biology of the Cell*, 22(8), pp.1290-1299.

Meng, M., He, S., Zhao, G., Bai, Y., Zhou, H., Cong, H., Lu, G., Zhao, Q. and Zhu, X. (2012). Evaluation of protective immune responses induced by DNA vaccines encoding *Toxoplasma gondii* surface antigen 1 (SAG1) and 14-3-3 protein in BALB/c mice. *Parasites & Vectors*, 5(1), p.273.

Mercier, C., Dubremetz, J., Rauscher, B., Lecordier, L., Sibley, L. and Cesbron-Delauw, M. (2002). Biogenesis of nanotubular network in Toxoplasma parasitophorous vacuole induced by parasite proteins. *Molecular Biology of the Cell*, 13(7), pp.2397-2409.

Mesquita, R., Ziegler, A., Hiramoto, R., Vidal, J. and Pereira-Chioccola, V. (2010). Real-time quantitative PCR in cerebral toxoplasmosis diagnosis of Brazilian human immunodeficiency virus-infected patients. *Journal of Medical Microbiology*, 59(6), pp.641-647.

Mi, H., Huang, X., Muruganujan, A., Tang, H., Mills, C., Kang, D. and Thomas, P. (2016). PANTHER version 11: expanded annotation data from Gene Ontology and Reactome pathways, and data analysis tool enhancements. *Nucleic Acids Research*, 45(D1), pp. D183-D189.

Mi, H., Muruganujan, A., Casagrande, J. and Thomas, P. (2013). Large-scale gene function analysis with the PANTHER classification system. *Nature Protocols*, 8(8), pp.1551-1566.

Middleton, M., Zukas, A., Rubinstein, T., Kinder, M., Wilson, E., Zhu, P., Blair, I., Hunter, C. and Pure, E. (2009). 12/15-Lipoxygenase-dependent myeloid production of interleukin-12 is essential for resistance to chronic toxoplasmosis. *Infection and Immunity*, 77(12), pp.5690-5700.

Miller, A., Brooks, G., McLeod, L., Ruwanpura, S. and Jenkins, B. (2014). Differential involvement of gp130 signalling pathways in modulating tobacco carcinogen-induced lung tumourigenesis. *Oncogene*, 34(12), pp.1510-1519.

Miraglia, M., Rodriguez, A., Barrionuevo, P., Rodriguez, J., Kim, K., Dennis, V., Delpino, M. and Giambartolomei, G. (2018). *Brucella abortus* traverses' brain microvascular endothelial cells using infected monocytes as a trojan horse. *Frontiers in Cellular and Infection Microbiology*, 8.

Molan, A., Nosaka, K., Hunter, M. and Wang, W. (2016). The role of *Toxoplasma gondii* as a possible inflammatory agent in the pathogenesis of type 2 diabetes mellitus in humans. *Family Medicine and Community Health*, 4(4), pp.44-62.

Molestina, R., El-Guendy, N. and Sinai, A. (2008). Infection with *Toxoplasma gondii* results in dysregulation of the host cell cycle. *Cellular Microbiology*, 10(5), pp.1153-1165.

Montoya, J. and Liesenfeld, O. (2004). Toxoplasmosis. *The Lancet*, 363(9425), pp.1965-1976.

Mungrue, I., Pagnon, J., Kohannim, O., Gargalovic, P. and Lusis, A. (2008). CHAC1/MGC4504 is a novel proapoptotic component of the unfolded protein response, downstream of the ATF4-ATF3-CHOP cascade. *The Journal of Immunology*, 182(1), pp.466-476.

Murphy, L. and Sarge, K. (2008). Phosphorylation of CAP-G is required for its chromosomal DNA localization during mitosis. *Biochemical and Biophysical Research Communications*, 377(3), pp.1007-1011.

Nagineni, C., Detrick, B. and Hooks, J. (2000). *Toxoplasma gondii* infection induces gene expression and secretion of interleukin 1 (IL-1), IL-6, granulocyte-macrophage colony-stimulating factor, and intercellular adhesion

molecule 1 by human retinal pigment epithelial cells. *Infection and Immunity*, 68(1), pp.407-410.

Nakashima, S. (2002). Protein kinase C (PKC): Regulation and biological function. *Journal of Biochemistry*, 132(5), pp.669-675.

Nam, H. (2009). GRA proteins of *Toxoplasma gondii*: Maintenance of host-parasite interactions across the parasitophorous vacuolar membrane. *The Korean Journal of Parasitology*, 47(Suppl), p.S29.

Napoli, M. and Flores, E. (2016). The p53 family orchestrates the regulation of metabolism: physiological regulation and implications for cancer therapy. *British Journal of Cancer*, 116(2), pp.149-155.

Nemzow, L., Lubin, A., Zhang, L. and Gong, F. (2015). XPC: Going where no DNA damage sensor has gone before. *DNA Repair*, 36, pp.19-27.

Ngô, H., Zhou, Y., Lorenzi, H., Wang, K., Kim, T., Zhou, Y., Bissati, K., Mui, E., Fraczek, L., Rajagopala, S., Roberts, C., Henriquez, F., Montpetit, A., Blackwell, J., Jamieson, S., Wheeler, K., Begeman, I., Naranjo-Galvis, C., Alliey-Rodriguez, N., Davis, R., Soroceanu, L., Cobbs, C., Steindler, D., Boyer, K., Noble, A., Swisher, C., Heydemann, P., Rabiah, P., Withers, S., Soteropoulos, P., Hood, L. and McLeod, R. (2017). Toxoplasma modulates signature pathways of human epilepsy, neurodegeneration & cancer. *Scientific Reports*, 7(1).

Niehus, S., Smith, T., Azzouz, N., Campos, M., Dubremetz, J., Gazzinelli, R., Schwarz, R. and Debierre-Grockiego, F. (2014). Virulent and avirulent strains of *Toxoplasma gondii* which differ in their glycosylphosphatidylinositol content induce similar biological functions in macrophages. *PLoS ONE*, 9(1), p.e85386.

Nishi, M., Hu, K., Murray, J. and Roos, D. (2008). Organellar dynamics during the cell cycle of *Toxoplasma gondii*. *Journal of Cell Science*, 121(9), pp.1559-1568.

Nozaki, T., Ali, V. and Tokoro, M. (2005). Sulfur-containing amino acid metabolism in parasitic protozoa. *Advances in parasitology,* 60, pp. 1-99.

Nunura, J., Vásquez, T., Endo, S., Salazar, D., Rodriguez, A., Pereyra, S. and Solis, H. (2010). Disseminated toxoplasmosis in an immunocompetent patient from Peruvian Amazon. *Revista do Instituto de Medicina Tropical de São Paulo*, 52(2), pp.107-110.

Okomo-Adhiambo, M., Beattie, C. and Rink, A. (2006). cDNA microarray analysis of host-pathogen interactions in a porcine in vitro model for *Toxoplasma gondii* infection. *Infection and Immunity*, 74(7), pp.4254-4265.

Olson, J., Wang, X., Pankratz, V., Fredericksen, Z., Vachon, C., Vierkant, R., Cerhan, J. and Couch, F. (2010). Centrosome-related genes, genetic variation, and risk of breast cancer. *Breast Cancer Research and Treatment*, 125(1), pp.221-228.

PANTHER Classification System. (2019). *PANTHER - Gene List Analysis*. [online] Available at: http://pantherdb.org/ [Last accessed 11 Mar. 2019].

Pappas, G., Roussos, N. and Falagas, M. (2009). Toxoplasmosis snapshots: Global status of *Toxoplasma gondii* seroprevalence and implications for pregnancy and congenital toxoplasmosis. *International Journal for Parasitology*, 39(12), pp.1385-1394.

Patidar, M., Yadav, N. and Dalai, S. (2016). Interleukin 15: A key cytokine for immunotherapy. *Cytokine & Growth Factor Reviews*, 31, pp.49-59.

Pavlou, G., Biesaga, M., Touquet, B., Lagal, V., Balland, M., Dufour, A., Hakimi, M. and Tardieux, I. (2018). Toxoplasma parasite twisting motion mechanically induces host cell membrane fission to complete invasion within a protective vacuole. *Cell Host & Microbe*, 24(1), pp.81-96.e5.

Pernas, L., Adomako-Ankomah, Y., Shastri, A., Ewald, S., Treeck, M., Boyle, J. and Boothroyd, J. (2014). Toxoplasma effector MAF1 mediates recruitment of host mitochondria and impacts the host response. *PLoS Biology*, 12(4), p.e1001845.

Pesci, E., Milbank, J., Pearson, J., McKnight, S., Kende, A., Greenberg, E. and Iglewski, B. (1999). Quinolone signaling in the cell-to-cell communication system of Pseudomonas aeruginosa. *Proceedings of the National Academy of Sciences*, 96(20), pp.11229-11234.

Petersen, E., Edvinsson, B., Lundgren, B., Benfield, T. and Evengård, B. (2006). Diagnosis of pulmonary infection with *Toxoplasma gondii* in immunocompromised HIV-positive patients by real-time PCR. *European Journal of Clinical Microbiology & Infectious Diseases*, 25(6), pp.401-404.

Peterson, P., Gekker, G., Hu, S. and Chao, C. (1995). Human astrocytes inhibit intracellular multiplication of *Toxoplasma gondii* by a nitric oxide-mediated mechanism. *Journal of Infectious Diseases*, 171(2), pp.516-518.

Pfaffl, M. (2001). A new mathematical model for relative quantification in real-time RT-PCR. *Nucleic Acids Research*, 29(9), pp.45e-45.

Pfaffl, M. (2002). Relative expression software tool (REST(C)) for group-wise comparison and statistical analysis of relative expression results in real-time PCR. *Nucleic Acids Research*, 30(9), pp.36e-36.

Pfaffl, M. (2003). *BestKeeeper Software - BioInformatics in kinetic PCR*. [online] Gene-quantification.de. Available at: https://www.gene-quantification.de/bestkeeper.html [Accessed 25 February 2017].

Pomares, C., Devillard, S., Holmes, T., Olariu, T., Press, C., Ramirez, R., Talucod, J., Estran, R., Su, C., Dubey, J., Ajzenberg, D. and Montoya, J. (2018). Genetic characterization of *Toxoplasma gondii* DNA samples isolated from humans living in North America: An unexpected high prevalence of atypical genotypes. *The Journal of Infectious Diseases*, 218(11), pp.1783-1791.

Pope, S. and Lässer, C. (2013). *Toxoplasma gondii* infection of fibroblasts causes the production of exosome-like vesicles containing a unique array of mRNA and miRNA transcripts compared to serum starvation. *Journal of Extracellular Vesicles*, 2(1), p.22484.

Primer Bank. (2006). *PrimerBank PCR Primers for Gene Expression Detection and Quantification*. [online] Available at: https://pga.mgh.harvard.edu/primerbank/ [Accessed 20 February 2017].

Pulzova, L., Bhide, M. and Andrej, K. (2009). Pathogen translocation across the blood-brain barrier. *FEMS Immunology & Medical Microbiology*, 57(3), pp.203-213.

Puzio-Kuter, A. (2011). The role of p53 in metabolic regulation. *Genes & Cancer*, 2(4), pp.385-391.

Radke, J. R., Behnke, M. S., Mackey, A. J., Radke, J. B., Roos, D. S., & White, M. W. (2005). The transcriptome of *Toxoplasma gondii*. *BMC biology*, *3*, pp. 26.

Ramakrishnan, S., Docampo, M., MacRae, J., Pujol, F., Brooks, C., van Dooren, G., Hiltunen, J., Kastaniotis, A., McConville, M. and Striepen, B. (2011). Apicoplast and endoplasmic reticulum cooperate in fatty acid biosynthesis in

apicomplexan parasite *Toxoplasma gondii*. *Journal of Biological Chemistry*, 287(7), pp.4957-4971.

Razakandrainibe, R., Combes, V., Grau, G. and Jambou, R. (2013). Crossing the wall: The opening of endothelial cell junctions during infectious diseases. *The International Journal of Biochemistry & Cell Biology*, 45(7), pp.1165-1173.

Reactome.org. (2019). *Home - Reactome Pathway Database*. [online] Available at: https://reactome.org/ [Accessed 14 June 2018].

Rezaei, F., Daryani, A., Sharifi, M., Sarvi, S., jafari, N., Pagheh, A., Hashemi, N. and Hejazi, S. (2018). miR-20a inhibition using locked nucleic acid (LNA) technology and its effects on apoptosis of human macrophages infected by *Toxoplasma gondii* RH strain. *Microbial Pathogenesis*, 121, pp.269-276.

Ribacke, U., Mok, B., Wirta, V., Normark, J., Lundeberg, J., Kironde, F., Egwang, T., Nilsson, P. and Wahlgren, M. (2007). Genome wide gene amplifications and deletions in *Plasmodium falciparum*. *Molecular and Biochemical Parasitology*, 155(1), pp.33-44.

RNeasy® Mini Handbook. (2012). 4th ed. [ebook] Qiagen. Available at: https://www.qiagen.com/ch/resources/resourcedetail?id=14e7cf6e-521a-4cf7-8cbc-bf9f6fa33e24&lang=en [Accessed 8 January 2017].

Rtprimerdb.org. (2008). *RTPrimerDB: the real-time PCR primer and probe database - Homepage*. [online] Available at: http://www.rtprimerdb.org/ [Accessed 23 February 2017].

Runkle, E.A., Antonetti, D.A., 2011. 'The blood-retinal barrier: Structure and functional significance' in Nag, S. (Ed.), *The Blood-Brain and Other Neural*

Barriers: Reviews and Protocols, Methods in Molecular Biology. Humana Press, Totowa, NJ, pp. 133–148.

Ruskin, J. and Remington, J. (1968). Immunity and intracellular infection: Resistance to bacteria in mice infected with a protozoan. *Science*, 160(3823), pp.72-74.

Rutkowski, J. and Brzezinski, B. (2013). Structures and properties of naturally occurring polyether antibiotics. *BioMed Research International*, 2013, pp.1-31.

Sabin, A. and Warren, J. (1942). Therapeutic effectiveness of certain sulfonamides on infection by an intracellular protozoon (Toxoplasma). *Experimental Biology and Medicine*, 51(1), pp.19-23.

Saçar, M., Bağcı, C. and Allmer, J. (2014). Computational prediction of microRNAs from *Toxoplasma gondii* potentially regulating the hosts' gene expression. *Genomics, Proteomics & Bioinformatics*, 12(5), pp.228-238.

Sakamuru, S., Attene-Ramos, M.S., Xia, M., 2016. Mitochondrial membrane potential assay. *Methods in Molecular Biology,* 1473, pp. 17–22.

Sanders, K., Fox, B. and Bzik, D. (2015). Attenuated *Toxoplasma gondii* therapy of disseminated pancreatic cancer generates long-lasting immunity to pancreatic cancer. *OncoImmunology*, 5(4), p.e1104447.

Schmidt, D., Hogh, B., Andersen, O., Hansen, S., Dalhoff, K. and Petersen, E. (2005). Treatment of infants with congenital toxoplasmosis: Tolerability and plasma concentrations of sulfadiazine and pyrimethamine. *European Journal of Pediatrics*, 165(1), pp.19-25.

Schubert-Unkmeir, A., Sokolova, O., Panzner, U., Eigenthaler, M. and Frosch, M. (2006). Gene expression pattern in human brain endothelial cells in response to *Neisseria meningitidis*. *Infection and Immunity*, 75(2), pp.899-914.

Schuster, F. (2002). Cultivation of *Plasmodium* spp. *Clinical Microbiology Reviews*, 15(3), pp.355-364.

Shapira, S., Gat-Viks, I., Shum, B., Dricot, A., de Grace, M., Wu, L., Gupta, P., Hao, T., Silver, S., Root, D., Hill, D., Regev, A. and Hacohen, N. (2009). A physical and regulatory map of host-influenza interactions reveals pathways in H1N1 infection. *Cell*, 139(7), pp.1255-1267.

Sher, A., Tosh, K. and Jankovic, D. (2016). Innate recognition of *Toxoplasma gondii* in humans involves a mechanism distinct from that utilized by rodents. *Cellular & Molecular Immunology*, 14(1), pp.36-42.

Sinai, A., Payne, T., Carmen, J., Hardi, L., Watson, S. and Molestina, R. (2004). Mechanisms underlying the manipulation of host apoptotic pathways by *Toxoplasma gondii*. *International Journal for Parasitology*, 34(3), pp.381-391.

Sinha, S. and Yang, W. (2008). Cellular signaling for activation of Rho GTPase Cdc42. *Cellular Signalling*, 20(11), pp.1927-1934.

Skariah, S. and Mordue, D. (2012). Identification of *Toxoplasma gondii* genes responsive to the host immune response during in vivo infection. *PLoS ONE*, 7(10), p.e46621.

Skillman, K., Daher, W., Ma, C., Soldati-Favre, D. and Sibley, L. (2012). *Toxoplasma gondii* profilin acts primarily to sequester G-actin while formins efficiently nucleate actin filament formation in vitro. *Biochemistry*, 51(12), pp.2486-2495.

Sonaimuthu, P., Ching, X., Fong, M., Kalyanasundaram, R. and Lau, Y. (2016). Induction of protective immunity against Toxoplasmosis in BALB/c mice vaccinated with *Toxoplasma gondii* rhoptry-1. *Frontiers in Microbiology*, 7.

Song, C., Chiasson, M., Nursimulu, N., Hung, S., Wasmuth, J., Grigg, M. and Parkinson, J. (2014). Metabolic reconstruction identifies strain-specific regulation of virulence in *Toxoplasma gondii*. *Molecular Systems Biology*, 9(1), pp.708-708.

Soni, A., Amisten, S., Rorsman, P. and Salehi, A. (2013). GPRC5B a putative glutamate-receptor candidate is negative modulator of insulin secretion. *Biochemical and Biophysical Research Communications*, 441(3), pp.643-648.

Soreq, H. and Wolf, Y. (2011). NeurimmiRs: microRNAs in the neuroimmune interface. *Trends in Molecular Medicine*, 17(10), pp.548-555.

Souza, A., Machado, F., Celes, M., Faria, G., Rocha, L., Silva, J. and Rossi, M. (2005). Mitochondrial damage as an early event of monensin-induced cell injury in cultured fibroblasts L929. *Journal of Veterinary Medicine Series A*, 52(5), pp.230-237.

Srinivasan, B., Kolli, A., Esch, M., Abaci, H., Shuler, M. and Hickman, J. (2015). TEER measurement techniques for in vitro barrier model systems. *Journal of Laboratory Automation*, 20(2), pp.107-126.

Stahl, W. and Kaneda, Y. (1998). Impaired thyroid function in murine toxoplasmosis. *Parasitology*, 117(3), pp.217-222.

Steed, E., Balda, M. and Matter, K. (2010). Dynamics and functions of tight junctions. *Trends in Cell Biology*, 20(3), pp.142-149.

Stewart, R., West, D., Wang, C., Weiss, H., Gal, T., Durbin, E., O'Connor, W., Chen, M. and O'Connor, K. (2016). Elevated integrin α6β4 expression is associated with venous invasion and decreased overall survival in non–small cell lung cancer. *Human Pathology*, 54, pp.174-183.

Sutterland, A., Fond, G., Kuin, A., Koeter, M., Lutter, R., van Gool, T., Yolken, R., Szoke, A., Leboyer, M. and de Haan, L. (2015). Beyond the association. *Toxoplasma gondii* in schizophrenia, bipolar disorder, and addiction: systematic review and meta-analysis. *Acta Psychiatrica Scandinavica*, 132(3), pp.161-179.

Suzuki, Y., Claflin, J., Wang, X., Lengi, A. and Kikuchi, T. (2005). Microglia and macrophages as innate producers of interferon-gamma in the brain following infection with *Toxoplasma gondii*. *International Journal for Parasitology*, 35(1), pp.83-90.

Szatanek, T., Anderson-White, B., Faugno-Fusci, D., White, M., Saeij, J. and Gubbels, M. (2012). Cactin is essential for G1 progression in *Toxoplasma gondii*. *Molecular Microbiology*, 84(3), pp.566-577.

Taddei, A., Giampietro, C., Conti, A., Orsenigo, F., Breviario, F., Pirazzoli, V., Potente, M., Daly, C., Dimmeler, S. and Dejana, E. (2008). Endothelial adherens junctions control tight junctions by VE-cadherin-mediated upregulation of claudin-5. *Nature Cell Biology*, 10(8), pp.923-934.

Taguchi, R., Tanaka, S., Joe, G., Maseda, H., Nomura, N., Ohnishi, J., Ishizuka, S., Shimizu, H. and Miyazaki, H. (2014). Mucin 3 is involved in intestinal epithelial cell apoptosis via N-(3-oxododecanoyl)-l-homoserine lactone-induced suppression of Akt phosphorylation. *American Journal of Physiology-Cell Physiology*, 307(2), pp.C162-C168.

Tao, S., Niu, L., Cai, L., Geng, Y., Hua, C., Ni, Y. and Zhao, R. (2018). N -(3-oxododecanoyl)- l -homoserine lactone modulates mitochondrial function and suppresses proliferation in intestinal goblet cells. *Life Sciences*, 201, pp.81-88.

Tartakoff, A. (1983). Perturbation of vesicular traffic with the carboxylic ionophore monensin. *Cell*, 32(4), pp.1026-1028.

Tateda, K., Ishii, Y., Horikawa, M., Matsumoto, T., Miyairi, S., Pechere, J., Standiford, T., Ishiguro, M. and Yamaguchi, K. (2003). The Pseudomonas aeruginosa autoinducer N-3-oxododecanoyl homoserine lactone accelerates apoptosis in macrophages and neutrophils. *Infection and Immunity*, 71(10), pp.5785-5793.

Teichmann, K., Kuliberda, M., Schatzmayr, G., Hadacek, F. and Joachim, A. (2012). In vitro determination of anticryptosporidial activity of phytogenic extracts and compounds. *Parasitology Research*, 111(1), pp.231-240.

Tenter, A., Heckeroth, A. and Weiss, L. (2000). *Toxoplasma gondii*: from animals to humans. *International Journal for Parasitology*, 30(12-13), pp.1217-1258.

Toxodb.org (2019). *ToxoDB: The Toxoplasma Genomics Resource*. [online] Available at: http://toxodb.org/ [Accessed 15 December 2017].

Trager, W., Zung, J. and Tershakovec, M. (1990). Initial extracellular development in vitro of erythrocytic stages of malaria parasites (*Plasmodium falciparum*). *Proceedings of the National Academy of Sciences*, 87(15), pp.5618-5622.

Trapnell, C., Williams, B., Pertea, G., Mortazavi, A., Kwan, G., van Baren, M., Salzberg, S., Wold, B. and Pachter, L. (2010). Transcript assembly and quantification by RNA-Seq reveals unannotated transcripts and isoform switching during cell differentiation. *Nature Biotechnology*, 28(5), pp.511-515.

TruSeq® Stranded mRNA Sample Preparation Guide. (2014). 5th ed. [ebook] Illumina Inc. Available at: https://support.illumina.com/content/dam/illumina-support/documents/documentation/chemistry_documentation/samplepreps_truseq/truseqstrandedmrna/truseq-stranded-mrna-sample-prep-guide-15031047-e.pdf [Accessed 12 June 2017].

Tseng, H., Huang, T., Wu, A., Chen, H., Liu, C. and Jong, A. (2015). How Cryptococcus interacts with the blood–brain barrier. *Future Microbiology*, 10(10), pp.1669-1682.

Tumova, L., Pombinho, A., Vojtechova, M., Stancikova, J., Gradl, D., Krausova, M., Sloncova, E., Horazna, M., Kriz, V., Machonova, O., Jindrich, J., Zdrahal, Z., Bartunek, P. and Korinek, V. (2014). Monensin inhibits canonical Wnt signaling in human colorectal cancer cells and suppresses tumor growth in multiple intestinal neoplasia mice. *Molecular Cancer Therapeutics*, 13(4), pp.812-822.

Tymoshenko, S., Oppenheim, R., Agren, R., Nielsen, J., Soldati-Favre, D. and Hatzimanikatis, V. (2015). Metabolic needs and capabilities of *Toxoplasma gondii* through combined computational and experimental analysis. *PLOS Computational Biology*, 11(5), p.e1004261.

Uchil, P., Pawliczek, T., Reynolds, T., Ding, S., Hinz, A., Munro, J., Huang, F., Floyd, R., Yang, H., Hamilton, W., Bewersdorf, J., Xiong, Y., Calderwood, D. and Mothes, W. (2014). TRIM15 is a focal adhesion protein that regulates focal adhesion disassembly. *Journal of Cell Science*, 127(18), pp.3928-3942.

Uchil, P., Quinlan, B., Chan, W., Luna, J. and Mothes, W. (2008). TRIM E3 ligases interfere with early and late stages of the retroviral life cycle. *PLoS Pathogens*, 4(2), p.e16.

Ueno, M. (2007). Molecular anatomy of the brain endothelial barrier: An overview of the distributional features. *Current Medicinal Chemistry*, 14(11), pp.1199-1206.

Veronesi, F., Santoro, A., Milardi, G., Diaferia, M., Branciari, R., Miraglia, D., Cioffi, A., Gabrielli, S. and Ranucci, D. (2017). Comparison of PCR assays targeting the multi-copy targets B1 gene and 529 bp repetitive element for

detection of *Toxoplasma gondii* in swine muscle. *Food Microbiology*, 63, pp.213-216.

Vichai, V. and Kirtikara, K. (2006). Sulforhodamine B colorimetric assay for cytotoxicity screening. *Nature Protocols*, 1(3), pp.1112-1116.

Vigorito, E., Kohlhaas, S., Lu, D. and Leyland, R. (2013). miR-155: an ancient regulator of the immune system. *Immunological Reviews*, 253(1), pp.146-157.

Vikström, E., Tafazoli, F. and Magnusson, K. (2006). Pseudomonas aeruginosa quorum sensing molecule N-(3 oxododecanoyl)-l-homoserine lactone disrupts epithelial barrier integrity of Caco-2 cells. *FEBS Letters*, 580(30), pp.6921-6928.

Vlachos, I., Zagganas, K., Paraskevopoulou, M., Georgakilas, G., Karagkouni, D., Vergoulis, T., Dalamagas, T. and Hatzigeorgiou, A. (2015). DIANA-miRPath v3.0: deciphering microRNA function with experimental support. *Nucleic Acids Research*, 43(W1), pp. W460-W466.

Vlachos, I.S., Hatzigeorgiou, A.G., 2017. Functional analysis of miRNAs using the DIANA tools online suite, in: Methods in Molecular Biology. Humana Press Inc., pp. 25–50.

Vlachos, I.S., Zagganas, K., ... Hatzigeorgiou, A.G., 2015. DIANA-miRPath v3.0: Deciphering microRNA function with experimental support. *Nucleic Acids Research*, 43, pp. W460–W466.

Vogler, M. (2011). BCL2A1: the underdog in the BCL2 family. *Cell Death & Differentiation*, 19(1), pp.67-74.

Wang, A., Nomura, M., Patan, S. and Ware, J. (2002). Inhibition of protein kinase Cα prevents endothelial cell migration and vascular tube formation in

vitro and myocardial neovascularization in vivo. *Circulation Research*, 90(5), pp.609-616.

Wang, J., Liu, X., Jia, B., Lu, H., Peng, S., Piao, X., Hou, N., Cai, P., Yin, J., Jiang, N. and Chen, Q. (2012). A comparative study of small RNAs in *Toxoplasma gondii* of distinct genotypes. *Parasites & Vectors*, 5(1), p.186.

Wang, L., Chen, H., Liu, D., Huo, X., Gao, J., Song, X., Xu, X., Huang, K., Liu, W., Wang, Y., Lu, F., Lun, Z., Luo, Q., Wang, X. and Shen, J. (2013). Genotypes and Mouse Virulence of *Toxoplasma gondii* Isolates from Animals and Humans in China. *PLoS ONE*, 8(1), p.e53483.

Wang, S., Zhang, Z., Wang, Y., Gadahi, J., Xu, L., Yan, R., Song, X. and Li, X. (2017). *Toxoplasma gondii* elongation factor 1-Alpha (TgEF-1α) is a novel vaccine candidate antigen against toxoplasmosis. *Frontiers in Microbiology*, 08.

Wang, X., Spandidos, A., Wang, H. and Seed, B. (2011). PrimerBank: a PCR primer database for quantitative gene expression analysis, 2012 update. *Nucleic Acids Research*, 40(D1), pp. D1144-D1149.

Wang, Z., Suo, X., Xia, X. and Shen, J. (2006). Influence of monensin on cation influx and NA+-K+-ATPase activity of *Eimeria Tenella* sporozoites i*n vVitro*. *Journal of Parasitology*, 92(5), pp.1092-1096.

Warnekulasuriya, M. (1998). Detection of *Toxoplasma gondii* in cured meats. *International Journal of Food Microbiology*, 45(3), pp.211-215.

Wei, H., Wei, S., Lindsay, D. and Peng, H. (2015). A systematic review and meta-analysis of the efficacy of anti-*Toxoplasma gondii* medicines in humans. *PLOS ONE*, 10(9), p.e0138204.

Weidner, J., Kanatani, S., Uchtenhagen, H., Varas-Godoy, M., Schulte, T., Engelberg, K., Gubbels, M., Sun, H., Harrison, R., Achour, A. and Barragan, A.

(2016). Migratory activation of parasitized dendritic cells by the protozoan *Toxoplasma gondii* 14-3-3 protein. *Cellular Microbiology*, 18(11), pp.1537-1550.

Weidner, J.M., Kanatani, S., Barragan, A., 2013. Rapid cytoskeleton remodelling in dendritic cells following invasion by *Toxoplasma gondii* coincides with the onset of a hypermigratory phenotype. *Cellular Microbiology,* 15, pp. 1735–1752.

Weiss, L.M., Kim, K., 2013. *Toxoplasma gondii: The model apicomplexan - Perspectives and Methods.* Second Edition. Elsevier Ltd.

Welton, N. and Ades, A. (2005). A model of toxoplasmosis incidence in the UK: evidence synthesis and consistency of evidence. *Journal of the Royal Statistical Society: Series C (Applied Statistics)*, 54(2), pp.385-404.

Winkelmann, E., Luo, H. and Wang, T. (2016). West Nile Virus infection in the central nervous system. *F1000Research*, 5, p.105.

Wolburg, H. and Lippoldt, A. (2002). Tight junctions of the blood–brain barrier. *Vascular Pharmacology*, 38(6), pp.323-337.

Xiao, J., Li, Y., Prandovszky, E., Karuppagounder, S., Talbot, C., Dawson, V., Dawson, T. and Yolken, R. (2014). MicroRNA-132 dysregulation in *Toxoplasma gondii* infection has implications for dopamine signaling pathway. *Neuroscience*, 268, pp.128-138.

Yang, N., Farrell, A., Niedelman, W., Melo, M., Lu, D., Julien, L., Marth, G., Gubbels, M. and Saeij, J. (2013). Genetic basis for phenotypic differences between different *Toxoplasma gondii* type I strains. *BMC Genomics*, 14(1), p.467.

Yarovinsky, F. (2014). Innate immunity to *Toxoplasma gondii* infection. *Nature Reviews Immunology*, 14(2), pp.109-121.

Zeiner, G., Norman, K., Thomson, J., Hammond, S. and Boothroyd, J. (2010). *Toxoplasma gondii* infection specifically increases the levels of key host microRNAs. *PLoS ONE*, 5(1), p.e8742.

Zhang, C., 2009. Novel functions for small RNA molecules. *Current Opinion in Molecular Therapeutics,* 11, pp. 641–51.

Zhang, X., Su, R., Cheng, Z., Zhu, W., Li, Y., Wang, Y., Du, J., Cai, Y., Luo, Q., Shen, J. and Yu, L. (2017). A mechanistic study of *Toxoplasma gondii* ROP18 inhibiting differentiation of C17.2 neural stem cells. *Parasites & Vectors*, 10(1).

Zimmermann, S., Murray, P., Heeg, K. and Dalpke, A. (2006). Induction of suppressor of cytokine signaling-1 by *Toxoplasma gondii* contributes to immune evasion in macrophages by blocking IFN-signaling. *The Journal of Immunology*, 176(3), pp.1840-1847.